The Handbook of Environmental Chemistry 38
Series Editors: Damià Barceló · Andrey G. Kostianoy

Tinglin Huang *Editor*

Water Pollution and Water Quality Control of Selected Chinese Reservoir Basins

Springer

The Handbook of Environmental Chemistry

Founded by Otto Hutzinger

Volume 38

More information about this series at http://www.springer.com/series/698

Water Pollution and Water Quality Control of Selected Chinese Reservoir Basins

Volume Editor: Tinglin Huang

With contributions by

Y. Cheng · H. Cong · R. Hu · T. Huang · X. Li · Y. Li · W. Ma · X. Qiu · J. Shi · X. Shi · X. Sun · Y. Sun · G. Wen · C. Xia · J. Xu · X. Yang · F. Zhang · H. Zhang · S. Zhou · Z. Zhou

Springer

Editor
Tinglin Huang
School of Environmental and Municipal Engineering
Xi'an University of Architecture and Technology
Xi'an, Shaanxi
China

ISSN 1867-979X ISSN 1616-864X (electronic)
The Handbook of Environmental Chemistry
ISBN 978-3-319-20390-4 ISBN 978-3-319-20391-1 (eBook)
DOI 10.1007/978-3-319-20391-1

Library of Congress Control Number: 2015951716

Springer Cham Heidelberg New York Dordrecht London

Printed on acid-free paper

Springer International Publishing AG Switzerland is part of Springer Science+Business Media (www.springer.com)

The Handbook of Environmental Chemistry Also Available Electronically

The Handbook of Environmental Chemistry is included in Springer's eBook package *Earth and Environmental Science*. If a library does not opt for the whole package, the book series may be bought on a subscription basis.

For all customers who have a standing order to the print version of *The Handbook of Environmental Chemistry,* we offer free access to the electronic volumes of the Series published in the current year via SpringerLink. If you do not have access, you can still view the table of contents of each volume and the abstract of each article on SpringerLink (www.springerlink.com/content/110354/).

You will find information about the

– Editorial Board
– Aims and Scope
– Instructions for Authors
– Sample Contribution

at springer.com (www.springer.com/series/698).

All figures submitted in color are published in full color in the electronic version on SpringerLink.

Aims and Scope

Since 1980, *The Handbook of Environmental Chemistry* has provided sound and solid knowledge about environmental topics from a chemical perspective. Presenting a wide spectrum of viewpoints and approaches, the series now covers topics such as local and global changes of natural environment and climate; anthropogenic impact on the environment; water, air and soil pollution; remediation and waste characterization; environmental contaminants; biogeochemistry; geoecology; chemical reactions and processes; chemical and biological transformations as well as physical transport of chemicals in the environment; or environmental modeling. A particular focus of the series lies on methodological advances in environmental analytical chemistry.

Series Preface

With remarkable vision, Prof. Otto Hutzinger initiated *The Handbook of Environmental Chemistry* in 1980 and became the founding Editor-in-Chief. At that time, environmental chemistry was an emerging field, aiming at a complete description of the Earth's environment, encompassing the physical, chemical, biological, and geological transformations of chemical substances occurring on a local as well as a global scale. Environmental chemistry was intended to provide an account of the impact of man's activities on the natural environment by describing observed changes.

While a considerable amount of knowledge has been accumulated over the last three decades, as reflected in the more than 70 volumes of *The Handbook of Environmental Chemistry,* there are still many scientific and policy challenges ahead due to the complexity and interdisciplinary nature of the field. The series will therefore continue to provide compilations of current knowledge. Contributions are written by leading experts with practical experience in their fields. *The Handbook of Environmental Chemistry* grows with the increases in our scientific understanding, and provides a valuable source not only for scientists but also for environmental managers and decision-makers. Today, the series covers a broad range of environmental topics from a chemical perspective, including methodological advances in environmental analytical chemistry.

In recent years, there has been a growing tendency to include subject matter of societal relevance in the broad view of environmental chemistry. Topics include life cycle analysis, environmental management, sustainable development, and socio-economic, legal and even political problems, among others. While these topics are of great importance for the development and acceptance of *The Handbook of Environmental Chemistry,* the publisher and Editors-in-Chief have decided to keep the handbook essentially a source of information on "hard sciences" with a particular emphasis on chemistry, but also covering biology, geology, hydrology and engineering as applied to environmental sciences.

The volumes of the series are written at an advanced level, addressing the needs of both researchers and graduate students, as well as of people outside the field of

"pure" chemistry, including those in industry, business, government, research establishments, and public interest groups. It would be very satisfying to see these volumes used as a basis for graduate courses in environmental chemistry. With its high standards of scientific quality and clarity, *The Handbook of Environmental Chemistry* provides a solid basis from which scientists can share their knowledge on the different aspects of environmental problems, presenting a wide spectrum of viewpoints and approaches.

The Handbook of Environmental Chemistry is available both in print and online via www.springerlink.com/content/110354/. Articles are published online as soon as they have been approved for publication. Authors, Volume Editors and Editors-in-Chief are rewarded by the broad acceptance of *The Handbook of Environmental Chemistry* by the scientific community, from whom suggestions for new topics to the Editors-in-Chief are always very welcome.

Damià Barceló
Andrey G. Kostianoy
Editors-in-Chief

Volume Preface

Reservoirs are important freshwater ecosystems providing water resources for several beneficial purposes, including agricultural irrigation, urban municipal water utilization, and drinking water supply. In China, there are more than 86,852 reservoirs, which play a vital role in providing a source of water to urban citizens, especially in arid and semi-arid regions.

This volume provides an overview of water pollution and water quality control of several selected Chinese reservoirs, named Jinpen Reservoir, Shibianyu Reservoir, Fenhe Reservoir, Zhelin Reservoir, and Zhoucun Reservoir. These reservoirs represent broad geographical distributions and different nutrition levels. In our research group, to ensure the security of drinking water supply, water pollution control has been systematically performed for 12 years. Drinking water supply is the main use of these reservoirs, with water-lifting aerators and bioremediation being the dominant management options. The main goals of water pollution investigation of Chinese reservoirs include monitoring cyanobacterial blooms, transformation of endogenous pollution (e.g., nitrogen, phosphorus, iron, and manganese) released from sediments, determining reservoir water/sediment microbial activity, and community compositions using biochemical and molecular technology. Meanwhile, water quality control and management of reservoirs using mixing–oxygenating technology combined with the bioremediation method, the technical background, the water quality improvement principles of water-lifting aeration, and the methods of designing and optimizing the structure of water-lifting aerators are discussed in this volume.

This volume is divided into four parts: (I) Water pollution of selected Chinese reservoirs, (II) Reservoir sediment contamination and its impact on water quality, (III) The mixing–oxygenating technology in situ controlling the reservoir water quality, and (IV) Microbial remediation method for polluted source water. This comprehensive volume can be used as a reference book by researchers and reservoir ecosystem managers.

We would like to thank all the authors and the publisher for their excellent work and insightful suggestions on the contents of this volume. We would also like to

express our gratitude to the reservoir management departments for their cooperation on water quality monitoring and water pollution controlling demonstration projects. With the progress of our research and practical engineering applications, we are expecting to publish an updated second edition of this volume some years down the line. In particular, we wish to acknowledge the foundation management departments, and the primary funding was provided by grants from the National Science and Technology Pillar Program (No. 2012BAC04B02), the Key National Natural Science Foundation of China (No. 50830303), and the National High-Tech Research and Development Program of China, also known as the "863 Program" (No. 2007AA06Z302).

Xi'an, P. R. China Tinglin Huang
April 2015

Contents

Part I
Water Pollution of Selected Chinese Reservoirs

Brief Introduction to the Selected Chinese Reservoirs

Gang Wen, Zizhen Zhou, Yang Li, and Tinglin Huang

Abstract Reservoirs are artificially formed in the bed of a river by building a dam, which intercepts the runoff. They have narrow surface but great depth, and the water level changes significantly during flooding. The mean depth of Chinese reservoirs is around 20–50 m.

China is a country with numerous lakes and reservoirs. There are more than 2300 lakes with individual areas of more than 1 km^2, and the total area is 70,988 km^2, with the fresh water of 2.25×10^{11} m^3. There are 86,852 reservoirs and the total volume is 4.13×10^{11} m^3. The total volume of fresh water in lakes and reservoirs is, therefore, 6.38×10^{11} m^3. They are the important fresh water source of drinking water in China.

Keywords Reservoirs • Pollution situation • Water quality • Sediments

1 Jinpen Reservoir

1.1 Location

Jinpen Reservoir (34°42′–34°13′N, 107°43′–108°24′E) is located in Zhouzhi County, Shaanxi Province, as shown in Fig. 1. It's about 1.5 km away from Heihe valley and 86 km away from Xi'an City. The reservoir is a huge water project used for urban water supply, agricultural irrigation, hydroelectric generation, and flood control. The flood design standard of the reservoir is 100-year flood ($Q = 3600$ m^3/s). The designed maximum water level is 594.0 m and the flood control level is 593.0 m.

G. Wen • Z. Zhou • Y. Li • T. Huang (✉)
School of Environmental and Municipal Engineering, Xi'an University of Architecture and Technology, Yanta Road 13, 710055 Xi'an, Shaanxi Province, P. R. China
e-mail: huangtinglin@xauat.edu.cn

T. Huang (ed.), *Water Pollution and Water Quality Control of Selected Chinese Reservoir Basins*, The Handbook of Environmental Chemistry 38,
DOI 10.1007/978-3-319-20391-1_1

Fig. 1 Jinpen Reservoir in Shaanxi Province

1.2 Basic Situation of the Watershed

1.2.1 Weather and Vegetation

Jinpen Reservoir has a warm temperate continental monsoon climate in the National Climate Division, with four distinct seasons. Meteorological disasters usually occur in summer and autumn. In spring and summer, a southeast monsoon blows fiercely. The area of Jinpen Reservoir in remote mountains belongs to the cold wet region, at an altitude of 1400 m, and the mean temperature is 8–10 °C. The precipitation in this area is more than 750 mm, which is the highest in Zhouzhi County.

1.2.2 Natural Resources

The animal resource is very rich in the Jinpen Reservoir basin. There are more than 40 kinds of animals, including leopard, sheep, deer, fox, and wild boar, and more than 230 kinds of birds, including golden pheasant, woodpecker, sparrow, magpie, and ring-necked pheasant. There are 174 kinds of forest pests. The fish have four orders, seven families, and 21 species, including carp, crucian carp, variegated carp, giant salamander, and so on.

The variety of plants is also quite rich in this area. The seed plants have 121 families, 640 genera, and 1550 species. The moss plants have 63 families, 142 genera, and 302 species. The phytoplanktons have eight divisions and 100 species, and there are plenty of ferns and lichens.

1.3 The Structure and Main Function of the Reservoir

1.3.1 The Structure

Jinpen Reservoir consists of a dam, a flood discharge tunnel, a spillway tunnel, a diversion tunnel, and a power station.

The dam is built from clay and gravel. The height, length, width, and altitude are 130 m, 433 m, 11 m, and 600 m, respectively. The clay core wall's altitude is 598.0 m, the top width is 7.0 m, and the maximum bottom width is 83 m.

The water inlet tower is used by the flood discharge tunnel, which is located on the left, the inlet's altitude is 545.0 m, and the gate size is 10×10 m. The body of the cave is used as a free-flow tunnel and the section size is 10×13 m, and its outlet's altitude is 493.2 m. The flow of this tunnel is designed to be 2421 m^3/s.

The spillway tunnel is located on the right, the inlet weir's altitude is 578.0 m, and its width is 12 m. The body of the cave used as a free-flow tunnel, the section size is 12×14 m–10×11 m, and its total length is 471.24 m. The design flow of the tunnel is 537 m^3/s.

The diversion tunnel is located on the right, and the height of inlet tower is 85.7 m. According to the water quality for urban water supply, three water intakes were set up at the top, middle, and bottom, at altitudes 571.0 m, 554.0 m, and 514.3 m, respectively. The diameter of the inlet tower is 3.5 m, and the outlet size is 2×2 m. The total length of this tunnel is 764.17 m. The design flow of this tunnel is 30.3 m^3/s.

The power station consists of three HLAL53-LI-120 water turbines, with a total capacity of 20,000 kW. The mean electric production is 73.08 million kWh per year.

The total volume of Jinpen Reservoir is 2×10^8 m^3 and the effective volume is 1.77×10^8 m^3. It is a deep canyon reservoir and the length of the main area is 3.5 km, the maximum depth is 90–105 m, and the mean depth is 60–95 m.

1.3.2 Main Function

Jinpen Reservoir is a large water project used for urban water supply, agricultural irrigation, hydroelectric generation, and flood control. The main water of Heihe abstraction works is from Jinpen Reservoir, the secondary source of water is Shitouhe Reservoir, and the spare source of water is from Shibianyu Reservoir. The distance of this project is 143 km, which can provide 4×10^9 m^3 water for Xi'an City per year.

1.4 The Water Quality of Jinpen Reservoir

1.4.1 The Pollution Status of Water Quality

Jinpen Reservoir is the main water source of Xi'an, and the water quality in the last 3 years is shown in Table 1. TN of the reservoir is around 2.0 mg/L, which is one times higher than that of the surface water environment quality standard (Class III). During the water stratification period in summer, pollutants are released to the water from sediments in anaerobic conditions and TN can reach 2.6 mg/L. TP of the reservoir has been lower than 0.05 mg/L in the last 3 years. The concentration of NH_4-N is quite low, even during the rainstorm period, but the concentration of NH_4-N can reach 0.65 mg/L during the water stratification period because of the release from sediment. The concentration of Fe has been relatively high in the last 3 years, and the release from sediment is responsible for the high iron concentration [1].

Table 2 shows the water quality of the same type of reservoirs in China. Compared to those reservoirs, the water quality of Jinpen Reservoir is of a medium pollution level. Overall, the pollution of Jinpen Reservoir is mainly caused by endogenous pollution, and TN and Fe are the main polluted parameters.

1.4.2 The Pollution Status of Sediment

Sediment samples were collected and analyzed. The pollution status of sediments in the main area of Jinpen Reservoir was assessed, and the result is shown in Table 3. In the sediment of Jinpen Reservoir, the concentrations of SOC, TN, and TP were similar to other reservoirs, but the concentration of Fe, which reached 147 mg/kg, was higher. The result that the bottom water can reach 2.5 mg/L in summer also showed that sediment release was the main reason for the higher Fe concentration. The concentrations of other heavy metals, such as Cd, Pb, and As, were very low and had little effect on the water quality [2–6].

The pollutants loads of other reservoirs are shown in Table 4, indicating that the concentrations of TP and SOC in Jinpen Reservoir are of a medium pollution level. Overall, the pollution of sediment in Jinpen Reservoir is of a medium level; endogenous pollution is the most important reason for water quality deterioration during the stratification period.

Table 1 Water quality status of Jinpen Reservoir in 2012–2014

Index	Year		
	2014	2013	2012
TN (mg/L)	2.050±0.1	1.850±0.2	1.900±0.15
TP (mg/L)	0.036±0.005	0.028±0.05	0.048±0.02
NH_4-N (mg/L)	0.280±0.02	0.152±0.08	0.182±0.02
TOC (mg/L)	3.120±0.1	2.852±0.05	3.005±0.3
Fe (mg/L)	0.300±0.05	0.320±0.02	0.280±0.08

Table 2 Water qualities of different drinking water reservoirs in China

Reservoir name	Fe (mg/L)	Mn (mg/L)	TP (mg/L)	TN (mg/L)	COD_{Mn} (mg/L)	The degree of eutrophication
Beisong Reservoir	0.70	0.12	0.08	1.81	2.9	Rich
Chaihe Reservoir	0.42	0.08	0.1	0.85	4.5	Rich
Dongfeng Reservoir	0.12	0.32	0.05	2.25	3.4	Middle
Dongyaxi Reservoir	0.84	0.45	0.07	0.96	2.65	Middle
Fuqiaohe Reservoir	0.33	0.08	0.07	0.69	4.78	Rich
Geyanhe Reservoir	0.32	0.18	0.01	0.24	2.37	Middle
Guandong Reservoir	1.11	0.51	0.04	1	3.6	Middle
Guanting Reservoir	0.45	0.24	0.11	4.97	5.8	Rich
Jiangkou Reservoir	0.15	0.09	0.01	1	1.05	Middle
Liangcha Reservoir	0.56	0.39	0.05	3.53	5	Rich
Qiaodun Reservoir	0.55	0.20	0.01	0.54	1.94	Poor
Menlou Reservoir	1.30	0.42	0.02	5.52	3.12	Middle
Shanmei Reservoir	0.62	0.15	0.12	1.62	4.1	Rich
Gaozhou Reservoir	–	–	0.01	0.88	1.68	Poor
Tangxi Reservoir	0.82	0.14	0.05	0.68	1.78	Middle
Xiashan Reservoir	0.55	0.04	0.06	2.23	6.13	Rich

Table 3 Concentrations of pollutants in the sediment of Jinpen Reservoir (mg/kg)

SOC (%)	TN	TP	Fe	Mn	Cd	Pb	As
2.29	810	703	147	70	1.2	8.5	6.4

Table 4 Pollutants concentrations in the sediment of other reservoirs

Reservoir name	TP (mg/kg)	SOC (%)
Miyun Reservoir	497–1239	–
Yuqiao Reservoir	437.50–478.37	2.13–2.39
Fenhe Reservoir	628.5–679.4	2.19–2.37
Qingshan Reservoir	41–96	1.20–1.72
Sanxia Reservoir	622	–
Xili Reservoir	1490	12.44

–: Not detected

2 Shibianyu Reservoir

2.1 Location

Shibianyu Reservoir (33°59′–34°00′N, 108°55′–108°56′E) is located in Wutai village, Chang'an area, Xi'an City. The basin area is 130 km^2, the average annual flow is 3.1 m^3/s, the designed flood flow is 420 m^3/s, and the total volume is 26 million m^3. The height of the dam is 82.5 m, the length is 285 m, and the total volume is 2.08 million m^3. A photo of Shibianyu Reservoir is shown in Fig. 2.

The Shibianyu River originates from Zhongnan Mountains to the north of Qinling Mountains. The geology is a rocky mountain area and the river basin coefficient is 2:1. The altitude ranges from 600 m to 2800 m. The mountain is high and steep on both sides, and the slope angle is more than 40°. The vegetation is poor in 4 km from the dam upstream to Guandi Temple and the vegetation is rich in 8 km from Guandi Temple to Qingcha. The vegetation area is about 60 % of all basins. The main tributaries include Dapiao River, Xiaopiao River, Longwozi River, and Daban River.

2.2 Basic Situation of the Watershed

2.2.1 Weather and Vegetation

There are two hydrological observation stations in Xianrencha and Guandi Temple. The average annual rainfall is 898 mm, the average annual runoff is 9.7×10^7 m^3, the average annual evaporation is 948.5 mm, the maximum runoff is 359 m^3/s, and the minimum runoff is 0.1 m^3/s.

The main vegetation includes broad-leaved deciduous forest, coniferous and broad-leaved mixed forest, and subalpine coniferous forest. There are 100 kinds of

Fig. 2 Shibianyu Reservoir

woody plants and 300 kinds of herbaceous plants. There are 30 kinds of mammals, 75 kinds of birds, ten kinds of reptiles, four kinds of amphibians, and 17 kinds of fishes.

2.2.2 Natural Resources

In this basin, there are more than 20 kinds of minerals, including marble, feldspar, dolomite, building gravel, vein quartz, and so on. There are igneous rock and metamorphic rock in the mountain area. More than 20 kinds of mineral products have already been found.

2.3 The Structure and Main Function of the Reservoir

2.3.1 The Structure and Storage Capacity

The dam of the reservoir is located in the north of Chang'an district, which is about 40 km away from Xi'an. The average annual runoff of the reservoir is 9.5×10^7 m^3 and the storage capacity of reservoir is 2.81×10^7 m^3. The annual water supply volume to Xi'an is 3×10^7 m^3 and the maximum daily water supply capacity is 4×10^5 m^3.

2.3.2 Main Function

It is a spare source of drinking water supply of Xi'an, which began to supply water to Xi'an in August 1990. The reservoir is a medium-sized reservoir and has comprehensive benefits such as irrigation, urban water supply, generating

electricity, and preventing flood. The reservoir lies in the second tributary of Feng River. The dam is 85 m high, at an altitude of 735 m, is 265 m long, and has a width of 7.5 m. Intake water holes are on the left bank of the dam, which is 448 m long, and their diameter is 3.6 m. The spillway tunnel lays on the right bank of the dam, and the total length, width, and height is 508 m, 7–8 m, and 10–12 m, respectively.

2.4 The Water Quality of Shibianyu Reservoir

2.4.1 The Pollution Status of Water Quality

Shibianyu Reservoir is a spare water source for Xi'an. The water quality in the past 3 years is shown in Table 5. The TN concentration was about 2.7 mg/L in the past 3 years, higher than that of Jinpen Reservoir. The TN concentration was as high as 4.0 mg/L in both flood season and the stratified period. The TP concentration of Shibianyu Reservoir maintained below 0.05 mg/L in the last 3 years. The TP concentration reached 0.09 mg/L due to the release of sediment in the stratification period. The NH_4-N concentration of Shibianyu Reservoir was also higher than that of Jinpen Reservoir, and the average annual concentration maintained at about 0.5 mg/L. The Fe and Mn concentrations of the reservoir have exceeded the limitations in the past 3 years; the average concentrations of Fe and Mn were about 0.4 mg/L and 0.2 mg/L, respectively. The Fe and Mn concentrations in the stratified period were much higher, with average concentrations reaching 0.62 mg/L and 0.72 mg/L, respectively [4, 5, 7].

In any case, the water quality of Shibianyu Reservoir was worse than that of Jinpen Reservoir. TN, NH_4-N, Fe, and Mn were at high risk of exceeding the national surface water quality standard (GB 3838–2002).

2.4.2 The Pollution Status of Sediment

Sediment samples were collected from Shibianyu Reservoir, and the analytic results are shown in Table 6. The nutrients of sediment were seriously polluted and the TN and TP concentrations were 1590 mg/kg and 1478 mg/kg, respectively. The concentrations were much higher than those of Jinpen Reservoir. The concentration of Fe in the sediment was up to 297 mg/kg and exceeded about two times that of Jinpen Reservoir, which was released from sediment in summer [8, 9]. Other heavy metals, such as Cd, Pb, and As, were at the same level as other drinking water reservoirs.

In other words, the sediment of Shibianyu Reservoir was seriously polluted by nitrogen, phosphorus, and Fe.

Table 5 Water quality of Shibianyu Reservoir in the past 3 years

Index	Years		
	2012	2013	2014
TN (mg/L)	2.80±0.3	2.67±0.2	2.75±0.2
TP (mg/L)	0.03±0.002	0.04±0.0005	0.04±0.004
NH_4-N (mg/L)	0.50±0.05	0.48±0.02	0.52±0.05
COD_{Mn} (mg/L)	3.22±0.25	3.32±0.3	3.11±0.3
Fe (mg/L)	0.45±0.05	0.36±0.01	0.42±0.05
Mn (mg/L)	0.21±0.02	0.18±0.04	0.19±0.002

Table 6 Pollutants concentrations in the sediment of Shibianyu Reservoir

SOC (%)	TN (mg/kg)	TP (mg/kg)	Fe (mg/kg)	Mn (mg/kg)	Cd (mg/kg)	Pb (mg/kg)	As (mg/kg)
3.32	1590	1478	297	70	2.2	4.5	8.4

3 Zhoucun Reservoir

3.1 Location

Zhoucun Reservoir (34°56′–34°57′N, 117°40′–117°41′E) was built in 1959 and began operation in June 1960. It is a provincial key medium-sized reservoir, and it is one of the five local medium-sized reservoirs in Zaozhuang City.

The total storage capacity of Zhoucun Reservoir is 8.404×10^9 m^3. It is an agricultural irrigation, flood control, and power generation reservoir. The catchment area is 121 km^2, which is a hilly watershed, with a begonia leaf-shaped basin, and the main stream length is 19.7 km. There are seven small reservoirs and eight ponds in the upstream area of the reservoir, which control a drainage area of about 14.91 km^2. A photo of Zhoucun Reservoir is shown in Fig. 3.

3.2 Basic Situation of the Watershed

3.2.1 Weather and Vegetation

Zaozhuang City is of the mid-latitude temperate continental monsoon climate, with four distinct seasons. The climate changes distinctly in different seasons. Spring climate is variable, southwest wind, less rainfall, often drought. Summer is composed of hot, humid air. Autumn has less cloud and rainfall. The weather of winter is cold and drought. The annual average temperature was 14.6 °C in 2012, 0.2 °C higher than the annual temperature in 2011. The average sunshine hours is 1947.6 h. The annual rainfall was 581.5 mm in 2012.

Fig. 3 Zhoucun Reservoir

3.2.2 Natural Resources

Fifty-seven kinds of ores have already been found within the territory of the Zaozhuang City, and 12 kinds of ores are found around the reservoir. Among them, the amount of coal is 1,717,710,000 tons; the recoverable amount of iron ores was 41,780,000 tons; the recoverable amount of copper ores is 980,000 tons; the recoverable amount of aluminum soil stones is 1,640,000 tons.

3.3 The Structure and Main Function of the Reservoir

3.3.1 The Structure and Storage Capacity

The length of dam is 1070 m and the maximum height is 29 m. The width and elevation of the dam are 6.0 m and 134.00 m, respectively. The flood control water level is 132.44 m and the corresponding storage capacity is 84.29×10^6 m^3. Drainage holes were built using C25 reinforced concrete box culvert under the dam, with the length of 119.1 m, and the designed flow is 14.1 m^3/s. Sub-three-hole spillway gates were designed, and the elevation of the bottom is 123.00 m. Three power plants were installed, with the power generation capacity of 350 kW.

3.3.2 Main Function

The total length of the irrigation area of the reservoir is 5.8 km, and it has eight branch canals. It has about 6866.667 ha of designed irrigation area. Fish breeding of the reservoir started from the 1980s, and the scale expanded rapidly. The fish breeding area has reached 20 % of the reservoir area and the network cases have exceeded 10,000. The net-case fish breeding has caused serious deterioration of the

water quality in the reservoir. To deal with this situation, the municipal water conservancy bureau developed the activity of clearing up renovation of the network case in 2008. After clearing up the network cases, the water quality of the reservoir has improved, but the sediments of the reservoir were polluted as well.

3.4 The Main Water Quality of Zhoucun Reservoir

3.4.1 The Pollution Status of Water Quality

There was a history of large-scale net-case fish breeding in Zhoucun Reservoir, which led to the fact that the water quality in this reservoir was relatively worse. Nitrogen, phosphorus, and organic pollution are quite heavy. As seen in Table 7, the TN concentration reached 2.5 mg/L in the past three years, due to the endogenous pollution [10, 11]. The average TP concentration of Zhoucun Reservoir in the past 3 years exceeded 0.05 mg/L, because of the release from sediment under anoxic conditions [12–14]. The TP concentration of the bottom regime reached up to 0.2 mg/L. The NH_4-N concentration of Zhoucun Reservoir was higher than that of Jinpen Reservoir. The COD_{Mn} concentration of Zhoucun Reservoir was nearly 5.0 mg/L, which is higher than that in both Jinpen Reservoir and Shibianyu Reservoir. The concentration of Fe in Zhoucun Reservoir was lower, and the average concentration did not exceed the national surface water quality standard (GB 3838–2002). However, the concentration of Mn was relatively high and the average concentration exceeded the national surface water quality standard (GB 3838–2002).

The water quality status of Zhoucun Reservoir is relatively worse. The phenomenon of stratification will cause the deterioration of the water quality in the whole reservoir.

3.4.2 The Pollution Status of Sediment

The results of sediment in Zhoucun Reservoir are shown in Table 8. It is obvious that the total organic carbon in the sediment of Zhoucun Reservoir was higher than that of other reservoirs, and the concentration was up to 7.36 %. The TN and TP concentrations of Zhoucun Reservoir were 890 mg/kg and 1158 mg/kg, respectively, which were lower than those of Shibianyu Reservoir but higher than that of Jinpen Reservoir. The Fe and Mn concentrations in the sediments of Zhoucun Reservoir were higher than those of Jinpen Reservoir and reached up to 280 mg/kg and 82 mg/kg, respectively [15–18].

In any case, the sediment of Zhoucun Reservoir was seriously polluted, especially organic matters, which was much higher than that in other drinking water reservoirs.

Table 7 Water quality of Zhoucun Reservoir in the past 3 years

Index	Years		
	2012	2013	2014
TN (mg/L)	2.57±0.03	2.67±0.03	2.36±0.2
TP (mg/L)	0.058±0.001	0.07±0.01	0.06±0.01
NH_4-N (mg/L)	0.53±0.005	0.85±0.06	0.72±0.005
COD_{Mn} (mg/L)	4.75±0.4	4.82±0.5	4.11±0.2
Fe (mg/L)	0.15±0.002	0.16±0.02	0.12±0.01
Mn (mg/L)	0.52±0.05	0.28±0.03	0.38±0.04

Table 8 Pollutants concentrations in the sediment of Zhoucun Reservoir

SOC (%)	TN (mg/kg)	TP (mg/kg)	Fe (mg/kg)	Mn (mg/kg)	Cd (mg/kg)	Pb (mg/kg)	As (mg/kg)
7.36	890	1158	280	82	4.2	6.4	2.6

4 Fenhe Reservoir

4.1 Location

Fenhe Reservoir (38°02′–38°07′N, 111°50′–111°55′E), as shown in Fig. 4, is located in Taiyuan City, Shanxi Province. The north-to-south distance is 15 km, and the total area is 32 km^2. The storage capacity of the reservoir is 700×10^8 m^3, equivalent to 13.5 times of the Ming Tombs Reservoir. The highest elevation is 1131.4 m. The construction of Fenhe Reservoir began in November 1958 and completed in 1960. The control drainage area of the reservoir is 5268 km^2, and the average annual inflow is 21.9 m^3/s. The designed flood inflow is 3670 m^3/s, and the total storage capacity is 7×10^8 m^3.

4.2 Basic Situation of the Watershed

4.2.1 Weather and Vegetation

Taiyuan City belongs to the temperate continental climate in the county, and the climate is arid. There is less rainfall, the temperature is relatively low, the wind force is relatively small, and the illumination is sufficient. Winter is long, cold, and dry, summer is hot and rainy, while Spring is windy. The annual average temperature is 7.1 °C–8.1 °C, the average annual rainfall is 428 mm, western wind is present throughout the year, and the annual average wind speed is 2.5 m/s. The total hours of sunshine are 2872.6 h.

Fig. 4 Fenhe Reservoir

4.2.2 Natural Resources

Natural resources in Taiyuan City include coal, iron, marble, silica, bauxite, limestone, graphite, marble, quartz, phosphorus, gypsum, mica, quartz stone, copper, gold, and so on. In particular, coal, iron, silicon, and marble are quite abundant. The resources mainly lie in the north and south ends of the territory, and the area of the coal field is 65 km^2. The tree population in Taiyuan City is dominated by coniferous forest, pine, white pine, spruce, and cypress. There are wild fruit trees, including *Prunus*, apricot, jujube, baccata, and mulberry. Wildlife animals include brown-eared pheasant, deer, musk deer, leopards, black stork, and white swan.

4.3 The Water Quality of Fenhe Reservoir

4.3.1 The Pollution Status of Water Quality

Fenhe Reservoir is the drinking water source of Taiyuan City, Shanxi Province. Water quality monitoring was carried out from 2008 to 2010, and the monitoring results are shown in Table 9. The water quality of Fenhe Reservoir is of a moderate pollution level. The TN concentration remained around 1.0 mg/L. The TP concentration maintained at a level around 0.04 mg/L–0.05 mg/L. The concentrations of COD_{Mn} and Fe were of a lower level, ranging from 2.75 mg/L to 3.22 mg/L and from 0.12 to 0.17 mg/L, respectively. In 2010, the concentration of Mn was the highest among the five reservoirs discussed in this chapter, reaching 0.48 mg/L. Especially in the bottom water of Fenhe Reservoir, the concentration of Mn reached 1.10 mg/L, which was due to the sediment release under anaerobic conditions.

4.3.2 The Pollution Status of Sediment

The sediment samples were collected in the main zone of Fenhe Reservoir. The analytic results are shown in Table 10. The organic carbon in the sediment of Fenhe

Table 9 Water qualities of Fenhe Reservoir in 2008–2010

Index	Year		
	2008	2009	2010
TN (mg/L)	0.96±0.12	1.27±0.1	1.16±0.2
TP (mg/L)	0.05±0.01	0.04±0.005	0.04±0.005
NH_4-N (mg/L)	0.54±0.06	0.45±0.01	0.62±0.1
COD_{Mn} (mg/L)	2.75±0.25	2.82±0.2	3.22±0.3
Fe (mg/L)	0.17±0.02	0.14±0.03	0.12±0.02
Mn (mg/L)	0.32±0.06	0.27±0.05	0.48±0.2

Table 10 Concentrations of pollutants in the sediment of Fenhe Reservoir

SOC (%)	TN (mg/kg)	TP (mg/kg)	Fe (mg/kg)	Mn (mg/kg)	Cd (mg/kg)	Pb (mg/kg)	As (mg/kg)
2.54	1090	665	118	68	11.42	2.4	1.6

Reservoir was 2.54 %, which is of a medium pollution level compared with that in other drinking water reservoirs, such as Jinpen Reservoir. However, the concentration of SOC in Fenhe Reservoir was much lower than that of Zhoucun Reservoir. The pollution degree of TN and TP in Fenhe Reservoir is of a medium level, and the contents were 1090 mg/kg and 665 mg/kg, respectively. The concentration of Cd in Fenhe Reservoir was about 12 times higher than the background concentration of Chinese lake sediment.

Overall, the sediment of Fenhe Reservoir is of a medium pollution level.

5 Zhelin Reservoir

5.1 Location

Zhelin Reservoir (29°14′–29°16′N, 115°12′–115°27′E), also known as "Zhelin Lake", is located at Jiujiang City, Jiangxi Province (Fig. 5). It is formed by the interception of Xiu River by the largest dam in Asia. The storage capacity of Zhelin Reservoir is 7.92×10^9 m^3. The reservoir consists of more than 990 islands and has picturesque and exquisite scenery.

Zhelin Reservoir is located at the northwest corner of Xiushui County, next to Wuning County and Yongxiu County. It is 80 km away from Nanchang (115°04′–115°40′N, 29°03′–29°18′E).

5.2 Basic Situation of the Watershed

5.2.1 Weather and Vegetation

The Zhelin Reservoir belongs to the subtropical monsoon climate. Rainfall is abundant, and the multi-year average precipitation is 1506 mm. The annual average

Fig. 5 Zhelin Reservoir in Jiangxi Province

temperature is 15 °C to 17 °C, and the annual extreme maximum and minimum temperature are 41.1 °C and −13.5 °C, respectively. The ice-free period of the area is generally 80–126 days.

In 2013, the total land area of Zhelin Reservoir is 2618.3 km^2, which is mainly forest land area (64.89 %), followed by grassland area (18.97 %) and water area (11.76 %).

In the region of Zhelin Reservoir, the plant community is abundant and there are more than 3500 species of higher plants.

5.3 The Structure and Main Function of the Reservoir

5.3.1 The Structure and Storage Capacity

Construction of the reservoir started in August 1958 and completed in 1975. It is the largest water storage project in Jiangxi Province. The dam controls an area of 9340 km^2, accounting for 63.5 % of the area of Xiu River basin. The annual average flow is 255 m^3/s. The designed elevation of Zhelin dam crest is 75 m (Wu Song). The designed flood level and low water level are 71.3 m and 50 m, respectively. The water area, storage capacity, water volume, and water level of Zhelin Reservoir are shown in Tables 11 and 12. The designed flood level is 70.13 m, and the corresponding storage capacity is 6.77×10^9 m^3. The average water depth of Zhelin Reservoir is 45 m, and the visibility is 11 m.

5.3.2 Main Function

At present, Zhelin Reservoir is mainly used for hydroelectric power, flood control, irrigation, large-scale water conservancy, and hydropower engineering. The total installed capacity is 420 MW, and the annual power output is 6.3×10^8 kWh.

Table 11 Water storage capacity and the corresponding water area of Zhelin Reservoir

Water level (m)	64	65	66	67	68	69	70	71	72	73
Capacity ($\times 10^8$ m^3)	47.2	50.17	53.18	56.4	59.9	63.44	67.2	71.11	75.08	79.2
Water area (km^2)	296.3	308.15	320.4	333	345.5	358.7	373.04	387.4	401.5	415.6

Table 12 Monthly changes of water level and water inflow in Zhelin Reservoir

Month	Jan.	Feb.	Mar.	Apr.	May	Jun.	Jul.	Aug.	Sep.	Oct.	Nov.	Dec.
Water level (m)	53.5	53.24	53.73	55.13	56.91	58.09	59.87	59.49	58.84	57.92	57.07	55.93
Water inflow ($\times 10^8$ m^3)	2.0	3.6	8.01	11.9	14.6	15.73	9.5	5.1	3.11	2.5	2.8	1.7

The flood control design standard of Zhelin reservoir is 1000-year flood. Zhelin Reservoir is mainly responsible for the flood control of the downstream tail area, the Beijing–Kowloon railway, and Yongxiu County.

Irrigation water was from the third auxiliary dam to Zhelin irrigation district. The main channel length is 54.92 km, and the designed flow is 30 m^3/s. The designed irrigation area is 320,000 mu, greatly improving the 17 townships in the region.

5.4 The Water Quality of Zhelin Reservoir

5.4.1 The Pollution Status of Water Quality

The water quality of Zhelin Reservoir is fine, meeting Class II of the national surface water quality standard (GB 3838–2002). But the monitoring results show that there is a seasonal deterioration phenomenon of the water quality in Zhelin Reservoir, especially during the stratification period in summer, which is due to the release of pollutants from the sediments. As shown in Table 13, the average TN concentration was within 1.0 mg/L in the last 3 years. In 2014, the average concentration of TN was 0.85 mg/L. From 2013 to 2014, the TN concentration reached 1.35 mg/L in the bottom water during the stratification period. The average concentration of TP in Zhelin Reservoir was below 0.025 mg/L, which had the same pattern as TN. The concentrations of NH_4-N, COD_{Mn} in the last 3 years were quite low, but the Fe and Mn concentrations were at a high risk of reaching important levels; for example, the concentration of Mn in vertical water reached 0.16 mg/L after the reservoir mixing in 2013, which already exceeded Class III of the national surface water quality standard (GB 3838–2002).

5.4.2 The Pollution Status of Sediment

Sediment samples of different sites were collected. The analytic results are shown in Table 14. The concentrations of SOC and TN in the main zone were slightly

Table 13 Water qualities of Zhelin Reservoir in 2012–2014

	Year		
Index	2012	2013	2014
TN (mg/L)	0.620±0.1	0.750±0.05	0.850±0.1
TP (mg/L)	0.022±0.04	0.025±0.01	0.024±0.04
NH_4-N (mg/L)	0.100±0.05	0.125±0.04	0.080±0.01
COD_{Mn} (mg/L)	2.680±0.2	2.500±0.02	2.820±0.12
Fe (mg/L)	0.122±0.03	0.168±0.05	0.150±0.02
Mn (mg/L)	0.060±0.01	0.072±0.01	0.080±0.02

Table 14 Concentrations of pollutants in the sediments of Zhelin Reservoir

	Index							
Site	SOC (%)	TN (mg/kg)	TP (mg/kg)	Fe (mg/kg)	Mn (mg/kg)	Cd (mg/kg)	Pb (mg/kg)	As (mg/kg)
Main zone	2.79	1360	2042	78.2	88.3	1.76	30.03	10.99
Convergence zone	1.85	1104	2053	158.4	103.5	2.66	55.3	7.89

higher than that of the convergence zone. The concentration of SOC in the main zone was higher than that of the other reservoirs discussed in this chapter, reaching 2.29 %. The concentrations of TP in the main zone and the convergence zone were nearly the same, but the concentration of TP of sediment in Zhelin Reservoir (2048 mg/kg) was much higher than that in the other reservoirs discussed in this chapter (with an average of 1200 mg/kg). The concentrations of heavy metals in the convergence zone were higher than that of the main zone, which was mainly due to the external input water with relatively high concentrations of heavy metals [19]. The sediments in the convergence zone were heavily polluted.

The monitoring results showed that the oxygen consumption rate of bottom water in the convergence area was much faster than that in the main zone during the stratification period, and the release potential of pollutants from sediments in the convergence area was also higher than the main zone.

Overall, the pollution of sediments in Zhelin Reservoir is also serious, and the sediment pollution load of the convergence area is higher than that of the main zone.

References

1. Min W, Sun XM, Huang SL, Tang XQ, Scholz M (2012) Laboratory analyses of nutrient release processes from Haihe River sediment. Int J Sediment Res 27:61–72
2. Fu J, Zhao C, Luo Y, Liu C, Kyzas GZ, Luo Y, Zhao D, An S, Zhu H (2014) Heavy metals in surface sediments of the Jialu River, China: Their relations to environmental factors. J Hazard Mater 270:102–109
3. Gao X, Chen CT (2012) Heavy metal pollution status in surface sediments of the coastal Bohai Bay. Water Res 46:1901–1911
4. Huang TL, Qin CH, Li X (2013) Studies on the seasonal variation and budget of nitrogen, phosphorus of the Shibianyu Reservoir. Xi'an Univ Arch and Tech (Natural science edition) 1:111–116 (in Chinese)
5. Huang TL, Qin C, Li X (2013) Studies on seasonal variation and sources of nitrogen and phosphorus in a canyon reservoir used as water source. Environ Sci 34:3423–3429 (in Chinese)
6. Usman AR, Alkredaa RS, Al-Wabel M (2013) Heavy metal contamination in sediments and mangroves from the coast of Red Sea: Avicennia marina as potential metal bioaccumulator. Ecotoxicol Environ Saf 97:263–270
7. Chen CH, Wang YX (2006) Release of phosphorus in sediment of a lake. Environ Sci Technol 29:15–16
8. Casamitjana X, Serra T, Colomer J, Baserba C, Pérez-Losada J (2003) Effects of the water withdrawal in the stratification patterns of a reservoir. Hydrobiologia 504:21–28
9. Huang TL, Li X, Rijnaarts H, Grotenhuis T, Ma W, Sun X, Xu J (2014) Effects of storm runoff on the thermal regime and water quality of a deep, stratified reservoir in a temperate monsoon zone, in northwest China. Sci Total Environ 485:820–827
10. Dehghan A, Dehghani A (2011) Experimental and theoretical investigation of thermal performance of underground cold-water reservoirs. Int J Thermal Sci 50:816–824
11. Wang S, Qian X, Han BP, Luo LC, Hamilton DP (2012) Effects of local climate and hydrological conditions on the thermal regime of a reservoir at Tropic of Cancer, in southern China. Water Res 46:2591–2604
12. Cao ZH (2013) Change law of water quality and water quality evaluation of Zhoucun reservoir (D) (in Chinese)

13. Cong HB (2007) Application of the technology of lifting water and aeration for improving water quality (D)
14. Huang TL, Li JJ (2007) Water lifting and aeration technology for improving raw water quality in Fenhe River Reservoir. Water Technol 4:13–16 (in Chinese)
15. Ma Y, Huang TL (2012) Water quality pollution and cause analysis of stratified reservoirs as urban water source. Value Eng 30:327–328 (in Chinese)
16. Ma Y, Guo QL, Huang TL (2013) Response characteristics of water quality to the seasonal thermal stratification in Jinpen reservoir along the Heihe river, Xi'an city in China. J Hydraul Eng 44:406–415 (in Chinese)
17. Ma Y, Tan P, Huang TL (2013) Sediment contaminant speciations and release characteristics of Fenhe Reservoir. City Town Water Suppl 1:73–78 (in Chinese)
18. Cao ZJ, Zhang X, Nanshan A (2011) Effect of sediment on concentration of dissolved phosphorus in the Three Gorges Reservoir. Int J Sediment Res 26:87–95
19. Zhou RY (2014) Study on the reservoir sediment multiphase interface transformation of phosphorus and heavy metal migration (D) (in Chinese)

Characteristics of Water Pollution in Typical Reservoirs

Gang Wen, Xuan Li, Xiaopeng Qiu, Ya Cheng, Yuankui Sun, and Tinglin Huang

Abstract Since the 1950s, the pollution of reservoirs has become serious. The water quality in reservoirs is deteriorating due to population growth, industrialization, and urbanization. In order to clarify the characteristics of water quality change in reservoirs, in-situ monitoring of water quality and phytoplankton were conducted in Jinpen Reservoir, Shibianyu Reservoir, Zhoucun Reservoir, and Zhelin Reservoir.

This chapter discusses the change of water quality in reservoirs in terms of eutrophication, algae pollution, and endogenous pollution. The results indicate that Zhelin Reservoir, Jinpen Reservoir, and Shibianyu Reservoir are in the middle eutrophic state, while Zhoucun Reservoir is in the eutrophic state. All the reservoirs suffer from algal blooms in July and August, with cyanobacteria dominating. Stratification, a very common phenomenon, occurs in the reservoirs mentioned above, can cause the decline of bottom dissolved oxygen, aquatic ecological environment deterioration, and the release of pollutants from sediment.

Keywords Eutrophication • Algal blooming • Stratification • Pollutants

1 Eutrophication

Lakes and reservoirs are important water resources for human survival [1]. However, since the 1950s, more nitrogen and phosphorus have been released into the water body, which led to serious eutrophication in lakes and reservoirs. Given the adverse effects on the sustainable development of social economy and environment, eutrophication has become an ubiquitous environmental problem worldwide and attracts more attention and recognition from many states [2].

G. Wen • X. Li • X. Qiu • Y. Cheng • Y. Sun • T. Huang (✉)
School of Environmental and Municipal Engineering, Xi'an University of Architecture and Technology, Yanta Road 13, 710055 Xi'an, Shaanxi Province, P. R. China
e-mail: huangtinglin@xauat.edu.cn

T. Huang (ed.), *Water Pollution and Water Quality Control of Selected Chinese Reservoir Basins*, The Handbook of Environmental Chemistry 38,
DOI 10.1007/978-3-319-20391-1_2

1.1 The Formation Mechanism of Eutrophication

Excessive nutrients are the key factor of eutrophication, with phosphorus being the crucial nutrient, followed by nitrogen, carbon, trace elements, and vitamins. The eutrophication process can be expressed as the following equation:

$$106CO_2 + 16NO_3^- + HPO_4^{2-} + 122H_2O + 18H^+ + \text{energy} + \text{trace elements} \rightarrow C_{106}H_{263}O_{110}N_{16}P_1(\text{algae protoplasm}) + 138O_2$$

The equation shows that phosphorus and nitrogen in the natural water bodies are the critical factors for the production of plankton biomass. Industrial wastewater, sewage, and farmland drainage contain large amounts of nitrogen and phosphorus, which could lead to increasing nutrients in water and cause vigorous growth of green plants and algae [3].

The relevant theories about the formation mechanism of eutrophication include the food chain theory and the life cycle theory.

(1) Food Chain Theory
This theory was proposed by Martin Shotton in 1997. It was believed that there are aquatic food chains in natural water. If zooplankton biomass decreases or their predation ability reduces, the algae growth amount will exceed consumption, which promotes eutrophication. Furthermore, the theory points out that increasing nutrition load is not the only reason for eutrophication. Some pollutants, such as persistent organic pollutants, can also affect the predatory ability of zooplankton and cause eutrophication [4].

(2) Life Cycle Theory
It is a widely accepted theory that plenty of compounds containing nitrogen and phosphorus are discharged into water bodies, and the original ecological balance is destroyed, which causes an excessive reproduction of algae. Algal blooms consume large amounts of dissolved oxygen, which makes plankton die due to the lack of oxygen. According to this theory, nitrogen and phosphorus are the fundamental reasons for eutrophication and algae are the main part of eutrophication.

According to the above two kinds of mechanisms for eutrophication formation, the reasons for eutrophication can be summarized as follows:

1. Water pollution is the primary cause of eutrophication. The pollution sources leading to eutrophication are generally around lakes and reservoirs, which can be exogenous sources or endogenous sources. Exogenous sources include point source pollution and non-point source pollution. Point source pollution usually refers to pollution discharged from drainage pipes, while non-point source pollution includes farmland drainage, river bank penetration, rain, and groundwater [5].
2. The hydraulic condition is one of the most important conditions that influence eutrophication. Eutrophication occurs in relatively closed water bodies, where water flow is slow and the water depth is shallow. Such conditions are suitable

for the growth of plants and algae. In deeper lakes or reservoirs, the hydraulic retention time is longer and a large number of pollutants can enrich at the bottom. Once stratification occurs, the bottom water will become anaerobic and nutrients will be released from the sediments.

3. Ecological imbalance promotes eutrophication. Microbial ecological imbalance also accelerates the eutrophication of water bodies. Microbes belong to disintegrators in the lake, and they can make use of organic pollutants derived from the producers and consumers in the food chain, thus maintaining water quality. However, if extensive organic matters enter into the water, dissolved oxygen will be consumed quickly and, thus, generate an anaerobic condition. Anaerobic conditions could not only destroy the food chain of lakes and reservoirs, but also intensify the phosphorus cycle.
4. Algal blooms form a vicious circle. Algal blooms make the optical radiation intensity attenuate rapidly along the depth, and causes the dissolved oxygen to decline. Algae would die from the lack of light and secrete algal toxin. The above phenomenon will lead to greater biological suffocation death and a loss of inhibiting ability to algae growth by ecological food chains. Meanwhile, it also contributes to the transformation of phosphorus in the water and further accelerates algal blooms [6].

1.2 The Assessment Method of Eutrophication

The eutrophic state depends primarily on factors such as total nitrogen (TN), total phosphorus (TP), biochemical oxygen demand in 5 days (BOD_5), chlorophyll-*a* (chla), and transparency (SD). The tropic state index (TSI), established by Carlson (1977) [7], is the most commonly used parameter, which includes TP, chla, and SD variables. The second most commonly used index is the lake evaluation index (LEI), proposed by Porcella. The two indexes both include chla, TP, and the absolute value of SD, so they are applicable to any lake or reservoir theoretically. According to the formulas (1–3), Table 1 gives the values of TP, chla, and SD corresponding to the TSI.

$$\mathrm{TSI} = 10(6 - \log_2 \mathrm{SD}) \tag{1}$$

$$= 10(6 - \log_2 7.7/\mathrm{chla}0.68) \tag{2}$$

$$= 10(6 - \log_2 48/\mathrm{TP}) \tag{3}$$

In China, the TLI proposed by Can is widely used, which includes chla, COD, TN, TP, and SD. The evaluation result is reliable if the TLI is combined with the trophic principal component analysis and hierarchical analysis. The TLI can be calculated by formula:

Table 1 Tropic state index (TSI) and its relevant parameters

TSI	Transparency (m)	Surface phosphorus concentration (mg/m^3)	Surface chlorophyll concentration (mg/m^3)
0	64	0.75	0.04
10	32	4.5	0.12
20	16	3	0.12
30	8	6	0.94
40	4	12	2.6
50	2	24	7.4
60	1	48	20
70	0.5	96	56
80	0.25	192	154
90	0.12	384	427
100	0.062	768	1183

Table 2 The assessment standard of eutrophication in lakes

	SD (m)	TP (mg/L)	TN (mg/L)	chla (μg/L)	BOD (mg/L)	COD (mg/L)
Oligotrophic	2	0.01	0.12	5	1.5	2
Middle oligotrophic	1.5	0.025	0.3	10	2	3
Mesotropher	1	0.05	0.6	15	3	4
Middle eutropher	0.7	0.1	1.2	25	5	7
Eutropher	0.4	0.5	6	100	15	20
Heavy eutropher	<0.1	>0.5	>6	>100	>15	>20

Table 3 The weight of each parameter

Parameter	chla	TP	TN	SD	COD
W_j	0.2663	0.1879	0.1790	0.1834	0.1834

$$\mathrm{TLI}(\sum) = \sum_{j=1}^{m} W_j \times \mathrm{TLI}(j) \tag{4}$$

TLI(Σ) is the comprehensive trophic status index; TLI (j) is the j-th parameter index of trophic status, as shown in Table 2; and W_j is the relative weight of the j-th trophic status index, as shown in Table 3.

The trophic status of the signal index is calculated by the following:

Table 4 Trophic state grading of lakes based on the weighted comprehensive trophic state index

	Oligotrophic	Mesotropher	Eutropher	Light eutropher	Middle eutropher	Heavy eutropher
Range of TLI	<30	30–50	>50	50–60	60–70	>70

Table 5 Chinese grade standards for eutrophication in lakes and reservoirs

	Trophic grade						
	I	II	III	IV	V	VI	
Assessment factors	Light eutropher	Light-middle eutropher	Middle eutropher	Middle-hyper eutropher	Hyper eutropher	Heavy hyper eutropher	T_{0i}
chla (μg/L)	≤1.0	≤2.0	≤4.0	≤10	≤65	>80	27
TP (mg/L)	≤0.0025	≤0.005	≤0.025	≤0.050	≤0.200	>0.600	0.157
TN (mg/L)	≤0.030	≤0.050	≤0.300	≤0.500	≤2.000	>4.600	1.247
COD_{Mn} (mg/L)	≤0.54	≤0.72	≤3.60	≤7.20	≤18	>48.78	13.14

$$\begin{aligned} \mathrm{TLI(Chla)} &= 10(2.5 + 1.086\ln \mathrm{Chla}) \\ \mathrm{TLI(TP)} &= 10(9.436 + 1.625\ln \mathrm{TP}) \\ \mathrm{TLI(TN)} &= 10(5.453 + 1.694\ln \mathrm{TN}) \\ \mathrm{TLI(SD)} &= 10(5.118 - 1.94\ln \mathrm{SD}) \\ \mathrm{TLI(COD)} &= 10(0.109 + 2.66\ln \mathrm{COD}) \end{aligned} \tag{5}$$

The unit of chla is mg/m^3, the unit of SD is m, and the units of the remainder are mg/L.

According to the value of the TLI, a series of consecutive values (0–100) are used to grade the trophic state of lakes or reservoirs (Table 4). Given that water pollution is gradual and continuous, a fuzzy mathematical method is considered to be reasonable to evaluate the trophic state of water. The concrete method is shown in Table 5

1.3 Trophic State Evaluation of Typical Reservoirs

1.3.1 Jinpen Reservoir

Chla, TP, TN, and COD_{Mn} are chosen as the surface water pollution control parameters of Jinpen Reservoir. The fuzzy comprehensive index method was used to estimate the trophic status in Jinpen Reservoir from 2008 to 2009. The monthly average results are shown in Table 6.

Table 6 Monthly average concentration of the pollution factors in Jinpen Reservoir

Month	chla	TP (mg/L)	TN (mg/L)	COD_{Mn} (mg/L)	Month	chla	TP (mg/L)	TN (mg/L)	COD_{Mn} (mg/L)
2008-03	0.89	0.015	1.08	2.27	2009-02	0.384	0.012	1.01	2.18
2008-04	1.71	0.025	1.14	2.75	2009-03	0.67	0.028	1.17	2.36
2008-05	3.39	0.05	1.43	3.16	2009-04	1.7	0.031	1.28	2.09
2008-06	3.643	0.035	1.05	3.04	2009-05	2.682	0.048	1.42	2.21
2008-07	3.294	0.032	1.36	3.29	2009-06	1.567	0.035	1.43	2.89
2008-08	15.76	0.05	1.44	3.48	2009-07	8.51	0.043	1.34	3.68
2008-09	5.37	0.061	1.381	3.43	2009-08	4.818	0.035	1.48	3.01
2008-10	2.48	0.035	1.26	2.88	2009-09	2.39	0.028	1.44	3.17
2008-11	1.828	0.024	1.25	2.90	2009-10	1.308	0.02	1.46	3.12
2008-12	0.97	0.014	1.09	2.56	2009-11	1.012	.0.011	1.27	3.04
2009-01	0.394	0.013	0.93	2.43	2009-12	0.848	0.008	1.18	2.68

Table 7 Fuzzy composite indexes for comprehensive evaluation of the nutrition in Jinpen Reservoir

Month	I	II	III	IV	V	VI	Results
2008-03	0.0282	0.1549	0.0750	0.4526	0.2894	0	Class IV (middle-hyper eutropher)
2008-04	0.0136	0.0801	0.2271	0.3871	0.2920	0	Class IV (middle-hyper eutropher)
2008-05	0	0.0410	0.1589	0.4119	0.3882	0	Class IV (middle-hyper eutropher)
2008-06	0	0.0477	0.3017	0.4329	0.2177	0	Class IV (middle-hyper eutropher)
2008-07	0	0.0421	0.2693	0.3156	0.3730	0	Class V (hyper eutropher)
2008-08	0	0.0046	0.1095	0.3385	0.5475	0	Class V (hyper eutropher)
2008-09	0	0.0083	0.2125	0.3376	0.4416	0	Class V (hyper eutropher)
2008-10	0	0.0807	0.2073	0.3783	0.3337	0	Class IV (middle-hyper eutropher)
2008-11	0.0080	0.0756	0.1215	0.4478	0.3472	0	Class IV (middle-hyper eutropher)
2008-12	0.0301	0.0998	0.1380	0.4466	0.2855	0	Class IV (middle-hyper eutropher)
2009-01	0.0142	0.1221	0.1383	0.5150	0.2104	0	Class IV (middle-hyper eutropher)
2009-02	0.0133	0.1228	0.1044	0.5012	0.2582	0	Class IV (middle-hyper eutropher)
2009-03	0.0188	0.0585	0.1963	0.3906	0.3358	0	Class IV (middle-hyper eutropher)
2009-04	0.0131	0.0877	0.1566	0.3735	0.3691	0	Class IV (middle-hyper eutropher)
2009-05	0	0.0855	0.0851	0.4237	0.4057	0	Class IV (middle-hyper eutropher)
2009-06	0.0151	0.0534	0.1813	0.3186	0.4315	0	Class V (hyper eutropher)
2009-07	0	0	0.2212	0.3096	0.4692	0	Class V (hyper eutropher)
2009-08	0	0.0239	0.2601	0.3828	0.3331	0	Class IV (middle-hyper eutropher)
2009-09	0	0.0649	0.2278	0.2559	0.4514	0	Class V (hyper eutropher)
2009-10	0.0211	0.0551	0.1847	0.2661	0.4730	0	Class V (hyper eutropher)
2009-11	0.0273	0.0688	0.1535	0.3677	0.3827	0	Class V (hyper eutropher)
2009-12	0.0255	0.0881	0.1187	0.4222	0.3455	0	Class IV (middle-hyper eutropher)

Using the weighted comprehensive trophic state index to evaluate the trophic status of Jinpen Reservoir, the evaluation results of each month are shown in Table 7.

The following conclusions can be drawn from Table 7: (1) The eutrophication degree of Jinpen Reservoir lies in the middle-hyper eutropher to hyper eutropher, which is consistent with the actual situation in water quality pollution; (2) The pollution and trophic status of Jinpen Reservoir are becoming serious.

Table 8 Weighted comprehensive trophic state index of Shibianyu Reservoir (2011)

Month	chla	TP	TN	COD_{Mn}	SD	Trophic state index	Trophic status
2011-03	1.3	0.033	2.2	3.5	2.2	39.8	Middle eutropher
2011-04	7.7	0.036	4.3	3.2	1.9	47.3	Middle eutropher
2011-05	10.6	0.038	3.7	2.9	1.7	47.9	Middle eutropher
2011-06	31.4	0.031	3.2	3.1	1.2	51.5	Light eutropher
2011-07	20.2	0.043	2.8	3.3	1.5	50.3	Light eutropher
2011-08	35.6	0.052	3.3	5.2	1	56.7	Light eutropher
2011-09	1.9	0.092	4.5	6.8	0.6	55.3	Light eutropher
2011-10	1.3	0.043	2.8	5.5	1.5	44.9	Middle eutropher
2011-11	1.1	0.036	2.1	4.5	2.0	41.0	Middle eutropher
2011-12	1.0	0.032	2.1	4.3	2.1	40.0	Middle eutropher

Table 9 Weighted comprehensive trophic state index of Shibianyu Reservoir (2012)

Month	chla	TP	TN	COD_{Mn}	SD	Trophic state index	Trophic status
2012-01	1.1	0.028	2.1	3.8	2.1	39.2	Middle eutropher
2012-02	1.0	0.023	2.0	3.7	2.1	38.1	Middle eutropher
2012-03	2.2	0.021	1.9	3.5	2.0	39.8	Middle eutropher
2012-04	5.9	0.025	4.3	3.0	1.8	45.3	Middle eutropher
2012-05	24.6	0.019	3.7	2.9	1.5	48.6	Middle eutropher
2012-06	44.7	0.036	3.1	4.1	1.2	54.2	Light eutropher
2012-07	27.8	0.033	2.5	3.5	1	51.8	Light eutropher
2012-08	41.6	0.032	2.3	3.6	0.6	54.6	Light eutropher
2012-09	52.2	0.075	3.6	6.2	0.4	62.7	Middle eutropher
2012-10	32.8	0.042	2.7	5.4	0.8	56.2	Light eutropher
2012-11	5.2	0.024	2.2	4.2	1.2	45.9	Middle eutropher
2012-12	1.2	0.021	2.1	3.3	1	40.5	Middle eutropher

1.3.2 Shibianyu Reservoir

Chla, TP, TN, and COD_{Mn} are chosen as the surface water pollution control parameters of Shibianyu Reservoir. The fuzzy comprehensive index method was used to estimate the trophic status in Shibianyu Reservoir from 2011 to 2013. The monthly average results are shown in Table 8.

It can be seen from Tables 8, 9, and 10 that the nutrient content of Shibianyu Reservoir is high. From October to April, the water temperature of the reservoir is low and the algal growth speed is restrained; thus, the transparency is high and the reservoir is in the middle eutropher [8]. With the temperature rising in May, algae in reservoir began to thrive. Diatom dominates in spring, and the peak of diatom biomass generally appears at the end of May. In summer, as the temperature rises further, harmful cyanobacteria (mainly *Microcystis aeruginosa*) begin to prevail. Depending on their strong adaptability in a wide range of temperature and illumination, cyanobacteria dominate for a long time until October. From May to September, algae grow quickly and the water transparency is reduced. Shibianyu Reservoir is, thus, in the hyper eutropher.

Table 10 Weighted comprehensive trophic state index of Shibianyu Reservoir (2013)

Month	chla	TP	TN	COD_{Mn}	SD	Trophic state index	Trophic status
2013-01	1.1	0.019	2.1	3.2	2.1	37.2	Middle eutropher
2013-02	1.1	0.021	2.1	3.1	2.2	37.2	Middle eutropher
2013-03	3.2	0.021	2.3	3.1	2.1	40.7	Middle eutropher
2013-04	6.1	0.032	3.7	3.2	2.0	45.6	Middle eutropher
2013-05	15.6	0.042	4.1	5.2	1.5	52.9	Light eutropher
2013-06	28.7	0.038	3.7	4.8	1.2	54.4	Light eutropher
2013-07	43.1	0.032	2.8	5.3	0.7	56.6	Light eutropher
2013-08	40.2	0.026	2.4	4.2	0.8	53.7	Light eutropher
2013-09	39.7	0.025	2.3	4.3	0.7	54.0	Light eutropher
2013-10	19.9	0.022	2.3	3.8	1.4	48.6	Middle eutropher
2013-11	5.2	0.042	2.7	3.5	1.8	45.9	Middle eutropher
2013-12	1.2	0.051	2.8	3.2	2.1	41.3	Middle eutropher

Table 11 Trophic status assessment of Zhoucun Reservoir

Month	chla	TN	TP	SD	COD	TLI(Σ)
12-04	38.03	71.36	40.79	47.64	39.26	82.68
12-05	25.11	66.52	33.06	45.36	46.92	81.67
12-06	58.81	63.27	33.06	52.18	46.00	83.38
12-07	70.45	61.40	49.94	65.42	54.72	85.12
12-08	71.97	69.36	49.94	64.24	54.33	85.58
12-09	65.76	70.52	44.32	59.24	48.75	84.76
12-10	64.63	68.27	45.02	55.75	45.55	84.55
12-11	55.47	69.78	42.45	52.80	34.79	82.87
12-12	54.13	70.45	33.06	47.64	42.82	83.44
13-02	48.59	70.85	33.75	32.64	32.61	83.23
13-03	43.13	72.09	35.67	49.33	37.02	82.25
13-04	39.24	70.45	36.26	53.22	38.56	81.89
13-05	41.38	67.81	38.43	53.22	39.58	82.23
13-06	52.19	59.23	46.00	57.82	56.40	84.48
13-07	65.31	65.67	62.18	62.43	54.76	85.94
13-08	62.60	70.39	44.32	66.67	48.84	84.20
13-09	59.59	71.10	44.32	60.45	38.75	83.31
13-10	58.73	68.64	48.64	55.03	41.45	84.11
13-11	56.86	65.84	44.32	47.64	39.39	83.87
13-12	55.18	65.22	42.45	43.97	32.85	83.02

1.3.3 Zhoucun Reservoir

The comprehensive nutrition state index was used to evaluate Zhoucun Reservoir. The results are shown in Table 11.

The results show that the comprehensive indices of trophic status in Zhoucun Reservoir from April 2012 to December 2013 are higher than 70, indicating that Zhoucun Reservoir belongs to the hyper eutropher and the water pollution is serious.

Table 12 The evaluation results of trophic status in Zhelin Reservoir (2008–2012)

Year	2008	2009	2010	2011	2012
TLI(∑)	43.14	51.28	48.27	38.45	43.73
Trophic status	Middle eutropher	Light eutropher	Middle eutropher	Middle eutropher	Middle eutropher

1.3.4 Zhelin Reservoir

According to the water quality results from 2008 to 2012, the evaluation results of trophic status are shown in Table 12: (1) Zhelin Reservoir belongs to the middle eutropher; (2) The trophic status index of Zhelin Reservoir increased from 2008 to 2009, but decreased from 2009 to 2011, and increased again from 2011 to 2012. This illustrates that the water environmental protection methods performed by the local government are not effective enough to control the eutrophication of Zhelin Reservoir.

1.4 Source Analysis of Nitrogen and Phosphorus in Typical Reservoirs

1.4.1 Shibianyu Reservoir

(1) Seasonal Variations of TN and TP

The TN content of Shibianyu Reservoir is high and the annual average concentration is 2.78 mg/L (Fig. 1a). The contents of TN are relatively low from December to February. The highest concentrations of TN are 4.3, 4.3, and 3.7 mg/L in the spring of 2011, 2012, and 2013, respectively. Storm runoff makes the concentration of TN rise sharply in summer. The highest TN concentrations during the storm runoff are 5.4 mg/L (September 19), 3.6 mg/L (September 3), and 4.1 mg/L (May 30) in 2011, 2012, and 2013, respectively. After the storm runoff, the concentration of TN reduces quickly. The TN concentration increases within a narrow range (from 2.2 to 2.9 mg/L) during the mixing period at the end of November 2013, but the phenomenon does not appear at the same time in 2011 and 2012.

The TP content can meet the national surface water quality standard (GB 3838–2002) (class III) throughout the year, and its annual average concentration is 0.038 mg/L (Fig. 1b). The TP concentration increases mainly in the period of summer storm runoff. The highest concentrations of TP are 0.19 mg/L (19 September), 0.13 mg/L (3 September), and 0.05 mg/L (30 May) in 2011, 2012, and 2013, respectively. The content of TP reduces quickly after the storm runoff. Similar to the variations in TN, TP rises at the end of November 2013 but did not increase in 2011 and 2012. To explore the reasons for the seasonal variations of phosphorus and nitrogen, ten monitoring points are selected upstream of the reservoir, as shown in Fig. 2.

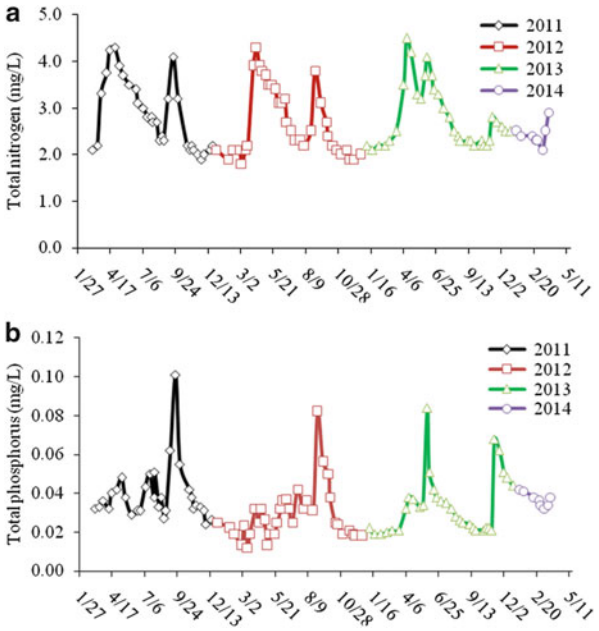

Fig. 1 Seasonal variations of TN and TP in Shibianyu Reservoir (2011–2014)

Fig. 2 Distribution of the monitoring points in Shibianyu Reservoir

(2) Cause Analysis of TN Increase in Spring

(1) Endogenous pollution survey

The thermal stratification of Shibianyu Reservoir disappeared at the end of November and then the reservoir entered the complete mixing period (Fig. 3a). During this period, the whole water is mixed and the temperature is low. The concentration of dissolved oxygen increases with the decreasing temperature and reaches a peak of 12.8 mg/L in winter (Fig. 3b). At this time, the reservoir has good self-purification ability and endogenous release is inhibited by dissolved oxygen. So, we can eliminate the impact of endogenous pollution on the nutrients concentration of Shibianyu Reservoir.

(2) Exogenous pollution survey

The flow into Shibianyu Reservoir is around 0.1 m^3/s in winter (Fig. 4). As the temperature increases during mid-March, the inflow of Shibianyu Reservoir increased because of upstream snowmelt, commonly known as spring flood. In this period, the rainfall is small enough. Since snowfall has becomes less in recent years, the flow is generally less than 10 m^3/s. After the rain, the inflow of Shibianyu Reservoir has a short period of increase and then remains at a stable flow (about 2 m^3/s). As shown in Table 13, with the increase of inflow, the TN concentration rises rapidly at the monitoring points (from S1 to S8) during mid-March. Especially at monitoring point S7, the TN concentration reached 6.58 mg/L. Until the end of May, TN started to decrease rapidly at the upstream monitoring points.

As shown in Table 14, the TN load upstream was estimated from March to May in 2011 and 2012. Despite the upstream water flow is relatively low, the TN concentration of the upstream water stays high over a long period. Due to the small water storage capacity of the reservoir, the upstream water has a great influence on the TN concentration of the reservoir. The upstream water causes TN to be increased by 0.6, 2.2, and 2.7 mg/L from March to May in 2011 and 1.6, 1.2, and 1.8 mg/L from March to May in 2012.

(3) Cause analysis of TN and TP increase

Influenced by the subtropical monsoon climate, the seasonal distribution of rainfall in Shibianyu Reservoir is uneven. As shown in Fig. 5, rainfall mainly concentrated in May to September, accounting for 80 % of the annual rainfall. The largest rainfall occurred in September (412 mm) and August (180 mm) from 2011 to 2013, respectively. The largest annual rainfall was 101.4, 81, and 92 mm from 2011 to 2013, respectively. In general, the inflow of the reservoir and rainfall were significantly positive correlated, especially during the rainy season. After the heavy rain in 2011–2013, the flood peak reached 100.4, 117.6, and 102.4 m^3/s, respectively. During the storm, the reservoir would experience a sharp change in the water level.

Large amounts of nitrogen and phosphorus entered into the reservoir and runoff is the main cause of the elevated concentration of TN and TP. Upstream flow and the content of nitrogen and phosphorus change greatly during storms; therefore, it is difficult to determine the exogenous pollutants accurately during the storm. However, when the reservoir flow is more than 100 m^3/s, the contents

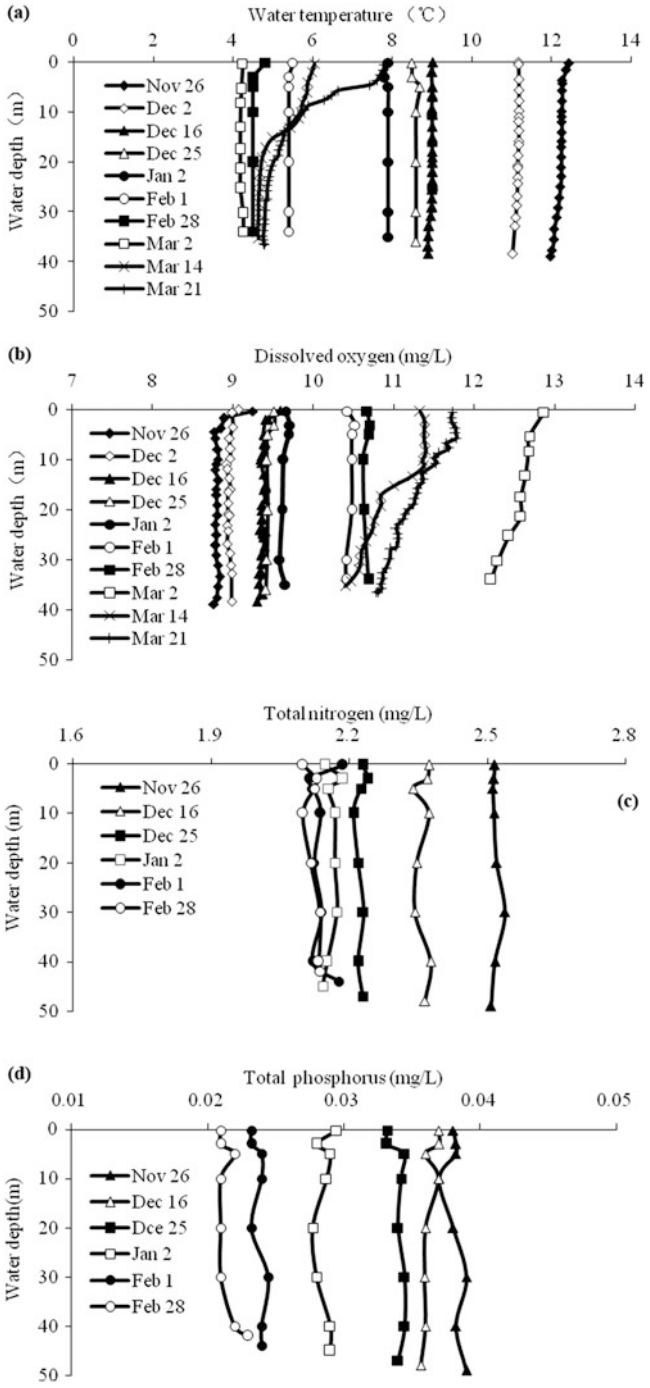

Fig. 3 Vertical distributions of temperature (**a**), dissolved oxygen (**b**), total nitrogen (**c**), and total phosphorus (**d**)

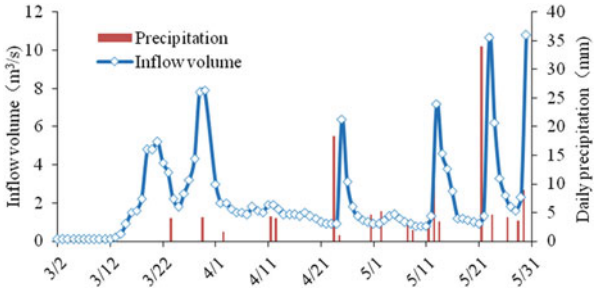

Fig. 4 Rainfall and inflow change curve in spring

Table 13 TN concentrations of upstream monitoring points (mg/L)

Monitoring point	February 28	March 5	March 20	April 3	April 25	May 10	May 19	June 3
S1	2.25	2.04	4.38	4.64	4.56	4.24	4.01	3.36
S2	2.26	2.06	4.86	4.89	4.62	4.31	4.34	3.19
S3	2.35	2.14	4.76	4.96	4.50	4.35	4.15	3.27
S4	2.49	2.15	4.62	4.82	4.18	4.41	3.92	3.09
S5	2.14	1.91	3.72	4.16	4.20	4.42	4.08	3.09
S6	2.31	1.91	3.71	4.13	4.00	5.02	3.93	3.20
S7	2.96	2.72	6.05	5.98	6.58	5.85	5.79	4.68
S8	2.10	1.83	3.81	4.39	4.19	4.25	4.01	3.36

Table 14 TN load of upstream in spring

	Rainfall (mm)	Reservoir inflow (10^4 m^3)	Average concentration (mg/L)	Month input (t)	Reservoir volume (10^4 m^3)	Increased concentration (mg/L)
2011-03	21.6	134	3.3	4.4	737	0.6
2011-04	35.3	445	4.1	18.2	818	2.2
2011-05	129.3	615	3.6	22.1	833	2.7
2012-03	16.3	604	3.7	22.3	1393	1.6
2012-04	34.0	409	4.5	18.4	1512	1.2
2012-05	86.5	691	3.4	23.5	1276	1.8

of TN and TP will rise with the increase of sediments in the runoff. The inflow nutrients load of storm runoff in 2011–2013 is shown in Table 15. The nutrients are mainly composed of particulate organic nitrogen and particulate organic phosphorus, which are easy to be settled. So, after the storm runoff, the TN and TP concentrations of the reservoir decline quickly and the endogenous pollution load increases.

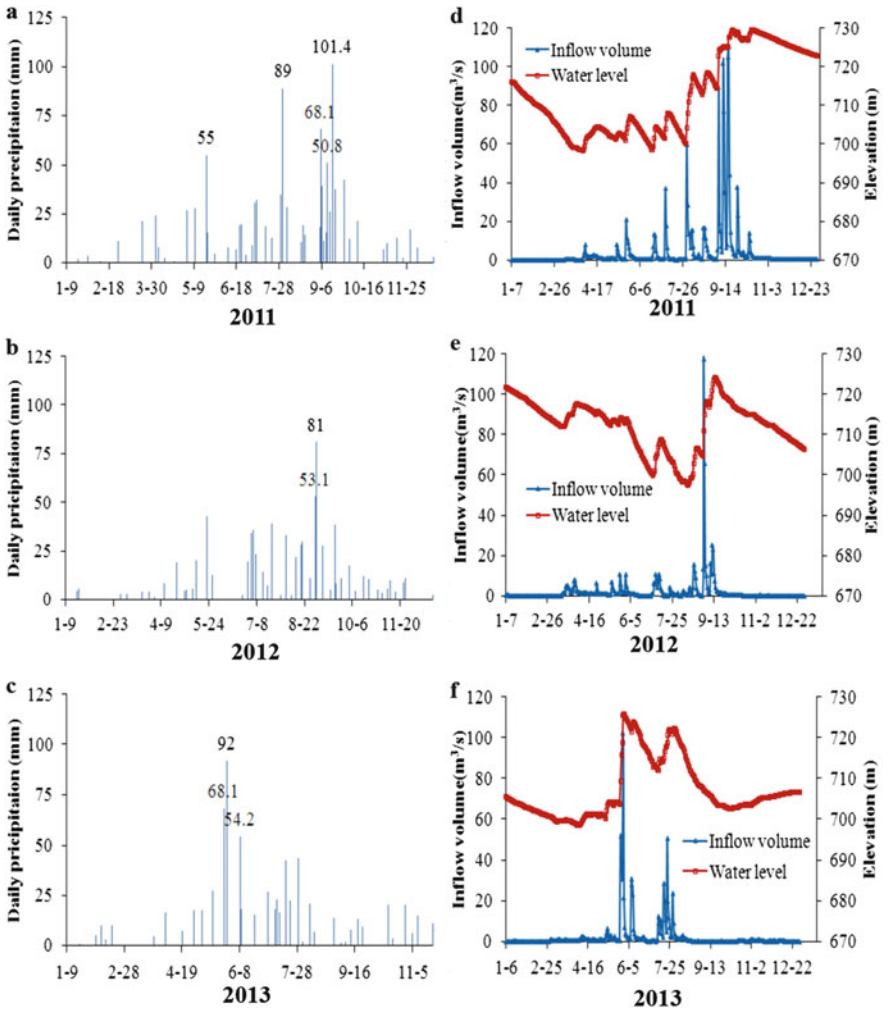

Fig. 5 Daily variations of rainfall, inflow, and water level (2011–2013)

1.4.2 Source Analysis of Nitrogen and Phosphorus in Zhoucun Reservoir

The TN concentration in Zhoucun Reservoir varies from 1.5 to 2.8 mg/L, with nitrate the major component (as shown in Figs. 6 and 7). The seasonal variation of the TN concentration is similar to that of nitrate. Their concentrations decline from spring to summer. In the late dry season, the concentrations of TN and nitrate would fall to the lowest levels. With the increase of rainfall in the rainy season, a number of exogenous nitrates enter into Zhoucun Reservoir, causing the concentrations of TN and nitrate to increase rapidly. In winter and spring, the concentration of TN is

Table 15 Inflow nutrients load of storm runoff

Year	Peak discharge (m^3/s)	Occurrence time	Inflow (10^4 m^3)	TN (mg/L)			TP (mg/L)		
				Inflow concentration	PTN/TN	Total input (t)	Inflow concentration	PTP/TP	Total input (t)
2011	110.4	18 September	4735	7.2/4.5	79 %	213.07	0.252/0.064	78 %	3.03
2012	117.8	1 September	1869	5.7/3.6	68 %	67.28	0.148/0.047	65 %	0.88
2013	102.0	29 May	1977	5.2/3.3	65 %	65.24	0.079/0.042	54 %	0.83

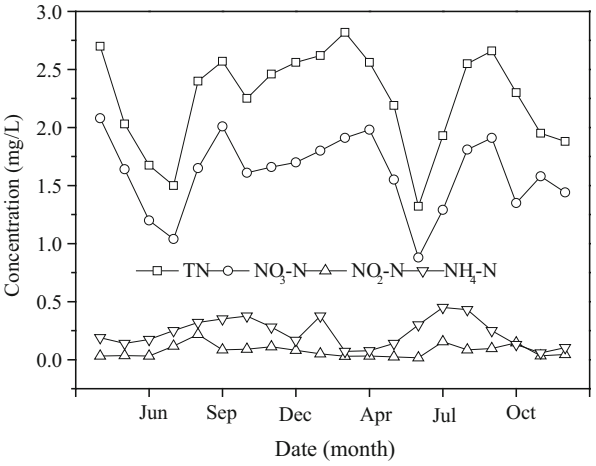

Fig. 6 Seasonal variations of nitrogen in Zhoucun Reservoir

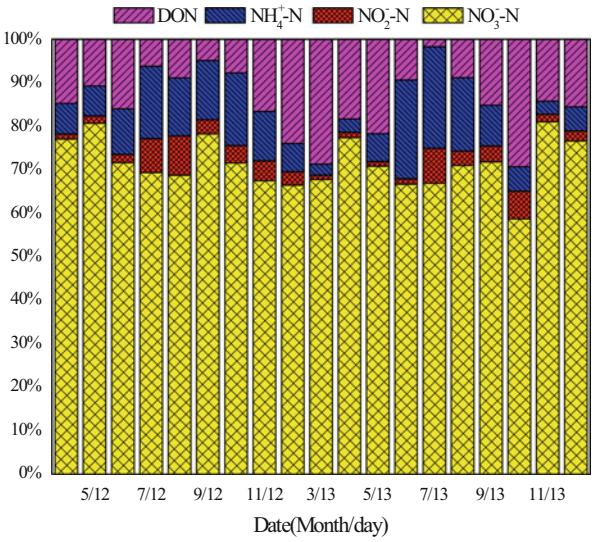

Fig. 7 Proportion of different species of nitrogen in Zhoucun Reservoir

stable, remaining around 2.5 mg/L. The concentration of nitrate is between 1.6 and 1.8 mg/L.

The concentrations of ammonia are in the range 0.2–0.5 mg/L, with the peak appearing in September or October each year. This is mainly due to the release of pollutants from sediment during May to October. Zhoucun Reservoir starts to form stratification in April, and the bottom water becomes anaerobic in May, which creates favorable conditions for the release of ammonia.

In September and October, stratification becomes weak and the thermocline moves down, which cause the original bottom water and ammonia to be released

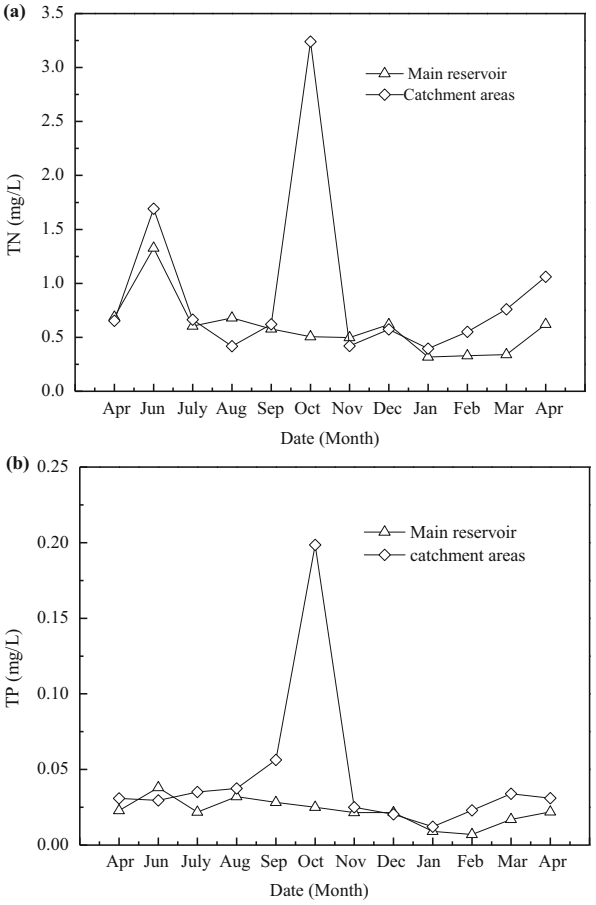

Fig. 8 Seasonal variations of TN and TP in Zhelin Reservoir

into the mixing layer. When the stratification is completely destroyed, ammonia will distribute homogeneously in the whole reservoir, and then ammonia will decline gradually due to the nitrification process.

1.4.3 Source Analysis of Nitrogen and Phosphorus in Zhelin Reservoir

Figure 8 shows the seasonal variations of TN and TP in Zhelin Reservoir and upstream. The concentrations of TN upstream and in the reservoir reach up to 1.33 and 1.69 mg/L, respectively, which are beyond the national surface water quality standard (GB 3838–2002) (class III). The average rainfall of Zhelin Reservoir is 1506 mm and 40–50 % of that occurs from April to June. Therefore, large amounts of pollutants are carried into the lake in June. The concentrations of TN in the major estuary, Wuning County, and fork entrance reach 1.8, 2.3, and 1.9 mg/L,

Table 16 Pollution load of Zhelin Reservoir in October 2013

Monitoring points	Region of influence (km^2)	Influence depth (m)	TN concentration (mg/L)	TP Concentration (mg/L)	TN load (t)	TP load (t)
Wuning County	7.26	5	5.72	0.336	207.6	13.29
Major estuary	3.36	5	3.93	0.26	44.39	4.37
Fork entrance	8.55	2.5	2.22	1.07	47.45	22.87
Shallow area	13.44	2.5	1.75	0.028	58.8	0.94
Summary	40.67				358.24	41.44

respectively. The concentration of TN in the reservoir is 1.33 mg/L. Therefore, rainfall runoff is the main cause of increased concentrations of TN and TP in Zhelin Reservoir.

The concentrations of TN and TP increased suddenly in October 2013, reaching 3.24 mg/L and 0.20 mg/L, respectively. Table 16 shows the estimation of pollution load according to the results of water quality in Zhelin Reservoir basin.

2 Algal Blooming

2.1 Harm of Algal Blooms

2.1.1 Effects on Drinking Water

(1) Algae-Induced Taste and Odor

Algae, fungi, and actinomycetes are the main sources of odor [9]. Different algae cause different types of odor. Algal growth secretes a lot of odor-producing compounds, which will be released after algae die. There are more than ten kinds of odor-producing compounds in eutrophic water. Geosmin and 2-methyl isopropyl alcohol (2-MIB) are the two major algae-induced odor compounds [10].

(2) Microcystin

Studies have shown that about 25–70 % of cyanobacteria can produce microcystin. The main species are *Microcystis aeruginosa*, *Anabaena flos-aquae*, and *Aphanizomenon flos-aquae* [11–13]. Microcystic toxins (MC), the most widely distributed toxins, are a group of seven peptide monocyclic liver toxins and have the closest relationship with human beings. They are also strong liver tumor-promoting agents. MC often exist in the algal cells and will be released into the water when the cells break up. MC have been found in drinking water all over the world. Events that animals die of microcystin have been reported in more than ten countries [14].

(3) Disinfection By-products
The issue of disinfection by-products has become a hot topic in current drinking water area [15]. Algal organic matter is the precursor of disinfection by-products. It could not only produce three trihalomethanes (THMs), but also the more harmful haloacetic acids (HAAs). All these disinfection by-products decrease the safety [16].

2.1.2 Effect on Water Treatment Systems

(1) Clogging Filters
The density of algae is close to that of water, which lets them remain suspended in water. Green algae, cyanobacteria, and diatom are the most common species in China.

Algae in the size range 2–200 μm have great effects on water plants. Since the density of algae is small, it is difficult to be removed by coagulation and precipitation [17]. A lot of residual algae will aggregate in the filter (especially slow filters) and form dense layers, which cause a reduction in the permeability of the filter. The gas released from the algae can also clog the filter, leading to the operation cycle being shortened and filter backwashed water increasing.

(2) The Increase of Chemical Cost
Much greater quantities of coagulants and disinfectants would be required due to the large amount of algae and algae-produced organic matter. Algal organic compounds could react with the hydrolysis products of coagulant (iron or aluminum salts) [18]. While the generating surface complex can prevent small particles from colliding with each other, it is, thus, inevitable to increase the dosage of coagulant to mitigate the impacts of surface complex [19].

2.1.3 Effect on Pipe Network and Water Quality

In order to control the number of bacteria generated in the water distribution network, the water from waterworks always maintain certain residual chlorine, even though bacteria still regrow in the water distribution network. The phenomenon is closely related to the nutrients in the effluent. The reproduction of bacteria causes water quality deterioration (e.g., as turbidity and chromaticity increase, the total number of bacteria increases). Algae and organic matter existing in the pipe network could promote the growth of bacteria and larger organisms, such as nematodes and sponge animals in the pipe network. It is very difficult to eliminate these animals, which can jam water meters and faucets. Algal metabolites can also react with the hydrolysis species during the coagulation process, which leads to greater coagulants consumption accordingly and increasing the water production cost. Furthermore, the generating complex can also cause pipeline corrosion and shorten the service life of the pipe network.

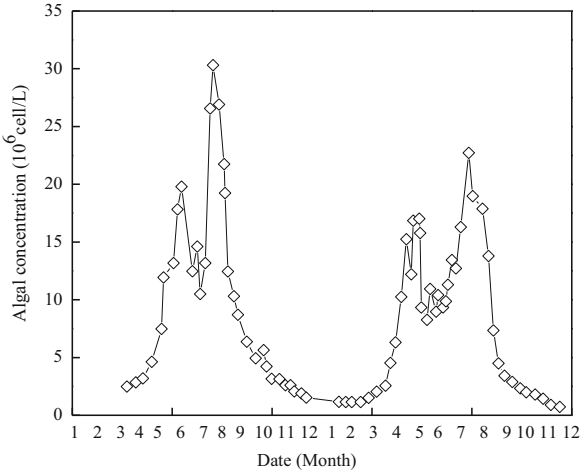

Fig. 9 Seasonal variation of algal abundance in the surface water of Jinpen Reservoir

In conclusion, algal blooming in lakes and reservoirs has a great influence on water quality, water plant operation, and the pipeline network. Thus, removing algae has become an important subject in controlling the water quality of reservoirs.

2.2 Algae Pollution of Jinpen Reservoir

2.2.1 Seasonal Variations of Algal Abundance

As an important producer in aquatic ecosystems, algal abundance and community can directly affect and indicate trophic status in reservoirs. Figure 9 shows that algal abundance distributed in a typical "saddle type" in Jinpen Reservoir during 2008–2009. In March 2008, the algal density in the surface water was less than 4×10^6 cells/L, while the value rapidly increased up to 22×10^6 cells/L in late May. The average daily growth rate is as high as 27.82×10^4 cells/(L·d). In July, algal abundance continued to rise and reached a peak at 30×10^6 cells/L. Algal blooming appeared in July and lasted for a month. Compared with that in 2008, less algal abundance was achieved in 2009 because of the different hydrological and meteorological factors. However, the duration of algal bloom (algal abundance $>10 \times 10^6$ cells/L) extended in 2009.

Regression analysis (Fig. 10) shows that there are positive correlations between algal abundance and TN or TP ($R^2 = 0.6546$, 0.4353, $p < 0.01$). In contrast, there is a negative correlation between algal abundance and water level ($R^2 = 0.209$, $p < 0.01$). Besides, the correlation between NH_4-N and algal abundance is poor.

Temperature is one of the most important influencing factors for algal growth, which can not only control the enzymatic reaction of photosynthesis and respiration intensity, but also influence other environmental factors and nutrients. TN/TP in Jinpen Reservoir fluctuates from 30 to 210, which indicates that phosphorus is the primary restrictive factor.

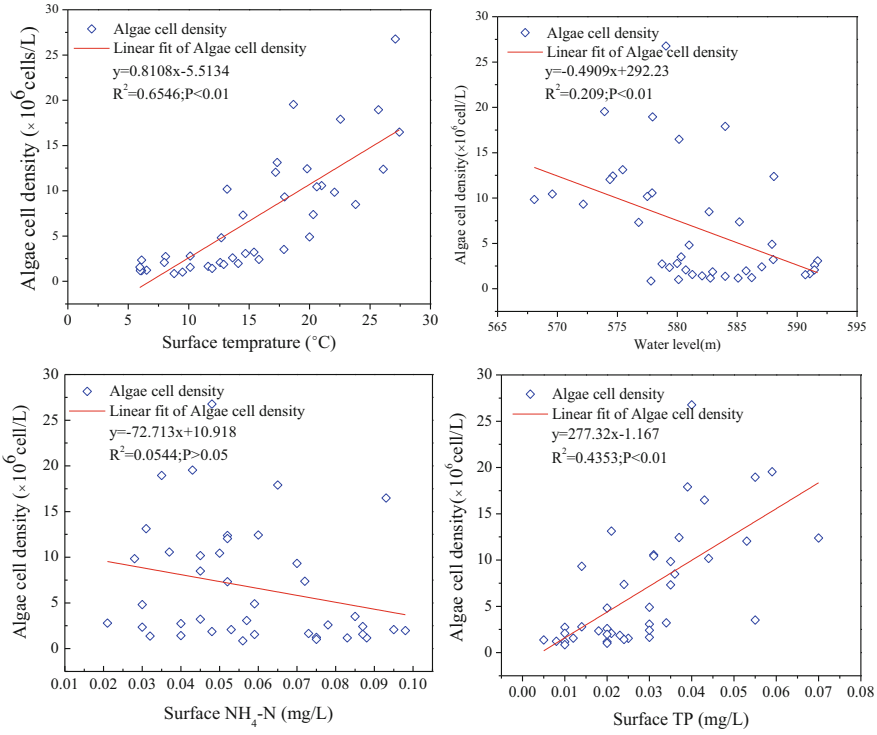

Fig. 10 Correlations between algal abundance and its influencing factors in the surface water of Jinpen Reservoir

The correlation between the water level and algal abundance is affected by many factors. On the one hand, fluctuation in the water level can change the nutrients concentration in the water (dilution or concentration). On the other hand, the turbulent effect involved in the fluctuation process can promote algal growth. With respect to the poor correlation between NH_4 and algal abundance, the authors proposed two reasons for this: (1) nitrogen released from sediment is far greater than the demand, although algal proliferation needs nitrogen to compound protein (algae tends to absorb organic nitrogen firstly, NH_4-N secondly, and finally NO_3-N); (2) NH_4 concentration of the surface water varies widely, since it is affected by many internal and external environmental factors, such as water temperature, pH value, air pressure, and wind speed.

2.2.2 Seasonal Variations of the Algal Community

Sixty-nine taxa belonging to five phyla (Bacillariophyta, Chlorophyta, Cyanophyta, Euglenophyta, and Xanthophyta) were identified. The most diverse groups include Chlorophyta (33 taxa), Bacillariophyta (20 taxa), and Cyanophyta (12 taxa). Euglenophyta and Xanthophyta only account for 5.80 %.

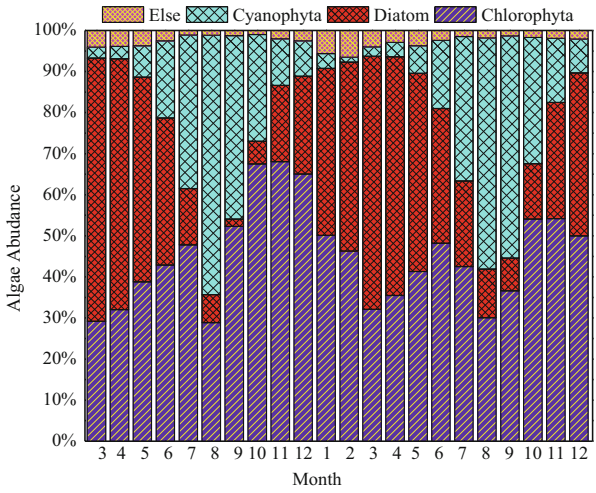

Fig. 11 Seasonal evolution of algal community structure in Jinpen Reservoir

Algal community succession also has obvious seasonal characteristics (Fig. 11). In spring, the dominant groups were Bacillariophyta (48–64 %), Chlorophyta (29–41 %), and Bacillariophyta (2–7.7 %). The major dominant species included *Cyclotella, Fragilaria*, and *Melosira*. In summer, the proportion of Cyanophyta (16–63 %) increased rapidly and Bacillariophyta decreased significantly. The prevalent algae evolved into the eutrophic status species: *Microcystis*, *Merismopedia*, *Chlorella*, and *Chroococcus*. During autumn, the proportion of Chlorophyta increased (37–68 %), while Cyanophyta decreased. The most popular species were *Chlorella*, *Scenedesmus*, *Chlorococcus*, and *Ankistrodesmus*. In winter, the proportion of Cyanophyta and Chlorophyta declined and Bacillariophyta returned to being prevalent.

Although the water temperature in Jinpen Reservoir was relatively low in the beginning of spring, algae began to grow rapidly due to the adequate nutrients supply and strong light intensity. During this period, some diatoms and green algae that are adaptable to low temperature became the dominant species. As the water temperature increased, algae began to grow and reached a peak in late spring for the first time in the year. After the beginning of summer, the water body became more stable due to the formation of thermal stratification. It was difficult for diatoms and other algae to remain in suspension and much of them would be lost by sedimentation. Considering the insufficient available nutrients in water, algal abundance declined at the beginning of summer. In July, the temperature increased rapidly and cyanobacteria began to grow and aggregate. Although the cyanobacteria recovered later than diatoms and green algae, the growth rate of cyanobacteria after its recovery was higher than that of diatoms and green algae. Besides, the thermal stability of genetic material and the photosynthesis system make cyanobacteria tolerant to high temperature. So, cyanobacteria took absolute superiority in algae competition in summer. In late August, algal abundance began to reduce after the

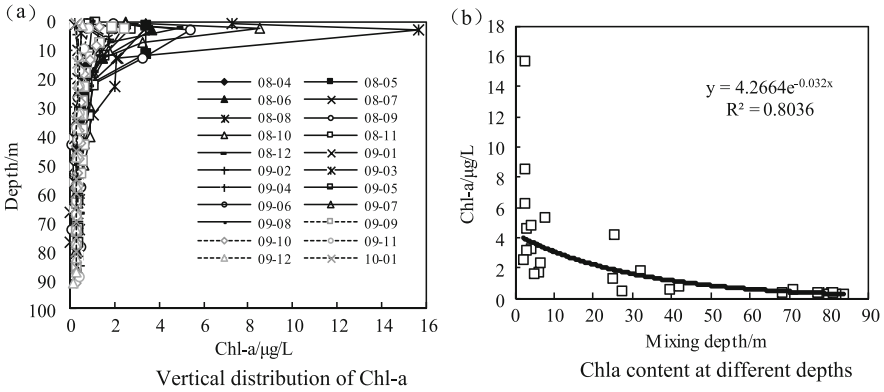

Fig. 12 Vertical distribution of chlorophyll-*a* concentration and correlation between its steady content and the water mixing depth in Jinpen Reservoir

"summer peak". The attenuation was mainly attributed to the increase of the respiration and photosynthesis rate. High temperature could raise the respiratory rate of algae, while the lack of available nutrients could reduce the photosynthesis rate. So, algal abundance decreased in the late summer. In autumn, due to the attenuation of light intensity and decreasing water temperature, Jinpen Reservoir began to mix and the proportion of diatoms increased. In winter, low temperature and low light intensity led algal abundance to fall sharply. Thus, the algae community succession characteristics in Jinpen Reservoir were as follows: "Diatom is dominant in spring and winter, while cyanobacteria and green algae are dominant in summer and autumn".

2.2.3 Vertical Distribution of Algae

Water temperature, illumination, and nutrient level are the key factors for algal growth. These factors are significantly different at different depths and have a great influence on the vertical distribution of algae.

To some extent, the vertical distribution of chlorophyll-*a* can represent the vertical distribution of algae. Figure 12a shows the vertical distribution of chlorophyll-*a* in 2008 and 2009 in Jinpen Reservoir. The maximum chlorophyll-*a* concentration in the upper layer (euphotic zone) appeared in July or August (9–16 μg/L), and the minimum occurred in January or February (0.2–0.34 μg/L). Seasonal variations of chlorophyll-*a* are similar to algal abundance, but were not synchronous. For example, when the algal density reached $(17–20) \times 10^6$ cells/L in the spring, the content of chlorophyll-*a* was still less than 4 μg/L. This was due to the low content of chlorophyll-*a* in diatoms. Furthermore, the phenomenon that the maximum chlorophyll-*a* did not appear in the surface water was mainly due to the light inhibition. Photosynthesis decreased rapidly with the increase of depth and the algal growth rate was seriously limited. In the thermocline, the chlorophyll-*a* content reduced to 0.2–0.3 μg/L quickly and reached a minimum in the hypolimnion layer (<0.2 μg/L).

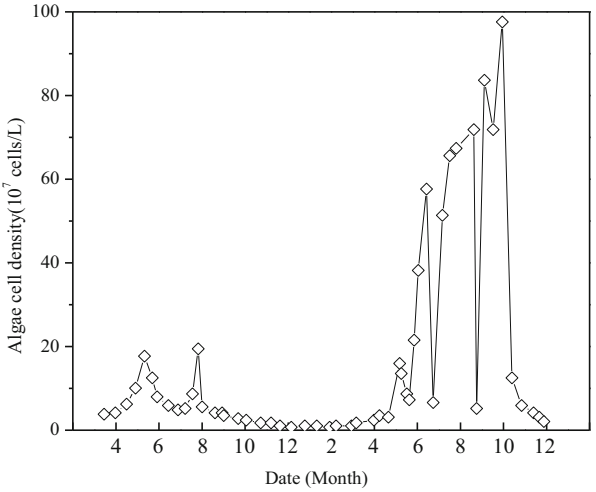

Fig. 13 Seasonal variations of algal abundance in Shibianyu Reservoir (2011.4–2012.12)

The mixing depth could directly affect the available light intensity and determine the distribution of algal biomass. The regression analysis shows that chlorophyll-*a* increases with the decline of mixing depth (Fig. 12b). There is a strong negative correlation between the two indexes ($y = 4.2664\text{e}{-}0.0323x$, $R^2 = 0.8036$). In July 2008, the mixing depth of Jinpen Reservoir was 2.54 m, and the corresponding chlorophyll-*a* was 6.29 μg/L. In August, the mixing depth increased to 2.61 m and chlorophyll-*a* was 15.7 μg/L. A similar phenomenon occurred in 2009. According to Diehl, when the mixing depth is lower than a certain limit, the algal settling velocity would be the primary factor influencing algal abundance. It could be expected that light inhibition is obvious at the surface, and slightly increasing the mixing depth will reduce the light intensity so as to weaken the light inhibition.

2.3 Algal Pollution in Shibianyu Reservoir

2.3.1 Algal Growth in Shibianyu Reservoir

High contents of nitrogen and phosphorus in Shibianyu Reservoir provide adequate nutrition for algal blooms. Water temperature, light, rainfall, and other environmental factors are also key factors for algal growth and community structure in Shibianyu Reservoir. The seasonal variations of algal abundance in 2011 and 2012 are shown in Fig. 13. Algae grew well from May to October. In spring, diatoms dominated and cyanobacteria were prevalent in summer.

Rainfall was frequent in the summer of 2011, which makes the water temperature and illumination intensity change continuously. Besides, due to the effect of dilution, rainfall played a key role in inhibiting algal growth, so algal blooms did not appear in 2011.

The rainfall in 2012 was close to the average level in Shibianyu Reservoir, so the algal dynamics in 2012 can typically reflect the common characteristics of algal

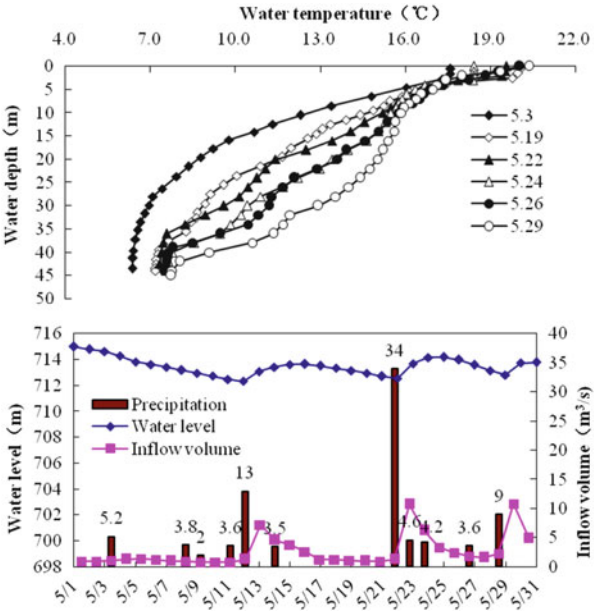

Fig. 14 Water temperature, rainfall, water level, and inflow in May (2012)

growth. It can be seen from Fig. 13 that algae pollution was serious in Shibianyu Reservoir in 2012. The diatoms started to grow rapidly from May and reached a peak in June. After a large rainfall (at the end of June), diatoms reduced. Cyanobacteria became dominant with the increase of water temperature and light intensity. Algal blooms were common from July to October in Shibianyu Reservoir. The algal abundance was as high as 1×10^8 cells/L. During this period, the reservoir had an obvious fishy smell, which seriously affected the water quality.

In order to further clarify the law of phytoplankton succession in Shibianyu Reservoir, algae were monitored frequently from May to October in 2012.

2.3.2 The Analysis of Algal Growth Characteristics and Influencing Factors

(1) Diatoms Growth Characteristics and Influencing Factors

Stratification started to appear in May in Shibianyu Reservoir, as shown in Fig. 14. During this period, rainfall was frequent and light, inflow changed little, and the water level fluctuated between 712 and 715 m. Due to the rainfall, the water temperature increased slowly in May. The surface water temperature was 17.59 °C and the temperature at the bottom was 20.35 °C. With the increase of water temperature and light intensity, the algae began to proliferate. In early May, chlorophyll-*a* was less than 3 μg/L. On May 19, chlorophyll-*a* increased up to 13.43 μg/L. The dominant species were *Cyclotella* and *Melosira*, which composed 26.26 % and 53.54 %, respectively. On May 22, the reservoir experienced a large

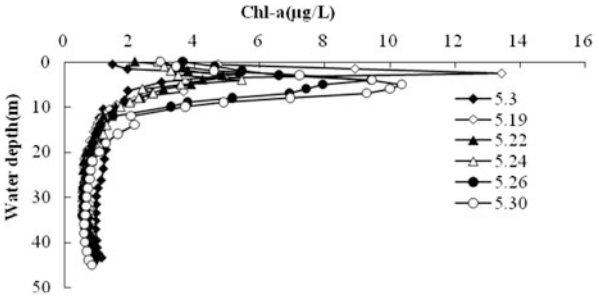

Fig. 15 Vertical distribution of algae in Shibianyu Reservoir in May (2012)

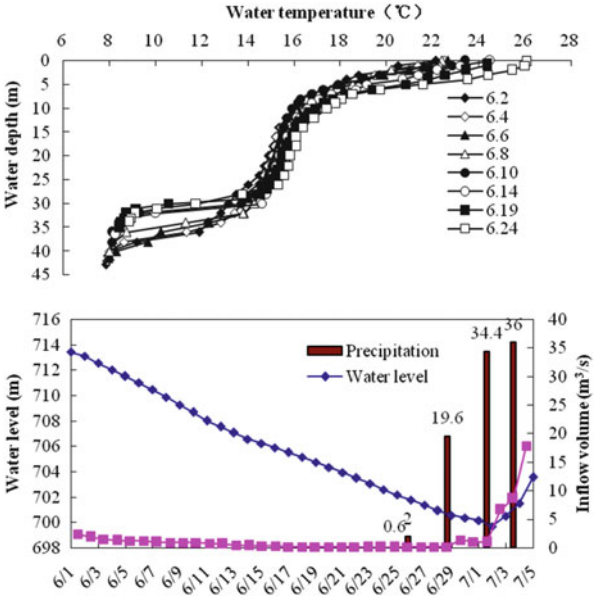

Fig. 16 Water temperature, rainfall, water level, and inflow in June (2012)

rainfall; thus, chlorophyll-*a* subsequently dropped to 4.84 μg/L. Then, the algal abundance increased again and the community changed. *Fragilaria* increased obviously and most of them gathered at a depth of 4–6 m (Fig. 15).

There was no rainfall in the Shibianyu Reservoir between late May and June 24. The water level dropped by 0.5 m/d. On June 1, the water level was 713.43 m and further declined to 700 m on July 2. Since July 2, continuous rainfalls have made the water level rise again. Changes of temperature, inflow, and water level are shown in Fig. 16.

It can be seen in Fig. 16 that stratification formed in June. On June 24, the water temperature was 26 °C and changed little below a depth of 10 m. Suitable temperature and enough light contributed to the rapid growth of algae (Fig. 17). The content of chla was about 50 μg/L and the algal abundance reached 5760×10^4 cells/L. The prevalent species was still *Fragilaria*, which occupied more than 80 %, but their individual size increased and the maximum diameter was close to 200 microns.

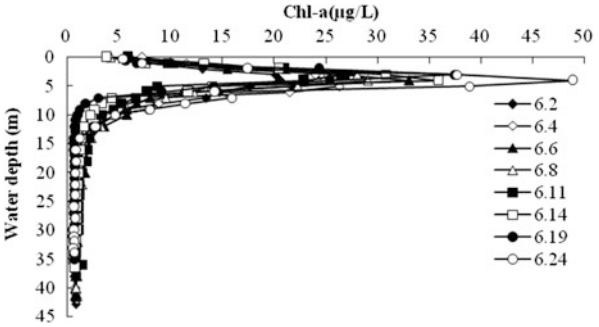

Fig. 17 Vertical distribution of algae in Shibianyu Reservoir in June (2012)

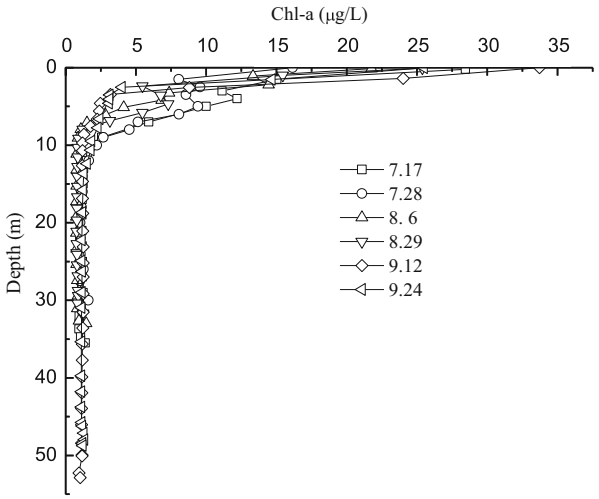

Fig. 18 Vertical distribution of cyanobacteria in Shibianyu Reservoir

(2) Distribution of Cyanobacteria

Figure 18 and 19 indicates that algal blooms were serious from July to October in Shibianyu Reservoir. A number of cyanobacteria often grouped together on the surface and algal abundance reached as high as 1×10^8 cells/L. As the water level decreased, the algal flocs would be left on the shore. In Shibianyu Reservoir, algal blooms were mainly composed of *Microcystis aeruginosa*, which occupied more than 90 %. Microcystis bloom is the most serious kind of water pollution. When it appears, the water gives off an unpleasant smell. Besides, algal toxin will be released after the algal cell fractures. Microcystis toxin is known as being the most harmful algal toxin.

The cause analysis of algal blooms in Shibianyu reservoir was investigated. Firstly, high contents of nitrogen and phosphorus in Shibianyu Reservoir provide sufficient nutrients for algae. Secondly, terrain conditions are suitable for algal growth: Adequate light is conducive to algal photosynthesis, and long hydraulic retention time also provides favorable conditions for algal blooms. Cyanobacteria can be prevalent for a long time due to its own competitive advantages: (1)

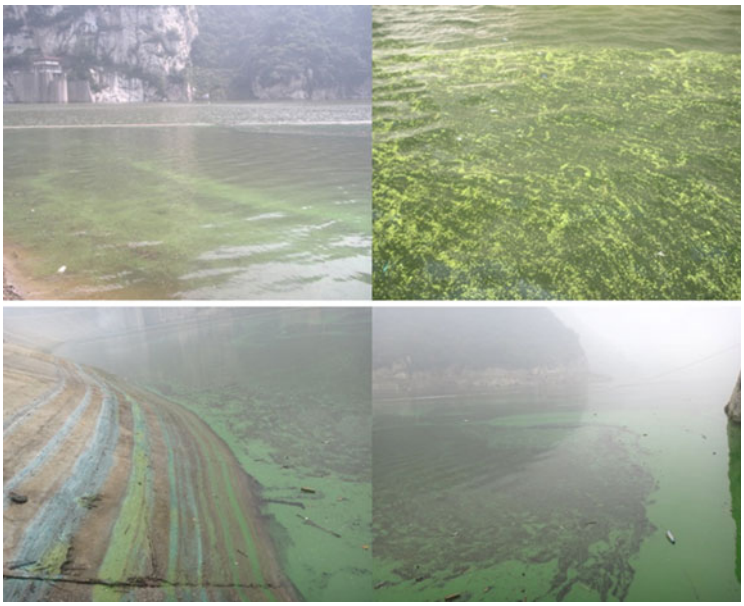

Fig. 19 Algal blooms in Shibianyu Reservoir (July–October)

Cyanobacteria can prevent light inhibition; (2) Cyanobacteria have higher nutrient affinity than others; (3) Cyanobacteria can mainly gather at the surface to a depth of 0.3 m by airbags regulation; (4) Cyanobacteria toxins have an inhibitory effect on other algae.

2.4 Algae Pollution of Zhoucun Reservoir

2.4.1 Algae Community Succession in Zhoucun Reservoir

A total of seven phyla, 57 genera, and 122 species were identified from April 2012 to November 2013. The total number was composed of 57 species of Chlorophyta, 28 species of Bacillariophyta, 25 species of Cyanophyta, three species of Euglenophyta, three species of Cryptophyta, two species of Xanthophyta, and three species of Pyrrophyta. Chlorophyta was the most important group in terms of species number (46.7 %), followed by Bacillariophyta (23 %), Cyanophyta (20.5 %), and the others. The algal abundance in Zhoucun Reservoir was very different in each season and at different depths.

In spring, Zhoucun Reservoir was dominated by Chlorophyta and Bacillariophyta. Specifically, the popular species were *Cyclotella*, *Synedra*, *Stephanodiscus*, *Cocconeis*, *Scenedesmus*, *Ankistrodesmus*, *Chlorococcales*, and *Chlamydomonas*. Chlorophyta was mainly distributed on the surface and Bacillariophyta was mainly distributed in the middle and bottom of the reservoir.

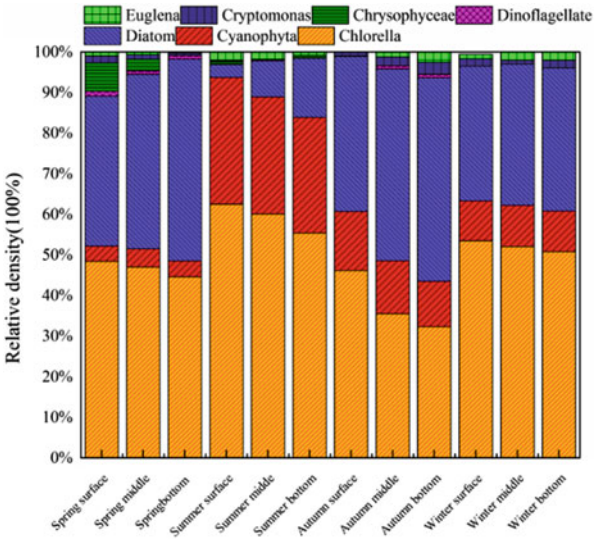

Fig. 20 Phytoplankton community succession in Zhoucun Reservoir

In summer, Cyanophyta dominated in the water, followed by Chlorophyta. The two species accounted for 80–90 % of the total. The vertical distribution of Chlorophyta presented a downward trend, while Bacillariophyta exhibited the opposite behavior. The prevalent species became less numerous and was mainly composed of *Chlorella*, *Microcystis*, *Anabaena*, and *Chroococcus*. *Microcystis* only dominated in the surface waters and the others were more common in the whole water.

In autumn, diatoms became dominant. The proportion of cyanobacteria and green algae decreased. The characteristics of the vertical distribution were similar to that in summer. The dominant genera were *Stephanodiscus*, *Synedra*, *Chlorella*, *Chroococcus*, *Lyngbya*, and *Anabaena*. *Chlorella* dominated in the whole water. Cyanophyta was mainly distributed in the surface and middle waters.

In winter, the phytoplankton community at different depths was similar. Green algae, diatoms, and cyanobacteria accounted for about 52 %, 30 %, and 14 %, respectively. The main prevalent species were *Synedra*, *Chlorella*, *Cyclotella*, *Chlamydomonas*, and *Chlorococcum* (Fig. 20).

The phytoplankton community varies with the change of trophic status. In general, *Chrysophyceae* and *Xanthophyta* are dominant in oligotrophic water. Dinoflagellates, Cryptophyta, and Bacillariophyta are prevalent in middle eutrophic water. Chlorella and Cyanophyta are popular in eutrophic water, while Chlorella and Cyanophyta are usually prevalent in the whole Zhoucun Reservoir, so the water quality of Zhoucun Reservoir can be judged as being eutrophic.

2.4.2 Seasonal Variations of Algal Abundance in Zhoucun Reservoir

The change of algal abundance in the surface water of Zhoucun Reservoir was unimodal. Seasonal variations of the vertical distribution were obvious.

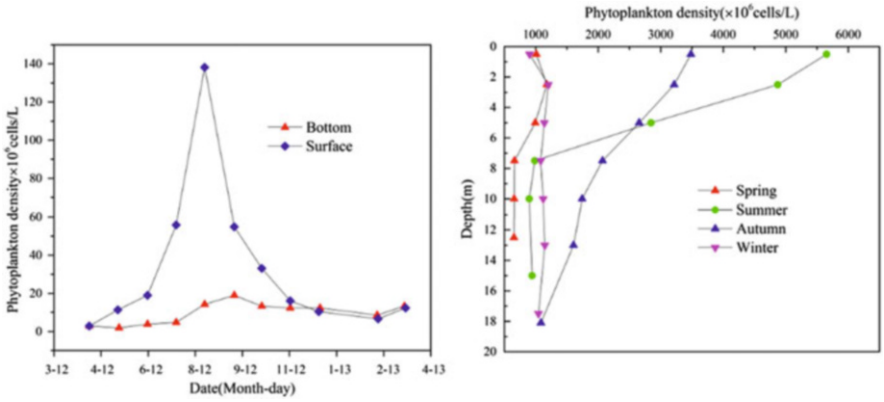

Fig. 21 Seasonal variations of algal abundance in Zhoucun Reservoir

In spring, the water temperature was still low while the light intensity increased. Algae started to grow on the surface. At the bottom, algal abundance changed little due to the low temperature and weak light intensity. Algal abundance in the surface layer was slightly higher than that at the bottom.

In summer, the water temperature and illumination both reached optimal conditions for algal growth. Meanwhile, the nutrient content was rich. The cell density of algae grew exponentially and the peak (1.39×10^8 cells/L) appeared in August. At the bottom, the cell density also increased, which was attributed to the deposition of algae. Illumination and water temperature dropped rapidly with the increase of depth, which makes the cell density of algae fall quickly in the vertical direction. Due to the influence of stratification, the water temperature changed little below 8 m. So, it follows that algal abundance changed little below 8 m in Zhoucun Reservoir.

The temperatures and light intensities fell in the autumn and the algal abundance decreased rapidly. Because there were still a large number of algae settling at the bottom, the algal abundance at the bottom was not significantly lower than that in summer. The vertical distribution in autumn was similar to the situation in summer because stratification still existed during this period.

Due to low temperature, weak light intensity, and short day time, the cell density of algae in the surface waters dropped to the lowest level throughout the year. The whole water mixed in the early winter, so there is no significant difference in algal abundance in the vertical direction (Fig. 21).

2.4.3 Analysis of Influencing Factors

Correlation and redundancy analysis were applied to explore the relationship between algal abundance and environmental factors. The algal abundance and water quality parameters are shown in Table 17. The serial numbers of dominant species are shown in Table 18.

Table 17 Algae and water quality in the surface water in Zhoucun Reservoir

Date	Algae abundance (million cells/L)	Chlorophyll-*a* (μg/L)	Rainfall (mm)	Water level (m)	Temperature (°C)	DO (mg/L)	pH	Turbidity (NTU)	TN (mg/L)	NO_3 (mg/L)	NO_2 (mg/L)	NH_4 (mg/L)	TP (mg/L)	N/P	Fe (mg/L)
12-04	3.26	3.32	36.5	125.00	15.7	9.44	8.68		3.24	3.08	0.032	0.290	0.037	87.6	0.149
12-05	1.08	1.01	8	124.57	22.6	8.53	8.53		2.44	1.84	0.035	0.548	0.023	105.9	0.015
12-06	23.97	22.50	9	123.94	25.2	10.52	8.72		2.61	1.20	0.032	0.075	0.023	113.5	0.031
12-07	77.74	65.71	271	125.22	28.2	14.59	10.16	33.8	2.60	1.04	0.217	0.450	0.065	40.2	0.149
12-08	93.71	75.58	200.5	125.47	27.2	10.29	10.07	18.2	2.40	1.13	0.217	0.060	0.065	36.9	0.236
12-09	48.63	42.66	110	127.63	23.2	7.25	9.86	9.3	2.57	2.01	0.084	0.550	0.046	55.9	0.200
12-10	23.51	38.43	9	127.82	20.3	9.69	8.48	7.74	2.25	1.61	0.090	0.375	0.048	46.8	0.118
12-11	10.26	16.54	59.5	127.66	12.7	10.40	8.3	5	2.46	1.66	0.112	0.680	0.041	60.0	0.087
12-12	11.14	14.62	39	127.47	6.5	11.65	8.11	3.5	2.56	1.70	0.080	0.167	0.023	111.0	0.030
13-02	6.93	8.78	12.5	127.06	3.8	10.77	8.35	2.5	2.20	1.80	0.051	0.375	0.024	93.2	0.015
13-03	11.43	5.31	10.5	126.82	7.6	11.93	8.5	3.3	2.82	1.91	0.029	0.072	0.027	104.4	0.026
13-04	1.19	0.94	21	126.48	11.9	10.05	8.36	3.4	2.56	1.98	0.032	0.078	0.028	91.4	0.026

Table 18 Spatial and temporal variations of dominant species in Zhoucun Reservoir

No.	Dominant species	Spring		Summer		Autumn		Winter	
		Surface layer	Bottom layer	Surface layer	Bottom layer	Surface layer	Bottom layer	Surface layer	Bottom layer
1	*Cyclotella*	+	+					+	+
2	*Stephanodiscus*	+					+		
3	*Ankistrodesmus*	+						+	
4	*Cocconeis*	+							
5	*Chlorella*			+	+	+	+	+	
6	*Synedra*		+		+		+	+	+
7	*Microcystis*			+		+			
8	*Lagerheimia longiseta*	+							
9	*Chlorococcum*								
10	*Oocystis*								+
11	*Chlamydomonas*							+	
12	*Anabaena*			+		+			
13	*Lyngbya*								
14	*Chroococcus*			+	+	+			
15	*Tabellaria*		+						
16	*Scenedesmus*	+							

Correlation analysis indicates that algal abundance was positively related to temperature, pH, turbidity, and TP, while it was significantly negatively correlated with the ratio of N/P (Table 19).

As shown in Table 20, the RDA analysis results can explain 91.9 % of the information of phytoplankton and environmental factors. The eigenvalues of axes 1 and 2 are 0.591 and 0.169, respectively. The correlation coefficient between environmental factors and phytoplankton is 1.

In the RDA sequence diagram, the angle between the arrows of algae depicts the relationship between different species. The smaller the angle, the higher the correlation. The same arrow direction indicates a positive correlation, while the opposite direction implies a negative correlation. The length of the arrow of environmental factors indicates their effects on phytoplankton. Figure 22 shows that TN, TP, and water level are the main factors influencing the phytoplankton community structure in Zhoucun Reservoir. TN, Mn, and NO_3^- have little effect on phytoplankton. *Chlorella*, *Chlamydomonas*, *Chroococcus*, and *Anabaena* were distributed in the first quadrant and there was a strong positive correlation with TN, turbidity, COD, TP, and pH. *Cyclotella*, *Synedra*, and *Stephanodiscus* were mainly distributed in the third quadrant and a strong negative correlation with TN, turbidity, COD, TP, and pH existed. *Scenedesmus* and *Chlorococcum* are negatively related to the water level, while *Ankistrodesmus* and *Lyngbya* have a strong relationship with Fe.

2.5 Algae Pollution in Zhelin Reservoir

2.5.1 Seasonal Variations of Algal Abundance

The algal abundance gradually increased as the temperature increased. In October, the water temperature at the surface was 26 °C, and the algal abundance reached a maximum of 2.25 million/L. In November, the water temperature and algal abundance rapidly decreased with the decreasing temperature. In January, the water temperature dropped to 11.8 °C and the algal abundance reached its minimum of the entire year. The monitoring station in the front of the dam is located in Yongxiu County. Due to the large area of Zhelin Reservoir, the period when algal abundance reaches a peak are different at each monitoring point. The maximum algal abundance appeared in the fork inlet of the lake and shallow water monitoring sites, reaching up to 4.2 million/L (Fig. 23).

The monitoring results showed that Zhelin Reservoir was still in a middle trophic status.

2.5.2 Characteristics of Algae Community Succession

The diatoms showed a rising trend after the first reduction from June 2013 to May 2014. In spring and winter, diatoms were prevalent and accounted for more than

Table 19 Correlation between algal abundance and environmental factors

	Algae abundance	Chlorophyll-*a*	Rainfall	Water level	Temperature	DO	pH	Turbidity	TN	NO_3	NO_2	NH_4	TP	N/P	Fe
Algae abundance	1.000														
Chlorophyll-a	0.953**														
Rainfall	0.457*	0.498*													
Water level	0.115	0.270	0.015												
Temperature	0.749**	0.687**	0.480*	−0.224											
DO	0.133	0.051	0.169	−0.077	−0.101										
pH	0.732**	0.637**	0.426	−0.166	0.893**	−0.043									
Turbidity	0.900**	0.897**	0.565*	−0.113	0.868**	−0.152	0.668**								
TN	−0.105	−0.160	−0.063	−0.319	−0.147	−0.130	−0.140	−0.127							
NO_3	−0.482*	−0.442	0.036	0.138	−0.317	−0.392	−0.173	−0.433	0.299						
NO_2	0.603**	0.738**	0.299	0.404	0.424	−0.067	0.401	0.624**	−0.246	−0.470*					
NH_4	0.010	0.169	0.076	0.417	0.209	−0.235	0.111	0.293	−0.175	0.181	0.390				
TP	0.703**	0.771**	0.679**	0.272	0.602**	−0.036	0.620**	0.900**	−0.301	−0.149	0.620**	0.219			
N/P	−0.640**	−0.700**	−0.597**	−0.228	−0.559*	−0.061	−0.613**	−0.851**	0.498*	0.292	−0.589**	−0.178	−0.955**		
Fe	0.635**	0.709**	0.469*	0.134	0.435	−0.046	0.592**	0.813**	−0.121	−0.166	0.482*	0.059	0.801**	−0.784**	1.000

Table 20 Statistical results of RDA

Axis	1	2	3	4
Eigenvalue	0.591	0.169	0.095	0.063
Cumulative percentage of species, %	59.1	76	85.6	91.9
Cumulative percentage of species and environmental correlation, %	59.1	76	85.6	91.9
Correlation of species and environment	1	1	1	1

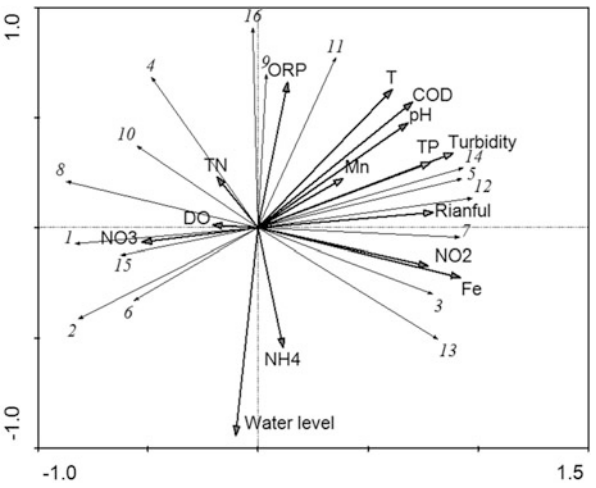

Fig. 22 RDA sequence diagram of phytoplankton and environmental factors in Zhoucun Reservoir

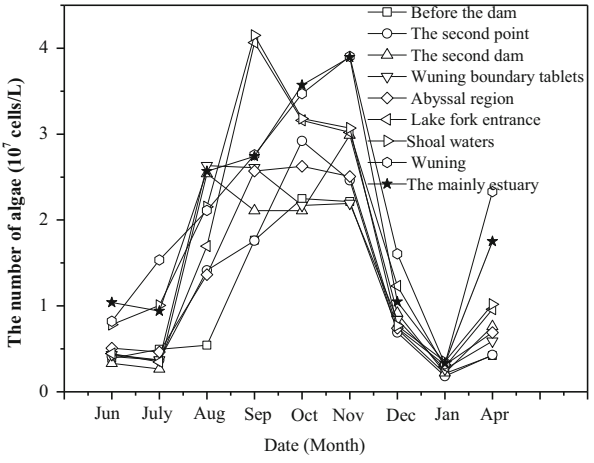

Fig. 23 Seasonal variations of algal abundance in Zhelin Reservoir (2013–2014)

50 %. The proportion of green algae was high throughout the year. In October and November, the proportion of green algae was up to 77.5 %. Cyanobacteria and Dinoflagellates had a low proportion throughout the year. The main limiting factors for algal growth in Zhelin Reservoir are nitrogen and phosphorus (Fig. 24).

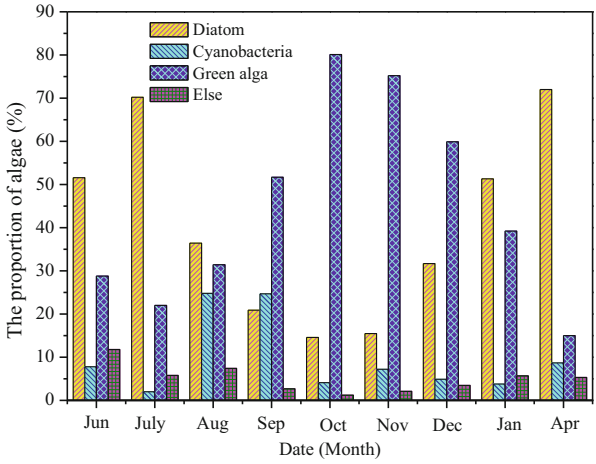

Fig. 24 Statistical analysis of algae species change in Zhelin Reservoir (2013–2014)

3 Odor and Substance-induced Olfactory

Odor is one of the earliest and most straightforward parameters that can be used to evaluate the quality of drinking water. Odor is a nerve stimulation integrated signal caused by olfactory-induced compounds in water acting on the person's nose, mouth, tongue, and other sensory peripherals [20]. The olfactory problem is a primary one. When people realize the odor of drinking water, the majority tend to believe that the water is poisonous and avoid using it.

Generally, the influence of water taste and odor is huge, which could affect the taste of water for drinking, reduce the quality of drinking water and aquatic products, cause disgust, nausea, and other unpleasant psychological effects, and reduce the aesthetic value of lakes and reservoirs. However, conventional water purification processes cannot remove the smell effectively. Some special odor control technologies or combined water purification processes are helpful in removing the taste and odor, but these will increase the cost of the water purification, thereby increasing the cost of living [21]. According to the US water industry statistics, 4.5–10 % of total revenue is used for solving taste and odor problems of drinking water.

3.1 The Odor Emergency Event in Huyan Waterworks

From mid-August, 2010, the Taiyuan municipal department received several water odor complaints from residents. They complained that the odor of drinking water is musty and the intensity of this mustiness increased after being boiled. The complaints mainly came from the west of Riverside Road Wanbailin and suburbs of the city. According to the distribution of water plants and the water supply network in

Taiyuan City, the problematic water came mainly from Huyan waterworks, whose raw water was taken from the Fenhe Reservoir.

According to the monitoring results for water quality, the water was musty before it flowed into the plant. So, the taste and odor of drinking water might come from the source water, namely the Fenhe Reservoir. To maintain social stability and protect public health, emergency measures were taken to eliminate the odor. Powder-activated carbon with a dosage of 14.4 mg/L was added to the aqueduct in front of plant at about 500 m intervals. After the implementation of emergency measures, the musty feeling was relieved but was not removed completely. Therefore, further studies on scientific and effective odor control technologies are needed.

Taste and odor reduces the quality of drinking water, causing the users discomfort and skepticism on the safety of drinking water, and, thus, leading to dissatisfaction and complaining. Besides, taste and odor in drinking water may affect human health or become a factor inducing certain diseases. If not resolved properly, the issue of taste and odor in drinking water will lead to unpredictable negative effects on Taiyuan residents, social stability, and industrial and agricultural production.

3.2 Identification and Analysis of Odor Compounds Sources

3.2.1 Identification of Odor Compounds

(1) Types of Odor Compounds

Given the various types of olfactory compounds, their detection is difficult due to the differences in molecular structure. The appropriate detection methods to identify the origin compounds causing odor should be selected based on their types [22]. According to the complaints from residents and the situation provided by Huyan waterworks, Taiyuan tap water has a musty odor. The in situ-collected raw water showed different intensities of mustiness. Some water samples became mustier after being sealed for some time. Therefore, must is the main odor type in the Fenhe Reservoir.

(2) Identification of Odor Compounds

Based on existing researches, compounds with a musty odor in natural water include geosmin, 2-methyl isobutyl camphane alcohol (2-methylisoborneol or 2-MIB), 2,3,6- trichloroanisole (2,3,6-trichloroanisole, or TCA), and 2-isopropyl-3-methoxypyrazine (IPMP) [23, 24]. Geosmin and 2-MIB are the main culprits in the musty water incident in China. The “drinking water health standards” of China (GB 5749–2006) sets geosmin and 2-MIB as the index of drinking water and its limit is 10 ng/L.

The detection technique is the headspace solid-phase microextraction/gas chromatography method. According to the water quality survey, the musty odor of raw water increases with standing time. In order to increase the concentration of the

Table 21 Test results of odor and taste compounds

	Tap water	Water of reservoir		
Test items	3-Sep	2-Sep	18-Sep	9-Oct
2-methyl isopropyl alcohol	17	40	64	25
Geosmin	–	–	–	–

odor compounds, the water samples were detected and analyzed after being left standing for 24 h. Table 21 shows the testing results of taste and odor compounds.

As shown in this table, the raw water contains 2-methylisoborneol with the highest concentration of 64 ng/L, but no geosmin was found. Meanwhile, 2-MIB, with a concentration of 17 ng/L, was detected from the effluent of Huyan water treatment plant on September 3, which suggests that 2-MIB is the main olfactory compound in Taiyuan tap water and Fenhe Reservoir.

(3) Physical and Chemical Properties of 2-MIB

The formula for 2-MIB is $C_{11}H_{20}O$ and its molecular weight is 168. According to the molecular structure, 2-MIB is saturated cyclic tertiary alcohol and its structure is similar to the pentagonal ring. The boiling point of 2-MIB is 196.7 °C and its solubility is 194.5 mg/L. The distribution ratio of 2-MIB in octanol and water K_{OW} is 3.13, which means that 2-MIB belongs to the semi-volatile, weakly polar molecules. 2-MIB is a micropolar fat-soluble compound which is insoluble in water. It is also soluble in methanol, acetone, hexane, methylene chloride, and other organic solvents. Since 2-MIB possesses a saturated cyclic structure, it is resistance to oxidation.

Different concentrations of 2-MIB show different types of odor. High concentration tastes camphor while low concentration tastes musty. People's sense of smell is extremely sensitive to 2-MIB and can sense the smell generated by trace 2-MIB. It is generally believed that the olfactory threshold of 2-MIB is 10 ng/L. However, the olfactory thresholds are affected by the tester's sensitivity, testing environment, and other factors. 2-MIB odor thresholds obtained by different researchers are different. Lalezary suggests that the 2-MIB olfactory threshold is 10 ng/L, while Ashitani gives the limit in the range 4–20 ng/L.

Currently, no researches indicate that 2-MIB causes direct harm to the human body, but the musty smell makes consumers uncomfortable. It is necessary to control the content of 2-MIB in water strictly. In Japan, the limit of concentration of 2-MIB is 10 ng/L in drinking water. In China, the "drinking water health standards" (GB 5749–2006) also defines 2-MIB as a reference index and the limit is 10 ng/L.

3.2.2 Sources of Olfactory-Induced Substances

Based on previous research results, 2-MIB in water mainly comes from actinomycetes and secondary metabolites of algae secretions [25]. Actinomycetes and small single-cell bacteria can produce 2-MIB. Cyanobacteria can also produce 2-MIB,

and the circumstances under low levels of cyanobacteria can cause water body odor. The common species of cyanobacteria that produce 2-MIB are *Ankistrodesmus*, *Phormidium*, *Oscillatoria*, *Phormidium*, and *Anabaena*.

It was found that the 2-MIB in Fenhe Reservoir came mainly from algae. The phenomenon of delayed odor release is due to the death of algae in dark conditions, which could cause intracellular olfactory substances to be released into the water.

3.3 Emergency Countermeasures for Controlling Algae-Induced Olfactory

The treatment processes adopted by Huyan water plant include "coagulation–sedimentation–filtration–disinfection", which are inefficient for odor removal. To improve odor removal, powdered activated carbon was added to the aqueduct every 800 m in the front of the Huyan water plant. After the addition of powdered activated carbon, the musty effluent from Huyan water plant decreased, but the mustiness in tap water was not eliminated. The concentration of 2-MIB in the water tanks was 17 ng/L on September 3, and this value is still higher than the permitted odor threshold. Because the dosing points of powdered activated carbon are near the water plant, the reaction time is very short and the adsorption capacity of activated carbon may not be fully exerted.

The odor problem caused by algae could not be removed efficiently by conventional water treatment processes. In order to select proper control schemes for taste and odor, many factors, such as the sources of odor-causing compounds, the current condition of the plant, and the urgent degree of processing, should be taken into consideration. The feasibilities of various 2-MIB removal techniques are discussed below:

1. Chemical oxidation: To our best knowledge, ozone is one of the most efficient oxidants for 2-MIB removal, since it can kill the algae effectively. This method is technically feasible, while the design and construction of an ozone system requires a long time, which makes it unsuitable for emergency odor treatment.
2. Adsorption: Although powdered activated carbon is widely used in water taste and odor control, the use of powdered activated carbon alone could not remove the odor of raw water.
3. Biological degradation: The olfactory-induced degradation microorganisms are crucial for this method, while the generation and accumulation of the microorganisms need a relatively long time. Thus, this method is also not suitable for emergency odor treatment.
4. Photocatalytic oxidation and ultrasonic radiation: Both of these techniques are still limited to the laboratory scale, and there is a long way to go before they can be considered for real applications.

In summary, it seems unrealistic to solve algae-induced olfactory emergencies by a single control technology. So, combined methods are considered to be the most suitable solutions to solve this problem. On the other hand, it is also difficult to

construct special emergency treatment plants due to the constraints of the existing water plant layout, pipe alignment, and power distribution. However, from another perspective, there is a great distance between water sources and water treatment plants. Therefore, combined with the experience of emergency treatment [26], odor control processes could be conducted in the aqueduct system. Accordingly, the "killing algae + adsorption" process is proposed.

Among the existing techniques, chemical oxidation is ideal for killing algae. The most commonly used oxidants include chlorine, chlorine dioxide, ozone, potassium permanganate, and copper salts. From the view of operating convenience and drug safety, potassium permanganate is the most suitable agent.

In conclusion, the process "potassium permanganate peroxidation + powdered activated carbon adsorption" was suggested to deal with odor emergencies. The mechanisms of the method involve two steps: (1) adding potassium permanganate into the raw water aqueduct system to damage algal cells and cause the release of 2-MIB in algae cells; (2) dosing powdered activated carbon to absorb the released 2-MIB.

4 Water Pollution Related to Stratification of the Reservoir

Stratification is a natural occurrence which occurs in reservoirs due to the change in water density with temperature at different depths. The stratification includes forward and reverse stratification [27]. Forward stratification means that the temperature of the upper layer is higher than that of the lower layer, and vice versa for reverse stratification.

Forward stratification is formed at the end of spring and early summer each year, due to the strong solar radiation warming the surface water quickly, so the density decreases, whereas the water temperature of the lower layer is relatively stable, remaining at a low level, and, thus, at a greater density. Due to the density difference between the upper and lower bodies of water, the interchange between the upper and lower water bodies is hindered, and a stable stratification is formed. Generally, the stratified water body is classified into three layers (Fig. 25): epilimnion, thermocline, and hypolimnion. The epilimnion is the top layer in a thermally stratified body of water, which is warmer and typically has a higher pH and higher dissolved oxygen concentration [28]. The hypolimnion is the dense, bottom layer of water in a thermally stratified body of water, and the hypolimnion is the coldest layer in summer. The thermocline is a thin but distinct layer, in which the temperature changes more rapidly with depth, and it is a transition layer between the epilimnion the and hypolimnion. A typical stratification structure is shown in Fig. 25.

Reverse stratification is possibly formed in cold winter. Due to the cold effect, the water temperature decreases and the density of the surface water also decreases as the water temperature drops to less than 4 °C; however, the water temperature remains stable (4 °C) at the bottom. Therefore, the density of the bottom water is

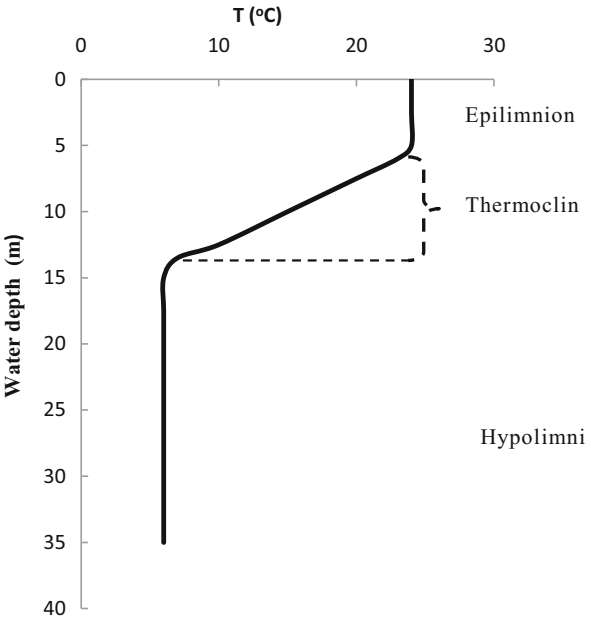

Fig. 25 Stratification in reservoirs

higher than that of the surface water, and the exchange of the upper and lower water bodies is hindered, so a stable reverse stratification is formed.

Storms and intense rainfall will destroy the stratification of a reservoir; as the water depth is small, the temperature stratification can be easily destroyed. When the water depth is less than 10 m, it is difficult to form a long-term stable stratification; even if it is formed, it is very fragile. When the water depth is greater than 30 m, it can form a long-term stable stratification. When the water depth is between 10 and 30 m, the stratification is weak and susceptible to wind, temperature, and other factors [29].

The stratification of a reservoir will deteriorate the water quality, including the decrease of DO in the bottom layer, the deterioration of the aquatic ecological environment, the release of contaminants from the sediments, and algal blooming [30, 31]. Due to the lack of water exchange between the upper and lower layers and the respiration of microorganisms and aquatic animals, oxygen in the lower layer gradually reduces close to zero eventually. Under anaerobic conditions, nutrients (N, P, organic matters) are released into the water, and, thus, increase the odor and transparency, and promote the growth of algae [32].

The basic characteristics of reservoirs are summarized as follows:

1. The hypoxia at the bottom of the reservoir: In most of the high-depth reservoir water, bottom oxygen consumption and temperature stratification will cause the bottom water layer to exhibit anaerobic and anaerobic conditions.
2. The release of pollutants from sediments under anaerobic environment: Under anaerobic conditions, it will lead to the release of ammonia, phosphorus, Fe, Mn,

and other heavy metal pollutants, and also result in color elevation, abnormal odor, and water quality deterioration.
3. The pollution derived from the water mixing: At the end of autumn or the beginning of spring, the reservoir will mix automatically, and the polluted bottom water will spread throughout the reservoir. For example, the frequent pollution of ammonia in the reservoir is due to the automatic mixing at the beginning of spring.
4. The algal blooming in the upper layer water: Most of the northern reservoirs have been used for regulation for years. Cyanobacteria blooms frequently due to the long retention time of water and poor mobility, combined with the endogenous release of nitrogen from sediments.
5. The cyclical pollution of water quality: In southern reservoir water, it is periodically contaminated with algae and organic matters in the hot summer season. In northern reservoir water, it is periodically contaminated with algae and organic pollutions in the hot summer season as well, but is also contaminated with high nitrogen and phosphorus, high chroma, and organic matters in winter and spring.

In the following, the effects of stratification on the water quality are discussed in detail in the four typical Chinese reservoirs.

4.1 The Stratified Characteristics of Jinpen Reservoir and Its Impact on Water Quality

4.1.1 The Seasonal Thermal Stratification Characteristics and Dynamics of Jinpen Reservoir

Figure 26 shows the vertical temperature change over a period of 2 years. From the spring, the temperature of air starts to increase and, also, the temperature of the surface water in Jinpen Reservoir gradually increases; however, the temperature of the bottom water increases slowly compared to that of upper layer water, which induces a significant difference between the upper layer water and the bottom layer water, and results in the formation of stratification. At the end of June, the three typical layers (epilimnion, thermocline, and hypolimnion) are formed, i.e., forward stratification. The temperature of the upper layer (epilimnion) changes with the variation of climate, and the highest temperature is around 27–28 °C in July and August. The bottom layer (hypolimnion) remains quite stable and the temperature is around 7 °C. In October, the temperature of the upper layer water starts to decrease with the decrease of air temperature. In January of the second year, the temperature of the upper layer water decreases by the same amount as that in the bottom water (7 °C); the water between the upper and bottom waters starts to mix automatically. With the arrival of spring warming, a new round of temperature stratification begins.

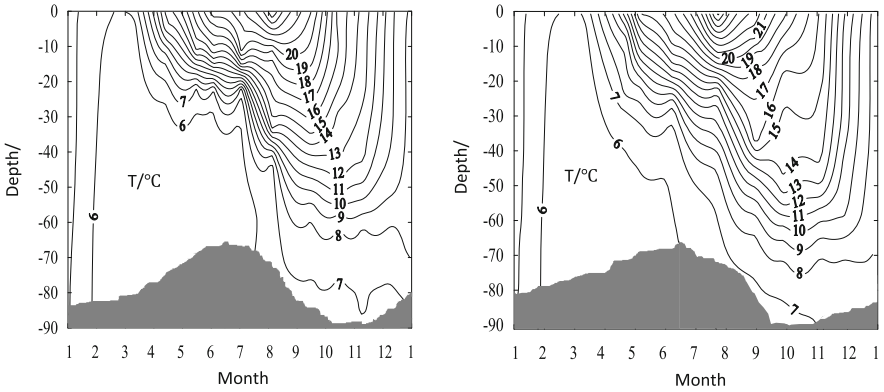

Fig. 26 Water temperature profiles in Jinpen Reservoir

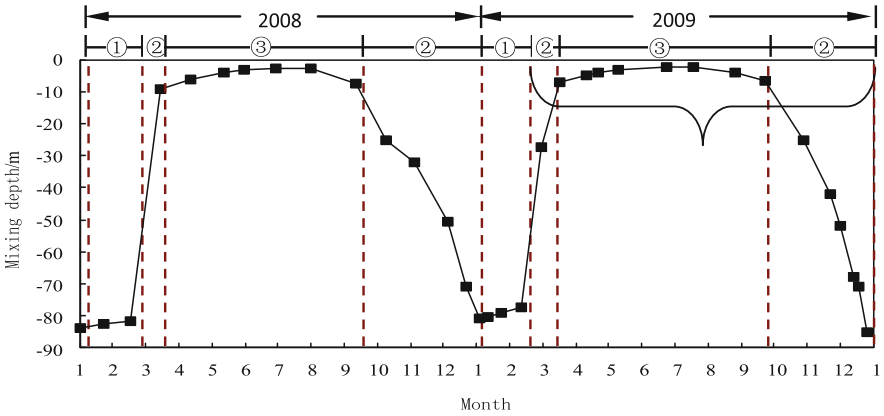

Fig. 27 Seasonal variation of mixing depth in Jinpen Reservoir (1. Mixing period, 2. Transition period, 3. Stratification period)

The surface mixed layer is a layer where this turbulence is generated by winds and surface heat fluxes. The surface mixed layer depth is defined as the range of depth where the temperature difference is not more than 1 °C from the top layer water [33]. The change of the mixed layer depth with season is shown in Fig. 27.

In recent years, the frequency of storm events has increased and they have a greater impact on a reservoir's thermal stratification structure. The influent, which carries large amounts of suspended solids, has an increased runoff and muddy bottom density, which leads to it sneaking into the bottom of the reservoir. As shown in Fig. 28, the mixing period is quite different in 2011–2012 due to the impact of storm runoff. For example, the water temperature at the bottom of the reservoir rose from 6.25°C to 12.66 °C by the end of July 2011 after the first heavy

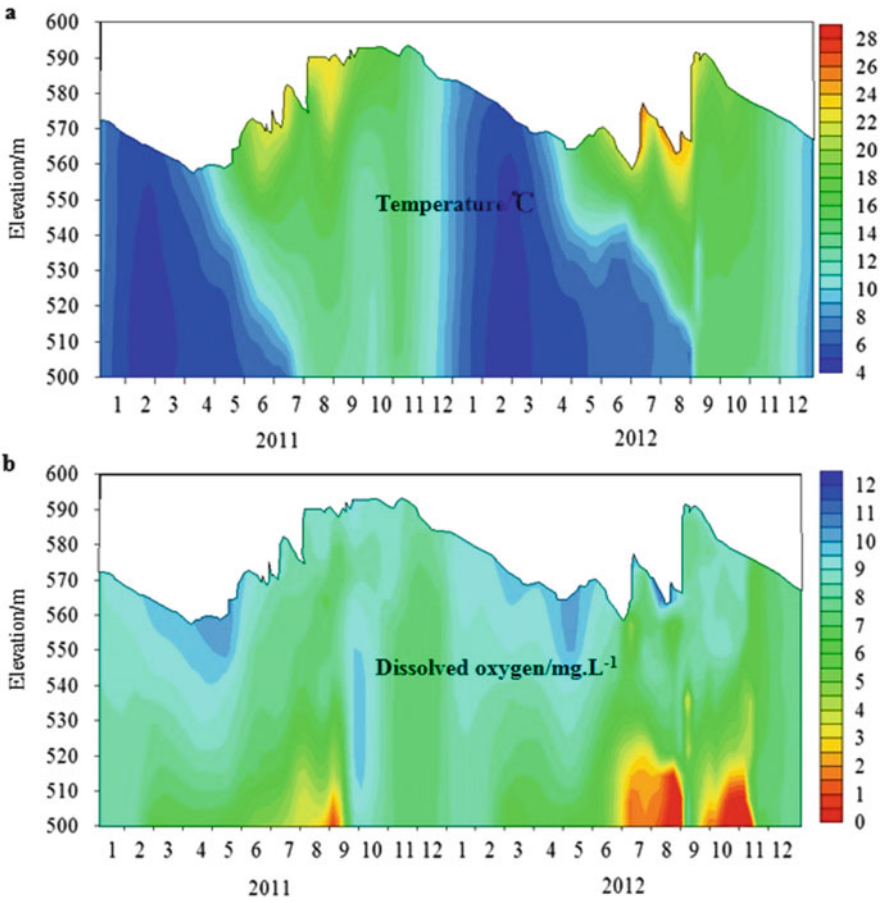

Fig. 28 Temperature and oxygen change in the vertical direction in Jinpen Reservoir (2011–2012)

rainfall and the surface water temperature also continued to decrease, so the reservoir mixed in advance. After the first rainfall in September 2011, the temperature difference of the upper and bottom layers in the main reservoir area reduced to 10.5 °C, and with the passage of time, the temperature difference between the upper and bottom layers in the main reservoir area was no longer changed. With the continuous rainfall, the temperature stratification in the main reservoir area has undergone a significant change: before rainfall, there is a greater temperature gradient at water depths from 0 to 17 m; after rainfall, the temperature of the bottom layer increased significantly, and the DO increased in the range of 0–30 m as well, which is due to the input of oxygen-rich water upstream undercurrent.

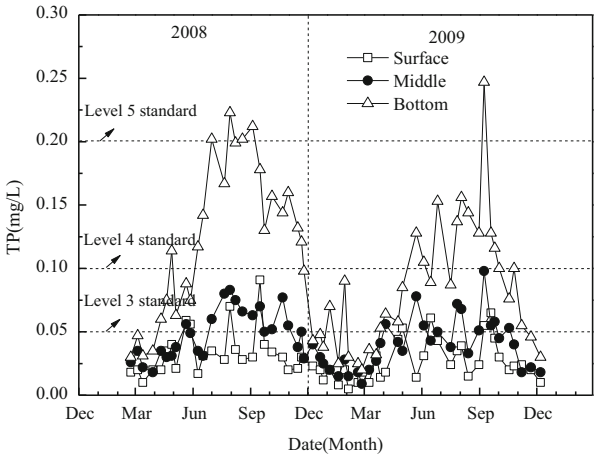

Fig. 29 Phosphorus concentration at different depths in Jinpen Reservoir

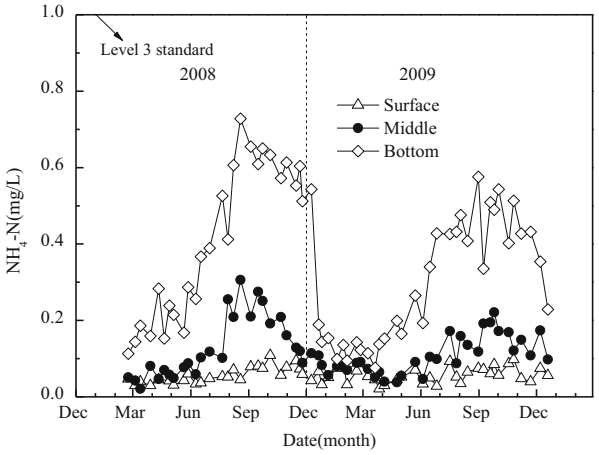

Fig. 30 Ammonia concentration at different depths in Jinpen Reservoir

4.1.2 The Water Quality Problems Derived from the Thermal Stratification of Jinpen Reservoir

(1) The Release of N and P Due to Thermal Stratification

With the seasonal water environment hypoxia, anaerobic conditions at the bottom of Jinpen Reservoir, and different forms of nitrogen, phosphorus fractions continued the "transformation–release–accumulation–diffusion" process in sediments under strongly reducing conditions, which accelerates the process of eutrophication in the entire reservoir area [34, 35]. Figures 29 and 30 show the changes in the spatial and temporal distributions of total phosphorus and ammonia in 2008 and 2009 in Jinpen Reservoir.

As shown in Figs. 29 and 30, during the stable thermal stratification period, the total phosphorus and ammonia increase rapidly with the increase of water depth. In this period, the water body between water layers is relatively stable vertically and do not blend, with the reservoir bottom water environment appearing seasonally in an anoxic/anaerobic state and different forms of nitrogen and phosphorus are released into the interstitial water, which then diffuses into the overlying water [36]. Once the mixing period begins, the nitrogen and phosphorus content of all the water layers tend to homogenize. The maximum concentration of phosphorus and ammonia occur in August and September each year in the bottom water. In March of the following year, the concentration of nutrients decreased to a minimum, corresponding to 0.223–0.247 mg/L (TP) and 0.576–0.728 mg/L (NH_4-N).

With respect to total phosphorus in the bottom water, it is higher than the national surface water quality standard (GB 3838–2002) (class III), and even reaches class V or worse than class V. The excessive periods are mainly from July to October annually. As can be seen from the results, it is clear that the main reason for total phosphorus excess is the release from sediments.

With respect to ammonia, although the concentration is always lower than the national surface water quality standard (GB 3838–2002) (class III) (1.0 mg/L), it shows a clear seasonal change pattern with the periodic alternation of a redox environment in Jinpen Reservoir. During the stable thermal stratification period, the concentration of ammonia always remains stable. Once the mixing period begins, the concentration of ammonia starts to decrease. As shown in Fig. 31, there is a negative correlation between the DO and the ammonia concentration in the bottom layer ($R^2 = 0.72$), and the ammonia concentration increases with the decrease of DO concentration. Comparatively, the correlation between total phosphorus and DO is quite weak ($R^2 = 0.32$).

In fact, the effect of the DO concentration on the concentration of total phosphorus is attributed to the change of water pH. Inorganic phosphorus accounts for about 65– 73 % of the sediment of Jinpen Reservoir, and it is the main form of released phosphorus. Inorganic phosphorus is composed of calcium phosphate (Ca-P: 50–55 %), iron and aluminum-bound phosphorus (Fe/Al-P: 26–31 %), and occluded phosphorus (OP). Ca-P is quite stable and is only released in acidic environments. O-P is also fairly stable and can be released in acidic and reductive conditions. With respect to the active Fe/Al-P, it can be significantly released under the condition of basic pH and lower DO. Under anaerobic conditions, Fe^{3+} is reduced to Fe^{2+} and phosphorus is released from Fe/Al-P in sediments, but the Fe^{2+} and PO_4^{3-} mainly accumulate in the particle gaps. Once the pH increases, OH^- ions would diffuse into the interstitial water and combine with Fe^{2+} to generate Fe $(OH)_2$ precipitation. The concentration of Fe^{2+} in the particle gaps will decrease, which then accelerates the dissolution reduction of Fe/Al-P and the release of total phosphorus into overlying water.

The release of total phosphorus under the condition of lower DO and higher pH can be expressed as follows:

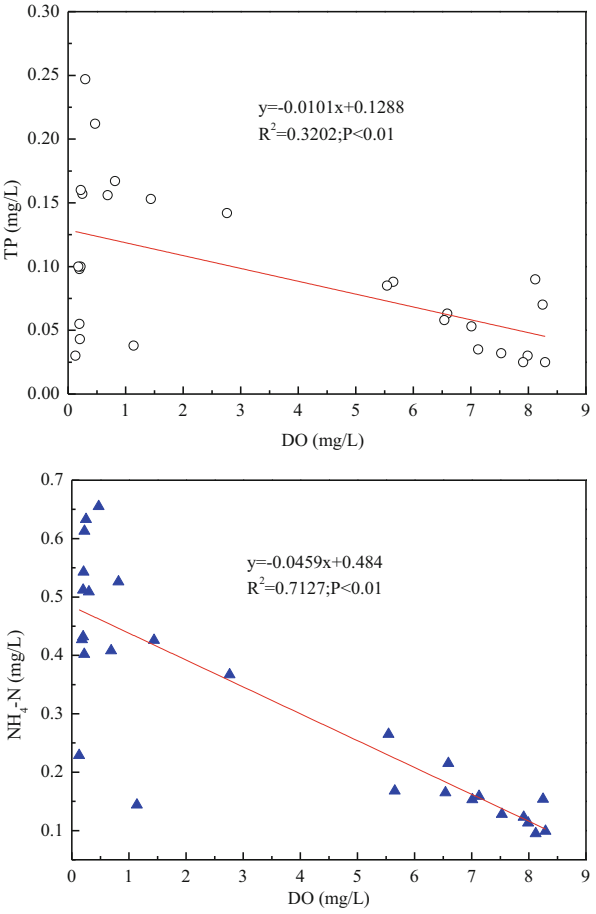

Fig. 31 Correlation between phosphorus/ammonia with oxygen at the bottom of Jinpen Reservoir

$$FePO_4 + 2OH^- + e^- \leftrightarrow PO_4^{3-} + Fe(OH)_2 \downarrow$$
$$Fe(OH)_2H_2PO_4 + 2OH^- + e^- \leftrightarrow PO_4^{3-} + Fe(OH)_2 \downarrow + 2H_2O$$

In the bottom of Jinpen Reservoir, the pH decreases gradually with the increase of anaerobic conditions. The release of total phosphorus from Fe/Al-P is hindered, so the increase of total phosphorus is attributed to the release of Ca-P.

(2) The Release of Heavy Metals Due to Thermal Stratification

The vertical distribution of total iron in Jinpen Reservoir is shown in Tables 22–25. The data show that the change in the concentration of total iron is closely related to the periodical thermal stratification of Jinpen Reservoir.

In spring, corresponding to the early period in the formation of thermal stratification, the reservoir is full of oxygen and is in a slightly alkaline state. Iron exists in the form of insoluble oxides and accumulates in the sediments. This process can be expressed as follows:

Table 22 The vertical distribution of total Fe in Jinpen Reservoir in March

Date	Depth (m)	Water temperature (°C)	DO (mg/L)	pH	Total Fe (mg/L)
2008-03-09	1.20	6.11	10.04	7.46	<0.03
2008-03-09	3.89	5.46	9.88	7.36	<0.03
2008-03-09	10.51	5.39	9.86	7.33	<0.03
2008-03-09	20.63	5.33	9.71	7.33	<0.03
2008-03-09	30.37	5.32	9.48	7.31	<0.03
2008-03-09	40.81	5.28	8.97	7.27	<0.03
2008-03-09	50.56	5.25	8.49	7.26	<0.03
2008-03-09	56.03	5.22	8.22	7.26	<0.03
2008-03-09	65.53	5.20	8.17	7.24	<0.03
2008-03-09	80.76	5.21	7.99	7.22	<0.03

Table 23 The vertical distribution of total Fe in Jinpen Reservoir in June

Date	Depth (m)	Water temperature (°C)	DO (mg/L)	pH	Total Fe (mg/L)
2008-06-30	2.84	21.06	8.50	8.57	<0.03
2008-06-30	12.87	19.95	7.28	7.62	<0.03
2008-06-30	22.73	6.96	6.44	7.04	<0.03
2008-06-30	32.54	6.10	6.60	6.83	<0.03
2008-06-30	42.70	5.84	5.89	6.78	0.033
2008-06-30	52.92	5.72	4.17	6.60	0.041
2008-06-30	62.74	5.69	3.22	6.49	0.058
2008-06-30	68.43	5.92	2.76	6.40	0.072

Table 24 The vertical distribution of total Fe in Jinpen Reservoir in October

Date	Depth (m)	Temperature (°C)	DO (mg/L)	pH	Total Fe (mg/L)
2008-10-11	0.80	16.40	8.16	7.96	0.068
2008-10-11	10.00	16.03	7.98	7.45	0.072
2008-10-11	20.00	15.25	6.39	7.16	0.083
2008-10-11	30.00	13.60	6.25	7.05	0.058
2008-10-11	40.00	13.33	5.79	6.92	0.072
2008-10-11	50.00	11.80	2.22	6.75	0.088
2008-10-11	60.00	8.22	1.57	6.49	0.096
2008-10-11	70.00	7.20	1.17	6.32	0.108
2008-10-11	82.00	6.90	0.43	6.27	0.144
2008-10-11	85.00	7.01	0.25	6.15	0.317

$$4Fe^{2+} + O_2 + 10H_2 \rightarrow 4Fe(OH)_2 \downarrow + 5H^+$$
$$Fe^{3+} + 3H_2O \rightarrow Fe(OH)_3 \downarrow + 3H^+$$

In this condition, the redox reaction occurs in the sediments and no release of iron into overlying water takes place. Therefore, the vertical concentration of the total iron water is very low in the reservoir (Table 22), and no excessive results of iron are found.

Table 25 The vertical distribution of total Fe in Jinpen Reservoir in January

Date	Depth (m)	Water temperature (°C)	DO (mg/L)	pH	Total Fe (mg/L)
2009-01-28	1.10	6.99	9.19	7.25	0.038
2009-01-28	5.14	6.96	9.03	7.21	0.033
2009-01-28	10.11	6.95	8.91	7.21	<0.03
2009-01-28	20.15	6.91	8.78	7.22	<0.03
2009-01-28	29.85	6.91	8.66	7.21	<0.03
2009-01-28	39.98	6.91	8.27	7.22	<0.03
2009-01-28	50.20	6.86	8.19	7.20	0.031
2009-01-28	59.55	6.83	8.27	7.21	<0.03
2009-01-28	64.98	6.72	8.28	7.20	<0.03
2009-01-28	74.00	6.52	8.26	7.19	0.041
2009-01-28	80.31	6.48	8.25	7.18	0.058

In summer, the iron concentration shows a different pattern (Table 23). With the development of thermal stratification, the dissolved oxygen begins to decay below the thermocline in water, and gradually turns into anaerobic conditions. The degradation of organic matter results in a slightly acidic water body. Fe in the sediment was reduced to dissolved Fe and migrated to the interstitial water layer, and then diffused into the overlying water driven by the concentration gradient. In this period, the characteristics of total iron in Jinpen Reservoir can be summarized as: the total iron concentration began to increase in the bottom of the reservoir, while it was still high in the upper water body, due to the higher dissolved oxygen content (oxidation state), plus the"bottleneck" of the thermocline, so the total iron concentration in the reservoir was still low.

In autumn, the dissolved oxygen continues to reduce due to the persistence of thermal stratification (Table 24). With the increased anaerobic level, the process of "transformation–release–diffusion" reached its peak, and the total iron concentration exceeded the national surface water quality standard (0.3 mg/L) (GB 3838–2002). Meanwhile, with the start of the local convection in the upper layer of the reservoir, the mixed layer depth increased, the range of the thermocline compressed, and the mass transfer was accelerated, which resulted in the increase of the total iron concentration. However, the total iron content in the water did not exceed the national surface water quality standard, due to the limited release and diffusion strength and the higher concentration of dissolved oxygen in the upper layer water.

In winter, the concentration of iron in the reservoir is shown in Table 25. In this stage, the reservoir was in a mixed and aerobic state, the water pH quickly increased up to a neutral–alkaline level, the release process of Fe was severely inhibited, and the concentration became uniform due to the convective mixing process. The total iron concentration decreased greatly.

In summary, before the period of mixing, the total iron content tended to increase in the water along the whole depth due to the thermal stratification, Fe release from the sediments was further enhanced, and the total iron concentration in

the water body of the bottom layer significantly increased. After mid-December, with the mixing depth increasing, the mass transfer resistance was significantly weakened and the total iron concentration accumulation in the reservoir bottom decreased. In early January, the dissolved oxygen concentration near the sediment rapidly increased up to 1 mg/L, and anaerobic conditions disappeared, so the release of iron slowed down. Once it reached the fully mixed period, the Fe release process became stagnant; however, a large amount of pollutants is carried up to the upper water body, due to the strong convective mixing; thus, the Fe content in the surface water rapidly increases. After that, the Fe concentration in the water remained at quite a low value, with a sustained oxygen-rich state in the reservoir.

4.2 The Stratified Characteristics of Shibianyu Reservoir and Its Impact on Water Quality

4.2.1 The Seasonal Thermal Stratification Characteristics and Dynamics of Shibianyu Reservoir

The vertical change of temperature in Shibianyu Reservoir is shown in Fig. 32. From March to May, it is the formation period of thermal stratification. During this period, the temperature in the upper layer water increased with increasing air temperature, but it increased slowly in the lower layer water body. In June, the water temperature of the upper layer water reached 20 °C, but the water temperature of the lower layer water was just 8 °C, giving a temperature difference of more than 12 °C. Stable stratification is formed in this period. Site S3 is located at the deepest point of the reservoir, the water temperature at the bottom is around 9 °C once the stable stratification period had been reached, and the low-temperature region is around 10 m deep (water temperature below 12 °C). Site S2 is a comparatively shallow point, and the water temperature is around 10 °C once the stable stratification period had been reached, and the low-temperature region is only about 5 m deep.

In general, when the reservoir surface water temperature drops below 10 °C, the reservoir will mix automatically. The results in 2011 and 2012 showed that the stratification of Shibianyu Reservoir is influenced by stormwater runoff. The main reasons for this are as follows:

1. The rainfall in Shibianyu Reservoir is concentrated, and mainly in the form of large storm runoff during rainstorms diving into the water body, increasing the mixing zone.
2. The temperature changes greatly in the reservoir during rainstorms, especially in case of continuous heavy rains. Water temperature differences during different rainfalls lead to changes in the undercurrent.
3. Heavy rain erosion could easily cause landslides, leading to water turbidity, and increasing the density significantly. When the density is higher than that of the bottom, the inflow will sneak into the bottom of the reservoir, resulting in complete destruction of the water stratification.

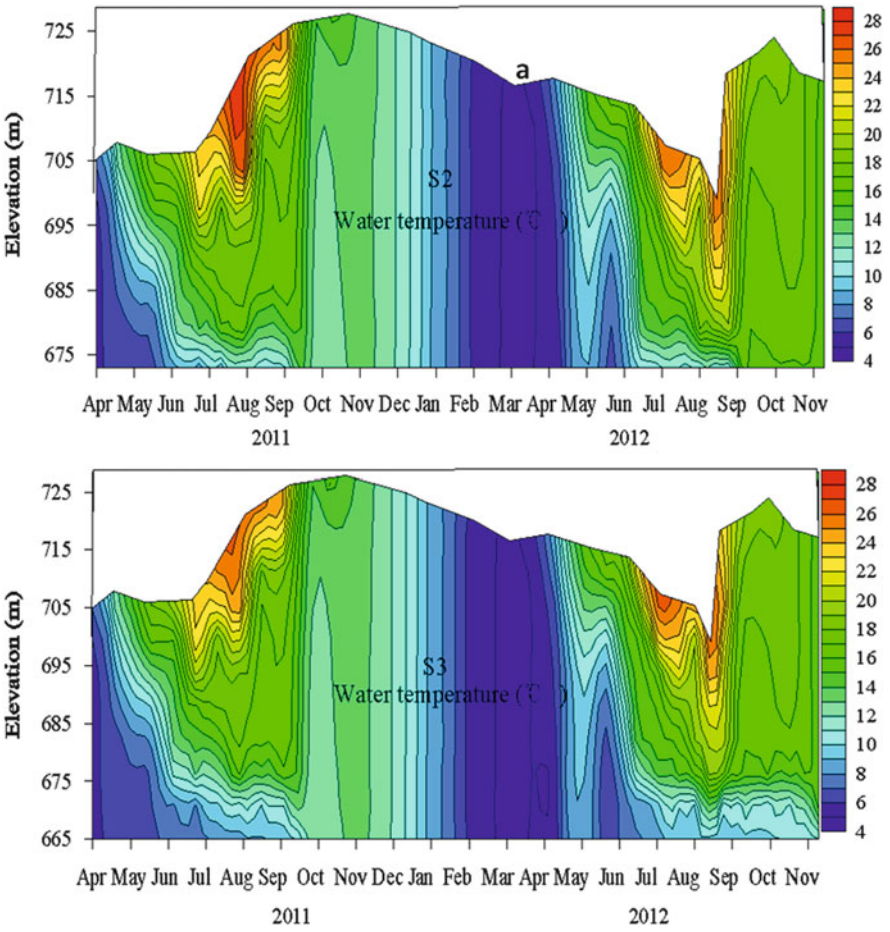

Fig. 32 Vertical distribution characteristics of water temperature in Shibianyu Reservoir (2011.3–2012.11)

The rainfall was a continuous heavy rainfall of 410 mm in September 2011, resulting in temperature decrease, and the runoff temperature changed greatly and the undercurrent position moved down, resulting in an increase of the mixed layer depth. In addition, the heavy rains leading to landslides, with high density water transferred into the reservoir, dived to the bottom of the reservoir, resulting in the mixing of the reservoir in advance. Due to the continuous rainfall, the water temperature stratification is not formed either.

In 2012, the rainfall intensity was weak compared to 2011, and the maximum rainfall occurred in August 31–September 1, with a peak flow of 117.6 m^3/s. After the storm runoff, the stratification was destroyed at the bottom of monitoring point

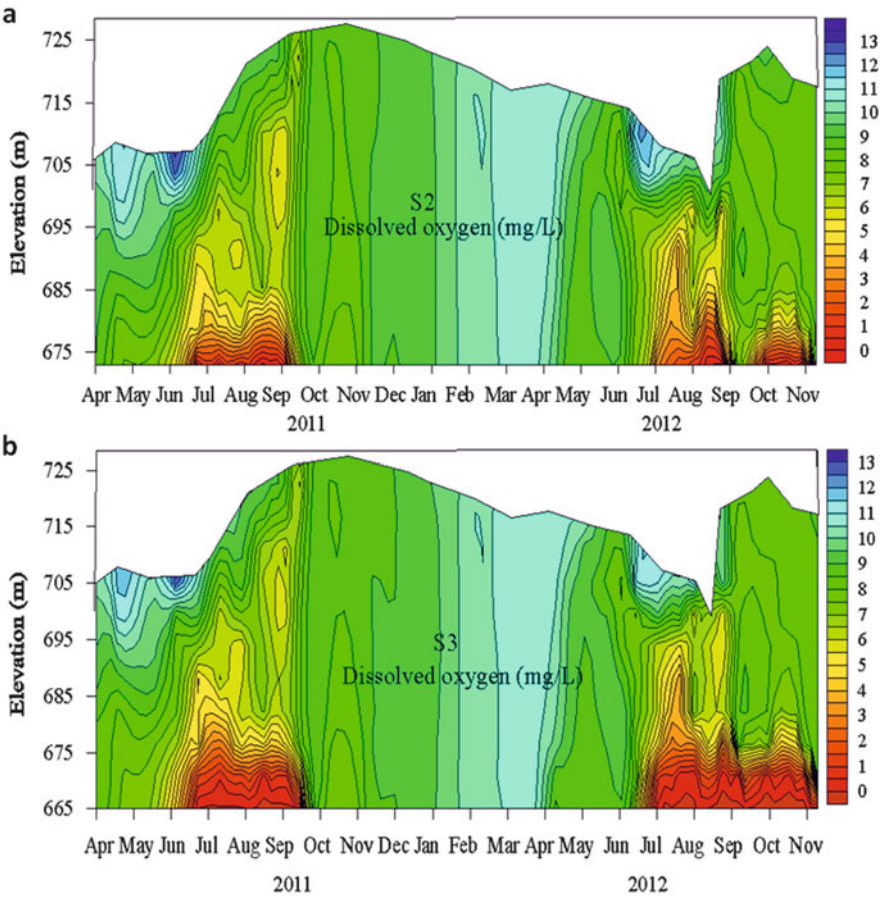

Fig. 33 Vertical distribution characteristics of dissolved oxygen in Shibianyu Reservoir (2011.3–2012.11)

S2, and the water temperature at the bottom increased from 10.44 °C to 14.22 °C, while the surface water temperature was about 20 °C. In early November, when the reservoir surface temperature dropped to about 14 °C, the water layer was fully mixed at monitoring point S2.

4.2.2 The Variation of Dissolved Oxygen Under Stratification

The seasonal variation of dissolved oxygen in Shibianyu Reservoir is shown in Fig. 33. There are significant seasonal variations of dissolved oxygen in Shibianyu Reservoir, which is affected by dynamic stratification. There is highly dissolved oxygen in the upper water of the reservoir, generally 8–10 mg/L. In addition, at the period of high algae, it would, to a certain extent, improve the dissolved oxygen in

the water due to oxygen production from algae photosynthesis. In the stratification formation period, with the increase of the temperature difference between the upper and lower layer waters, the oxygen mass transfer rate continues to decrease, resulting in the gradual decrease of dissolved oxygen. By the end of May, the water formed a stable thermal stratification, and the dissolved oxygen of the bottom water rapidly reduced from 8 mg/L to zero after 20 days, due to the consumption of sediments and lower-layer water. The anaerobic area is mainly located in a low-temperature region. There is a larger anaerobic zone at S3.

In September 2011, the stratification was destroyed in advance, as a result of storm runoff, and the dissolved oxygen increased rapidly at the bottom of the reservoir. The reservoir temperature stratification is no longer formed again due to the continuous rainfall. The DO of the entire reservoir remained around 8 mg/L.

By the end of August 2012, the stratification was totally destroyed at site S2 after a heavy rainstorm. The dissolved oxygen of the bottom water increased from 0 mg/L to 6 mg/L. Afterwards, the reservoir encountered less rainfall and higher temperature, and the reservoir water returned to a stratified state again due to the consumption of sediments and lower-layer water. In November, the reservoir water mixed again at site S2 and, correspondingly, maintained an aerobic state. At site S3, the bottom water remained in an anaerobic state after the heavy rainfall in August 2012, and a water-lifting aerator was implemented to increase the concentration of dissolved oxygen. After 1 month of running the water-lifting aerator, the dissolved oxygen at the bottom increased greatly.

4.2.3 The Variation of pH Under Stratification

The pH value of the water body, namely the hydrogen ion concentration index, is a reflection of the water quality conditions (pH). The seasonal changes in the reservoir can not only change the chemical speciation of substances in raw water, the migration and transformation process, and the metabolic activity of aquatic organisms, but also affect the urban water supply system. So, the pH value has been seen as an important indicator of water quality.

The pH of water depends on the changes in the vertical distribution of water alkalinity, photosynthesis, microbial activity, the distribution difference of soluble ion, and the dissolved oxygen in reservoir sediments.

The seasonal vertical distribution of pH in Shibianyu is shown in Fig. 34. During the mixing period, the pH of the upper- and lower-layer water is almost the same. With the formation of stratification, pH differences in the vertical distribution become more and more obvious. The pH of water bodies decreases with increasing water depth, and the pH of surface water is higher and exhibits alkaline characteristics. Especially in the period of algal blooming, the pH of surface water is close to 10, which is mainly attributed to the fact that algae photosynthesis in surface water absorbs carbon dioxide and destroys the balance of the water body $\left(CO_3^{2-}/HCO_3^{-}/CO_2\right)$, and causes pH increase of the surface water.

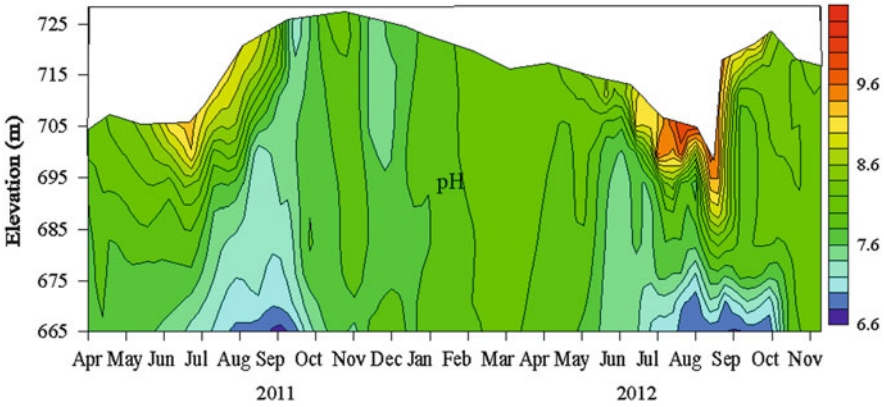

Fig. 34 Vertical distribution characteristics of pH in Shibianyu Reservoir (2011.3–2012.11)

In 2011, no algae outbreak was found in the reservoir due to the effects of rainfall; however, in 2012, algal blooming was quite serious, so the pH value of the upper water from May to October in 2012 was higher than that in 2011. The drastic decrease of the pH value within 5–15 m is mainly due to the weakened algae photosynthesis.

The pH in the bottom water is usually acidic (6.6–7.0), especially in the stable stratification period of the reservoir, which is mainly due to the acidic intermediates and formed sulfide derived from the anaerobic decomposition of organic matter and sulfate.

4.2.4 The Variation of Conductivity Under Stratification

Conductivity is a parameter for characterizing the soluble ions, which is closely related to the amount of inorganic acids, bases, salts, and other substances contained in the water. At low concentrations of these substances, the conductivity increases with increasing ion concentration. Conductivity is not only affected by the ionic content in water, but also affected by the temperature and viscosity of the water. Generally, the conductivity of natural water is between 50 and 500 μS/cm. Some of these ions are involved in redox reactions, which will consume dissolved oxygen in water. Because the stratified water bodies will directly affect the diffusion of ions in the water, it follows that stratification is closely associated with conductivity changes in reservoirs.

The conductivity of Shibianyu Reservoir varies with depth, as shown in Fig. 35. The figure shows that during spring, no difference was observed with respect to the conductivity in the vertical distribution. From May to September, with the gradual formation of stratification, the difference in conductivity in the vertical distribution increases, showing first decreases and then increases over water depths. There is a higher conductivity at the bottom of the reservoir. In summer, the conductivity is

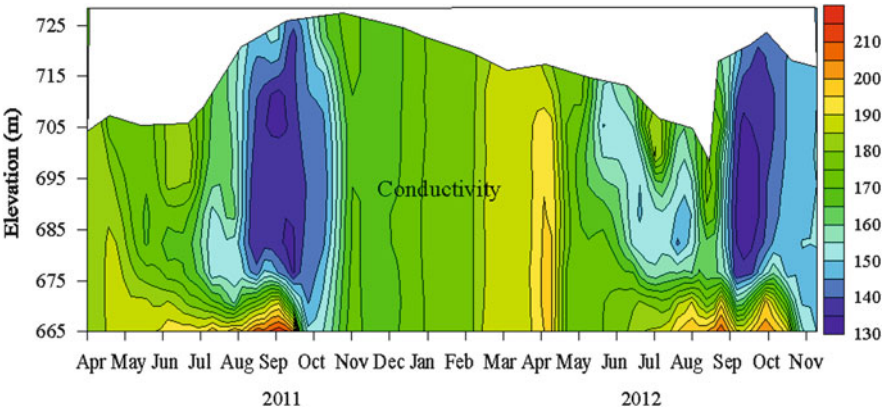

Fig. 35 Vertical distribution characteristics of conductivity in Shibianyu Reservoir (2011.3–2012.11)

relatively lower during periods of rain, but the conductivity is higher during periods without rain due to the strong water evaporation.

The transfer of dissolved oxygen between the upper- and lower-layer water is hindered after the formation of stratified water in the reservoir. The dissolved oxygen of the bottom water continues to decrease due to the oxygen consumption of sediments and bottom water. At the end of June, the dissolved oxygen at the bottom of the reservoir dropped to 0 mg/L. Under anaerobic conditions, the release of pollutants in sediments resulted in the increase of ion concentration in the lower-layer water, and, therefore, the conductivity of the lower-layer water also increases.

Conductivity has a minimum value within a certain water depth range, which is mainly due to the undercurrent from the upstream runoff (low conductivity) during stratification, resulting in a lower conductivity compared to the upper- and lower-layer water. Therefore, the vertical distribution of conductivity in the reservoir is closely related to water stratification and upstream undercurrent.

4.2.5 The Water Quality Problems Derived from the Thermal Stratification of Shibianyu Reservoir

During stratification, the mass transfer of dissolved oxygen between upper- and lower-layer water is fully hindered. The DO of the bottom water maintains an anaerobic state during stratification.

With the formation of the anaerobic environment at the bottom of the reservoir, the release of pollutants in sediments began, and the concentrations of nitrogen, phosphorus, and other nutrients began to increase in the lower-layer water of the reservoir (as shown in Fig. 36). In early August, the total phosphorus content was 0.12 mg/L, and the concentration of ammonia increased up to 0.7 mg/L at the bottom of the reservoir. At the same time, the concentration of iron and manganese

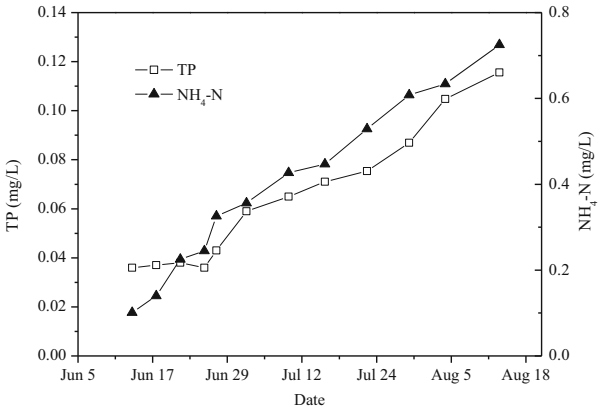

Fig. 36 Release curve of ammonia and phosphorus at the bottom of Shibianyu Reservoir during stratification

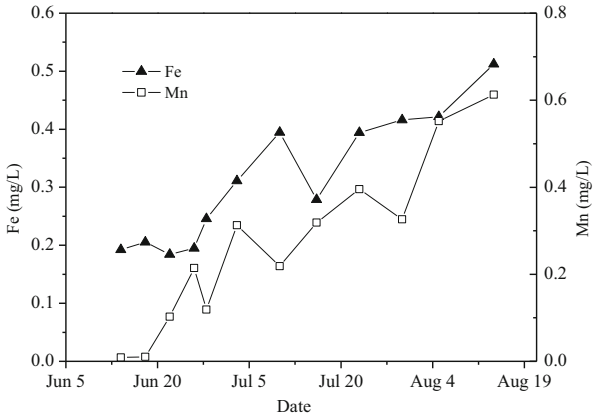

Fig. 37 Release curve of iron and manganese at the bottom of Shibianyu Reservoir during stratification

in the bottom water began to increase, until mid-August, when the concentration of iron and manganese exceeded the national surface water quality standard by 1–2 times (as shown in Fig. 37). With the extension of the anaerobic environment in the bottom water, the release of contaminants in the sediment was enhanced further.

4.3 The Stratified Characteristics of Zhoucun Reservoir and Its Impact on Water Quality

4.3.1 The Thermal Stratification Characteristics of Zhoucun Reservoir

The temperature variations of Zhoucun Reservoir from 2012 to 2013 are shown in Fig. 38. The surface temperature of Zhoucun Reservoir changes clearly with season, where the maximum is in the summer in July and August (up to 31 °C),

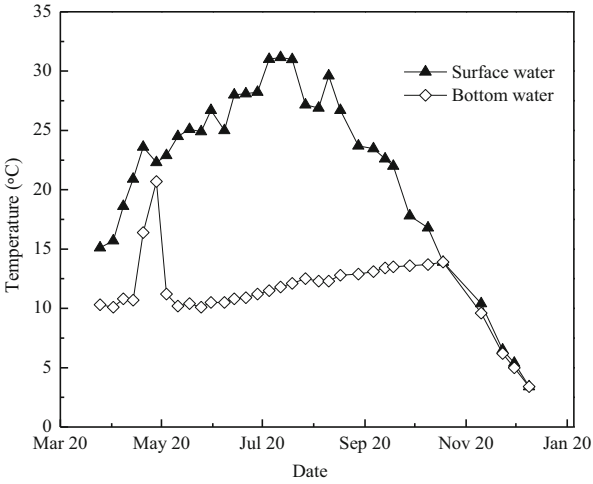

Fig. 38 Water temperature changes at the surface/ bottom ofZhoucun Reservoir (2012–2013)

and the lowest temperature appears in January (4 °C). The temperature change in the bottom water is not obvious, which stayed around 10 °C from April to November, slightly increased up to about 13 °C in summer, and reached a minimum of 4 °C in January.

Padisak has proposed a method to determine the stratification of a reservoir (RWCS), as follows:

$$\mathrm{RWCS} = (D_h - D_s)/(D_4 - D_5).$$

D_s—surface temperature of the water;
D_h—bottom temperature of the water;
D_4—water density at 4 °C;
D_5—water density at 5 °C.

The stratification standard is as follows: at RWCS>20, it is the stratification period; at RWCS≤20, it is the mixed period. The change of RWCS value with seasons is shown in Fig. 39. From April to October, the RWCS value is higher than 20, so it is the stratification period. From November to March of the following year, the RWCS value is lower than 20, so it is the mixed period. The Zhoucun Reservoir exhibited the same stratification mode year on year. Based on the results in the most recent 2 years, the stratification period can be classified into three periods, namely the stratification formation period, the stratification stable period, and the stratification weakness period. In April and May, it is the stratification period; from June to September, it is the stratification stable period; in October and November, it is the stratification weakness period.

The vertical distribution of physical and chemical parameters varied in different periods. The temperature change in different periods is shown in Fig. 40. In the stratification formation period, the ranges of the epilimnion, thermocline, and hypolimnion are 0–7 m, 7–10 m, and 10 m to the bottom, respectively. In the

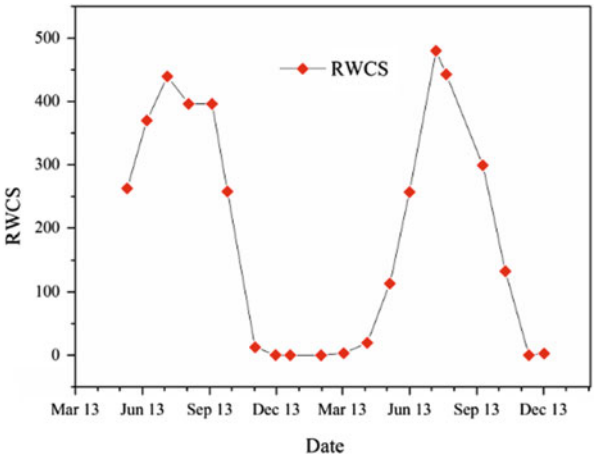

Fig. 39 Seasonal variations of RWCS in Zhoucun Reservoir

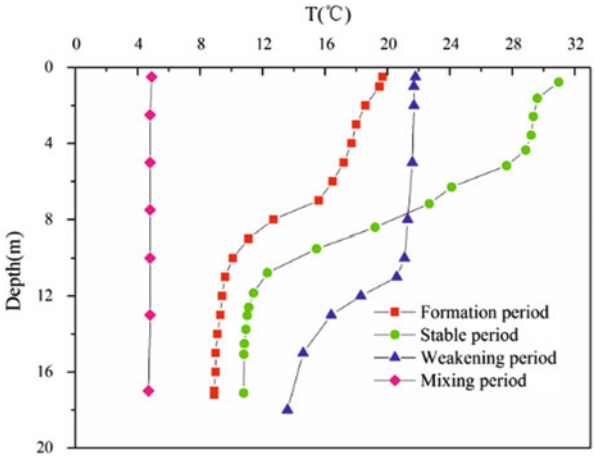

Fig. 40 Vertical distribution of water temperature at different periods in Zhoucun Reservoir

stratification stable period, the ranges of the epilimnion, thermocline and hypolimnion are 0–5 m, 5–10 m, and 10 m to the bottom, respectively. In the stratification weakness period, the upper water was mixed and the temperature was always the same, and the thermocline moved down gradually until it was totally mixed, namely the mixed stratification period.

4.3.2 The Variation of Dissolved Oxygen Under Different Periods

The DO change in different periods is shown in Fig. 41. Because many factors affect the DO concentration of a water body, especially algae photosynthesis, in order to better obtain representative results, the dissolved oxygen concentration

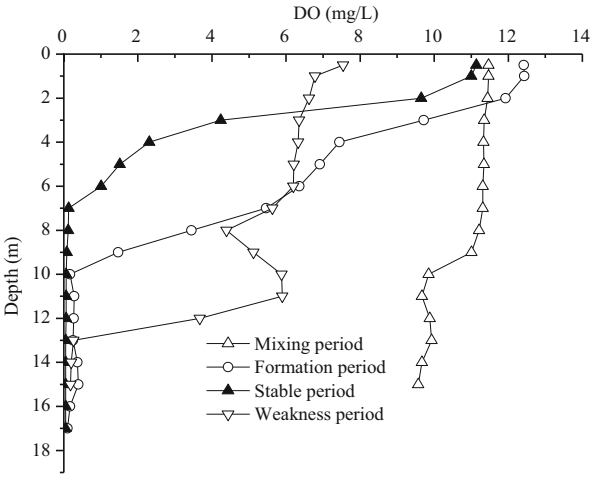

Fig. 41 Vertical distribution of dissolved oxygen at different periods in Zhoucun Reservoir

(Fig. 41) was measured on a sunny morning at 10:00 AM in May, August, October, and December. As shown in Fig. 41, the vertical distribution of DO in the stratification formation period and the stratification stable period is quite similar. In the surface water, the DO concentration was as much as 12 mg/L due to the photosynthesis of algae. However, the DO concentration rapidly decreased to zero between 2 and 6 m, since the photosynthesis weakened with water depth. Comparatively, the difference in DO change between the stratification formation period and the stratification stable period is that the decrease rate of DO in the stratification stable period is more rapid in the thermocline, which is due to the algal blooms in this period, resulting in reduced water clarity. In the stratification weakness period, parts of the water body are already mixed, and the DO concentration of a mixed water body is higher (6 mg/L), but the water body without mixing below the thermocline water remains in anaerobic conditions (DO is 0 mg/L). In the mixed period, the DO concentrations of the surface and bottom waters showed little difference.

4.3.3 The Variation of pH Under Different Periods

The pH of Zhoucun Reservoir water is in the range of 7.2–9.0, and shows a significant seasonal change with the stratification period (as shown in Fig. 42). As shown in Fig. 42, the water is alkaline, which is due to the strong light intensity, inducing strong algae photosynthesis and consumption of the carbon dioxide in the water. The vertical distribution of pH is quite different at different stratification periods, which is quite similar to the temperature behavior. The pH in the bottom water decreased gradually from the stratification formation period to the stratification weakness period, which is mainly due to the fact that the reservoir is always in anaerobic conditions during the stratification period, and the nitrogen, phosphorus, organic matters, sulfide, iron, and manganese were released into the water body and induced pH decrease.

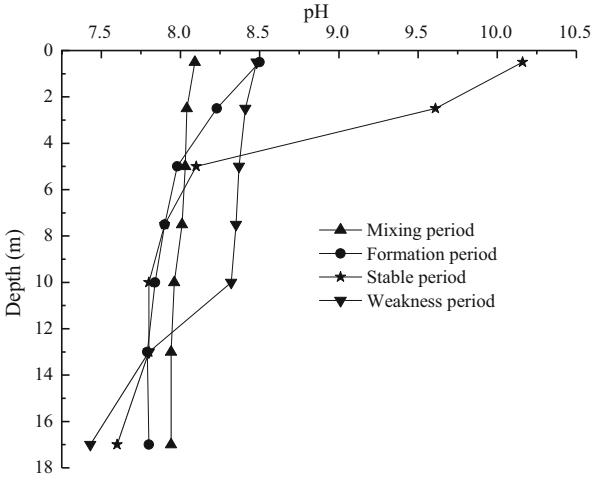

Fig. 42 Vertical distribution of pH at different periods in Zhoucun Reservoir

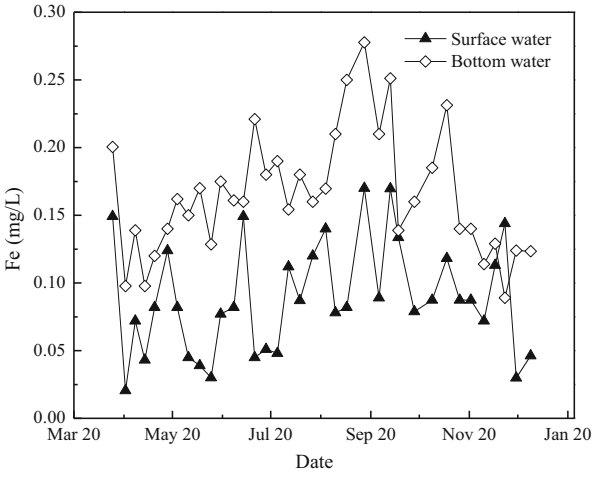

Fig. 43 Change of iron concentration at the surface/bottom waters at different periods in Zhoucun Reservoir

4.3.4 The Water Quality Problems Derived from the Thermal Stratification

(1) The Seasonal Change of Iron in Zhoucun Reservoir

The variation of iron concentration in Zhoucun Reservoir with time is shown in Fig. 43. It clearly shows that the concentration of iron is in the range 0.02–0.35 mg/L. There is a slight difference in iron concentration between the surface and bottom water bodies, and the iron concentration in the bottom water is slightly higher than that of surface water, which is due to the release of iron from the sediments under anaerobic conditions. Overall, the iron concentration in Zhoucun Reservoir is not very high, which is lower than the national surface water quality standard (GB

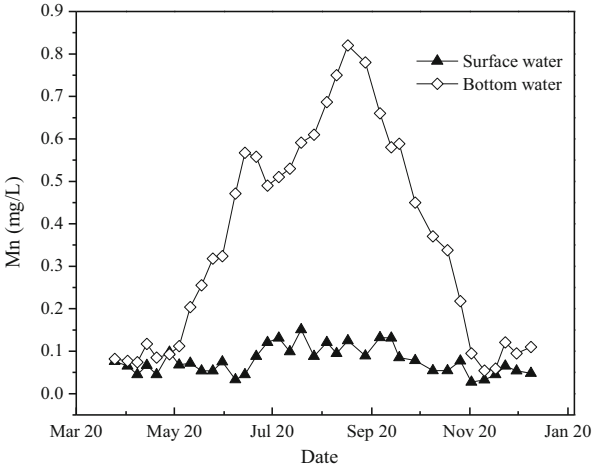

Fig. 44 Change of manganese concentration at the surface/bottom waters at different periods in Zhoucun Reservoir

3838–2002) (class III, the corresponding iron concentration is 0.3 mg/L), conforming to the class III source water standard.

(2) The Seasonal Change of Manganese in Zhoucun Reservoir

The variation of manganese concentration in Zhoucun Reservoir with time is shown in Fig. 44. The figure clearly shows that the concentration of manganese is in the range 0–0.8 mg/L. In September and October each year, the manganese pollution is quite serious and reaches a maximum, about 0.7–0.8 mg/L, which is about 7–8 times higher than the national surface water quality standard (GB 3838–2002) (class III). Comparatively, the manganese concentration in Zhoucun Reservoir is a little lower from January to May, approximately 0.1 mg/L. From the beginning of June, the massive release of manganese from sediments starts, and, at the end of August, the manganese concentration in the bottom water reaches a maximum. There is a high risk of manganese excess in the mixed period due to the massive release of manganese from the sediments. For example, once the water was just completely mixed, the manganese concentration reached 0.18 mg/L in both surface and bottom water bodies in November 11, 2012, exceeding 1.8 times the national surface water quality standard (GB 3838–2002) (class III). In November 4, 2013, the manganese concentration of the bottom water reached 0.21 mg/L, exceeding 2.1 times the national surface water quality standard (GB 3838–2002) (class III). After complete mixing, the manganese concentration in water gradually decreased and reached 0.1 mg/L in December.

(3) The Vertical Change of Manganese in Zhoucun Reservoir

The vertical change of manganese concentration in Zhoucun Reservoir in different periods is shown in Fig. 45. In the mixed period and stratification formation period, there is no obvious vertical change of manganese concentration. However, in the stratification stable period and stratification weakness period, the vertical distribution of manganese is apparently different. In the water layer below the thermocline,

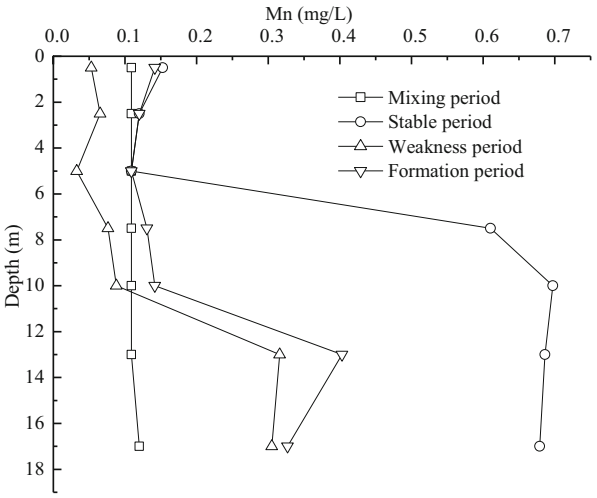

Fig. 45 Vertical distribution of manganese concentration (2012–2013)

the manganese concentration is significantly higher than that of the water layer above this layer, which is attributed to the higher manganese release rate compared with the diffusion rate. The manganese concentration below the thermocline was 0.63 and 0.72 mg/L in 2012 and 2013, respectively. In the stratification weakness period, the manganese concentration in the upper mixed water decreased due to the oxidation and dilution effect. The manganese concentration in the bottom water increased slightly due to the manganese release from the sediments and the decrease of unmixed water volume.

4.4 The Stratified Characteristics of Zhelin Reservoir and Its Impact on Water Quality

4.4.1 The Thermal Stratification Characteristics of Zhelin Reservoir

The vertical temperature change of Zhelin Reservoir is shown in Fig. 46a. The water depth of the monitoring position is around 42 m. As seen in Fig. 46a, the thermal stratification started from the April. At this time, the temperature difference between the surface layer water and the bottom layer water was around 8 °C. Until summer, the stable stratification was fully formed and the temperature difference between the surface layer and the bottom layer was 22 °C. In the fall, the surface water would get cold continuously, and the vertical temperature difference was more and more homogenous. Until early January in the following year, the water body was totally mixed and the vertical distribution of the water quality parameters was the same.

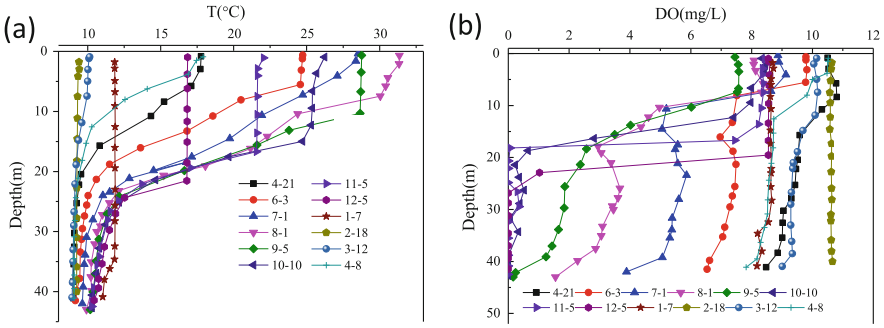

Fig. 46 Vertical distribution of water temperature and dissolved oxygen in Zhelin Reservoir (2012–2013)

The vertical DO change of Zhelin Reservoir is shown in Fig. 46b. During the thermal stratification period (from April to December), the DO concentration decreased with the increase of water depth. In the surface layer water, the DO concentration is always quite high (around 8 mg/L), due to the storm effect. In the middle layer water, the DO concentration gradually decreased, due to the lack of photosynthesis and the storm effect. In the bottom water, the DO concentration continuously decreased to a minimum value, due to the consumption of sediments and organic matters in water bodies. The DO concentration was around 2 mg/L in August. Until early January of the following year, the water mixing started and the vertical DO concentration in water tended to be consistent and reached the saturation level (>8 mg/L) under the local temperature conditions.

4.4.2 The Water Quality Problems Derived from the Thermal Stratification

(1) The Seasonal Change of TN and TP in Zhelin Reservoir

The seasonal change of TN and TP is shown in Fig. 47. The maximum concentration of annual TN and TP was 1.30 and 0.14 mg/L, respectively. The maximum concentration of TN occurred in the flood season in June, which was attributed to the inflow of surface runoff, carrying an amount of pollutants. Although the concentration of TP increased slightly during the flood season, the maximum concentration of TP occurred in the stable thermal stratification period, but not in the flood season. The main reason for TP increase is the release of manganese from the sediments under anaerobic conditions. The TP concentration reached a maximum before the mixing period. In January of the following year, the reservoir was totally mixed, and the TN and TP concentrations reduced to minimums of 0.4 and 0.01 mg/L, respectively.

During the stratification period, the bottom water was in an anaerobic state, and the redox potential also decreased. Therefore, nitrogen and phosphorus were

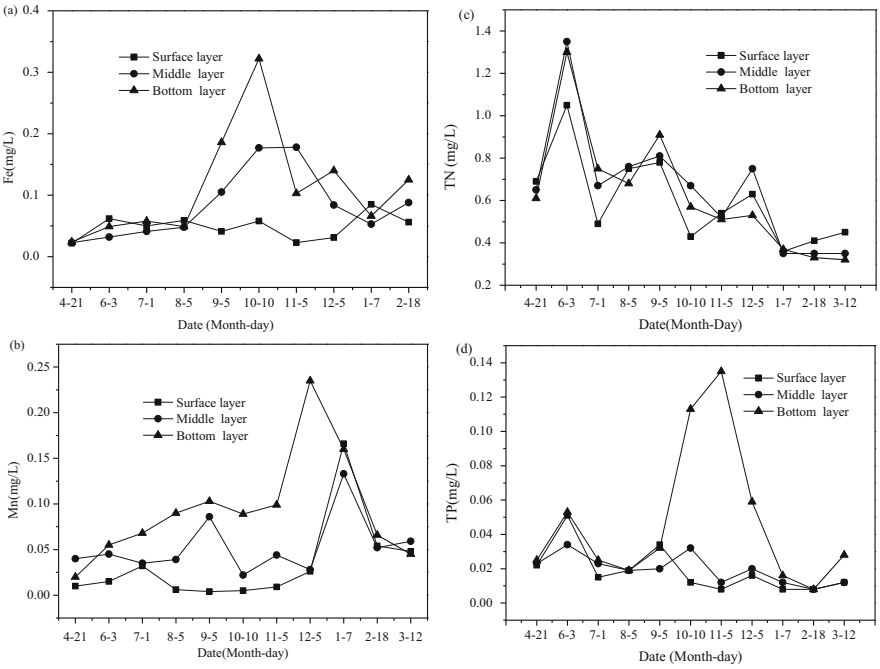

Fig. 47 Dynamics of nitrogen, phosphorus, iron, and manganese in Zhelin Reservoir

released into the overlying water. Comparatively, the release of TN is not as significant, since the water is slightly polluted in the reservoir, which was confirmed by the laboratory simulation experiments, and the maximum release concentration of TN was just 1.50 mg/L. In regards to TP, the main reason for the massive increase of TP in the reservoir is the release from the sediments under anaerobic conditions.

(2) The Seasonal Change of Iron and Manganese in Zhelin Reservoir

Fe and Mn are quite active elements, and their existence is easily affected by the environment in the sediment–water interface. The seasonal change of iron and manganese is shown in Fig. 47. The maximum concentrations of Fe and Mn were 0.32 and 0.34 mg/L, respectively, which occurred at the bottom of the water body under the stable stratification period. The minimum concentrations of Fe and Mn were 0.1 and 0.16 mg/L, respectively, when reaching the mixing period.

Fe and Mn were also at low levels before August (the Fe and Mn concentrations were lower than 0.1 mg/L), when the water was in an oxygen-rich state. After August, the bottom water body was in an anaerobic state, and the concentration of Fe and Mn increased continuously and exceeded the surface water quality standard. In January of the following year, the reservoir was fully mixed, and the concentration of Fe was at a low level, but the concentration of Mn was in an excessive state.

5 The Sulfide Pollution in the Reservoir

Sulfides include water-soluble hydrogen sulfide, acid-soluble metal sulfide, as well as insoluble sulfide and organic sulfide [37]. Hydrogen sulfide has a strong smell of rotten eggs, which can cause unpleasantness when the water contains a few milligrams per liter of hydrogen sulfide. Hydrogen sulfide is toxic, which can harm cytochrome oxidase, cause tissue hypoxia, and even threaten life. In addition, hydrogen sulfide is easily oxidized by bacteria to form sulfuric acid, which corrodes metal equipments and pipes. The latest results showed that acid-volatile sulfide plays a major role in the chemical activity of heavy metals in sediment and their bioavailability [38]. Therefore, sulfide is an important indicator of water pollution. In the following, with Zhoucun Reservoir as an example, the pollution characteristics and source analysis of sulfide are illustrated.

5.1 The Seasonal Variation of Sulfide in Zhoucun Reservoir

Figure 48 shows the seasonal variation of sulfide in Zhoucun Reservoir in 2012 and 2013. There is a similar variation in the trend of sulfide in the hypolimnion of Zhoucun Reservoir in 2012 and 2013. In the mixing period and the stratification formation period, there is no sulfide in the water. From late July, a rapid release of sulfide occurred in the sediments, and reached a peak of about 2.5 mg/L before the mixing period. In May, the DO of the bottom water in Zhoucun Reservoir dropped to zero, which provided the essential condition for sulfide release; but, at this time, the water pH was 8, and the redox potential was 180 mV, with organic matter in the hypolimnion being quite less, which inhibited the release of sulfide from the sediments. Until late July, a large number of sulfides were released from the sediments due to the increased organic matters in sediments, the decrease of redox potential (−200 mV), and the formation of a reductive environment.

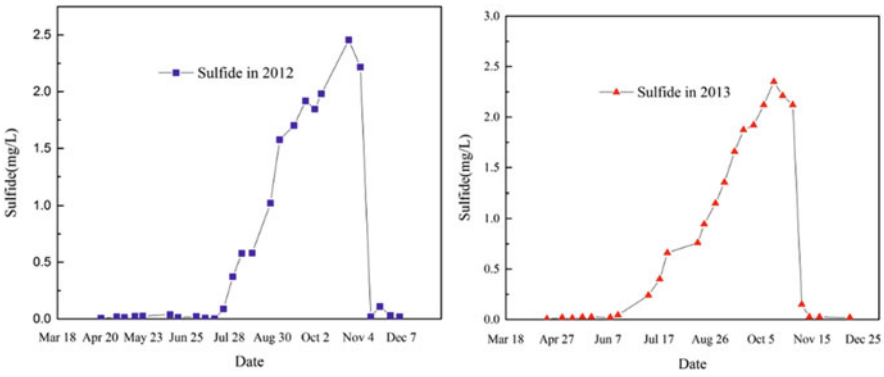

Fig. 48 Dynamics of sulfide in Zhoucun Reservoir

Table 26 The content of sulfur in the sediments of Zhoucun Reservoir

Sample	Unit	1	2	3	4	5
Bottom sediment in Zhoucun Reservoir	mg/L	9.378	7.424	12.637	12.427	12.599
Bottom sediment in Shibianyu Reservoir	mg/L	0.9631				
Dry mud content in Zhoucun Reservoir	mg	0.8853	0.7006	1.1927	1.173	1.1894

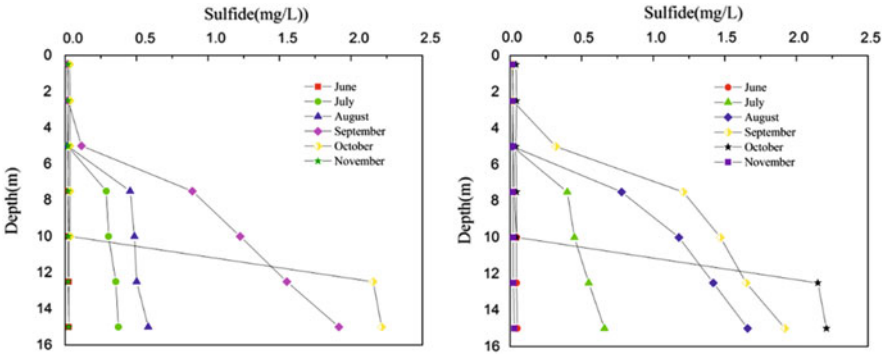

Fig. 49 Vertical distribution of sulfide in Zhoucun Reservoir

As shown in Table 26, there is a higher amount of sulfide (ten times higher) in the sediments of Zhoucun reservoir compared with that in Shibianyu Reservoir. That is the reason why the sulfide is excessive in Zhoucun Reservoir.

In the reservoir, because most of the sediments were in a reduced state, the sulfate will be reduced to sulfide by the sulfate-reducing bacteria. In the sediment of reservoirs, there are a lot of anaerobic microorganisms, including sulfate-reducing bacteria. Sulfate-reducing bacteria can reduce sulfate and generate sulfide in the decomposition of organic matter. In the case of plenty of sulfate in the sediments, the sulfide production rate is often directly proportional to the concentration of organic matter in the sediment. The results showed that the production of sulfide occurred in the surface sediments, which contained a lot of organic matter. In addition, it was found that the higher the content of organic matter in the sediments, the greater the sulfide production rate.

5.2 The Vertical Distribution of Sulfide in Zhoucun Reservoir

The vertical distribution of sulfide in Zhoucun Reservoir in 2012 and 2013 is shown in Fig. 49. As can be seen, the distribution of sulfide in water bodies showed an obvious stratification. The sulfide concentration in the epilimnion is almost zero,

due to the aerobic state. The release of sulfide began from July. During the early period, the release rate is slower than the diffusion rate, resulting in the same sulfide concentration at different water depths in the hypolimnion.

Until September, the sulfide release rate increased, and the sulfide concentration rose with the increase of water depth. The maximum sulfide concentration reached 1.8 mg/L at the bottom of the reservoir. In October, in the stratification weakness period, mixing occurred in the upper layer water and dissolved oxygen increased, while sulfide was removed by oxidation. However, it still maintained a high sulfide concentration in the bottom water, since the water environment was still in a reducing state.

References

1. Wisniewska M, Luscinska M (2012) Long-term changes in the phytoplankton of Lake Charzykowskie. Oceanol Hydrobiol Stud 41:90–98
2. Freeman AM, Lamon EC, Stow CA (2009) Nutrient criteria for lakes, ponds, and reservoirs: a Bayesian TREED model approach. Ecol Model 220:630–639
3. North RL, Smith REH, Hecky RE, Depew DC, Leon LF, Charlton MN, Guildford SJ (2012) Distribution of seston and nutrient concentrations in the eastern basin of Lake Erie pre- and post-dreissenid mussel invasion. J Great Lakes Res 38:463–476
4. Zhao JY, Ramin M, Cheng V, Arhonditsis GB (2008) Competition patterns among phytoplankton functional groups: how useful are the complex mathematical models? Acta Oecologica-Int J Ecol 33:324–344
5. Reichwaldt ES, Ghadouani A (2012) Effects of rainfall patterns on toxic cyanobacterial blooms in a changing climate: between simplistic scenarios and complex dynamics. Water Res 46:1372–1393
6. Smith VH, Schindler DW (2009) Eutrophication science: where do we go from here? Trends Ecol Evol 24:201–207
7. Carlson RE (1977) A trophic state index for lakes1. Limnol oceanogr 2:361–369
8. Naselli-Flores L, Barone R (2012) Phytoplankton dynamics in permanent and temporary Mediterranean waters: is the game hard to play because of hydrological disturbance? Hydrobiologia 698:147–159
9. Parinet J, Rodriguez MJ, Sérodes JB (2013) Modelling geosmin concentrations in three sources of raw water in Quebec, Canada. Environ Monit Assess 185:95–111
10. Ho L, Hoefel D, Bock F, Saint CP, Newcombe G (2007) Biodegradation rates of 2-methylisoborneol (MIB) and geosmin through sand filters and in bioreactors. Chemosphere 66:2210–2218
11. Devlin J, Edwards O, Gorham P, Hunter N, Pike R, Stavric B (1977) Anatoxin-a, a toxic alkaloid from Anabaena flos-aquae NRC-44h. Can J Chem 55:1367–1371
12. Harada K, Ogawa K, Kimura Y, Murata H, Suzuki M, Evans WR, Carmichael WW (1991) Microcystins from Anabaena flos-aquae NRC 525–17. Chem Res Toxicol 4:535–540
13. Krishnamurthy T, Carmichael W, Sarver E (1986) Toxic peptides from freshwater cyanobacteria (blue-green algae). I. Isolation, purification and characterization of peptides from Microcystis aeruginosa and Anabaena flos-aquae. Toxicon 24:865–873
14. Ghernaout B, Ghernaout D, Saiba A (2010) Algae and cyanotoxins removal by coagulation/flocculation: a review. Desalination Water Treat 20:133–143
15. Chang H, Chen C, Wang G (2013) Characteristics of C-, N-DBPs formation from nitrogen-enriched dissolved organic matter in raw water and treated wastewater effluent. Water Res 47:2729–2741

16. Zamyadi A, Ho L, Newcombe G, Bustamante H, Prévost M (2012) Fate of toxic cyanobacterial cells and disinfection by-products formation after chlorination. Water Res 46:1524–1535
17. Carrick HJ, Schelske CL (1997) Have we overlooked the importance of small phytoplankton in productive waters? Limnol Oceanogr 42:1613–1621
18. Zamyadi A, Fan Y, Daly RI, Prévost M (2013) Chlorination of Microcystis aeruginosa: toxin release and oxidation, cellular chlorine demand and disinfection by-products formation. Water Res 47:1080–1090
19. Fleming LE, Rivero C, Burns J, Williams C, Bean JA, Shea KA, Stinn J (2002) Blue green algal (cyanobacterial) toxins, surface drinking water, and liver cancer in Florida. Harmful Algae 1:157–168
20. Watson SB, Brownlee B, Satchwill T, Hargesheimer EE (2000) Quantitative analysis of trace levels of geosmin and MIB in source and drinking water using headspace SPME. Water Res 34:2818–2828
21. Sagehashi M, Shiraishi K, Fujita H, Fujii T, Sakoda A (2005) Ozone decomposition of 2-methylisoborneol (MIB) in adsorption phase on high silica zeolites with preventing bromate formation. Water Res 39:2926–2934
22. Munoz R, Sivret EC, Parcsi G, Lebrero R, Wang X, Suffet IH, Stuetz RM (2010) Monitoring techniques for odour abatement assessment. Water Res 44:5129–5149
23. Dzialowski AR, Smith VH, Huggins DG, DeNoyelles F, Lim NC, Baker DS, Beury JH (2009) Development of predictive models for geosmin-related taste and odor in Kansas, USA, drinking water reservoirs. Water Res 43:2829–2840
24. Yan Z, Zhang Y, Yu J, Yuan H, Yang M (2011) Identification of odorous compounds in reclaimed water using FPA combined with sensory GC-MS. J Environ Sci 23:1600–1604
25. Peter A, Köster O, Schildknecht A, Gunten U (2009) Occurrence of dissolved and particle-bound taste and odor compounds in Swiss lake waters. Water Res 43:2191–2200
26. Zat M, Benetti AD (2011) Removal of the odoriferous compounds geosmin and 2-methylisoborneol from drinking water by the processes of cascade aeration, air stripping and nanofiltration. Engenharia Sanitaria E Ambiental 16:353–360
27. Yu H, Tsuno H, Hidaka T, Jiao C (2010) Chemical and thermal stratification in lakes. Limnology 11:251–257
28. Wang S, Qian X, Han BP, Wang QH, Ding ZF (2011) Physical limnology of a typical subtropical reservoir in south China. Lake Reservoir Manag 27:149–161
29. Shuka L, Cullaj A, Shumka S, Miho A, Duka S, Bachofen R (2011) The spatial and temporal variability of limnological properties of Bovilla reservoir (Albania). Water Resour Manag 25:3027–3039
30. Lee YG, Kang JH, Ki SJ, Cha SM, Cho KH, Lee YS, Park Y, Lee SW, Kim JH (2010) Factors dominating stratification cycle and seasonal water quality variation in a Korean estuarine reservoir. J Environ Monit 12:1072–1081
31. Mueller B, Bryant LD, Matzinger A, Wueest A (2012) Hypolimnetic oxygen depletion in eutrophic lakes. Environ Sci Tech 46:9964–9971
32. Hanson D, Austin D (2012) Multiyear destratification study of an urban, temperate climate, eutrophic lake. Lake Reservoir Manag 28:107–119
33. Boegman L, Loewen MR, Hamblin PF, Culver DA (2008) Vertical mixing and weak stratification over zebra mussel colonies in western Lake Erie. Limnol Oceanogr 53:1093–1110
34. Baharim NH, Ismail R, Omar MH (2011) Effects of thermal stratification on the concentration of iron and manganese in a tropical water supply reservoir. Sains Malaysiana 40:821–825
35. Beutel MW, Horne AJ, Taylor WD, Losee RF, Whitney RD (2008) Effects of oxygen and nitrate on nutrient release from profundal sediments of a large, oligo-mesotrophic reservoir, Lake Mathews, California. Lake Reservoir Manag 24:18–29
36. Fillos J, Swanson WR (1975) The release rate of nutrients from river and lake sediments. Water Pollut Control Fed 47:1032–1042

37. Roden EE, Tuttle JH (1992) Sulfide release from estuarine sediments underlying anoxic bottom water. Limnol Oceanogr 37:725–738
38. Liu J, Yan C, Macnair MR, Hu J, Li Y (2007) Vertical distribution of acid-volatile sulfide and simultaneously extracted metals in mangrove sediments from the Jiulong River Estuary, Fujian, China. Environ Sci Pollut Res 14:345–349

Typical Reservoir Pollution Source Analysis

Xinxin Shi, Weixing Ma, Xuan Li, Ya Cheng, and Tinglin Huang

Abstract Exogenous and endogenous pollutions are the two main kinds of pollution sources that result in the deterioration of water quality in reservoirs. Exogenous pollution is derived from the environment surrounding reservoirs, including industrial wastewater, sewage runoff, solid waste, meteoric waters, and surface runoffs from urban, agriculture, and pastoral areas. Endogenous pollution is mainly caused by the pollutants released from sediments, the fecundity and death of phytoplankton and aquatic plants, and aquaculture. The pollution source analysis contributes to a deep research on the mechanism, process, and control of reservoir pollution, and provides basic theory and technology supports for improving the water quality. In recent years in China, with the further understanding about the importance of water protection, especially with the significant progress of water protection, the exogenous pollution of water sources has been or is being effectively controlled. Endogenous pollution becomes the dominant factor affecting water quality. In this chapter, the exogenous and endogenous pollution sources, classification, and status in China are concretely discussed and four reservoirs in China named Jinpen, Shibianyu, Zhoucun, and Fenhe were examined to elaborate these issues. For exogenous pollution, the pollution sources, main pollutants, and the load of every kind of exogenous pollutant in Shibianyu Reservoir were shown to indicate that runoff after rainfall scour was one of the main reasons for TN and TP increase. For endogenous pollution, pollutants release from sediment caused by forward temperature stratification in Heihe Reservoir and backward temperature stratification in Fenhe Reservoir were analyzed. The results showed that temperature stratification would result in the release of nitrogen and phosphorus from sediment. Moreover, endogenous pollution caused by algae reproduction and aquaculture in Zhoucun Reservoir were also discussed point for point and the data indicated that the algae in this reservoir were highly correlated with temperature, pH, turbidity, and total phosphorus, but inversely correlated with the ratio of nitrogen and phosphorus. Decades of cage culture was one main reason for the heavy pollution in sediment of Zhoucun Reservoir.

X. Shi • W. Ma • X. Li • Y. Cheng • T. Huang (✉)
School of Environmental and Municipal Engineering, Xi'an University of Architecture and Technology, Yanta Road 13, 710055 Xi'an, Shaanxi, P. R. China
e-mail: huangtinglin@xauat.edu.cn

T. Huang (ed.), *Water Pollution and Water Quality Control of Selected Chinese Reservoir Basins*, The Handbook of Environmental Chemistry 38,
DOI 10.1007/978-3-319-20391-1_3

Keywords Exogenous pollution • Endogenous pollution • Sediments • Algal blooming • Aquaculture

1 Exogenous Pollution

Exogenous pollution is the water pollution caused by sources outside of lakes and reservoirs, including sewage runoff, industrial wastewater, polluted branches, surface runoffs from agriculture and pastoral areas, and so on. Exogenous pollution is also grouped into point source pollution and non-point source pollution based on the differences in pollution sources and properties. The point source pollution comprises sources which intensively discharge the pollutant in the long term and significantly threaten the water environment. The non-point source pollution comprises the sources scattered over the water drainages. At present, point source pollution is basically well under control. The pollutants largely come from non-point source pollution, such as the surface runoffs from agriculture, the erosion from urban or deforested land, mining, and air pollution. Here, taking Shibianyu Reservoir as an example, the pollution properties, main pollutants, and contamination load of exogenous pollution are introduced.

1.1 Exogenous Pollution Properties in Shibianyu Reservoir

Surrounding Shibianyu Reservoir, there are thick woods and diverse vegetation, which play important roles in water conservation. Above the reservoir dam, the length of the trunk stream is 30 km. The main branches include Dapiao stream, Xiaopiao stream, Longwozi stream, and Dabancha stream with lengths of 6–7 km. The pollution properties depend on the pollution sources [1, 2]. For Shibianyu Reservoir, runoff pollution particularly comes from the following: (1) The sewage runoff and household waste from upstream towns. A field survey found that the toilets in upstream towns were mainly squat toilets which were built on the shores of streams. Moreover, sewage runoff was directly discharged into ditches. These are sources of nitrogen and phosphate. (2) The flow of a water-diversion project. The flow of a water-diversion project from Qianyou River that disembogues into Shibianyu Reservoir is one of the potential pollution sources. (3) A quarry placed upstream of the reservoir. Rock dregs from the quarry not only destroyed the natural environment, but also easily lead to water pollution of the reservoir. A large fire at the quarry containing thousands of tons of used tires resulted in severe pollution of the adjacent water course by the products of pyrolysis.

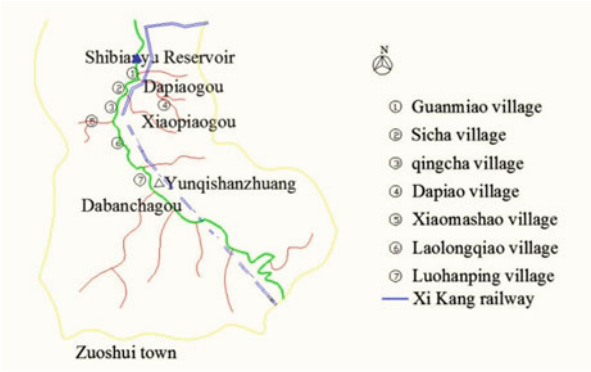

Fig. 1 Map of sample points dispersed upstream of Shibianyu Reservoir

1.2 Main Pollutants in Shibianyu Reservoir

The main pollutants of exogenous pollution in Shibianyu Reservoir include nitrogen, phosphorus, and organic matter. There are nine sample points distributed from the head of Shibianyu to the entrance of the reservoir (Fig. 1), which are used to monitor the water quality changes.

The water quality of upstream of Shibianyu Reservoir from 2011 to 2012 are as follows:

(1) Nitrogen

The total nitrogen (TN) concentration in runoff upstream of Shibianyu Reservoir was of a high level and changed with the season (Table 1). In spring, the TN concentration (about 4 mg/l) is the highest; after that, the concentration declined, but remained above 2 mg/l. The changes of TN were almost consistent between upstream and inside the reservoir, which indicated that the TN concentration in the reservoir was largely affected by the flow from upstream.

The changes in ammonia concentration (NH_3-N) are shown in Table 2. On sunny days, the NH_3-N in runoff from upstream was at a low level, which basically satisfied the environmental quality standard for surface water: I standard. After rainfall, the NH_3-N increased significantly, which indicated that NH_3-N mainly came from domestic living pollution and surface soil pollution along the flow. However, the increase of NH_3-N was much lower than that of TN, which illustrated that the nitrogen pollutants from upstream largely existed as nitrate and inorganic nitrogen.

(2) Phosphorus

The changes of total phosphorus concentration (TP) are shown in Table 3. The TP was of a low level and changed little with seasons. On sunny days with runoff from upstream, TP ranged from 0.008 to 0.029 mg/l. After rain, TP increased slightly, but this concentration was still slightly lower than that inside Shibianyu Reservoir. After rainfall runoff, TP at the entrance of the reservoir increased significantly, which resulted from the flow from rainfall runoff that

Table 1 TN seasonal concentration of the upstream of Shibianyu Reservoir (average values of 2011 and 2012)

	Runoff	1	2	3	4	5	6	7	8	9	Reservoir
Spring	S	3.9	3.7	3.8	3.8	1.7	3.7	3.9	4.9	3.7	3.6
	R	4.1	4.0	3.9	4.0	1.8	3.7	3.5	5.1	3.9	3.9
Summer	S	2.8	2.7	2.7	2.8	2.2	2.6	2.6	3.7	2.8	3.0
	R	2.7	2.9	3.1	3.7	2.5	3.0	3.0	4.3	2.9	3.1
Autumn	S	2.2	2.3	2.2	2.4	1.8	2.7	2.6	3.1	2.6	2.5
	R	2.4	2.5	2.5	2.6	1.9	2.8	2.7	3.6	2.9	2.6
Winter	S	1.9	2.0	2.0	2.1	1.5	1.7	2.0	2.5	2.2	2.1
	R	2.0	2.1	2.0	2.1	1.7	2.2	2.1	2.8	2.2	2.0

S stands for runoff on a sunny day
R stands for runoff after a rainy day

transported into the bottom layer of water in the reservoir due to gravity, and mixed with the concentrated phosphorus released from sediment. These results indicated that high TP in the reservoir was mainly caused by endogenous pollution.

(3) COD_{Mn}

The average value of COD_{Mn} in runoff from upstream on sunny days was about 2 mg/l, which was lower than that in the reservoir (Table 4). This means that the organic matter in the reservoir largely came from endogenous pollution, such as algae rapid propagation and organic pollutants released from sediment.

(4) Alkalinity

The alkalinity in runoff upstream of Shibianyu Reservoir was of a low level, and the changes of alkalinity with season were almost consistent between upstream and inside the reservoir. It is a little high in spring and the lowest in summer (Table 5). There were large changes of alkalinity among sample points upstream. The alkalinity is especially low in Dabancha-Longwozigou (the average value is 20 mg/l, calculated by $CaCO_3$). However, the alkalinity in Jishi increased and was close to that of the reservoir. Rainfall significantly affected the alkalinity. Normally, the alkalinity in all sample points decreased after rainfall, which has low alkalinity (normally below 10 mg/l). Therefore, rainfall may be the main reason for the decrease of the alkalinities in the reservoir and in the upstream sample points.

1.3 Exogenous Pollution Load in Shibianyu Reservoir

(1) Domestic Pollution Load

Domestic discharge load comes from solid waste, sewage, and excrement. The main parameters include TN, TP, and COD_{Cr}. Due to the scattered villages

Table 2 NH_3-N seasonal concentration of the upstream of Shibianyu Reservoir (average values of 2011 and 2012)

	Runoff	1	2	3	4	5	6	7	8	9	Reservoir
Spring	S	0.043	0.049	0.049	0.055	0.049	0.060	0.137	0.095	0.060	0.154
	R	0.189	0.133	0.150	0.144	0.032	0.111	0.027	0.066	0.049	0.139
Summer	S	0.147	0.164	0.153	0.215	0.204	0.187	0.153	0.227	0.210	0.249
	R	0.210	0.158	0.312	0.181	0.295	0.249	0.221	0.267	0.443	0.281
Autumn	S	0.089	0.093	0.101	0.112	0.124	0.115	0.109	0.114	0.153	0.149
	R	0.102	0.106	0.132	0.153	0.168	0.212	0.214	0.193	0.215	0.198
Winter	S	0.116	0.100	0.072	0.122	0.066	0.111	0.123	0.118	0.122	0.145
	R	0.212	0.284	0.206	0.212	0.223	0.200	0.217	0.200	0.273	0.184

S stands for runoff on a sunny day
R stands for runoff after a rainy day

Table 3 TP seasonal concentration of the upstream of Shibianyu Reservoir (average values of 2011 and 2012)

	Runoff	1	2	3	4	5	6	7	8	9	Reservoir
Spring	S	0.010	0.010	0.014	0.014	0.014	0.019	0.017	0.021	0.023	0.048
	R	0.019	0.014	0.019	0.019	0.023	0.032	0.023	0.027	0.034	0.062
Summer	S	0.010	0.012	0.010	0.010	0.012	0.016	0.012	0.014	0.023	0.042
	R	0.016	0.016	0.020	0.029	0.024	0.029	0.029	0.029	0.046	0.051
Autumn	S	0.012	0.013	0.012	0.014	0.017	0.018	0.017	0.022	0.025	0.033
	R	0.021	0.022	0.023	0.026	0.026	0.030	0.029	0.031	0.041	0.042
Winter	S	0.008	0.010	0.009	0.012	0.011	0.015	0.010	0.013	0.022	0.019
	R	0.010	0.009	0.013	0.016	0.015	0.014	0.021	0.022	0.030	0.021

S stands for runoff on a sunny day
R stands for runoff after a rainy day

Table 4 COD_{Mn} seasonal concentration of the upstream of Shibianyu Reservoir (average values of 2011 and 2012)

	Runoff	1	2	3	4	5	6	7	8	9	Reservoir
Spring	S	2.3	2.0	2.0	1.9	2.2	1.6	2.2	2.0	2.2	2.7
	R	3.6	3.1	2.7	3.1	2.9	3.0	3.7	3.6	4.1	3.0
Summer	S	2.5	1.8	1.8	1.9	1.6	2.2	1.9	1.8	2.0	3.3
	R	3.3	3.6	3.7	3.5	2.6	3.0	3.6	3.2	3.7	3.5
Autumn	S	2.2	2.3	2.4	2.3	2.1	2.4	2.5	2.6	2.2	3.7
	R	2.9	2.9	3.0	3.3	2.6	3.0	3.2	3.7	3.6	6.2
Winter	S	2.1	2.2	2.1	2.4	1.9	2.4	2.3	2.1	2.2	4.0
	R	3.0	3.2	3.3	2.8	2.9	3.3	3.5	3.2	3.3	4.1

S stands for runoff on a sunny day
R stands for runoff after a rainy day

upstream of Shibianyu Reservoir, the discharge coefficients were chosen as below based on Chinese national statistics (Table 6).

Based on the above coefficients, the discharged TN, TP, and organic pollutants from upstream villages were estimated and are shown in Tables 7, 8, and 9, respectively. The quantity of TN, TP, and organic pollutants were 9.61, 2.21, and 43.40 t per year, respectively. TN and organic pollutants mainly came from the residents' excrement. TP largely originated in domestic solid waste. Therefore, rational treatment for resident's excrements and domestic solid waste is the key point to control the quantities of the discharged pollutants.

(2) Agricultural Pollution Load

Agricultural pollution load comes from livestock breeding and plants farming. The area for plants farming surrounding Shibianyu Reservoir is relatively small, and the usage of chemical fertilizers and pesticides was really very small. Thus, plants farming makes little effect on the reservoir water quality. Moreover, there was no large-scale breeding industry. The total numbers of livestock and poultry upstream of Shibianyu Reservoir were 139 and 3200, respectively.

(3) Rainfall Scour Pollution Load

The vegetation coverage was relatively high upstream of Shibianyu Reservoir. In normal conditions, soil erosion was not serious. The appearance of exogenous pollutants was largely during rainstorm runoff. For example, in 2011, from July to September, the rainfall in Shibianyu reached 706.6 mm, among which 422.5 mm occurred in September and was mainly due to storms (Fig. 2). A large amount of sand and humus were carried into the reservoir due to the storm flush and landslides in September. The monitor results indicated that the runoff after rainstorm resulted in the significant increase of turbidity and organic pollutant concentration. At the same time, TN and TP were also much higher than the standard limits. Moreover, the pollutants were mainly insoluble, which were appropriate to precipitate to the bottom of the reservoir and absorb nitrogen and phosphorus during precipitation (Table 10). This precipitation would result in a substantial increase of the endogenous pollution load [1, 2].

Table 5 Seasonal alkalinity of the upstream of Shibianyu Reservoir (average values of 2011 and 2012)

	Sample	1	2	3	4	5	6	7	8	9	Reservoir
Spring	S	22.9	28.2	22.9	26.43	57.9	38.8	41.4	54.6	42.2	50.5
	R	21.1	23.8	22.9	28.2	34.6	27.3	38.2	41.7	37.6	45.9
Summer	S	17.1	17.1	17.1	22.0	41.7	49.3	44.2	45.4	34.2	37.2
	R	16.0	16.0	16.0	20.9	24.6	33.4	34.6	36.9	30.2	33.6
Autumn	S	17.3	17.5	17.6	18.2	42.6	33.2	36.5	38.2	35.2	35.6
	R	15.2	16.1	15.9	16.9	27.6	30.2	31.4	33.2	33.0	33.1
Winter	R	19.7	20.9	20.9	24.6	51.7	41.8	45.5	56.6	38.1	42.6
	S	17.6	18.1	18.3	19.5	35.4	29.3	30.53	37.8	36.4	40.7

S stands for runoff on a sunny day
R stands for runoff after a rainy day

Table 6 Related discharge coefficients

Pollution source	Coefficients (kg/cap · a)		
	TN	TP	COD_{Cr}
Sewage	0.56	0.16	5.99
Excrement	3.06	0.524	19.8
Solid waste	2.09	0.63	

Table 7 The estimated values of nitrogen discharged from residents

Village	Population	Sewage (t/a)	Excrement (t/a)	Solid waste (t/a)	Total (t/a)
Guanmiao	381	0.21	1.17	0.80	2.18
Dapiao	206	0.12	0.63	0.43	1.18
Sicha	382	0.21	1.17	0.80	2.18
Qingcha	151	0.08	0.46	0.32	0.86
Xiaomashao	212	0.12	0.65	0.44	1.21
Laolongqiao	166	0.09	0.51	0.35	0.95
Luohanping	185	0.10	0.57	0.39	1.06
Total	1683	0.94	5.15	3.52	9.61

Table 8 The estimated values of phosphorus discharged from residents

Village	Population	Sewage (t/a)	Excrement (t/a)	Solid waste (t/a)	Total (t/a)
Guanmiao	381	0.06	0.20	0.24	0.50
Dapiao	206	0.03	0.11	0.13	0.27
Sicha	382	0.06	0.20	0.24	0.50
Qingcha	151	0.02	0.08	0.10	0.20
Xiaomashao	212	0.03	0.11	0.13	0.28
Laolongqiao	166	0.03	0.09	0.10	0.22
Luohanping	185	0.03	0.10	0.12	0.24
Total	1683	0.27	0.88	1.06	2.21

Table 9 The estimated values of organic matters discharged from residents

Village	Population	Sewage (t/a)	Excrement (t/a)	Solid waste (t/a)
Guanmiao	381	2.28	7.54	9.83
Dapiao	206	1.23	4.08	5.31
Sicha	382	2.29	7.56	9.85
Qingcha	151	0.90	2.99	3.89
Xiaomashao	212	1.27	4.20	5.47
Laolongqiao	166	0.99	3.29	4.28
Luohanping	185	1.11	3.66	4.77
Total	1683	10.08	33.32	43.40

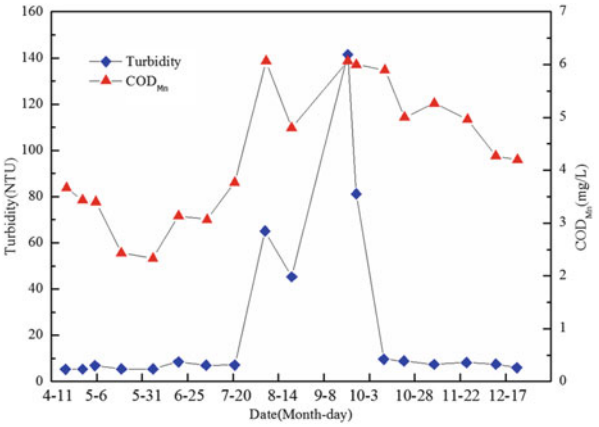

Fig. 2 Turbidity and COD_{Mn} during rainfall runoff period in Shibianyu Reservoir

Table 10 Estimated pollutant load during the rainfall runoff period in September

Pollutant	Concentration (mg/L)	Load in reservoir (t)	Insoluble matter (%)
Phosphorus	0.086	4.54	54
TN	3.56	187.97	41
COD_{Mn}	6.54	345.31	37

2 Endogenous Pollution

Endogenous pollution is one of the biggest concerns in the topic of water research all over the world. The US Environmental Protection Agency defined endogenous pollutants as the hazardous soil and organic matters or minerals from humans or the environment, which precipitate on the bottom water through soil erosion, atmospheric deposition, riverbank erosion, or mineralization. Actually, the general endogenous pollution is the total hazardous matters including all kinds of nutrients and pollutants which accumulate long term in the bottom water caused by natural or human factors. Sediment, as the home of whole matters in water, was not only an "accepter" but also a "donor" in certain conditions. Endogenous pollution has significant effects on a lot of water sources.

Endogenous pollution of reservoirs has the following characteristics: (1) The pollution area is large. The sediment would be a pollution source in certain conditions, such as in summer stable stratified time. The areas of reservoirs are normally large, from several square kilometers to several hundreds or thousands of square kilometers, so the endogenous pollution in a reservoir is similar to that of non-point source pollution. For example, the area of Lake Volta is 8482 km^2 and that of Guanting Reservoir in China is 230 km^2. (2) The pollution effect is lasting. Endogenous pollution in reservoirs is normally accompanied by sediment accumulation, with which the endogenous pollution grows and finally becomes the main factor of pollution. (3) Pollutants release pathway and quantity are uncertain. Pollutants release depends on environmental conditions, and with different

conditions, the amount of released pollutants is different. For example, for shallow reservoirs, the release of pollutants in sediment could be caused by storms; for deep water reservoirs, storms may only affect the surface water, and the release of pollutants in sediment may be mainly caused by the effects of aquatic organisms and the environment in the bottom water.

Endogenous pollution exists in most of the lakes and reservoirs in China. In Hang Zhu, the endogenous pollution load of Xi Lake is 41 % higher than that of exogenous pollution. In Dian Lake, the nitrogen accumulated in sediment is 7.8 times higher than in exogenous pollution, and phosphorus is 15.6 times greater. Even if the lakes and reservoirs were protected very well, such as Xili Reservoir and Guanting Reservoir, endogenous pollution is still the main cause of bad water quality in certain seasons. From the 1970s to the present, a great deal of research on endogenous pollution has been carried out, most of which focus on the cycle and transformation of the pollutant element and combined with eutrophication.

2.1 Endogenous Pollution Caused by Pollutants in Sediment

Both forward and backward stratification of water could cause the entrance of pollutants from the sediment into the water. Recently, periodic deterioration of water quality resulted from thermal stratification. For example, in Guizhou Province, the water of Hongfeng Reservoir and Baihua Reservoir turned black with odorous foam in summer, with TN, TP, and sulfur increasing, pH decreasing, and dead fish. This condition lasted from 10 to 30 days and seriously threatened the water supply safety. The long-term anaerobic environment in the bottom of deep water reservoirs caused by stratification is another reason for the deterioration of water quality. For example, Liuxihe Reservoir in Guangdong Province (average depth is 22 m and the maximum depth is 73 m), only in December and January was the reservoir in a mixed state. In the north of China, the backward stratification in winter would cause the deterioration of water quality in spring when the water mixed, such as Fenghe Reservoir in Taiyuan. Here, taking Fenhe and Heihe Reservoirs as examples, the endogenous pollution caused by sediment in introduced in detail.

2.1.1 Pollutants Release from Sediment in Heihe Reservoir Caused by Forward Stratification

(1) Seasonal Stratification Structure in Heihe Reservoir

As shown in Fig. 3a and b, in 2008 and 2009, the temperature changes of the water in Heihe Reservoir were coincident with that of the air temperature, but with a slight lag. The water temperature fluctuated from 5.5 to 27 °C. In the bottom water, the temperature fluctuated very little, and was stable at around 5.5–7 °C. On the vertical

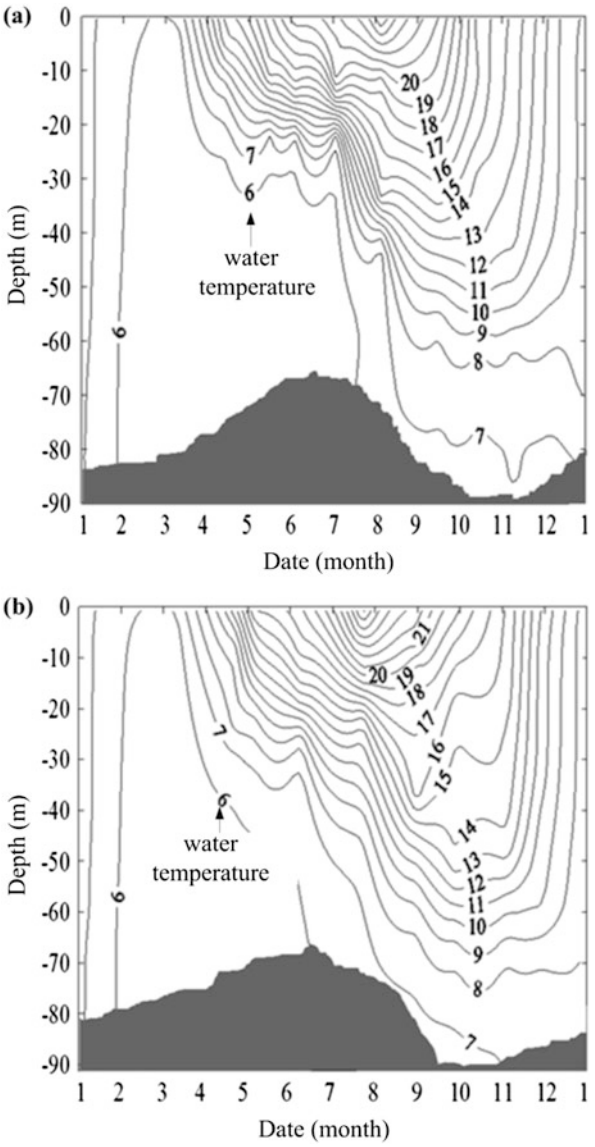

Fig. 3 The temperature changes with the water depth in vertical of Heihe Reservoir in 2008 (a) and 2009 (b)

profile, there is an obvious seasonal character presenting in the gradient distributions of the water temperature [3].

In spring, the low temperature stage finished in Heihe Reservoir and the warming stage started. The temperature of the surface water in the reservoir increased constantly, and there were no obvious changes of the temperature in the bottom water. Therefore, the temperature variation between the surface and bottom

water increased constantly, and the water in the reservoir transitioned to a stratification structure.

In summer, the growing temperature resulted in the further increase of heat flux on the surface water. The temperature in the upper layer increased sharply, but that in the bottom layer increased slowly. There was obvious forward stratification on the vertical profile. In June 2008 (Fig. 3a), at depths from 12 to 15 m, the temperature variation was small, and below a depth of 30 m, it was an isothermal layer. Between the two depth ranges, it was the thermocline depth at which the average temperature gradient was more than 1 degree per meter, and the maximum temperature variation was as high as 10–14 °C. In comparison, during the same period in 2009, at the thermocline depth, the temperature gradient was smaller (0.5–0.8 degrees per meter). The depth of the isothermal layer decreased (below 35 m), but the stratification was still very obvious. In July and August, a double thermocline layer presented in some regions of water, due to the heat exchanged between the air and water surfaces.

In autumn, the temperature stopped increasing and decreased instead. However, the stratification still existed. With the air temperature decreased, the water distributed heat to air and the water temperature decreased. The upper water gradually dived due to the increase in density. Convection on the vertical profile resulted in uniform temperature in the upper water. At the same time, the temperature variation in the temperature layer decreased and finally became consistent. The temperature of the bottom water stayed at about 7 °C. Therefore, the range of temperature became smaller and smaller with the increase of the range of vertical convection.

In winter, the temperature variation between the upper and bottom waters further decreased. The stratification structure was gradually lost and the reservoir started to transform to the isothermal stage. At the beginning of January, the whole reservoir mixed and the strong convection on the vertical profile promoted heat exchange between the upper and bottom waters. The water lost its heat gradually with the decreasing air temperature, which resulted in the temperature dropping in the whole water body. During winter time, Heihe Reservoir did not freeze and the minimum temperature was 5–5.5 °C in late February. When spring comes again, a new cycle of temperature evolution starts.

(2) DO Changes Resulted from the Heat Stratification in Heihe Reservoir

In reservoirs, DO mainly comes from three sources: air, photosynthesis by aquatic organisms, and runoff of the reservoir. DO is usually consumed by the organic matters decomposition catalyzed by microbes, organic matters in sediment, respiration of aquatic creatures, and other oxidation of reductive matters [4]. DO depends on the relative strength of oxygen input and oxygen expending, and is affected by water temperature, water quality, water kinetics, and oxygen partial pressure.

The DO changes profile is shown in Fig. 4a and b. Because of the dynamic stratification structure of water, the DO distribution in Heihe Reservoir also changed seasonally. During the heat stratification and transition period (from March to December), the DO concentration decreased with the water depth. It is

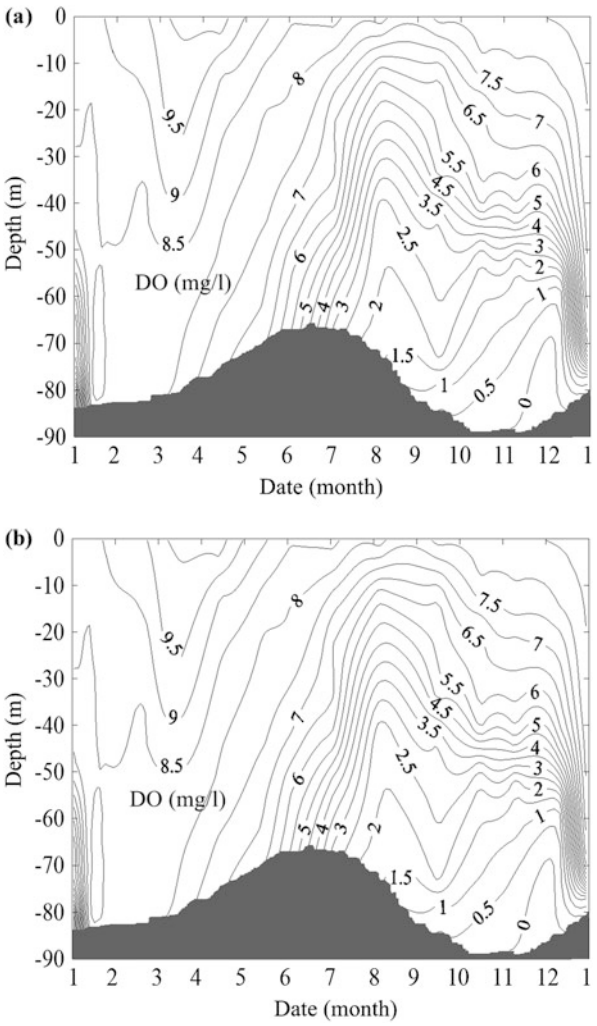

Fig. 4 DO profile in Jinpen Reservoir in 2008 (**a**) and 2009 (**b**)

easy for surface water to reaerate due to its direct connection with air and the mixing process by wind. The DO concentration in the surface water is basically consistent with the saturated DO in air. At depths from 2 to 10 m in summer and autumn, the DO in surface water usually supersaturated, which resulted from algae reproduction and exuberant photosynthesis. With increasing depth, it is hard to reaerate due to the limited algae production with low temperature and light. At the same time, the water continually expended oxygen, such that the DO concentration decreased constantly. At the bottom of the reservoir, the DO concentration became the lowest in the whole water, which resulted from being far away from atmosphere, continual oxygen expenditure by organic matter (mainly from sediment), mineralization, and decomposition.

In water, the oxygen transfer is usually slow and mainly depends on water exchange. If the water flows between upper and bottom waters exchange sufficiently in the reservoir, the oxygen consumption mechanism would turn into the oxygen recovery mechanism. Once the exchange was hampered, the water in the bottom would turn into an oxygen deficit. Steady temperature gradients hamper the exchange of matter between upper and bottom waters and make the water turn anoxic. In March, after the heat stratification begins to form, DO in the bottom of Heihe Reservoir was 8 mg/l and decreased to 2 mg/l in July, then to 0.5 mg/l in September, then to the minimum of about 0.1 mg/l. At the beginning of January, the DO recovered to 8 mg/l due to the whole water mixing in the reservoir. Thus, the DO vertical profile depends on the seasonal temperature stratification.

(3) The Release of Nitrogen and Phosphorus in Heihe Reservoir

Nitrogen and phosphorus are the significant elements to evoke eutrophication and algae reproduction. There are many geochemical processes on the interface of water, sediment, and microorganisms with the two elements, which make good sense to the water quality changes in reservoirs. With the appearance of seasonal oxygen deficit in the bottom of Heihe Reservoir, the nitrogen and phosphorus with several kinds of states undergo processes as follows: transition, release, accumulation, and diffusion, which promote the process of eutrophication.

As shown in Fig. 5, during heat stratification period, TN and TP sharply increased with depth. And during the isothermal period, the variation of TN and TP on the vertical profile sharply decreased and became consistent. The maximum of TP and ammonia–nitrogen (NH_3-N) shown in August or September were 0.223–0.247 mg/l and 0.576–0.728 mg/l, respectively. And the minimum of TP and ammonia–nitrogen (NH_3-N) shown in March were 0.02–0.03 mg/l and 0.076–0.113 mg/l, respectively.

From April to December, the TP concentration in the bottom of the reservoir is 1.06–4.94 times higher than the limit value (0.05 mg/l) in class III for lakes and reservoirs of the environmental quality standard of surface water (GB 3838–2002). The worst was class V or exceeded class V. The TP concentration in the upper water of reservoir is 1.06–1.82 times higher than the limit value of class II from July to October. Endogenous release is the main inducement for TP exceeding the limits periodically.

Compared to TP, although the NH_3-N concentration did not exceed the limit value (1.0 mg/l) in class III of the environmental quality standard of surface water (GB 3838–2002), with the oxidative–reductive cycle in Heihe Reservoir, NH_3-N changed with season. It is worth noting that, in August and September, after the TP concentration reached the maximum value, the TP maintained with the oxygen further decreased. However, from August to December, the NH_3-N concentration remained at a high level and did not decrease until the mixing period. As shown in Fig. 6, there was an obvious negative correlation between the DO and NH_3-N concentrations ($R^2 = 0.7127$). But the correlation between DO and TP concentrations ($R^2 = 0.3203$) was not as strong as that of DO and NH_3-N concentrations.

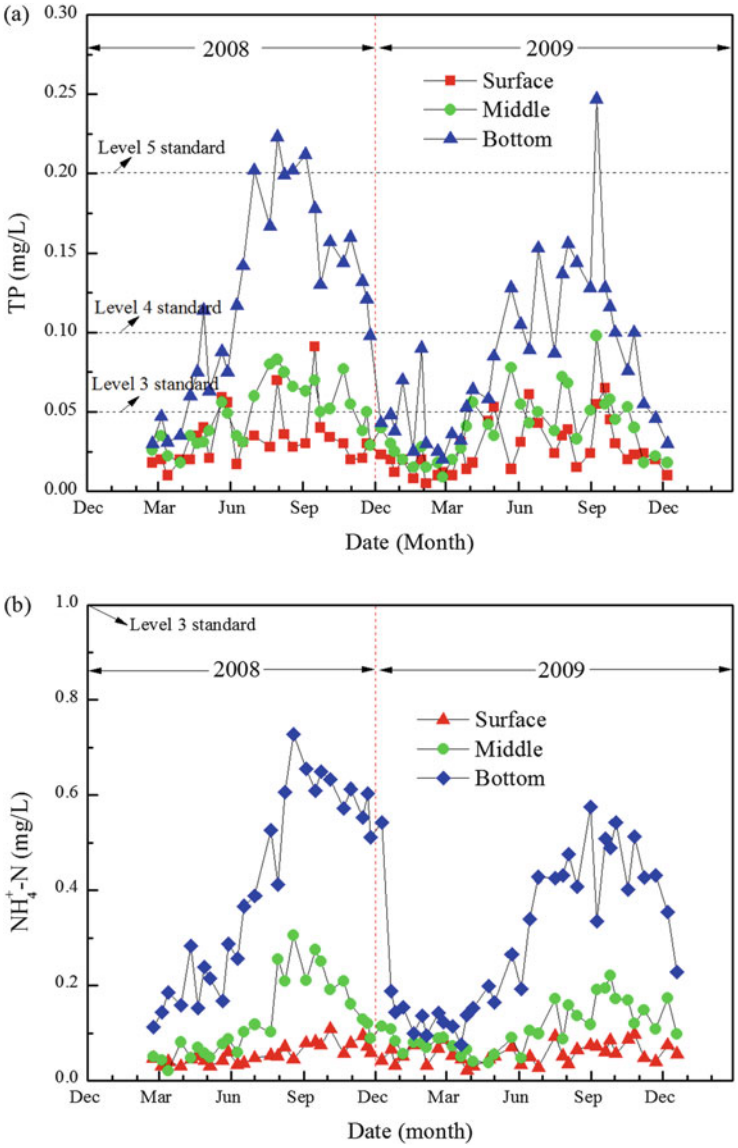

Fig. 5 The changes of TP (**a**) and ammonium (**b**) concentrations with date in Heihe Reservoir

In fact, the different response between TP and NH_3-N to DO is mainly due to the changes of the water pH. pH is not the main factor which would affect NH_3-N release. Even in the extreme pH (3 or 10) conditions, the NH_3-N release quantity did not undergo a large change. However, it is different to TP. In the sediment of Heihe Reservoir, inorganic phosphorus accounted for 65–73 %, from which the phosphorus in water was largely released. Inorganic phosphorus was composed of

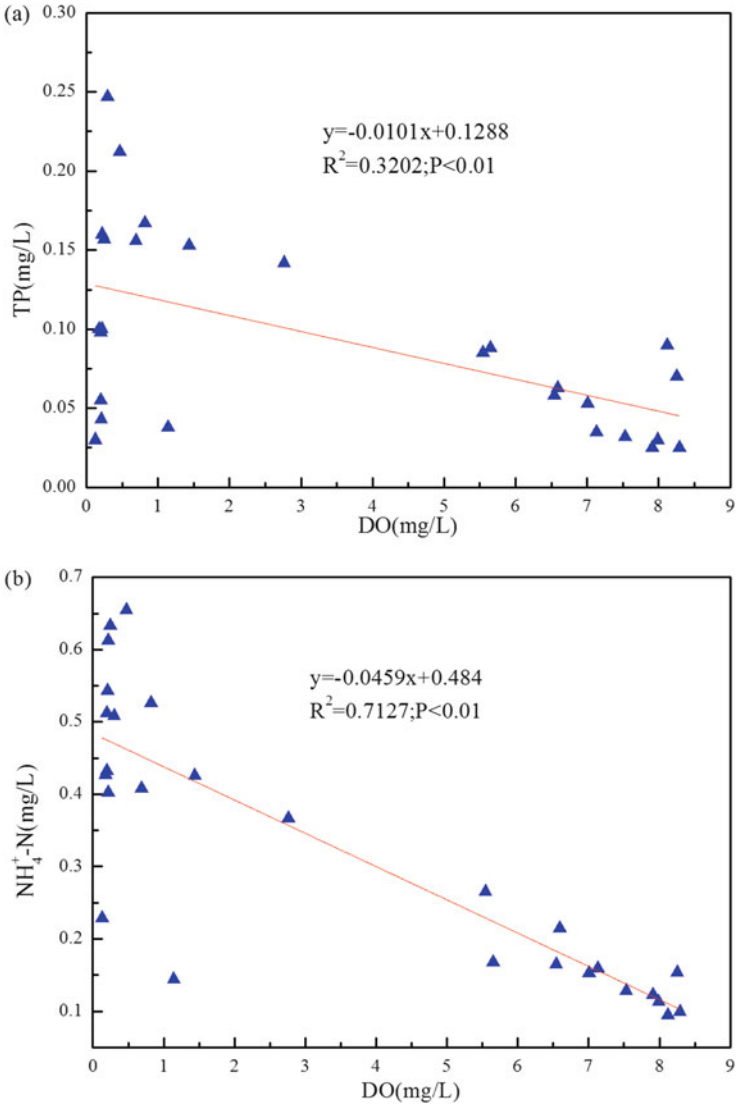

Fig. 6 The correlation of TP (**a**) and ammonium (**b**) with DO in Heihe Reservoir

Ca-P (50–55 %), Fe/Al-P (26–31 %), and occluded phosphate (O-P, 14–24 %). Ca-P is normally steady and dissolved in an acidic environment. O-P is only dissolved in strongly acidic and reductive solutions. Fe/Al-P is active and easy to release, and high pH and low DO promote its release. In anaerobic conditions, Fe^{3+} is reduced to Fe^{2+}; at the same time, the phosphorus in Fe/Al-P begins to be released. However, because of the accumulation of Fe^{2+} and PO_4^{3-}in the pore water of sediment, the diffusion resistance increased, which limited the phosphorus release. When the pH

is relatively high, Fe^{2+} turns to $Fe(OH)_2$, which promotes the rate of phosphorus release. This process is shown as follows:

$$FePO_4 + 2OH^- + e^- \leftrightarrow {PO_4}^{3-} + Fe(OH)_2 \downarrow$$

$$Fe(OH)_2H_2PO_4 + 2OH^- + e^- \leftrightarrow {PO_4}^{3-} + Fe(OH)_2 \downarrow + 2H_2O$$

Moreover, with oxygen consumption, the pH in the bottom water gradually increases and the Fe/Al-P release pathway is hampered. Ca-P would dissolve to a certain extent. TP release is a complicated issue, because it is affected by many factors and different kinds of phosphorus have various contributions to the phosphorus concentration in overlying water.

(4) The Release of Metal Pollutants in Heihe Reservoir

The seasonal temperature stratification structure in a reservoir directly or indirectly affected the water environmental characteristics. Behaviors at the interface between water and sediment of the sensitive oxidation–reduction elements, such as Fe and Mn, could be indicators of the changes in the water environment [5].

Vertical distributions of the total Fe concentration during different seasons in Heihe Reservoir are shown in Tables 11, 12, 13, and 14. The monitoring results indicated that the total Fe change rule was closely related to the cycled heat stratification in the reservoir. In spring, at the beginning of the heat stratification, oxygen was plentiful in the bottom water and the pH was a little alkaline [6]. In these conditions, an insoluble high valence iron compound with weak transfer ability was formed on the surface of the sediment and accumulated. The oxidation and reduction of iron compounds proceeded in the sediment and did not diffuse into the overlying water. Therefore, the total iron in the vertical water column was very low and not higher than the standard value.

In summer (Table 12), with the formation of heat stratification structure, below the thermocline, the oxygen declined and the water environment turned anaerobic and anoxic. The decomposition of organic matter made the water acidic and the high valent Fe as the electron acceptor was reduced to low valent. The low valent Fe as ions has strong transfer ability, which then diffused to the pore water in sediment and was transferred into overlying water by concentration gradients. Therefore, in this period, the Fe concentration in the middle and bottom waters began to increase. But in the upper water, the Fe concentration was still very low, due to the higher DO concentration and the bottleneck of thermocline on the vertical profile.

In autumn (Table 13), with the heat stratification being maintained and the DO concentration in the bottom of the reservoir decreasing further, the "transfer–release–diffusion" process of Fe was intensified. The total iron concentration in the bottom water was above the standard value limit (0.3 mg/l) in the environmental quality standard of surface water (GB 3838–2002). At the same time, with the convection in the upper water and decrease of the thermocline thickness, there is a little increase of the total iron concentration in the vertical water column, which was not above the standard value limit due to higher DO and the limited release and diffusion.

Table 11 The vertical distribution of total iron concentration in Heihe Reservoir in spring

Date	Depth (m)	Temperature (°C)	DO (mg/L)	pH	Total iron (mg/L)
2008-03-09	1.20	6.11	10.04	7.46	<0.03
2008-03-09	3.89	5.46	9.88	7.36	<0.03
2008-03-09	10.51	5.39	9.86	7.33	<0.03
2008-03-09	20.63	5.33	9.71	7.33	<0.03
2008-03-09	30.37	5.32	9.48	7.31	<0.03
2008-03-09	40.81	5.28	8.97	7.27	<0.03
2008-03-09	50.56	5.25	8.49	7.26	<0.03
2008-03-09	56.03	5.22	8.22	7.26	<0.03
2008-03-09	65.53	5.20	8.17	7.24	<0.03
2008-03-09	80.76	5.21	7.99	7.22	<0.03

Table 12 The vertical distribution of total iron concentration in Heihe Reservoir in summer

Date	Depth (m)	Temperature (°C)	DO (mg/L)	pH	Total iron (mg/L)
2008-06-30	2.84	21.06	8.50	8.57	<0.03
2008-06-30	12.87	19.95	7.28	7.62	<0.03
2008-06-30	22.73	6.96	6.44	7.04	<0.03
2008-06-30	32.54	6.10	6.60	6.83	<0.03
2008-06-30	42.70	5.84	5.89	6.78	0.033
2008-06-30	52.92	5.72	4.17	6.60	0.041
2008-06-30	62.74	5.69	3.22	6.49	0.058
2008-06-30	68.43	5.92	2.76	6.40	0.072

Table 13 The vertical distribution of total iron concentration in Heihe Reservoir in autumn

Date	Depth (m)	Temperature (°C)	DO (mg/L)	pH	Total iron (mg/L)
2008-10-11	0.80	16.40	8.16	7.96	0.068
2008-10-11	10.00	16.03	7.98	7.45	0.072
2008-10-11	20.00	15.25	6.39	7.16	0.083
2008-10-11	30.00	13.60	6.25	7.05	0.058
2008-10-11	40.00	13.33	5.79	6.92	0.072
2008-10-11	50.00	11.80	2.22	6.75	0.088
2008-10-11	60.00	8.22	1.57	6.49	0.096
2008-10-11	70.00	7.20	1.17	6.32	0.108
2008-10-11	82.00	6.90	0.43	6.27	0.144
2008-10-11	85.00	7.01	0.25	6.15	0.317

In winter, during the isothermal period, the whole reservoir was anoxic and the pH recovered to neutral and mildly alkaline. The release of Fe was hampered and the Fe concentration became uniform with convection. The Fe concentration in the vertical column decreased.

Table 14 The vertical distribution of total iron concentration in Heihe Reservoir in winter

Date	Depth (m)	Temperature (°C)	DO (mg/L)	pH	Total iron (mg/L)
2009-01-28	1.10	6.99	9.19	7.25	0.038
2009-01-28	5.14	6.96	9.03	7.21	0.033
2009-01-28	10.11	6.95	8.91	7.21	<0.03
2009-01-28	20.15	6.91	8.78	7.22	<0.03
2009-01-28	29.85	6.91	8.66	7.21	<0.03
2009-01-28	39.98	6.91	8.27	7.22	<0.03
2009-01-28	50.20	6.86	8.19	7.20	0.031
2009-01-28	59.55	6.83	8.27	7.21	<0.03
2009-01-28	64.98	6.72	8.28	7.20	<0.03
2009-01-28	74.00	6.52	8.26	7.19	0.041
2009-01-28	80.31	6.48	8.25	7.18	0.058

2.1.2 Pollutants Release from Sediment in Fenhe Reservoir Caused by Backward Stratification

In the middle of March 2005, the tap water from Fenhe Reservoir presented a yellow color and with fishy and rusty smell. The water monitor results showed that the ammonia concentration dramatically increased to 1.4 mg/l. After an increased dosage of chlorine, the residual chlorine kept decreasing. At the same time, the Fe and Mn concentrations in the water also increased.

The ammonium in water consumes a lot of chlorine and forms chlorinated disinfection byproducts, which are very harmful to humans. Based on the Chinese environmental quality standards for surface water, the highest tolerable value for an urban drinking water source is 1 mg/l. Moreover, the Chinese Ministry of Construction ruled for the water quality for class I that the ammonium and nitrite concentrations in drinking water should be below 0.5 mg/l and 0.1 mg/l, respectively. The European Community ruled guideline value for the concentration of ammonium in drinking water is 0.05 mg/l.

(1) Exogenous Pollution Analysis

Upstream of Fenhe Reservoir, the population was sparse and there were no large-scale enterprises discharging pollutants. Therefore, the water pollution did not result from industrial water discharge. In winter, the flow upstream was frozen and cut off, so there is no pollutant coming from runoff. Furthermore, the population of the town located upstream was only 20,000 and the domestic sewage was discharged discontinuously. However, the ammonium concentration in the water at the entrance of the domestic sewage was only 0.7 mg/l. Thus, domestic sewage was not the main reason for ammonium increase. Therefore, the sudden increase of ammonium should not be caused by exogenous pollution.

(2) Endogenous Pollution Analysis

March is a usual period in which ammonium was above the limit value, because the water was frozen and the reaeration pathway was hampered. The water became anoxic finally because of the consumption of oxygen by sediment in the reservoir. In this condition, the nitrogen compounds in the sediment were decomposed into ammonium, which diffused into water. At the same time, Fe and Mn dissolved in the water, which made the color turn to yellow. Moreover, in winter, the temperature in the bottom water was about 4 °C and the density of the water at this position was the greatest. The temperature in the upper water was near 0 °C and the density of the water was low. Then, the density stratification was formed, which resulted in the lack of exchange between the upper and bottom waters and the ammonium stayed in the bottom layer. At this time, the ammonium concentration in the upper water was low due to the lack of water exchange. However, in spring, after the ice melted, the temperature in the upper water increased to 4 °C and the water started to sink by gravity. Finally, with the assistance of wind, the water contained concentrated ammonium in the bottom water mixed with the whole water in the reservoir, which resulted in the ammonium concentration increasing sharply. Based on the monitor data, on March 15th, 2005, the ice in Fenhe Reservoir started to melt, and on March 17th, the ammonium concentration increased.

In order to testify the above hypothesis, the sediment in Fenhe Reservoir was analyzed, and the oxygen consumption experiments in sediment and water and ammonium release imitation experiments of sediment release were carried out.

(3) Sediment Analysis

In September 2005, the mud at 10 cm in sediment of the reservoir was analyzed by a bottom sampler. The distances from the sampler points to the dam were 0.3, 1.0, 1.7, and 2.5 km. The four samples were named as #1, #2, #3, and #4. The appearance of the mud samples is shown in Fig. 7. From sample #1 to #4, the color became weaker and weaker. Samples #1–#3 were ash black, and sample #4 was yellow. Sample #4 was of low viscosity and mainly constituted large particles of sand. The pH was measured directly. After that, the mud sample was dried and ground, and total organic matter, nitrogen, phosphorus, iron, and manganese were analyzed (Table 15). The concentrations of organic matter, nitrogen, and iron in samples #1–#3 were moderate, except for low manganese concentrations. The concentrations of organic matter and nitrogen in sample #4 were 30 % lower than those in samples #1–#3. The reason for the variation between samples #1–#3 and #4 was that the upstream depth sharply decreased at sample #4, which resulted in the increase of the flow rate, so that the clay, with plenty of organic matter, was hard to precipitate.

(4) Oxygen Consumption Experiments in Sediment and Water

An oxygen consumption experiment in sediment was carried out in winter at the sample points. The sediment samples were put in a bottle of volume 1000 ml. The sediment depth in the bottle was 5 cm, with a flat surface. The distilled water was slowly injected into the bottle and the initial DO was tested. Then, the lid of the bottle was fitted tightly and there was no air in the bottle. The bottle was placed at the bottom of the reservoir and removed after 25–28 h. The DO was tested again.

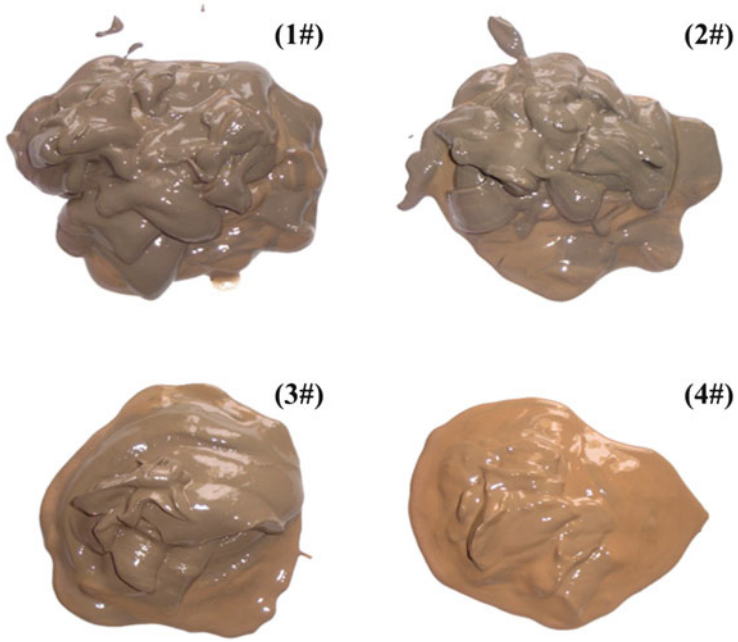

Fig. 7 Photos of sediment in Fenhe Reservoir

Table 15 The sediment composition of Fenhe Reservoir

Sample	pH	Organic matter (%)	Kjeldahl nitrogen (%)	TP (mg/kg)	Fe (mg/g)	Mn (mg/g)
#1	7.31	2.28	0.12	617	43.91	0.94
#2	7.18	2.36	0.15	667	44.41	0.94
#3	7.13	2.63	0.13	622	45.87	0.84
#4	7.28	1.76	0.1	590	42.55	0.99

There are four sample points along the axial direction of the reservoir and the distance between two adjacent points was 500 m (named 1, 2, 3, and 4). The rate of oxygen consumption in sediment (S_{DO}, mg/(m^{2}h)) was calculated using the following equation:

$$S_{DO} = \frac{(C_0 - C_e) \cdot V}{A \cdot T}$$

where C_0 is the initial DO concentration (mg/l), C_e is the final DO concentration, V is the bottle volume (l), A is the cross-sectional area (m^2) of the bottle, and T is time (h).

The rates of oxygen consumption in Fenhe Reservoir are shown in Table 16. The values of S_{DO} were relatively high and the average S_{DO} value was 11.8 mg/(m^2 h).

Table 16 The oxygen consumption in sediment of Fenhe Reservoir

Sample	Water volume (L)	Initial DO (mg/L)	Final DO (mg/L)	Experimental bottle area (m^2)	Time (h)	Oxygen consumption rate (mg/(m^2 h))
1	720	9.28	3.39	0.008065	37.0	14.21
2	730	8.9	3.16	0.008065	37.2	13.99
3	730	9.47	5.28	0.008065	41.0	9.25
4	735	10.51	5.96	0.008065	41.2	10.06

S_{DO} in sample #1 was the highest (14.21 mg/(m^2 h)) and that in sample #2 was the next highest. These results were consistent with the sediment mud analysis.

The oxygen consumption experiment in water was carried out as follows: first, the water from Fenhe Reservoir was put into a bottle and the initial DO concentrated was tested. Then, similarly to the experiment of oxygen consumption in sediment, the lid of the bottle was fitted tightly and there was no air in the bottle. The bottle was placed into the reservoir and removed after 22 days. The DO was tested again. There were three samples at depths of 1, 6, and 12.5 m, which denoted the upper, middle, and bottom waters in the reservoir. The rate of oxygen consumption in water (W_{DO}, mg/(l · d)) was calculated using the following equation:

$$W_{DO} = \frac{C_0 - C_e}{T}$$

where T is the time (d), C_0 is the initial DO concentration (mg/l), and C_e is the final DO concentration.

The rate of oxygen consumption in water is shown in Table 17 and the value was in the range 0.06–0.159 mg/(l · d). The variation among different layers may result from the different temperatures. The temperatures of the upper and bottom waters were 1 °C and 4 °C, respectively.

Based on the rate of oxygen consumption in sediment and water, it is entirely possible that the water in Fenhe Reservoir became anoxic at a certain depth when the surface water was frozen.

(5) Ammonium Release Imitation Experiment in Anaerobic Conditions

The ammonium release simulation experiments were carried out in the laboratory. First, 1000 ml of sediment from Fenhe Reservoir was put into a bottle with volume 5 ml. Second, 3500 ml of water from Fenhe Reservoir was slowly injected into the bottle. Then, the bottle was placed in a refrigerator at a temperature of 4 °C. Third, oxygen or nitrogen gas was injected into the bottle when needed by the experiment and the DO concentration was tested and adjusted twice every 24 h. There are four DO gradients: 0–1, 1–2, 2–3, and 3–4 mg/l, and the results are shown in Fig. 8.

As shown in Fig. 8, when the DO concentration decreased below 2 mg/l, the sediment release rate was relatively fast and, on the sixth day, the released ammonium concentration was higher than 1 mg/l. However, when the DO concentration

Table 17 The oxygen consumption of Fenhe Reservoir

Water	Initial DO (mg/L)	Initial date	Final DO (mg/L)	Final date	Time (d)	Oxygen consumption rate (mg/(L · d))
Surface	11.75	1–20	10.39	2–11	22.28	0.061
Middle	11.2	1–20	9.6	2–11	22.28	0.072
Bottom	11.47	1–20	7.92	2–11	22.28	0.159

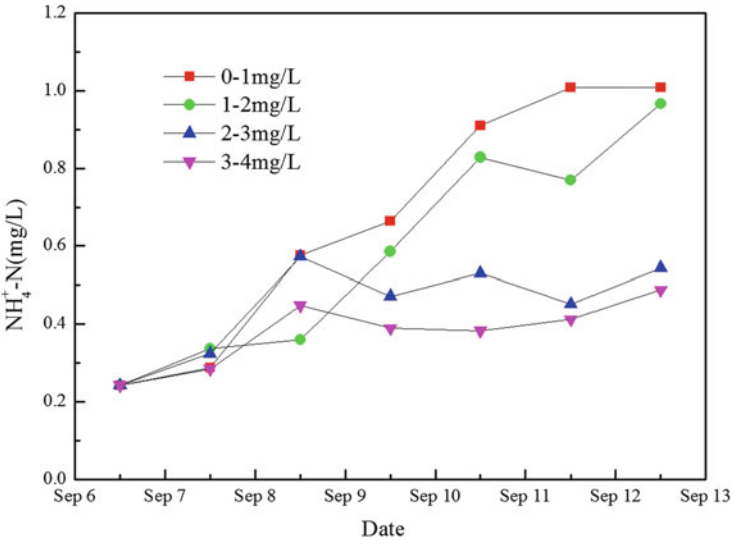

Fig. 8 Ammonium release from the sediment of Fenhe Reservoir

was 2–4 mg/l, on the sixth day, the released ammonium concentration was only 0.5 mg/l.

The truth of ammonium release was that ammonium adsorbed on the interface of sediment and water stopped turning into nitrite and accumulated in the water. There were various inorganic nitrogen translations on the interface of the sediment and water. The major place for mass cycle between the sediment and water was at a depth of 0–2 cm of sediment. It was always anaerobic inside the sediment, and in this condition, the organic matters containing nitrogen was turned into ammonium by ammonibacteria. The ammonium first went into the pore water in sediment and then diffused into overlying water. If there was enough oxygen in the overlying water, the ammonium would turn into nitrate by nitrification, which resulted in the increase of nitrate concentration in overlying water. The nitrate would diffuse back into the pore water by the concentration gradient and be converted to nitrogen gas by denitrification in anaerobic conditions. When there is little oxygen in overlying water, both nitrification and denitrification were hampered or stopped. Then, ammonium with high concentration would be accumulated in the pore water in sediment and overlying water.

Therefore, based on the monitor and experimental results, the accumulation and release of concentrated ammonium during the frozen period may be the main reason for the sharp increase of ammonium in Fenhe Reservoir.

2.2 *Endogenous Pollution Caused by Phytoplankton Death and Reproduction*

Eutrophication, algae reproduction and death, and water bloom are other main reasons for the deterioration of water quality in reservoirs [7]. Heat stratification played an important role in the growth of phytoplankton and evolution of community structure. Steady heat stratification structure may result in water bloom; thus, serious water bloom often happened in summer. In the mixing period of reservoirs, with the decrease of temperature, most of the algae were died, deposited, and decomposed, which resulted in fast expenditure of the oxygen in water. The residual algae which were not completely decomposed would deposit on the surface of sediment, which would increase the oxygen expenditure in sediment [8]. Furthermore, during the process of harmful algae decomposition, extracellular microcystins would be released into the water, which would endanger the water supply security.

2.2.1 Eutrophication Caused by Algae Reproduction in Zhoucun Reservoir

(1) Algae Species in Zhoucun Reservoir

There were seven phyla, 57 genera, and 122 species in Zhoucun Reservoir based on the monitor results during April 2012 to November 2013. *Chlorophyta*, cyanobacteria, and *Bacillariophyta* accounted for90.1 %. *Chlorophyta* was the most common and accounted for 46.7 %, including 26 genera and 57 species. Cyanobacteria accounted for 20.5 %, including 13 genera and 25 species. *Bacillariophyta* accounted for 23 %, including 13 genera and 28 species. And *Pyrrophyta*, *Euglenophyta*, *Chrysophyta*, and *Cryptophyta* accounted for 1.6 %, 5.7 %, 0.8 %, and 1.6 % respectively (Table 18).

In spring, *Chlorophyta* and *Bacillariophyta* were the most common. The dominant genera were *Cyclotella*, *Synedra*, *Stephanodiscus*, and *Cocconeis*, which belonged to *Bacillariophyta*, and *Scenedesmus*, *Ankistrodesmus*, *Chlorococcum*, and *Chlamydomonas* belonged to *Chlorophyta*. The dominant genera of *Chlorophyta* were mainly distributed in the surface water and the dominant genera of *Bacillariophyta* were mainly distributed in the middle and bottom waters. On the vertical profile, from the upper to the bottom waters, *Chlorophyta* decreased from 48.4 to 44.6 %, but *Bacillariophyta* increase from 36.9 to 49.7 % (Table 19).

Table 18 Algae species in Zhoucun Reservoir

Phyla	Class	Order	Family	Genera
Cyanophyta	*Cyanophyceae*	*Chroococcales*	*Chroococcaceae*	*Microcystis*, *Chroococcus*, *Coelosphaerium*, *Merismopedia*, *Dactylococcopsis*
		Hormogonales	*Nostocaceae*	*Anabaenopsis*, *Nostoc*, *Anabaena*
			Oscillatoriaceae	*Spirulina*, *Oscillatoria*, *Phormidium*, *Lyngbya*
Cryptophyta	*Cryptophyceae*		*Cryptomonadaceae*	*Cryptomonas*
Pyrrophyta	*Dinophyceae*	*Peridinales*	*Ceratiaceae*	*Ceratium*
			Peridineaceae	*Peridinium*
Chrysophyta	*Chrysophyceae*	*Chrysomonadales*	*Mallomonadaceae*	*Mallomonas*
Xanthophyta	*Xanthophyceae*	*Heterotrichales*	*Tribonemataceae*	*Tribonema*
Bacillariophyta	*Centricae*	*Coscinodiscales*	*Coscinodiscaceae*	*Melosira*, *Cyclotella*, *Coscinodiscus*
	Pennatae		*Fragilariaceae*	*Tabellaria*, *Synedra*
		Biraphidinales	*Naviculaceae*	*Gyrosigma*, *Frustulia*, *Navicula*
			Cymbellaceae	*Cymbella*
		Monoraphidinales	*Achnanthaceae*	*Cocconeis*
		Aulonoraphidinales	*Nitzschiaceae*	*Nitzschia*
Euglenophyta	*Euglenophyceae*	*Euglenales*	*Euglenaceae*	*Euglena*
Chlorophyta	*Chlorophyceae*	*Volvocales*	*Chlamydomonadaceae*	*Chlamydomonas*, *Chlorogonium*
			Volvocaceae	*Gonium*, *Pandorina*, *Eudorina*
			Haematococcaceae	*Rhodella L.V.Evans*
		Tetrasporales	*Palmellaceae*	*Sphaerocystis R. Chodat*
			Coccomyxaceae	*Fusioidea*
		Chlorococcales	*Chlorococcaceae*	*Chlorococcum*, *Golenkinia*, *Schroederia*
			Chlorellaceae	*Chlorella*, *Tetraedron*
			Oocystaceae	*Ankistrodesmus*, *Attheya*
			Sorastraceae	*Tetrachlorella*
			Hydrodictyaceae	*Pediastrum*
			Scenedesmaceae	*Scenedesmus*, *Tetrastrum*
	Conjugatophyceae	*Desmidiales*	*Desmidiaceae*	*Closterium*, *Penium*

Table 19 The changes of dominant genera with time and space in Zhoucun Reservoir

		Spring		Summer		Autumn		Winter	
	Dominant genera	sur.	bot.	sur.	bot.	sur.	bot.	sur.	bot.
1	*Cyclotella*	+	+					+	+
2	*Stephanodiscus*	+					+		
3	*Ankistrodesmus*	+						+	
4	*Cocconeis*	+							
5	*Chlorella*			+	+	+	+	+	
6	*Synedra*		+		+		+	+	+
7	*Microcystis*			+		+			
8	*Chodatella*	+							
9	*Chlorococcum*								
10	*Oocysts*								+
11	*Chlamydomonas*							+	
12	*Anabaena*			+		+			
13	*Lyngbya*								
14	*Chroococcus*			+	+	+			
15	*Tabellaria*		+						
16	*Scenedesmus*	+							

sur. stands for the surface layer of the reservoir
bot. stands for the bottom layer of the reservoir

In summer, *Cyanophyta* was the most common and *Chlorophyta* was the next most common, which, together, accounted for 80–90 % of all algae, whereas the ratio of *Bacillariophyta* decreased. On the vertical profile, the ratio of *Chlorophyta* decreased from the upper to the bottom waters and *Cyanophyta* was in reverse [9]. The algae species in summer was limited and the dominant genera were *Chlorella*, which belonged to *Chlorophyta*, and *Microcystis*, *Anabaena*, and *Chroococcus*, which belonged to *Cyanophyta*. *Microcystis* was mainly distributed on the upper water and the others were found throughout the water body.

In autumn, the ratio of *Cyanophyta* and *Chlorophyta* declined and the distributions on the vertical profile were the same as those in summer. The dominant genera were *Stephanodiscus* and *Synedra, which belonged* to *Bacillariophyta*, *Chlorella*, which belonged to *Chlorophyta*, and *Chroococcus*, *Lyngbya*, and *Anabaena*, which belonged to *Cyanophyta*. *Chlorella* was found all over the reservoir and the dominant genera of *Cyanophyta* was distributed in the upper and middle waters.

In winter, the community structure of phytoplankton in whole water was similar. *Cyanophyta*, *Chlorophyta*, and *Bacillariophyta* accounted for 14 %, 52 %, and 30 % respectively. The dominant genera were *Cyclotella* and *Synedra*, which belonged to *Bacillariophyta*, and Chlorella, *Chlamydomonas*, and *Chlamydomonas*, which belonged to *Chlorophyta*. The distributions of the dominant genera on the vertical profile were the same as those in spring.

The community structure of phytoplankton was changed with the eutrophication condition. Normally in a dystrophic reservoir, the dominant genera were

Chrysophyceae and *Xanthophyta*. In a mesotrophication reservoir, the dominant genera were dinoflagellates, *Cryptomonas*, and *Bacillariophyta*. And in a eutrophic type reservoir, the dominant genera were *Cyanophyta* and *Chlorophyta*. In Zhoucun Reservoir, in summer, the dominant genera were *Cyanophyta* and *Chlorophyta*, which were distributed in the upper and middle waters. These results indicated that Zhoucun Reservoir belonged to the eutrophic type reservoir.

(2) Temporal and Spatial Variation of Algae Abundance in Zhoucun Reservoir
The intensity change of phytoplankton in Zhoucun Reservoir was of a unimodal distribution every year [10]. The change in the bottom water was small but very obvious on the vertical profile.

In spring, although the light time increased, phytoplankton in the upper water still grew slowly, due to the low temperature. The density of phytoplankton in the bottom water remained unchanged because of low temperature and limited light. Thus, on the vertical profile, the density of phytoplankton in the upper water was a little higher than that in the bottom water (Fig. 9).

In summer, the temperature and light reached the best values for phytoplankton growth and there were plenty of nutrients in Zhoucun Reservoir, which resulted in the density of phytoplankton growing exponentially. The maximum density of phytoplankton was reached in August (1.39×10^8 cell/l). The density of phytoplankton decreased quickly due to the decrease of temperature and light with depth. Above a depth of 8 m, the density of phytoplankton changed little due to the relatively even temperature and abundant sunshine.

In autumn, the density of phytoplankton in the upper water decrease rapidly due to the decline in temperature and limited sunshine. In the bottom water, the density of phytoplankton did not decrease obviously because of the phytoplankton sedimentation from the upper water. On the vertical profile, the density of phytoplankton was distributed similarly to that in summer.

In winter, the density of phytoplankton declined to the lowest level in the whole year because of the low temperature and weak light. Due to the "turnover" phenomenon in Zhoucun Reservoir that happened in the autumn of 2012, the upper and the bottom waters mixed and there was no obvious difference in the density of phytoplankton on the vertical profile.

(3) The Relation Between Algae and Water Quality in Zhoucun Reservoir
To simplify the experiment, only the phytoplankton species and environmental factor in upper water were analyzed because the phytoplankton was concentrated in the upper layer of the reservoir. The relation between algae and water quality in the upper layer of Zhoucun Reservoir is shown in Table 20. The dominant genera of phytoplankton are shown in Table 19 and the results of the analyses are shown in Table 21 and Fig. 10.

As shown in the correlational analysis, the algae in Zhoucun Reservoir were highly correlated with temperature, pH, turbidity, and total phosphorus, but were inversely correlated with the ratio of nitrogen and phosphorus.

The first two axes of the results in the redundancy analysis (RDA) included information of 91.9 % between phytoplankton and environmental factors. The

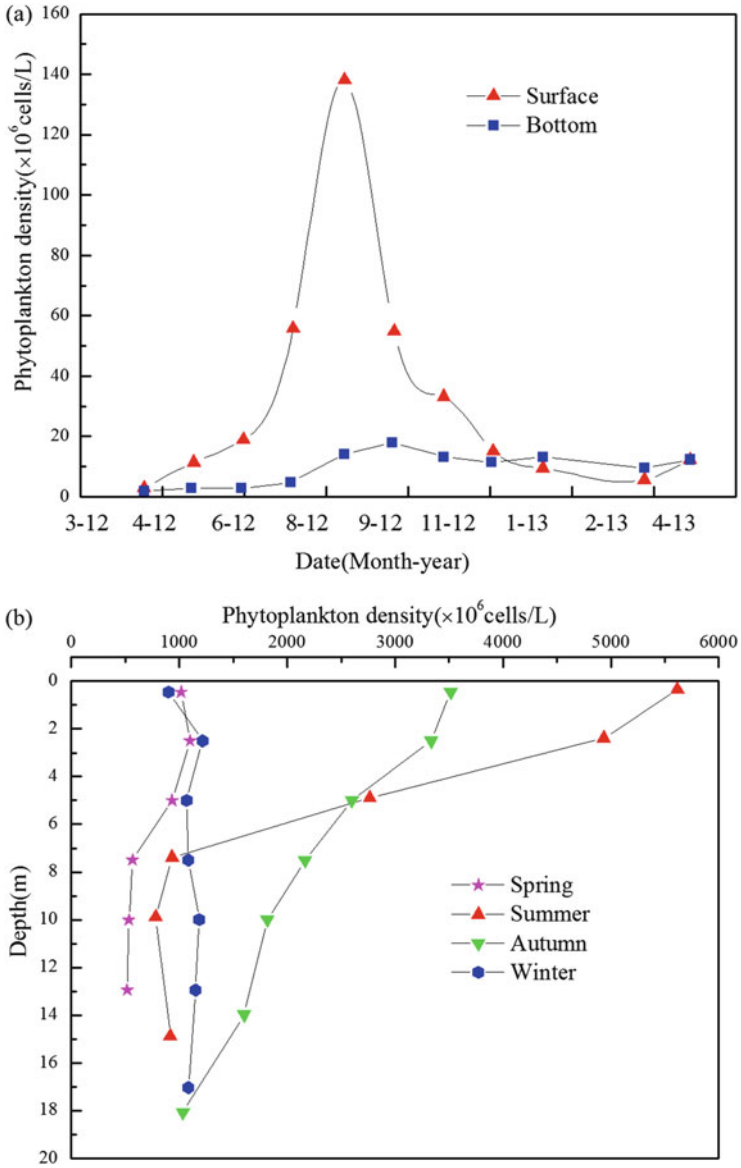

Fig. 9 The algae abundance changes with time (a) and space (b) in Zhoucun Reservoir

characteristic values of axes 1 and axes 2 were 0.591 and 0.169, respectively. The correlation coefficient between environmental factors and phytoplankton was 1 (Table 22).

In the RDA ordination diagram, the angle between two arrows of dominant genera stands for the correlation of the two algae species; the higher angle, the

Table 20 The water quality of the surface layer in Zhoucun Reservoir

Date	Algae abundance (10^4 cells/L)	Chlorophyll (μg/L)	Rainfall (mm)	Water level (m)	Temperature (°C)	DO (mg/L)	pH	Turbidity (NTU)	TN (mg/L)	NO_3^- (mg/L)	NO_2^- (mg/L)	NH_4^+ (mg/L)	TP (mg/L)	N/P	Fe (mg/L)
Apr-12	326	3.32	36.5	125.00	15.7	9.44	8.68		3.24	3.08	0.032	0.290	0.037	87.6	0.149
May-12	108	1.01	8	124.57	22.6	8.53	8.53		2.44	1.84	0.035	0.548	0.023	105.9	0.015
Jun-12	2397	22.50	9	123.94	25.2	10.52	8.72		2.61	1.20	0.032	0.075	0.023	113.5	0.031
Jul-12	7774	65.71	271	125.22	28.2	14.59	10.16	33.8	2.60	1.04	0.217	0.450	0.065	40.2	0.149
Aug-12	9371	75.58	200.5	125.47	27.2	10.29	10.07	18.2	2.40	1.13	0.217	0.060	0.065	36.9	0.236
Sep-12	4863	42.66	110	127.63	23.2	7.25	9.86	9.3	2.57	2.01	0.084	0.550	0.046	55.9	0.200
Oct-12	2351	38.43	9	127.82	20.3	9.69	8.48	7.74	2.25	1.61	0.090	0.375	0.048	46.8	0.118
Nov-12	1026	16.54	59.5	127.66	12.7	10.40	8.3	5	2.46	1.66	0.112	0.680	0.041	60.0	0.087
Dec-12	1114	14.62	39	127.47	6.5	11.65	8.11	3.5	2.56	1.70	0.080	0.167	0.023	111.0	0.030
Feb-13	693	8.78	12.5	127.06	3.8	10.77	8.35	2.5	2.20	1.80	0.051	0.375	0.024	93.2	0.015
Mar-13	1143	5.31	10.5	126.82	7.6	11.93	8.5	3.3	2.82	1.91	0.029	0.072	0.027	104.4	0.026
Apr-13	119	0.94	21	126.48	11.9	10.05	8.36	3.4	2.56	1.98	0.032	0.078	0.028	91.4	0.026

Table 21 The correlation of algae abundance and environmental factors in Zhoucun Reservoir

	Algae abundance	Chlorophyll	Rainfall	Water level	Temperature	DO	pH	Turbidity	TN	NO_3^-	NO_2^-	NH_4^+	TP	N/P	Fe
Algae abundance	1.000														
Chlorophyll	0.953**														
Rainfall	0.457*	0.498*													
Water level	0.115	0.270	0.015												
Temperature	0.749**	0.687**	0.480*	−0.224											
DO	0.133	0.051	0.169	−0.077	−0.101										
pH	0.732**	0.637**	0.426	−0.166	0.893**	−0.043									
Turbidity	0.900**	0.897**	0.565*	−0.113	0.868**	−0.152	0.668**								
TN	−0.105	−0.160	−0.063	−0.319	−0.147	−0.130	−0.140	−0.127							
NO_3^-	−0.482*	−0.442	0.036	0.138	−0.317	−0.392	−0.173	−0.433	0.299						
NO_2^-	0.603**	0.738**	0.299	0.404	0.424	−0.067	0.401	0.624**	−0.246	−0.470*					
NH_4^+	0.010	0.169	0.076	0.417	0.209	−0.235	0.111	0.293	−0.175	0.181	0.390				
TP	0.703**	0.771**	0.679**	0.272	0.602**	−0.036	0.620**	0.900**	−0.301	−0.149	0.620**	0.219			
N/P	−0.640**	−0.700**	−0.597**	−0.228	−0.559*	−0.061	−0.613**	−0.851**	0.498*	0.292	−0.589**	−0.178	−0.955**		
Fe	0.635**	0.709**	0.469*	0.134	0.435	−0.046	0.592**	0.813**	−0.121	−0.166	0.482*	0.059	0.801**	−0.784**	1.000

* stands for the significance less than 0.01
** stands for the significance less than 0.05

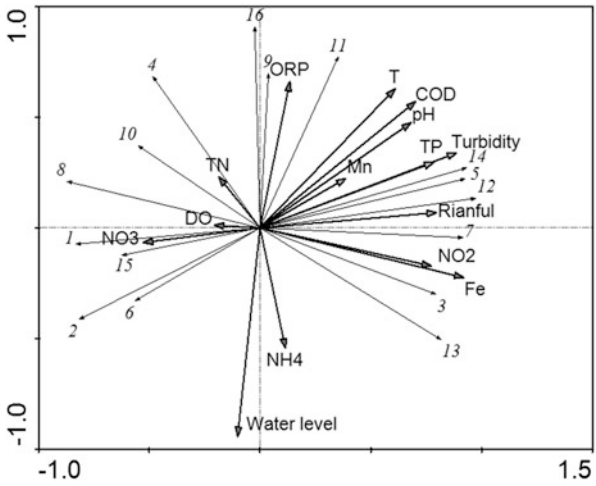

Fig. 10 The RDA diagram between phytoplankton and environmental factors of the reservoir

Table 22 RDA statistical results

Axis	1	2	3	4
Characteristic value	0.591	0.169	0.095	0.063
Accumulative species percentage (%)	59.1	76	85.6	91.9
Accumulative percentage of the correlation of species and environment (%)	59.1	76	85.6	91.9
The correlation of species and environment	1	1	1	1

higher correlation. The same arrow direction stands for a positive correlation and the reverse arrow direction stands for a negative correlation. The length of the environmental factor arrow stands for the impact of each factor on the dominant genus and the angle stands for the correlation between the factor and the dominant genus [11]. As shown in Fig. 10, T, TP, and water level were the main factors affecting the phytoplankton community structure in Zhoucun Reservoir. TN, Mn, and NO3- had minimal impact on the phytoplankton community structure. *Chlorella* and *Chlamydomonas*, which belonged to *Chlorophyta*, and *Chroococcus* and *Anabaena*, which belonged to *Cyanophyta*, were in the first quadrant. These kinds of algae and T, turbidity, COD, TP, and pH showed strong positive correlation. *Cyclotella*, *Synedra*, and *Stephanodiscus*, which belonged to *Bacillariophyta*, were mainly distributed in the third quadrant and showed strong negative correlations with T, turbidity, COD, TP, and pH. Moreover, *Scenedesmus* and *Chlorococcum* in *Chlorophyta* and water level showed negative correlations. *Ankistrodesmus* and *Lyngbya* showed strong correlations with iron [12].

2.3 Endogenous Pollution Caused by Aquaculture

High-density cage fish culture needs a large quantity of bait to be put into the reservoir. The fish bait, as nutrients, will partly be eaten as food by fish and partly be distributed into the water and deposited onto the sediment, resulting in secondary pollution [13]. If the cage culture exceeds the environmental carrying capacity, the water quality will be deteriorated and have a fishy odor, which heavily endangers people's lives and health.

Modern cage culture is an intensified culture method which cultures fishes in a cage made of metal or other chemical material mesh and, in China, started from the 1970s. At the beginning, the natural plankton in the reservoir was used as bait and, later, the plankton was replaced by artificial synthetic diet. Although cage culture has a lot of advantages, such as less investment, high yield, and accessible fishing, the harmful effect of the culture on the water environment became more and more serious with unrestricted increase of the culture scale and strength, which included the pollution of baits, metabolite waste, fish medicine, and so on [14].

Recently, the effects of residual baits and metabolite wastes on the water quality became more and more highlighted and are mainly as shown below:

(1) Baits increased the N and P nutrients concentration. N and P nutrients in baits and fishy waste, suspended particles, and organic matters became the main sources of eutrophication. The bait of cage carp culture included 36 % protein, in which 62.3 % and 22 % of N and P were discharged in the water of the reservoir. Almost all studies indicated that TP and TN concentrations in the culture region were higher than those in normal water, and the greater the density of the cage culture, the greater the TP and TN increases. Most of the studies showed that inorganic nitrogen was ammonia based and there was a lot of organic nitrogen. Moreover, the TP concentration increased with depth, which resulted from the deposition of carbon-containing matters.
(2) Suspended solids decreased the DO concentration and transparency. The quantity of suspended solids increased by residual baits, fish waste, and fish disturbance. On the other hand, the nutrient increase prompted the reproduction of plankton, which also resulted in the increase of the quantity of suspended solid and the decrease of water transparency. In series, the decrease of water transparency would result in the weak photosynthesis of phytoplankton and low DO concentration.
(3) Culture changed the physicochemical character of sediment. The transition and deposition of substrates in sediment were changed by cage culture. Additional deposition of TP and TN from the residual bait resulted in the surface layer in sediment turning anaerobic, in which conditions, a lot of harmful gas released by the sulfate reduction is catalyzed by bacteria.

2.3.1 Water and Sediment Pollution Caused by Aquaculture in Zhoucun Reservoir

(1) Cage Culture in Zhoucun Reservoir

Zhoucun Reservoir was built in 1959 and began operation in 1960. It is a middle-sized (84×10^6 m^3) reservoir which is based on agriculture irrigation and flood control, combined with electricity generation and fish culture. Cage culture in Zhoucun Reservoir began in the 1980s and thrived in the 1990s, with 20 % of the reservoir area and more than 10,000 cages in peak season. The high-density culture surpassed the environmental bearing capacity and resulted in the deterioration of water quality and large economic losses. For this situation, in 2008, cage rectification was carried out by the water conservancy bureau of Zaozhuang. Almost all cages in the reservoir were cleared and the water quality was relatively improved. However, because years of pollutants deposited on the sediment was not cleared and upstream of the reservoir was polluted heavily, the water pollution condition was still challenging in Zhoucun Reservoir.

(2) The Effects of Cage Culture on the Sediment

After more than 30 years of cage culture, there were large amounts of baits, fertilizers, medicines for fish, and fish waste in the sediment, which were potential pollution sources and could be released into the overlying water, yielding appropriate condition resulting in water bloom. The concentrations of organic matters, TP, sulfide, and sulfate-reducing bacteria are shown as below:

(I) Organic matters and TP

The concentrations of organic matters and TP in the sediment of seven reservoirs in China are shown in Table 23. The concentration of organic matter in the sediment of Zhoucun Reservoir was largely higher than that of other reservoirs. Moreover, TP concentration in the sediment of Zhoucun Reservoir was lower than that of Miyun Reservoir and Xili Reservoir, but much higher than that of Fenhe Reservoir, Yuqiao Reservoir, and Qingshan Reservoir. When the DO concentration was below 1 mg/l, the phosphorus in sediment would release and the TP concentration in overlying water could be 0.25 mg/l and 0.51 mg/l in winter and in summer, respectively, exceeding the limit value (0.05 mg/l) in class III of water. These results indicated that the sediment in Zhoucun Reservoir was under a heavy pollutants load, which seriously endangered the water quality and has attracted great attention.

(II) Sulfide

Sulfide concentration in the sediment of Zhoucun Reservoir was ten times higher than that of Shibianyu Reservoir (Table 24), which resulted in not only the sulfide concentration exceeding the standard level in September, but also the water becoming odorous.

Table 23 The comparison of contents of TP and organic matter in Zhoucun and other reservoirs in China

Reservoir name	TP (μg /g)	Organic matter (%)
Zhoucun	513.28 ~ 1157.26	5.85 ~ 10.17
Miyun	497 ~ 1239	-
Yuqiao	437.50 ~ 478.37	2.13 ~ 2.39
Fenhe	628.5 ~ 679.4	2.19 ~ 2.37
Qingshan	41 ~ 96	1.20 ~ 1.72
Sanxia	622	-
Xili	1490	12.44(VSS)

Table 24 The quantity of sulfide in sediment

Sample	Unit	1	2	3	4	5
Sediment from Zhoucun Reservoir	mg/l	9.378	7.424	12.637	12.427	12.599
Sediment from Shibianyu Reservoir	mg/l	0.9631				
Dry mud from Zhoucun Reservoir	mg/mg	0.8853	0.7006	1.1927	1.173	1.1894

(III) Sulfate-reducing bacteria

The colony count of sulfate-reducing bacteria in the sediment of Zhoucun Reservoir was 4.5×10^4 cfu/g and the water content was 82.34 %, which equaled 2.5×10^5 cfu/g in dry mud. Moreover, the sulfate concentration in the water of Zhoucun Reservoir was 50–60 mg/l, which meant that, in anoxic conditions, the sulfate would be easily turned to sulfide by sulfate-reducing bacteria. Monitor data showed that the rates of oxygen consumption in winter (temperature equaling 4 °C) and summer (temperature equaling 10 °C) were 1.6 mg/($m^2 \cdot d$) and 1.9 mg/($m^2 \cdot d$), respectively, in the sediment of the reservoir, which meant that there was an anoxic condition for sulfate reduction.

References

1. Huang T, Li X, Ma W, Qin C, Zhang Y (2014) Dynamic characteristics of nutrients and causal analysis in eutrofic reservoir: a case study of Shibianyu reservoir. Desalination Water Treat 52 (7–9):1624–1635
2. Huang T, Li X, Rijnaarts H, Grotenhuis T, Ma W, Sun X, Xu J (2014) Effects of storm runoff on the thermal regime and water quality of a deep, stratified reservoir in a temperate monsoon zone, in Northwest China. Sci Total Environ 485:820–827
3. Wang S, Qian X, Han B, Luo L, Hamilton DP (2012) Effects of local climate and hydrological conditions on the thermal regime of a reservoir at tropic of cancer, in Southern China. Water Res 46(8):2591–2604

4. Cong H, Huang T, Chai B, Zhao J (2009) A new mixing–oxygenating technology for water quality improvement of urban water source and its implication in a reservoir. Renew Energy 34 (9):2054–2060
5. Gale PM, Reddy KR, Graetz DA (1992) Mineralization of sediment organic matter under anoxic conditions. J Environ Qual 21(3):394–400
6. Lovley DR, Phillips EJ, Lonergan DJ (1991) Enzymic versus nonenzymic mechanisms for iron (iii) reduction in aquatic sediments. Environ Sci Technol 25(6):1062–1067
7. O'Neil JM, Davis TW, Burford MA, Gobler CJ (2012) The rise of harmful cyanobacteria blooms: the potential roles of eutrophication and climate change. Harmful Algae 14:313–334
8. Xiao L, Wang T, Hu R, Han B, Wang S, Qian X, Padisák J (2011) Succession of phytoplankton functional groups regulated by monsoonal hydrology in a large canyon-shaped reservoir. Water Res 45(16):5099–5109
9. Reichwaldt ES, Ghadouani A (2012) Effects of rainfall patterns on toxic cyanobacterial blooms in a changing climate: between simplistic scenarios and complex dynamics. Water Res 46(5):1372–1393
10. Liu L, Liu D, Johnson DM, Yi Z, Huang Y (2012) Effects of vertical mixing on phytoplankton blooms in Xiangxi Bay of Three Gorges Reservoir: implications for management. Water Res 46(7):2121–2130
11. Te SH, Gin KY (2011) The dynamics of cyanobacteria and microcystin production in a tropical reservoir of Singapore. Harmful Algae 10(3):319–329
12. Joung S, Oh H, Ko S, Ahn C (2011) Correlations between environmental factors and toxic and non-toxic Microcystis dynamics during bloom in Daechung Reservoir, Korea. Harmful Algae 10(2):188–193
13. Stirling HP, Dey T (1990) Impact of intensive cage fish farming on the phytoplankton and periphyton of a Scottish freshwater loch. Hydrobiologia 190(3):193–214
14. Cornel GE, Whoriskey FG (1993) The effects of rainbow trout (Oncorhynchus mykiss) cage culture on the water quality, zooplankton, benthos and sediments of Lac du Passage, Quebec. Aquaculture 109(2):101–117

The Protection of Chinese Water Reservoirs

Gang Wen, Tinglin Huang, and Haibing Cong

Abstract Source water protection is the prerequisite for drinking water safety, and a reliable source of water is the guarantee for a safe water supply. Source water protection is via administrative, legal, economic and technical methods, and management to ensure the quality and quantity of source water. This chapter mainly elaborates on the protection of source water reservoirs based on the three following aspects: planning, division, and management. Protection planning includes isolation protection engineering planning, ecological restoration planning, and emergency capability planning. The division of protection areas is introduced based on three aspects: principle, method, and signs. The protection management includes water quality monitoring and evaluation, pollution management, ecological management, and integrated water management. In addition, three examples of reservoir water protection are illustrated, providing a reference for reservoir protection.

Keywords Reservoir protection • Management • Protection areas division

1 Planning of Reservoir Water Protection

1.1 The Main Contents of Reservoir Water Protection

Source water protection is the prerequisite for a drinking water supply, and reliable source water is the guarantee for a safe water supply. Source water protection is via administrative, legal, economic and technical means, rational development, and management to ensure the quality and quantity of water. In terms of water, overall planning, utilization, and stress-effective should be considered to avoid overexploitation and water depletion. Meanwhile, in terms of water quality, effective means should be taken to prevent water pollution and other public hazards, to reduce and eliminate harmful substances, and to strengthen the supervision and management of water pollution control.

G. Wen • T. Huang (✉) • H. Cong
School of Environmental and Municipal Engineering, Xi'an University of Architecture and Technology, Yanta Road 13, 710055 Xi'an, Shaanxi Province, P. R. China
e-mail: huangtinglin@xauat.edu.cn

T. Huang (ed.), *Water Pollution and Water Quality Control of Selected Chinese Reservoir Basins*, The Handbook of Environmental Chemistry 38,
DOI 10.1007/978-3-319-20391-1_4

Source water protection methods include legal regulatory measures, and management and technical measures. Some aspects are as follows:

1. The legislations for protecting source water should be strengthened and water protection regulations should be developed and improved.

   There are many water protection laws such as the "Water Law of the People's Republic of China", "Water Pollution Prevention and Control Law of the People's Republic of China", and the "Environmental Protection Law of the People's Republic of China". Meanwhile, local governments have also developed related water protection regulations or requirements in accordance with the actual situations in their regions. These legal documents and regulations are the guarantee of water conservation efforts. Water conservation should be based on and take advantage of these laws and regulations to promote the necessity and importance of water conservation, and also raise people's awareness of water protection. Enforcement of water protection laws should be enhanced and carried out strictly according to the laws. In the process of improving our regulatory system to protect drinking water sources, the successful experience of foreign countries combined with the actual situations in China should be considered. On the one hand, existing Chinese laws and regulations can be revised and improved under these circumstances. On the other hand, the relevant laws and regulations should be supplemented.
2. Implement unified management of the watershed and strictly control the emission of pollutants in the basin.

   Unified planning of water supply, drainage, and sewage treatment in the basin should be taken. In accordance with the pollutants bearing capacity of the basin, we should control the amount of total pollutants and solve the contradictions and conflicts between water supply and drainage. The layout of urban and industrial areas in the basin should be rationally planned [1]. Industry and farming which are likely to cause pollution, such as chemical, petroleum, mining, electroplating, and animal husbandry, should be moved to downstream towns.
3. Strengthen the water protection and reduce non-point source pollution.

   Soil erosion, siltation, and underground runoff reduction will lead to a decrease of the normal flow and reduce the safety of water supply [2]. Therefore, it is essential to strengthen the regulation and prevent the destruction of vegetation in the upper river. At the same time, human and animal sewage, spraying pesticides and fertilizers, and other activities, which may cause a wide range of non-point source pollution, should be avoided. Therefore, we should strengthen the human and animal management in the basin, limit the use of persistent and highly toxic pesticides, and make good use of intensive fertilization and other measures.
4. Enhance the monitoring and management of water quantity and quality.

   In terms of water quantity, it is essential to conduct surface water hydrological observations and forecasting. In the terms of water quality, a water pollution study should be conducted and evaluated to establish the water pollution

monitoring network to understand the water pollution situation and dynamics of various pollutants in time to prevent the contamination of source water.

5. Improve the technical levels of water protection.

   Based on the investigation of water pollution, researches should be carried out for different types of water pollutants in the migration and transformation of its pollution range, extent, and trends, to establish water quality models for different water sources and water quality prediction methods. We should adopt a more scientific method for calculating the amount of available source water in the basin, develop source water carefully, and ensure a reliable water supply.

1.2 The Isolation Planning for Protecting Reservoir Water

1.2.1 Source Water Protection District and Protective Measures

To prevent the intake points and their surrounding waters from contamination, the docking of fishing boats, swimming, and all activities that may contaminate water should be prohibited within a radius of no less than 100 m, and clear signs should be set in place.

To prevent the contamination of source water directly, it is forbidden to discharge industrial wastewater and domestic sewage into intake points from 1000 m upstream to 1000 m downstream. Waste residue should not be stacked within the scope of protection, and hazardous chemicals must be far away from warehouses. Special reservoirs and lakes for drinking should be enrolled into protection, depending on the specific circumstances [3–5].

In less than 10 m range outside water production districts, it is forbidden to set residential areas, livestock farms, and seepage toilets and pits, and must maintain good healthy conditions.

1.2.2 The Division of Water Protection Areas

The areas of water and land which are designated and required special protection to combat pollution of drinking water sources and ensure the quality of the water environment are called drinking water source protection areas. They are generally classified as first-grade protection areas, secondary-grade protection areas, and extended protection areas. The first-grade protection areas should meet the drinking water hygiene requirements, while the secondary-grade protection areas are mainly set to meet the water quality requirements under normal situations and ensure that there is enough time and buffer zones to take emergency measures under emergency situations. Extended protection areas are set to ensure the protection of drinking water sources and water quality [6, 7]. The protection scopes should include reservoir areas and a certain range of lands. The division method of protection areas is detailed in Sect. 4.2.

1.3 The Ecological Restoration Planning on Protecting Reservoir Water

For the ecological safety of source water protection areas, ecological restoration and ecological construction should be conducted to improve the natural purification capacity of protection areas, promote ecological cycles, and improve and protect the water quality of source water.

The ecological protection and restoration of source water has two basic contents, namely the protection of the water environment and the restoration of the aquatic ecosystem. Protection and restoration are conducted simultaneously. Firstly, the protection of the aquatic environment means protecting the water and wading sections, including protecting water quality and the pollution. Secondly, it is essential to take engineering measures to repair damaged water ecology and turn it into a virtuous circle.

1.3.1 Functions of Aquatic Ecosystems

Aquatic ecosystems include aquatic plants, animals, microorganisms, and aquatic environments. They are an organic whole and play different roles in water cycling and water self-purification processes.

In short, higher plants have the ability to purify water directly, while at the same time provide suitable habitat and food for other species, and promote the virtuous cycle of the ecological environment. Fish, protozoa, and metazoan can prey algae effectively to control eutrophication. The blooming of phytoplankton (algae) can pollute water and should be absolutely controlled. Herbivorous and carnivorous fish can eat higher plants, so fish and small animals should be appropriately controlled. On the other hand, their presence will prevent the overgrowth of certain higher plants to maintain the ecological balance. In the process of carrying out environmental protection and restoration, we should maintain the ecological balance and regulate the species and quantities moderately.

1.3.2 The Protection and Restoration of the Aquatic Ecosystem

The destruction of ecosystems is due to two reasons. On the one hand, it is due to the changes of abiotic environmental factors, making the environment deterioration and causing species extinction. On the other hand, the food chain is interrupted, and the balance in the proportion of biological populations is damaged. Some organisms are severely weakened or even die, whereas certain biological populations overgrow.

For source water, the objectives of ecosystem protection and restoration are water protection and water purification. Therefore, water ecological environment

protection and restoration of aquatic plants should be conducted. Specific measures are as follows [8]:

1. Control the input of exogenous pollution and protect the environments of biological survival. Reduce the effect of toxic and hazardous pollutants on aquatic organisms. Reduce the input of organic pollutants to prevent excessive decomposition of organic matters, which can consume oxygen in water and result in an anaerobic state, causing aquatic ecological deterioration.
2. Strengthen the protection of water and soil, and reduce the input of sediments. Sediment will cover aquatic organisms and plants to reduce water transmittance and hinder the photosynthesis of aquatic plants.
3. Control algal blooming. Cyanobacteria blooms can reduce the transmittance of lakes and available light. Furthermore, algae can adhere to the surface of the water plants, not only seriously hampering the exchange of materials during photosynthesis, but also leading to large populations of microorganisms, causing decay and death of aquatic plants. Mechanical harvesting, biological control, drug control, and other methods should be used to control algae [9].
4. Control the density of herbivorous and carnivorous fish, maintain the balance of the aquatic food chain, moderately feed the fish, and control algae growth.
5. Prohibit the destructive or excessive harvesting of aquatic organisms, and protect the normal process of reproduction.
6. Harvest the higher plants moderately to prevent excessive growth and water marsh.
7. Human-assisted and human-induced restoration methods can be used to remediate the destroyed aquatic environment. Human assistance is used to promote the natural recovery of aquatic plants. There are several methods of human assistance: manufacturing the shoal geographical environment conducive to plant growth, clearing up the bottom sediment, improving the light conditions, eliminating storm washing, and so on. Human-induced restoration means artificially planting aquatic plants.
8. Maintain the water levels of lakes and reservoirs, and protect the environment of biological diversity. Rational use of water resources should be arranged in the dry season.

1.4 The Emergency Planning on Protecting Water Reservoirs

To avoid or prevent the pollution of drinking water source and protect the water safety of residents, emergency projects should be constructed. The main contents of emergency projects include: construct an emergency system of source water and ensure effective operation of the system; develop emergency plans for drinking water source.

1.4.1 The Monitoring and Early Warning System of Source Water

Pollution can be divided into two types: conventional pollution and outburst pollution. Under normal circumstances, due to changes in environmental conditions and other natural causes, the outbreak of contamination belongs to conventional pollution, such as the outbreak of cyanobacteria. Outburst pollutions are caused by the input of chemicals, toxins, and other harmful substances due to sudden incidents, such as chemicals leakage in a traffic accident [10,11]. Outburst pollutions in drinking water sources include:

1. Large amounts of sewage are discharged into the upstream river, contaminating the drinking water source;
2. The security incidents in upstream drinking water sources result in highly toxic and harmful chemicals polluting the drinking water source;
3. Pollution incidents caused by human activities: water pollution incidents caused by urban and industrial enterprises;
4. Other activities, such as genetically modified organisms, pathogenic microorganisms, and viruses causing highly aggressive, infectious contamination events.

The water pollution emergency has the features of urgency, danger, and uncertainty. If it is not treated with a timely response and handling, it will bring great harm. So, we must strengthen the monitoring capacity and control of toxic and hazardous chemical contaminants, construct water quality forecasting and incident warning systems, and strengthen the management capacity of drinking water source [10]. The early warning systems are built based on the following four aspects:

1. Achieving the governmental guarantee. To establish the water supply emergency system, develop the scientific emergency plan, and resolve the drinking water pollution emergency.
2. Providing the technical support. Improve the mobile, rapid response, and automatic forecasting ability of the monitoring system, to achieve water quality automatically in key areas, waters, and water supply sources. It includes studies on how to select and protect emergency water sources, and how to disinfect and treat the emergency water supply.
3. Providing personnel guarantee. Invite expertise from universities, research institutes, and construction teams to ensure timely handling of the water pollution emergency.
4. Establishing a rapid and reliable water quality information processing system. Achieving and tracking the water quality information quickly and accurately, maintaining a 24-h service hotline in the relevant departments. Problems can be reported promptly and handled in a timely fashion once the water pollution emergency occurs [12,13].

1.4.2 Construction of the Emergency Source Water and Protection System

Constructing an alternative source of water is quite important. For a city with an urban population of over 200,000 and using surface water as drinking water source, warning and emergency plans should be established in continuous drought years. The alternative source water should be chosen based on the following principles. Firstly, the water should be have good sensory properties, including looking, smelling, and tasting; secondly, the water quality of the selected source water should be tested and meet the national source water standards.

In recent years, water pollution emergencies occurred frequently, and have a great influence on the water supply. How to avoid and solve these unexpected problems becomes quite important. So, water quality monitoring and warning system should be established.

2 Division of Reservoir Water Protection Areas

Drinking water protection areas refers to a certain areas of water and land designated to prevent drinking water sources from contamination and ensure the water quality of source water. Division of source water protection areas, setting up signs to clarify, and warning and reminding the boundaries of protection areas are very effective management tools to protect drinking water sources, and are the requirements of relevant laws and regulations. The State Environmental Protection Agency issued the "Technical Guideline for Delineating Source Water Protection Areas" [6], which clearly indicates the standard techniques and methods of delineating drinking water source protection areas.

Due to the acceleration of industrialization, the surrounding environments of many drinking water sources are contaminated, and water shortages in many cities are caused by water pollution. Therefore, drinking water source protection is imminent, and the division of drinking water source protection areas is an effective protective method. On one hand, protection areas should be large enough to meet the requirements of water quality protection. On the other hand, it should be as small as possible to reduce the negative impact of water source protection areas on the local economy.

2.1 The Division Principles of Source Water Protection Areas

The setting and division principles of drinking water source protection areas are as follows:

1. National regulations require that drinking water source protection areas should be set in drinking water sources. Drinking water source protection areas are divided into surface water source protection areas and groundwater source protection areas.

   Source water protection areas should include certain water areas and land areas. Drinking water source protection areas are generally classified as first-grade protection areas, second-grade protection areas, and extended protection areas in necessity. The source water intake point is the center of all protection areas. The "Surface Water Quality Standard" requires that source water protection is the priority target [14,15].
2. Water quality in source water protection areas must meet the water quality health standard and water environment quality standard.

   The water quality in first-grade protection areas should meet water quality standards (class II) in the "Surface Water Quality Standard" [16]. The water quality in secondary-grade protection areas should meet water quality standards (class III) in the "Surface Water Quality Standard" [16], while the water quality of water entering the first-grade protection areas should meet the water quality standards (class II) in the "Surface Water Quality Standard" [16].
3. Determine the technical indicators for delineating source water protection areas. The following factors should be considered [17,18]:

   Local geographical, hydrological, meteorological, and geological characteristics, hydrodynamic characteristics, the type of water pollution, pollution characteristics, the distribution of the drainage area, the size of water sources, and water demand should be considered. The range of source water protection areas should be quantitatively predicted and determined according to the above-mentioned characteristics in different areas.
4. Prevent direct pollution by human activities near the source water protection areas. Guarantee the water quality conforming to the regulated requirements under normal circumstances. Prepare urgent remediation methods and buffer areas to deal with water pollution emergency situations.
5. Balance the relationship between source water protection and economic development. Under the condition of ensuring water quality of protection areas, the source water protection areas should be as small as possible.

2.2 Division Method of Source Water Protection Areas

2.2.1 The Classification of Water Sources

Water sources made up of lakes and reservoirs are classified based on their sizes. Reservoirs with a storage capacity less than 0.1 million m^3 are defined as small reservoirs, 0.1–1 million m^3 are defined as medium-sized reservoirs, and more than 100 million m^3 are defined as large reservoirs. Lakes are classified based on the

surface area: lakes with surface areas less than 100 km^2 are defined as small reservoirs and others are defined as medium- and large-sized lakes.

2.2.2 Division of Protection Areas

(1) First-grade protection areas

1. Scope of water areas

   The whole water areas in small reservoirs and lakes are designated as first-grade protection areas. Model calculation methods are used to determine the scope of first-grade protection areas in medium and large lakes and reservoirs. When parts of water areas in medium and large lakes and reservoirs are designated as first-grade protection area, water hydrodynamic (flow, diffusion) characteristics and water quality analysis should be done to determine the scope of protection areas, where the water should meet the water quality standards (class II) in the "Surface Water Quality Standard" [16].

   In general, the first-grade protection areas are those with a radius of 300 m from the intake point in small lakes and medium-sized reservoirs, and with a radius of 500 m in large reservoirs and lakes.

2. Scope of land areas

   The land in the first-grade protection areas is designated to ensure the water quality in the protection areas, and the scope is determined by the following method. The land 200 m above the normal water level is the protection area in lakes and reservoirs. The depth range of first-grade protection areas is not lower than the health protection range of the drinking water source.

(2) Secondary-grade protection areas

1. Scope of water areas

   The secondary-grade protection areas are determined through model analysis and calculation. The radial distance from secondary-grade protection areas to the first-grade protection areas should be greater than that of the desired distance of pollutant attenuation from the class III to class II water quality standard [16]. With respect to small lakes and reservoirs, all the water areas outside first-grade protection areas are secondary-grade protection areas. With respect to large reservoirs, the water areas of secondary-grade protection areas are not less than 2000 m away from the first-grade protection areas.

2. Scope of land areas

   The land scope of secondary-grade protection areas is determined according to the major environmental problems.

   (a) When the non-point source pollution is the main pollution source, the depth range of secondary-grade protection areas are determined based

on the physical geography, environmental characteristics, and environmental management. The land boundary of secondary-grade protection areas cannot exceed the scope of the corresponding watershed basin. When the source water is seriously affected by non-point sources pollution, the seriously polluted regions should be classified into secondary-grade protection areas to facilitate effective control of these pollutants.

(b) Based on the terrain analysis. With regards to small reservoirs, the entire upstream watershed can be set as the secondary-grade protection areas. The secondary-grade protection areas of small lakes and medium reservoirs are above the normal water level and at a 2000 m horizontal distance. Large reservoirs can designate the areas less than 3000 m away from the first-grade protection areas as the secondary-grade protection areas.

(3) Extended protection areas

According to the scope of lakes and reservoirs basins, the distribution of pollution sources, and the influence on drinking water sources quality, the areas outside secondary-grade protection areas can be set as extended protection areas.

2.3 The Signs of Source Water Protection Areas

2.3.1 Classification of Source Water Protection Area Signs

The signs of source water protection areas are divided into several types:

1. Landmark of source water protection areas

   The landmark has two main functions: firstly indicating the boundary of source water protection areas, and secondly warning passers that cross the source water protection areas should be strictly in accordance with the relevant laws and regulations.
2. Warning signs of source water protection areas

   Traffic warning signs are mainly applied to source water protection areas in the transportation field, which are divided into road warning signs and waterways warning signs. The main function is to alert passing traffic vehicles, pedestrians, and boats to drive carefully in source water protection areas. As the traffic warning signs are mainly set in traffic roads or waterways, they should meet the regulations and standards of national road traffic acts.

3. Billboards of source water protection areas

   Billboards are set for the education of people to protect source water. The main contents and setting positions are flexible. It is essential to place the billboards in a prominent location.

2.3.2 The Content of Source Water Protection Area Signs

1. Landmark of source water protection areas

   Unify the signs of source water protection areas as much as possible. The contents of protection area signs are presented on the front and back sides. The front contents of signs are constituted of symbols, names of protection areas, and supervision and management information (including telephone hotline). The back is composed of graphical representations and regulations of the source water protection areas. The range is shown based on the "Technical Guideline for Delineating Source Water Protection Areas" [6], with clear graphical illustrations. The regulations are shown based on the "Water Pollution Prevention Law" and the "Water Pollution Control Act Implementation Rules".
2. Warning signs of source water protection areas

   Traffic warning signs of source water protection areas are divided into road warning signs and waterways warning signs, according to different modes of transportation.

   (a) The road warning signs of source water protection areas

   The form and structure of road warning signs are set according to the relevant content in "Road Traffic Signs and Markings" (GB 5768). The left part of the road warning signs is the graphical sign of source water protection areas, while the right part is written with "You have entered the XX source water X level protection area with XX km", to warn passing vehicles and pedestrians to show careful driving behaviors and inform about the distance.

   (b) The waterways warning signs of source water protection areas

   The form and structure of the waterways warning signs are set according to the relevant content in "Inland Navigation Aids" (GB 5863). The waterways warning signs of source water protection areas use the private labels in GB 5863. The shape of special provisions is regulated in GB 5863; for first-grade source water protection areas, the upward side of warning signs comprises source water protection areas graphic signs, and the downward side is written with "The source water first-grade protection areas prohibit ships from entering". For secondary-grade and extended protection areas, the upward side of warning signs comprises source water protection areas graphic signs, and the downward side is written with "You have entered the XX drinking water source X level protection area with XX km" to warn passing vehicles and pedestrians to show careful driving behaviors and inform the distance.

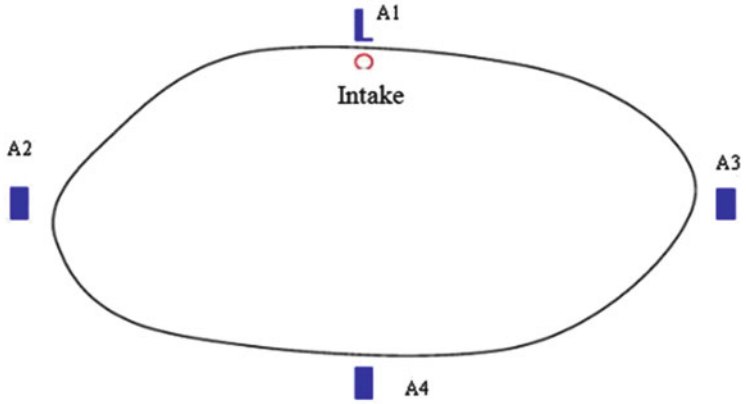

Fig. 1 The landmark setting schematic of small reservoirs and reservoirs with a single function of water supply

3. Billboards of source water protection areas

   The billboards of source water protection areas are mainly designed for public education by local governments. Except for the graphical signs of protection areas, other content is not mandatory.

2.3.3 The Position of Source Water Protection Area Signs

1. The landmarks position of source water protection areas

   (a) The landmarks location of first-grade protection areas

   For small reservoirs (reservoir volume less than 0.1 million m^3) and reservoirs with a single function of water supply, according to the boundary of the reservoir, the landmarks are established on the side of land area (as shown by points A1, A2, A3, and A4 in Fig. 1).

   For medium and large lakes and reservoirs, according to the designated range (for small and medium-sized lakes and reservoirs, with a radius range of 300 m from the water intake; for large reservoirs and lakes, with a radius range of 500 m from the water intake), the landmarks are established on the side of land area in the first-grade protection areas (points A1 and A2 in Figs. 2 and 3).

   (b) The landmarks location in land of first-grade protection areas

   In the land of the boundary of designated first-grade protection areas, the landmarks are established according to the setting position in water areas.

   Within the designated range, landmarks should be established based on the actual situation of the population and activities.

   Landmarks can be established based on physical geography, environmental characteristics, and environmental management.

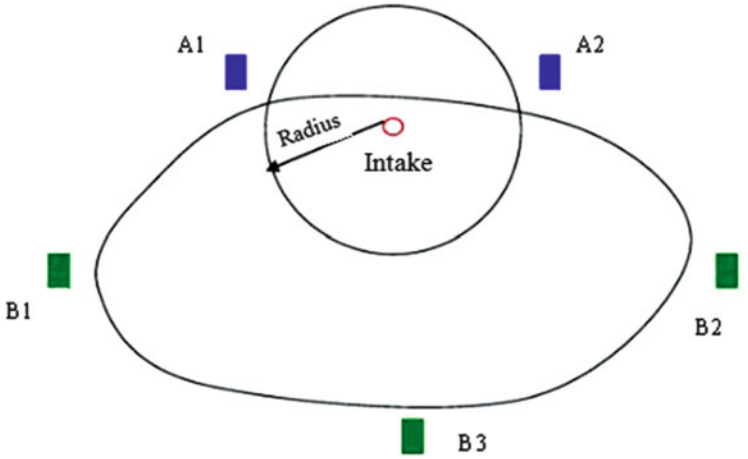

Fig. 2 The landmark setting schematic of small lakes and medium reservoirs

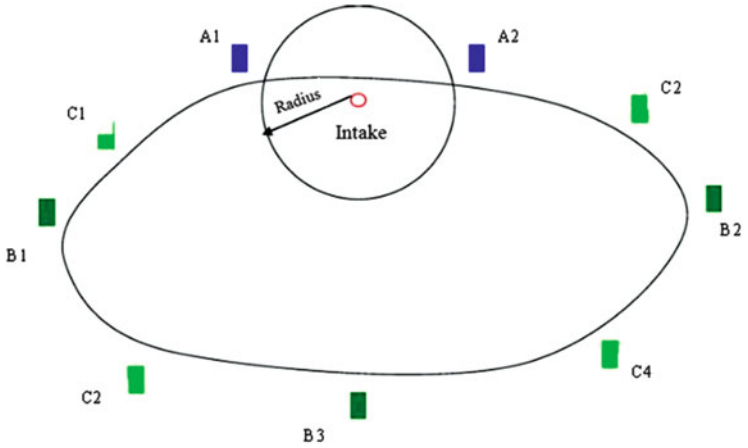

Fig. 3 The landmark setting schematic of large reserviors

(c) The landmarks location of secondary-grade protection areas

For small lakes and medium reservoirs, according to the delineation of the boundary waters of the reservoir, the landmarks are separately established on the side of land area (as shown by points B1, B2, and B3 in Fig. 2).

For medium and large lakes and reservoirs, according to the designated range, the landmarks are separately established on the side of land area in the secondary-grade protection areas (as shown by points B1 and B2 in Fig. 3). If the external distance of first-grade protection areas is more than 3000 m, the landmark can be set in an appropriate position (as shown by points C1 and C2 in Fig. 3).

(d) The landmarks location in land of secondary-grade protection areas

In the boundary of designated protection areas, the landmarks are established according to the setting position of landmarks in water areas.

Within the designated range, landmarks should be established based on the actual needs of the population and activities (such as intersections, green leisure areas, and so on). Landmarks can be established based on physical geography, environmental characteristics, and the need of environmental management.

(e) The landmarks location of extended protection areas

The landmarks location of extended protection areas are established based on the secondary-grade protection areas.

2. The traffic warning signs position of source water protection areas

The traffic warning signs are set up on the road entrance of source water protection areas. As traffic warning signs are used in roads or waterways, the specific setting positions should comply with the relevant requirements of GB 5768 and GB 5863.

3. The billboards position of source water protection areas

The setting positions of the billboards in source water protection areas should meet the relevant requirements of GB/T 15566 and GB 5768.

3 Management of Reservoir Water Protection

3.1 The Monitoring and Evaluation of Water Quality

The purpose of monitoring water quality involves grasping the dynamic changes of water quality and providing accurate and reliable information for subsequent assessment. Based on these results, rational water utilization and pollution control methods could be determined. In general, water quality monitoring and assessment include the arrangement of monitoring points, the determination of monitoring parameters, the monitoring frequency, and the evaluation of water quality.

1. Monitoring parameters

The monitoring parameters vary widely with different source water, and they should be determined by both the standard of source water environmental quality and the actual polluted situation. At present, according to the general environmental quality standard, the monitoring parameters can be divided into three categories [19]:

(a) Routine monitoring parameters. These parameters include potassium, sodium, calcium, magnesium, sulfate, chloride, bicarbonate, pH, total dissolved solids, total hardness, oxygen consumption, ammonia, nitrate, nitrite, total phosphorus, total nitrogen, dissolved oxygen, and so on.

(b) Harmful substances. In general, these parameters include mercury, chromium, tin, copper, lead, zinc, arsenic, and so on. With regard to the organic hazardous substances, phenol, cyanide, and other harmful industrial substances are often included.
(c) Bacteria. The bacteria monitoring point should be set in control points. For some specific pollution components, some special parameters should also be monitored. For lakes and reservoirs, in order to know the eutrophication level, the ecological situation should be analyzed. The parameters include bacteria, algae phytoplankton, biomass, aquatic animals, and plants.

2. Monitoring network layout

The monitoring network layout often includes the determination of monitoring cross-section, monitoring vertical line, and monitoring points.

(a) The determination of monitoring cross-section. Water quality monitoring sections are divided into three types: the reference section, the monitoring section, and the cut section.

The reference section is placed upstream of the river or pollution source, which is set to determine the pollution source and measure the water quality of a river before entering the contaminated area.
The monitoring cross-section is used to find out specific water quality conditions or specific sources of water pollution, which is mainly set downstream of the river (500–1000 m away from the residential or industrial zone), or set at the entrance/exit and representative positions of lakes and reservoirs. In addition, more monitoring sections should be set up in lakes and reservoirs according to their sizes.
The cut section is used to assess the effects of mixing dilution, which is generally located downstream 1500 m away from the last city discharge point.

(b) The determination of monitoring vertical lines. In each monitoring section, several monitoring vertical lines should be set, and the numbers are based on the width of the monitoring section. If the width of the water surface is below 50 m, one vertical line is needed at the congested line location; if the width of the water surface is 50–100 m, two vertical lines are set at the right and left, respectively; if the width of the water surface is 100–1000 m, three vertical lines are set at the left, middle, and right, respectively; if the width of the water surface is above 1500 m, five vertical lines should be set.
(c) The determination of monitoring points. Many monitoring points should be set at different water depths in a vertical line, and the exact number depends on the vertical depth. If the water depth is less than 5 m, one monitoring point under the water surface of 0.3–0.5 m is necessary; if the water depth is 5–10 m, two monitoring points should be set under the water surface of 0.3-0.5 m and above the bottom of 1 m, respectively; if the water depth is 10–50 m, three monitoring points are needed under the water surface of 0.3–0.5 m, above the bottom of 1 m, and the middle water, respectively; while

when the water depth is more than 50 m, more sampling points should be added accordingly. With regards to the deeper reservoirs and lakes, the sampling point at the layer of the thermocline should be considered, if there is one.

3. Monitoring frequency. The sampling frequency should be able to reflect the time changes of water quality. Under normal circumstances, the monitoring frequency should be once per month, and not less than 12 times per year. The sampling times can be reduced appropriately for smaller scales of source water.
4. Water quality evaluation. Water quality evaluation should be refined using the water quality monitoring data and the water quality standard. The evaluation of surface water should be based on "the surface water environment quality standards" and "drinking water quality standards". The water quality of source water should meet the class III standard of "the surface water environment quality standards". The water quality of source water in the first-grade protection areas should meet the class II standard of "the surface water environment quality standards", and source water in the secondary-grade protection areas should meet the class III standard of "the surface water environment quality standards.

To achieve a comprehensive evaluation of water quality and, thus, prevent and control water pollution effectively, suitable water quality evaluation methods should be selected. At present, there are several methods used for water quality assessment, including statistics, comprehensive index method, mathematical statistics, and Hamming's method [20].

3.2 The Management of Pollutant in Water Source Protection Areas

To prevent pollution and manage the water quality of source water protection areas, measures should be adopted according to the "Water Pollution Prevention and Control Law of the People's Republic of China" and "Pollution Prevention and Control Regulations of Drinking Water Sources Protection Areas". The detailed methods are as follows:

1. Set up the special administrative agencies and enhance the unified management of the river basin and unified planning;
2. Lay down the corresponding regulations or laws on water pollution prevention and control, and step up publicity efforts to expand the social impact;
3. Formulate and improve the source water quality standard and the relevant emission standards;
4. Adopt the economic measures, such as increasing the charge of water drainage and water supply;
5. Strengthen the patrol, surveillance, monitoring, and management of source water protection areas. Ban all facilities and activities from the violation of

regulations in accordance with the "Pollution Prevention and Control Regulations of Drinking Water Sources Protection Areas";
6. Investigate the pollution source and pollutants characteristics, and take effective measures to control the pollution source and pollutants;
7. Strengthen the management of ships and tourism on the source water surface, which may induce the movement of pollution, and improve the wastewater and waste collection treatment facilities of the ship. Strengthen education and management, and ensure wastewater can be tackled properly.

3.3 The Ecological Management of Source Water Protection Areas

Ecological management should grasp the dynamic variation of the ecological environment based on the investigation of the ecological environment, and then certain methods are adopted to maintain a good ecological environment.

1. Monitor the dynamic change of the ecosystem factors in source water protection areas, such as the species, quantity, and distribution of biological animals, the protection areas, and the vegetation type of lakeside zones.
2. Monitor the environmental factors in source water protection areas, such as temperature, light, water temperature, water quality, and sediment deposition.
3. Analyze the dynamic change of biological factors to find out the reasons for the deterioration of ecological systems over time.
4. Analyze the dynamic change of environmental factors to determine the causes of ecological destruction and find out the methods to prevent the deterioration of ecological systems.
5. Strengthen the patrol management of ecological systems in source water protection areas, prevent damage to the forest shelter belt, and protect the vegetation in the basin. Harvest the aquatic organisms properly, and ensure the normal reproduction of aquatic plants in the source water protection areas.

4 Examples of Reservoir Water Protection

Although the water quality of about 60 % of lakes and reservoirs can meet the water standard (class II), some source waters are far from satisfactory, such as those reservoir waters including Miyun Reservoir in Beijing, Jiangdong water areas in Xiamen, and Yunlong Reservoir in Kunming. To reduce the environmental pollution load, source water protection areas are established and delineated. However, the division of source water protection areas is based on geographic space instead of internal mechanisms, making it less effective to protect source water. Taking Huangpu River as an example, the protection areas of Huangpu River were set

early in 1985 and enlarged later in 1999. However, the water quality of Huangpu River is far from satisfactory, as the permanganate index is higher than that of drinking water quality. At present, several works on controlling point pollution and delineating drinking water protection areas have been successfully conducted.

4.1 Shenzhen Experience

Shenzhen city has undergone rapid economic development, but at the same time, the environments are seriously polluted. Due to the overlooking of environmental protection in the early period of economic development, all the reservoirs and river basins are polluted to some extent.

There are no large rivers or lakes in Shenzhen; therefore, more than 70 % of water is taken from other cities, which seriously limits the economic development. The government has paid more attention to protecting reservoirs and several methods have been undertaken. In 2001, the situation of reservoirs and river basins was assessed in detail and "Water Protection Ordinance" and "Source Water Protection areas" were published. Twenty-seven drinking water protection areas were set at different grades. Take Xili Reservoir as an example. On one hand, an isolation project has been set up to reduce the pollution resource. On the other hand, a patrol has been established to intensify the supervision of populations and vehicles entering the source water protection areas.

Xili Reservoir is located at the west of Shenzhen city, with a catchment area of 29 km^2, a total storage capacity of 4.2 million m^3, and annual water supply of 10 million m^3. Xili Reservoir is an important intake point of the water supply network and is also a main regulation reservoir. Therefore, the water quality of Xili Reservoir has a direct influence on the drinking water quality of Shenzhen. The government had invested vast amounts of money and implemented many projects to improve the water quality. At present, a large amount of pipes has been built around the reservoir to collect municipal wastewater and early-stage rainfall. The scale of this project is huge and around 3 billion RMB has been spent to protect the Xili Reservoir water.

4.2 Beijing Experience

Since 1999, to solve water shortage, eutrophication, and other ecological problems in Beijing Miyun Reservoir, extraordinary measures have been undertaken, including a strict source water protection system being established; three green ecological barriers (ecological rehabilitation, ecological construction, and ecological protection) have been formed; 30 ecology-friendly small river basins have been constructed; methods for controlling wastewater, rubbish, toilets, environment, and rivers have been put into practice simultaneously. On the other hand, the return

of rice fields to land plays an important role in increasing the amount of water and reducing the pollution from chemical fertilizers and pesticides. Moreover, fish breeding (1 hm^2 areas) was cancelled and commercial buildings (around 11,000 m^2) were pulled down. At the same time, the reservoir is managed in a closed style with a protective net around it. In addition, biological technologies were carried out by releasing algae-eating fishes into the reservoir. Based on the above comprehensive control methods, the amount of water in Miyun Reservoir has increased up to 110 million m^3 from 65 million m^3 in 2004, and the water quality can meet the national source water standard (class II). Due to the implementation of reservoir water protection areas and fishing ban policy, the water quality has been improved significantly.

4.3 Jinpen Reservoir Protection

As the main drinking water source of Xi'an city, the water quality of Jinpen Reservoir is directly related to the public health of a population of 3 million and the sustainable economical development of Xi'an city. Therefore, it is of great significance to investigate and clarify the present pollution, and then make specific plans for protecting the reservoir water. Some measures have been taken to protect Jinpen Reservoir, which are listed as follows:

1. Make efforts to return cultivated land to forests, prohibit hunting, and plant trees on mountains. There is a positive correlation between water quality in rivers and land utilization in the river basin. Pollution control in river valleys can be enhanced by increasing forest areas, which plays a positive role in preventing soil erosion and reducing dusts. Planting more forests is encouraged, or plant trees and grasses where it is suitable.
2. Control the population size by relocating the residents. Overpopulation is the main reason for environmental destruction, and controlling the population size by settling them in another place is under operation. Currently, there are 3520 homes and 13,452 people in Jinpen Reservoir basin, making it difficult and cost to relocate so many people at once. The relocation project is carried out step by step. Firstly, the relocation project including 334 homes and 1576 people had finished by the end of April, 2000. Then, the second phase of the relocation project including 159 homes and 590 people in the first-grade and secondary-grade protection areas was carried out: 88 homes and 321 people in Mazhao Town were settled at the end of 2012, while the other 71 homes and 269 people in Louguan Town were settled at the end of 2013. Thirdly, the relocation in the extended protection areas will be carried out later according to economic and social development.
3. The domestic wastewater and garbage must be treated on-site, collected separately, utilized comprehensively, and treated harmlessly. At the same time, efforts to treat polluted water and other wastewaters have been made, such as:

the upgrading of rural toilets, the treatment of domestic garbage, the upgrading of the drainage system, the comprehensive use and recovery of wastewater, and the sorting and recycling of domestic garbage.

4. Ecological agriculture and pollution-free agricultural bases are established to prevent pollution from chemical fertilizers and pesticides. To reduce soil erosion and adjust the industrial structure, scientific farming, ecological agriculture, and the construction of pollution-free agricultural bases are encouraged. Poisonous pesticides are banned in the Jinpen Reservoir protection areas. Moreover, the use of chemical fertilizers and pesticides are restricted, and the application of biological control strategies are promoted and encouraged.
5. Enforce the related laws and consolidate the management of source water protection areas. The government enforces the control of pollution sources and the administrative procedures of pollutant-emission outlets. The unlawful act of discharging dirty water into Jinpen Reservoir would be punished severely. It is forbidden to dig sand, collect stones, and mine in the protection areas. Enterprises are enforced to cease.
6. Improve the public's awareness. It is difficult to change the over-consumption of resources, heavy pollution, unsustainable way of life, and production for a long time. Therefore, seminars, posters, and other media have been used to advocate the importance and urgency of source water protection. At the same time, people in the protection areas are guided to create a civilized and clean living environment. They are encouraged to fully participate in the process of source water protection, and arouse the awareness of environmental protection.

References

1. Chen ZH (2008) The research of western ecological compensation mechanism. Minorities Press, Beijing (in Chinese)
2. Xia Q, Chen YQ, Liu XB (2004) Benchmark water quality and water quality standards. China Standard Press, Beijing (in Chinese)
3. Davies JM, Mazumder A (2003) Health and environmental policy issues in Canada: the role of watershed management in sustaining clean drinking water quality at surface sources. J Environ Manage 68(3):273–286
4. Walsh G, Wepener V (2009) The influence of land use on water quality and diatom community structures in urban and agriculturally stressed rivers. Water SA 35(5):579–594
5. Stonestrom DA, Scanlon BR, Lu Z (2009) Introduction to special section on impacts of land use change on water resources. Water Resour Res 45(7)
6. HJ/T338-2007 (2007) Technical guideline for delineating source water protection areas. (S) The state environmental protection administration
7. Liang J, Peng XC, He T (2009) Research on the prevention and cure countermeasure of drinking water sources in lake reservoirs. Guangdong Agric Sci 7:181–185 (in Chinese)
8. China's wetland protection plan of action (2002) Wetland utilization and protection of Shanghai seminar. (R) Shanghai (in Chinese)
9. Liu PB (2007) Studies on protection and management of drinking water sources in Beijing. China Water Res 10:138–140+134 (in Chinese)

10. Zhang ZT, Cao Q, Xie T (2013) Design of water quality monitoring and warning system of drinking water source. Environ Protect Sci 01:61–64 (in Chinese)
11. Mao N, Liu R, Li HH, Ning GF (2013) Development and application of water quality monitoring and warning management information system for drinking water sources. China's Environ Manag 05(05):30–34 (in Chinese)
12. Duan LQ, Guo RR (2013) Introduction to water quality monitoring and early warning system in the application of water source of drinking water. J Henan Sci Technol 8(15):185 (in Chinese)
13. Liu WL, Dai J, Zhang JD (2011) Establishing drinking water monitoring warning system. Ind Safety Environ Protect 37(3):15–16 (in Chinese)
14. Zhao HL, Chen DH, Zhang LP (2008) A study on zoning system for drinking water source protection. Shanghai Environ Sci 4(27):167–169 (in Chinese)
15. Zhou XH, Jiang HP (2009) Study on division of conservation areas for drinking water and on protective measures for Chitian reservoir. Water Res Protect 6(25):8–12 (in Chinese)
16. GB3838-2002 (2002) Environmental quality standards for surface water. (S) The state environmental protection administration
17. Tang X, Nian FH (2011) Research on the prevention and cure countermeasure of drinking water sources in lake reservoirs-select Daxi reservoir as an example. Guangdong Chem Ind 214(38):115–116 (in Chinese)
18. He T, Peng XC, Bai ZY, Liang J (2009) Comparison of division method for reservoir drinking water protected area. Resource Dev Market 25(2):122–123, +185(in Chinese)
19. Zhou YX, Li WP (2008) Groundwater quality monitoring and assessment. Hydrogeol Eng Geol 1:1–11 (in Chinese)
20. Wu Y, Chen Z, Li Z (2008) Genotoxicity evaluation of drinking water sources in human peripheral blood lymphocytes using the comet assay. J Environ Sci 20(4):487–491

Part II
Reservoir Sediment Contamination and its Impact on Water Quality

Overview of Reservoir Sediment Contamination

Jinlan Xu, Chao Xia, Zizhen Zhou, Ruizhu Hu, and Tinglin Huang

Abstract The concentration of inorganic phosphorus (IP) in the surface sediment of each of the studied reservoirs ranged from 208.8 to 636.7 mg/kg. The concentration of Fe/Al-P in the surface sediment in the four reservoirs ranged from 82.1 to 216.7 mg/kg, and the average value was 129.6 mg/kg, accounting for 11.54–18.1 % of the sediment total phosphorus (STP) content. The highest proportion of IP is observed in Yuqiao Reservoir, and Jinpen Reservoir had the lowest proportion. In addition, the results indicated that the Ca–P concentrations of the four reservoir sediments are in the range 180.7–303.4 mg/kg, with an average value of 247.1 mg/kg, accounting for 22.33–37.1 % of the STP. The content of organic phosphorus (OP) in the reservoir surface sediment is in the range 64.2–201.8 mg/kg, accounting for 9.85–18.52 % of STP content. The ion exchange nitrogen (IE-N) content (mg/kg) in reservoirs is significantly different. The IE-N content of Shibianyu Reservoir is much higher than that of other reservoirs, accounting for 18.35 % of the total nitrogen (TN). The IE-N in the studied reservoirs accounted for 15.33–18.35 % of the TN. IE-N exists in three different speciations: the concentration of ammonia is much higher than that of nitrate and nitrite, and the concentration of nitrite is the lowest. The cloning and sequencing results showed that microorganisms were made up of ten major categories, including *shaped bacillus*, *Chloroflexi*, *Verrucomicrobia*, *Bacteroides*, *Acidobacteria*, *thick wall bacteria*, *actinomycetes*, *Gemmatimonadetes*, *Nitrospirae*, and *Planctomycetes*, in the Jinpen Reservoir sediments.

Keywords Reservoir • Sediments • Physical properties • Chemical properties • Microbial community

J. Xu • C. Xia • Z. Zhou • R. Hu • T. Huang (✉)
School of Environmental and Municipal Engineering, Xi'an University of Architecture and Technology, Yanta Road 13, 710055 Xi'an, Shaanxi Province, P. R. China
e-mail: huangtinglin@xauat.edu.cn

T. Huang (ed.), *Water Pollution and Water Quality Control of Selected Chinese Reservoir Basins*, The Handbook of Environmental Chemistry 38,
DOI 10.1007/978-3-319-20391-1_5

1 Physical Properties of Reservoir Sediment

1.1 Particle Size of Sediment

Fine particles have greater surface areas than larger particles. They have a stronger adsorption capacity, easily absorb more phosphorus compounds in water, and hinder the sediment interstitial water absorption of the phosphate in the water layer. Kim and other studies have found that the order of the absorption capacity of sediment and adsorption efficiency and adsorption rate in Wuli Lake and Gong Lake is: clay > fine sand > coarse sand > silt [1]. The distribution of sediment particles influences the degree of porosity. Large porosity is conductive to the spread of diffusion and migration of sediment, and also benefits oxygen to diffuse into the deeper sediment. Liu found that the content of iron, aluminum, and phosphorus increased with larger particle sizes combined with sediments. In general, the content of calcium-binding phosphorus in fine sandy sediments is higher [2].

1.2 The Color of Sediment

Samples were taken from Zhoucun Reservoir located in Zaozhuang City, Shandong Province; a hand-held GPS positioning system was used to find the reservoir's origin. Six sediment samples were taken by a Peterson sampler. The sampling depth is 10–15 cm below the sediment surface. The samples were placed in sealed polyethylene bags and taken to the laboratory as soon as possible. The specific sampling points are shown in Fig. 1. Table 1 shows the distance between the sampling points and the dam, as well as the water depth.

The sediment samples were placed in a beaker, left to stand, and the supernatant liquid was removed by syringe. Then, the sediment samples were spread on paper to dry. The detailed characteristics are shown in Table 2.

It was found that the color of sediment gradually becomes black with the increase of water depth: the color of sample 5 is the blackest and that of sample 2 is brown. Sample 1 has the greatest fish odor, and the deep water area sediment has a sulfide odor. The color of deep water area sediment, especially for samples 5 and 6, became black. However, the color becomes light after standing in the air. Therefore, it is inferred that the deep water area sediments is in anaerobic conditions, as the color changed due to the lack of oxygen. We can conclude that the color of the Zhoucun Reservoir sediments is obviously blacker than the other two reservoirs (Jinpen Reservoir and Shibianyu Reservoir). The color of the sediments of the other two reservoirs is brown and they do not have an obvious stench, and the degree of stickiness is significantly greater than that of Zhoucun Reservoir.

Sampling point	latitude	longitude	Sampling point	latitude	longitude
1	34°57′8.8″N	117°39′53.06″E	4	34°56′48.06″N	117°40′38.96″E
2	34°57′3.41″N	117°40′7.41″E	5	34°56′39.37″N	117°40′55.9″E
3	34°56′56.56″N	117°40′22.62″E	6	34°56′32,66″N	117°41′9.74″E

Fig. 1 The location of sediment sampling points in Zhoucun Reservoir

Table 1 The location and depth of sediment sampling points in Zhoucun Reservoir

Sampling points	1	2	3	4	5	6
Distance to the dam, m	2500	2000	1500	1000	500	100
Depth of water, m	7	7	10	10	13	10

1.3 Moisture Content of Sediment

The moisture content of the Zhoucun Reservoir sediment is about twice that of the sediments from Jinpen Reservoir and Shibianyu Reservoir, while the moisture content of sediments in Jinpen Reservoir and Shibianyu Reservoir are closer (Table 3).

2 Chemical Properties of Reservoir Sediments

2.1 The Status of Phosphorus in the Sediments

1. Mineral states: iron phosphate, aluminum phosphate, calcium phosphate, and magnesium phosphate are the types of mineral phosphorus. Mineral states also have a phosphorus component and residual phosphorus. The relative content of

Table 2 Sensory traits description of sediment sampling points in Zhoucun Reservoir

Item	1	2	3	4	5	6
Overlying water	The water is high in quantity and limpidity. Some plankton can be seen	The water is high in quantity and limpidity. Much plankton, including plankton of size 1 mm, can be seen	Small quantity of overlying water	The water is high in quantity and limpidity. Some plankton can be seen	Small quantity of overlying water. No plankton can be seen	Small quantity of overlying water, black in color, and hard to clarify
The shape of sediment	The sediment is light in color and soft	The sediment is lightest in color, massive, including subtilis, tree branches, and conch	The surface of the sediment is light in color, after stirring; the sediment turns black and sticky internally	The sediment is black in color and soft internally	The sediment is dark black in color and sticky	The sediment is dark black in color and sticky
The smell of sediment	Sediment has a bad smell	It is stenchy	It has a lot of stench	It has a little stench	It has minimum stench, with the smell of sulfide	It is stenchy, with the smell of sulfide
Dry sediment	It is hard to break down into smaller particles	It is hard to break down into smaller particles	It is hard to break down into smaller particles	After grinding, it is still black in color	After grinding, it is still black in color	After grinding, it is still black in color

Table 3 The moisture content of Jinpen Reservoir, Shibianyu Reservoir, and Zhoucun Reservoir

Name of reservoir	Moisture content (%)
Jinpen Reservoir	40–50
Shibianyu Reservoir	35–45
Zhoucun Reservoir	75–85

minerals in the sediment is determined by the sources and the pH. Acidic sediments contain high concentrations of iron and aluminum oxides, from which it is easy to form aluminum iron phosphate. In neutral–alkaline sediments, the calcium carbonate contents are high and it is easy to form calcium phosphate.

2. Substitutable states: this refers to phosphoric acid or phosphate anion, which can be adsorbed on the sediment. $H_2PO_4^-$ and HPO_4^{2-} are the most common substitution phosphates. Since the negative charge increases with the decrease of pH, the substitution phosphorus generally decreases with increasing pH.
3. Soluble: phosphorus which is dissolved in interstitial water is orthophosphate. Metals and phosphates form soluble complexes.

Table 4 TP concentration (mg/kg) and the different speciations in four reservoirs

Name of reservoir	TP	IP	OP	Fe/Al-P	Ca-P
Yuqiao Reservoir	652.3	208.8	83.4	118.2	241.9
Fenhe Reservoir	766.5	362.7	121.7	101.4	180.7
Jinpen Reservoir	711.3	302.6	64.2	82.1	262.4
Shibianyu Reservoir	1358.6	636.7	201.8	216.7	303.4

Researchers have divided inorganic phosphorus in sediments into calcium phosphorus (Ca-P), aluminum phosphate (Al-P), iron phosphate (Fe-P), organic phosphorus (OP), reductive phosphorus (Re-P), and residual phosphorus (residual-P). Organic phosphorus is similar to some known organic phosphorus compounds in organisms, such as plant hormones, nucleic acids, phospholipids, phosphoprotein, and phosphate metabolism [3].

1. IP: the content of inorganic phosphorus (IP) in the surface sediments of the studied reservoirs ranged from 208.8 to 636.7 mg/kg (as shown in Table 4), accounting for 65.32–73.24 % of the total phosphorus content of STP. The results indicated that IP is the primary element in the sediment. The highest content of IP is that in Shibianyu Reservoir, and the lowest is in Yuqiao Reservoir.
2. Fe/Al-P: Fe/Al-P is the phosphorus bound to Al, Fe, Mn oxides, and hydrates. It is the main speciation of bioavailable phosphorus, and can be utilized by microorganisms, which change with redox conditions [4, 5]. As the oxidation–reduction potential (ORP) reduced, the ferric iron combined with phosphate in sediment is reduced to ferrous iron, and the phosphorus bound to iron is released into the interstitial water and then transferred to the overlying water. So, Fe/Al-P is the main speciation of phosphorus release and transformation in sediment [6]. As can be seen in Table 4, the contents of Fe/Al-P in the surface sediments of the four reservoirs are between 82.1 mg/kg and 216.7 mg/kg, and the average value is 129.6 mg/kg, which accounts 11.54–18.1 % of the STP content. The highest proportion is that in Yuqiao Reservoir, and the lowest proportion is that in Jinpen Reservoir. When the ORP is reduced in the multiphase interface, Fe/Al-P bound phosphorus is released to the overlying water due to the reduction of dissolved iron [7].
3. Ca-P: Ca-P is also called apatite phosphorus, contained in the primary mineral particles, and it is consists of particle phosphorus. Generally, Ca-P has little effect on the content of phosphorus in the overlying water, but can be easily released at low pH [3]. Only under the condition that CO_2 is adequate or the pH is lower can Ca-P be released. The results show that the contents of Ca-P in the four reservoir sediments are between 180.7 and 303.4 mg/kg, and the average value is 247.1 mg/kg, accounting for 22.33–37.1 % of STP. The highest proportion is in Yuqiao Reservoir, whereas the lowest proportion is in Shibianyu Reservoir. The average pH value of the reservoirs is about 8.0, showing a distribution that the surface is high and the underlying water is low. Sediment

at the bottom of the reservoir will lead to an anaerobic or anoxia environment when stratification occurs because stratification prevents oxygen transfer from the upper to the lower layers. The pH will decrease to 6 at the interface of the bottom sediment because small molecule organic acids are formed under anaerobic conditions. As a result, Ca-P is released due to the weak acidic environment of sediment at the bottom. It is a potential risk of the release of Fe/Al-P under the condition of weak acid environment.

According to the above results, Ca-P is the dominant IP in the surface sediment of the reservoir, accounting for about 70 % of the IP. The content of Ca-P depends on the geochemical background and the pH value [2]. TP is dominated by IP.

4. OP: organic phosphorus (OP) is the main constituent of phosphorus in sediment. It can be converted into bioavailable phosphorus [8]. The contents of OP in the surface sediment of the four reservoirs are between 64.2 and 201.8 mg/kg, accounting for 9.85–18.52 % of the total phosphorus content. The highest proportion is found in Fenhe Reservoir, and the smallest proportion in Jinpen Reservoir. The results show that 50–60 % of OP can be converted into bioavailable phosphorus by microorganisms [8]. OP also has a potential threat to the overlying water and can accelerate the eutrophication trend.

2.2 Nitrogen in Sediments and its Geometrical Status

The nitrogen in sediment can be divided into transformed nitrogen and untransformed nitrogen. Transformed nitrogen can be released in the water under specific environmental conditions, since the attachment to sediments surface or combination capacity is its weakness. Untransformed nitrogen can enter the mineral grid of sediment and wrap in larger particles of the endothecium. Untransformed nitrogen cannot participate in the nitrogen cycle [9]. Therefore, the content of transformed nitrogen in sediment intuitively reflects the maximum content of the nitrogen cycle in sediment [10]. The distribution of transformed nitrogen in natural sediment can clearly reveal the contribution of the nitrogen cycle and can establish a theoretical basis on controlling endogenous contamination of source water.

(1) The Distribution Characteristics of IE-N (Ion Exchangeable Nitrogen)
IE-N is an absorbable nitrogen but has the weakest capacity for combining with sediment. It is the most active part in sediment. IE-N is quite important for the nitrogen cycle in sediment. The content and release of IE-N are influenced by temperature, salinity, pH, DO, organic matter, and biological disturbance. It is not only correlated with these factors, but is also directly correlated with the construction, character, and granularity of sediment [10].

Among the three different speciations of IE-N that exist, the content of ammonium is much higher than that of nitrate and nitrite. The content of nitrite is the lowest because it is the intermediate product and corresponding instability.

Different from the marine sediment, ammonium in the reservoir sediment is the main speciation of IE-N [10]. This is mainly attributed to the fact that benthos played an important role in biogeochemical cycling in marine creatures, including microorganisms, protozoa, small animals, and large animals. The feeding of benthos and nutrients in ocean sediment had inalienable relations. The composition of biological systems in reservoir sediment is relatively simple compared with marine sediments. Microorganisms play a main role in cycling nitrogen. The distribution of microorganisms is different in different reservoirs.

(2) The Distribution Characteristics of WAE-N (Weak Acid Extractable Nitrogen)

WAE-N is the carbonate combined with nitrogen. The WAE-N content and distribution are affected by many factors, especially the pH and sediment grain size. It is not easy for $CaCO_3$ to dissolve in the district of high carbonate content because the content of sediment organic carbon (SOC) is low and the pH is stable [9]. The carbonate content in the source water reservoir sediment is higher than that in marine sediments. However, the content of SOC is lower and the mineralization is relatively weak, which lead to a higher WAE-N content.

(3) The Distribution Characteristics of SAE-N (Strong Alkali Extractable Nitrogen)

SAE-N consists of nitrogen-bonded Fe/Mn oxides. Its formation and distribution are mainly controlled by the redox environment in sediment [9]. The different contents of SAE-N in each point reflect the diversity of redox conditions. The highest proportion of TN in Fenhe Reservoir is 29.62 %, whereas the lowest was found in Shibianyu Reservoir. Therefore, the complicated environment of sediment has a significant effect on SAE-N formation [9].

(4) The Distribution Characteristics of SOE-N (Strong Oxidant Extractable Nitrogen)

SOE-N is the transformable speciation of nitrogen, containing mainly organic nitrogen. The distribution of SOE-N is related to the sediment origin, organic matter content, particle size, input rate of organic matter, deposition rate, and redox environment. The SOE-N content is the highest content in transformable nitrogen. The content of SOE-N is listed in Table 5. The order is as follow: Shibianyu Reservoir 706.7 mg/kg, Yuqiao Reservoir 314.2 mg/kg, Fenhe Reservoir 304.9 mg/kg, and Jinpen Reservoir 259.9 mg/kg. The lower content of SOE-N in Jinpen Reservoir is related to the higher water depth.

2.3 Sediment Organic Carbon in Sediment and its Present Status

SOC is an important constituent part of the sediment. SOC mainly includes protein, aliphatic, carbonyl, lipids, and polysaccharide. As shown in Table 6, the highest organic matter content is that found in Shibianyu Reservoir, which reached 5.82 %.

Table 5 TN concentration (mg/kg) and their different speciations at the four reservoirs

Name of reservoir	TN	IE-N	WAE-N	SAE-N	SOE-N
Yuqiao Reservoir	732.5	112.3	113.8	192.2	314.2
Fenhe Reservoir	1032.4	179.9	241.8	305.8	304.9
Jinpen Reservoir	562.9	85.9	120.9	96.2	259.9
Shibianyu Reservoir	1692.2	310.6	395.6	279.3	706.7

Table 6 SOC proportion (%) and their different speciations at the four reservoirs

Name of reservoir	SOC	Protein	Aliphatic	Carbonyl	Lipids	Polysaccharide
Yuqiao Reservoir	2.88±0.24	22.4	4.7	30.4	13.6	28.9
Fenhe Reservoir	3.02±0.18	10.8	15.6	29.3	7.9	36.4
Jinpen Reservoir	2.29±0.11	14.5	10.2	27.9	19.1	28.3
Shibianyu Reservoir	5.82±0.21	13.4	22.6	24.6	8.3	31.1

It also suggests that the sediment pollution of Shibianyu Reservoir is the most serious among the four reservoirs. The sediment pollution degree of Jinpen Reservoir is not heavy: the organic matter content is only 2.29 %. Polysaccharide accounts for about 30 % and it has the largest proportion of organic matter in the reservoirs, the second highest is the carbonyl compounds, and the least is the lipids.

2.4 Metal Elements in the Sediments and its Geometrical Status

In recent years, more cities have chosen reservoirs as a source water of drinking water, due to the shortage of groundwater supply. However, the development of industry brings more heavy metal pollution. Iron, aluminum, and manganese are the main pollutants. The presence of heavy metals in drinking water has the potential to harm human health. Related studies show that iron and manganese are the active metals, which allows them to participate in geochemical cycles [11]. Organics bonded iron and manganese in the reservoir sediments have a strong adsorption capacity to phosphorus. Thus, the study on heavy metals and its morphology is of great significance for the protection of source water.

The main combined speciations of heavy metals include: exchangeable iron (F1), carbonate combined iron (F2), iron (manganese) oxide bound iron (F3), organic matter and sulfide combined iron (F4), and residual lattice combined iron (F5).

The results are shown in Fig. 2. The concentration of total iron is up to 297 mg/kg in Shibianyu Reservoir, and F3 accounts for 43.3 % of the total iron. The results also indicate that F3 is the easiest to release to the water under anaerobic conditions. The proportion of F3 in Jinpen Reservoir is higher as well. Studies have shown that F3, F4, and F5 can release iron to the overlying water under anaerobic conditions, and F1 and F2 can absorb iron and phosphorus in water.

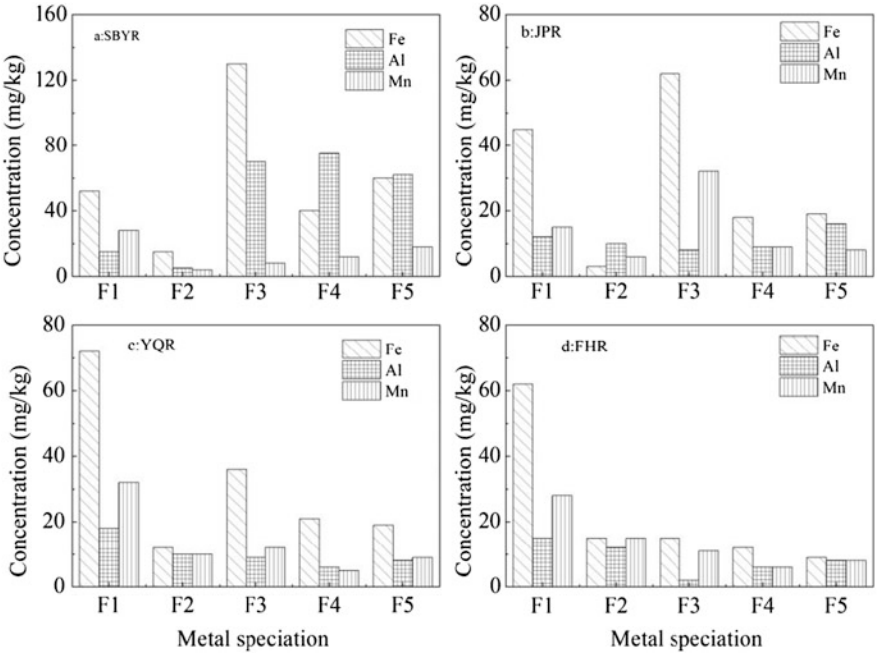

Fig. 2 The concentration of Fe, Al, and Mn in the four reservoirs: (**a**) Shibianyu Reservoir; (**b**) Jinpen Reservoir; (**c**) Yuqiao Reservoir; (**d**) Fenhe Reservoir

The content of aluminum in sediment decreased under anaerobic conditions, which is consistent with the trend of iron. F3, F4, and F5 released aluminum to the overlying water, while F1 and F2 absorbed aluminum from the overlying water.

The release and adsorption of manganese are shown in Fig. 2. Manganese in sediments is released to the overlying water. However, it is F3 manganese that is absorbed on the surface of sediment. The change of manganese is different from that of iron and aluminum because the manganese has strong sensitivity to the redox condition. Therefore, the manganese is released from sediments. The release mechanism of manganese is different from that of iron and aluminum.

3 Biological Properties of Sediment

3.1 Microbial Community in Jinpen Reservoir

Denaturing gradient gel electrophoresis (DGGE), cloning and sequencing techniques were used to analyze the diversity of the microbial community structure in Jinpen Reservoir. The results are shown in Table 7. The major categories (10) were

Table 7 Microbial cloning sequencing results of surface sediment in Jinpen Reservoir

Phylum	Class	Amount	Proportion, %	Total, %
Proteobacteria	*Gammaproteobacteria*	59	40.97	59.02
	Deltaproteobacteria	8	0.69	
	Betaproteobacteria	23	15.97	
	Alphaproteobacteria	2	1.39	
Chloroflexi	*Anaerolineae*	4	2.78	3.47
	Dehalococcoidetes	1	0.69	
Verrucomicrobia	*Subdivision*	4	2.78	5.56
	Verrucomicrobiae	4	2.78	
Bacteroidetes	*Flavobacteria*	5	3.47	15.28
	Sphingobacteria	4	2.78	
		13	9.03	
Acidobacteria	*Acidobacteria*	4	2.78	2.78
Firmicutes	*Clostridia*	2	1.39	1.39
Actinobacteria	*Actinobacteria*	2	1.39	1.39
Gemmatimonadetes	*Gemmatimonadetes*	2	1.39	1.39
Nitrospira	*Nitrospira*	1	0.69	0.69
Planctomycetes	*Planctomycetacia*	2	1.39	1.39
OD1		1	0.69	0.69
		3	2.08	2.08

detected, namely *Proteus, Chloroflexi, Verrucomicrobia, Bacteroides*, *Acidobacteria*, *Firmicutes, Actinobacteria, Gemmatimonadetes, nitrification pylori*, and *Planctomycetes*. *Proteus* was the dominant group (59.02 %). *Proteus* is also the dominant bacteria in the Kuroshio source region [12], Dongping lake [13] and Jiaozhou Bay. Few studies on the microbial community structure of sediments in water reservoirs have been carried out. Many results showed that *γ-Proteobacteria* is the dominant group of microorganisms in marine sediments. In addition, studies have shown that *α-Proteobacteria* groups are the dominant bacteria [11]. In this study, *β-Proteobacteria* is the second most dominant flora (15.97 %) in the surface sediments of Jinpen Reservoir. Studies have shown that *β-Proteobacteria* groups are a typical freshwater biomass [14], consistent with the nature of Jinpen Reservoir. *Green Bay bacteria door* is often found in groups with high organic matter content and low moisture environment. The content of *Chloroflexi bacteria* is relatively low (3.47 %) in sediment containing 2.29 % organic matter and 44.72 % moisture. *Firmicutes* bacilli can be used as an indicator of land-based sources of pollution groups, often used in coastal environmental pollution monitoring [15]. In this study, *Firmicutes* species accounted for only 1.39 % of microbial communities. The result shows that the reservoir water protection measures are better and there are no coastal environmental problems. *δ-Proteobacteria* groups and *ε- Proteobacteria* are considered to be the role of sulfate-reducing bacteria taxa. In this study, *δ-Proteobacteria* accounts for 0.69 %. *ε-Proteobacteria* is not detected. *Acidobacteria* is generally a non-primitive bacterial taxa, mainly the introduction of the external environment, which is often

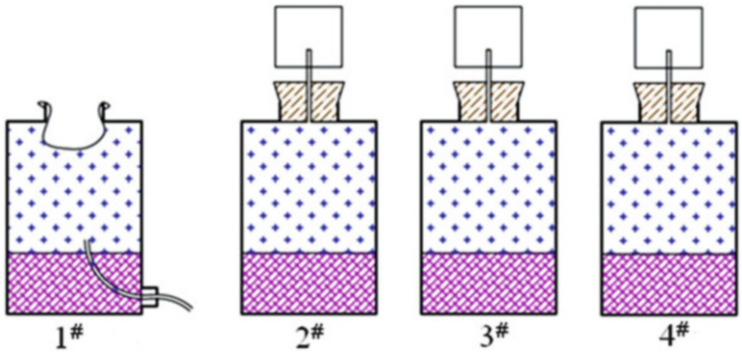

Fig. 3 Schematic of the reactors

considered to be present in a strong acidic environment of heavy metals [16]. In this study, *Acidobacteria* were also detected (2.78 %), although the content is lower, but it is responsible for the higher concentration of heavy metals in a multiphase interface system [17, 18].

3.2 Microbial Community Structure Analysis in Xi'an Shibianyu Reservoir

Four parallel reactors were designed (as shown in Fig. 3). Water samples were collected from the overlying water. Sediment samples were disposed in the bottom reactors. Gas collection bags were provided at the top of the reactors.

The dissolved oxygen in overlying water in the No. 1 reactor was determined, and it changed over time. When the dissolved oxygen decreased to 2 mg/L (on the 9th day), the No. 2 reactor was opened. When the dissolved oxygen decreased to 1 mg/L (on the 37th day), the No. 3 reactor was opened. When the dissolved oxygen decreased to approximately 0 mg/L (on the 88th day), the No. 4 reactor was opened. The surface layer, the intermediate layer, and the underlying sediments in the No. 2 reactor were taken out for testing. The sediments in the surface layer, intermediate layer, and bottom layer were labeled as 2S, 2M, and 2B, respectively. Similarly, 3S, 3M, 3B and 4S, 4M, 4B were labeled as the sediments in the surface layer, intermediate layer, and bottom layer of the No. 3 and No. 4 reactors.

Total DNA was extracted from the sediment samples for the analysis of bacteria, denitrifying bacteria, and methane bacteria. Polymerase chain reaction (PCR) was amplified for DGGE to obtain the samples of bacteria, denitrifying bacteria, and methane bacteria in DGGE fingerprints (Fig. 4). As can be seen from the bacterial DGGE profiles in these ten samples, the overall numbers of strips were richer. But their locations had no significant differences in 2M, 2B and 3S. The brightness of some bands, such as A, F, and C, increased. The DGGE atlas of denitrifying

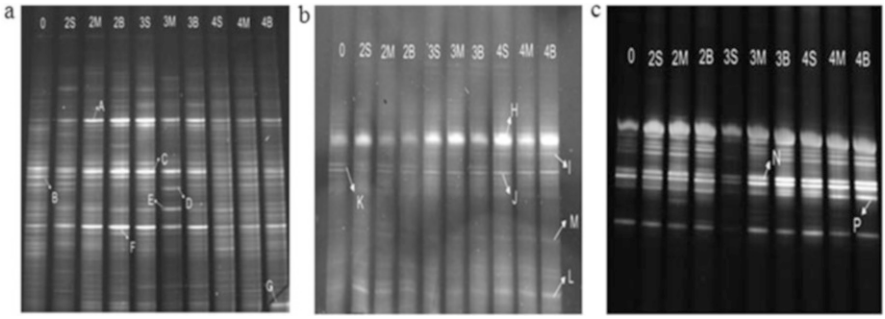

Fig. 4 The DGGE profiles: (**a**) bacteria, (**b**) denitrifying bacteria, (**c**) methane bacteria

Table 8 Identification results of the bacteria, denitrifying bacteria, and methane bacteria in the sediments

Band	Species	Similarity, %	Sequence length, bp
A	*Acinetobacter* spp.	100	161
B	Uncultured bacterium	100	160
C	Uncultured *Vibrio* spp.	99	160
D	Uncultured *Anoxybacillus* spp.	100	160
E	*Anoxybacillus flavithermus*	100	160
F	*Comamonas* spp.	98	182
G	Uncultured bacterium	100	154
H	Uncultured bacterium	95	127
I	*Comamonadaceae* bacterium	93	113
J	Uncultured bacterium	97	127
K	Uncultured bacterium	93	127
L	*Leptothrix cholodnii* SP-6	93	127
M	Uncultured bacterium	92	133
N	Uncultured *Methanosaeta* spp.	99	292
P	Uncultured *archaeon*	100	292

bacteria and the number of total bands were lower. The position difference was not obvious. The DGGE atlas of methane bacteria and the overall number of strips meant that it was more than bacteria and less than denitrifying bacteria. There was no significant difference in their position. But in the five samples in the post, the intensity of the bands were enhanced.

16S rDNA sequencing of the strips which were labeled in Fig. 4 were tested. The sequence results were compared with those in the GenBank database (Table 8).

The diversity indexes of bacteria, denitrifying bacteria, and methanogenic bacteria in each sediment sample were calculated, and the results are shown in Table 9. There was no significant difference between bacteria A with the continuous decrease of DO concentration. The denitrifying bacteria in the experiment began to decrease as the DO concentration decreased to 2 mg/L. The diversity index of denitrifying bacteria of sediment in the surface layer, middle layer, and bottom

Table 9 The diversity indexes of bacteria, denitrifying bacteria, and methane bacteria in the sediment

Name of samples	0	2S	2M	2B	3S	3M	3B	4S	4M	4B
Bacteria	0.74	0.75	0.69	0.87	0.78	0.69	0.74	0.70	0.67	0.67
Denitrifying bacteria	0.45	0.33	0.43	0.41	0.22	0.20	0.25	0.37	0.42	0.42
Methanogens	0.58	0.87	0.92	0.92	0.54	0.82	0.83	0.82	0.88	0.88

layer decreased, and then increased again at the end of the experiment, under the condition of DO<1 mg/L. It was conducive for the growth, reproduction, and accumulation of the denitrifying bacteria. The diversity index of methane bacteria in sediment increased significantly at the beginning of the experiment, due to the concentration of DO being below 2 mg/L (aerobic conditions) [19, 20].

References

1. Jin XC, Wang SR, Jiang X (2004) Preliminary study of three dimension model of the lake water sediment interface. Res Environ Sci 17(Suppl):1–5 (in Chinese)
2. Liu QM, Liu M, Xu SY (2002) Distribution feature of inorganic phosphorous in tidal sediments at different grain sizes taken from Shanghai coastal zone. Mar Environ Sci 21 (3):29–33 (in Chinese)
3. Mlynarczyk N, Bartoszek M, Polak J, Sulkowski WW (2013) Forms of phosphorus in sediments from the Goczałkowice Reservoir. Appl Geochem 37:87–93
4. Ruttenberg KC (1992) Development of a sediment extraction method for different forms of phosphorus in marine sediments. Limnol Oceanogr 37(2):1460–1482
5. Ruban V, Brigault S, Demare D (1999) An investigation of the origin and mobility of phosphorus in freshwater sediments from Bort-Les-Orgues Reservoir, France. J Environ Monit 1(4):403–407
6. Chai BB (2008). Study on pollutant release and multi phase interface between water and sediment. Masters degree at Xi'an University of Science and Technology (in Chinese)
7. Zhou ZM, Huang TL, Cong HB (2007) Algae removal by combined process of water-lifting aeration and biological contact oxidation. China Water Wastewater 23(15):13–16
8. Rydne E (2000) Potentially mobile phosphorus in Lake Erken sediment. Water Res 34 (7):2037–2042
9. Ma HB, Song JM, Xia X (2003) Nitrogen forms and their functions in biogenchemical cycling in Bohai Sea sediments. Geochemistry 32(1):48–54 (in Chinese)
10. Lü XX, Song JM, Li XG, Yuan HM, Zhan TR, Li N, Xl G (2005) Geochemical characteristics of nitrogen in the southern Yellow Sea surface sediments. J Mar Syst 56(1–2):17–27
11. Hewson I, Fuhrman J (2004) Richness and diversity of bacterioplankton species along an estuarine gradient in Moreton Bay, Australia. Appl Environ Microbiol 70(6):34–25
12. Wei YL, Wang P, Zhao MX (2010) A preliminary study of microbial diversity of the top sediment from the MD 062–3047. Adv Earth Sci 25(2):212–219 (in Chinese)
13. Song HN, Du BH, Zhang MY, Fu WZ, Lu XM, Li ZH, Ding YQ (2010) Effect of environmental factors on bacterial community in lake Dongping sediment. Acta Microbiol Sinica 50 (8):1065–1071 (in Chinese)
14. Eiler A, Bertillsson S (2004) Composition of freshwater bacterial communities associated with cyanobacterial blooms in four Swedish lakes. Environ Microbiol 6(12):1228–1243

15. Fujioka R (2001) Monitoring coastal marine waters for spore-forming bacteria of faecal and soil origin to determine point from non-point source pollution. Water Sci Technol 44(7):181–188
16. Barns S, Cain E, Sommerville L (2007) Acidobacteria phylum sequences in uranium contaminated subsurface sediments greatly expand the known diversity within the phylum. Appl Environ Microbiol 6(12):23–31
17. Auer MT, Auer NA, Barkdoll BB, Bornhorst TJ (2014) 4.18—The Great Lakes: nutrients, sediments, persistent pollutants, and policy perspectives for a sustainable future. Earth Systems and Environmental Sciences
18. Song HN, Du BH, Zhang MY (2010) Effect of environmental factors on bacterial community in Lake Dongping sediment. Acta Microbiologica Sinica 50(8):1065–1071 (in Chinese)
19. Ting DS, Appan A (1996) General characteristics and fractions of phosphorus in aquatic sediments of two tropical reservoirs. Water Sci Technol 34(7–8):53–59
20. Qian YC, Liang XQ, Chen YX (2010) Significance of biological effects on phosphorus transformation processes at the water–sediment interface under different environmental conditions. Ecol Eng 37(6):816–825

Characteristics of Pollutants Released from Reservoir Sediments

Jinlan Xu, Chao Xia, Zizhen Zhou, Yang Li, Fan Zhang, and Tinglin Huang

Abstract Nitrogen is not only a basic constituent element of life, but it is also one of the key elements causing eutrophication. It has an important effect on nutritional status and water quality in lakes and reservoirs. Inorganic nitrogen, including ammonia (NH_4^+) and nitrate (NO_3^-), often occurs following nitrification and denitrification reactions in a multiphase interface with the change of dissolved oxygen (DO) and redox. In addition, the extent of heavy metals is diffused from sediments to overlying water. It may cause potential harm to the water quality of the reservoir. This chapter is separated into two parts: (1) The release of nitrogen and phosphorus from sediment is investigated in typical Chinese reservoirs; (2) The release of metals from sediment is investigated in typical Chinese reservoirs.

Keywords Release • Nitrogen and Phosphorus • Sediments • Reservoir • Heavy Metals

1 The Release of Nitrogen in Sediment

Dissolved inorganic nitrogen (DIN), such as NO_3^-, NO_2^-, and NH_4^+, and some organic nitrogen (Org-N) originating from dead species as well as N_2 dissolved in water, can be assimilated by specific species. Org-N and NH_4^+ in water infiltrate sediment by diffusion and settle to form endogenous nitrogen. However, some Org-N is mineralized to NH_4^+, and other Org-N become Org-N sinks. Obviously, the cycle of nitrogen in a multiphase interface is a multibiochemical process, as shown in Fig. 1 [1, 2]. Current studies mainly focus on the speciations of nitrogen, the ecological significance of various speciations, the cycle of various nitrogen, nitrification and denitrification, and factors influencing reservoirs [3–7].

J. Xu • C. Xia • Z. Zhou • Y. Li • F. Zhang • T. Huang (✉)
School of Environmental and Municipal Engineering, Xi'an University of Architecture and Technology, Yanta Road 13, 710055 Xi'an, Shaanxi Province, P. R. China
e-mail: huangtinglin@xauat.edu.cn

T. Huang (ed.), *Water Pollution and Water Quality Control of Selected Chinese Reservoir Basins*, The Handbook of Environmental Chemistry 38,
DOI 10.1007/978-3-319-20391-1_6

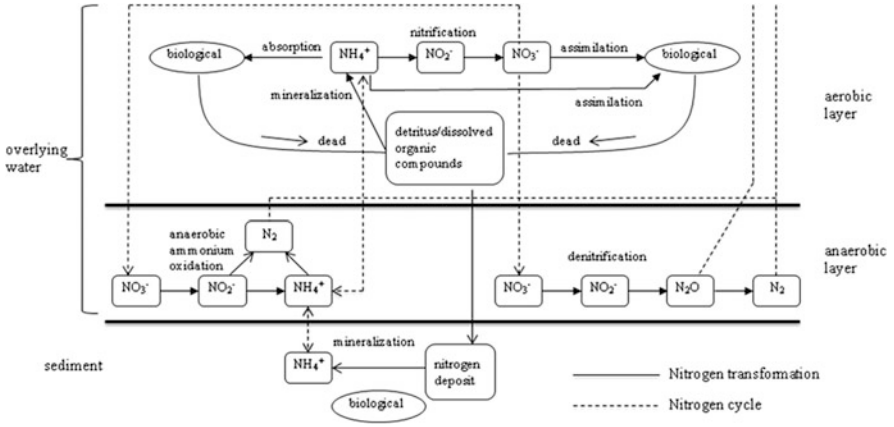

Fig. 1 The cycle of nitrogen in a multiphase interface

1.1 Jinpen Reservoir

(1) Reservoir Situation

The plane of Jinpen Reservoir is in an S-shaped bend, belonging to the Canyon Reservoir, and the main channel is narrow, as shown in Fig. 2. The reservoir has two entrance tributaries and one water outlet. Therefore, the sampling points are along the length direction of the main channel. In addition, the sampling points are placed in the tributaries of the entrance near the water intake. The 17 sampling points are all shown in the terrain map.

The 17 sampling sediments are mixed evenly, placed into a brown jar, which is then filled with anoxic water and aerated by purity N_2, sealing the bottle mouth using a rubber plug, avoiding light and with the temperature set at 7 °C–8 °C. The experimental conditions are shown in Table 1.

(2) The Release of Nitrogen

There are 24 experimental bottles, from which the pollutant indexes are determined at a certain time. The average value is considered as the result of measurement, and the concentrations of total nitrogen and ammonia in overlying water are obtained. The determination results are shown in Fig. 3.

It can be seen from Fig. 3 and Table 2 that the ammonia increased gradually in overlying water under the anaerobic condition and reached a balance after 60 h. The maximum concentration is 3.5 mg/L, the release rate is 13.68 mg/(m^2·d), and the release rate of total nitrogen is 30.24 mg/(m^2·d). The experimental results show that the release of ammonia and total nitrogen is very significant in the sediment of Jinpen Reservoir. The release of pollutants can reach a balance when the dissolved oxygen concentration is less than 0.5 mg/L. The release of pollutants into overlying water seriously affects the water quality of overlying water.

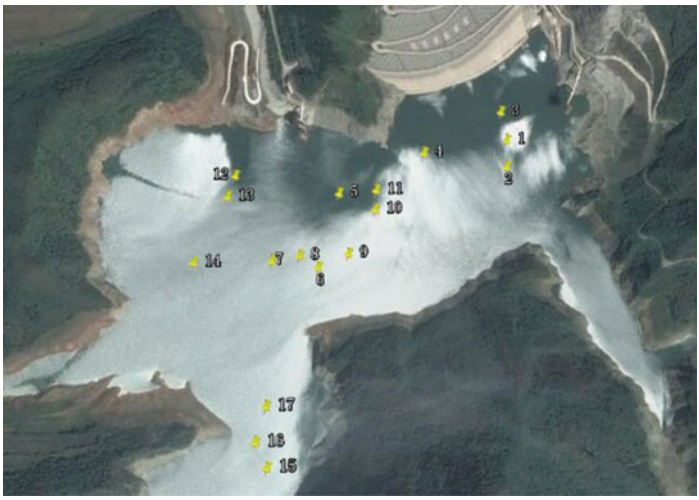

	latitude	longitude		latitude	longitude
1	34°2′45.41″N	108°12′20.90″E	10	34°2′41.62″N	108°12′7.02″E
2	34°2′43.16″N	108°12′20.29″E	11	34°2′43.12″N	108°12′7.48″E
3	34°2′47.94″N	108°12′21.03″E	12	34°2′46.61″N	108°11′54.51″E
4	34°2′45.30″N	108°12′12.66″E	13	34°2′45.04″N	108°11′53.41″E
5	34°2′43.56″N	108°12′3.94″E	14	34°2′40.07″N	108°11′49.38″E
6	34°2′37.59″N	108°12′0.76″E	15	34°2′23.38″N	108°11′53.26″E
7	34°2′38.92″N	108°11′56.62″E	16	34°2′25.39″N	108°11′52.54″E
8	34°2′38.88″N	108°11′59.24″E	17	34°2′27.83″N	108°11′53.97″E
9	34°2′38.32″N	108°12′3.74″E			

Fig. 2 The sampling points layout of Jinpen Reservoir

Table 1 The experimental control conditions

	DO	Temperature	Light
Control condition range	≤0.5 mg/L	7–8 °C	Avoiding light

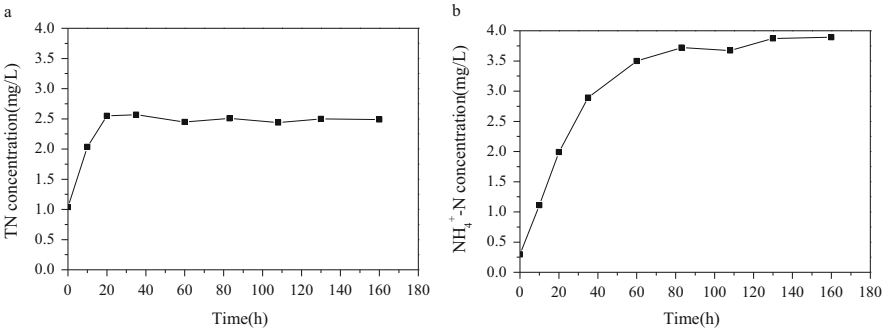

Fig. 3 Concentration variation of total nitrogen (**a**) and ammonia (**b**) in overlying water

Table 2 The results of the release experiment

Item	Balanced release time (h)	Initial concentration (mg/L) (average value)	Limit release concentration (mg/L) (average value)
Ammonia	58.5	0.296	3.345
Total nitrogen	34.5	1.037	3.572

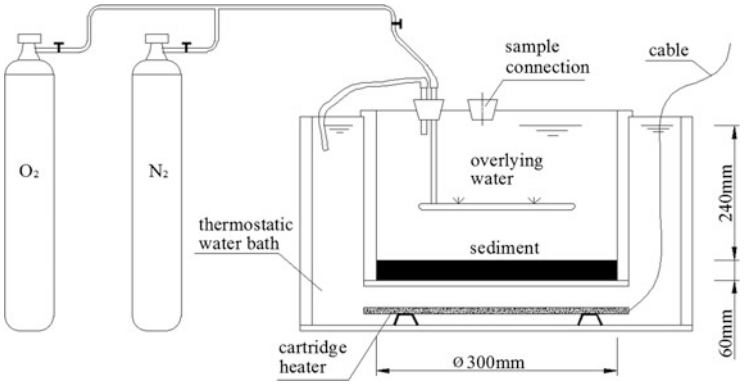

Fig. 4 Diagram of the experimental device

(3) Effect of Microorganisms on Nitrogen Release

The experimental water was taken from water above 50 cm of the interface between water and sediment in Jinpen Reservoir. Water samples were kept at 4 °C after filtration by a 0.450-μm membrane. Sediment samples were collected from below 30 cm of the interface between sediment and water in Shibianyu Reservoir using a Pedersen sampler, then sand and stone were sieved by a 0.9 -mm Nylon 20 mesh, and, finally, the sediment was dried of water using a syringe. The experimental device is shown in Fig. 4. 60 mm of sediment and 240 mm of overlying water were placed in the experimental barrels. The experiment was divided into a sterile group and a non-sterile group. The deactivation was performed by heating for 2 h at 70 °C. At the start of the experiment, 85 mL of chloroform was added to the water in the barrels. The overlying water quality was measured at a certain time interval.

Figure 5 shows the change of dissolved oxygen with time. The DO concentration in the non-sterile group decreased faster than that in the sterile group, which decreased to below 2 mg/L in 25 days. The result shows that the presence of microorganisms can accelerate the consumption of dissolved oxygen. The concentration of ammonia in the non-sterile group increased sharply to 2.5 mg/L when overlying water reached an anaerobic stage. The release rate of ammonia reached 50.18 mg/(m^2·d). However, the concentration of ammonia in the sterile group increased to 1 mg/L (Table 3).

As shown in Fig. 6, the ammonia concentration of the non-sterile group increased sharply up to 2.5 mg/L. The release rate reached 50.18 mg/(m^2·d) during

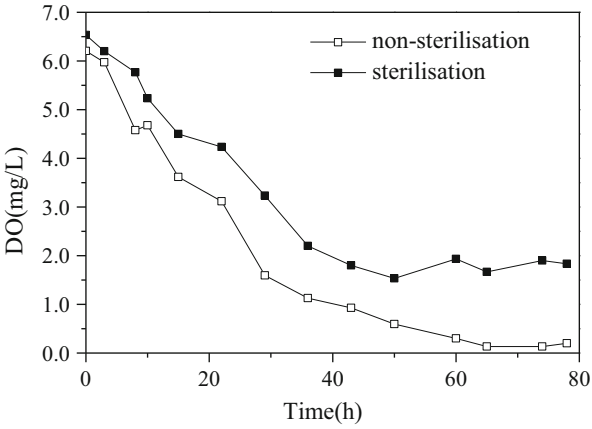

Fig. 5 The variation of DO concentration in overlying water

Table 3 The release rate of total nitrogen and ammonia experiment

Item	Balanced release rate (mg/(d·m^2))	Standard deviation	Average release rate (mg/(d·m^2))	Standard deviation
Ammonia	13.68	0.22	6.96	0.81
Total nitrogen	30.24	0.08	5.52	0.52

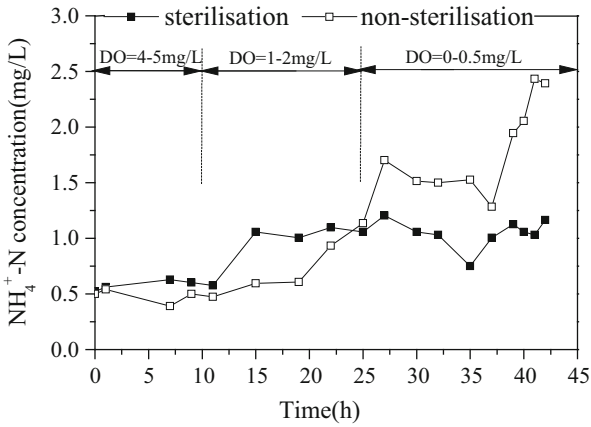

Fig. 6 The variation of ammonia concentration in overlying water

the anaerobic stage. However, the concentration of ammonia in the sterilized group increased slowly to 1 mg/L. Overall, the concentration of ammonia of overlying water in the non-sterile group shows a downward trend (Fig. 7), decreasing from 2.0 mg/L to 0.028 mg/L after 40 days. The downward trend of the non-sterile group is less than that of the sterile group, falling only to 1.3 mg/L.

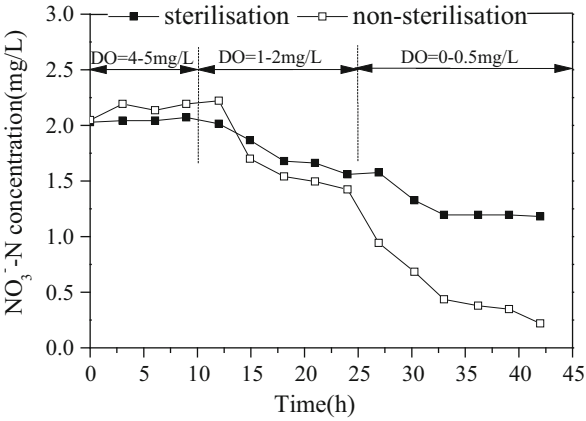

Fig. 7 The variation of nitrate concentration in overlying water

1.2 Shibianyu Reservoir

(1) Reservoir Situation

Shibianyu Reservoir is the emergency source water of Xi'an. It began to supply water in August 1990. The reservoir dam is located in Hao River of Shibianyu upstream near the north slope of Qinling Mountain. It is 40 km from Xi'an. The catchment area above the dam is 282 km^2. The average annual runoff is 95,000,000 m^3. The total storage capacity is 28,100,000 m^3. The volume of supply water to Xi'an is 30,000,000 m^3, and the maximum daily supply capacity is 400,000 m^3. The average annual rainfall is 898 mm. The average annual runoff is 97,000,000 m^3. The average evaporation is 948.5 mm (601 evaporation pan), and the maximum measured runoff is 359 m^3/s (June 8, 2002). The largest dry flow is 0.1 m^3/s, and the largest survey of historical flood flow is 650 m^3/s.

(2) The Release of Nitrogen

The experimental overlying water and sediment are both collected from Shibianyu Reservoir. Surface sediment (0–30 cm) was collected by a Pedersen grab sampler, whereas overlying water was collected 1 m below the reservoir's water surface (DO>8 mg/L). The sediment and overlying water were carried back to the laboratory and kept at low temperature until use. Two liters of sediment were loaded at the bottom of the reactor and 8 L of raw water was slowly injected into the reactor using the siphon method.

As shown in Fig. 8, the concentration of ammonia in overlying water increased gradually over time, reaching 10 mg/L after 90 days. However, the concentration of nitrate decreased, finally reaching zero. The release rate of ammonia in sediment is 10.77 mg/ (m^2·d). The total nitrogen in surface, middle, and bottom sediment decreased to 28.4 %, 34.3 %, and 31.1 %, respectively (Fig. 9).

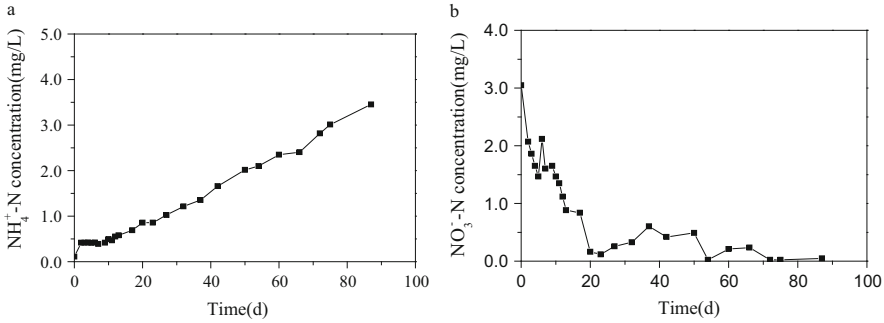

Fig. 8 The concentration of ammonia (**a**) and nitrate (**b**) in overlying water

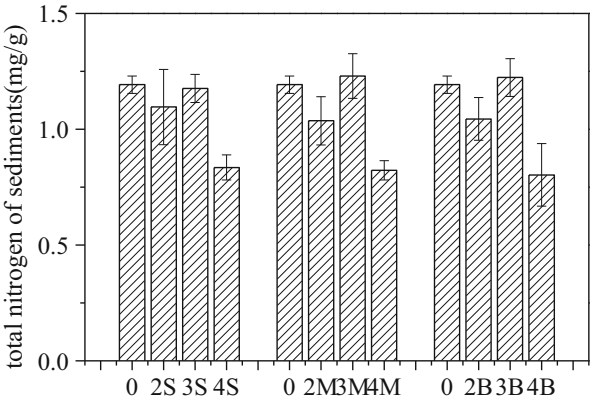

Fig. 9 The concentration of total nitrogen in sediment

(3) Effect of Microorganisms on Nitrogen Release

The experimental water was taken from water above 50 cm of the interface between water and sediment in Shibianyu Reservoir. The water samples were kept at 4 °C after filtration by 0.45-μm membrane. Sediment samples were collected from below 30 cm of the interface between sediment and water in Shibianyu Reservoir using a Pedersen sampler, then sand and stone were sieved by a 0.9-mm Nylon 20 mesh, and, finally, the sediment was dried of water using a syringe, mixing, and preservation. The experimental device is shown in Fig. 4. The experimental mud and water were divided into two groups, the non-sterile group and the sterile group, by ultraviolet irradiation. The total number of bacteria before and after was determined by the MPN method. The physicochemical properties and deactivation rate are listed in Table 4.

The experiment was divided into sterile and non-sterile groups. Each group had two parallel series, and each series comprised ten experimental bottles. The sediments of the sterile group and the non-sterile group were loaded into brown jars

Table 4 The physicochemical properties and deactivation rate after UV irradiation in Shibianyu Reservoir

TN concentration (mg/g)	TP concentration (mg/g)	Organic matter (%)	Moisture content (%)	Total bacteria (cells/g)		Rate of sterile (%)
				Non-sterile	Sterile	
1.168	0.813	3.296	42.649	2×10^4	15	99.93

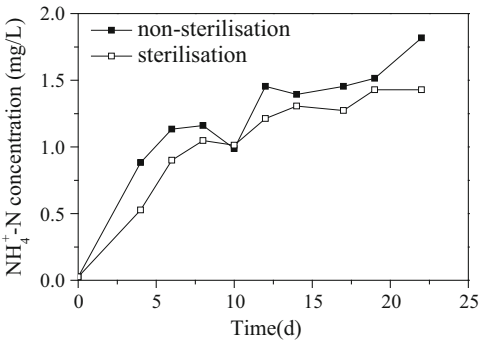

Fig. 10 The concentration trend of ammonia in overlying water

with 6 cm inner diameter and 250 mL volume. 150 mL of raw water from the reservoir was slowly injected into the bottle along the bottle wall above the sediment using the siphon method, avoiding disturbance of the bottom sediment. The reaction bottle is sealed and preserved by avoiding light in the freezer, adjusting the temperature to 7 °C–8 °C. The overlying water quality was measured at a certain time interval.

As shown in Fig. 10, the concentration of ammonia in overlying water in the non-sterilized group increased gradually, reaching 1.8 mg/L after 20 days. The concentration of ammonia in the sterilized group increased gradually with time, reaching a balance with the concentration of 1.4 mg/L after 15 days. The concentration of dissolved organic matter in overlying water increased when the concentration of ammonia in the non-sterilized group increased gradually and released into overlying water. The concentrations of ammonia and UV_{254} show a significant positive correlation, as shown in Fig. 11 ($R^2 = 0.8061$). However, the concentration of ammonia in the sterilized group in overlying water and the dissolved organic matter have a weak correlation ($R^2 = 0.301$), as shown in Fig. 12.

With the anaerobic environment intensified, denitrification accelerates gradually, which results in a significant decrease of the total nitrogen of overlying water in 19 days (Fig. 13), reaching a minimum value of 0.597 mg/L. After that, the concentration of total nitrogen began to rise again. As the experiment proceeded, the concentration of nitrate in the non-sterile group showed a downward trend (Fig. 14), decreasing from 1.242 to 0.028 mg/L. The concentration of nitrite was quite low, but the concentration of nitrite in the non-sterilized group was higher than that in the sterilized group (Fig. 15).

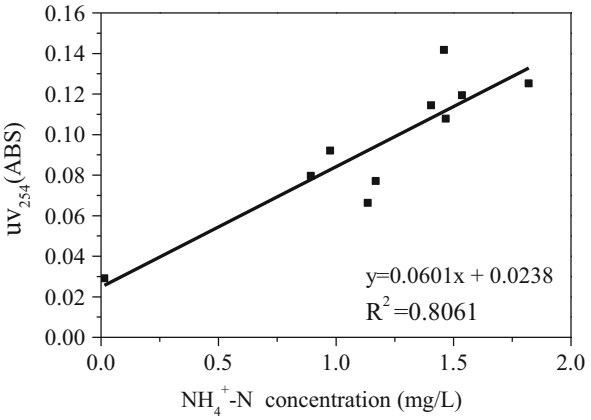

Fig. 11 Correlation analysis of ammonia concentration and UV_{254} change in the non-sterilized group

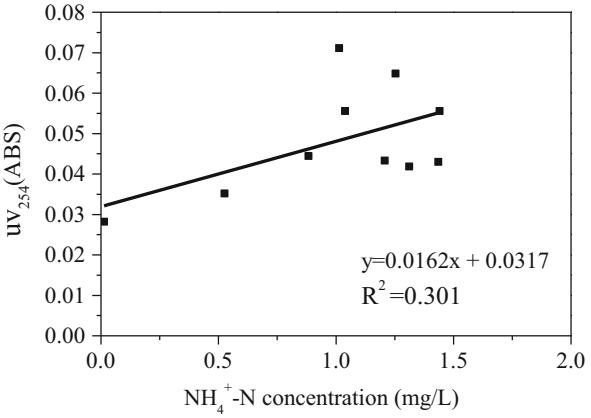

Fig. 12 Correlation analysis of ammonia concentration and UV_{254} change in the sterilized group

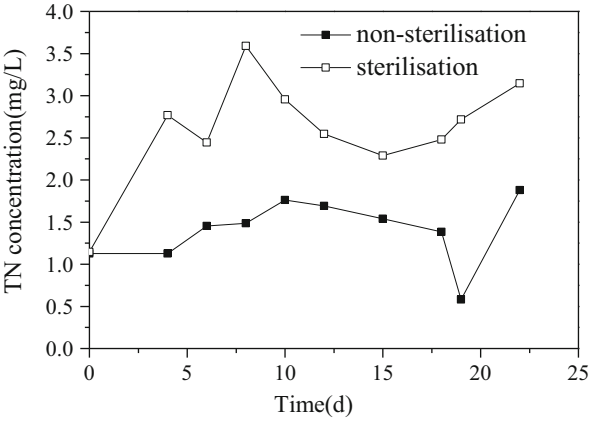

Fig. 13 The variation trend of TN concentration in overlying water

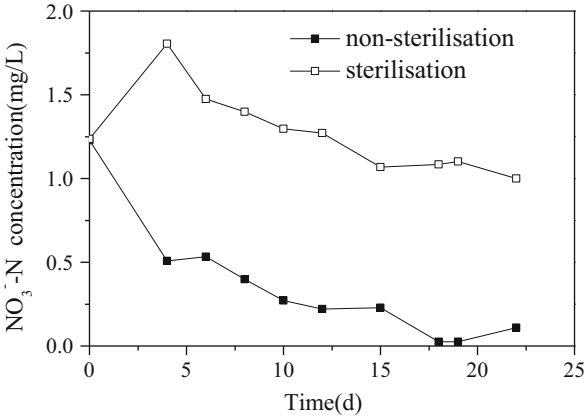

Fig. 14 The variation trend of NO_3^- concentration in overlying water

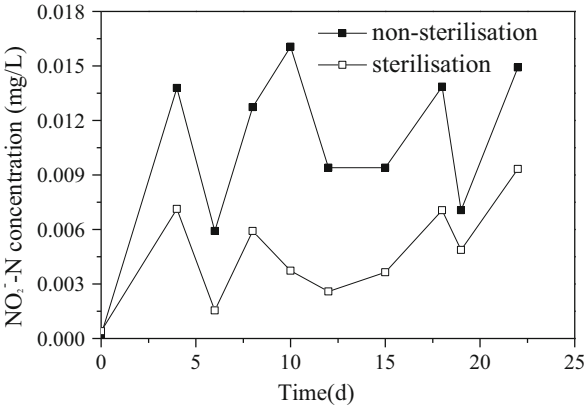

Fig. 15 The variation trend of NO_2^- concentration in overlying water

The main factors that influenced denitrification include the nitrate concentration in water and sediment, carbon availability, temperature, dissolved oxygen concentration and penetration depth, redox potential, block material (such as S^{2-}) concentration, pH, salinity, light, benthic disturbance, and plant community characteristics. The results of sulfate and dissolved oxygen in overlying water are shown in Figs. 16 and 17. With the decrease of DO concentration in a multiphase interface, the concentration of sulfate in the non-sterilized group decreased significantly from 10.99 to 4.22 mg/L, a percentage of 60.61 %. However, sulfate only drops 30.88 % in the sterilized group. The oxygen consumption rate of the non-sterilized group was significantly higher than that of the sterilized group, which indicates that the presence of microorganisms in sediment would result in the consumption of DO. The anaerobic condition accelerated the release of ammonia and resulted in the accumulation of ammonia in overlying water in the non-sterilized group.

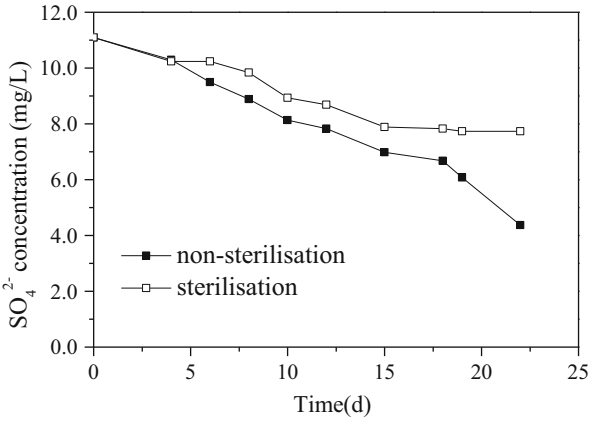

Fig. 16 The variation trend of SO_4^{2-} in overlying water

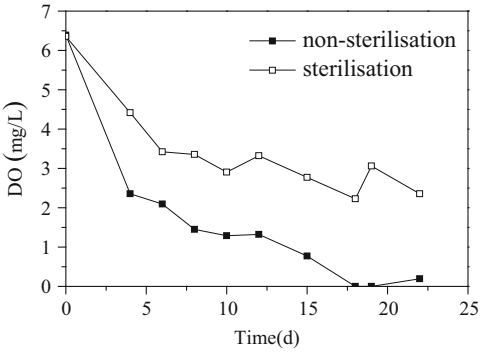

Fig. 17 The variation of DO concentration in overlying water

1.3 Zhoucun Reservoir

(1) Reservoir Situation

The water collecting area of the reservoir is 121 km^2. The basin is a pure hill area, and the upstream of the reservoir has seven small reservoirs and eight small embankments. The total control watershed area of the seven reservoirs is 14.91 km^2. The dam of the reservoir is 1070 m in length. The maximum height of the dam is 29 m, the width is 6.0 m, and the elevation is 134.00 m. A detailed description of this reservoir can be found in Chap. 1.

Ten sediment samples were taken from different positions near the main reservoir area using a Pedersen sampler. The specific sampling points distribution is shown in Fig. 18. The sampling depth of sediment is 10–15 cm below the interface between water and sediment.

(2) The Release of Nitrogen

The reactors are two glass bottles with 25 cm diameter and a volume of 25 L, wrapped with black cloth. The bottle mouth is sealed by a rubber plug, which is arranged on the pressure balance hole and aeration holes. The water is injected into

	latitude	longitude		latitude	longitude
1	34°56′34.88″N	117°45′3.25″E	6	34°56′46.79″N	117°40′54.94″E
2	34°56′41.95″N	117°41′7.63″E	7	34°56′53.80″N	117°40′59.10″E
3	34°56′49.60″N	117°41′13.22″E	8	34°57′0.90″N	117°41′3.60″E
4	34°56′34.43″N	117°40′47.66″E	9	34°56′47.25″N	117°40′41.83″E
5	34°56′40.11″N	117°40′50.8″E	10	34°56′59.47″N	117°40′51.09″E

Fig. 18 The location of sampling points in Zhoucun Reservoir

the reactor along the bottle wall using the siphon method, avoiding disturbances to the bottom sediment samples. The ratio of sediment thickness and water height is 1:4. The concentration of DO in the reactor declined to 3 mg/L by purging N_2. The reactor is sealed and placed at a constant temperature (4 or 10 °C) in a culture box.

The concentration of ammonia in water showed a rapid increasing trend. Microbial activity at 4 °C is lower than that at 10 °C because the concentration of NH_4^+ reached 6.09 mg/L and 6.89 mg/L at 4 °C and 10 °C, respectively. Therefore, the microbial activity promotes the release of NH_4^+, and the release rates of NH_4^+ are 18.9 mg/($m^2 \cdot d$) and 19.9 mg/($m^2 \cdot d$) at 4 °C and 10 °C, respectively (Fig. 19).

As shown in Fig. 20, overlying water soon showed hypoxia due to the rapid decline of the DO concentration in the reactor. Hypoxia can lead to the process of denitrification in the water, so the concentration of NO_3^- decreased rapidly. The decay rates in the reactor at 4 °C and 10 °C are 1.1 mg/($m^2 \cdot d$) and 2.0 mg/($m^2 \cdot d$), respectively. This result indicates that the higher the temperature of the water, the higher the activity of denitrifying bacteria, and the denitrification is faster. At the same time, NO_2^- accumulation appeared in the overlying water because the reductase competitive ability of nitrate is higher than that of nitrite reductase. Low temperature restrains the activity of denitrifying bacteria, so the accumulation of NO_2^- at 4 °C is slower than that at 10 °C, and the cycle is also longer. With the process of denitrification, NO_3^- and NO_2^- concentrations of overlying were close to 0 mg/L.

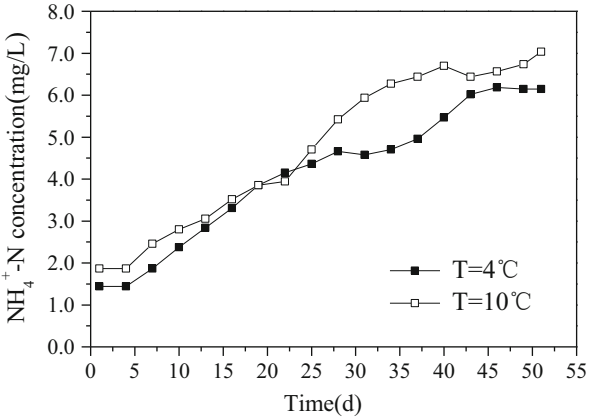

Fig. 19 The release characteristics of NH_4^+ in overlying water

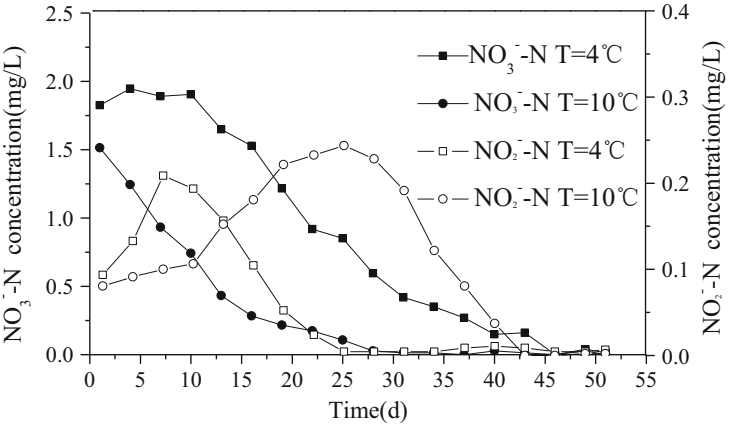

Fig. 20 The variation of NO_3^- and NO_2^- in overlying water

2 The Release of Phosphorus in the Sediments

Phosphorus (P) is one of the most important elements in the interface between water and sediment. It is also one of the key elements resulting in the eutrophication of lakes and reservoirs. The exchange process between sediments and phosphorus comprise very complex physical, chemical, and biological processes, and their interactions include the biological cycle of phosphorus, the re-suspension of particles, and the adsorption and desorption of dissolved phosphorus. The phosphorus recycling process of a water–sediment multiphase interface is a complex process, including oxidation and reduction, adsorption of the dissolved minerals, and the

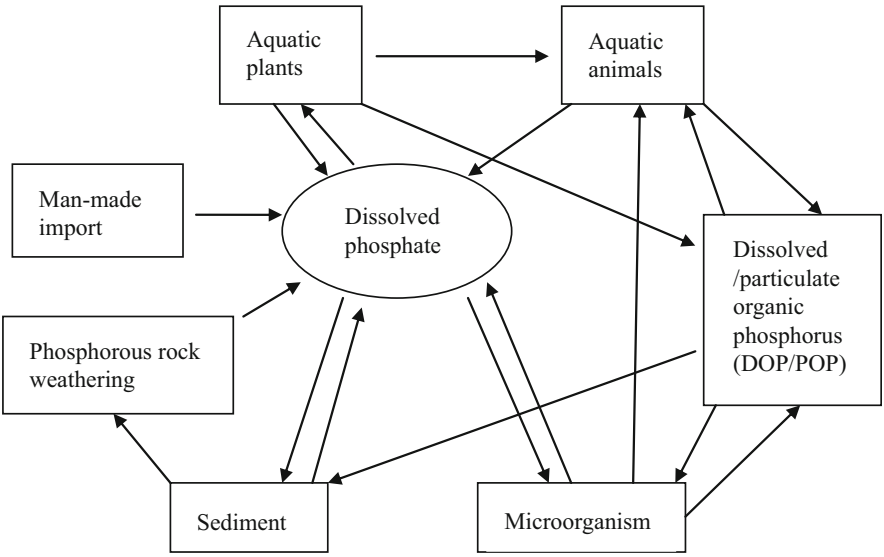

Fig. 21 Diagram of the phosphorus cycle in lakes and reservoirs

metabolism of bacteria and microbes occur in the process. This process includes hydrodynamic or biological disturbances, and may make the sedimentary phosphorus re-activate and release, becoming the endogenous reason which can influence the load in the water body. The simple cycle of phosphorus in a water–sediment multiphase interface can be seen in Fig. 21.

Phosphorus can be divided into orthophosphate, polymeric phosphate, and organic phosphorus. Orthophosphate is the most stable condition and can be absorbed directly by microbes. In addition, studies have shown that the release of phosphorus sediment mainly exists in the speciation of phosphate. Therefore, research on the concentration of PO_4^{3-} in the water and its variation has important significance [8]. Under normal circumstances, the concentration of PO_4^{3-} in the overlying water reaches 1–2 mg/L. Regardless of whether under the anaerobic environment or the aerobic environment, sediment is a phosphorus sink, and when the concentration of PO_4^{3-} in the overlying water is less than 1 mg/L, the sediment become the source of phosphorus under anaerobic conditions [9, 10].

The release of phosphorus in sediment is influenced by many factors, such as the speciation of phosphorus in the sediment and environmental factors. Environmental factors like temperature, dissolved oxygen, pH, ORP, disturbance, and others are considered more and more in the release of phosphorus in sediment and will be further studied [11]. Elevated temperatures will promote the microbial and benthic animals' activities and decomposition of organic matter in sediment, and the consumption of dissolved oxygen is accelerated in the water. The overlying water body in an anaerobic condition can result in a lower ORP, which results in the release of phosphorus-bound iron hydroxide in the sediment. Moreover, the increase of temperature will accelerate the release rate of phosphorus [12]. In

addition, with the increase of pH in the water, the release of phosphorus is increased significantly. From what has been discussed above, the factors that influence phosphorus release, such as dissolved oxygen, pH, and ORP, are due to the following reasons theoretically: (1) Under anaerobic conditions, with the decrease of ORP, Fe^{3+} is reduced to Fe^{2+}, making the iron-bound P release, as shown in Eqs. (1) and (2); (2) At higher pH values, OH^- will produce substitution on phosphate based on the principle of solubility, making the iron- and aluminum-bound phosphorus release, as shown in Eqs. (3) and (4).

$$FePO_4 - e \leftrightarrow Fe^{2+} + PO_4^{3-} \quad (1)$$

$$Fe(OH)_2H_2PO_4 - e \leftrightarrow Fe^{2+} + PO_4^{3-} + 2H_2O \quad (2)$$

$$FePO_4 + 3OH^- \leftrightarrow Fe(OH)_3 \downarrow + PO_4^{3-} \quad (3)$$

$$AlPO_4 + 3OH^- \leftrightarrow Al(OH)_3 \downarrow + PO_4^{3-} \quad (4)$$

The phosphorus firstly goes into the pores of the sediment, and then runs into the overlying water body due to the disturbance caused by microorganisms and bottom-dwelling organisms and storms caused by resuspension [13]. The current study on the transformation of phosphorus in a multiphase interface focuses on four aspects: (1) The relationship between the sediment and the overlying water quality; (2) The shape and grade determination of phosphorus in water and sediments; (3) The adsorption and release characteristics of phosphorus in the sediment; (4) The impact factor of phosphorus release and adsorption in the water.

2.1 Shibianyu Reservoir

(1) The Release of Phosphorus

Methods of sampling and research are the same as in Sect. 5.3.2 (2). The change of soluble phosphate in No. 1 reactor with time is shown in Fig. 22. The concentrations

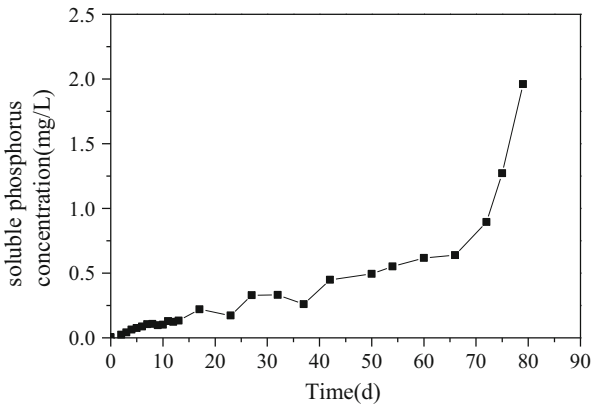

Fig. 22 The variation of soluble phosphate concentration in overlying water

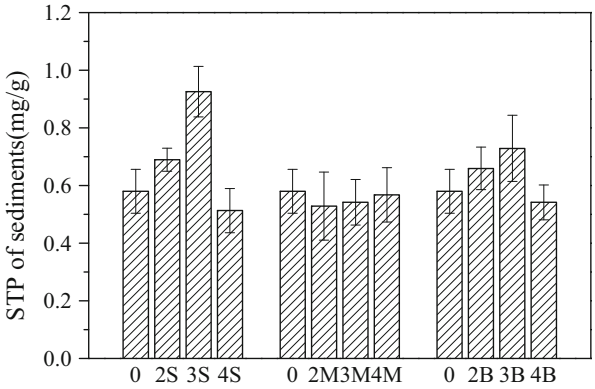

Fig. 23 Total phosphorus content in sediment

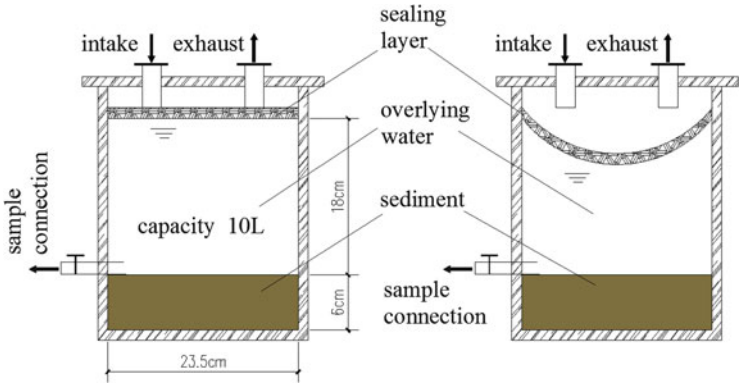

Fig. 24 Diagram of the experimental device

of soluble phosphate in overlying water accumulated gradually, and reached 2 mg/L on the 70th day.

With the experiment proceeding, the concentration of dissolved oxygen in overlying water continually decreases, as shown in Fig. 23. The total content of phosphorus in the sediment did not reduce obviously compared with the initial content of phosphorus. However, the phosphorus content in the surface sediment is more evident, because the total phosphorus content in the surface sediment of No. 3 reactor increased obviously and reached 0.93 mg/g on the 37th day.

(2) Effects of ORP and Microbes on the Release of Phosphorus in the Sediment of Shibianyu Reservoir

Three 10 L organic glass containers were used as reactors for the static release test (Fig. 24). The No. 1 reactor was used as the control reactor. In the No. 1 reactor, raw water and sediment were added in a ratio of 1:3. 2.5 L of sediment were added to the organic glass container, and 7.5 L of raw water was evenly injected along the

reactor wall using a siphon. The reactor was sealed after the raw water had been added. For the No. 2 reactor, sediment was inactivated using chloroform (2.5 L of sediment mixed evenly with 1 L of chloroform for 24 h). The raw water was inactivated by high-temperature treatment (at 121 °C, 30 min). The No. 3 reactor was filled with water and then 500 g of sodium sulfite was homogeneously added in order to keep low ORP.

(1) Changes of phosphorus concentration in sediment
The results are shown in Table 5. In different reaction conditions, the concentration of phosphorus decreased by different degrees. The No. 3 reactor maintains low ORP under reducing conditions, the concentration of Fe/Al-P in sediment decreased by 53.77 %, IP decreased by 53.83 %, and TP decreased by 50.78 % after the reaction, which is higher than that of No. 1 reactor in natural controlled oxygen. The results show that Fe/Al-P and IP in sediment were released to the water in strong reducing conditions. In No. 2 reactor, the concentration of Fe/Al-P decreased by 29.50 %, and the concentration of IP decreased by 31.96 %, which is lower than that of No. 1 reactor. The concentration of TP was slightly higher than that of No. 1 reactor. However, the concentration of OP decreased by 13.07 %, which is much lower than that of No. 1 reactor. This result shows that sterilization may inhibit the decomposition and transformation of OP in the sediment. In No. 1 and No. 3 reactors, the alkaline phosphatase activity (APA) of sediment is higher than that in raw sediment. In No. 3 reactor, a large amount of phosphorus is released under reductive conditions. The APA of sediment is higher in No. 3 reactor than that in No. 2 reactor. The results indicated that it is more suitable for alkaline phosphatase under reductive conditions and can promote the growth of reproductive microbial communities.

(2) Phosphorus concentration of overlying water
The experiment lasted 85 days. The concentrations of TP and PO_4^{3-} in overlying water increased from zero to 0.185 mg/L and 0.181 mg/L, respectively, in the No. 1 natural oxygen consumption reactor (Figs. 25 and 26). In No. 2 reactor (sterilization), the corresponding concentrations of TP and PO_4^{3-} in overlying water increased up to 0.358 mg/L and 0.116 mg/L, respectively. In the No. 3 anaerobic reactor, the corresponding concentrations of TP and PO_4^{3-} in overlying water were 1.031 mg/L and 0.580 mg/L, respectively. The significant difference in phosphorus concentration in the three reactors indicated that environmental conditions have great influence on phosphorus release from sediment.

The concentration of soluble iron (Fe^{2+}) in the overlying water was monitored, and the results are shown in Fig. 27. It was found that the changing trend of Fe^{2+} concentration is roughly the same as that of PO_4^{3-}. This shows that PO_4^{3-} and Fe^{2+} in the overlying water are related. In No. 3 reactor, the content of Fe/Al-P decreased obviously after the reaction, which indicated that the

Table 5 Different speciations of phosphorus in sediment before and after reaction

	Original sediment	No. 1 reactor		No. 2 reactor		No. 3 reactor	
Speciations	Concentration, mg/kg	Concentration, mg/kg	Reduction, %	Concentration, mg/kg	Reduction, %	Concentration, mg/kg	Reduction, %
Fe/Al-P	284.82±0.02	194.19±0.21	33.75	200.80±0.05	29.50	104.12±0.17	53.77
Ca-P	12.40±0.01	0.98±0.05	92.06	1.18±0.02	90.48	0.59±0.06	95.24
IP	300.44±0.02	220.16±0.12	34.45	204.42±0.23	31.96	197.73±0.31	53.83
OP	23.09±0.09	10.43±0.23	54.83	20.07±0.02	13.07	12.40±0.04	46.31
TP	334.08±0.04	219.01±0.07	30.17	219.01±0.18	34.44	164.44±0.22	50.78
APA	36.02±0.23	42.79±0.12	−18.80	23.53±0.04	34.68	46.36±0.14	−28.71

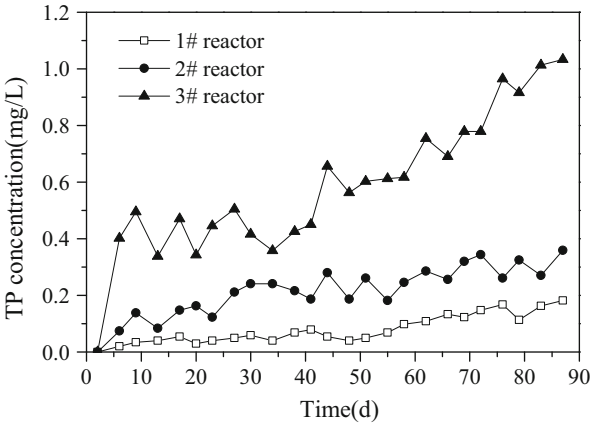

Fig. 25 The variation of total phosphorus concentration in overlying water

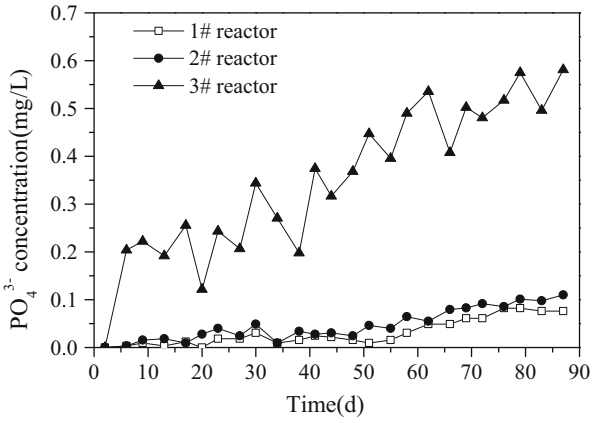

Fig. 26 The variation of PO_4^{3-} phosphorus concentration in overlying water

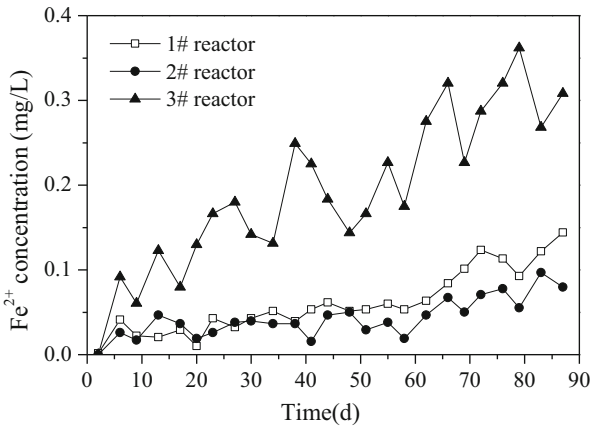

Fig. 27 The variation of Fe^{2+} concentration in overlying water

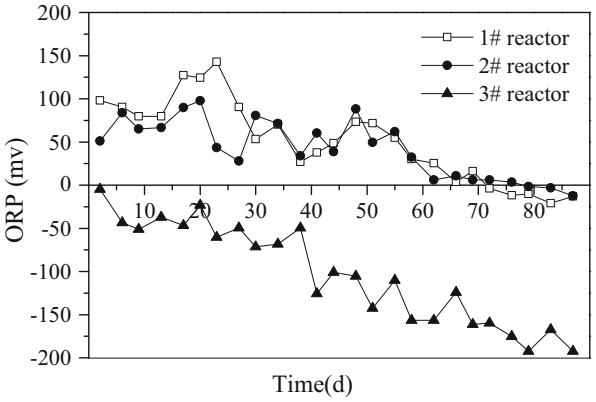

Fig. 28 The variation of ORP in overlying water

strong reducing conditions can promote the decomposition of Fe/Al-P in the sediment into Fe^{2+} and PO_4^{3-}.

(3) Effects of ORP on phosphate release from sediment
As shown in Fig. 28, during the test, when ORP in No. 1 reactor decreased from 100 mv to −20 mv, the concentration of TP in overlying water increased from 0 to 0.36 mg/L, PO_4^{3-} increased from 0 to 0.12 mg/L, and Fe^{2+} increased from 0 to 0.14 mg/L. At the same time, when ORP in No. 3 reactor continued to reduce to −200 mv, the concentration of TP in overlying water increased from 0.079 to 1.03 mg/L, PO_4^{3-} increased from 0.002 to 0.58 mg/L, and Fe^{2+} increased from 0 to 0.14 mg/L; the increases were more significant than those in No. 1 reactor.

This result may indicate that there is a negative correlation between the overlying water ORP value and the concentration of TP, PO_4^{3-}, and Fe^{2+}. The lower the ORP value, the higher the content of TP, PO_4^{3-}, and Fe^{2+}. The change of phosphorus is shown in Table 5. In overlying water, ORP is lower than 0 mv, and iron- and aluminum-bound phosphorus (Fe/Al-P) in sediment can be released to the overlying water in the speciation of dissolved phosphate.

(4) Effect of microorganisms on phosphate release from sediment
Under sterilization conditions (No. 2 reactor), although the ORP value reduced from the initial 51.8 mv to −8.9 mv (Fig. 28), the accumulated growth rate of PO_4^{3-} in the overlying water is only slightly higher than that in No. 1 reactor. The concentration of Fe^{2+} is slightly lower than that in the No. 1 control reactor (Fig. 27). This indicated that the sterilization limited the concentrations of non-soluble phosphorus in the overlying water and reduced the microbial nutrition absorption of phosphorus in water. The speciations of phosphorus (Table 5) shows the amount of OP in No. 2 reactor reduced less than No. 1 reactor, which illustrates that the sterilization conditions can inhibit the release of OP in the sediment, whereas it cannot inhibit the release of Fe/Al and phosphorus. At the same time, the before and after phosphate reductase activity reduced in No. 2 reactor. The results show that the number of phosphobacteria in No. 2 reactor is much less than that in No. 1 reactor.

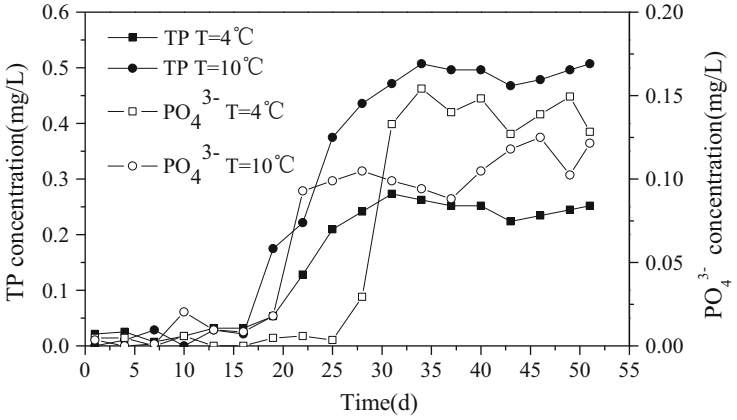

Fig. 29 The release of TP and PO_4^{3-} in sediment

2.2 Zhoucun Reservoir

(1) The Release of Phosphorus

As can be seen from Fig. 29, the phosphorus in sediment started to be released when the DO concentration was lower than 1 mg/L. The concentration of TP in the overlying water was 0.25 mg/L and 0.51 mg/L in the two conditions (no matter whether 4 °C or 10 °C), respectively. The release rate of TP at 10 °C is higher than that at 4 °C because higher temperature accelerated the reduction of dissolved phosphorus and the speed of the displacement reaction, and also intensified the benthic activity [14]. The release rates of TP were 19.2 mg/($m^2 \cdot d$) and 18.9 mg/($m^2 \cdot d$). However, the release rate of PO_4^{3-} at 4 °C is slightly higher than that at 10 °C. The main reasons for this were that the pH of overlying water at 4 °C was higher than that at 10 °C. Higher pH and lower DO would produce a synergistic effect on the release of PO_4^{3-}.

(2) The Effect of Microbes on the Release of Phosphorus

The experimental apparatus is shown in Fig. 30. The simulation experimental device is divided into six compartments, of which three lattices are the sterilization boxes, equipped with an ultraviolet sterilizing lamp, and the other three lattices are not sterilized boxes. Sediments in the sterilization box were heated at 70 °C for 2 h. The experimental box of each grid is connected to a gas release device, which can pass nitrogen and oxygen and control the dissolved oxygen concentration. The concentration of dissolved oxygen in the aerobic phase is controlled to be in the range 7–8 mg/L, and the dissolved oxygen is controlled to be below 1 mg/L in the anaerobic stage. The test temperature is 30 °C. Control of the pH value in part of the experimental box is needed. The specific control conditions are shown in Table 6. Water samples were extracted through the sampling port using a syringe to measure the dissolved phosphorus and total phosphorus. Determination of the phosphatase

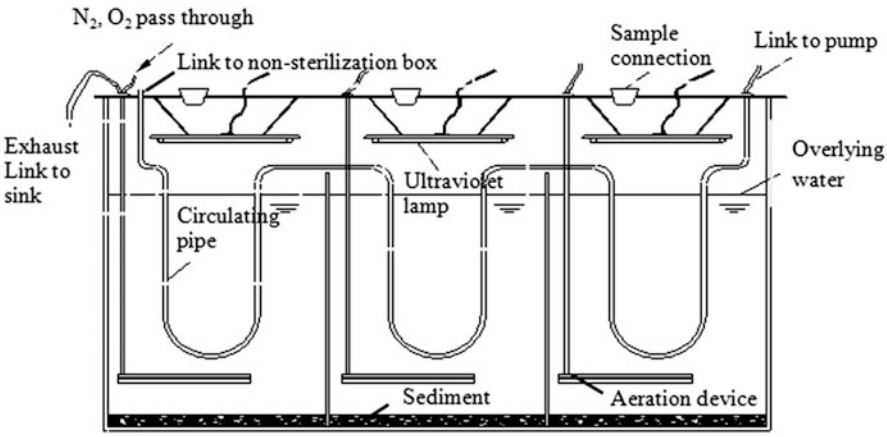

Fig. 30 Sediment release simulation—sterilization box

Table 6 Control conditions of the six reactors

Number	No. 1	No. 2	No. 3	No. 4	No. 5	No. 6
Microbial status	Sterilization	Sterilization	Sterilization	Non-sterilization	Non-sterilization	Non-sterilization
pH of overlying water	6.5	No control	9.1	6.5	No control	9.1

and organic phosphorus fractions in the original sediment was performed under aerobic and anaerobic conditions, respectively.

As shown in Fig. 31, the release of phosphorus from the sediment in No. 1 sterilization box and No. 4 non-sterile box did not occur under the weak acid aerobic conditions. Microorganisms played an important role in phosphorus release under anaerobic conditions. The release of phosphorus occurred in No. 4 non-sterile box, and the release rate of phosphorus is 0.41 mg/(m^2·d) in the early stages of anaerobic conditions. Also, the release strength increases gradually with time. The average release rate reaches 2.14 mg/(m^2·d) after 10 days. A minor release of phosphorus occurs in No. 1 sterilization box during the early stages of anaerobic conditions, but this process lasts only 6 days, and it then remains at a very low level.

When the pH is 9.1, the process of phosphorus release is shown in Fig. 32. The release of phosphorus in the non-sterile experiment box is faster than that in the sterile box. The release of phosphorus in the sterile box is obviously behind that of the non-sterile experiment box. There is no phosphorus release in the first 20 days. It can be proven that microorganisms play an important role in phosphorus release.

The effect of microorganisms on the pH value of water is shown in Fig. 33. During the aerobic phase, the pH value is about 7.5. During the anaerobic stage, the pH value of water increases to the highest value of 8.35 in the non-sterile box. However, the pH values of water slightly decreased under the sterilization

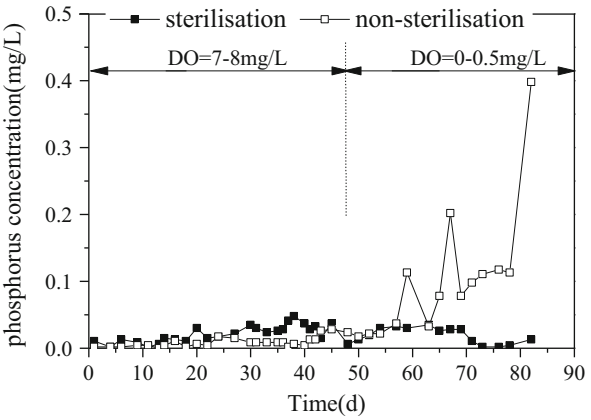

Fig. 31 The concentration of phosphorus in overlying water (pH = 6.5)

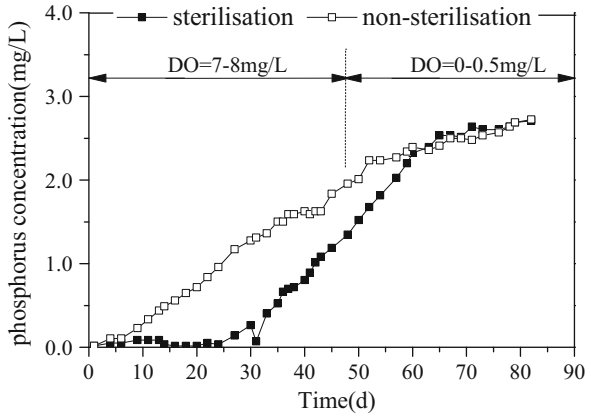

Fig. 32 The variation of phosphorus in overlying water (pH = 9.1)

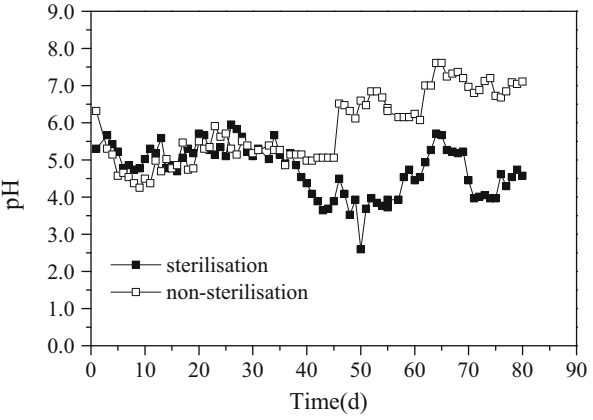

Fig. 33 The variation of pH in overlying water

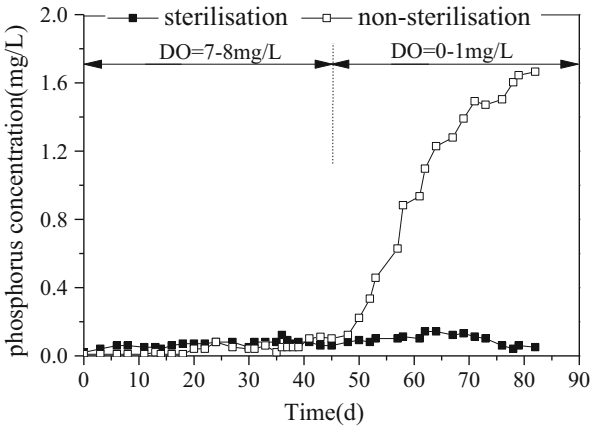

Fig. 34 The concentration of phosphorus in overlying water

conditions, maintaining at around 7.2. This shows that microbial metabolic processes lead to an increase of the pH value, which promotes phosphorus release. The comprehensive effect of microorganisms on phosphorus release is shown in Fig. 34. It can be seen from Fig. 34 that, during the aerobic stage, there is no phosphorus release at pH 7.5 in either the sterilization box or the non-sterilized box. During the anaerobic stage, the release of phosphorus in the non-sterilization box is significant. The concentration increases to a highest value of 1.85 mg/L. The average release rate reaches 8.60 mg/(m^2·d). The phosphorus release in the sterilization box is slow; for example, the highest release concentration is only 0.11 mg/L after 12 days.

3 The Release of Iron and Manganese in Sediment

Heavy metal pollution is a global environmental problem, which is particularly serious in industrial countries and emerging developing countries. With the development of electroplating, tanning, corrosion, dyes, and other industries, more and more heavy metal wastewater flow into water bodies to cause serious harm to animals, plants, and the environment [15, 16]. Heavy metals are important and potentially harmful contaminants. Heavy metals, which are different from other pollutants, require a special focus on the results from their persistent environmental hazards, geochemical cycles, and ecological risks [17].

The vast majority of heavy metals flow into water through various path, then quickly turn from the aqueous phase into the solid phase, and then bind to suspended solids and sediments. During the process of runoff, the heavy metals combined with the suspended solids will transform into the sediments with weakening intensity of the flow turbulence. Sediment, which is the fate of water pollutants, has an important impact on the structure and services of water ecosystems. Heavy metals are important pollutants in aquatic sediments because they are

potentially harmful and difficult to degrade, as well as being easy to magnify and accumulate in living bodies. Heavy metals are considered an important indicator of water pollution because, in sediment, they have characteristics such as high abundance and easy accurate detection [18–20].

The studies of domestic scholars on the reservoirs of iron and manganese pollution show that: the distribution of iron and manganese changed with seasons as well as reservoir temperature stratification. High concentrations of iron and manganese mainly appear in the middle and bottom layers of reservoirs during the period of temperature stratification, which is closely related to the hypoxia in the bottom layer and pH decrease. Also, secondary pollution is caused by the release of iron and manganese in sediments. The concentration of iron and manganese in reservoirs exceed the standard levels during summer time, as the temperature of the reservoir stratifies significantly. It is difficult for surface dissolved oxygen to enter the bottom reservoirs through the thermocline. The concentration of dissolved oxygen of the bottom layer is consumed by organic, benthic organisms and reducing pollutants [21–23]. The DO concentration of the underlying water consistently decreases with pH declines. The concentration of iron and manganese in bottom sediments are released, so the concentrations of iron and manganese in the overlying water increased. In winter and spring, the temperature tends to be isothermal and the temperature difference is small. The whole water body presents an oxidized state when the DO concentration and pH of the water is high. Under oxidizing conditions, iron and manganese have a weak migration behavior due to forming insoluble compounds. Gradually, they settle in the vicinity of the reservoir bottom sediment and water interface, and accumulate in the surface of sediment, leading to an increase in deposits of iron and manganese content, while in overlying water, their corresponding concentrations decrease [16, 24, 25].

3.1 Iron Release of Jinpen Reservoir

The influence of redox environment and pH on the release of iron in sediments was investigated. The research methods of this part are the same as previous reports [26, 27]. The concentrations of iron in No. 1–3 test reactors are shown in Fig. 35. As seen in Fig. 35, during the aerobic phase, no iron was released in the experimental reactors. This is also proof that phosphorus release under aerobic conditions at a high pH value is mainly metathesis rather than dissolution. Under anaerobic conditions, a smaller amount of Fe was released from sediment. During the anaerobic period, the concentration of Fe dramatically increased to 0.50 mg/L on the 8th day in the reactor with pH 6.5. Fe^{2+} released from the sediment will take some time to migrate and be entered into the water body, so the Fe^{2+} and TDP concentrations are synchronized over time. It also proves that phosphorus release is a reduction reaction shown in Eqs. (5) and (6) under conditions of low pH. The concentration of iron began to increase to 0.43 mg/L in a dozen days after the anaerobic period in the reactor with pH 8. Because the precipitation reaction as

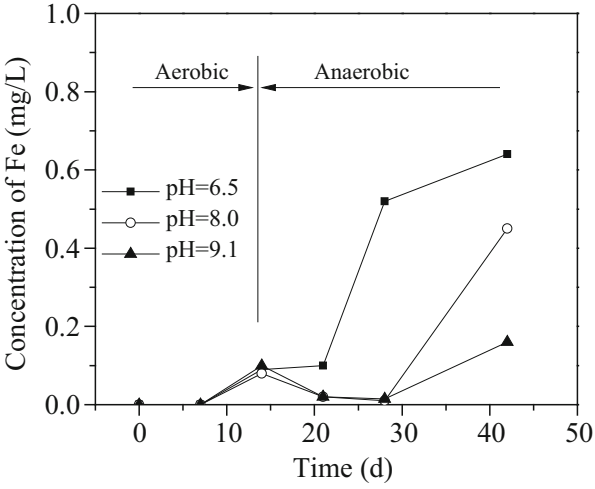

Fig. 35 Release of Fe in sediment under different pH values of 6.5, 8.0 and 9.1

shown in Eq. (7) had occurred, this delayed the increase of the Fe^{2+} concentration. The Fe concentration was low in the reactor with pH 9.1, and the maximum Fe concentration did not exceed 0.10 mg/L. The reason for this is that the equilibrium concentration of Fe^{2+} is only 0.017 mg/L, and the reaction shown in Eq. (7) is carried out thoroughly. Therefore, Fe^{2+} does not present under high pH values.

$$FePO_4^- - e- \rightleftharpoons Fe^{2+} + PO_4^{3-} \tag{5}$$

$$Fe(OH)_2H_2PO_4^- + e- \rightleftharpoons Fe^{2+} + PO_4^{3-} + 2H_2O \tag{6}$$

$$FePO_4 + 3OH^- \rightleftharpoons Fe(OH)_3 \downarrow + PO_4^{3-} \tag{7}$$

Thus, Fe^{3+} is reduced to Fe^{2+} under anaerobic conditions. Therefore, the concentration of iron in the water depends on the pH value. For instance, when the pH value is higher than 8.5, the equilibrium concentration of Fe^{2+} is lower than 0.27 mg/L, as determined by the $Fe(OH)_2$; while at low pH conditions, the anaerobic environment will promote the transformation from Fe^{3+} to Fe^{2+} in sediment [28, 29].

The research methods of this part are the same as in previous reports [30, 31]. This study is a simulation experiment based on Jinpen Reservoir sediment and the results are shown in Fig. 36.

As can be seen in Fig. 36, Fe is released significantly up to 0.05 mg/L under natural conditions (non-sterile) during the anaerobic period while the rate of the release was only 1.04 mg/(d · m^2).

Only trace Fe was released, and the maximum release concentration was only 0.015 mg/L under sterile conditions. The experimental results showed that the metabolism of microorganisms under anaerobic conditions would accelerate the release speed of Fe in sediments. In aerobic environments (the DO concentration is 4–5 mg/L), the Fe^{2+} concentration in the overlying water was very low, and tended

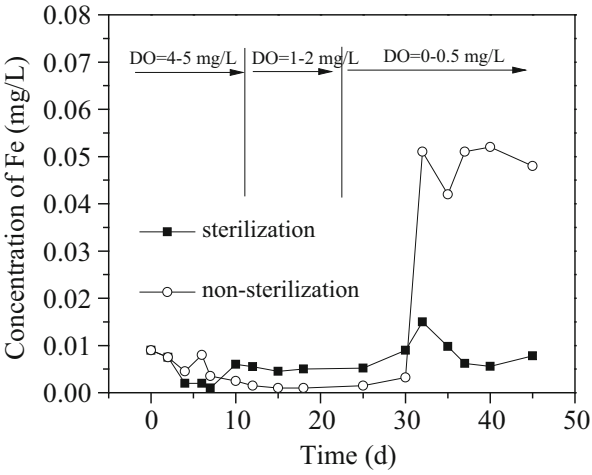

Fig. 36 Effects of microbes on the release of Fe under different DO concentrations

to decrease. The water of Fe^{2+} was oxidized to $Fe(OH)_3$ under aerobic conditions. $Fe(OH)_3$ was deposited on the sediment surface. No iron release occurred during the anoxic phase (DO = 1–2 mg/L) under both sterile and non-sterile conditions.

3.2 Manganese Release in Jinpen Reservoir Sediment

(1) The Influence of Redox Condition on Mn Release in Sediment

The Mn concentrations in No. 1–3 reactors are shown in Fig. 37. As can be seen, the release amount increased rapidly under anaerobic conditions at pH 6.5. In about 28 days, the release reached a maximum value of 3 mg/L, and tended to reach a release balance. The release of manganese was very low under aerobic and anoxic conditions, and the maximum was only 1.70 mg/L. However, 1.14 mg/L of manganese is released under anaerobic conditions at pH 8, which was lower than the corresponding value at pH 6.5. There was no release of Mn under aerobic conditions. There was basically no release of manganese under three conditions (aerobic, anoxic, and anaerobic) at pH 9.1. The possible reasons for the above phenomenon are that manganese in nature is mainly of the form $MnO_2 \cdot H_2O$. MnO_2 can be reduced to soluble Mn^{2+} (as seen in Eq. (8)) at low pH, so manganese is easy to release.

$$MnO_2 + 4HCl = MnCl_2 + Cl_2 + 2H_2O \tag{8}$$

This was the reason for the release of manganese under aerobic or anoxic conditions at pH 6.5. Meanwhile, manganese can also be reduced under reducing and anaerobic conditions, as shown in Fig. 37. There was no release of manganese under anaerobic conditions at pH 9.1. The reasons for this is that $Mn(OH)_2$ and

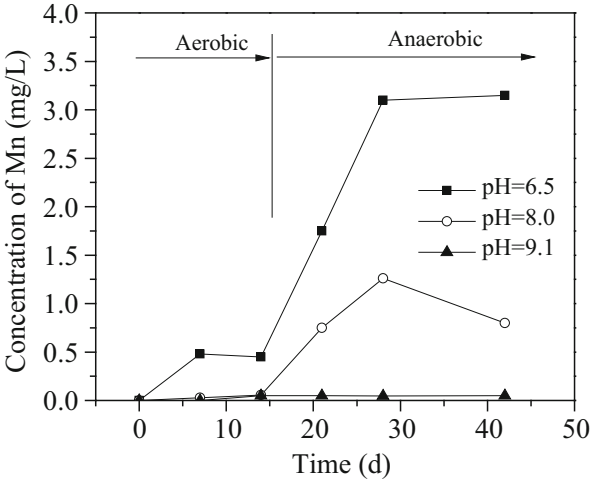

Fig. 37 Characteristics of Mn release in sediment under different pH values of 6.5, 8.0 and 9.1

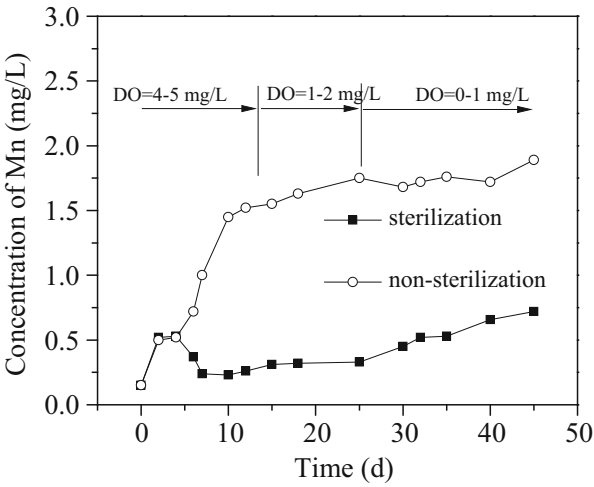

Fig. 38 Microbes effects on the release of Fe (sterilization and non-sterilization)

$Mn_3(PO_4)_2$ are insoluble in water and easy to produce precipitation at pH 9.1. In addition, OH^- and PO_4^{3-} concentrations were higher in the test reactors at pH 9.1, and Mn^{2+} transfers into sediment under anaerobic reduction. Therefore, manganese becomes undetectable in the overlying water [32, 33].

Thus, manganese can be released in acid reductive or anaerobic reductive acidic conditions. However, manganese cannot be released when the pH value is higher.

(2) The Effect of Microbes on the Release of Manganese in Sediment

As can be seen from Fig. 38, the manganese of sediment in Jinpen Reservoir was released to a large extent under high dissolved oxygen concentration (DO = 4–5 mg/L) conditions for non-sterile reactors. The highest concentration of Mn^{2+} in water reached 1.37 mg/L. At the same time, the pH of water decreased from 7.35 to

6.30. In weak acidic conditions, Mn in sediment was reduced and released (as seen in Eq. (8)). The concentration of manganese was only 0.62 mg/L under sterile conditions, which is lower than the corresponding value under non-sterile conditions. The results suggest that the microbial metabolism speeded up the release of manganese. The reason for this is that the presence of microorganisms may have further reduced the oxidation–reduction potential of the environment, leading to more Mn^{2+} being released and reduced.

3.3 The Release of Iron and Manganese in Shibianyu Reservoir and Zhoucun Reservoir

Sediment samples were collected from Shibianyu Reservoir and Zhoucun Reservoir for the simulation experiment. The concentrations of total iron (TFe) and total manganese (TMn) in the overlying water are shown in Fig. 39. The maximum concentration of Fe in the overlying water occurred in the reactors loaded with Zhoucun Reservoir sediment. The concentration of total iron increased dramatically to the highest value of 1.33 mg/L in 20 days, after which it decreased to 0.6–0.7 mg/L. The Fe concentration in Shibianyu Reservoir was 0.92 mg/L, which is lower than that in Zhoucun Reservoir (the maximum release intensity is 1.33 mg/L), and both were higher than that in Jinpen Reservoir (the maximum release intensity is 0.5 mg/L).

The concentration of manganese in the overlying water in the reactors all showed a sharp increase at first, then quickly reduced to a certain stable value, and finally showed a steady downward trend. The concentration of manganese in the overlying water reached the maximum on the 20th day. The maximum concentration of Mn in Zhoucun Reservoir was 1.55 mg/L, while the maximum concentration of Mn in Shibianyu Reservoir was 1.33 mg/L. They were both lower than that in Jinpen Reservoir (the maximum release is 3 mg/L).

Based on the above analysis, the following conclusion can be obtained: in the sediment samples under static and airtight conditions, Fe and Mn will be released into the overlying water. The study of Marc and others confirmed that the interactions between the iron oxide and the phosphate are the main mechanisms of release and absorption [34–36]. Under anaerobic conditions, the soluble phosphorus and manganese showed a consistent positive correlation with the results of Marc et al. When released to the maximum value of 1.5 mg/L, sediment will adsorb iron from the overlying water. So, the concentrations of Fe and Mn in the overlying water decreased drastically. After that, the concentrations of phosphorus in the overlying water began to decrease drastically. The falling of Fe and Mn concentrations in the overlying water was consistent in the falling of phosphorus concentration. This result showed that Fe and Mn settled in sediments through the oxidation–reduction reaction to form FeOOH and MnOx when phosphorus was released into the overlying water. The available Fe and Mn drastically decreased because Fe and Mn in the overlying water transform into the combined state. Meanwhile, the

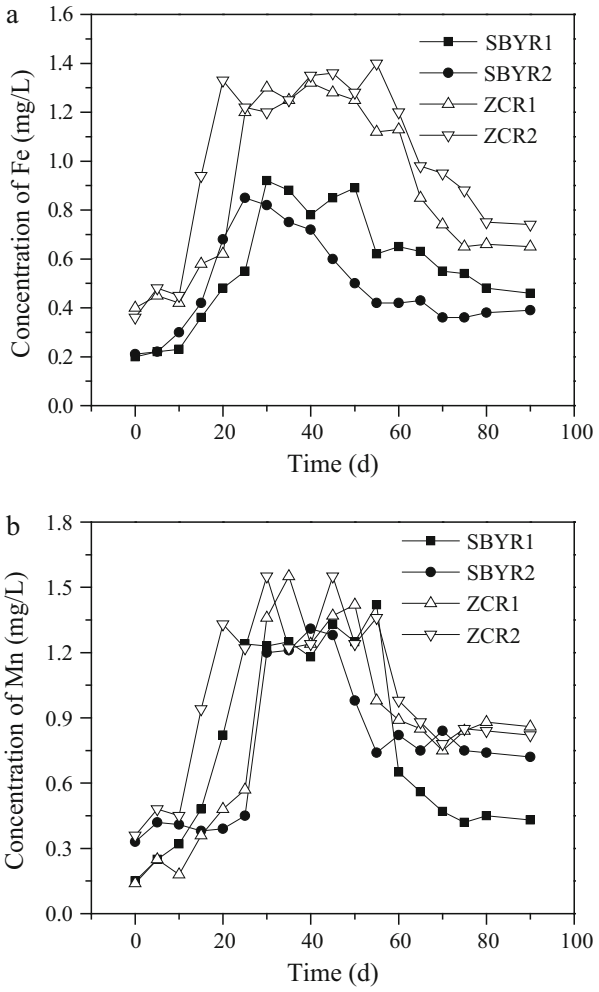

Fig. 39 Concentrations of Fe and Mn in the overlying water. **a** Fe release characteristics in Shibianyu Reservoir and Zhoucun Reservoir, **b** Mn release characteristics in Shibianyu Reservoir and Zhoucun Reservoir

concentration of phosphorus in the overlying water sharply reduced because a large gathering of FeOOH and $Al(OH)_3$ adsorbed phosphorus from overlying water. Olaf, whose findings also indicated that MnOx on FeOOH coatings may promote the absorption of phosphate precipitation or even together, which was consistent with the results of this experiment.

3.4 Release of Iron and Manganese in Zhelin Reservoir

Iron and manganese are redox-sensitive elements. The migration of Fe and Mn in the interface between sediment and water reflect the redox conditions. The release

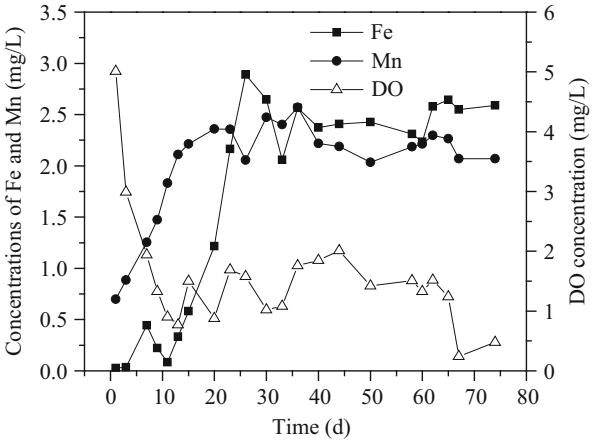

Fig. 40 Release concentrations of Fe and Mn in Zhelin Reservoir

of Fe and Mn in sediment in the main area of the reservoir was investigated. The monitoring results are shown in Fig. 40. It can be seen from the figure that Fe and Mn were released significantly, with their maximum release concentrations reaching 2.89 mg/L and 2.57 mg/L, respectively, when the dissolved oxygen in the water is down to about 1 mg/L. The release of iron in Zhelin Reservoir was significantly higher than that in Jinpen Reservoir, Shibianyu Reservoir, and Zhoucun Reservoir. The release concentration of Mn was lower than that of Jinpen Reservoir and higher than those of Shibianyu Reservoir and Zhoucun Reservoir. Research has shown that Fe-P will be substantially released under anaerobic conditions. So, the increase of the Fe concentration was often accompanied by the increase of the phosphorus release concentration. The results further confirmed this rule: when the release of Fe reaches a peak, the TP reaches a high level too. As the release time prolonged, the concentrations of Fe and Mn were slightly decreased, which may be due to the release of other ions in sediment or contaminants reacting with Fe and Mn and forming insoluble compounds that are deposited again.

3.5 Comparison of Iron and Manganese Release

Table 7 shows the quantities of iron and manganese released in the studied reservoirs. Among the four typical reservoirs, Zhelin Reservoir has the largest amount of iron release, 2.89 mg/L. The largest amount of manganese released was from Jinpen Reservoir, reaching 3 mg/L. The experimental results show that the main factors that influence the release in sediment are dissolved oxygen, pH and the action of microorganisms. In large reservoirs, the stratification period is long. With the influence of oxygen consumption of water and sediment at the bottom of

Table 7 The released amounts of Fe and Mn in typical reservoirs

Name of reservoir	Release content	
	Fe (mg/L)	Mn (mg/L)
Jinpen Reservoir	0.50	3.00
Shibianyu Reservoir	0.92	1.33
Zhoucun Reservoir	1.40	1.55
Zhelin Reservoir	2.89	2.57

the water body, which goes into an anaerobic state, the water pH and microbials react, so that changes will occur, leading to the release of sediment.

4 Release Characteristics of Heavy Metals in Sediment

According to the literature, the release of heavy metals was studied in surface water, such as Zhenhe River, Dayihe River, Yellow River, Songhuajiang River, Chaohu Lake, Taihu Lake, Nanhu Lake, Huangpujiang River, Yangtze Delta, south of the Yellow Sea, and other water bodies. The following conclusions were obtained: (1) Surface water is contaminated complexly by heavy metals, with severe contamination of Pb in mining areas, moderate pollution of Hg, and slight pollution of Zn. (2) Influenced by water environmental conditions, heavy metals mostly exist in suspended solids and sediment. The content of heavy metals in general suspended particulate matter is several times higher than that in sediment, and hundreds of times higher than dissolved heavy metals in water. (3) The content of heavy metals in lake tributaries is generally higher than that in lakes, and estuarine pollution is more serious. (4) The concentration of heavy metals in water is relevant to the pH value. It is easy to precipitate into the sediment under alkaline conditions, while it is easy to release under acidic conditions. (5) The content of heavy metals in the Yangtze River estuary waters is that it is higher in the dry season than in the flood period, and higher at the bottom than at the surface. Also, a variety of heavy metals is in good correlation, indicating that they have the same source. This shows that understanding heavy metal release in sediment has a significant meaning to improving water quality.

4.1 Distribution of Heavy Metals in Sediment in Fenhe Reservoir

(1) Distribution of Heavy Metals in Sediment Under Microbial Action
The environmental effects of heavy metals in sediment and their chemical speciation are closely related. Further studies show that there is a certain degree of correlation between the chemical solvent extraction method and the environmental

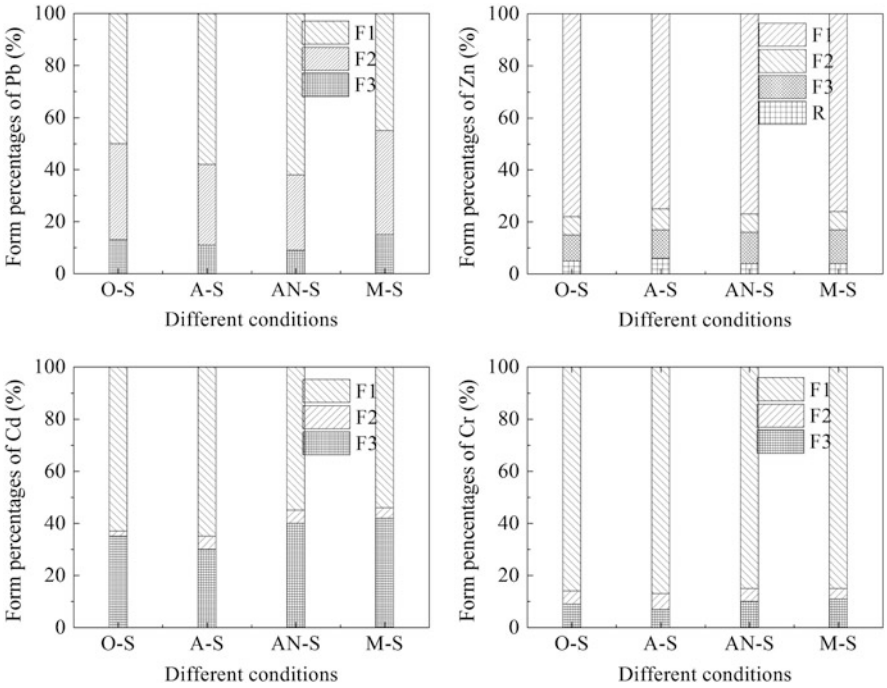

Fig. 41 Microbial effects on heavy metals speciation in sediments

and ecological effects of heavy metals. Therefore, for the BCR extraction method, F1 includes water-soluble, exchangeable, and carbonate fractions heavy metals, F2 is iron and manganese oxide bound to heavy metals, and F3 is organic and sulfide phase bound to heavy metals. All of these have potential environmental effects.

The impact of microorganisms on the distribution and concentration of heavy metals in Fenhe Reservoir is shown in Fig. 41. Under non-sterile conditions, after pretreatment to different samples (original, aerobic, anaerobic, plus reduction of pharmacy), the proportions of Cd between F1, F2 and F3 and the total T [(F1+F2+F3)/T] are 31.37 %, 35.71 %, 55.56 % and 46.89 % respectively. And under sterile conditions, the proportions increase accordingly to 0.90 %, 7.14 %, 26.48 % and 13.02 %, respectively. The results indicate that the potential environmental effects of Cd in sediment have been further strengthened when microorganisms participate in the reaction, especially under anaerobic conditions.

Under the pretreatment conditions in different samples, the proportion of Cd binding speciations of F1 to the total content (F1/T) respectively increase accordingly to 5.75 %, 6.88 %, 20.13 %, and 13.92 %, compared to sterile conditions. So, the exchangeable Cd (F1) as a percentage of the total increase is the main reason that leads to the increase of the [(F1+F2+F3)/T] ratio. Cd and organic matter in the binding capacity of sediment is much weaker than other heavy metals (such as Cu and Zn). The order of stability constants of binding to organic matter is as follows:

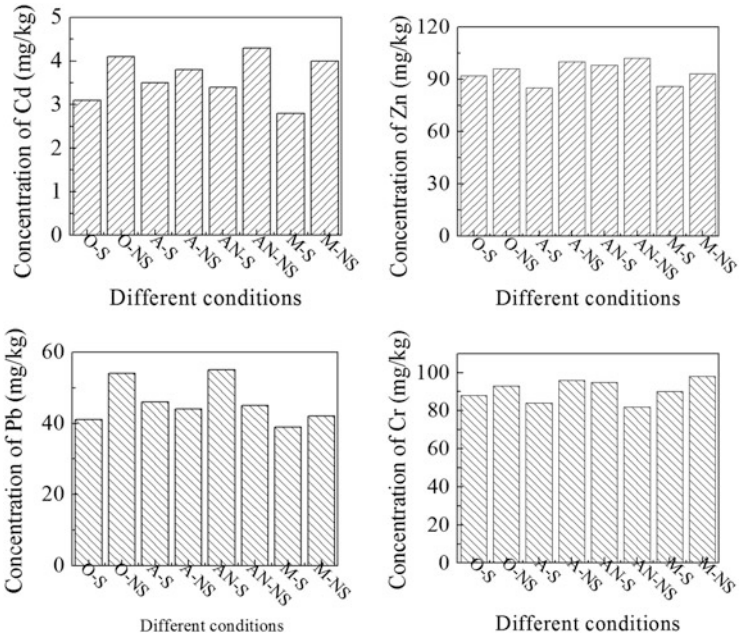

Fig. 42 Heavy metal concentrations in the sediment samples under different pretreatment conditions

Cd (log K = 5.45) <Zn (log K = 7.15) <Cu (log K = 12.60) [37]. Organic matter in sediment can be utilized by the microorganisms for mineralization decomposition. Thus, the combination of Cd with organic matter will be looser and easier to dissociate from organic-bound matter. It follows that the content in water-soluble, exchangeable, and carbonate fraction (F1) speciations will increase rapidly.

When the potential environmental effects of various speciations of heavy metals are strengthened by microbial action, the extent of migration and the diffusion of heavy metals will be increased from sediment to overlying water through the sediment–water interface. It can be seen from the changing content trends of heavy metal in sediments that, as the [(F1+F2+F3)/T] ratio increases, and under pretreatments of different samples (original, aerobic, anaerobic, plus the reduction agent), the total amount of Cd in sediment decreases respectively by 15.24 %, 11.11 %, 36.84 % and 27.78 % (Fig. 42), compared with sterile conditions.

For Zn, the microorganisms cause the [(F1+F2+F3)/T] values to increase by 1.58 %, 9.18 %, 1.66 % and 1.33 %, compared to sterile conditions. In the pretreatment and aerobic conditions, the change in the values of Zn is consistent with the change in the values of Cd. This is under the action of microorganisms, as the [(F1+F2+F3)/T] ratio increases (Fig. 42).

Pb is highest among the four heavy metals bound on iron and manganese oxides, which is 12.21 times that of Cd, 10.73 times that of Zn, and 3.28 times that of Cr, respectively (Fig. 41). There is strong absorption between iron, manganese oxides,

and lead due to a stable complex constant [38, 39]. Microbial effects on the distribution of lead are similar to the distribution of Cd and Zn. That is, the ratios of [(F1+F2+F3)/T] increase by 6.76 % and 11.18 %, respectively, under the actions of microorganisms action. It is worth noting that the [(F1+F2+F3)/T] ratios increase by 3.48 % and 6.06 %, respectively, for chemical control under aerobic and anaerobic conditions. This could be interpreted as: different sources (biogenic and non-biogenic nature) of iron and manganese oxides had differences in the adsorption capacity of lead [40]. Under aerobic and anaerobic chemical control conditions (sterilized), a strong migration activity (such as F1) of lead is strongly adsorbed on the surface of iron and manganese oxides, which restrict the relocation and diffusion of lead through the interface between sediment and water. Therefore, the total amount of lead in sediment is higher than that under microorganisms conditions (Fig. 42). Other chemical redox conditions which replace the action of microorganisms have become a major factor in controlling the potential environmental effects of lead in sediment.

For Cr, the microbial action on its potential environmental effects is weak. The changes in the [(F1+F2+F3)/T] values are 0.81 %, 1.65–2.22 % and 3.61 %. Under anaerobic conditions, microbial effects on the [(F1+F2+F3)/T] values are similar to the variation trend of lead in aerobic and anaerobic chemical control conditions. The effect of the [(F1+F2+F3)/T] value variation trend on the total Cr in sediment is the same as the three metals mentioned above (Fig. 42).

(2) The Bioavailability Content of Heavy Metals in Sediment

The bioavailability of heavy metals in sediment is further explored by the EDTA single extraction method under different pretreatment conditions. Extractable speciations characterize the bioavailability of heavy metals, including water-soluble, exchangeable, organic weakly bound speciations, and other speciations of heavy metals. The results of previous studies show that the proportion of the bioavailability to the total (B/T) generally does not exceed 5 % when the EDTA single extraction method is used [41].

Under different sample pretreatment conditions, the bioavailability of heavy metals in sediments in Fenhe Reservoir is shown in Fig. 43. The average B/T values of Cd and Pb are 20.42 % and 32.89 %, respectively, which indicated a strong bioavailability and potential environmental effects. The B/T values of Zn and Cr are less than 5 %, and the results are similar to previous reports. The linear relation between the values of (F1+F2+F3)/T and B/T of four heavy metals in sediments is showed in Fig. 44. The linear relation between (F1+F2+F3)/T (X) and B/T (Y) is $Y = 0.806X–0.0816$ ($R^2 = 0.7427$). For Pb, the B/T and [(F1+F2+F3)/T] values present a common changing trend (Figs. 41 and 44); that is, (F1+F2+F3)/T] and B/T increase because of microbial action under the reduced condition of adding reducing agent, and the potential environmental effects also increase. However, chemical redox conditions instead of microbial action became the main factors controlling the potential environmental effects of lead in sediment.

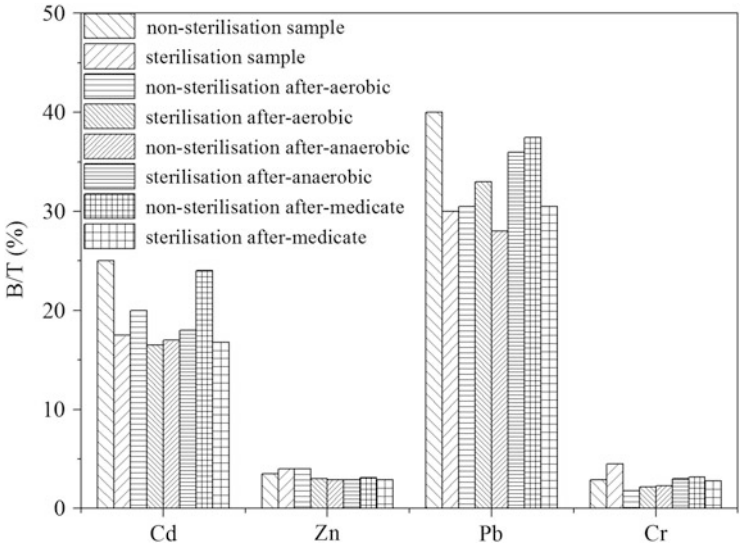

Fig. 43 The bioavailability content of heavy metals accounted ratio of the total (B/T)

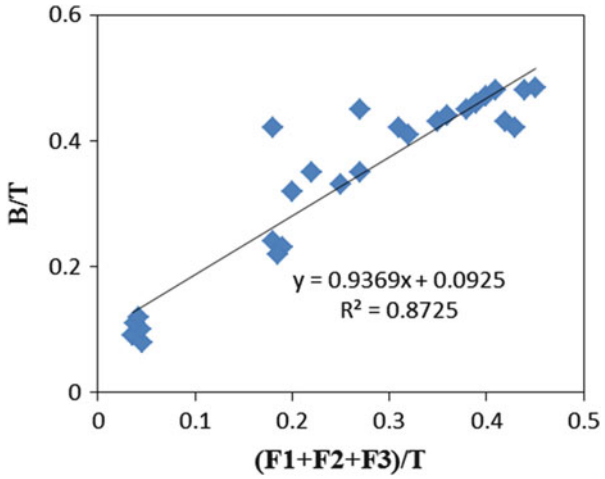

Fig. 44 The correlation analysis of (F1+F2+F3)/T and B/T

(3) Summary

1. The potential environmental effects of Cd and Zn in sediment increase under microbial actions. In addition, chemical redox conditions instead of microbial action became the main factors controlling the potential environmental effects of lead in sediment.
2. The average proportion of the bioavailability of Cd and Pb of the total (B/T) are 20.42 % and 32.89 %, respectively, while the Zn and Cr B/T values are less than 5 %.

3. The potential environmental effects of heavy metals have a direct impact on the variation of the total amount of heavy metals in sediment. On the sediment–water interface, the diffusion of heavy metals will also be increased with the enhancement of the potential environmental effects of heavy metals in various speciations, and it may cause potential harm to the water quality of the reservoir to some extent.

4.2 Distribution Characteristics of Heavy Metals in Jinpen Reservoir Sediment

(1) Assessment of Heavy Metals Content in Jinpen Reservoir and Its Potential Ecological Risk

The contents of four heavy metals, Cd, Zn, Cr, and Pb, in sediment of Jinpen Reservoir are shown in Fig. 45. The Cr and Cd contents are higher and are 1.28 and 1.79 times the average content of heavy metals in Chinese lake sediment [42]. The contents of Zn and lead are lower, among which the Zn content (96.95 ± 3.29 mg/kg) is only 60.35 % of the background values in Chinese lake sediment. The above data show that pollution of Cd and Cr are obvious in sediment of Jinpen Reservoir.

The potential ecological risk index method proposed by Hakanson is introduced to assess the potential ecological risk of the four heavy metals in sediment in order to further illustrate the pollution level and potential ecological harm of heavy metals in sediment. This method can evaluate heavy metal pollution at the point where sediment is deposited, considering not only the content of heavy metals in sediment, but also links to the ecological, environmental, and toxicological effects

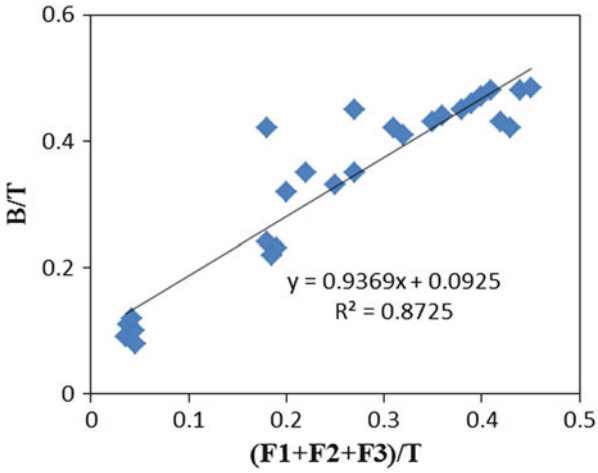

Fig. 45 Concentrations of heavy metals in the sediment of Jinpen Reservoir

Table 8 The classification standard of the potential ecological risk of heavy metals

Single pollution factor $\mathbf{C_f^i}$	Degree of contamination	Single potential ecological risk index	Accumulation of potential ecological risk index (RI)	Degree of potential ecological risk
$\mathbf{C_f^i} < 1$	Low	$\boldsymbol{E_r^i}<40$	$\mathbf{RI}< 150$	Slight
$1 \leq \mathbf{C_f^i} < 3$	Moderate	$40 \leq \boldsymbol{E_r^i} < 80$	$150 \leq \mathbf{RI} < 300$	Moderate
$3 \leq \mathbf{C_f^i} < 6$	Higher	$80 \leq \boldsymbol{E_r^i} < 160$	$300 \leq \mathbf{RI} < 600$	Strong
$\mathbf{C_f^i} \geq 6$	Highest	$160 \leq \boldsymbol{E_r^i} < 320$	$\mathbf{RI} \geq 600$	Strong
		$\boldsymbol{E_r^i} \geq 320$		Extremely strong

of heavy metals using a comparable equivalent property index classification method. The potential ecological risk index (RI) relates to the individual pollution factor, heavy metal toxicity, and response factors of individual potential ecological risk factors, which can be expressed in the following equation:

$$\mathrm{RI} = \sum_{i=1}^{n} E_r^i = \sum_{i=1}^{n} T_r^i C_f^i = \sum_{i=1}^{n} T_r^i C_s^i / C_n^i \tag{9}$$

In this equation, RI is the potential ecological risk index; E_r^i is the individual potential ecological risk index; T_r^i is the toxic response index of certain metals; C_f^i is the single pollution index; C_s^i is the concentration of heavy metals in surface sediments; and C_n^i is the background value. In this study, the reference value is used from the world's highest background values of heavy metals in sediment in the previous period of industrialization.

The classification criteria of the heavy metal pollution index and ecological risk are shown in Table 8. According to this standard, the potential ecological risk of heavy metals in sediment is evaluated, and the results are shown in Table 9. The results show that the accumulation potential ecological risk index (RI) of the four heavy metals in sediment is 110.53. Table1 shows that the accumulation potential ecological risk in Jinpen Reservoir sediment is slight. The single pollution index of Zn, Pb, and Cr is between 1 and 2, which is moderate pollution. And the single pollution index of Cd is 3.36, showing strong pollution. From the assessment of the potential ecological risk of the four heavy metals, the individual potential ecological risk factor of Cd is much larger than the other three heavy metals, reaching 100.80, with a heavier individual ecological harm. However, the other three heavy metals show only low single ecological harm. The evaluation results indicate that the secondary pollution of Cd in sediment may occur and brings severe security risks to the water quality and safety of Jinpen Reservoir. So, the intensity and attention of environmental governance in sediment of Jinpen Reservoir should be further strengthened.

Table 9 Single pollution factor, potential ecological risk index, and degree of potential ecological risk of heavy metals

Element	Measured value (mg/kg)	Background value (mg/kg)	Single pollution factor	Degree of contamination	Toxic response factor	Single potential ecological risk index	Degree of single potential ecological risk
Cd	1.68±0.81	0.5	3.36	Heavier	30	100.80	Heavier
Zn	96.95±3.29	80	1.21	Moderate	1	1.21	Low
Pb	28.07±10.87	25	1.12	Moderate	5	5.61	Low
Cr	87.05±9.33	60	1.45	Moderate	2	2.90	Low

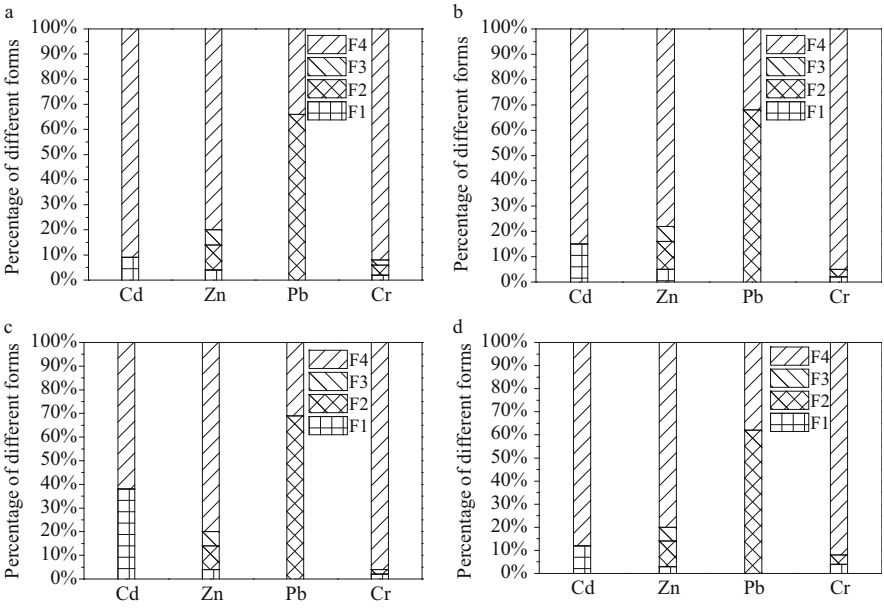

Fig. 46 Percentage concentration of different speciation of heavy metals in sediment

(2) Distribution of Heavy Metals in Jinpen Reservoir Sediment

The environmental effects of heavy metals in sediment and soil are closely related to its speciation of occurrence. Further studies show that there is a correlation between the results made by chemical solvent extraction and environmental effects of heavy metals. It is generally believed that all heavy metals extracted have potential environmental effects. For reservoirs, three speciations of heavy metals in the sediment include soluble and exchangeable speciation (F1, acid extraction), reducible speciation (F2, hydroxylamine hydrochloride extraction reduction), and oxidized speciation (F3, hydrogen peroxide oxidation extraction). Environmental effects and transformation capabilities of heavy metals will change. A lot of metals will flow into the overlying water body to cause secondary pollution of the water quality. In this process, various speciations of heavy metals in sediment have different diffusion abilities from sediment to the water body. Soluble and ion exchange heavy metals have strong diffusion ability. The residual speciation of heavy metals has weak environmental effects, and it can stably exist in sediment.

The distribution of heavy metals in Jinpen Reservoir sediment is shown in Fig. 46. In four sampling points (I–IV), various speciations of heavy metals in sediment have similar distribution rules, in which the percentage of the residual lead is the lowest. The result indicated that the potential environmental effects of lead in sediment are also the most obvious. Soluble, exchangeable, and oxidized lead is almost below the detection limit. The vast majority of lead existed in reducible speciation. This indicates that the migration and transformation tendency of lead in sediment (F1, F2, F3, and residual) leaned toward reducible speciations in deep reservoirs with average depths of 90 m, because the sediment–water interface

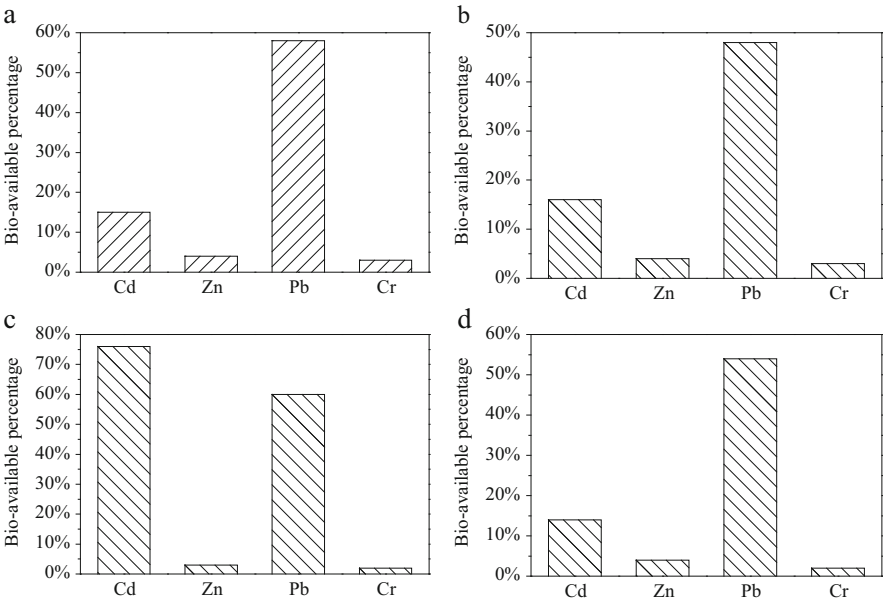

Fig. 47 The bioavailability concentrations of heavy metals in sediment

is under a long-term reduction of the physical and chemical conditions of hypoxia. Iron and manganese oxides are more closely bound to lead (mainly existing in reducible speciations) due to strongly combined constants [38, 39]. This is another reason for the higher percentage of lead-reducible speciations.

At different sampling points, the percentage of Cr in three speciations (F1, F2, and F3) in sediment is between 4.2 and 7.9 %, which is lower than the other three heavy metals. Therefore, its potential environmental effect is also weak. The percentage of residual Zn shows little difference among all the sampling points, remaining at about 80 %. In each sampling point, the percentage of residual Cd is between 71.4 and 90.5 %, which is higher than the residual Pb and Zn. However, particular attention needs to be paid to the fact that Cd exists mainly in soluble and exchangeable (F1) speciations. However, F1-binding Cd is easier to release upwards from pore water to the overlying water, thereby directly harming the water quality.

(3) Bioavailability of Heavy Metals in Sediment

The bioavailability of heavy metals in sediment is further explored based on the sequential extraction experiment of heavy metals in Jinpen Reservoir sediment. EDTA single extraction is used to characterize the bioavailability of heavy metals, including soluble, exchangeable, and organic weakly bound speciations, etc. [41].

Studies show that the proportion of bioavailability to the total content (B/T) generally does not exceed 5 % when characterizing the bioavailability of heavy metals in soil or sediment using EDTA single extraction [43]. However, the bioavailability of heavy metals in Jinpen Reservoir sediment (Fig. 47) shows that

the B/T value of Pb is 50–60 % at each sampling point. The B/T value of Pb is significantly higher than those of the other heavy metals at sampling point III. The B/T value of Cd is more than 10 % at all sampling points. The B/T value at sampling point III is up to 76.2 %, which is significantly different to the previous study. The results of heavy metals speciations shows that the percentage of residual lead is the lowest using the continuous extraction method. In addition, Cd in sediment mainly exists in the F1 binding speciation, which is easier to migrate. The bioavailability of Cd and Pb in Jinpen Reservoir sediment is high, which has strong potential environmental dangers.

(4) Summary

1. Cr and Cd content in sediment of Jinpen Reservoir is high, and is 1.28 and 1.79 times the background values in Chinese reservoirs, respectively.
2. The potential ecological risk of Cd in sediment is much larger than that of the other heavy metals, which is 100.8, with a strong ecological harm. Cd is the major contributor causing increasing potential ecological risk in Jinpen Reservoir.
3. Reducible lead is accelerated to transforming in sediments due to the special physical and chemical conditions. Except for the residual speciation of Cd, Cd present in soluble and exchangeable speciations are easier to release to the overlying water from pore water in sediment, thereby directly harming the reservoir.
4. The B/T values of Zn and Cr in sediment are less than 5 % at each sampling point, and the potential environmental effects are weak. The B/T values of lead are within the range 50–60 %. The B/T values of Cd are greater than 10 %, with a maximum of 76.2 %. These data show that the bioavailability of Pb and Cd in sediment is higher, with strong potential environmental harm.

4.3 Release of Heavy Metals in Shibianyu Reservoir and Zhoucun Reservoir

(1) Release of Copper in Sediment

The Tessier morphological changes of heavy metals in sediment and ion concentrations in the overlying water of Shibianyu Reservoir and Zhoucun Reservoir are measured. The ion concentration of heavy metals in overlying water is shown in Fig. 48.

Reactions are carried out during a period of 90 days. The result shows that the concentration of Cu^{2+} in the overlying water has little variation at different times between the reactors. The maximum release of Cu^{2+} in Shibianyu Reservoir and Zhoucun Reservoir are 45 and 52 μg/L, respectively. In the same reactor, changes of Cu^{2+} in overlying water during the whole experimental phase are very significant. The concentration of Cu^{2+} in the overlying water increases sharply,

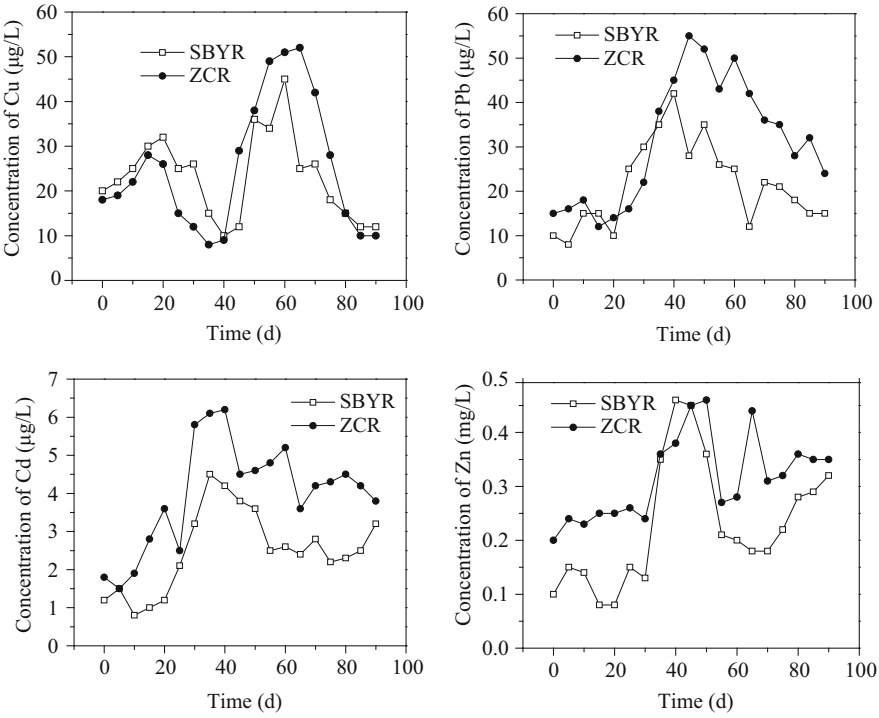

Fig. 48 Heavy metals release of Shibianyu Reservoir and Zhoucun Reservoir

maintaining a value of 30 μg/L in about 20 days. After 45 days, the concentration of Cu^{2+} continues to increase to approximately 50 μg/L, and then decreases to 10 μg/L at the end of the reaction.

Changes of the Pb^{2+} concentration in the overlying water are shown in Fig. 49. The concentration of Pb ions in the overlying water decreases slightly at 10 days. From 15 to 40 days, the concentration of Pb ions in each reactor increases sharply to 42 μg/L and 55 μg/L in Shibianyu Reservoir and Zhoucun Reservoir, respectively. The concentrations of Pb ions in the overlying water reaches the maximum value at around 38 days. Although the change in the Pb ions concentration is not as regular as that of Cu, it can be found that the concentration of Pb ions in different reactors have a two increase trend, a stable behavior, and a two decrease period. And if the concentration of Pb ions in the overlying water is seen as a function of time (d), the concentration of Pb ions has two maxima at about 12 days and 42 days, respectively. The results indicate that the Pb ions concentration in overlying water is related to environmental conditions.

The concentrations of Cd^{2+} in overlying water are shown in Fig. 50. The concentrations of Cd ions in overlying water in each reactor differ from each other during the experiment. The maximum release of Cd in the sediment of Shibianyu Reservoir and Zhoucun Reservoir is 6.2 μg/L and 4.5 μg/L, respectively.

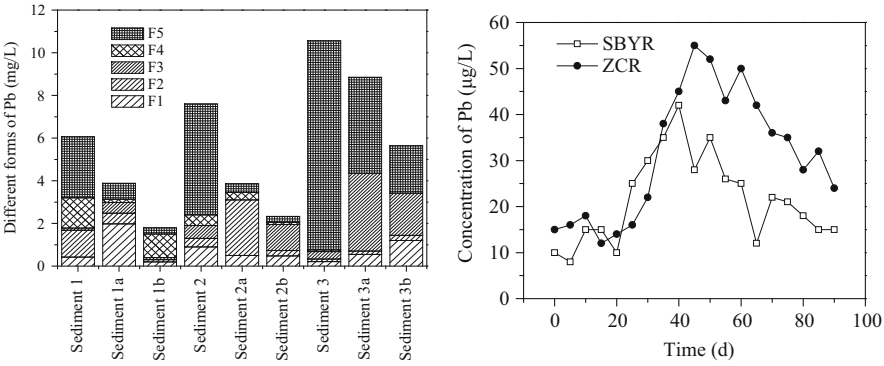

Fig. 49 Release of Pb in sediment of Shibianyu Reservoir and Zhoucun Reservoir

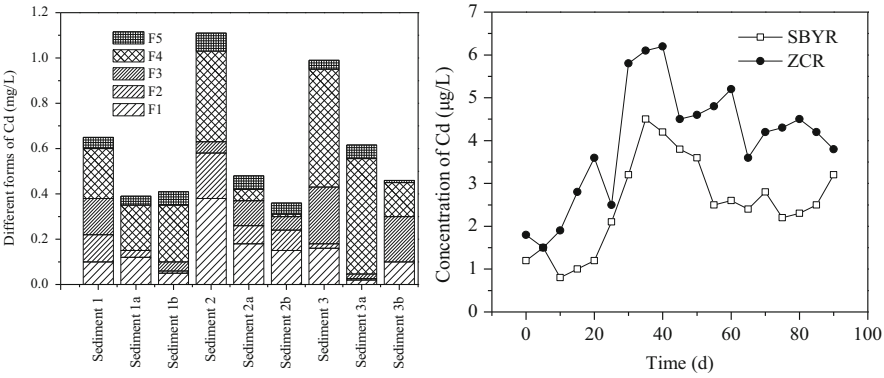

Fig. 50 Release of Cd in sediment of Shibianyu Reservoir and Zhoucun Reservoir

However, concentration of Cd in overlying water has the same trend as Pb during the same period. The result indicates that the transport and transformation processes of Cd to overlying water are related to environmental conditions.

The total amount of Cu in two sediments decreases after the reaction, which decreases more in the Zhoucun Reservoir sediment. The reduction of Cu in sediment indicates that part of Cu can release into the overlying water under anaerobic conditions. It is also observed that the concentration of exchangeable fractions of metal Cu (F1) in sediment increases more than before. The concentration of exchangeable (F1), carbonate bound (F2), iron (manganese) oxide fraction (F3), and organic-bound and bound to sulfide (F4) decreases more than before. Exchangeable and carbonate bound to Cu slightly decreased. Organic-bound to Cu in Zhoucun Reservoir sediment also reduced. The reduction in residue lattice bound (F5) of Cu in two sediments is not large.

The concentration of Cu^{2+} in the overlying water increased sharply, maintaining a value of 28 μg/L at 20 days. After 45 days, it increased to approximately 50 μg/L,

and then decreased to 10 μg/L at the end of the reaction. It is known that the decrease of Cu in sediment is mainly in the metal-exchangeable and carbonate-bound speciations. The reduction of Cu in sediment of reactors does not seem to be much different. This phenomenon is similar to the concentration of Cu^{2+} in overlying water. Cu in sediment will release to the overlying water under anaerobic conditions. Exchangeable and carbonate bound to copper is the major speciation. This process is not affected by the content of copper in the overlying water.

(2) Release of Lead in Sediment

The total amount of lead in sediment reduced compared with before (Fig. 49). The total amount of lead in the sediment of Shibianyu Reservoir decreased significantly. The reduction in the content of lead in sediment shows that a part of lead released to the overlying water under anaerobic conditions. No obvious variation was observed in exchangeable lead. The content of carbonate-bound lead in two sediments is low, and the changes are not evident. Iron (manganese) oxide-bound lead is reduced. Organic-bound and sulfide-bound lead in Zhoucun Reservoir increased compared to before, while organic-bound and sulfide-bound lead in Shibianyu Reservoir reduced. Residual bound lead in sediment reduced after the reaction; the change is the most obvious among all the speciations of lead.

The concentrations of Pb^{2+} in the overlying water are shown in Fig. 49. The concentration of Pb^{2+} is slightly lower in overlying water at 10 days. From 15 to 40 days, the concentration of Pb^{2+} increases sharply. At 38 days, the concentration of Pb^{2+} reaches its maximum value. The changes in Pb^{2+} concentration indicates that the concentration of Pb^{2+} in overlying water is related to the environmental conditions. The result shows that the decomposition and release of lead in sediment occurs mainly in the form of the residual speciations. This result indicates that the residual bound lead in sediment will be affected by the environmental conditions in the overlying water. A large amount of lead was released into the overlying water.

(3) Release of Cadmium in Sediment

The content of cadmium in sediment by the Tessier morphological method is shown in Fig. 50. The total amount of cadmium and Tessier form of cadmium in sediment was reduced compared to before. The largest reduction was for the organic matter and sulfide-bound cadmium, followed by metal-exchangeable cadmium. Varying speciations of cadmium will be released to the overlying water under anaerobic conditions. The total cadmium in sediment decreased.

The concentrations of Cd^{2+} in the overlying water are shown in Fig. 50. Temporal and spatial variations show that the transport and transformation processes of cadmium in sediment into overlying water are affected by the environmental conditions.

(4) Release of Zinc in the Sediment

The content of zinc in sediment by the Tessier morphological method is shown in Fig. 51. The total Zn and metal-exchangeable Zn in Shibianyu Reservoir sediment reduced, while the Zn content in Zhoucun Reservoir sediment increased correspondingly. Carbonate-bound, iron (manganese) oxide-bound, organic matter, and

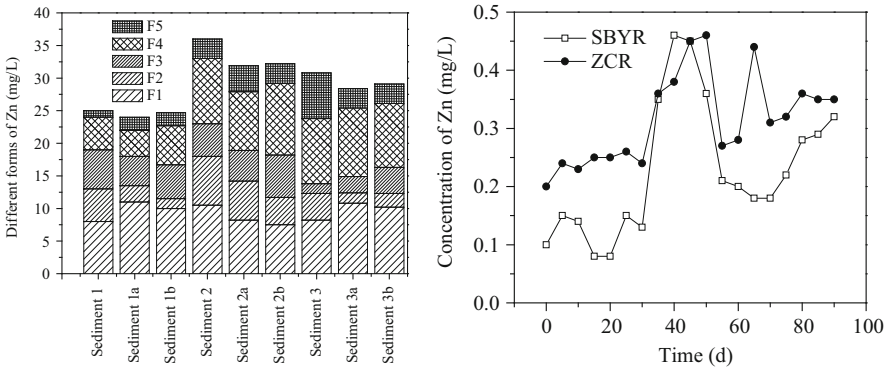

Fig. 51 Release of Zn in sediment of Shibianyu Reservoir and Zhoucun Reservoir

sulfide-bound, residual Zn contents all reduced, while carbonate-bound and residual speciation reduces to a greater extent.

The concentrations of Zn^{2+} in the overlying water are shown in Fig. 51. The release of Zn^{2+} in Shibianyu Reservoir sediment is lower than that in Zhoucun Reservoir at 20 days. After that, the release of Zn^{2+} increased in Shibianyu Reservoir sediment. The highest concentration of Zn^{2+} was 0.45 mg/L in two sediments at 40 days. From 50 to 60 days, the concentration of Zn^{2+} shows a tendency to decline. The result shows that zinc in sediment will be released into the overlying water after 30 days. The released zinc in sediment is mainly in carbonate-bound and residual-bound speciations.

(5) Release of Arsenic in Sediment

Figure 52 shows that the total amount of arsenic in the sediment decreases. The maximum reduction occurs in sediment of Shibianyu Reservoir. The largest reduction is organic matter and sulfide-bound (F4) and metal-exchangeable (F1) arsenic. The reduction of arsenic in organic arsenic of Zhoucun Reservoir is larger than that of Shibianyu Reservoir. However, the reduction of exchangeable arsenic in sediment of Shibianyu Reservoir is also significant. This phenomenon indicates that organic and exchangeable arsenic in sediment mainly diffuse to the overlying water under the anaerobic environment. The reduction of carbonate-bound (F2) and iron (manganese) oxide-bound arsenic is lower than the sulfide-bound and exchangeable arsenic. However, the content of carbonate-bound and iron (manganese) oxide-bound arsenic in the sediment is the lowest. This result shows that carbonate-bound and iron (manganese) oxide-bound arsenic is easy to release into the overlying water under anaerobic conditions.

The concentration of As^{2+} in the overlying water during the experiment is shown in Fig. 52. The changes in the arsenic ion concentration in the overlying water is more obvious, showing a trend of decreasing at first, then increasing, and, finally, decreasing sharply. There is a slight increase at 10 days and a sharp increase from 25 to 38 days. From 42 to 65 days, the concentration of As^{2+} in the overlying water becomes stable and the variation range is 35–45 μg/L. After that, the

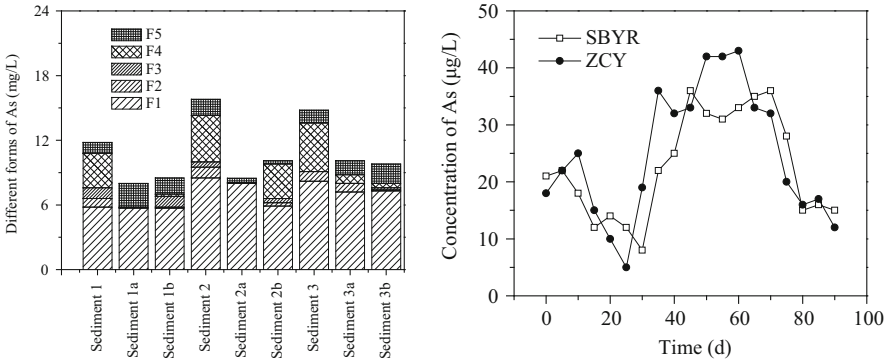

Fig. 52 Release of As in sediment of Shibianyu Reservoir and Zhoucun Reservoir

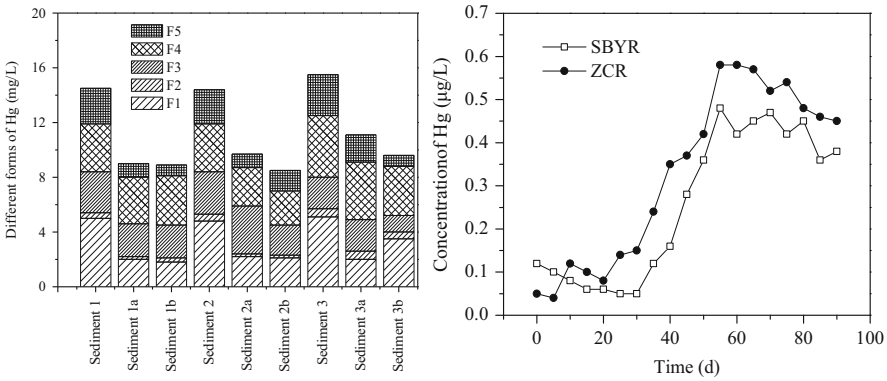

Fig. 53 Release of Hg in sediment of Shibianyu Reservoir and Zhoucun Reservoir

concentration of As^{2+} drastically reduces. The results indicate that arsenic in the sediment may be firstly released into the overlying water and then adsorbed again into sediment.

(6) Release of Mercury in Sediment

Before and after the experiment, the contents of mercury in sediment by the Tessier morphological method are shown in Fig. 53.

The total mercury content decreases in the sediment in the end of the reaction, and the reduction in Zhoucun Reservoir is greater than that in Shibianyu Reservoir. In the reactor of Shibianyu Reservoir, exchangeable, iron (manganese) oxide-bound, and residual mercury reduce more, while exchangeable, iron (manganese) oxide-bound, organic-bound, and residual mercury have greater reduction in sediment in the Zhoucun Reservoir reactor. These results illustrate that exchangeable, iron (manganese) oxide-bound, and residual mercury will be substantially released to the overlying water.

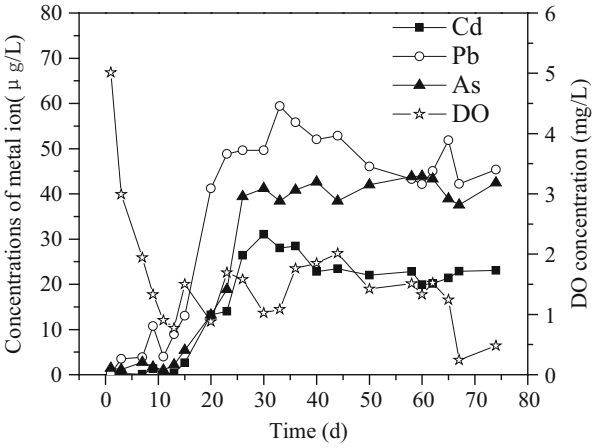

Fig. 54 Release of heavy metals in sediment of Zhelin Reservoir

The concentrations of Hg^{2+} in the overlying water are shown in Fig. 53. During the experiment, the change in Hg^{2+} concentration in overlying water is greater, showing an increasing trend at first, then decreasing.

4.4 Release of Heavy Metals in Zhelin Reservoir

The concentration of Cd, Pb, As, and other elements showed a trend of increase at first and then decrease (Fig. 54). The maximum release of lead reaches 59.40 μg/L, the maximum release of arsenic reaches 43.88 μg/L, and the maximum release of cadmium reaches 31.00 μg/L (far beyond the limit of 5.00 μg/L). When natural water bodies mix together, it is obvious that cadmium exceeded the limit, while lead and arsenic did not.

The limitations of Fe, Mn, Pb, As and Cd in the national surface water quality standard (GB 3838–2002) for class III water are 0.3 mg/L, 0.1 mg/L, 50 μg/L, 50 μg/L and 5 μg/L, respectively. The results show that the release strength of Fe, Mn and Cd in Zhelin Reservoir sediment is high, exceeding the limitations.

5 The Interaction of Pollutants in the Process of Release

5.1 Correlation of Iron and Phosphorus Release

Studies have shown that microorganisms can promote the release of phosphorus, which accelerates the reduction of iron. The concentration of soluble iron has significant meaning to investigate the cycle transformation of phosphorus in the water–sediment interface.

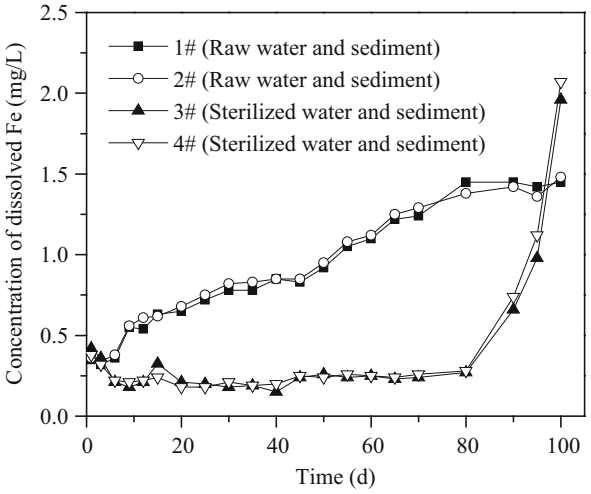

Fig. 55 Variation of soluble iron concentration in overlying water

Figure 55 shows the concentration of soluble iron in overlying water during the experimental process. As can be seen, the concentration of soluble iron in overlying water is similar to soluble phosphorus; that is, the concentration of soluble iron does not apparently release, remaining basically at 0.2–0.4 mg/L, with slight fluctuations during the aerobic phase. The concentrations in No. 1 and No. 2 reactors are slightly higher than those in No. 3 and No. 4 reactors. After entering the anaerobic stage, the concentrations of soluble iron increased significantly in No. 1 and No. 2 reactors containing microorganisms, and it remained stable at about 1.3 mg/L after the balance of release. However, the soluble iron concentration showed no significant changes in the anaerobic stage in No. 3 and No. 4 reactors without microorganisms. The result indicates that microorganisms accelerate the release of iron. It also illustrates that the presence of microorganisms plays a role in the release of soluble iron.

After adding strong reducing agents, the release becomes apparent, and the maximum release rate reached 49.64 mg/(d·m^2). The final concentration of soluble iron reached above 2.2 mg/L in the reactor. A strong reducing agent is added to promote the release of soluble iron.

Microorganisms play an important role in the direct reduction of iron during anaerobic conditions. Fe^{3+} is an electron acceptor in anaerobic biological reactions. The microorganism can use electrons, which are transferred from the process of assimilating organic matter, and directly reduce the ferric iron to ferrous iron and ATP. In this process, the non-specific iron reductase combined with the electron transport in cells plays a major role [44]. Microbial metabolism plays a crucial and decisive role in the oxidation–reduction potential of the aqueous layer.

The concentration of soluble phosphorus and soluble iron is further investigated in No. 1 and No. 2 reactors containing microorganisms. The results are shown in Figs. 56 and 57. It can be seen that soluble phosphorus and soluble iron show a

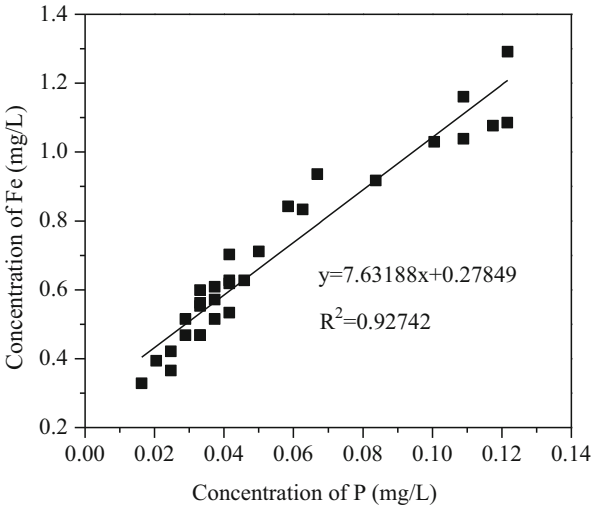

Fig. 56 Correlation analysis of iron and phosphorus in sediment of No. 1 reactor

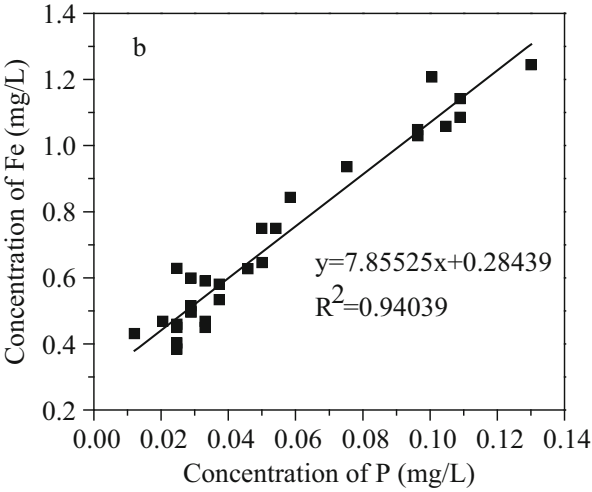

Fig. 57 Correlation analysis of iron and phosphorus in sediment of No. 2 reactor

significant positive correlation, and the correlation coefficients are 0.9299 and 0.9424, respectively. The positive correlation of two concentrations could be simply illustrated from Fig. 57. Inorganic phosphorus compounds like Fe-P in sediment is reduced and dissolved under redox conditions. The concentration of dissolve phosphate of pore water increased when Fe-P is reduced to the dissolved form. It migrated into the overlying water under concentration gradient action. This process is a classical theory of reservoirs and lakes. This process is related to electron donor and acceptor, reaction potential order, microorganisms, and other complex factors in a multiphase interface system. Figures 58 and 59 show that the relationship between the migration and transformation of phosphorus in a

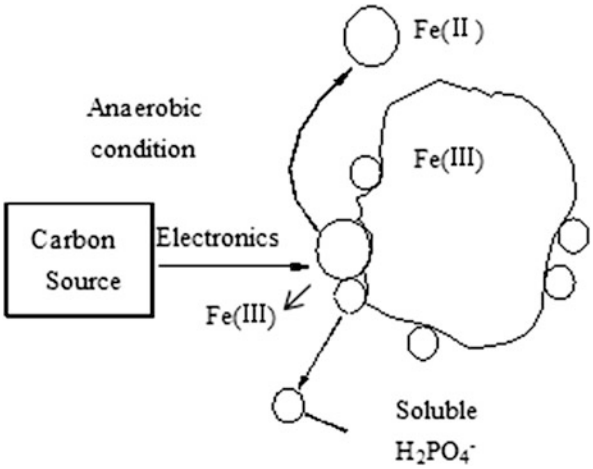

Fig. 58 Mechanism of soluble phosphorus and soluble iron

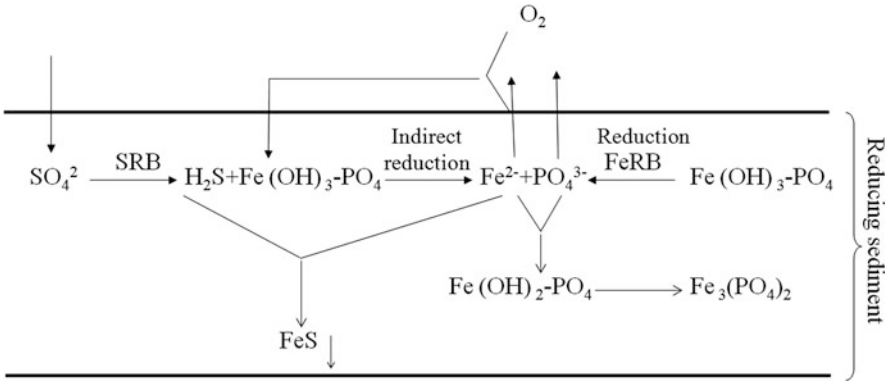

Fig. 59 The relationship of sulfate and iron reduction and the release of dissolved phosphate (SRB is sulfate-reducing bacteria; FeRB is Fe-reducing bacteria)

multiphase interface, the concentration of sulfate, the role of sulfate-reducing bacteria, and the release of soluble iron and dissolved phosphate.

5.2 The Relationship Between Nitrogen Transformation and Other Pollutants Transformation

The nitrogen cycle in the sediment interface is one of the main processes in reservoirs, which has a significant impact on the nutritional status and water quality

of the reservoir. Nitrogen in sediment is mainly organic nitrogen. The concentration of nitrogen in sediment mainly depends on the primary productivity and is strongly correlated to organic carbon (Org-C). Nitrogen released from sediment goes into the interstitial water at first, and then spreads further to the pore water and the overlying water. Diffusion is driven by the concentration gradient on the surface. Nitrogen mainly releases in the speciation of ammonium (from the degradation of nitrogenous organic compound). Ammonium is rapidly oxidized to NO_2^- and NO_3^- under aerobic conditions. The NO_2^- and NO_3^- contents in pore water are very low, and most of them are converted to N_2 by denitrification because the concentration of DO tends to zero in the sediment.

The transformation of nitrogen in the water–sediment interface is controlled by physical–chemical factors and biological processes. The release of nitrogen depends on the decomposition of nitrogen compounds, mainly related to the DO concentration, oxidation–reduction potential (ORP), C/N ratio, cation exchange capacity (CEC), temperature, and hydrodynamic conditions. Biotransformation dominated in the biogeochemical cycle of nitrogen. Microbes are important for driving the nitrogen cycle. They ensure that the nitrogen cycle is not interrupted and maintain nitrogen balance of the ecosystem. For the absence of anthropogenic disturbance lakes, microbes play a very important role in the process of nitrogen input and release into the atmosphere. The nitrogen cycle driven microbially is not isolated, but is closely related to the cycle of carbon, oxygen, sulfur, phosphorus, and other nutrients, and is affected by a variety of metals and organic chemicals. Many redox reactions of the nitrogen cycle are carried out in the metabolism of microorganisms, and particular enzymes catalyzers of such reactions. Thus, the gene and its corresponding enzyme are important objectives of the study for microbial processes in the nitrogen cycle [45].

Sediment plays a very important role in the transfer of nitrogen compounds in reservoirs. Nitrogen in sediment is only buried in a small part, and the majority of nitrogen can be regenerated by mineralization and released by early diagenesis to NH_4^+, NO_3^-, and NO_2^-. Early diagenesis refers to all reactions occurring within the solid sediment and its contained interstitial water when the temperature of sediment (sedimentary rock) is not obviously higher than the normal temperature (25 °C). Bacterial involvement in the degradation of organic matter is a distinctive feature of early diagenesis. The early diagenetic driver is organic matter decomposition and oxidation reaction. This process is often near the interface of sediment and water. Oxidation and decomposition restrict part of the organic debris used by organic matter, and determine the rates of nutrients released into the overlying water. According to the difference of the final electron acceptor in the oxidation process of organic matter, early diagenesis can be divided into three zones: (1) Strong oxidation zone: oxygen as a final electron acceptor; (2) Anoxic zone: the NO_3^-, MnO_2, and Fe_2O_3 as the final electron acceptor; (3) The anaerobic zone: SO_4^{2-}as the final electron acceptor. The dissolution and settlement process of different substances occurred in these zones greatly, which affect the flux of soluble components [46].

When organic matter is decomposed by different heterotrophic bacteria in sediment, it generates NH_4^+, which has an important impact on diagenesis. When NH_4^+ is released into the solution, NH_4^+ can be re-oxidized, or recombined into organic compounds, or adsorbed to particulate matter, or diffused into the other regions of sediment with concentration gradients. Absorption of the particulate matter on NH_4^+ generally comes in two speciations: (1) Exchangeable adsorption: ion exchange occurs on the physical surface of the particles; (2) Fixed adsorption: adsorption on the inside of particulate matter, into the lattice structure, and cannot replaced by other cations. Generally, the concentration of NH_4^+ increases as the depth increases, stabilizes to a certain extent, and then decreases as the depth increases. When the concentration is particularly high, NH_4^+ may re-precipitate into authigenic minerals. In the anoxic zone, the main reaction of transfer NH_4^+ is usually ion exchange reaction between particles. Quantitative description of NH_4^+ adsorption is an important role for nutrient cycling and diagenesis.

NH_4^+ generated in ammonification can transform into NO_3^- in the role of denitrifying bacteria. This kind of denitrification is also an important process in the nitrogen cycle, and it connects the relationship between nitrogen mineralization and N_2 loss from sediments through denitrification. The ecological effect on nitrification is detoxification (for organisms) in a high concentration of NH_4^+, and consumption of dissolved oxygen, as well as oxygen depletion at the bottom of the water body. Denitrification reduces the load of nitrogen going from land to water, and, to some extent, limits the primary productivity of the water body. Nitrification and denitrification have been proved to occur together in sediments. The rate of nitrification is usually determined by the availability of O_2 and NH_4^+. Seasonal changes of denitrification are determined by the available NO_3^-. Therefore, the denitrification rate is constrained by nitrification, which is interdependent between nitrification and denitrification. Factors of controlling the nitrification and denitrification rates mainly include temperature, redox environment in sediments, and dissolved oxygen concentration in the overlying water. The depth of O_2 penetration into the sediment determines the area where nitrification occurs. The depth of the oxidized region is related to the O_2 consumption rate. The elevation of temperature usually accelerates the O_2 consumption. Under normal circumstances, in the winter, the temperature is low, and the dissolved O_2 concentration of overlying water is high. Blending both the bottom and top layers of the water causes the situation that the sediment is in a strong oxidizing environment, so nitrification is significant. In the spring and summer, the temperatures rises, the biological activity at the bottom of water is strengthened, and the concentration of dissolved oxygen in the overlying water decreases, so that the sediment is in a reducing environment. Although the rising temperature reduces nitrification and denitrification, denitrification is relatively dominant. In addition, bioturbation can greatly promote the nitrification and denitrification processes. Organisms can accelerate the nitrogen gas to escape from inorganic nitrogen compounds. Nitrification and denitrification decreases accordingly due to increasing salinity [46].

So far, researches on the biogeochemical cycling of nitrogen in reservoirs have made some achievements, but there are also many problems. Various interrelated processes of nitrogen migration and transformation in reservoirs constitute a complex open-loop system. Different environmental factors will affect the specific process of the reaction. More than one reaction can use the same speciation of nitrogen. The exchanging amount of nitrogen in the three interfaces of sediment–water–atmosphere is difficult to quantify. The facts mentioned above have increased the difficulty of the study.

5.3 Effects of Iron and Manganese Cycling on Interfacial Release

There exists a variety of interfaces in the water–sediment system, including the water–sediment interface, oxidation–reduction interface, and water–sediment–organism interface. The water–sediment interface is a relatively fixed geological interface based on the phase. The interface interaction process is a comprehensive reaction in physical, chemical, and biological interactions. The oxidation–reduction interface is a chemical interface which has redox indicators as criterion in the water–sediment system, and its spatial position is unstable. In the 1980s, Davison proposed a boundary conversion mode of iron oxide, the manganese oxide reduction cycle, according to thermodynamic stratified principles of reservoirs. It is worth noting that the seasonal migration of the boundary layer controls the cycle of iron and manganese. The redox boundary layer is a special environment interface. It is a transition zone changing from oxidizing conditions to reducing conditions in the surface water environment. However, the boundary is not a tangible, visible geological interface, but is a typical chemical interface. Its presence status changes with the nature of the water body, water chemistry characteristics, seasonal transition, and other environmental conditions changes. More detailed studies have been carried out by other domestic scholars.

Iron and manganese cycling in the interface of sediment in reservoirs is mainly driven by the degradation of organic matter. The cycle includes four parts: reduction, diffusion, oxidation, and deposition. At a certain depth, iron and manganese act as an oxidant in the process of degradation of organic matter, and is reduced to form the dissolved iron and manganese in pore water. The dissolved iron and manganese in pore water also diffuse and migrate into the overlying water driven by the concentration gradient, and are oxidized to iron and manganese oxide in the sediment surface, forming particulate speciations of iron and manganese oxide enrichment. However, the cycle of iron and manganese is restricted not only by the water–sediment interface in the reservoir, but also by the impact of the redox boundary layer. In the non-hypoxic season, the redox boundary layer is located near the sediment–water interface. The cycle of iron and manganese results in the enrichment of iron and manganese on the surface of sediment. When seasonal

hypoxia occurs in the reservoir, the redox boundary layer migrates up to the overlying water from sediment seasonally. The iron and manganese interface extends upwards into the overlying water to result in seasonal release on the sediment surface of iron and manganese and iron and manganese enrichment in anoxic water bodies [47].

In addition, the migration of iron and manganese is restricted by the redox conditions of a water body. When the water body is in good oxygenated condition, the oxidation–reduction boundary coincides with the water–sediment geological interface. The circulation of iron and manganese is near the water–sediment interface in the overlying water, and do not affect the overlying water. The concentrations of iron and manganese in overlying water are very low, and there is no significant diffusion and release of pollutants. When the water stratification occurs and the bottom is in the anoxia condition, iron and manganese in pore water migrate upward to the overlying water. The redox boundary moves into the water, leading to a massive release of iron and manganese in sediment into the overlying water.

At the end of the stratification period, the anoxia condition disappears from the bottom, and the redox boundary returns to the sediment. A strong release of iron and manganese comes to an end. Concentrations of dissolved iron and manganese in the water tend to stabilize at a low value. Thus, it constitutes seasonal migration of a redox boundary in lakes. Iron and manganese cycling is controlled by the redox boundary and the water–sediment interface.

Seasonal remigration of iron and manganese after deposition in reservoirs will change the environmental record of sediment. Trace elements in sediment also exhibit the migration phenomenon after deposition. Trace elements in sediment and iron and manganese records show a related vertical fluctuation. Due to the impact of iron and manganese oxide on the adsorption of trace elements, the interface cycling of iron and manganese affects the migration of trace elements.

The remobilization of manganese in early diagenesis in the sediment is much fiercer than in iron. Manganese has priority to act as the primary oxidant in the decomposition of organic matter because the oxidation potential of manganese is higher than that of iron. The diffusion and migration of manganese is stronger than that of iron. The oxidation rate of manganese is lower than that of iron. Therefore, it is more stable for manganese than iron in the water, as well as showing a longer retention time than iron. Overall, the redox cycle of manganese is more intense than that for iron and has a more significant impact on the water body. In the degradation process of organic matter, part of the sulfate is reduced to S^{2-}. When the reduced iron and manganese diffuse towards the overlying water, Fe^{2+} and S^{2-} form the iron sulfide. Thus, it inhibits the release from the pore water to the overlying water. The migration of iron is blocked due to the reduction of sulfate [48].

The study shows that iron and manganese, especially manganese, can enrich in the vicinity of the interface water and the extent of its enrichment will be higher over time. So, it may form tuberculosis of iron and manganese oxide in the reservoir. Soluble nutritive salt is adsorbed and precipitates, resulting in reduced emissions to water bodies. On the other hand, it will have a significant impact on the

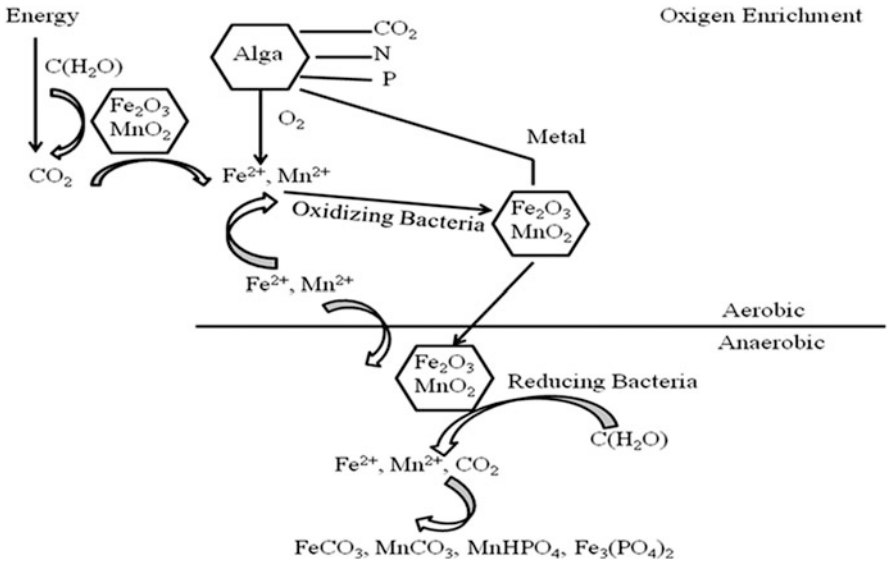

Fig. 60 Iron and manganese recycling transformation process of water, sediment, and biological systems

water quality. Especially during seasonal hypoxia, it leads to increasing concentrations of iron and manganese throughout the lake, and causes water pollution due to iron and manganese seasonal release. Thus, the cycle of iron and manganese on the water–sediment interface of reservoirs is both an important symbol of conversion of redox conditions and an important condition for material migration in the interface.

Abnormal behavior on the elements interface and microbials are closely linked. Iron and manganese are not only important elements forming microbial intracellular enzymes and cofactors, but they dominate microbial respiration and metabolism in the extracellular space due to their special changing characteristics. Iron valence is between divalent and trivalent, while manganese valence is between divalent and tetravalent. These changes lead to iron and manganese oxides to be dissolved and re-mineralized, and coupling with carbon, nitrogen, phosphorus, sulfur, and metal cycling phase in nature. As shown in Fig. 60, on the surface of the water, algal cells photosynthesis and the atmosphere provide adequate oxygen. The biochemical oxidation of iron and manganese ions, the adsorption of metal ions, and organic light degradation on iron and manganese oxide surface occur. In the oxygen-free water–sediment interface, the processes of degradation of organic matter, which takes iron and manganese oxides as electron acceptors, occur in microbes. Part of the iron and manganese diffuse upwards into the oxidation zone to re-enter the cycle with the pore water, and others have the reaction of secondary mineralized fixation with the metal ions in the speciation of carbonate salt, phosphate, and sulfide. The reaction between microorganisms and iron and manganese depends on the chelating dissolution of extracellular active matter. Mineral process accelerates

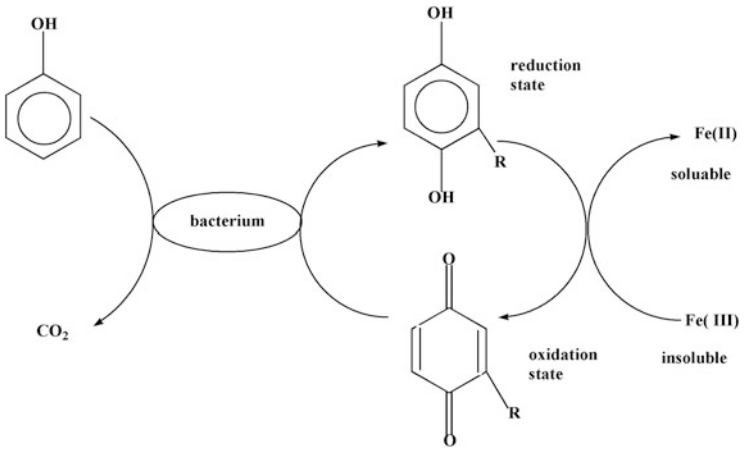

Fig. 61 Extracellular electron transfer of bacteria on reduction Fe^{3+}

biological processes. On the other hand, it depends on the catalysis of electron transfer, also forming a kind of extracellular electron transport chain which can adapt to harsh environmental conditions. Figure 61 is a schematic showing the role of the extracellular electron transfer [49].

Algae is a major manufacturer of organic matter in the water as well as being a water-oxidized environment maker, interdependent with iron and manganese minerals. Nitrogen cycling mainly relies on the nitrogen bacteria and cyanobacteria. Phosphorus is absorbed in the algal cells by the photosynthetic process in the speciation of nutrients. During the process of degradation of algal cells, phosphorus and carbon dioxide precipitate into minerals combined with solution element products, such as $MnHPO_4$, $MnCO_3$, $FeCO_3$, and $Fe_3(PO_4)_2$. Under the organic-rich conditions, metallic elements are further fixed in the speciation of sulfide precipitation with the role of sulfate-reducing bacteria. Fe^{2+}/Fe^{3+}, Mn^{2+}/Mn^{4+}, Fe/Mn and other parameters not only reflect the water body status, but take advantage of environmental mineral material to adjust Fe^{2+}/Fe^{3+}, Mn^{2+}/Mn^{4+} and Fe/Mn because of the good biocompatibility of iron and manganese oxides. It is entirely possible to solve complex organic and metal contamination to realize the pollution control of water bodies [49].

References

1. Trimmer M, Nicholls JC, Deflandre B (2003) Anaerobic ammonium oxidation measured in sediment along the Thames Estuary, United Kingdom. Appl Environ Microbiol 69(11):6447–6454
2. Zehr JP, Ward BB (2002) Nitrogen cycling in the ocean: new perspectives on processes and paradigms. Appl Environ Microbiol 68(3):1015–1024

3. Ma HB, Song JM, Lv XX, Yuan HM (2003) Nitrogen forms and their functions in recycling of the Bohai Sea sediments. Geochimica 32(1):48–54 (in Chinese)
4. Lv XX, Song JM, Li XG (2005) Geochemical characteristics of nitrogen in the southern Yellow Sea surface sediments. J Mar Syst 56:17–27
5. Casey RE, Taylor MD, Klaine SJ (2004) Localization of denitrification activity in macropores of a riparian wetland. Soil Biol Biochem 36:563–569
6. Tanaka T, Guo LD, Deal C, Tanaka N, Whitledge T, Murata A (2004) N deficiency in a well oxygenated cold bottom water over the Bering Sea shelf: influence of sedimentary denitrification. Cont Shelf Res 24:1271–1283
7. Wang JL, Yang N (2004) Partial nitrification under limited dissolved oxygen conditions. Process Biochem 39:1223–1229
8. Owens PN, Walling DE (2002) The phosphorus content of fluvial sediment in rural and industrialized river basins. Water Res 36:685–701
9. Bostom B, Andersen JM, Fleischer S, Jansson M (1988) Exchange of phosphorus across the sediment–water interface. Hydrobiologia 170:229–244
10. Bostr MB, Aderser JM, Broberg B (1988) Bioavailability of different phosphorus forms in freshwater systems. Hydrobiologia 170:133–155
11. Sondergaard M, Jensen JP, Jeppesen E (2003) Role of sediment and internal loading of phosphorus in shallow lakes. Hydrobiologia 506–509:135–145
12. Torrent J, Schwertmann U, Barron V (1994) Phosphate sorption by natural hematites. Eur J Soil Sci 45:45–51
13. Hosomi M, Okada M, Sudo R (1982) Release of phosphorus from lake sediments. Environ Int 7(2):93–98
14. Bertuzzi A, Faganeli J, Welker C, Brambati A (1997) Benthic fluxes of dissolved inorganic carbon, nutrients and oxygen in the Gulf of Trieste (Northern Adriatic). Water Air Soil Pollut 99(1–4):305–314
15. Salati S, Moore F (2010) Assessment of heavy metal concentration in the Khoshk River water and sediment, Shiraz, Southwest Iran. Environ Monit Assess 164:677–689
16. Usman AR, Alkredaa RS, Al-Wabel M (2013) Heavy metal contamination in sediments and mangroves from the coast of Red Sea: *Avicennia marina* as potential metal bioaccumulator. Ecotoxicol Environ Saf 97:263–270
17. Dehghan A, Dehghani A (2011) Experimental and theoretical investigation of thermal performance of underground cold-water reservoirs. Int J Therm Sci 50:816–824
18. Wang Z, Yao L, Liu G, Liu W (2014) Heavy metals in water, sediments and submerged macrophytes in ponds around the Dianchi Lake, China. Ecotoxicol Environ Saf 107:200–206 (in Chinese)
19. Yang J, Chen L, Liu LZ, Shi WL, Meng XZ (2014) Comprehensive risk assessment of heavy metals in lake sediment from public parks in Shanghai. Ecotoxicol Environ Saf 102:129–135 (in Chinese)
20. Zhou ZM, Shen CH, Zhang JF, Tu F (2009) Assessment of heavy metal pollution in the sediments of Shanmei Reservoir Valley. J Huaqiao University (Natural Science) 4:22–27 (in Chinese)
21. Casamitjana X, Serra T, Colomer J, Baserba C, Pérez-Losada J (2003) Effects of the water withdrawal in the stratification patterns of a reservoir. Hydrobiologia 504:21–28
22. Huang TL, Li X, Rijnaarts H, Grotenhuis T, Ma W, Sun X, Xu J (2014) Effects of storm runoff on the thermal regime and water quality of a deep, stratified reservoir in a temperate monsoon zone, in Northwest China. Sci Total Environ 485:820–827
23. Huang TL, Qin C, Li X (2013) Studies on seasonal variation and sources of nitrogen and phosphorus in a canyon reservoir used as water source. Huan jing ke xue= Huanjing kexue/[bian ji, Zhongguo ke xue yuan huan jing ke xue wei yuan hui "Huan jing ke xue" bian ji wei yuan hui 34:3423–3429 (in Chinese)

24. Fu J, Zhao C, Luo Y, Liu C, Kyzas GZ, Luo Y, Zhao D, An S, Zhu H (2014) Heavy metals in surface sediments of the Jialu River, China: their relations to environmental factors. J Hazard Mater 270:102–109
25. Gao X, Chen CTA (2012) Heavy metal pollution status in surface sediments of the coastal Bohai Bay. Water Res 46:1901–1911
26. Venkatramanan S, Chung SY, Ramkumar T, Gnanachandrasamy G, Kim TH (2015) Evaluation of geochemical behavior and heavy metal distribution of sediments: the case study of the Tirumalairajan river estuary, southeast coast of India. Int J Sediment Res 30:28–38
27. Whittleston RA, Stewart DI, Mortimer RJ, Burke IT (2013) Enhancing microbial iron reduction in hyperalkaline, chromium contaminated sediments by pH amendment. Appl Geochem 28:135–144
28. Azam HM, Finneran KT (2013) Ferric iron amendment increases Fe (III)-reducing microbial diversity and carbon oxidation in on-site wastewater systems. Chemosphere 90:1435–1443
29. Nickel M, Vandieken V, Bruechert V, Jørgensen BB (2008) Microbial Mn (IV) and Fe (III) reduction in northern Barents Sea sediments under different conditions of ice cover and organic carbon deposition. Deep Sea Res Part II: Top Stud Oceanogr 55:2390–2398
30. Paul L, Herrmann S, Koch CB, Philips J, Smolders E (2013) Inhibition of microbial trichloroethylene dechorination by Fe (III) reduction depends on Fe mineralogy: a batch study using the bioaugmentation culture KB-1. Water Res 2013(47):2543–2554
31. Preat A, Mamet B, Di Stefano P, Martire L, Kolo K (2011) Microbially-induced Fe and Mn oxides in condensed pelagic sediments (Middle-Upper Jurassic, Western Sicily). Sediment Geol 237:179–188
32. Aquilina A, Homoky WB, Hawkes JA, Lyons TW, Mills RA (2014) Hydrothermal sediments are a source of water column Fe and Mn in the Bransfield Strait, Antarctica. Geochim Cosmochim Acta 137:64–80
33. Elliott A, Plach J, Droppo I, Warren L (2014) Collaborative microbial Fe-redox cycling by pelagic floc bacteria across wide ranging oxygenated aquatic systems. Chem Geol 366:90–102
34. Fernandes SO, Gonsalves MJ, Michotey VD, Bonin PC, LokaBharathi P (2013) Denitrification activity is closely linked to the total ambient Fe concentration in mangrove sediments of Goa, India. Estuar Coast Shelf Sci 131:64–74
35. Keene AF, Johnston SG, Bush RT, Burton ED, Sullivan LA, Dundon M, McElnea AE, Smith CD, Ahern CR, Powell B (2014) Enrichment and heterogeneity of trace elements at the redox-interface of Fe-rich intertidal sediments. Chem Geol 383:1–12
36. Komlos J, Kukkadapu RK, Zachara JM, Jaffe PR (2007) Biostimulation of iron reduction and subsequent oxidation of sediment containing Fe-silicates and Fe-oxides: Effect of redox cycling on Fe (III) bioreduction. Water Res 41:2996–3004
37. Takenaga H, Aso S (1975) Studies on the physiological effect of humic acid (Part 9). Stability constants of cation-nitrohumic acid chelates. J Soil Sci Plant Nutr 46:349–354
38. Ramos L, González MJ, Hernández LM (1999) Sequential extraction of copper, lead, cadmium and zinc in sediments from Ebro river (Spain): relationship with levels detected in earthworms. Bull Environ Contam Toxicol 62:301–308
39. Yu KC, Chang CY, Tsai LJ, Ho ST (2000) Multivariate analysis on heavy metal binding fractions of river sediments in southern Taiwan. Water Sci Technol 42:193–199
40. Mario V, John B, Garrison S (2005) Mechanisms of Pb (II) sorption on a biogenic manganese oxide. Environ Sci Technol 39:569–576
41. Tarvainen T, Kallio E (2002) Baselines of certain bioavailable and total heavy metal concentrations in Finland. Appl Geochem 17:975–980
42. Hua LP, Hua L, Gao J, Zhang ZX, Yin XX, Zhu FY, Wang XD (2006) Heavy metal pollution of sediments of lakes in china. Soils 38(4):366–373
43. Quevauviller P, Lachica M, Barahona E (1998) Certified reference material for the quality control of EDTA- and DTPA-extractable trace metal contents in calcareous soil (CRM 600). Fresenius J Anal Chem 360:505–511
44. Zhang XH (1999) Iron cycles in water sources. Water Wastewater Eng 11:005

45. Zeng J, Yang LY, Xiao L, Yin DQ, Qin BQ (2007) Biogeochemical cycling of nitrogen in lakes and the role of microorganisms in conversion of nitrogen compounds. J Lake Sci 19 (4):382–389 (in Chinese)
46. Lv XX, Song JM (2003) Morphology and ecological significance of nitrogen in marine sediments [J]. Mar Sci Bull 45(5):101–111 (in Chinese)
47. Luo SS, Wan GJ (1999) New progress in the study of Fe, Mn and S systems at the sediment-water interface of lakes on Yunnan-Guizhou plateau. Geology-Geochemistry 27(3):47–63 (in Chinese)
48. Luo SS, Wan GJ, Huang RG (2003) Characteristics of Fe, Mn, S cycle at the sediment-water interface of Yangzong lake, Yunnan province. Urban environ Urban Eco 16(5):75–78 (in Chinese)
49. Zheng WY, Li HR (2005) Bio-chemistry process of iron and manganese recycling in water-mineral-microbe system. Nonferrous Metals 57(3):67–70 (in Chinese)

Impact of Contaminated Sediment on the Water Quality of Typical Reservoirs

Jinlan Xu, Chao Xia, Zizhen Zhou, and Tinglin Huang

Abstract The sediment in reservoirs is mainly derived from the sedimentation of suspended grains, such as organic particles and inorganic minerals, carried by runoff scouring from vegetation. There are three parts in this chapter: (1) Effects of pollutants released from sediment on water quality; (2) Effects of metals released from sediment on water quality; (3) Algal blooms and their impact on water quality. The decrease of the oxidation–reduction potential (ORP) in a multiphase interface under anaerobic conditions resulted in the increase of soluble ferrous hydroxide. Phosphate combining with iron hydroxide in sediment is released to interstitial water and then diffused into the overlying water. In addition, the metabolism of microbes resulted in the decrease of the ORP in anaerobic conditions, promoting the release of soluble iron in sediment and then causing the huge release of phosphorus. The release of endogenous phosphorus from sediment under anaerobic conditions resulted in the significant increase of PO_4^{3-} in the overlying water. The release of phosphorus from sediment depends on the conditions of the ORP.

Keywords Water quality • Reservoir • Sediment • Nitrogen and phosphorus • Algal bloom

1 Effect of Nitrogen Release from Sediment on Water Quality

1.1 Interstitial Water Quality and Nitrogen Speciation in Sediment

Tangyu Reservoir is located in Tangyu town, Lantian County, Shaanxi Province, with an artificial dam in the Stone Gate. It was built in 1975 from national investment, has a north–south length of 1500 m, greatest width of 400 m, and a

J. Xu • C. Xia • Z. Zhou • T. Huang (✉)
School of Environmental and Municipal Engineering, Xi'an University of Architecture and Technology, Yanta Road 13, 710055 Xi'an, Shaanxi Province, P. R. China
e-mail: huangtinglin@xauat.edu.cn

T. Huang (ed.), *Water Pollution and Water Quality Control of Selected Chinese Reservoir Basins*, The Handbook of Environmental Chemistry 38,
DOI 10.1007/978-3-319-20391-1_7

Table 1 Distances of the sampling points in Tangyu Reservoir

	Distance (m)		Distance (m)		Distance (m)
S_2–S_1	280	S_5–S_1	670	S_8–S_1	930
S_3–S_1	400	S_6–S_1	835	S_9–S_1	1100
S_4–S_1	515	S_7–S_1	900	S_{10}–S_1	1110

S_1 as for the origin

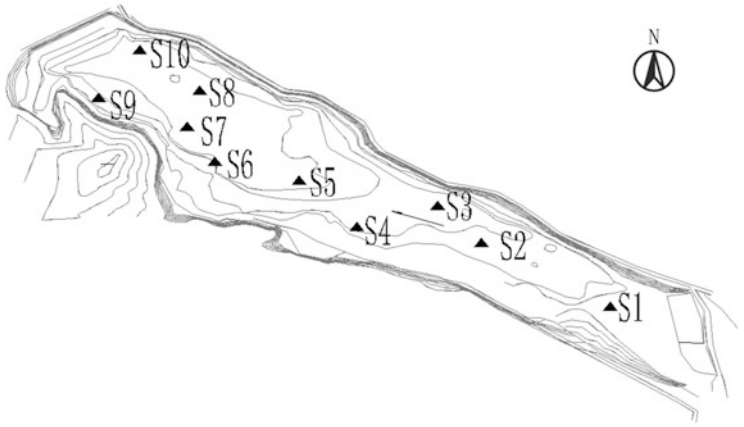

Fig. 1 The locations of the sampling points in Tangyu Reservoir, Xi'an City

total area of 3.7 km^2. The maximum design water depth is 32.58 m, and it has a total storage capacity of 4,480,000 m^3. It was mainly used for irrigation at the beginning of its user, but in recent years, the reservoir has served as a drinking water source due to water shortage.

A total of ten representative sampling points at the upstream, midstream, and downstream sections were selected in this study (Table 1). The surface sediment samples were collected by a Pedersen grab type sampler, sealed in the bags, and cryopreserved. The distribution of the sampling points is shown in Fig. 1.

The moisture content, ignition loss, and organic content of sediment were determined in the ten sampling points (Fig. 2). The water quality of the interstitial water in sediment was further analyzed (Fig. 3).

It can be seen from Figs. 2 and 3 that the differences in the moisture content in sediment are small (with an average of 43 %) due to the different geographic positions and environment conditions. The maximum sediment total nitrogen (STN) is 2.6 mg/g at sampling point S_{10}, while the minimum STN is 1.4 mg/g at sampling point S_6. The average STN is 2.1 mg/g. The maximum SOC is 5.3 % and the minimum SOC is 2.8 %, with an average of 3.8 %. The TN concentration of interstitial water at S_3, S_6, S_7, and S_8 are 18.5 mg/L, 8 mg/L, 7.5 mg/L, and 10.5 mg/L, respectively. The depth of these four sampling points is larger. The concentration of ammonium in interstitial water at S_3, S_4, S_6, and S_7 are 4.9 mg/L, 4.2 mg/L, 5.1 mg/L, and 3.9 mg/L, respectively. The water quality at these sampling points is

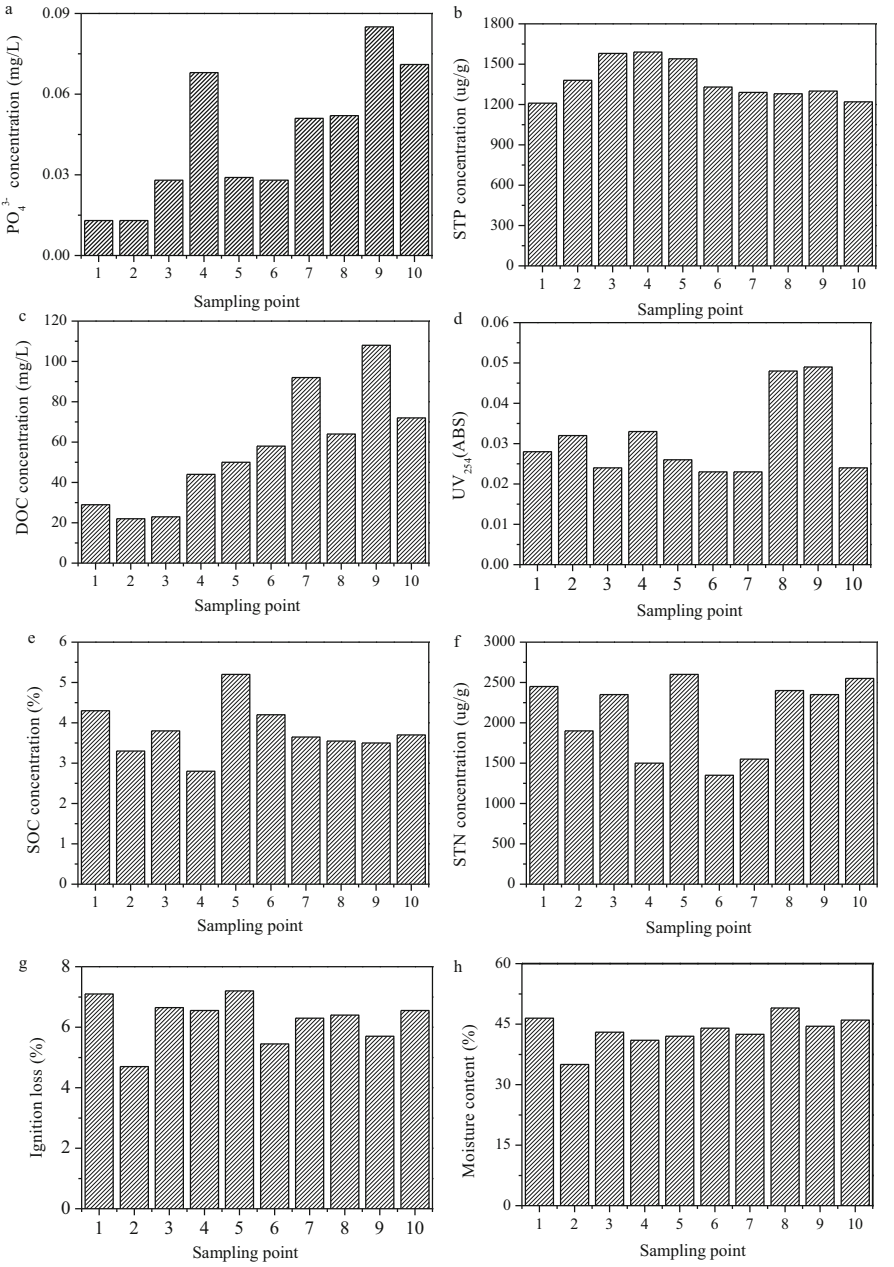

Fig. 2 Water quality of the interstitial water and physicochemical properties of sediment

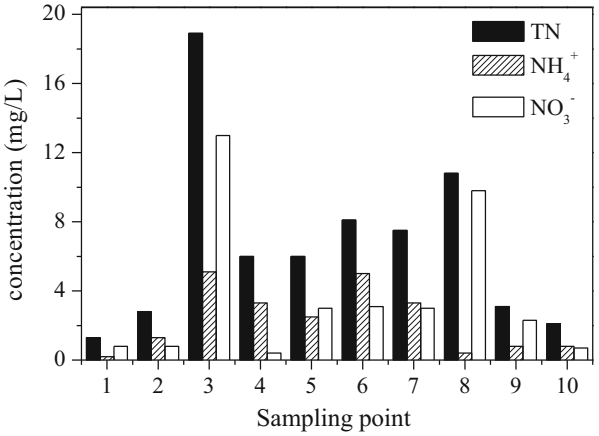

Fig. 3 Interstitial water quality of the sampling points

significantly worse than at the other sampling points, especially regarding TN and NH_4^+. The results indicated that the dissolved oxygen concentration is lower as the water depth becomes greater, which accelerates the release of pollutants [1].

The content of different speciations of nitrogen in reservoirs was determined [2]. The results are shown in Table 2, indicating that the proportion of transformed nitrogen (TF-N) to the total nitrogen is different at the different locations. For S_3, S_8, S_9, S_4, and S_6, the concentration order is WAF-N>SAE-N>IE-N. For S_5 and S_7, the concentration order is WAE-N>IE-N>SAE-N. In these seven sampling points, it can be seen that the proportion of WAE-N ranks next to SOE-N; only the proportions of SAE-N and IE-N are slightly different. There are greater differences between S_{10}, S_1, and S_2 and these seven sampling points, following the rules SAE-N>WAE-N>IE-N for S_1 and S_2, and IE-N>WAE-N>SAE-N for S_{10}. It can be seen that the complexity and irregularity of nitrogen speciation in water reservoir sediment. The ranges of total nitrogen, transformed nitrogen, and SOE-N values in sediment are 1392–2591 μg/g, 549.24–1278.48 μg/g, and 382.52–835.73 μg/g, respectively. However, the content of nitrogen increased with the decrease of sediment particles. As shown in Table 2, there is a good positive correlation between the three speciations of nitrogen and the organic content in sediment. The water quality of the interstitial water and physicochemical properties of the sediment of each sampling point are shown in Table 3, indicating that the content of TF-N is negatively correlated with the TOC content in the interstitial water ($r = -0.806$, $n = 10$, $p < 0.05$). TF-N was released to the water during the mineralization of organic matter; thus, the transferable contents in these sediments decreased, but the TOC content in the interstitial water increased [3]. Therefore, the lower the content of TF-N in the sediment, the higher the content of TOC in the interstitial water. It can be seen that the TN concentration in the sediment and the ammonium content in the interstitial water have a good negative correlation ($r = -0.647$, $n = 10$, $p < 0.05$). That is, along with the decrease of TN concentration, the ammonia concentration increased. This result indicated that TN in the sediment was converted to ammonia.

Table 2 The content of extracted nitrogen and the proportion of the total nitrogen

Sampling point	IE-N		WAE-N		SAE-N		SOE-N		Transformed nitrogen	
	Content (μg/g)	Proportion (%)	Proportion (%)	Content (μg/g)	Proportion (%)	Content (μg/g)	Proportion (%)	Content (μg/g)	Proportion (%)	Content (μg/g)
S_1	13.89	0.57	40.77	1.66	84.40	3.45	835.73	34.11	974.79	39.79
S_2	10.11	0.53	45.91	2.41	61.80	3.24	431.42	22.62	549.24	28.80
S_3	51.10	2.11	153.54	6.34	85.94	3.55	751.10	31.02	1041.69	43.01
S_4	69.47	4.58	93.42	6.16	72.47	4.78	482.19	31.79	717.55	47.31
S_5	136.47	5.32	152.64	5.95	74.05	2.88	777.43	30.28	1140.59	44.42
S_6	33.65	2.42	90.44	6.50	65.13	4.68	382.52	27.48	571.74	41.07
S_7	72.37	4.64	98.33	6.31	59.73	3.83	502.88	32.26	733.30	47.04
S_8	63.44	2.56	93.71	3.78	68.12	2.75	583.74	23.58	809.00	32.68
S_9	37.35	1.60	190.21	8.13	85.76	3.67	551.77	23.59	865.09	36.98
S_{10}	313.39	12.10	184.34	7.11	82.29	3.18	698.45	26.96	1278.48	49.34

Table 3 The correlation coefficient of each speciation of nitrogen in sediment with other physical and chemical indicators of water quality

	Sediment index				Interstitial water quality				
Speciations	Moisture content	LOI	Organic matter	Particle size	TN	NO_3^-	NO_2^-	NH_4^+	TOC
IE-N	0.253	0.336	0.178	−0.187	−0.254	−0.171	−0.183	−0.202	−0.148
WAE-N	0.314	0.218	0.177	−0.401	0.154	0.1833	−0.620	−0.022	−0.028
SAE-N	0.374	0.464	0.144	−0.306	0.101	0.1304	−0.290	−0.289	−0.572
SOE-N	0.435	0.827	0.575	−0.516	0.141	0.205	0.154	−0.373	−0.545
Transformed nitrogen	0.464	0.734	0.487	−0.509	0.036	0.116	−0.117	−0.329	−0.806
TN	0.437	0.509	0.427	−0.732	0.153	0.294	0.165	−0.647	−0.593

$n = 10, p < 0.05$

Combining the measured data of the reservoir and in terms of the ten sampling points, the order is in accordance with the influence degree of the nitrogen cycle that is influenced by the four nitrogen speciations, which is as follows: SOE-N>WAE-N>IE-N and SAE-N. This is different from the theoretical order (IE-N, WAE-N, SAE-N, SOE-N), in that SOE-N has the greatest impact.

1.2 The Contributions of Existing Speciations of Nitrogen in the Sediment to Release in the Multiphase Interface

The sediment and overlying water in Shibianyu Reservoir were regarded as research objects in this simulation experiment. The content of various speciations of nitrogen in sediment were tested after the experiment, in order to study how much the various speciations of nitrogen in sediment contribute to the release of nitrogen in the multiphase interface. Various speciations and proportions of nitrogen in sediment have important effects on the overlying water quality.

The results are shown in Fig. 4. The major speciations of nitrogen release in sediment are IE-N, WAE-N, and SOE-N. Their proportions are 41.55 %, 55.17 %, and 53.67 %, respectively. IE-N is adsorbed nitrogen with the weakest ability to combine with sediment, but it is also the most "active" section in sediment. 90 % of IE-N occurs in the form of ammonia. Ammonia is the first product of organic nitrogen mineralization, so its release is very significant. The change of WAE-N is affected by many factors, especially pH and sediment grain size. The composition distribution of grain size in sediment is shown in Fig. 5. 90 % of the particle sizes are smaller than 39.78 μm, and the distribution is mainly between 15.65 and 39.78 μm, which indicates that the WAE-N is easy to be utilized, participate in the multiphase interface cycle, and release to the overlying water by biological

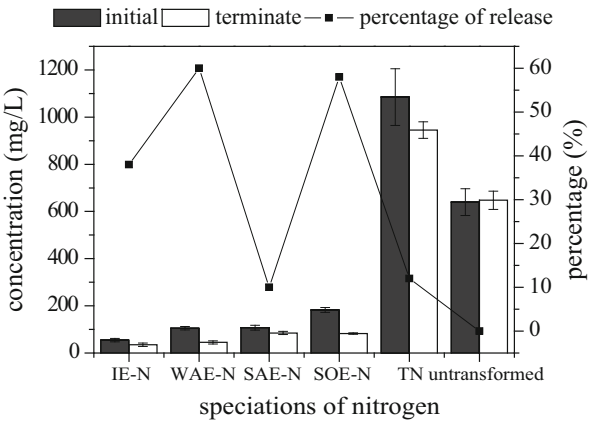

Fig. 4 The change of each nitrogen speciation before and after release in sediment

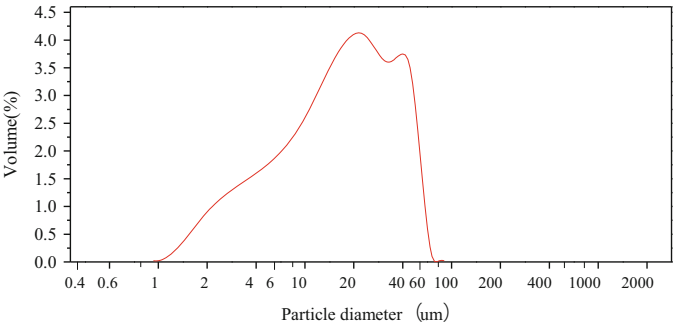

	Volume/%					
Diameter	10	25	50	75	80	90
μm <	3.21	6.76	15.65	27.39	33.01	39.78

Fig. 5 The distribution of the mechanical composition of sediment

	Volume/%					
Diameter	10	25	50	75	80	90
μm<	3.21	6.76	15.65	27.39	33.01	39.78

processes. SAE-N is the nitrogen combined with iron/manganese oxides. The formation and distribution of SAE-N is mainly controlled by the redox conditions of sediment. SOE-N is mainly related to the source of matter and the sedimentary environment. The main factors include the granularity, velocity of organic matter transporting to sediments, deposition rate, and the ORP environment of sediment. At the end of the experiment, the DO concentration in the multiphase interface is close to 0 mg/L, the ORP is lower, and the grain size composition is fine, which makes organic nitrogen easy to be mineralized, decomposed, and released to the overlying water (Pavanelli and Sellil 2013).

2 Effect of Phosphorus Release from Sediment on Water Quality

2.1 The Speciation and Other Physicochemical Properties of Phosphorus in Sediment and the Correlation Analysis of Interstitial Water Quality

The contents of different speciations of phosphorus in sediment were determined (Ruttenburg 1992), and the results are shown in Fig. 6. The content of inorganic

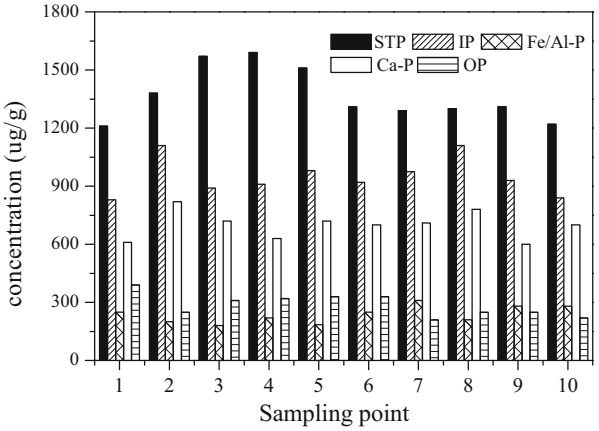

Fig. 6 The speciation of each sampling point

Table 4 The phosphorus speciation of sediment samples, interstitial water quality, and the correlation analysis of physicochemical properties

	STP	Fe/Al-P	Ca-P	IP	OP
Moisture content	−0.39	0.18	−0.45	−0.47	0.07
Loss on ignition (LOI)	0.20	0.10	0.22	−0.03	−0.30
Particles	0.32	0.06	0.11	0.45	−0.37
STN	−0.15	−0.24	−0.13	0.29	0.50
SOC	0.01	0.45	−0.22	−0.21	−0.32
DOC	0.21	0.83**	−0.25	0.14	−0.61*
Interstitial water PO_4^{3-}	−0.06	0.61*	−0.31	−0.05	−0.55

Notes: the Pearson correlation coefficient is analyzed using the OriginPro software in the table, and the number of samples is $n = 10$. * represents significant correlation at the 0.05 level, ** represents significant correlation at the 0.01 level

phosphorus (IP) in the surface sediment of each sampling point was between 835.73 and 1136.74 μg/g, accounting for 65.32–73.24 % of STP. The result indicated that IP is the main speciation of TP in sediment. The content of IP and STP followed the same trend. The maximum value is at sampling point S_8, and the minimum value is at sampling point S_1. The content of Fe/Al-P ranged from 165.09 to 327.07 μg/g, with an average of 241.34 μg/g, accounting for 12.61–22.92 % of STP. The maximum value of Fe/Al-P is at sampling point S_7, while the minimum value of Fe/Al-P is at sampling point S_3. The content of Ca-P ranged from 610.94 to 826.70 μg/g, with an average of 711.98 μg/g, accounting for 46.44–60.24 % of STP. The maximum value of Ca-P is at sampling point S_2, and the minimum value of Ca-P is at sampling point S_1. The content of OP ranged from 15.32% to 31.90%. The maximum OP is at sampling point S_1, and the minimum OP is at sampling point S_8.

The phosphorus speciations of the interstitial water and the physicochemical properties of sediment are shown in Table 4. It can be seen that the physicochemical indexes of sediment have a weak correlation with the phosphorus speciations. Only

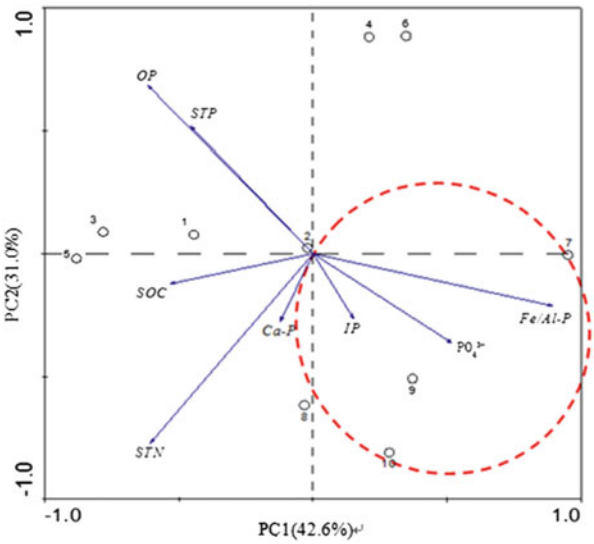

Fig. 7 Principal component analysis of the interstitial water quality and phosphorus speciation, as well as its physicochemical properties

the concentrations of DOC and PO_4^{3-} have a significant correlation with the Fe/Al-P content in interstitial water (the correlation coefficients are 0.83 and 0.61). This proved that Fe/Al-P in sediment contributed greatly to the PO_4^{3-} content in interstitial water. The grain size of sediment has a certain correlation with the content of STP and IP (the correlation coefficients are 0.32 and 0.45). The distribution of particle size is an important factor affecting the content of STP and IP. The correlation coefficient of STM and OP in sediment is 0.50. The content of SOC and STP in sediment and other speciations, except for Fe/Al-P, have a poor correlation. In contrast, the concentrations of DOC and Fe/Al-P in interstitial water have a better correlation, which suggests that the speciation of Fe/Al-P in sediment and SOC in sediment may be homologous. The sediment of reservoirs is mainly derived from the sedimentation of suspended grains, such as organic particles and inorganic minerals, carried by runoff scouring from good vegetation, which is consistent with the actual vegetation conditions upstream of the reservoir basin [4].

The phosphorus speciation and physicochemical properties of sediment and the PO_4^{3-} content of interstitial water are shown in Fig. 7. The first two principal components of the eight principal component factors are present. The variances are 42.6 % and 31 % (the total variance is 73.6 %). There are significant differences in the ten sampling points distributed in different quadrants. Among them, Fe/Al-P and SOC in sediment make greater contributions to the first principal component. Fe/Al-P is relevant to the first spindle positively, while SOC is relevant to the first spindle negatively. The sampling points S_9 and S_{10} distribute in the fourth quadrant, the sampling point S_7 is located at a junction of the first and fourth quadrants, and sampling point S_8 is placed in the third quadrant close to the fourth quadrant. It can

be clearly seen that the four points (S_7, S_8, S_9, S_{10},) are influenced greatly by IP, Fe/Al-P, and SOC. The content of PO_4^{3-} in the interstitial water of the four sampling points is relatively higher among the ten sampling points. The results indicated that Fe/Al-P is the most active phosphorus speciation in sediment and is easily released. Therefore, Fe/Al-P can also be an auxiliary index for determining the potential of phosphorus release in sediment.

2.2 *The Contributions of Existing Speciations of Phosphorus in Sediment to the Release in the Multiphase Interface*

The study investigated the source of phosphate in interstitial and overlying water and provided the basis on judging the eutrophication level of reservoirs.

2.2.1 The Release from Sediment in Tangyu Reservoir

The content of STP in sediment is closely related to the content of PO_4^{3-} in overlying water. Through static simulation experiments, the release characteristics of different phosphorus speciations from sediment were explored under the conditions of different DO and ORP, and the results are shown in Figs. 8 and 9.

As shown in Fig. 8, the concentration of DO is below 0.5 mg/L in the first 5 days due to the oxygen consumption by the sediment and overlying water. The concentration of PO_4^{3-} in overlying water increased under anaerobic conditions. The concentration of PO_4^{3-} increased rapidly, and then reached a maximum value at 24 days. During the period of 24–30 days, the concentration of PO_4^{3-} decreased and then remained stable, and the release of phosphorus reached an equilibrium. The ORP in the multiphase interface decreased under anaerobic conditions, resulting in the release of soluble ferrous hydroxide. Phosphate combined with iron hydroxide in sediment was released into interstitial water, which then diffused

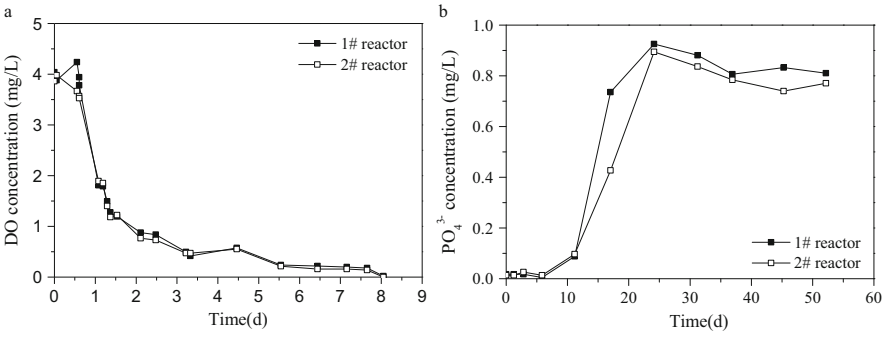

Fig. 8 The concentration of DO (**a**) and PO_4^{3-}change (**b**)

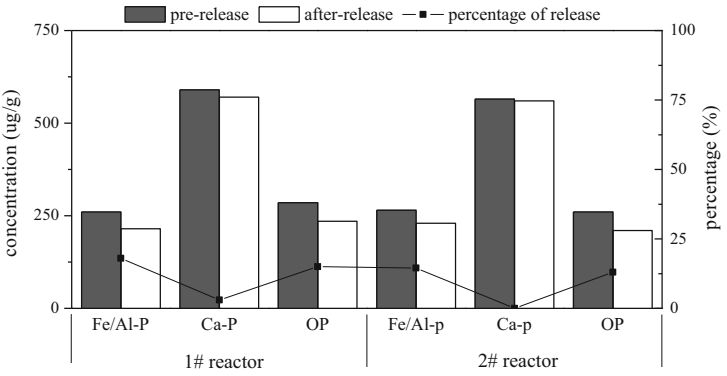

Fig. 9 The content of different phosphorus species in sediment before and after release

into the overlying water. In addition, the metabolism of microbes resulted in the decrease of ORP in anaerobic conditions, promoted the release of soluble iron in sediment, and then caused the huge release of phosphorus [5]. Therefore, the release of endogenous phosphorus in sediment under anaerobic conditions increased the content of PO_4^{3-} in the overlying water. The release of phosphorus in sediment depends on the condition of the ORP.

The content of phosphorus in sediment was determined before and after release. The results showed that STP and phosphorus were released to some extent. As shown in Fig. 9, the release of Fe/Al-P is higher than that of Ca-P. The Fe/Al-P release proportions of S_1 and S_2 were 17.12 % and 14 %, respectively, while the release proportions of Ca-P were only 3 % and 0.55 %, respectively. OP had a certain degree of release (15.76 % and 13.58 %), but its release proportion is less than that of Fe/Al-P (the Fe/Al-P content accounted for about 20 %, while the OP content accounted for about 30 % in STP). Anaerobic conditions are favorable for the release of Fe/Al-P. It can be found that the content of Fe/Al-P in the sediment make the greatest contribution to the release of PO_4^{3-} in the water, which was consistent with the results of the static release simulation experiment.

2.2.2 The Static Release Simulation Results of Sediment in Fenhe Reservoir

The concentration change of PO_4^{3-} in overlying water can be seen in Fig. 10. The PO_4^{3-} concentration of No.1 and No.2 reactors in overlying water only has variations under aerobic conditions. The release of endogenous phosphorus in sediment was not obvious. However, the PO_4^{3-} concentration increased gradually up to 0.12 mg/L and 0.13 mg/L on the 30th day under anaerobic conditions. The release rate increased from 0.42 mg/(d·m^2) to 2.09 mg/(d·m^2). The content of released PO_4^{3-} increased significantly.

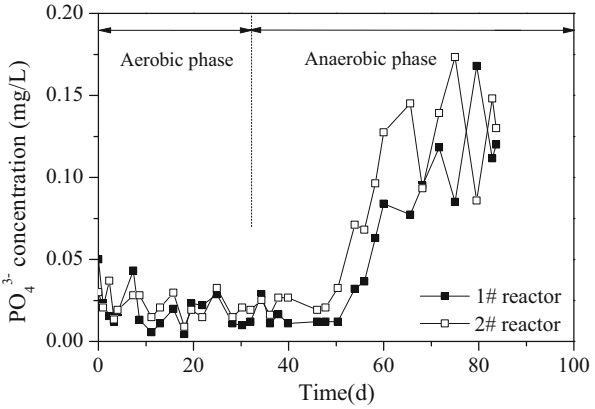

Fig. 10 The PO_4^{3-} concentration in overlying water

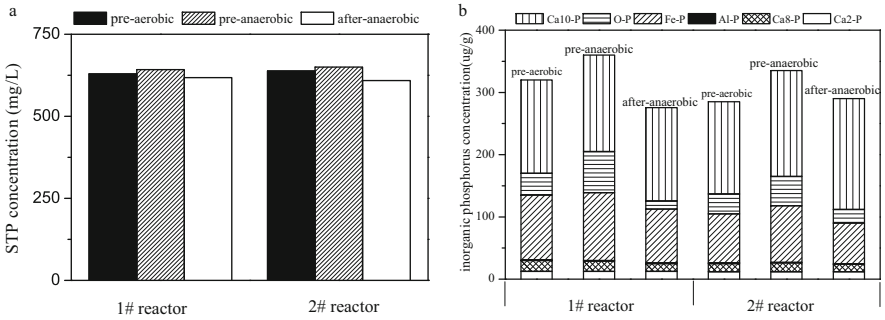

Fig. 11 The content of STP and its species before and after release

The contents of STP and inorganic phosphorus in sediment are shown in Fig. 11. The part of STP in the sediment of the two reactors is released to overlying water at the end of the anaerobic process. The content of STP decreased slightly, showing reductions of 3.69 % and 5.15 % in the two reactors, respectively. The results were consistent with the content of PO_4^{3-} in overlying water. After the anaerobic stage, the content of OP in these two reactors both decreased significantly. Because the concentration of DO and ORP in the multiphase interface are both lower in the anaerobic stage, insoluble iron/manganese metal oxide that speciations occluded organic phosphorus are dissoluted and desorbed, and PO_4^{3-} is released to the overlying water. In addition, the content of Fe/Al-P in the sediments of No.1 and No.2 reactors decreased significantly in the anaerobic stage. Fe/Al-P reduced by 21.9% in No.1 reactor, while Fe/Al-P reduced by 19.5% in No.2 reactor. Besides the occluded organic phosphorus, Fe/Al-P is also an important source leading to the increase of the PO_4^{3-} concentration, which is consistent with the static release simulation results of Tangyu Reservoir.

3 The Release Characteristics of Heavy Metals from Sediment

In this section, the effect of the redox conditions on the heavy metals distribution in the sediment of Tangyu Reservoir was investigated. In addition, the migration and transformation of heavy metals between the sediment and water interface was explored.

3.1 Materials and Methods

Representative sediment samples were collected from the shallow fresh sediment within 30 cm. Sediment samples were dried at 75 °C–80 °C, and were screened through a 1-mm nylon mesh to remove sand, stones, and other particulate matter. Then, the samples were digested by mixed acid. The mixing acid composition is: HNO_3/$HClO_4$/HF, with a volume ratio of 2:1:1. 0.1g sediment samples were added to 5 mL of mixed acid. The samples were placed in a special Teflon-lined cup digestion tank. The digestion tank was placed in a 180°C oven for 12 h.

Studies of redox conditions on the heavy metals distribution followed specific experimental steps: mix the collected sediment samples with water, with a ratio of 1/4 (V/V), 2 h of high-temperature (121 °C) heat sterilization, and then the experiment was divided into aerobic and anaerobic stages. High-purity oxygen and nitrogen were used to adjust the dissolved oxygen concentration in the reactor. The concentration of dissolved oxygen in the aerobic phase was controlled at 7–8 mg/L. After 23 days, the dissolved oxygen concentration decreased to less than 0.5 mg/L using pure nitrogen. The anaerobic phase was maintained for 92 days.

At the end of the anaerobic or aerobic phase, the sediment samples were taken from the reactors and dried at 75 °C–80 °C. Within a certain time interval in the anaerobic or aerobic phase, a certain volume of overlying water was collected from the reactor. Then, the samples were immediately filtered through a 0.45μm filter. The heavy metals in sediment samples and the contents of all speciations were measured by ICP-MS (Finnigan MAT Company ELEMENT).

3.2 Results and Discussion

The concentration of chromium in the overlying water decreased from 12.36 g/L to 5.35 g/L by the 17th day under aerobic sterilization conditions. The concentrations of cadmium and lead decreased from the initial values of 3.72 μg/L and 20.54 μg/L to 0.06 μg/L and 0.39 μg/L at the end of the aerobic process, respectively. Copper also showed a similar variation trend (as shown in Fig. 12). The results show that the migration of Cr, Cu and Cd are significantly reduced. The concentrations of Co,

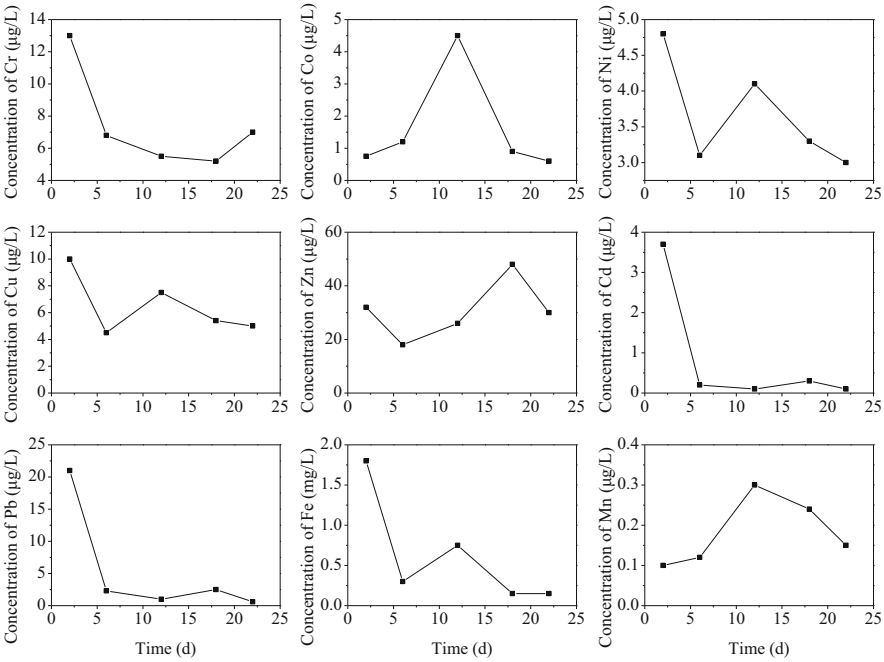

Fig. 12 Concentrations of heavy metals in overlying water during the aerobic incubation

Zn and Mn showed similar variation trends. The concentration of chromium in overlying water increased from the initial value of 4.64 g/L to 8.57 g/L after 20 days in the anaerobic process (Fig. 13). With longer anaerobic time, Pb and Cd in the overlying water showed a similar trend, increasing from 0 g/L to 5.33 g/L and 0.38 g/L rapidly, respectively. Under anaerobic conditions, the mobility of Cr, Cd and Pb in sediment could be enhanced. In the post-anaerobic period, the concentrations of Pb, Cd and Fe in overlying water increased rapidly and completely changed to be different from the aerobic phase. Fe and Mn oxides act as high valence electron acceptors, and the transformation processes were involved in the reduction of pollutants. Pb is easily absorbed by oxides. The relationships among the linear rules between the overlying water Cd and Pb contents (y, μg/L) with the Fe content (x, mg/L) were: $y = 2.3672\text{x} + 0.4976$ ($R^2 = 0.8669$) and $y = 3.43\text{x}$—0.6416 ($R^2 = 0.9906$), respectively.

Heavy metals in sediment at the sediment–water interface which experienced peak fluxes may have the following formula: $f(x)_t=(x_t\text{-}x_0)\times V/A$.

Under different environmental conditions, according to Eq. (1), in conjunction with Figs. 12 and 13, heavy metals that have a significant release phenomenon in the sediment–water interface in the investigated objects were observed. The release fluxes calculation of heavy metals in the sediment–water interface under different environmental conditions is as follows:

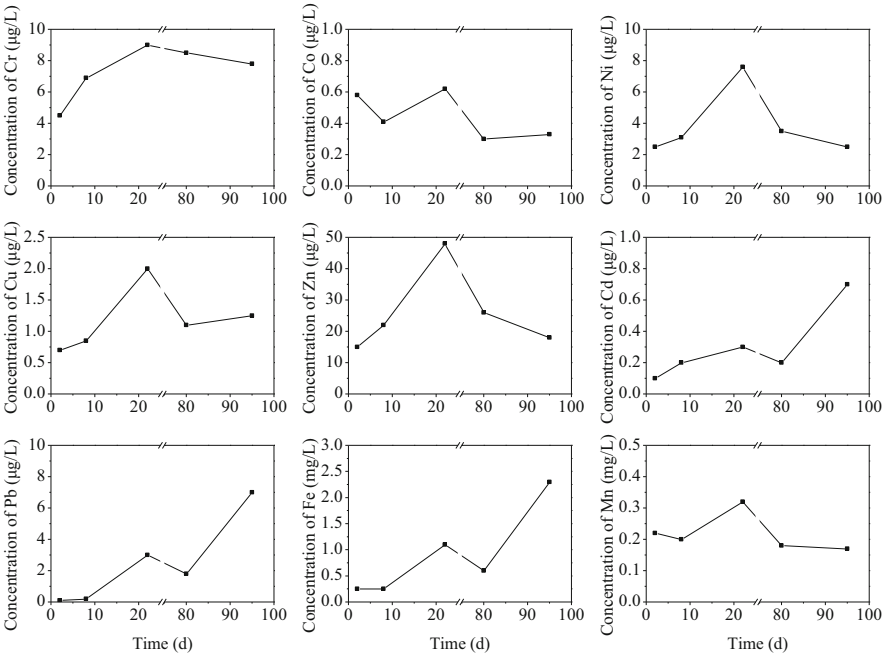

Fig. 13 Concentrations of heavy metals in overlying water during the anaerobic incubation

Table 5 Fluxes of the heavy metals between the sediment and water interface during different redox conditions (ng/cm^2)

Conditions	Co	Zn	Mn	Fe	Cr	Ni	Cu	Pb	Cd
Aerobic conditions	13.38	55.61	247	–	–	–	–	–	–
Anaerobic conditions	–	–	–	738.08	16.87	18.41	4.39	25.70	2.74

As can be seen from Table 5, under aerobic conditions, the concentrations of Co, Zn, and Mn reached their maximum values on the 15th day in the overlying water. Under anaerobic conditions, Pb, Cd and Fe reached the maximum in overlying water at the end of the anaerobic stage. The release of other heavy metals reached a peak on the 20th day under anaerobic conditions. Fe and Mn fluxes were much larger than the other heavy metals. The maximum flux of zinc was 55.61 ng/cm^2. The maximum flux of cadmium reached 2.74 ng/cm^2.

The impacts of redox conditions on the distribution of heavy metals in sediment were investigated. Various speciations (F1, F2, and F3) were examined by BCR sequential extraction procedure methods. During the aerobic process, the proportion of the F1 dropped from 22.85 % to 15.21 %. F1/T of cadmium increased up to

17.39 % under anaerobic conditions because the mobility was strengthened under anaerobic conditions. The conclusion was consistent with the variation of cadmium concentration in the overlying water (Fig. 12). F1/T of cadmium significantly reduced under aerobic conditions because the binding capacity between cadmium and organic matter in the sediment was much weaker than that of other heavy metals (such as Cu and Zn, etc.). Therefore, F1/T of cadmium in sediment can be observed more significantly under non-sterile conditions than that in sterile experimental conditions. Soluble, exchangeable F1-bound cadmium was more easily released to the overlying water than that of reducible (F2) and oxidizable (F3) cadmium. Therefore, the impact of cadmium in sediment on water quality was higher than that for other heavy metals under the particular geochemical conditions.

A similar phenomenon also occurred for lead in sediment. The most significant speciation was F2. During the aerobic process, F2/T of lead in sediment dropped from 36.42 % to 30.04 %. However, F2/T of lead increased up to 33.70 % after the anaerobic process. Under aerobic conditions, the concentration of lead in the overlying water decline rapidly (Fig. 13). The result indicated that the release of lead was significantly enhanced under anaerobic conditions (Fig. 13). The maximum flux of lead was up to 25.70 ng/cm^2. The concentrations of lead in the overlying water were consistent with the variation of F2/T in sediment. The F2/T of lead changed when the aerobic conditions became anaerobic conditions, which can explain why the reducible F2 migration was accelerated in the sediment–water interface.

Besides residual chromium, chromium mainly existed in organic and sulfide phase (F3) speciations. Variations of chromium F3/T are similar to F2/T of lead and F1/T of cadmium. F3/T of chromium decreased under aerobic conditions. However, F3/T of chromium increased under anaerobic conditions. Various speciations of F1, F2, and F3 have potential environmental effects on the water quality, so the variations of F3/T in sediment under different environmental conditions showed corresponding mobility of chromium and environmental effects. The concentration of chromium in overlying water verified the above conclusions (Fig. 13).

The potential environment affects various speciations of Cr, Cd, and Pb, of which the concentrations decrease under aerobic conditions, which is not in accordance with other studies. It was explained by the complexity of physical and chemical conditions, as well as biogenic and non-biogenic components in different reservoir sediment samples. For Co, Ni, Cu, and Zn, the trends and characteristics of the [(F1+F2+F3)/T] values are similar to the F1/T values of Cd, F3/T values of Cr, and F2/T values of Pb under aerobic or anaerobic conditions, respectively. However, the effects of redox conditions on the distribution of various speciations were not obvious (Fig. 14). The concentrations of Co, Ni, Cu and Zn in the overlying water were much lower than that of Cd, Cr and Pb under different environmental conditions.

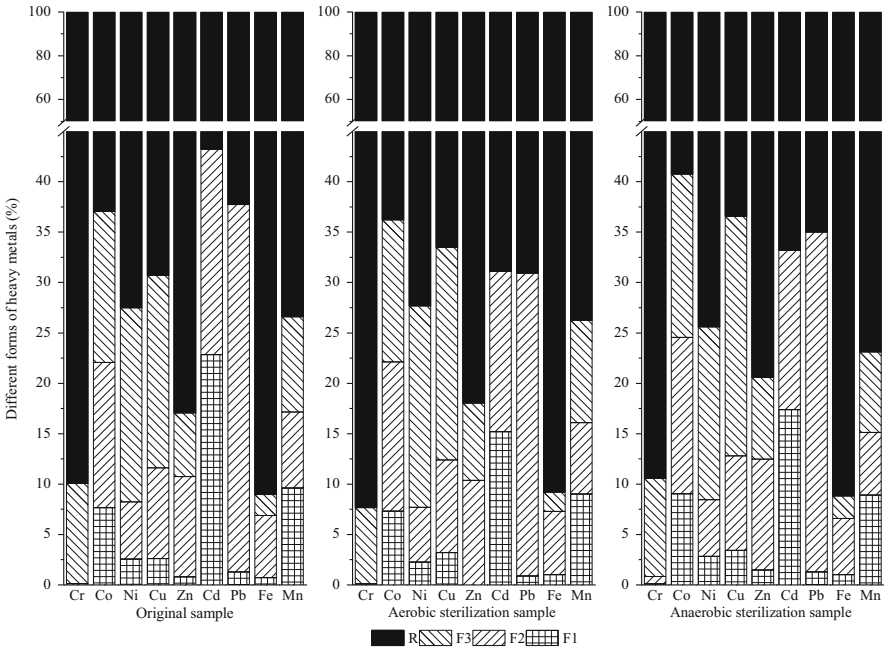

Fig. 14 The percentage of the heavy metals under different redox conditions

4 Algal Blooms and Odor

4.1 Algal Bloom and Its Impact on Water Quality

4.1.1 Algae Species

Algae in botany is listed as algae, and has developed into an independent discipline, simply called algae.

Algae have common features, although there are natural algae groups. Algae can be defined by the fact that the majority of algae have chlorophyll. They live in a planktonic way. Algae are autotrophic microorganisms that are capable of photosynthesis, releasing oxygen to absorb inorganic elements in water into their own organisms. Their body size is generally 2–200 μm, and regular individuals or groups are observed to be a little green by microscope. Algae are a kind of plant with no real roots, stems, or leaves. They are a compost of unicellular and multicellular groups. The shapes of algae are filamentous, branched fronds, and so on. Only a few have similar tissue differentiation in roots, stems, and leaves. The colors and shapes of algae are quite different in the different types. Its simple structure is considered to be the minimum plant. Single cells can reproduce spores or zygotes [6]. They are important organic producers in water. Therefore, algae play an important role in maintaining water balance in the ecosystem, as they are

primary producers in the metabolism and energy cycle and because the community structure of algae and their growth amount are directly influenced by the water ecological environment change [7].

All algae except cyanobacteria are eukaryotes. Eukaryotic algae have chloroplasts, including chlorophyll a, b, c, d, β-carotene, and lutein. Algae are photosynthetic autotrophs and can undergo reproduction through photosynthesis. Algae growth requires sunlight. The growth pH range is from 4 to 10, while the optimum pH is 6–8. The majority of algae are warm, and some algae can thrive in hot springs at temperatures of 85 °C. Some are able to grow in ice. The optimum growth conditions for algae are as follows: water containing 0.2–0.3 mg/L nitrogen and 0.05–0.1 mg/L of phosphate, water temperature 12–20 °C, and water turbidity less than 50–80 NTU. Therefore, in lakes, reservoirs, and rivers, in which water flows slowly, and under certain conditions, algal blooms will occur. Of course, this will induce many new problems, when as such water bodies are used as the water source. Therefore, the effect of algae on water quality was further explored in order to take effective measures to ensure safe drinking water.

Algae are widely distributed in rivers and lakes, ponds, ditches, alkali salt lakes, moist soil, leaves, bark, walls, and even snow surfaces. Algae have a very close relationship with human life and the living environment. There are about 2100 species of algae in total, and more than 27,000 kinds. According to their cell structure and reproductive and genital construction, algae can be divided into different phylum. Hu et al. summarized the classification system of algae, which is shown in Table 6 [6].

Table 6 Classification system of algae

R. E. Lee grading system (1999)	C. Van Den Hoek grading system (1995)	L. E. Graham grading system (2000)
1. *Cyanophyta*	1. *Cyanophyta=Cyanobacteria*	1. *Cyanobacteria (Chloroxybacteria) (Prochlorophytes)*
2. *Prochlorophyta*	2. *Prochlorophyta=Chloroxybacteria*	2. *Glaucophyta*
3. *Glaucophyta*	3. *Glaucophyta*	3. *Euglenophyta*
4. *Rhodophyta*	4. *Rhodophyta*	4. *Cryptophyta*
5. *Chlorophyta*	5. *Heterokontophyta*	5. *Haptophyta*
6. *Euglenophyta*	6. *Haptophyta*	6. *Dinophyta*
7. *Dinophyta*	7. *Cryptophyta*	7. *Ochrophyta*
8. *Cryptophyta*	8. *Dinophyta*	8. *Rhodophyta*
9. *Chrysophyta*	9. *Euglenophyta*	9. *Chlorophyta*
10. Prymnesiophyta	10. *Chlorarachniophyta*	
11. *Bacillariophyta*	11. *Chlorophyta*	
12. *Xanthophyta*		
13. *Eustigmatophyta*		
14. *Raphidophyta*		
15. *Phaeophyta*		

Most floating algae are unicellular planktonic species. They are physiologically similar to the plant cell, just smaller in size and suspended in a liquid medium. There are different dominant algae genera in different types of nutrient conditions. Algae in oceans are mainly diatoms. The cyanobacteria microcystis and diatom in freshwater are generally recognized as typical representatives of eutrophic lakes.

There are many types of algae plants, which can be summarized as the following types:

1. Types with foot (amoeba type): Include the golden algae, algae, and armor, a few species of green algae. The protoplast extends pseudopodia and is movable without cell walls.
2. Flagella type (floating type): They have cells with cell walls, periplasmic, or capsule shells. They can perform active movement. They can be divided into single cell type flagella and flagellar type groups. They include dinoflagellates, hidden algae, euglena, and the majority of golden algae.
3. Glue group type (groups indefinite type): They cannot move. They belong to nutrition reproduction. After cell division, they are buried in a common plastic inner, and can continue to grow. They have no definite number of cells.
4. Spherical cell type (non-floating type): They have vegetative cells of non-flagellated form. They can be a single cell or a certain number of cells linked to groups of various shapes. This is prevalent in planktonic algae.
5. Filamentous body: They can form multicellular plant cells through division in cross-section. Except for euglena, other algae also belong to this type. They can be divided into unbranched filamentous and branching filamentous types.

4.1.2 Algal bloom and Its Harm

Water body eutrophication leads to algal blooms in lakes and reservoirs. Algal blooms of lakes and reservoirs often show the following features ([8]):

1. Algal blooms in water. The most prominent manifestations of eutrophication are large numbers of algae. In general, there are millions or more fronds per liter of eutrophic water. Algal blooms affect the ecosystem structure of the water body but also cause difficulties in the operation and management of water purification plant waterworks, which cannot guarantee the quantity and quality and even lead to the end of water production in severe conditions.
2. Abnormal odor. More than ten species have been identified as being produced by odorous eutrophic water. Algae are the main odorous material produced. These algae can emit stench smells around the lake, which gives a feeling of discomfort, and can impact and annoy people's normal lives directly.
3. Release toxic substances into the water body. Algae, especially *cyanobacteria*, can release a variety of algal toxins to the water during their metabolic process of dying. Algal toxins are strong toxicological, which could threaten the lake, reservoir water environment and even the entire ecosystem. For example, *cyanophyta* indefinite cavities *pluvialis* (*co-closp haeriumd ubium*),

M. aeruginosa (Mcrocy tisaeruginosa), blooms of anabaena (a nabaena f losaquae) can release algal toxins, liver toxins, neurotoxins and other toxic substances. In addition, hydrogen sulfide, methane, ammonia and other toxic gases can be produced in eutrophic water during hypoxia.

4. Seriously overabundance of nutrients. Organic pollution, total nitrogen, total phosphorus, and dissolved phosphorus (DP) are found at high concentrations in eutrophication water, which also shows low transparency and deterioration of water quality.
5. Lake and reservoir water ecosystems degrade sharply. Biome characteristics in lakes reflect the ecological conditions and nutritional status of water bodies. The species and structure of aquatic organisms head towards reverse succession with the degradation of aquatic ecosystems in lakes and reservoirs. The number of species of non-tolerance reduce or even disappear. The biological indicators can quickly and accurately determine the degree of eutrophication of lakes and reservoirs.

4.2 Microcystins in Water

Microcystis blooms are the most pontential and serious category for water pollution. If the bloom is severe, the lake will become thick indigo blue-green, and the balance of aquatic ecosystems will be destroyed. The formation of algal blooms, especially *cyanobacteria*, will cause a releasing of a variety of algal toxins after the rupture of cell, such as *microcystins genus* (*Microcystis*), *Anabaena* (*Anabaena*), *Oscillatoria genus* (*Oscillatoria*), *Nostoc genus* (*Nostoc*), *Aphanizomenon* (*Aphanizomenon*) and partly *cruentum genus* (*Nodularia*). Algal bloom frequency and amplitude are also increasing with the intensification of eutrophication. Toxic algal blooms and biosecurity threat have drawn increasingly widespread attention.

Studies confirm that algal toxins have potential inhibition of important human regulatory enzymes (protein phosphatase 1 and 2A), which can lead humans, livestock, and wildlife to acute and chronic poisoning and even death. In addition, a strong lure promotes a cancer of the liver effect. Microcystin LR (MCLR) is known to be a cyanobacterial toxin of the most toxic and largest acute hazard in fresh water. Many countries have established a drinking water standard MCLR limit according to the World Health Organization recommendations (WHO 2004): the maximum allowable amount is 1.0 μg/L. Conventional drinking water treatment technology cannot effectively remove algal toxins because microcystin is toxic and widely distributed, with a stable chemical structure [9]. Therefore, algal toxins pose a serious threat to drinking water. Microcystin contamination of water bodies has become a global environmental problem that has increasingly drawn people's attention [10]. Eutrophication and algal toxins increasing pollution has been getting worse. How to effectively control algae toxin pollution has become a problem in the field of water supply.

Currently, the studies of algal toxins have mostly been conducted on microcystin and focused on the situation of microcystin contamination, chemical structure, physical, and chemical properties. The mechanism of toxic effects, separation and analysis methods, water treatment process removal methods, and other aspects have also been investigated.

4.2.1 Status of Algal Toxin Contamination

Cyanobacteria is widely distributed around the world, from the polar ice cold lakes to hot springs above 70 °C. The algae may exist almost anywhere in the world where there is light and water. In many countries or regions, algal toxins can be detected in natural waters. For example, in the Rivers of Berlin, the microcystin concentration was between 0.14 and 119 ng/L [11]; in the French Grand-Lieu Lake, the highest microcystin concentration is 5.06 ng/g dry weight of pure algae in September [12]. In Belgian natural waters, bioassays showed 870 ng of microcystin per gram of dry weight algae [13]. In Thailand, in reservoirs and ponds, per gram of dry weight water containing microcystin were 0.7–0.8 mg in blooms [14]. In South Korea's lakes, per gram of dry weight water contained 20–1500 ng of algal toxins in blooms (Park 1998). Taiwan's reservoirs and lakes in blooms contained 0.11–10.06 μg of microcystin per gram of dry weight water.

In China, in the 1960s, there was already a cyanobacteria bloom appearing in Taihu. In the early 1980s, more than half of the lake areas among 34 surveyed Chinese lakes showed eutrophication [15]. Since the 1990s, the national freshwater eutrophication of water bodies became more serious. 60 % of natural freshwater lakes have different degrees of eutrophication (Zhang 2001), and the scope is also expanding. Besides Yunnan Dianchi Lake, Jiangsu Taihu and Anhui Chaohu have experienced serious pollution of cyanobacteria blooms. The Yangtze and the Yellow River's many lakes and reservoirs have also undergone varying degrees of algal blooms, and algal toxin has been detected ([16–18]). For example, in the Dianchi Lake area, cyanobacterial blooms microcystin (MC) was controlled at a concentration of 0.8 μg/L from May 2000 to April 2001. In October 2000 in Jiangxi Poyang Lake, the average concentration of microcystin was 0.89 μg/L. In July 2001, 2.7–14.2 μg/L of MC was detected in the raw water of four waterworks in Wuxi City. The MCLR concentrations of six samples in Dianshan Lake were in the range 0.044–0.136 μg/L during June to October of 2002. In September 2003 in Guanting, the algae toxin concentration extracted was up to 3.13 mg per gram of dry weight of river. These lakes and reservoirs are important sources of drinking water. The release of algal toxins after algae die and the slow degradation in natural water bodies cause hidden dangers to human health. To some extent, the problem of microcystin pollution has become a global water quality problem.

4.2.2 Algal Toxin Types, Structures, and Properties

There are many different types of algal toxins, including liver toxins, neurotoxins, and lipopolysaccharide endotoxins. Liver toxins are divided into microcystins and nodularins, which are the most toxic. At present, the most common pollution is microcystin algae toxin (also known MCYST, called MC). MC is the secondary metabolite of certain species or strains of cyanobacteria generated by monocyclic heptapeptide hepatotoxins. MC is of large molecular weight (800–1100). The basic structure is ring (D-alanine -LX-red-β-methyl isobutyl-D--LY-ADDA-D-aspartate glutamate-*N*-methyl isobutyl dehydroalanine), as shown in Fig. 15 ([19]; Rinehart 1994).

ADDA (3-amino-9-methoxy-2, 6, 8-trimethyl-10-phenylmethyl-4, 6-dienoic acid) shown in Fig. 15 is an expression of the biological activity of algal toxin essential groups. The ADDA amino acid's conjugated dimensional structure will affect its toxicity and methylation of other amino acids, which can produce different isomers. More than 70 kinds of microcystins have been found (Law 2003). The most common and with greatest toxicity are MCLR, MCRR, MCYR, L, R, and Y, which represent bright histidine, arginine, and tyrosine.

Since a cyclic structure and double bonds interval are present, MC is very stable in water [20], non-volatile, resistant to pH change, and easily dissolved in water. The solubility of MC in water can be 1000 mg/L or more. MC cannot be easily be adsorbed on the particle suspended solids or sediments. MC is not hydrolyzed in several common enzymes, such as pepsin, chymotrypsin, and insulin, and remained stable for longer periods (27 days) in deionized water. MC has a good thermal stability, as it is still not destroyed when heated to 300 °C. Dried MC can be preserved for several years at room temperature. The molecular structure of MC

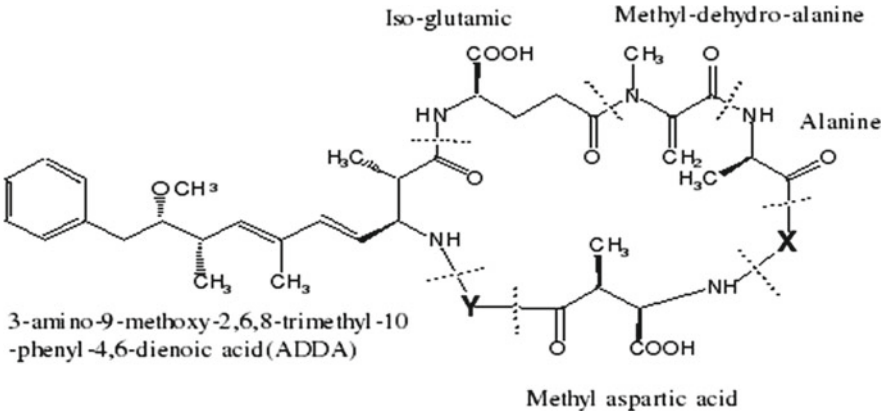

Microcystin-LR：X= Leu（L），Y= Arg（R）
Microcystin-RR：X= Arg（R），Y= Arg（R）
Microcystin-YR：X= Tyr（Y），Y= Arg（R）

Fig. 15 The structural formula of microcystin

contains carboxyl, amino, and amido. Therefore, MC has different ionization tendencies at different pHs [21].

For example, the charge of MCLR is positive monovalent at pH <2.09, the net charge is zero at 2.09<pH<2.19, the net charge is negative monovalent at 2.19<pH<12.48, and the net charge is negative bivalent at pH>12.48.

Therefore, the bioaccumulation effects of MC are small under high pH (>8) conditions of water bloom (Maagd 1999). Meanwhile, the MC molecule ADDA groups are β, γ double bond, and susceptible to oxidation and biodegradation in the presence of light ([22]; Ones 1994; Tsuji 1993; [23]).

4.2.3 Production Mechanism of Algal Toxins

The reason for algae producing MC and the control factor for this is one of the most important focuses of research. Though it is still not certain why cyanobacteria produce toxins, the physiological role of algal toxins is mainly evolution and self-protection, which seems to have become a consensus. There are two main viewpoints about the MC mechanism [24]. First, environmental factors affect or alter the toxicity. The other is genetically determined, which is why microcystins were divided into strains and strain-free.

There are many environmental factors that affect microcystin synthesis. They are mainly light, temperature, pH, and nutrients. Although temperature and light both have effects on the toxin, the influence of temperature is greater than the others. Van der Westhuizen found that *M. aeruginosa* UV-006 strains of toxicity were different at different temperatures. The contents of three kinds of toxins are also different. Temperature does not change the structure of toxin, but can change the concentration of the toxin. The temperature at high light intensity has little effect on the production of toxins [25], while at low light intensity, the temperature can affect the production of toxins. Thus, in Utkilen and Gjolme's view, light is an important factor limiting toxins, or even the only factor. To find out which factor plays a dominant role, there is no consensus. And in nutrients, different types of nutrients have different effects. The impact of nitrogen and carbon is not significant, but the effect of phosphorus is obvious. Trace elements including Al, Cd, Cr, Cu, Mn, Ni, and Sn have no effect on producing toxin, while the effects of Fe and Zn are very obvious [26]. These environmental factors primarily control the production of toxins by acting on the rate of cell division rather than being a direct effect of metabolic pathway that the toxin produced. There is a linear correlation between the rate of cell division and the toxin production rate.

Those who back toxin genes determinism believe that microcystis with strains (Toxic Strains) and without strains (Nontoxic Strains) have different genes [27]. Toxicity is determined by gene, and the differences between microcystis with strains (Toxic Strains) and without strains (Nontoxic Strains) depends on whether there exists an enzyme genome which is synthesized by one or several encoding toxins [28]. Microcystin synthesis may be affected by the peptide synthetase, which is adjusted by genes directly and can be adjusted by genes indirectly.

Environmental factors affect the toxin synthesis by affecting the activity of the enzyme [29]. DNA fragments Mcy producing microcystin have been isolated from the chromosome of a microcystin. It is found that those algae species which can produce microcystins algae all contain the Mcy gene. Microcystin synthesis is controlled by them, and it is a catalytic synthesis of the peptide synthesis enzyme complex body, but algae that do not produce microcystin, some of which also contain the Mcy gene [30], show that the change of environmental factors can regulate and control gene expression.

Genetic determinism or environmental determinism are not individually isolated; in fact, they are interrelated and interacting. Although genetic factors have important and direct roles in physiological control for toxic algae toxin, environmental factors can directly affect gene expression under specific conditions, thus indirectly controlling toxigenic characteristics. Under certain environmental conditions, toxic algal strains can produce mutations in toxigenic algae. Toxigenic strains of algae under certain environmental conditions may not produce poison.

4.2.4 Transformation of Algal Toxins in the Water

Typically, microcystis produces and exists within the cyanobacterial cells. Only after algal cell aging, death, or rupture will algal toxins be released into the water.

For pure cultures of microcystis, substantial laws of its toxicity change is in the logarithmic growth phase. MC is mainly present in the cells, increasing in concentration, in the late logarithmic growth phase. Among MCRR, MCYR, and MCLR, the increase in the amount of MCRR is the largest when it reaches maximum growth; the total toxin levels continue to increase. However, the occurrence of redistribution makes a large number of MC cells appear in the environment. After entering the stable period, both intracellular and extracellular toxins begin to decline. Most of the MC is released into the aquatic environments when freshwater algae reach the highest level and dissolution occurs. At that moment, the amount of microcystin in the solids (including algae and other microorganisms) and the amount of microcystin in water are in an opposite directions relationship [20].

Another experimental study showed that the water solubility of microcystin is only 10 % to 20 % of the total in the cyanobacteria logarithmic growth period. It was quickly dissolved without algicidal agents or other conditions. The concentration of microcystin in most water is 0.1–10 μg/L. The cell toxin is much higher ([31]; Lawton 1998).

Zhang et al. studied the fate of algal toxin in natural waters. It was found that light degradation is the main way to reduce the concentration of alga toxic in natural waters. However, microbial degradation, bioaccumulation, and adsorption of particulate matter are also the causes of algae toxin maintaining a low concentration [32]. Cyanobacterial toxins within the cells in sunlight can change the side-chain double bonds isomer ADDA, while the toxicity is significantly reduced. The half-life is about l0 days, but the pure microcystin in sunlight is stable. The existence of

soluble cytochrome humus and other photosensitizers in water can increase the rate of photolysis [33].

The biodegradation of MC is also the main transformation pathway. MC chemical properties are stable, and not easily broken by eukaryotes and bacteria peptidase. However, MC molecules ADDA groups have unsaturated double bonds, which can be degraded by some special bacteria in natural waters [22]. Jin et al added Dianchi Lake sediment into MC extract, which completely disappeared after 5–7 days (Jin 2002). Cousins et al found that natural waters can generate the most degrading MCLR in a week. MC can remain stable over 27 days in deionized water, while in natural sterilized water, the period of stability is 12 days [34]. The study shows that MC can be released into the water gradually, and be degraded under the action of light and microorganisms. However, this process is slow, and usually lasts a few days to several weeks.

The algal toxin that is produced by cyanobacteria cells is released into natural water bodies because of the large amount of dilution in water bodies and the effect of light and microbial degradation. It is generally maintained at a lower concentration in natural waters. However, a substantial rise of microcystin happened in water after algal blooming, thereby threatening the safety of drinking water.

4.2.5 Harm of Algal Toxins

The current findings suggest that the target organ of microcystin is the liver [35]. MC can affect two cell types of the liver, namely liver hepatocytes and macrophages, cells with high selectivity and great biological activity.

MC can strongly inhibit the activity of protein phosphatases after it enters the liver cells. In addition, an increase in the protein kinase activity resulted in excessive intracellular phosphorylation of many proteins in cells to break the balance of intracellular protein phosphorylation/dephosphorylation. Such biochemical effects are further amplified through the cell signaling system to change in a variety of enzyme activities. It also resulted in a series of physiological disorders of intracellular biochemical reactions to cause liver damage to the cytoskeleton, leading to liver hemorrhage and necrosis, and, finally, leading to death.

Microcystin can harm the liver macrophages and induce the generation of interleukin-1 (IL-1). IL-1 induced acute inflammation in further substances, such as prostaglandins, thromboxane, and tumor necrosis factor (TNF-δ). These substances led to liver damage and necrosis [36]. In addition, MC is a potential tumor-promoting agent, which can affect the epigenetic process by intercellular communication and signal transduction-induced tumors [37].

Animals, through direct contact or via drinking water containing the MC, will suffer from diarrhea, vomiting, fatigue, shortness of breath, loss of appetite, mouth or eye discharge, and other symptoms, and even experiencing liver enlargement and pathological lesions, bleeding, or necrosis, and dying due to respiratory obstruction [38–40]. The water containing toxins can cause skin and eye irritation and headaches, dizziness, nausea, vomiting, and other symptoms.

In recent years, many countries and regions of the world observed that MC contamination events can cause livestock poisoning. For example, some soldiers from England showed flu-like symptoms, and some soldiers were indicators of elevated liver enzymes in 1991 after training in cyanobacteria-contaminated water due to the presence of microcystins in water [41]. In February 1996 in Brazil, 126 people show symptoms of acute or subacute liver poisoning, of which 60 died of liver failure when microcystin-contaminated water was used as kidney dialysis [42,43]. In China, there are examples of 100,000 cases of primary liver cancer deaths each year. A high incidence of primary liver cancer in the Haimen, Qidong, and Fusui regions is related to local residents' long-term drinking of water containing trace amounts of microcystin in shallow ponds and rivers. An epidemiological survey found that the incidence of primary liver cancer was positively correlated with the algal toxin levels in drinking water ([44]; Ueno 1996). Studies have shown that algal toxins can promote tumors, and chronic toxic effects of algal toxins pose a serious threat to human health.

4.3 Algal Growth and Reproduction Characteristics in Shibianyu Reservoir

From November 2012 to November 2013, the algal cell density and chlorophyll-a concentration of Shibianyu Reservoir were continuously monitored.

4.3.1 The Annual Variation of Algal Cells Number in Shibianyu Reservoir

As shown in Fig. 16, the algae density in April reached the first peak during the stratification formation period. Algal growth reached the second peak during the stable stratification period in September, as shown in Figs. 16, 17 and 18.

As shown in Fig. 16, the growth peak of algae occurred during the stratification period and the stable stratification period. The algal cell density was less than 3×10^6 cells/L in the stratified reservoir formation period in March. Algal blooms occur after April with the gradual increase of temperature. The cell density gradually increased due to the propagation characteristics of the diatom. Algae mainly grow in the depth range of 2–5 m. The highest cell density increased up to 17.63×10^6 cells/L in the stratification formation period (April 14th), as shown in Fig. 6. The dominant species was diatoms. The algal cell density decreases rapidly, affected by rain in mid-May. The minimum density was 1.6×10^6 cells/L. The density of algae also gradually increased with increasing light intensity and temperature. In July, the number of algae was maintained at 17×10^6 cells/L. The algal density increased rapidly from the beginning of August. The highest density of algae was 39×10^6 cells/L in August, and in the second peak of algae density, the

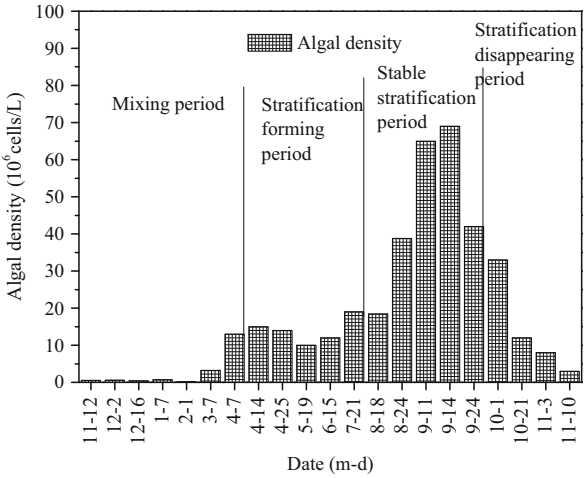

Fig. 16 Algae density changes throughout the year in Shibianyu Reservoir

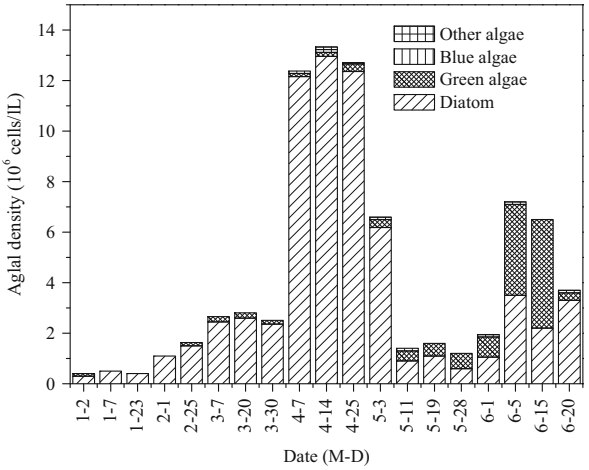

Fig. 17 Dominant species change from January to June in Shibianyu Reservoir

algal cell density reached 69×10^6 cells/L in the stable stratification period on September 14th. There was a serious "bloom" phenomenon, as shown in Fig. 18. The dominant species was green cyanobacteria. The weak light intensity and temperature decreased due to the continuous rains in September, so the algal growth was restricted. The algal density decreased gradually. The number of algae decreased rapidly because of the rain due to the dilution effect. The water temperature was not suitable for the growth of algae after the mixing period, so the algal cell density decreased. The maximum value was 1.53×10^6 cells/L, and the main advantage of algae species was diatom, which maintained at a low level.

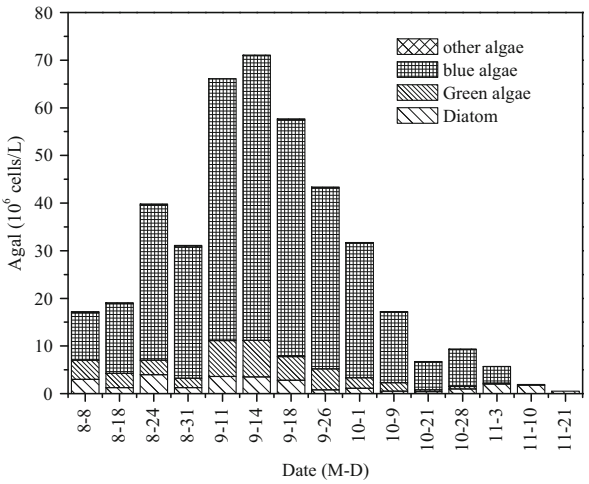

Fig. 18 Dominant species change from July to November in Shibianyu Reservoir

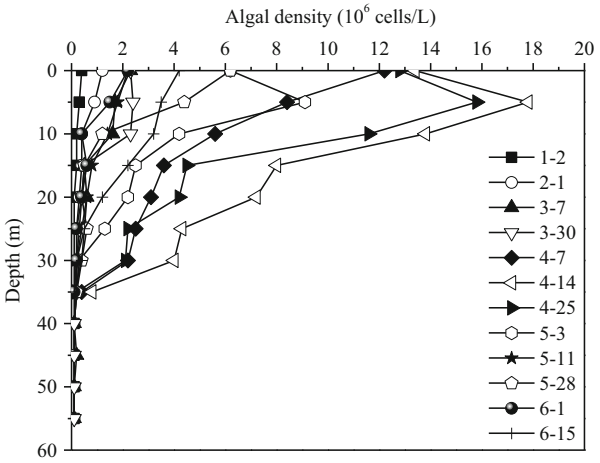

Fig. 19 Vertical variation of algae density

4.3.2 The Vertical Variation of Algal Density in Shibianyu Reservoir

Different cell densities and chlorophyll-a were monitored, as shown in Figs. 19 and 20.

Chlorophyll-a is an important component of algae cells, which can reflect the number of algae and water quality to some extent by measurement of the chlorophyll-a concentration. The chlorophyll-a concentration is closely related to the amount of algae in water.

As can be seen in Figs. 19 and 20, the diatom growth was mainly between 2 m to 5 m. In the stratification formation period (April 14th), the algae density reached a maximum value (17.6×10^6 cells/L) at a depth of 3 m, while the highest

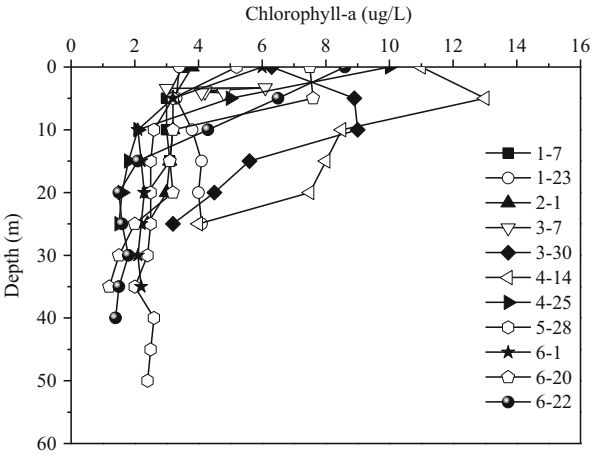

Fig. 20 Vertical variation of chlorophyll-a of diatom

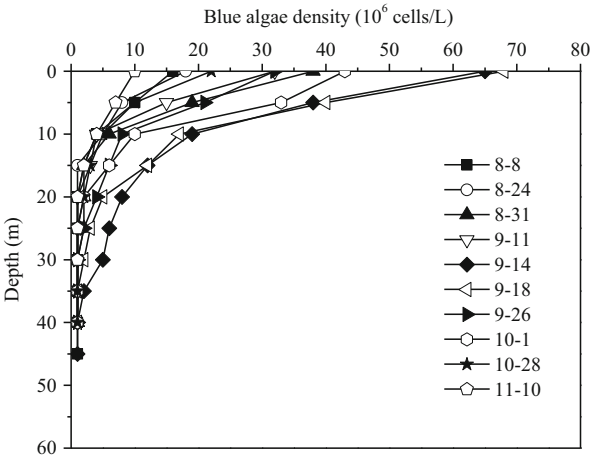

Fig. 21 Vertical variation of algae density in the blooming period

chlorophyll-a concentration reached 12.84 μg/L. The dominant species were diatoms, as the water temperature was 13.7 °C. The algae density was no more than 10×10^6 cells/L with the increase of algal density and decrease of water depth, especially below 15 m. The concentration of chlorophyll-a was less than 7 μg/L, and it declined quickly, especially at the bottom of the water body, and the maximum cell density was no less than 1×10^6 cells/L. The concentration of chlorophyll-a was 2 μg/L.

In the stable stratification period, the cell density increased as the temperature gradually increased. Green cyanobacteria began blooming, as shown in Figs. 21 and 22.

The TN concentration was up to 2.84 mg/L and the TP concentration reached 0.04 mg/L because the light intensity and water temperature gradually increased,

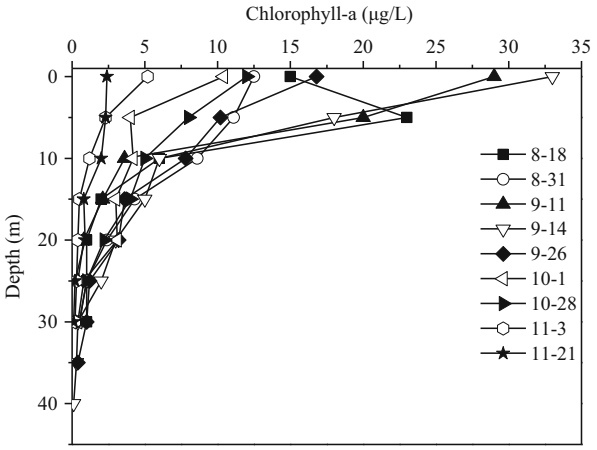

Fig. 22 Vertical variation of chlorophyll-a during the blooming period

and also because of the greater amount of nutrients of Shibianyu Reservoir in the stable stratification stage. The cell density was about 17×10^6 cells/L and chlorophyll-a was 19 μg/L in the stable stratification of the surface water. The algal cell density in the surface water reached 38×10^6 cells/L in August and the value of chlorophyll-a was 23.4 μg/L. The second peak of algae density in September reached 69.28×10^6 cells/L. Algae mainly ranged from the surface water to a depth of 2 m. The concentration of chlorophyll-a was 33.56 μg/L. It can also explain that the density of algal cells can be largely reflected by the concentration of chlorophyll-a. The algal density increased with decreasing depth; especially under depths of 20 m, the algal density remained at a very low level.

The algal density was influenced by light intensity and temperature [45–48]. However, greater light intensity does not mean more vigorous growth of algae. Greater cell density and algal growth requires appropriate water temperature and light conditions. The algal density can be very intuitive to showing how many algae there are in water and the bloom intensity. During the eutrophic water bloom, the algae density continuously increased when severe water blooms are observed. The algal density of phytoplankton is more than 20×10^6 cells/L when algae are blooming. It can be seen that there is a serious "bloom" phenomenon in Shibianyu Reservoir [49–51]. The number of algal cells decreased significantly after water entered the mixing period due to the decrease of light intensity and water temperature.

References

1. Micić V, Kruge MA, Hofmann T (2013) Variations of common riverine contaminants in reservoir sediments. Sci Total Environ 458–460:90–100
2. Ma HB, Song JM, Yuan HM (2003) Nitrogen forms and their functions in recycling of the Bohai Sea sediments. Geochimica 32(1):48–54 (in Chinese)

3. Lauren SC, Maria GP, William MB, Amy TS, James MM (2012) Nitrogen cycling within suboxic and anoxic sediments from the continental margin of Western North America. Mar Chem 128–129:12–254.
4. Pavanelli D, Selli L (2013) Effective size characteristics of suspended sediment and nutrient concentrations during flood events in the reno river tributaries. Pro environ sci 19: 723-732
5. Ruttenberg KC (1992) Development of a sediment extraction method for different forms of phosphorus in marine sediments[J]. Limnol Oceanoger 37(2): 1460-1482
6. Huang TL, Yan S, Chai BB, Liu H (2011) Phosphorus forms and its distribution in source water reservoir sediment. J Tianjin University 44(7):607–612 (in Chinese)
7. Huang TL, Chai BB, Qiu ES, Zhu WH (2010) Microbial effects on phosphorus release from sediments on the multi-phase interface of water-sediment-biofacies. J Basic Sci Eng 18 (1):61–70 (in Chinese)
8. Hu HJ, Wei YX (2006) Chinese freshwater algae—systems, classification and ecology. Science Press, Beijing (in Chinese)
9. Kangkang (2007) Proliferation of algae and TN/TP Correlation. Chongqing: Urban Construction and Environmental Engineering, Chongqing University
10. Peng JJ, Li CH, Huang XH (2004) City eutrophication causes and characteristics. Ecol Sci 23 (4):370–373
11. Chow CWK, Drikas M, House J, Burch MD, Velzeboer RMA (1999) The impact of conventional water treatment processes on cells of the cyanobacterium *Microcystis aeruginosa*. Water Res 33(15):3253–3262
12. Haider S, Naithani V, Viswanathan PN, Kakkar P (2003) Cyanobacterial toxins: a growing environmental concern. Chemosphere 52(1):1–21
13. Fromme H (2000) Occurrence of cyanobacterial toxins~microcystins and anatoxina in Berlin water bodies with implications to human health and regulations. Environ Toxicol 15 (2):120–130
14. Vezie C (1998) Variation of microcystin content of cyanobacterial blooms and isolated strains in Lake Grand-Lieu. Microb Ecol 35(2):126–135
15. Wirsing B (1998) First report on the identification of microcystin in a water bloom collected in Belgium. Syst Appl Microbiol 21(1):23–27
16. Mahakhjant A (1998) Detection of microcystins from cyanobacterial water blooms in Thailand fresh water. Physiol Res 46:25–29
17. Park HD, Iwami C, Watanabe MF, Harada K, Okino T, Hayashi H (1998) Temporal Variabilities of the concentrations of Intra-and extracellular microcystin and toxic microcystis species in a hypertrophic lake, lake Suwa, Japan[J]. Environ. Toxic. water quality, 13(1): 61-72
18. Shen JG (2001) Contamination of microcystin toxicity mechanisms and detection methods. Prevent Med Inform 17(1):10–11.
19. Zhang WH, Xu XQ, Qiu CQ (2001) Advance in study on microcystins in aquatic environment. Res. Environ. Sci. 14(2): 57-62 (in Chinese)
20. Chen Y, Zhang YS, Lin YD (2002) Taihu Lake Basin Water microcystin content survey. China Public Health 18(12):1455–1456 (in Chinese)
21. Mu LN, Chen CW, Yu SZ, Liu JL, Wu YY, Zhu WC (2000) Taihu Lake water content of microcystin survey research and treatment methods. China Public Health 16(19):803–804 (in Chinese)
22. Xu HB, Sun M, Sui HX (2003) Dynamics of fish in the Jiangxi Poyang Microcystin Contamination. Health Res 32(3):192–197 (in Chinese)
23. Sivonen K (1996) Cyanobacterial toxins and toxin production. Phycologia 35(1):12–24.
24. Rinehart KL (1994) Structure and biosynthesis of toxins from blue-green algae(cyanobacteria) [J]. Appl. Physiol, 76(6): 1759-1762
25. Law LA, Robertson PKJ, Cornish BJPA (2003) Processes influencing surface interaction and photocatalytic destruction of microcystins on titanium dioxide photocatalysts[J]. Catal, 213 (1): 109-113

26. Watanabe MF, Tsuji K (1992) Release of heptapeptide toxin (Microcystin) during the decomposition process of Microcystis aeruginosa. Nat Toxins 1:48–53
27. Rivasseau C, Martins S, Hennion MC (1998) Determination of some physiochemical parameters of microcystins (cyanobacterial toxins) and trace level analysis in environmental samples using liquid chromatography. J Chromatogr 799(1–2):155–169
28. De Maagd PGJ, Hendriks AJ, Seinen W, Sijm DTHM (1999) pH-dependent hydrophobicity of the cyanobacteria toxin microcystin-LR[J]. Wat. Res., 33(3): 677-680
29. Tsuji K, Watanuki T, Kondo F, Watanabe MF, Nakazawa H, Suzuki M, Uchida H, Harada KI (1997) Stability of microcystins from cyanobacteria. 4. Effect of chlorination on decomposition. Toxicon 35(7):1033–1041
30. Ones GJ, Orr PT (1994) Release and degradation of microcystin following algaecide treatment of a microcystis aeruginosa bloom in a recreational lake. As determined by HPLC and protein phosphatase inhibition assay[J]. Wat. Res., 28(4): 871-876
31. Tsuji K, Naito S (1993) Stability of microcystins from cyanobacteria: effect of light on decomposition and isomerization[J]. Environ. Sci. technol., 28(1): 173-177
32. Kaya K, Sano T (1998) A photodetoxification mechanism of the cyanobacterial hepatotoxin microcystin-LR by ultraviolet irradiation. Chem Res Toxicol 11(3):159–163
33. Chen YP (2005) Efficacy and mechanism of Fenton role in the removal of microcystins. Fuzhou University Graduate Thesis 1: 6
34. Utkilen H, Gjolme N (1998) Energy the dominating controlling factor for microcystin production in Microcystis aeruginosa. Compilation of abstracts. 4th International Conference on Toxic Cyanobacteria 63
35. Min L, Ying L, Shunzhang Y (2001) Effects of nitrogen, phosphorus, iron, zinc on microcystis aeruginosa growth and toxin production. Shanghai Environ Sci 20(4):166–170
36. Borner T (1998) Microcystins synthetase: gene and enzyme. 4th International Conference on Toxic Cyanobacteria 58
37. Meipner K, Kittmann E, Borner T (1996) Toxic and non-toxic strains of the cyanobacterium *Microcystis aeruginosa* contain sequences homologous to peptide synthetase genes. FEMS Microbiol Lett 135:295–303
38. Zhu GC, Wu LX (2005) Microcystins in drinking water limits and biological pretreatment control. Water Suppl Drain 31(2):17–20
39. Nishizawa T, Asayama M, Fujii K, Harada K, Shirai M (1999) Genetic analysis of the peptide synthetase genes for a cyclic heptapeptide microcystin in Microcystis spp. Eur J Biochem 126 (3):520–529
40. Lahti K, Rapala J, Fardig M, Niemela M, Sivonen K (1997) Persistence of cyanobacterial hepatotoxin, microcystin-LR in particulate material and dissolved in lake water. Water Res 31 (5):1005–1012
41. Zhang WH, Song LR, Xu XQ, Liu YD, Zhang XH (2004) A preliminary study of microcystin toxin fate in natural waters. Resour Environ Yangtze River Basin 13(1):84–88 (in Chinese)
42. Feitz AJ, Waite TD, Jones GJ, Boyden BH, Orr PT (1999) Photocatalytic degradation of the blue green algal toxin Microcystin-LR in a natural organic aqueous matrix. Environ Sci Technol 33(2):243–249
43. Jin LN, Zhang WH, Zheng L, Xu XQ (2002) Biodegradation of microcystin in dianchi lake aquatic environment. China Environ. Sci., 22(2): 189-192 (in Chinese)
44. Cousins IT, Bealing DJ, James HA, Sutton A (1996) Biodegradation of microcystin-LR by indigenous mixed bacterial populations. Water Res 30(2):481–485
45. Miura GA (1991) Hepatotoxicity of microcystin-LR in fed and fasted rates. Toxicon 29 (3):337–346
46. Harada K (1996) Trace analysis of microcystins. Phycologia 35(Suppl 6):36–41
47. Humpage AR, Falconer IR (1999) Microcystin-LR and liver tumor promotion: effects on cytokinesis, ploidy, and apoptosis in cultured hepatocytes. Environ Toxicol 14:61–75

48. Boudrez A, Evens K, Beullens M, Wealkens E, Stalmans W, Bollen M (1999) Identification of MYPT1 and NIPP1 as subunits of protein phosphatase 1 in rat liver cytosol. FEBS Lett 455:175–178
49. Guzman RE, Solter PF (1999) Hepatic oxidative stress following prolonged sublethal Microcystin-LR exposure. Toxicological Pathology 27:582–588
50. Vasconcelos VM, Pereira E (2001) Cyanobacteria diversity and toxicity in a wastewater treatment plant (Portugal). Water Research 35:1354–1357
51. Lawton LA, Codd GA (1991) Cyanobacterial (blue-green algae) toxins and their significance in U.K. and European waters. J Institut Water Environ Manag 5:460–465
52. Hirooka EY, Pinotti MHP, Tsutsumi T, Yoshida F, Ueno Y (1999) Survey of microcystins in water between 1995 and 1996 in Parana, Brazil using ELISA. Nat Toxins 7(3):103–109
53. Jochimsen EM, Carmichael WW, An JS, Cardo DM, Cookson ST, Holmes CEM, Antunes MBD, de Melo DA, Lyra TM, Barreto VST, Azevedo SMFO, Jarvis WR (1998) Liver failure and death after exposure to microcystins at a hemodialysis center in Brazil. N Engl J Med 338:873–878
54. Yu SZ (1995) Primary prevention of hepatocellular carcinoma. J Gastroenterol Hepatol 10:674–682
55. Ueno Y, Nagata S, Tsutsumi T (1996) Detection of microcystins, a blue-green algal hepatotoxins, in drinking water sampled in Haimen and Fusui, endemic areas of primary liver cancer in china, by highly sensitive immunoassay[J]. Carcinogenesis 17: 1317-1321
56. Donatella P, Lavinia S (2013) Effective size characteristics of suspended sediment and nutrient concentrations during flood events in the Reno River tributaries (Northern Italy). Procedia Environ Sci 19:723–732
57. Feng TG, Wan XN (2006) Eutrophic lakes and repair technology of harm. Soil Water Conserv 13(2):145–147
58. Hao ZW, Xu XQ (2001) Determined by HPLC with solid phase extraction of trace microcystin. Anal Chem 29(5):522–525
59. Jin XQ, Chen WM (2005) Microcystin in Taihu Lake and its relationship with plankton. China Environ Sci 25(1):28–31
60. Otsuka S, Suda S, Li RH, Watanabe M, Oyaizu H, Matsumoto S, Watanabe MM (1999) Phylogenetic relationship between toxic and non-toxic strains of genus Microcystis based on 16S to 23S internal transcribed spacer sequence. FEMS Microbiol Lett 172:15–21
61. Wu W, Qu JH, Chen JZ, Hu GD, Li H (2002) Toxicological effects on fish liver. China Environ Sci 22(1):67–70 (in Chinese)
62. Zhao I, Wang X, Xie Q, Cheng K, Li YY, Wu HY, Zhao J, Gan XS (1999) Dopant “blooms” microcapsules filled isolation and identification of toxins. Central China Normal University (Natural Science) 33(2):250–254 (in Chinese)

Part III
The Mixing-Oxygenating Technology In Situ Controlling the Reservoir Water Quality

Methods of Reservoir Water Pollution Control and Water Quality Improvement

Tinglin Huang, Xuan Li, Ya Cheng, and Xinxin Shi

Abstract In this chapter, the common technical methods, including physical, chemical, and ecological control techniques, for improving the water quality of lakes and reservoirs are briefly introduced. The physical control technologies mainly include the mixing–oxygenating technology, dilution and scour, sediment dredging, and coverage. The chemical control technologies mainly include phosphorus precipitation and passivation, restoration of acidified lakes or reservoirs, and sediment oxidation. The ecological control technologies mainly include bioremediation, phytoremediation, and biomanipulation remediation. By analyzing and comparing the tested data, for water sources such as reservoirs, the mixing–oxygenating technology is more suitable for decreasing endogenous pollution and controlling eutrophication.

Keywords Pollution control • Physical control • Chemical control • Ecological control

1 The Physical Controlling Techniques

1.1 The Mixing–Oxygenating Technology

1.1.1 Surface Aeration System

Surface aeration occurs by means of disturbing the surface layer of water bodies and increasing contact between air and water in order to dissolve the oxygen in the air into the water. A common surface aerator is shown in Fig. 1.

A top-down approach is used by mechanical axial flow pumps to set up a circulation pattern. A floatation platform and a frame are used to support an electric motor, gearbox and drive shaft, and large propeller (1.8–4.6 m diameter), by which water of the surface layer in the lakes or reservoirs is pushed downwards and a circulation pattern is created, preventing thermal stratification. Surface spray units

T. Huang (✉) • X. Li • Y. Cheng • X. Shi
School of Environmental and Municipal Engineering, Xi'an University of Architecture and Technology, Yanta Road 13, 710055 Xi'an, Shaanxi Province, P. R. China
e-mail: huangtinglin@xauat.edu.cn

T. Huang (ed.), *Water Pollution and Water Quality Control of Selected Chinese Reservoir Basins*, The Handbook of Environmental Chemistry 38,
DOI 10.1007/978-3-319-20391-1_8

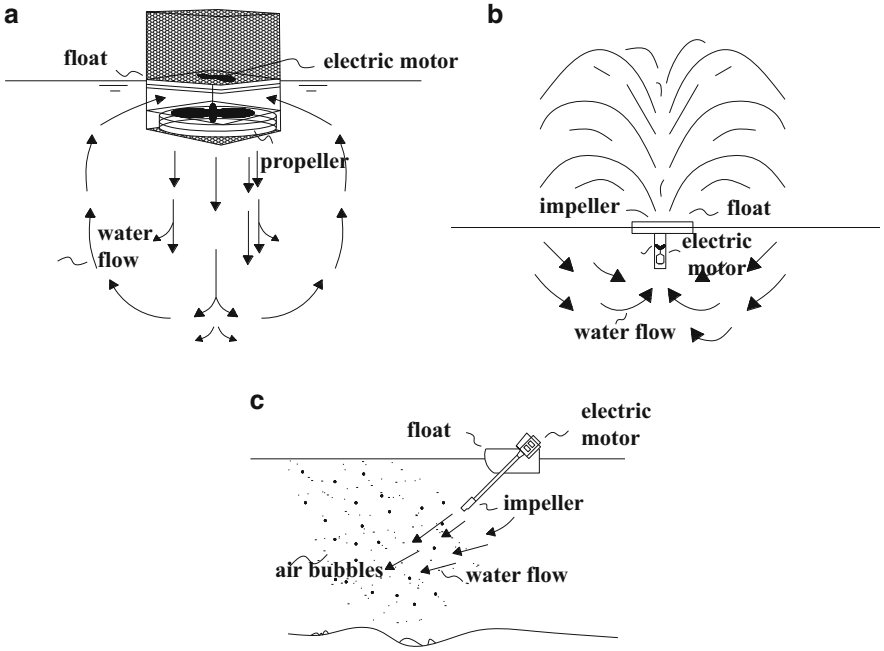

Fig. 1 Diagram of mechanical axial flow pumps (**a**), surface spray (**b**), and impeller-aspirator systems (**c**)

use a float to support an electric motor-driven impeller. The rapidly spinning impeller pulls water up a vertical tube and throws it out in an umbrella or fountain shape above the lake or reservoir surface. Atmospheric reaeration occurs during this process. Impeller-aspirator systems consist of an electric motor-driven impeller at the bottom of a hollow shaft extending at an angle down into the water. The air is propelled by the rotating impeller.

Surface aeration technology has a better effect for shallow lakes or reservoirs, but for deep reservoirs, the water cycling mainly occurs in the upper and middle layers. Thus, a surface aeration system is normally used for controlling cyanobacterial blooms, which commonly occur in the upper layer of water bodies.

1.1.2 Hypolimnetic System

A hypolimnetic system introduces oxygen into the water at the bottom of the lake or reservoir, while keeping the natural stratification in order to preserve the habitat for the fauna living in the cold waters at the bottom of the lake or reservoir [1] and avoid the possible production of evil-smelling gases by incomplete oxidation of organic matter, which could have a strongly negative impact on the recreational use of the lake or reservoir. In such conditions, optimal management of the hypolimnetic system faces two contrasting requirements which need to be properly

balanced. The first requirement is to provide an adequately oxygen supply, which is possible only through large water discharge volumes by the jets. The second requirement is to limit the rate of deep water mixing, which is responsible for the alteration of thermal stratification. The supply of oxygen to the hypolimnion is relatively slow because of the small surface area available in the aeration apparatus across which the oxygen transfer is made. For water bodies with large hypolimnia or large surface areas, several factors must be considered.

The size of hypolimnetic aerators is largely dependent on the following factors: consumption rates, the requirement of dissolved oxygen, volume of deep water, time, and so on. The oxygen supply rate should not be less than the oxygen consumption rate. The oxygen consumption rate can be obtained by measuring the decrease of dissolved oxygen of the deep water and can be calculated as:

$$O_2 = \frac{DO_{t_1} - DO_{t_2}}{t_2 - t_1} h. \tag{1}$$

In this equation, O_2 represents the consumption rate of oxygen, g/(m^2·d); t_1 and t_2 are the starting and ending times of monitoring, respectively, d; DO_{t1} represents the dissolved oxygen concentration at the beginning of water column stratification; DO_{t2} represents the concentration of dissolved oxygen before dropping to 1 mg/L at a certain time, mg/L; and h represents the average depth of deep water, m. Moreover, the air requirements can be calculated according to the following formula:

$$Q = \frac{O_2 A_h \times 10^{-3}}{1.205 m Y_A}. \tag{2}$$

In this equation, Q represents the air requirement, m^3/d; A_h represents the area of the deep layer; Y_A represents the percentage of oxygen in the air; m is the oxygen utilization efficiency; 1.205 is the air density, kg/m^3; and 10^{-3} is the conversion factor, g/kg.

Hypolimnetic aerators can be further classified into two basic groups: full lift and partial lift. Full lift system transfer water from the hypolimnion to the surface, and then back to the hypolimnion. This system tends to be less prone to causing nitrogen supersaturation in the hypolimnion than the partial lift system (Fig. 2).

1.1.3 Destratification Systems

Destratification is a type of artificial circulation that completely mixes stratified water in a lake or reservoir from top to bottom in order to eliminate or prevent summer stratification [2]. It is possible to provide the required oxygen in situ by artificially mixing the lake or water bodies. It has been shown that the primary mechanism of oxygen transfer is at the water surface, even if compressed air is used as the mixing medium. Riddick summarized the device as: “an aerator should be

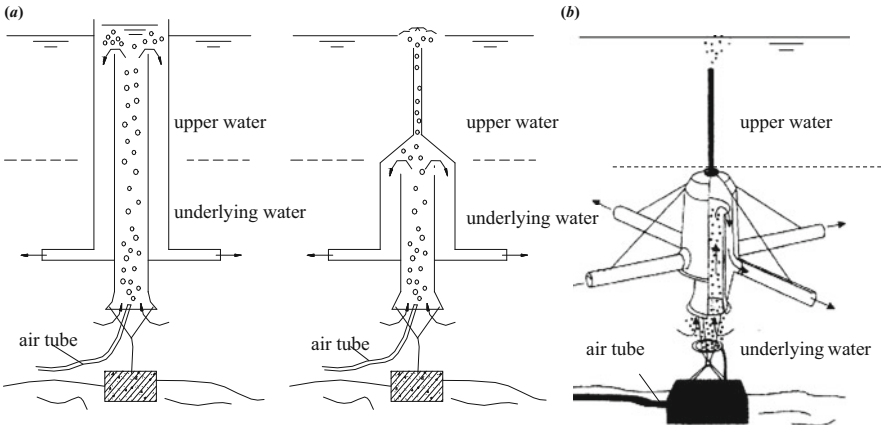

Fig. 2 Schematic diagram of a deep water aeration device of the air ascension type: full lift system (**a**), partial lift system (**b**)

regarded as a cheap, uncomplicated and relatively efficient device for pumping water". There are mainly two techniques: air diffuser and hydraulic gun.

1. Air diffuser systems
   There are two purposes of air mixing: the first is that it can mix the water of upper and lower layers, and the second is to destroy the water column and supply oxygen. The air mixture is transmitted via compressed air into the water, and the oxygen will be released in the form of small bubbles. The rising bubbles would bring the lower water to the surface, and then surface waters would be forced to migrate down. It can promote water mixing and increase the concentration of the dissolved oxygen. At the same time, the contact between bubbles and water can oxygenate the water body directly. The air mixing device is shown in Fig. 3.

   Besides destroying the stratification, raising the water dissolved oxygen content, and improving the water quality of the anaerobic problems, mixing–oxygenating can control the eutrophication. Most of the algae need for photosynthesis to make them stay on the surface for light. Their floating growth mechanism ensures their floatation and more gather as a result of surface brightness. The liquidity of reservoirs is small, which results in the algae steadily staying on the surface of the water, receiving sufficient light and multiplying rapidly. Air mixing can make algae migrate to the lower water body without light, which inhibits their growth and makes them die. To achieve this purpose, two conditions must be satisfied: the mixing intensity should be large enough to resist the algae's floatation speed, and the water depth should be large enough so that the algae have plenty of time to stay in deep waters. Otherwise, the activate algae will circulate to the surface, which is not only unable to control algae, but also promotes algae breeding, because the nutrients originally located at the bottom are brought up to the surface water.

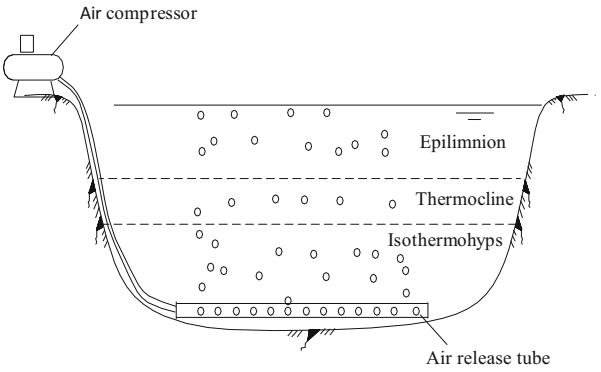

Fig. 3 Schematic diagram of a mixing–oxygenating filling device

2. Hydraulic gun systems
   A hydraulic gun is a device that can mix water and promote circulation. It's structure is shown in Fig. 4.

   A hydraulic gun consists of a straight cylinder, gas chamber, float, and anchor pier. It is installed in the water vertically. Its key component is the air chamber, which consists of an inverted U glyph water seal device. The compressor transfers the compressed air into the gas chamber continuously. When the air inside the air chamber builds up under the water seal chamber and finally breaks the water seal, it would squirt inside the tube and combine into a large gas flare, which is then accelerated in the cylinder, forming piston flow, and causes the water to rise in the cylinder. The cylinder continuously inhales water, which is transferred to the surface. The lifting water mixing causes increasing temperature, decreasing density, and diffusion around all horizontal directions. Water can be drawn into the bottom layer and up to the surface as great a distance as 1–2 km.

   Pumping mixing intermittently launches large gas bombs to push the rising water. Its mixing efficiency is lower than the free rising water in a small bubble. But a hydraulic gun should be designed and arranged appropriately, otherwise the mixing effect will be too small. For example, if the gas bomb of the hydraulic gun is big, but the contact area with water is small, then hydraulic gun itself will not be able to perform the function of filling oxygen.

   A hydraulic gun's effect on water quality improvement is shown as below:

- Controlling the eutrophication. Circulate the upper algae to the lower and restrain the photosynthesis of algae.
- Raising the water-dissolved oxygen and resolving the anaerobic problems [3].

1.2 Dilution and Scour

Dilution and scour are two common techniques for controlling the water quality. The purpose of dilution is to reduce the pollutant concentration by introducing a

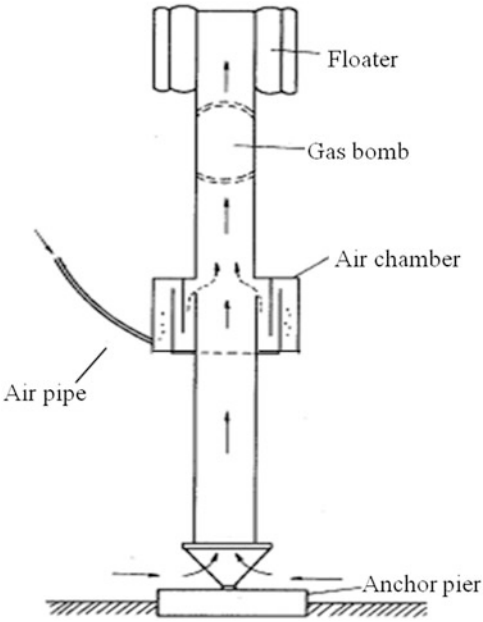

Fig. 4 The structure of hydraulic gun systems

part of water with a low concentration of pollutants and discharge water with a high concentration of pollutants. The purpose of scour is to eliminate water biomass and displace the water. In Nanjing Xuanwu Lake, West Lake of Hang Zhou, and Dian Lake in Kunming Lake of China, they all adopt outflow water diversion to dilution and scour. This technology can effectively reduce the concentration of pollutants and the load and concentration of algae. On the other hand, dilution and scour can also affect the deposition rate of pollutants to sediment. During the process of high-speed dilution or flushing, the deposition proportion of pollutants to the sediment will decrease. But if the dilution rate is inadequate, the concentration of pollutant may increase instead. The design and calculation of dilution and wash is according to the following model.

1. Completely mixed model
   Small lakes and reservoirs can be calculated by the completely mixed model. To disregard the influence of sediment deposition and release, the empirical formula of the retention coefficient for washing is:

$$R = \frac{1}{1 + \sqrt{\rho}}. \tag{3}$$

   In this equation, ρ is the water exchange or flushing rate. a^{-1} is equal to the ratio of the introduced water flow to the water volume of lakes or reservoirs.

After the start of scour, the pollutants concentration in the lake or reservoir decreases gradually, which is a transient process. Based on the material balance equation, the pollutant concentration can be calculated as follows:

$$C_t = C_{\text{in}} + (C_0 - C_{\text{in}})e^{-\rho t}. \tag{4}$$

In this equation, C_t is the pollutants concentration in the lake or reservoir at time t after scouring, C_{in} is the influent concentration, and C_0 is the initial concentration.

If the time for dilution and scour is too long, after reaching steady-state conditions, the equilibrium concentrations of pollutant can be calculated as below:

$$C = \frac{L}{H\rho}(1 - R) = \frac{L}{H\left(\rho + \sqrt{\rho}\right)}. \tag{5}$$

In this equation, L is the area load of pollutant, which is equal to the ratio of the total amount of introduced pollutant in unit time to its area, and H is the average depth.

The actual dilution process is more complex. Some factors such as the direction of flow, the wind, and the shape of lakes or reservoirs will affect the dilution effect. Dilution can also produce some additional effects, such as the growth of cyanobacteria.

2. Plug flow model

The dilution of rivers can be described by the plug flow model. We assume that the original flow of the river is Q_0, the introduced flow is Q_{in}, and C_{in} is the pollutant concentration. The hypothesis is that a stream of water mix, precipitation, and degradation has not happened or its effect can be neglected. Before and after mixing, the mass conservation equation is:

$$(Q_{\text{in}} + Q_0)C = Q_{\text{in}}C_{\text{in}} + Q_0C_0. \tag{6}$$

In the above equation, C is the mixed pollutants concentration.

If the highest permitted concentration of pollutant in the river is C_{p}, the required flow of clean water to flush the polluted river is Q_{in}. When calculating clean water carried on sewage, the flux of the river is Q_0:

$$Q_{\text{in}} = \frac{(Q_{\text{in}} + Q_0)C_{\text{p}} - Q_0C_0}{C_{\text{in}}} \text{ or } Q_0 = \frac{(Q_{\text{in}} + Q_0)C_{\text{p}} - Q_{\text{in}}C_{\text{in}}}{C_0}. \tag{7}$$

1.3 Sediment Dredging and Coverage

1.3.1 Sediment Dredging

Sediment dredging is an effective technology to restore water quality. A large number of pollutants accumulate in the sediment, including nutrients, hard-decomposed deleterious organic compounds, heavy metal ions, etc. [4]. For example, in the Dian Lake sediment, the amount of accumulated nitrogen and phosphorus are 7.8 times and 15.6 times higher than that of exogenous input, respectively [5]. Under certain conditions, these harmful pollutants are released into the water and affect the ecology in the water or accumulate in organisms through the food chain. Sediment dredging is an important aspect of the control of water pollutants.

1. Survey on sediment dredging
   Investigation of sediment distribution and thickness, including calculating the volume of sediment dredging and grasping the property of sediment, is essential preparatory work of sediment dredging. For lakes and reservoirs of small areas of less than 40 ha, a sampling interval measuring 15 m is appropriate, and for larger lakes and reservoirs, the sampling point interval can be set to 30 m. The mud sample measurement can be used with the diameter of the dial is 0.9–1.6 cm steel drill detection layer depth and thickness of sediment. When silt sediment is composed of a high organic matter content and low density, the measurements in the bottom of floating mud can be used a 200-KHz sounder. Water depth measurement is carried out during periods of peace. When the water depth is less than 10 m, the water depth measurement error and the pollution soil sampling depth error is not more than 10cm.
2. The sediment dredging technique selection
   Generally, there are two methods of dredging. One is dredging after the water is drained, and then bulldozers, scrapers, and hydraulic dredges are used to scoop the mud. This method can only be applied to small lakes and reservoirs that allow temporary water blackout. The second is dredging with water, which includes mechanical dredging and hydraulic dredging.
3. The treatment of water in mud
   The volume of mud pumped from the bottom of reservoirs or lakes is several times larger than that of sediment. The mud precipitates in the yard and a large amount of water drains outside, which contains a lot of pollutants released from the sediment. Whether the water needs to be treated and how depends on the composition of pollutants in the residual water, the quality and function of the receiving water, and economic analysis. The yard residual water treatment process should be simple, cost-effective, and suitable for high-flow residual water treatment.
4. The disposal of dredged mud
   The dredged mud contains a variety of harmful pollutants; thus, it cannot be directly piled up and needs to be treated in order to prevent the spread of pollutants. The mud utilization should obey the rules as below: the combination

of mud treatment and application development, concentrated use and scattered utilization, and short-term interests and long-term benefit [6].

1.3.2 Sediment Covering

There are two functions for sediment covering. One of the functions is to prevent the release of sediment contaminants, such as nitrogen, phosphorus, organic matter, iron, and manganese. The other is to control the overgrowth of aquatic plants. The release of pollutants from the sediment includes two processes: firstly, the pollutants diffuse to the surface of solid particle and dissolve into the pore water. Secondly, the concentrated pollutants diffuse into the water body from the pore water. In some cases, the diffusion process restricts the release of sediment. Furthermore, activities of fish or benthic fauna and water waves caused by disturbances will accelerate the migration of contaminants to the water body. Increase overlay can effectively impede the activities of benthic fauna in the sediment surface, prevent disturbance on the muddy water, greatly decrease the spread of the migration effect, and then prevent the release of sediment contaminants.

2 The Chemical Control Technology

2.1 Phosphorus Precipitation and Passivation

2.1.1 The Principle of Phosphorus Precipitation and Passivation

The precipitation and passivation technologies can be used in sediment with a high concentration of phosphorus. Chemical precipitation is a method that easily adds hydrolysis inorganic salts to the water in order to remove phosphorus by precipitation. Passivation is the method that adds excess hydrolysis inorganic salts to the water body and lets their hydrolysis product form a thin layer and covers with the sediment surface to block and adsorb the phosphorus released from the sediment. At present, due to the stability under anaerobic conditions and the high efficiency of capture of inorganic granular phosphorus, aluminum sulfate is mainly used to precipitate and passivate the phosphorus in sediment. Furthermore, aluminum sulfate has no toxic threat to life in the water in the general dosage range. The effect of the precipitation technique is fast, but this management has a limited shelf life. Thus, it is generally recommended for use as a temporary measure.

2.1.2 The Implementation Methods of Phosphorus Precipitation and Passivation

There are two ways to determine the dosage of aluminum salt. For the first method, with the purpose of removing the phosphorus in water through precipitation, the dosage can be calculated by experimental results in the lab. When implemented, the dosage should be gradually increased until the removal of phosphorus meets the requirements. For the first method, with the purpose of adsorbing phosphorus released from sediment, the dosage should match the amount of released phosphorus from sediment, so as to achieve long-term control of endogenous phosphorus. This requires analyzing and determining the amount of phosphorus released from a certain thickness of sediment. The dosage can be determined through theoretical calculations or experiments. Considering the safety of creatures in water, the drugs need to be dosed in the deep water region and avoid contact with creatures in shallow water. The determination of the optimal dosage involves the change of hydrogen ion concentration (pH), the carbonate alkalinity, and the toxicological effects of aluminum ions. The concentration of dissolved aluminum ion will rise rapidly if the pH value is below 5.5.

Therefore, it was suggested to maintain the concentration of dissolved aluminum ions at 550 μg/L or less because studies have shown that there are no significant short-term and long-term toxicological effects for fish at this concentration. However, there are virtually no detailed studies about the toxicological effects of aluminum ions on water ecology or a detailed study on chronic toxicology and biological accumulation. The biggest drawback of this technique is that it is dramatically affected by the pH value. For example, in the acid rain or acid deposition region, acidic water may cause the pH value to drop dramatically, resulting in a precipitation state where aluminum becomes dissolved aluminum ions, and precipitated phosphorus may be dissolved again or suspended in the water, which increases the rich nutrition phenomenon.

2.2 Remediation of Acidified Lakes or Reservoirs

The acidification of lakes or reservoirs is mainly caused by acid rain. Therefore, the fundamental approach is to reduce the emissions of SO_2 and NO_x so as to reduce the amount of acid rain. When the pH value of the water is below 5.6, carbon dioxide in the water will reach an equilibrium with its vapor in the air, and the water is considered to be in the acidified state. The pH value of some acidified lakes or reservoirs can even reach 4.0–4.5. The acidification of water results in the disappearance of acid-sensitive species, the loss of biodiversity, and makes the mass circulation slow down. After acidification, the organic matter cannot be decomposed, and pollutants begin to accumulate. Moreover, acidification often

results in the decrease of the number of fish, and even the extinction of some species.

Adding lime is a convenient way to quickly repair acidified lakes and reservoirs. It has been successfully applied in the United States, Canada, Europe, and other countries, and has been widely recognized as a successful method. Lime material comprises powder limestone ($CaCO_3$), quick lime (CaO), slaked lime [$Ca(OH)_2$], and so on. The dissolution rate of $CaCO_3$ is slow, so it will not cause a sharp change in the pH. The addition of lime can adjust the pH of water, improve fish growth conditions, and make some of the acid-sensitive species recover in the relative short term. However, within a few years, it is difficult to return to the state of the species composition before acidification. This method has some effects on lakes or reservoirs with long hydraulic retention time, and the cost is very high. However, the long-term effectiveness is hard to estimate. Moreover, groundwater was used to regulate the pH of acidified lakes or reservoirs in Wisconsin [7], because groundwater normally has higher hardness and alkalinity. The advantage of this method is that the cost is relatively low and the water is easy to supply to maintain the lakes or reservoirs in a certain pH range.

2.3 The Oxidation of Sediment

Sediment oxidation is a method that can remove the organic matter, nitrogen, and phosphorus by injecting an oxidizer into the sediment. The depth of oxidation is up to 10–20 cm [8]. Common oxidants for sediment include calcium nitrate [$Ca(NO_3)_2$], ferric chloride ($FeCl_3$), and lime [$Ca(OH)_2$]. Calcium nitrate is used as an electron acceptor, which is used to remove nitrogen and is easier to penetrate into the inner layer of sediment than oxygen. Ferric chloride can react with hydrogen sulfide to form more ferric hydroxide, and then improve the efficiency of phosphorus passivation. Lime can raise the pH value to maintain a level appropriate for microbial denitrification [9].

Sediment oxidation can also be seen as a substitute technique of passivation treatment by aluminum salt. The difference between the two techniques is that the passivation treatment is only applied to the surface of the sediment, and the sediment-oxidizing reagent is injected into inner layer of sediment. Water organisms are seldom affected by the oxidation of sediment, which has more long-term effects. However, sediment oxidation can only control the endogenous release of phosphorus caused by the anaerobic sediment reduction, and it has no effect on the release of phosphorus caused by pH and temperature.

3 Ecological Control Technology

3.1 Bioremediation

Microorganisms have a strong power to degrade organic pollutants. It has been known that there are hundreds of thousands of environmental pollutants, most of which are organic compounds. Microorganisms are able to reduce the toxicity of pollutants or make them completely harmless by decomposition and transformation [10]. There are two main modes of microbial degradation: the first is microbial degradation by the secretion of extracellular enzymes; the second is degradation by intracellular enzymes after the pollutants have been absorbed into the microbial cells. The bioremediation for sediment polluted by heavy metals is the focus of this part.

1. The transformation of heavy metals by bioremediation
   Mercury, lead, tin, selenium, arsenic, and other metal or metalloid ions lose toxicity under microbial metabolism. There are several paths for the transformation of heavy metals, including methylation, reduction, and oxidation, as shown in Table 1.

3.2 Phytoremediation

1. The mechanism of the removal of organic pollutants by phytoremediation
   Plants have great removal effects against hydrophobic organic matter, such as benzene, toluene, ethylbenzene, and xylene. Moreover, some plant enzymes can

Table 1 The transformation of heavy metals by microorganisms

Mechanism	Metal or metalloid	Microorganism
Methylation	As(V)	*Aspergillus*, *Mucor*, *Fusarium*, *Paecilomyces, methanogens*
	Cd(II)	*Pseudomonas*
	Te(IV)	*Pseudomonas*
	Se(IV)	*Pseudomonas*, *Aspergillus*, *Penicillium*, *Candida*
	Sn(II)	*Pseudomonas*
	Hg(II)	*Bacillus*, *Clostridium methane*, *Aspergillus*, *Neurospora genus*
	Pb(IV)	*Pseudomonas*, *Aeromonas*
Oxidation	As(III)	*Pseudomonas*, *Actinomyces*, *Bacillus gas production*
	Sb(III)	*Antimony bacterial genera*
	Cu(I)	*Ferrooxidans*
Reduction	As(V)	*Chlorella*
	Hg(II)	*Pseudomonas*, *Escherichia*, *Aspergillus*, *Staphylococcus*
	Se(IV)	*Corynebacterium* spp., *Streptococcus* spp.
	Te(IV)	*Salmonella*, *Shigella*, *Pseudomonas*

rapidly degrade organic matter. Plants also have a large root system, which carries rich microbes. Plants play an important role during microbial metabolism, which accelerates the biological decomposition of pollutants [11].

2. The mechanism of controlling eutrophication by phytoremediation
   Plants control eutrophication mainly through the competitive system between aquatic plants and algae [12]. Aquatic plants can absorb the nutrients which are necessary for algae, such as nitrogen and phosphorus, to control the growth of algae.
3. The mechanism of regulation of the aquatic ecosystem
   Higher hydrophytes is the microbial carrier and habitat of aquatic animals. There are abundant microbial and animal species in higher hydrophytes. Aquatic plants can weaken the wind and waves, promote the settlement of suspended particles, prevent sediment resuspension, and decrease the release of pollutants in sediment. Aquatic plants will release oxygen by photosynthesis, which can increase the dissolved oxygen in the water and improve the water ecological environment. Furthermore, higher hydrophytes could cover light to restrain the growth of algae.

References

1. Gafsi M, Kettab A, Djehiche A, Goteicha K (2015) Study of the efficiency of hypolimnetic aeration process on the preservation of the thermal stratification. Desalin Water Treat 1–7 (ahead of print)
2. Schladow SG (1993) Lake destratification by bubble-plume systems: design methodology. J Hydraul Eng 119(3):350–368
3. Harris LA, Hodgkins C, Day MC, Austin D, Testa JM, Boynton W, Van Der Tak L, Chen NW (2015) Optimizing recovery of eutrophic estuaries: impact of destratification and re-aeration on nutrient and dissolved oxygen dynamics. Ecol Eng 75:470–483
4. Akcil A, Erust C, Ozdemiroglu S, Fonti V, Beolchini F (2015) A review of approaches and techniques used in aquatic contaminated sediments: metal removal and stabilization by chemical and biotechnological processes. J Clean Prod 86:24–36
5. Guo ZR (2003) Key task and strategy of pollution control of Dianchi lake. Yunnan Environ Sci 22(2):5–7 (in Chinese)
6. DelValls TA, Andres A, Belzunce MJ, Buceta JL, Casado-Martinez MC, Castro R, Riba I, Viguri JR, Blasco J (2004) Chemical and ecotoxicological guidelines for managing disposal of dredged material. TrAC Trends Anal Chem 23(10):819–828
7. Zhang XH (2002) The water environment restoration engineering principle and application. Chemical Industry Press, Beijing, pp 48–51 (in Chinese)
8. Dacey JW, Howes BL (1984) Water uptake by roots controls water table movement and sediment oxidation in short spartina marsh. Science 224(4648):487–489
9. Masscheleyn PH, Delaune RD, Patrick WH Jr (1990) Transformations of selenium as affected by sediment oxidation-reduction potential and pH. Environ Sci Technol 24(1):91–96
10. Amoroso MJ, Abate CM (2012) Bioremediation of copper, chromium and cadmium by actinomycetes from contaminated soils. In: Bio-geo interactions in metal-contaminated soils. Springer, Heidelberg, pp 349–364
11. Anderson TA, Cuthie EA, Walton BT (1993) Bioremediation in the rhizosphere. Environ Sci Technol 27:2630–2636
12. Qin B, Yang L, Chen F, Zhu G, Zhang L, Chen Y (2006) Mechanism and control of lake eutrophication. Chin Sci Bull 51(19):2401–2412

Water Quality Improvement Using Water-Lifting Aeration Technology

Tinglin Huang, Xin Sun, Xuan Li, Haibing Cong, and Ya Cheng

Abstract This chapter introduces the technical background and water quality improvement principles of water-lifting aeration, and describes the methods of designing and optimizing the structure of a water-lifting aerator. The mixing and oxygenation performance of a water-lifting aerator is analyzed using established mathematical models of hydrodynamics and oxygen transfer for the aeration chamber of a water-lifting aerator. Application conditions for controlling the internal water quality pollution and algal blooms by using water-lifting aeration technology are analyzed and discussed. With the help of the computational fluid dynamics (CFD) method, the flow fields outside a water-lifting aerator are numerically simulated, and the effective radius of the algae inhibition zone analyzed and determined. The proper installation height and outflow configuration of a water-lifting aerator are also numerically analyzed and optimized.

Keywords Water-lifting aerator • Principle • Pollution control • Algae inhibition

1 Introduction of Water-Lifting Aeration Technology

1.1 Background of Water-Lifting Aeration Technology

Eutrophication of lakes and reservoirs has been an important research topic for water scientists and engineers involved with water pollution control and drinking water safety worldwide [1–3]. The main reasons for water eutrophication are point source pollution, such as urban sewage and industrial wastewater, and non-point source pollution, such as agricultural production, soil erosion, and the internal water quality pollution of lakes and reservoirs [4]. Indirect reasons for eutrophication are the hydrological and hydraulic characteristics of lakes and reservoirs. Pollutants such as organic matter, nitrogen, and phosphorus are transported to lakes and reservoirs through rivers [5, 6]. Meanwhile, lakes and reservoirs have the

T. Huang (✉) • X. Sun • X. Li • H. Cong • Y. Cheng
School of Environmental and Municipal Engineering, Xi'an University of Architecture and Technology, Yanta Road 13, 710055 Xi'an, Shaanxi Province, P. R. China
e-mail: huangtinglin@xauat.edu.cn

T. Huang (ed.), *Water Pollution and Water Quality Control of Selected Chinese Reservoir Basins*, The Handbook of Environmental Chemistry 38,
DOI 10.1007/978-3-319-20391-1_9

characteristics of large capacity and weak fluidity. Nutrients continue to accumulate in the water and sediment, thereby providing adequate nutrition for algae and other phytoplankton.

Density stratification over the water depth occurs easily in deep-water lakes and reservoirs. Once the water is stratified, the exchange between the upper water and the lower water is limited, and the oxygen concentration in the latter gradually decreases due to the insufficient supply of oxygen. Under anaerobic conditions, a lot of organic and inorganic pollutants can be released from the sediment. The effect of these reactions is a deteriorated aquatic ecological environment [7].

New ideas for in-situ remediation and improvement technologies for lakes and reservoirs having the above-mentioned water quality problems are emerging worldwide [6, 8–12]. They are usually utilized to prevent the occurrence of eutrophication and the release of internal pollutants and to inhibit such problems at the source. In-situ remediation and improvement technologies for lakes and reservoirs have many advantages, such as low investment requirements, working quickly and cleanly with no side effects, and energy-saving operation [13–15].

Mixing and oxygenation using compressed air is one such clean and energy-saving in-situ water quality improvement technology [5, 6, 13, 14, 16–20]. The mixing and oxygenation technology does not add any physical, chemical, or biological issues. Thus, it cannot introduce side effects and does not destroy the aquatic chemical balance or biological environment. There are three main types of in-situ mixing and oxygenation technologies for water quality control, namely, deep aeration–oxygenation, rising plume of air bubbles, and water lifting with pumps or water jets [7].

Deep aeration is also called hypolimnion aeration, by which only the lower water body is oxygenated rather than mixing the upper and lower water bodies. This technology is dedicated to increasing dissolved oxygen in the lower water body and to inhibiting the release of pollutants from sediments [21–24]. However, deep aeration does not spread oxygenated water to the surrounding zone due to small-scale water circulation and it cannot directly control algal growth.

Mixing by bubble plume is achieved by releasing compressed air into the water in the form of small bubbles through diffusers installed at the bottom of lakes and reservoirs [16, 17]. When the air bubbles rise, the lower water is entrained and carried upwards by the bubble plume. Then, it spreads around on the surface area and flows down after local mixing with the surface water, thus forming a kind of vertical circulation. The induced vertical circulation can destroy the thermal stratification [25]. Oxygen is transferred into the water during the bubble flow. Meanwhile, the algae in the surface water can be transported to the middle and lower waters outside of the bubble plume, where the algal growth is inhibited due to the decrease in light intensities and water temperatures [26]. However, the range of the mixing zone is limited, and the requirements for the installation of air tubes are relatively higher, so it is difficult to implement this technology in large deep reservoirs and lakes.

An air-lifting aerator is a straight cylinder with an aeration chamber in its lower part [27]. Compressed air is injected into the aeration chamber, and once the

aeration chamber is full, the air will be released instantly, resulting in the formation of a large air piston in the central rising tube and then the plug flows upwards in the straight rising tube. The bottom water is sucked from the lower part of the air-lifting aerator continuously, and is carried upwards in the rising tube. Then, it spreads around on the surface area, leading to the vertical circulation and mixing. The effective mixing area outside the air-lifting aerator is also limited. Currently, the application of this technology lacks any theoretical guidance, which is a considerable problem for its successful application [28]. In addition, air-lifting aeration itself has no function for direct oxygenation.

Recently, the water-lifting aeration technology has been developed for the in-situ water quality improvement and eutrophication control of lakes and reservoirs [5, 6, 13–15, 20, 29]. The water-lifting aerator combines the advantages of the air-lifting aerator, and can mix the upper and lower waters and directly oxygenate the water, expanding its technical capabilities. In recent years, Huang et al. carried out systematic and comprehensive theoretical studies of the structure and performance of water-lifting aerators, as well as an applied study of their control of eutrophication and inhibition of algal growth and pollutant-release from sediments.

1.2 The Water Quality Improvement System of Water-Lifting Aeration

As shown in Fig. 1, the water quality improvement system of water-lifting aeration consists of water-lifting aerators, air compressors, and air conveying pipes.

The water-lifting aerators are usually arranged in the entire reservoir or in the vicinity of the reservoir outlet. The distances between water-lifting aerators can be determined by the effective scope of a single water-lifting aerator, which depends on the aerator's configuration, air flow rate, water depth, and applied purpose of water-lifting aeration. The mechanisms and scope of algae inhibition and

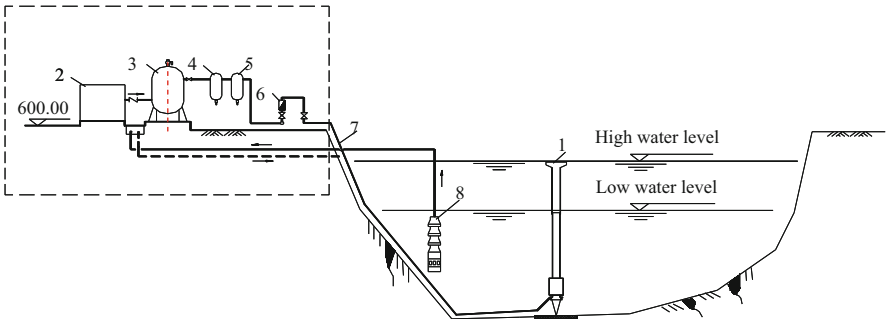

Fig. 1 Water quality improvement system of water-lifting aeration. (*1*) Water-lifting aeration, (*2*) air compressor, (*3*) air cylinder, (*4*) prefilter, (*5*) oil filter, (*6*) flowmeter, (*7*) air supply pipeline, (*8*) cooling water pump

destratification are different; the optimization of the water-lifting aeration system can be done by numerical simulation of the hydrodynamics and water quality.

1.3 The Design and Optimization of a Water-Lifting Aerator

Figure 2 shows the diagram of a typical water-lifting aerator. The main part consists of the straight ascending tube installed vertically in the water, along with air supply pipes, an air diffusor, aeration chamber, return chamber, air vessel, water-tight compartment, and anchor pier [20, 30].

The ascending tube is a straight pipe with an inlet near the bottom and an outlet near the surface. The aeration chamber, return chamber, and air vessel are wrapped in the annular space outside the lower section of the ascending tube. The top air vessel is connected to the ascending tube via microholes on the tube's wall, and the bottom air vessel is separated from the ascending tube by a seal plate. The air-releasing pipe is a circular perforated pipe located below the inlet of the aeration chamber. There is a row of holes with diameters of 2–3 mm downward of the air-releasing pipe. The water-tight compartment is a hollow buoy used to provide buoyancy and to ensure that the water-lifting aerator stands vertically in the water. The anchor pier is a heavy concrete unit resting on the bottom of a reservoir (or lake), used to anchor the water-lifting aerator.

1.3.1 The Structural Design

1. Ascending tube

   The ascending tube is a cylindrical straight unit for conveying water flow. The inlet of the ascending tube has a horn-shaped mouth for decreasing the local flow resistance and weakening the disturbance of the sediment by the suction. The vertical distance between the tube's inlet and the reservoir bottom is nearly 2 m. The outlet of the ascending tube consists of a submerged straight or mushroom tube near the water surface.

   In order to make the water-lifting aerator adapt to any change in water level, the length of the ascending tube can be adjusted automatically. Therefore, the ascending tube can be designed with two segments: the lower segment is fixed to the anchor pier with steel chains and the upper segment is hung below the upper water-tight compartment. The upper segment is connected to the lower segment by a socket. The upper segment is sheathed outside the lower segment, and can float by sliding on the wall of the lower segment. The maximum floating height of the ascending tube is restricted by a ring anchor fixed on the top of the lower segment, as shown in Fig. 2.

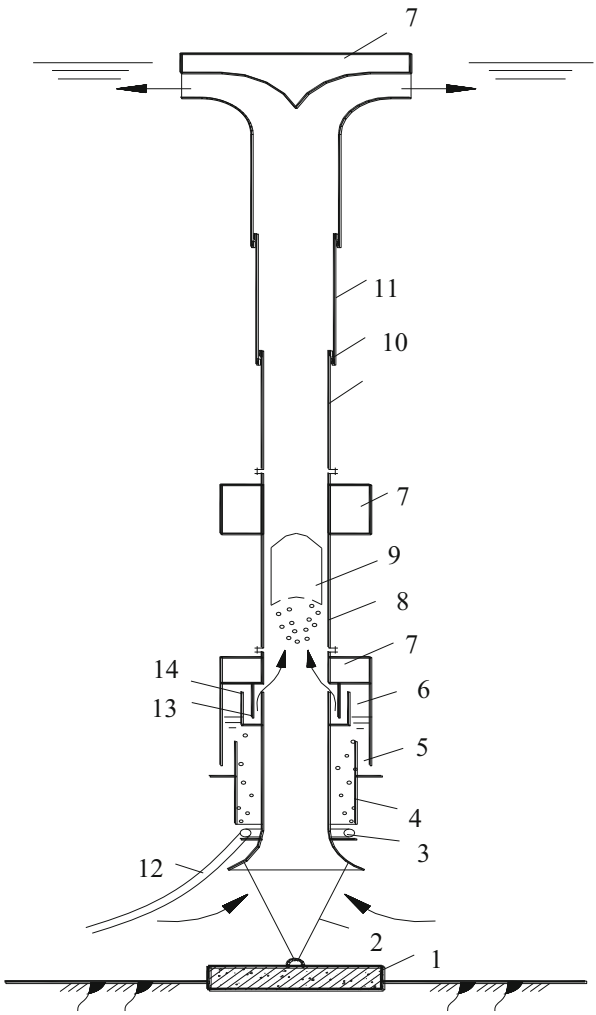

Fig. 2 Structural diagram of a water-lifting aerator. (*1*) Anchor pier, (*2*) steel chains, (*3*) air diffusers, (*4*) aeration chamber, (*5*) return chamber, (*6*) air vessel, (*7*) water-tight compartment, (*8*) ascending tube, (*9*) air piston, (*10*) lock ring, (*11*) slide tube, (*12*) air supply pipe, (*13*) seal plate, (*14*) overflow plate

2. Aeration chamber

The aeration chamber (Fig. 3a) is divided into three annular zones by the overflow plate and seal plate. The innermost annular zone is surrounded by the vertical seal plate and the central ascending tube's wall. The two other annular zones are the void air zone and the valid air zone. The air in the valid air zone can flow into the ascending tube and form the air piston. The water level declines as the air is released into the aeration chamber. When the water level drops to the bottom of the seal plate, the air in the top aeration chamber will flow into the ascending tube instantaneously, and the water level in the aeration chamber increases again.

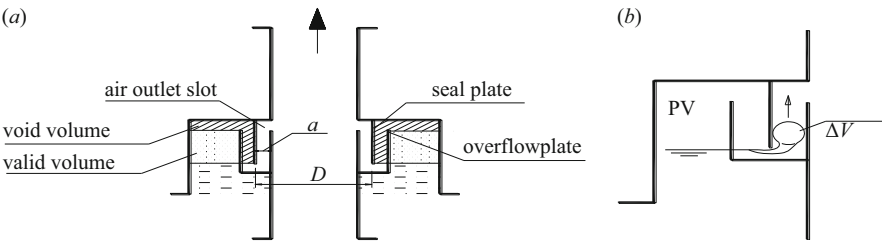

Fig. 3 Structural graph of the aeration chamber of a water-lifting aerator. (*a*) Overall configuration of the aeration chamber, (*b*) detailed configuration of the air outlet slot

The effective volume of the aeration chamber should be large enough to ensure formatting of the air piston over a certain distance in the rising tube. The diameter of a rising air piston accounts for about 75 % of the ascending tube's diameter (d). The volume of an air piston must be larger than that of a sphere with a diameter of $0.75d$. The effective volume of the aeration chamber also determines the volume of the air piston and the releasing frequency of the air piston, which affects the velocity of the water flow in the rising tube. A detailed analysis of the optimized aeration chamber volume appears in Sect. 3.1.

3. Return chamber

The aeration chamber is a place for air–water contact and oxygen transfer. A circular perforated pipe is installed below the aeration chamber. Released air bubbles are in contact with the water in the aeration chamber, oxygen in the air bubbles is then transferred to the water, and the undissolved air gradually accumulates in the air zones. As the air bubbles rise in the aeration chamber, the water is carried upwards by the rising air bubbles, the anoxic water is then sucked into the aeration chamber through the aerator's inlet, and the oxygenated water is circulated to the lower zone of the reservoir through the return chamber.

The bubble plume spreads with a certain width, so the width of the aeration chamber should be less than that of the bubble plume, otherwise, a local circulation can be generated near the aerator's inlet. In order to control the velocity of water flow downwards in the return chamber and prevent the air bubbles from flowing back to the water through the return chamber, the width and height of the return chamber should be carefully determined. Calculation of the flow rate in the aeration chamber will be described in Sect. 1.3.2.

In order to weaken the flow fluctuations in the aeration and return chambers, radial separation guide plates are set to separate the annular space. The rising tube, the outer cylinder of the aeration chamber, and the outer cylinder of the return chamber are connected together with the guide plates. Generally, at least four guide plates should be set. Ring baffles are set at the outlet of the return chamber to guide the outflow horizontally and to prevent the formation of a short flow between the outlet of the return chamber and the inlet of the aeration chamber.

4. Suspension method

   A water-lifting aerator is suspended in the water with the help of the buoyancy force provided by the water-tight compartment or resin foam. The water-tight compartment is usually made from rigid materials. The lower segment of a water-lifting aerator can slide on the inner wall of the upper segment. If the segments are too long, they should be divided into several subsegments and made separately before installation. The lower subsegments can be connected by a flange and the upper subsegments can be connected using a socket. The upper water-tight compartment is set near the water surface.

1.3.2 Optimization of the Aeration Chamber

1. The effects of aeration chamber configuration on the formation of an air piston

   Only when the configuration of the aeration chamber is reasonable can the air piston be formed in the ascending tube by quickly releasing the air in the aeration chamber as a whole. Otherwise, the air in the aeration chamber can only spill in the form of medium-sized air bubbles. The water-lifting performance will be poor if the air piston is not formed. Experimental results show that whether the air piston can be formed depends on the volume of the aeration chamber (V), the width of the air outlet (a), the diameter of the seal plate (D), and the submerged depth of the aeration chamber (H_0). The greater the V, the smaller the a, D, and H_0, and the easier it is for the air to overflow one time.

   As shown in Fig. 3b, when the water level drops to the bottom edge of the seal plate, the air pressure inside the seal plate and the water pressure outside the seal plate are equal (P), and then the first air bubble with a volume of ΔV is released. If the original position is filled by the air in the aeration chamber, a continuous bubble flow will then be formed and all the air in the aeration chamber will finally be released. If the original position is filled by the water in the air outflow slot, the residual air in the aeration chamber will then be retained in the chamber and cannot be released after the first bubble.

   Whether the vacated space is filled by the air or the water depends on their respective volumes. If the volume of air in the aeration chamber is greater than that of water in the air outflow slot, the vacated space will be filled by the air in the aeration chamber. The air pressure in the aeration chamber and the water pressure at the bottom edge of the seal plate are equal (P), and the air pressure in the aeration chamber suddenly drops by ΔP_1, defined as follows:

$$\Delta P_1 = \frac{\Delta V}{V} P. \tag{1}$$

   As the first bubble rises, the water pressure near the bubble is less than P. The water pressure drop is marked as ΔP_2. The greater the ΔV, the greater the ΔP_2 due to more difficult filling. The greater the water volume in the air outflow slot, the smaller the pressure drop due to easier filling. Therefore, the volume of the

air bubble and the width of the air outflow slot can be approximately expressed as follows:

$$\Delta P_2 \propto \frac{\Delta V}{aD}. \tag{2}$$

After the release of the first air bubble, the air pressure in the aeration chamber drops to $P - \Delta P_1$, and the water pressure near the bubble wake drops to $P - \Delta P_2$. If the ΔP_1 is greater than the ΔP_2, the air pressure in the aeration chamber will be less than the water pressure in the air outlet slot, and the vacated space of the first bubble wake will be filled by the water in the air outflow slot. So, the condition for releasing all the air in the aeration chamber is:

$$\Delta P_1 < \Delta P_2. \tag{3}$$

2. Model of the minimum air chamber volume

For a specific water depth (H_0) and diameter of the ascending tube, the width of the air outlet (a) should be chosen to be as small as possible to make the air in the aeration chamber pass through the air outlet within 1–2 s and with an average flow velocity of less than 3–5 m/s. The challenging task of designing the aeration chamber is how to determine the proper volume of the aeration chamber under the conditions of known a, D, and H_0. Combining Eqs. (1)–(3) yields the following relationship:

$$V > kaDP.$$

The minimum volume of the aeration chamber can be calculated as follows:

$$V = k(a + a_0)^{\alpha}(D + D_0)^{\beta}(10.3 + H_0)^{\gamma} + b, \tag{4}$$

where k, a_0, D_0, b, α, β, and γ in Eq. (4) are undetermined constants.

By changing the values of a, D, and H_0, corresponding values of V can be obtained and the relationship between V and the combined values of a, D, and H_0 can be developed. The undetermined constants in Eq. (4) can be calibrated against the experimental data using the Marquardt method. After performing programmed computation, the values of the undetermined constants k, c_0, D_0, b, α, β, and γ are 0.0002, 0.0168, 0.209, 0.001079, 1, 1, and 2.59, respectively.

The minimum required value of the volume of the aeration chamber (V) can be calculated by substituting values of a, D, and H_0 in Eq. (4). Figure 4 shows the minimum values of V under different values of a. As shown in Fig. 5, the prediction errors of V are within ± 10 %, indicating that the predicted results agree well with the actual results. Thus, the empirical formula expressed with Eq. (4) is feasible and can be used to determine the optimized volume of the aeration chamber.

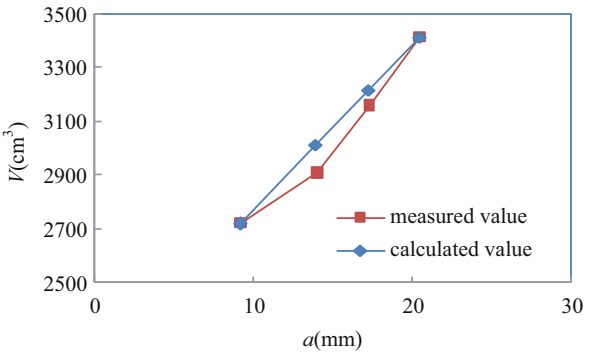

Fig. 4 Relationship between V and a

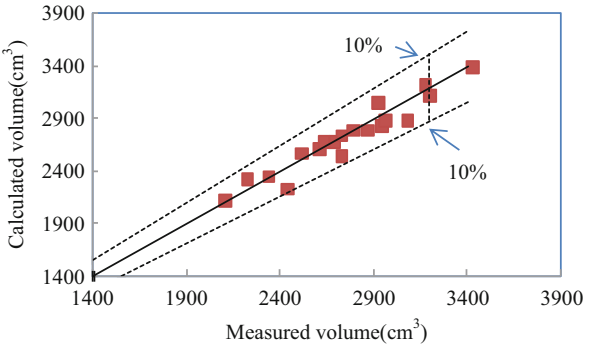

Fig. 5 Comparison of calculated and measured volumes of the aeration chamber

2 Principles of Water Quality Improvement Using a Water-Lifting Aerator

2.1 Operating Procedures

The operating procedures of a water-lifting aerator are as follows.

Compressed air is continuously released into the aeration chamber through the air diffusers. Some oxygen in the air is transferred to the water as the air rises in the form of microbubbles in the aeration chamber. At the same time, water is carried upwards by air bubbles in the aeration chamber, and the oxygenated water then returns to the reservoir bottom through the return chamber. Undissolved air accumulates in the top zone of the aeration chamber, so the water is forced to flow out from the air zone by the accumulated air, causing the water level to gradually go down in the aeration chamber. When the water level drops to the bottom edge of the seal plate, the air in the aeration chamber will instantaneously pass through the bottom edge of the seal plate and flow into the ascending tube through the air outlet. Then, the aeration chamber will be refilled with water.

Air released from the aeration chamber will combine and form a large air piston in the ascending tube, the air piston will occupy the entire cross-section of the

ascending tube and rises quickly, forming a plug flow upwards. The water flow will firstly be accelerated until the air piston goes out of the ascending tube; subsequently, the water flow will be decelerated due to the flow resistance until the formation of the next air piston. The water in the bottom of the reservoir will be sucked by the rising air in the ascending tube and then transported to the surface zone of the reservoir; the water lifted from the reservoir bottom will mix with the water near the reservoir surface and then spread sideways, thus allowing mixing between the upper and lower water layers.

2.2 Principles of Water Quality Improvement

A water-lifting aeration system has direct functions of oxygenating and mixing.

As described in Sect. 2.1, compressed air is released into the water in the aeration chamber, some oxygen in the air bubbles will be transferred to the water in the aeration chamber, and the oxygenated water will return to the reservoir bottom through the return chamber and form a local water circulation in the anoxic bottom zone. The dissolved oxygen concentration is low in the bottom zone and the pressure of the compressed air is high, so high oxygen transfer efficiency can be expected.

Driven by the air piston, the water flow upwards is developed in the ascending tube of a water-lifting aerator, the lower water will be transported to the surface area, and this causes the water flow downwards outside the water-lifting aerator and, hence, water flow upwards inside the aerator and water flow downwards outside the aerator form the circulating water flow in the reservoir. For stratified lakes and reservoirs, when the lower water is transported to the upper zone, the mixture of the lower water and upper water is still heavier than the background upper water, so the upper water will be pushed down gradually. On the other hand, outflow from the aerator will also flow horizontally due to its kinetic energy; this will enlarge the mixing zone and promote the vertical water circulation in a reservoir. Moreover, a strong sucking flow near the inlet of the aeration chamber will then be developed by the pulse flow of high velocity within a short time, and this also affects the water far from the aerator.

Using the water-lifting aeration technology, the oxygen concentration of the lower water can be increased by oxygenating the lower water directly or transporting the upper water of high oxygen concentration by vertical circulation. Once the anoxic condition of the lower water is improved due to increased oxygen concentration, the dissolving and releasing of pollutants from sediment under anaerobic reducing conditions will thus be inhibited. Oxidative decomposition of organic matter in sediment will be promoted.

Most algae mainly grow in the well-lit surface water, and they will sink very slowly after maturation. However, *Microcystis aeruginosa*, one of the dominant algae in most drinking water reservoirs, can float upwards in the water due to its special buoyancy adjustment mechanism, which gives it more opportunities for

growth and reproduction in the surface water. Water circulation generated by water-lifting aeration can be used to control the algal growth by three mechanisms. Firstly, the algae in the surface water can be transported to the lower water by the circulating water flow. They cannot photosynthesize in the dark environment and will gradually die. If the renew rate of the surface water due to the generated circulation is greater than the rate of algal growth, the algae cannot reproduce. Secondly, low temperatures are not conducive to algal growth, so it will be inhibited by the temperature change caused by the water circulation generated by the water-lifting aeration. When the lower water is transported to the surface zone, the temperature of the surface water will fall, so the growth of algae remaining in the surface water will be inhibited. Thirdly, the light penetration will be weakened in the lower water, and this will inhibit the growth of algae.

Air diffusers, the aeration chamber, return chamber, and air vessel are highly integrated in a water-lifting aerator. The water-lifting aerator has functions of oxygenating the lower water and mixing the upper and lower water layers, which can then be used to effectively control the release of pollutants from sediment and the excessive growth of algae in the surface water.

3 Mixing and Oxygenation Performance of a Water-Lifting Aerator

3.1 Water Flow Velocity Model

The water flow rate of a water-lifting aerator directly affects the mixing performance, which is dependent on several factors, such as the air flow rate, the diameter and length of the ascending tube, and the volume of the aeration chamber. This section provides an analysis of the forces acting on the water flow, establishes a mathematical model to calculate the water flow velocity, and provides a validation of the established model.

With the air piston formed intermittently, the water flow velocity in the ascending tube changes periodically. Each cycle of the water flow can be divided into two stages. The first stage is defined as the acceleration stage, in which an air piston is formed and drives water upwards with acceleration until it rushes out of the ascending tube. The second stage is defined as the deceleration stage, in which water in the ascending tube rises with deceleration until the next air slug forms.

3.1.1 Model Development

1. Model of water flow velocity in the acceleration stage

   The flow in the acceleration stage is characterized as a gas–liquid two-phase slug flow. When the air piston rises, some water will flow downwards in the form

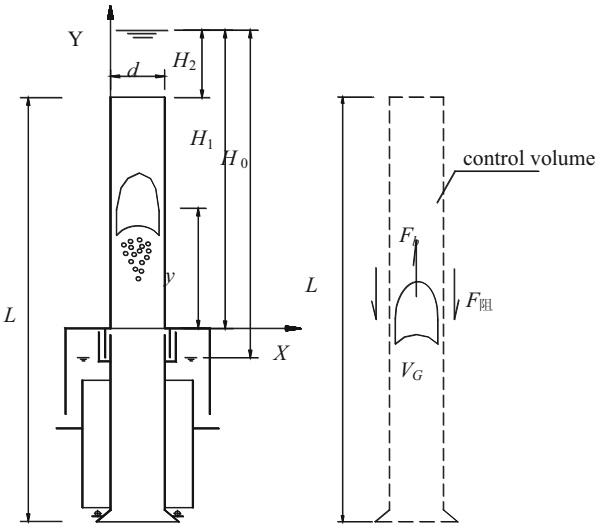

Fig. 6 Forces acting on the fluid in the ascending tube of a water-lifting aerator

of a water film in the small gap between the air piston and the wall of the ascending tube [31]. The flow of the rising air piston and the water flow are not synchronized; there is a relative sliding movement between the air flow and the water flow. The water between the inlet and outlet of the ascending tube is chosen as a control volume, as shown in Fig. 6.

In this stage, the buoyancy force and friction resistance act together on the control volume [30]. Using Newton's second law, the following momentum equation can be obtained:

$$F = F_{\mathrm{b}} - F_{\mathrm{f}} = ma = m\frac{dv}{dt} = m\frac{dv}{dy}\frac{dy}{dt} = mv\frac{dv}{dy}, \tag{5}$$

where F_{b} is the buoyancy force acting on the control volume from the air piston, N; F_{f} is the friction resistance acting on the control volume from the wall, N; a is the acceleration of the control volume, m/s^2; v is the rising velocity of the control volume, m/s; y is the height between the air piston and the top of the aeration chamber, m, $y \in [0, H_1 - H_2]$; H_1 is the height between the top of the aeration chamber and the water surface, m; H_2 is the submerged water depth at the top of the aeration chamber, m; t is the time, s; m is the mass of the control volume, kg.

The buoyancy force can be expressed as follows:

$$F_{\mathrm{b}} = V_{\mathrm{G}}\rho_{\mathrm{L}}g, \tag{6}$$

where ρ_{L} is the water density, kg/m^3; g is the gravity acceleration, m/s^2; V_{G} is the volume of the air piston at a specified height, m^3.

The initial volume of the air piston is the effective volume of the air chamber (V_0), and it will increase due to the reduction of the water pressure as the air

piston rises. The rising of the air piston is very rapid; therefore, the expansion of the air piston can be approximately treated as an adiabatic process and expressed as follows:

$$P_0 V_0^{1.402} = P_1 V_G^{1.402},$$

where P_0 is the absolute air pressure in the aeration chamber, Pa; V_0 is the effective air volume of the aeration chamber, m^3; P_1 is the absolute pressure of the air piston at a specified height (y), Pa.

Rearranging the above equation gives:

$$V_G = V_0 (P_0/P_1)^{1/1.402} = V_0 \frac{(10.33 + H_0)^{0.713}}{(10.33 + H_1 - y)^{0.713}},$$

where H_0 is the height between the bottom of the aeration chamber and the water surface, m.

Substituting V_G into Eq. (6) yields the buoyancy force acting on the control volume:

$$F_b = \frac{(10.33 + H_0)^{0.713}}{(10.33 + H_1 - y)^{0.713}} V_0 \rho_L g. \tag{7}$$

The friction resistance from the tube's wall is equal to the water weight equivalent to the water head loss in the ascending tube:

$$F_f = h_\xi \rho_L g A = \left(\zeta_i + \zeta_o + \lambda \frac{L}{d}\right) \frac{v_L^2}{2g} \rho_L g A = \frac{\zeta A \rho_L}{2} v_L^2, \tag{8}$$

where h_ξ is the water head loss in the ascending tube, m; A is the cross-sectional area of the ascending tube, m^2; ζ_i and ζ_o are the local resistance coefficients of the inlet and outlet of the ascending tube; ζ is the total flow resistance coefficient; L is the length of the ascending tube, m; d is the diameter of the ascending tube, m; v_L is the water flow velocity, m/s; λ is the friction coefficient of the ascending tube's wall, relating to the water flow velocity (v_L).

The mass of the control volume in the ascending tube can be calculated as follows:

$$m = (V - V_G)\rho_L + \frac{10.33 + H_0}{10.33} V_0 \rho_G \tag{9}$$

where ρ_G is the air density under standard atmospheric pressure, kg/m^3; V is the volume of the control volume, m^3.

Substituting Eqs. (7)–(9) into Eq. (5) gives the ordinary differential equation of velocity of the control volume with the height from the top of the aeration chamber to the air piston (y):

$$\frac{dv}{dy} = \frac{B_1 V_0 \rho_L g - 0.5\zeta A \rho_L v_L^2}{[(V - B_1 V_0)\rho_L + B_2 V_0 \rho_G]v}, \tag{10}$$

where $B_1 = (10.33 + H_0)^{0.713}/(10.33 + H_1\text{-}y)^{0.713}$, $B_2 = 1 + 0.097H_0$.

The velocity of the air piston (v_G) is greater than that of the control volume (v). According to the principle of momentum, the following relationship can be obtained:

$$V_0\rho_G^{'}v_G + (V - V_G)\rho_L v_L = \left(V_0\rho_G^{'} + (V - V_G)\rho_L\right)v, \tag{11}$$

where $\rho_G^{'}$ is the air density at the air pressure in the aeration chamber, kg/m^3.

The velocity of the air piston can be expressed as follows:

$$v_G = 1.2v + v_\infty, \tag{12}$$

where v_∞ is the velocity of the air piston in still water:

$$v_\infty = 0.345\sqrt{gd}$$

Substituting Eqs. (11) and (12) into Eq. (10), the values of v, v_G, and v_L at different values of y and t can be determined by using a numerical differential method.

2. Model of the water flow velocity in the deceleration stage

In the deceleration stage, only friction resistance from the tube's wall acts on the control volume, the mass of the control volume is constant, and the water flow velocity is equal to the velocity of the control volume. Substituting Eqs. (8) and (9) into Eq. (5) gives the equations of motion of the control volume in the deceleration stage:

$$\frac{dv_L}{dt} = -\frac{\zeta}{2L}v_L^2. \tag{13}$$

The integral equation is as follows:

$$t = -\int_{v\max}^{v_L} \frac{2L}{\zeta v_L^2} dv_L, \tag{14}$$

where v_{max} is the maximum water flow velocity at the end of the acceleration stage.

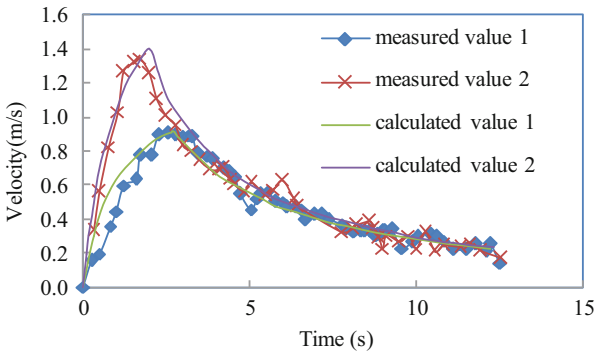

Fig. 7 Water flow velocity with time in the ascending tube of a model water-lifting aerator under different chamber volumes ($V_1 = 17$ cm^3, $V_2 = 1600$ cm^3)

3.1.2 Model Validation

In order to verify Eqs. (10) and (13), the water flow velocities in the ascending tube at different stages were measured with an ultrasonic flowmeter at a sampling rate of 0.25 s. The measured water flow velocities were compared with the velocities calculated under different conditions. Figure 7 shows the water flow velocities in the ascending tube under two air chamber volumes. The calculated water flow velocities fit the measured values very well, which indicates that the developed water flow velocity models are feasible.

3.1.3 Relationship Between Water Flow Rate and Process Parameters

Using the developed mathematical models of water flow velocity, the water flow velocity and water flow rate of a water-lifting aerator can be calculated under different structural and operational parameters. Based on the calculated results, the water flow velocity and water flow rate of a water-lifting aerator monotonically increase with the diameter, length, submerged depth of the aeration chamber, and air flow rate of the aerator. Figure 8 shows the relationship between the average water flow velocity and the air flow rate.

The optimum chamber volume V_{op} is related to the air flow rate Q, length of the water-lifting aerator L (water depth), and chamber position H_1. For a water-lifting aerator with a certain length and diameter, under a fixed air flow rate, the maximum water flow velocity can be obtained at an optimum chamber volume V_{op} (Fig. 9).

The relationship equations of the average water flow velocity under different conditions are listed in Table 1.

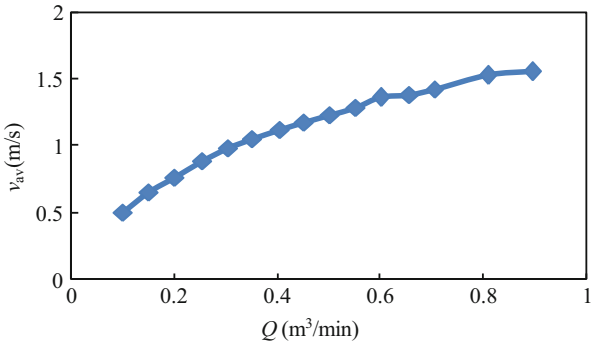

Fig. 8 Relationship between the average water flow velocity and air flow rate Q

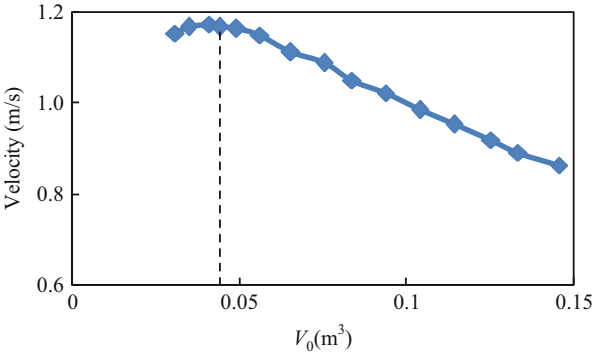

Fig. 9 Relationship between the average water flow velocity and the effective volume of the aeration chamber V_0

3.2 Model of Oxygen Transfer in the Aeration Chamber

3.2.1 Model Development

According to the double-film theory, a water film is present on the surface of air bubbles and the oxygen is first transferred to the water film, being in the condition of saturated dissolved oxygen with the concentration of C^*, whereas the dissolved oxygen concentration in the main water flow is C. The concentration of the dissolved oxygen gradually increases in the main water flow with increasing water flow (as shown in Fig. 10).

The dissolved oxygen (DO) concentration is a function of the position z. Taking a thin layer of the aeration chamber with a height of Δz as the control volume, the DO balance in the control volume is analyzed. Assuming that the dissolved oxygen in the control volume is only transferred from the air bubbles, the following DO balance can be expressed:

Total dissolved oxygen out of the control volume = total dissolved oxygen into the control volume + transferred dissolved oxygen from the air bubbles in the control volume.

Table 1 The relationship equations of the average water flow velocity of the ascending tube v_{av} (or water flow rate Q_w) and structural parameters or operational variables of a water-lifting aerator

Relationship	Regressed equation	Precision	Notes
v_{av}–H_1	$v_{av} = -A_1 \cdot H_1^2 + B_1 \cdot H_1 + C_1$	$R^2 = 0.9892$	L, H_2 are constant, relative position of aeration chamber to the tube is varied
v_{av}–L	$v_{av} = -A_2 \cdot L^2 + B_2 \cdot L + C_2$	$R^2 = 0.9906$	H_2 is constant, L, H_1 vary synchronously (water depth is varied)
v_{av}–V_0	$v_{av} = A_3 \cdot V_0^3 - B_3 \cdot V_0^2 + C_3 V_0 + D$	$R^2 = 0.997$	Air flow rate is constant, aeration chamber volume is varied
v_{av}–Q	$v_{av} = A_4 \cdot \ln Q + B_4$	$R^2 = 0.996$	Aeration chamber volume is constant, air flow rate is varied
Q_w–d	$Q_w = -A_5 \cdot d^2 + B_5 \cdot d - C_5$	$R^2 = 0.9996$	Length of the water-lifting aerator is constant, diameter of ascending tube is varied
V_{op}–H_1	$V_{op} = A_6 \cdot H_1^2 - B_6 \cdot H_1 + C_6$	$R^2 = 0.9792$	L, H_2 are constant, relative position of aeration chamber to the tube is varied
V_{op}–L	$V_{op} = -A_7 \cdot L^2 + B_7 \cdot L + C_7$	$R^2 = 0.9932$	H_2 is constant, L, H_1 vary synchronously, namely, water depth is varied
Vop–Q	$Vop = A_8 \cdot Q + B_8$	$R^2 = 0.9936$	Aeration chamber volume is constant, air flow rate is varied

Notes: A_i, B_i, C_i, D_i are positive constants

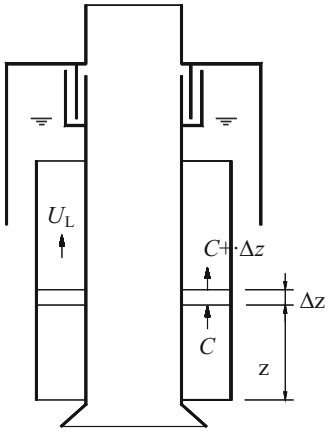

Fig. 10 Simplified diagram of the aeration chamber for studying the oxygen mass transfer model

By setting the dissolved oxygen concentration into the control volume as C, then the dissolved oxygen concentration out of the control volume is $C + \partial C/\partial z \cdot \Delta z$.

The dissolved oxygen transferred from the air film per unit time and per unit volume can be calculated as $K_L a(C^* - C)$, where K_L and a are the total area of air bubbles per unit control volume and the oxygen mass transfer coefficient on the gas–liquid interface, respectively.

Setting the cross-sectional area of the aeration chamber as A, the DO balance in the control volume can be expressed as follows:

$$\left(C + \frac{\partial C}{\partial z} \cdot \Delta z\right) A U_{\mathrm{L}} = A U_{\mathrm{L}} C + K_{\mathrm{L}} a (C^* - C) A \cdot \Delta z.$$

Making $\Delta z \rightarrow 0$, transforming the above equation leads to:

$$\frac{\partial C}{\partial z} = \frac{K_{\mathrm{L}} a}{U_{\mathrm{L}}} (C^* - C), \tag{15}$$

where C is the DO concentration in water, mg/L; C^* is the saturated DO concentration in the water film, mg/L; z is the distance from the calculated position to the bottom of the aeration chamber, m; $K_{\mathrm{L}}a$ is the total mass transfer coefficient, s^{-1}; U_{L} is the water flow velocity in the aeration chamber, m/s.

According to Henry's law, the saturated DO concentration in the water film is:

$$C^* = H_{\mathrm{A}} Y_{\mathrm{A}} P = H_{\mathrm{A}} Y_{\mathrm{A}} \left(1 + \frac{H_3 - z}{10.33}\right), \tag{16}$$

where H_{A} is the Henry's constant, (mg/L)/atm; Y_{A} is the oxygen mole fraction in bubbles; P is the total pressure of bubbles, atm; H_3 is the distance from the bottom of the aeration chamber to the water surface, m.

Assuming that the flow in the aeration chamber is a push flow, then substituting Eq. (16) into Eq. (15) gives:

$$C = (C_{\mathrm{in}} - A_1)\exp(-k_1 z) - k_3 z + A_1, \tag{17}$$

where $A_1 = k_2 + k_3/k_1$, $k_1 = K_{\mathrm{L}}a/U_{\mathrm{L}}$, $k_2 = H_{\mathrm{A}}Y_{\mathrm{A}}/(1 + H_3/10.33)$, $k_3 = H_{\mathrm{A}}Y_{\mathrm{A}}/10.33$; C_{in} is the dissolved oxygen concentrations of water at the entrance of the aeration chamber.

In Eq. (17), the unknown parameters are the total mass transfer coefficient $K_{\mathrm{L}}a$ and the water flow velocity in the aeration chamber U_{L}, and their determination methods will be introduced in Sect. 3.2.2.

3.2.2 Determination of Model Parameters

1. *The total mass transfer coefficient* $K_{\mathrm{L}}a$

   The total mass transfer coefficient $K_{\mathrm{L}}a$ is related to the air flow rate in the aeration chamber, bubble diameter, water flow velocity, temperature, oxygen diffusion coefficient, and other factors. Referring to the models introduced in the related literature [32], these parameters can be calculated as follows:

$$\frac{\Phi}{(1-\Phi)^4} = 0.2(Bo)^{1/8}(Ga)^{1/12}Fr, \tag{18}$$

$$d_b = 26(Bo)^{-0.5}(Ga)^{-0.12}(Fr)^{-0.12}D, \tag{19}$$

$$a = 0.33(Bo)^{0.5}(Ga)^{0.1}\Phi^{1.13}D^{-1}, \tag{20}$$

$$K_L = 0.5(Se)^{0.5}(Bo^*)^{3/8}(Ga^*)^{1/4}D_L d_b^{-1}, \tag{21}$$

where, Bo, Ga, Fr, Se, Bo^*, and Ga^* are dimensionless numbers, $Bo = (gD^2\rho_L/\gamma)$, $Ga = (gD^3/{v_L}^2)$, $Fr = U_G/\sqrt{gD}$, $Se = (v_L/D_L)$, $Bo^* = (g{d_b}^2\rho_L/\gamma)$, and $Ga^* = (g{d_b}^3/{v_L}^2)$; Φ is the ratio of air bubbles in the mixture of air and water; d_b is the average diameter of air bubbles, m; a is the gas–liquid two-phase contact area per unit volume of water, m^2/m^3; K_L is the oxygen mass transfer coefficient, m/s; D is the equivalent diameter of the aeration chamber, equal to the square root of the cross-sectional area of the aeration chamber divided by $\pi/4$, m; D_L is the molecular diffusion coefficient of oxygen in water, m^2/s; v_L is the kinematic viscosity of water, m^2/s; γ is the surface tension of water, kg/s^2; U_G is the local superficial air flow velocity, equal to the air flow rate divided by the cross-sectional area of the aeration chamber under local conditions, m/s.

Once the superficial compressed air flow velocity U_G (or flow) in the aeration chamber is known, the cross-sectional area and the total mass transfer coefficient $K_L a$ can be calculated with Eqs. (18)–(21).

2. *Water flow velocity in the aeration chamber*

The water flow rate in the aeration chamber is directly related to the air flow rate, the height of the aeration chamber, the cross-sectional area of the aeration chamber, and the inlet and outlet forms of the aeration chamber. Referring to the introduced empirical formula in the related literature [32], the water flow rate can be calculated as follows:

$$Q_L = 5.14h^{0.698}{Q_G}^{0.459}5.75^{D/2}, \tag{22}$$

where Q_L is the water flow rate in the aeration chamber, L/s; h is the height of the aeration chamber, m; Q_G is the air flow rate (converted to that under pressure in the aeration chamber), L/s.

Laboratory tests were carried out to check the feasibility of Eq. (22). From Table 2, the calculated and measured values of water flow rates in the aeration chamber were basically in agreement, but the calculated water flow rates were larger than those measured in the cases of large air flow rate, which is mainly caused by poor outflow from the return chamber.

So far, all unknown parameters in Eq. (17) and the increment of the DO concentration between the inlet and outlet of the aeration chamber can be calculated. In order to accurately calculate $K_L a$ and Y_A, the aeration chamber can be divided by several segments in the flow direction, and the segment's length can be set as 1 m. The values of $K_L a$ and Y_A for each segment can be

Table 2 Water flow rates in the aeration chamber

Q_G (L/s)	0.11	0.17	0.22	0.28
Q_L (measured)	1.04	1.17	1.26	1.30
Q_L (calculated)	1.25	1.52	1.70	1.90

calculated separately and the oxygen concentration of the front segment's outlet (C_{out}) is regarded as that of the following segment (C_{in}).

3.2.3 Model Validation

1. *Experimental measurement*
   Tap water was first added to a water tank, and aqueous solution of Na_2SO_3 was gradually added. Then, the water in the tank was stirred and the dissolved oxygen concentration was measured until the DO concentration decreased to zero. A water-lifting aerator was put in the water tank and a DO probe was placed at half depth. When operating the water-lifting aerator, the DO concentration in the water tank was measured every 5 min. The total amount of water in the tank was 710 L, the water temperature was 11 °C, and the air flow rates were 800 and 1000 L/h.
2. *Model calculations*
   The inlet DO concentration C_{in} changed continuously in the aeration chamber, and the increment of dissolved oxygen in the aeration chamber varied with time. After calculation, the water in the water tank could be completely circulated once after 12 periods of releasing the air piston. In order to calculate the oxygen concentration easily, the water tank was simplified to a non-ideal reactor equivalent to 12 completely mixed reactors in series (Fig. 11). A zero-order reaction occurred in 1–12 reactors. According to the principle of mass balance, for the nth reactor, the increment of DO concentration during the time period of Δt is equal to the net amount of DO entering the reactor during Δt, which can be determined by subtracting the amount of outflow from that of inflow in this period. The relationship is as follows:

$$V_n\left[C_{n(t+\Delta t)} - C_{n(t)}\right] = C_{n-1(t)}Q\Delta t - C_{n(t)}Q\Delta t.$$

The relationship of dissolved oxygen concentration between any two adjacent reactors in the system of 1–12 reactors can be expressed as follows.

$$C_{n(t+\Delta t)} = \frac{C_{n-1(t)}Q\Delta t + C_{n(t)}(V_n - Q\Delta t)}{V_n}, \tag{23}$$

where Q is the average flow rate in the water-lifting aerator, C_n is the dissolved oxygen concentration of any reactor in C_2–C_{12}; V_n is the volume of the nth aerator.

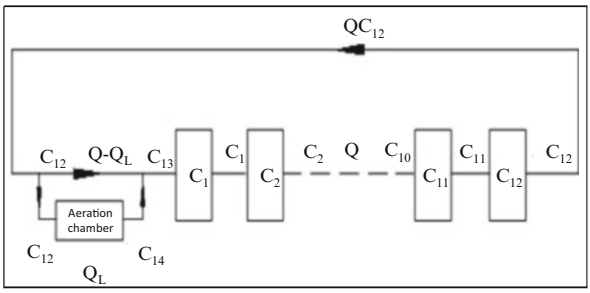

Fig. 11 Flume model of non-ideal reactors

C_{12} and C_{14} are the dissolved oxygen concentrations of the inflow and outflow of the aeration chamber, and their relationship can be expressed with Eq. (17), hence:

$$C_{14} = (C_{12} - A_1)\exp(-k_1 z) - k_3 z + A_1.$$

C_{13} is obtained by the weighted average of C_{12} and C_{14}:

$$C_{13} = \frac{Q_L C_{14} + (Q - Q_L)C_{12}}{Q}, \tag{24}$$

where Q_L is the water flow rate in the aeration chamber of a water-lifting aerator, and is calculated by Eq. (22).

C_1 is obtained by C_{13} using Eq. (23).

At $t = 0$, $C_1\,(0) = C_2\,(0) = \ldots = C_{13}\,(0) = C_{14}\,(0) = 0$. Taking the time interval Δt as 1 s, the dissolved oxygen concentration for each reactor can be calculated at different times. A DO analyzer probe is located at the position of #6 reactor. Therefore, the calculated dissolved oxygen concentration of C_6 is regarded as the measured one in the experiments.

As can be seen from Fig. 12, the measured values are in good agreement with the calculated values. The measured values are slightly lower only at high dissolved oxygen concentrations. The reason for this is probably excessive dosing of Na_2SO_3. Dissolved oxygen in the water is consumed at high dissolved oxygen concentrations.

3.3 Hydrodynamic Model for the Aeration Chamber

In Sect. 3.2, the water flow rate in the aeration chamber was calculated using the proposed empirical model [32]. However, the application of this empirical model is conditional. This section describes a one-dimensional two-phase flow model for the aeration chamber of a water-lifting aerator [33–35]. The model includes the flow

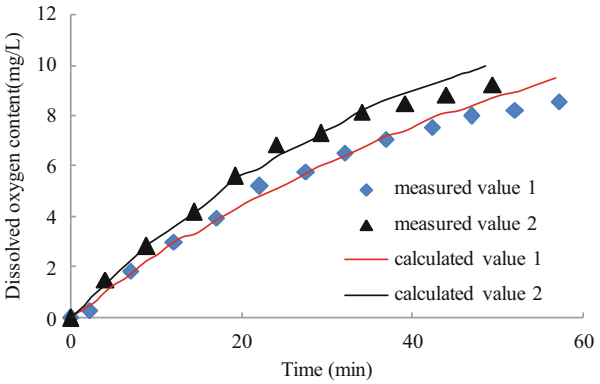

Fig. 12 Comparison of calculated and measured dissolved oxygen concentrations under different air flow rates ($Q_1 = 0.8$ m^3/h, $Q_2 =$ 1 m^3/h)

rate balance equation, mass conservation equation, momentum balance equation, and energy or pressure balance equation.

3.3.1 Model Development

The aeration chamber can be divided into four parts: the ascending zone, descending zone, the gas–liquid separation zone, and the outflow zone (Fig. 13). The flow in the ascending zone of a chamber is gas–liquid two-phase flow, in which the density of the mixture is less than that of water, and the flow in the descending zone is a single water flow. Driven by the pressure difference caused by the difference inflow density between the ascending zone and the descending zone, the water flows from the ascending zone to the descending zone.

A hydraulic model of one-dimensional gas–liquid two-phase flow was established according to the equilibrium between the driving force and drag force acting on the gas–liquid two-phase fluid. The driving force is induced by the gas holdup or density difference between the ascending zone and the descending zone, and the drag force is induced by the wall friction and local flow resistance.

1. *Balance equation for the ascending zone*

   Mass conservation equation:

$$Q_{lr} = A_r V_{lr} \varepsilon_{lr}, \tag{25}$$

$$Q_{gr} = A_r V_{gr} \varepsilon_{gr}. \tag{26}$$

   The relationship between the superficial velocity and actual velocity is as follows:

$$U_{gr} = V_{gr} \varepsilon_{gr}, \tag{27}$$

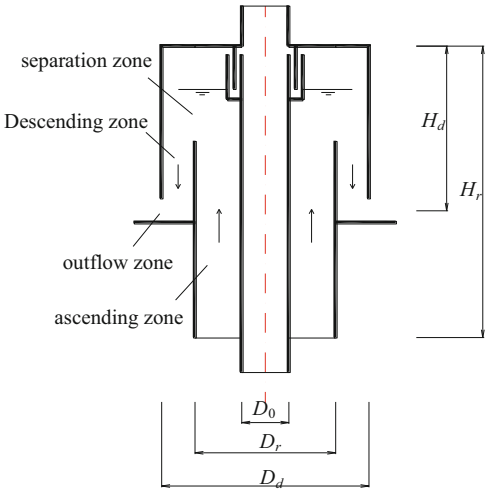

Fig. 13 Diagram of the aeration chamber for studying the hydrodynamic model

$$U_{lr} = V_{lr}\varepsilon_{lr}. \tag{28}$$

The air flow rate at the air diffusers can be calculated by Eq. (29):

$$Q_{gr} = \frac{P_{\text{atm}}}{P_{\text{atm}} + 10^{-5}\rho_l g h_1'} Q_{\text{gatm}}. \tag{29}$$

The pressure drop in the ascending zone includes the gravity pressure reduction and the pressure loss due to the wall friction, and the momentum equation can be expressed as:

$$\left(\frac{dP}{dz}\right)_r = -\left(\rho_l\varepsilon_{lr} + \rho_g\varepsilon_{gr}\right)g - \left(\frac{dP}{dz}\right)_{fr}. \tag{30}$$

The pressure drop caused by the wall friction in the ascending zone can be expressed as follows:

$$\left(\frac{dP}{dz}\right)_{fr} = \frac{W_{lr}\tau_{plr}}{A_r}. \tag{31}$$

The relationship between the water holdup and the gas holdup is:

$$\varepsilon_{lr} + \varepsilon_{gr} = 1. \tag{32}$$

The other equations are:

$$A_r = \frac{\pi\left(D_r^2 - D_0^2\right)}{4}, \tag{33}$$

$$W_{lr} = \pi(D_r + D_0), \tag{34}$$

where Q is the flow rate, m^3/s; A is the cross-sectional area, m^2; V is the actual velocity, m/s; ε is the gas holdup; U is the superficial velocity, m/s; P is the pressure, N/m^2; $h_1^{'}$ is the water depth where the air difussors are located, m; g is the local gravity acceleration, m/s^2; ρ is the density, kg/m^3; $\frac{dP}{dz}$ is the pressure gradient, Pa/m; τ_p is the shear stress, N/m^2; W is the wet perimeter, m; D is the diameter, m.

The meanings of the subscripts are: r is the ascending zone; d is the descending zone; l is the liquid; g is the gas; atm is the standard atmospheric pressure; f is the wall friction; 0 is the central cylinder.

Similar equations for the descending zone correspond to Eqs. (25)–(34).

2. *Local pressure loss*

The pressure loss at the top of the aeration chamber can be expressed as:

$$\Delta P_{\text{top}} = \frac{1}{2}\rho_l K_t V_{lr}^2. \tag{35}$$

The pressure drop at the outlet of the descending zone can be expressed as:

$$\Delta P_{\text{out}} = \frac{1}{2}\rho_l K_E V_{lr}^2, \tag{36}$$

where ΔP_{top} and ΔP_{out} are the pressure drops caused by the local turning of flow at the top of the ascending zone and at outlet of the descending zone; K_t and K_E are the pressure loss coefficients at the top of the ascending zone and at outlet of the descending zone.

3. *Relationship of flow rates*

The flow rate in the ascending zone is equal to that in the descending zone:

$$Q_{lr} = Q_{ld} \Rightarrow A_r U_{lr} = A_d U_{ld}. \tag{37}$$

4. *Friction resistance on the wall*

The frictional resistance on the wall of the ascending zone is:

$$\tau_{plr} = \frac{1}{2} f_{lr} \rho_l V_{lr}^2, \tag{38}$$

$$f_{lr} = 0.079 Re_r^{-0.25}, \tag{39}$$

$$Re_r = \frac{D_{eqr} V_{lr} \rho_l}{\mu_l}, \tag{40}$$

where f is the friction coefficient; Re is the Reynolds number; μ is the viscosity, kg/(m·s); D_{eq} is the equivalent diameter to the same cross-section, m.

The frictional resistance on the wall of the descending zone can also be calculated.

5. *The energy balance equation or pressure balance equation*

The energy balance or pressure balance of the two-phase flow must be met:

$$\Delta P_1 + \int_r \frac{dP}{dz} = \int_d \frac{dP}{dz} + \Delta P_{\text{top}} + \Delta P_{\text{out}}. \tag{41}$$

6. *The pressure difference between the inlet and outlet*

The height difference between the inlet and outlet results in the difference of the static pressure caused by potential energy, which can be expressed as:

$$\Delta P_1 = \rho_l g (H_r - H_d), \tag{42}$$

where ΔP_1 is the pressure difference between the inlet and outlet, N/m^2; H is the height, m.

Combining the above equations gives:

$$\begin{aligned} &2g\left[\left(\varepsilon_{ld} + \frac{\rho_g \varepsilon_{gd}}{\rho_l} - 1\right) H_d - \left(\varepsilon_{lr} + \frac{\rho_g \varepsilon_{gr}}{\rho_l} - 1\right) H_r\right] \\ &\quad = \left(\frac{f_{ld} W_{ld} H_d A_r^2}{A_d^3 \varepsilon_{ld}^2} + \frac{f_{lr} W_{lr} H_r}{A_r \varepsilon_{lr}^2}\right) U_{lr}^2 + (K_t + K_E) V_{lr}^2. \end{aligned} \tag{43}$$

Since $\rho_g << \rho_l$, $\varepsilon_{gd} < 1$, $\varepsilon_{gr} < 1$, $\frac{\rho_g \varepsilon_{gd}}{\rho_l} \approx 0$, $\frac{\rho_g \varepsilon_{gr}}{\rho_l} \approx 0$.

Simplifying Eq. (43) yields:

$$\begin{aligned} &2g\left(\varepsilon_{gr} H_r - \varepsilon_{gd} H_d\right), \\ &= 0.316\left(\frac{\rho_l}{\mu_l}\right)^{-0.25} U_{lr}^{1.75} \left[\left(\frac{D_r^2 - D_a^2}{D_d^2 - D_r^2}\right)^{1.75} \frac{(D_d - D_r)^{-1.25} H_d}{\left(1 - \varepsilon_{gd}\right)^{1.75}} + \frac{(D_r - D_o)^{-1.25} H_r}{\left(1 - \varepsilon_{gr}\right)^{1.75}}\right] \\ &\qquad + \frac{(K_t + K_E)}{\left(1 - \varepsilon_{gr}\right)^2} U_{lr}^2. \end{aligned} \tag{44}$$

The water flow velocity and gas holdup in the aeration chamber can be predicted from Eq. (44) with the real-domain method of Matlab, but the pressure loss coefficients of K_E and K_t need to be known before using this equation.

Based on the field data of hypolimnetic aerators installed in Lake Prince and Lake Western Branch, Burris et al. proposed the relationship of $K_t = 4.7U_{lr}^{-1.4}$ [21], and Brodkey and Hershey suggested $K_t = 0.5$ [36] according to the experimental results of oxygen transfer. Fried and Idelchick suggested that $K_E = 2.9$ (pressure loss coefficient at the inlet of the ascending zone $K_{\text{in}} = 1.4$, pressure loss coefficient at the outlet of the descending zone $K_{\text{in}} = 1.5$) [37].

3.3.2 Determination of Model Parameters

Before using use Eq. (44), the relationship between the gas holdup and superficial air velocity and water flow velocity also needs to be developed. The gas holdup in the ascending zone can be calculated with Eq. (45) [38]:

$$\varepsilon_{gr} = \frac{4Q_g}{\pi\left(D_r^2 - D_o^2\right)(V_{lr} + V_b)} = \frac{U_{gr}}{(V_{lr} + V_b)}. \tag{45}$$

Wüest et al. also proposed the following relationship between V_b and r_b:

$$\begin{aligned}
&\text{When } r_b < 7 \times 10^{-4}\text{m}, \ V_b = 4474 {r_b}^{1.357};\\
&\text{When } 7 \times 10^{-4}\text{m} \le r_b \le 5.1 \times 10^{-3}\text{m}, \ V_b = 0.23;\\
&\text{When } r_b > 5.1 \times 10^{-3}\text{m}, \ V_b = 4.202 {r_b}^{0.547},
\end{aligned}$$

where V_b is the rising velocity of air bubbles, m/s; r_b is the radius of air bubbles, m.

As previously described, many empirical equations are combined in the hydrodynamic model for the aeration chamber, so the water flow velocity and gas holdup in the aeration chamber can be accurately predicted with the developed hydrodynamic model by choosing the proper empirical equations according to different experimental conditions.

3.3.3 Model Validation

1. Experimental methods

   In order to verify the developed hydrodynamic model for the aeration chamber, a series of experiments were conducted in a model water-lifting aerator. The water flow velocity was measured indirectly with a pitot tube. Pitot tubes were installed at several cross-sections of the descending tube of a lab-scale aerator. Several piezometric tubes were also installed on the outer walls of the ascending zone and descending zone to determine the gas holdups in the ascending zone and descending zone. The nozzles of piezometric tubes and pitot tubes were connected to differential pressure meters with latex hoses to determine the pressure difference.

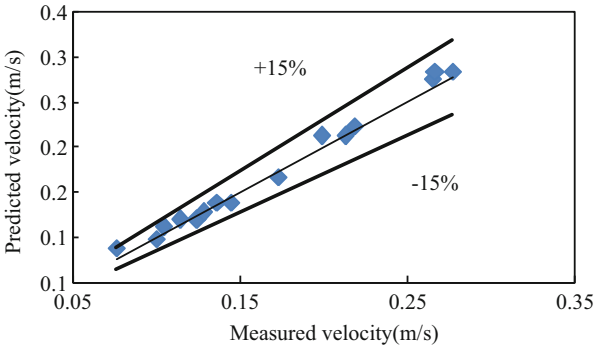

Fig. 14 Comparison of the measured and predicted superficial water flow velocities in the ascending zone

2. Model validation

Based on the measured water flow velocities and gas holdups and calculated air flow velocities from the air flow rate in the aeration chamber, the gas–liquid two-phase flow drift flux model for these aeration conditions was calibrated with Eq. (46):

$$\frac{U_{gr}}{\varepsilon_g} = 0.8027\left(U_{gr} + U_{lr}\right) + 0.2711. \tag{46}$$

The values of coefficients C_0 and U_{BT} are roughly in accordance with those in other related literature.

Figure 14 shows that the errors of the predicted and measured water flow velocities were within the range of ±15 %. The prediction errors of gas holdup were also within ±15 %. These results indicate that the developed hydrodynamic model has strong applicability to predict the water-lifting performance in an aeration chamber of a water-lifting aerator.

4 Internal Pollution Control by Water-Lifting Aeration

The water-lifting aeration technology can be used to inhibit the release of contaminants by increasing the dissolved oxygen concentration, which can be achieved by oxygenating the anoxic water and mixing the upper and lower waters. Thus, the premise of using the water-lifting aeration technology is that the bottom water in a reservoir is anoxic or anaerobic. At present, it is generally recognized that the anaerobic condition is the key to the release of pollutants from sediment [4, 7], but the critical dissolved oxygen concentration for the massive release of pollutants from sediment is uncertain. In order to determine the specific application conditions restraining the release of contaminants from sediment using water-lifting aeration, comparative studies were conducted on the releasing rates of pollutants under different conditions of dissolved oxygen concentration.

4.1 Application Condition of Inhibiting the Release of Ammonia Nitrogen

It is always shown to be anaerobic in the sediment; nitrogenous organic matter can be transformed into ammonia nitrogen by the ammonifying bacteria and releasing it into the overlying water [39]. When the overlying water is aerobic, ammonia nitrogen will be transformed into nitrate nitrogen by nitrification, and nitrate nitrogen will seep back to the surface sediment to be transformed into nitrogen by denitrification in a hypoxia state, thus completing the whole process of nitrification and denitrification [40, 41]. However, when the overlying water is anaerobic, ammonia nitrogen released from the sediment can be transformed into nitrate nitrogen smoothly, which will cause the accumulation of ammonia nitrogen [42–44]. What dissolved oxygen concentration in overlying water can hinder the nitration of ammonia nitrogen and cause the accumulation of ammonia nitrogen? The results as shown in Fig. 6 in Sect. 1.1 of Chap. 6 indicate that the accumulation of ammonia nitrogen is caused when the dissolved oxygen concentration in water is less than 2 mg/L. Therefore, the application condition of inhibiting the release of ammonia nitrogen from sediment with water-lifting aeration is a dissolved oxygen concentration less than 2 mg/L.

4.2 Application Condition of Inhibiting the Release of Phosphorus

The release of phosphorus in sediment is not only affected by dissolved oxygen, but is also controlled by the pH value. Experiments of phosphorus release were conducted under combined conditions of different pH values and dissolved oxygen concentrations. The pH values of the three simulated experiments were 6.5, 8, and 9.1, respectively. The dissolved oxygen concentration fell gradually from 5 to 4 mg/L in 20 days, from 4 to 3 mg/L in 10 days, from 3 to 2 mg/L in 10 days, from 2 to 1 mg/L in 12 days, and from 1 to <1 mg/L in 38 days.

In the release experiments, the sediment and water samples were obtained from the main channel of Heihe Reservoir. The algae and other plankton were filtered through a 0.45-μm membrane, eliminating their effects on the experimental results. The reactors, comprising three organic glass columns with diameter and height of 300 mm, were placed in a closed and opaque water tank under a constant temperature of 30 °C. O_2 and N_2 were bubbled into the reactors to maintain the required concentration of dissolved oxygen in the overlying water. The pH value in the overlying water was adjusted with 0.1 M NaOH and HCl solutions.

Figure 15 shows the results of phosphorus concentrations in the overlying water under different experimental conditions.

When the pH was 6.5, the concentration of dissolved oxygen decreased from 5 to 1 mg/L in 65 days, and the release rate of phosphorus was zero. When the DO

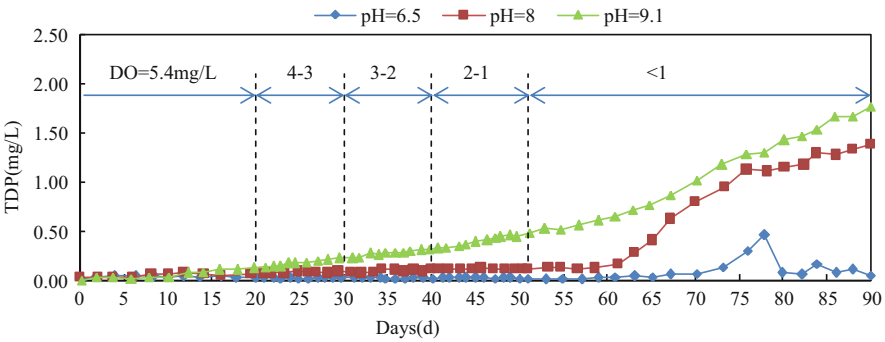

Fig. 15 Effects of dissolved oxygen concentration and pH on the release of phosphorus

concentration was less than 1 mg/L, phosphorus began to release at an average rate of 9.3 mg/(d m^2). This is because the iron combined with phosphorus in sediments was reduced and dissolved ($Fe^{3+} \rightarrow Fe^{2+}$), and that makes phosphate, which is combined with iron ($FePO_4$), dissolved, and released into the water. However, the release of phosphorus is unstable [45–47].

When the pH was 8, the release rate of phosphorus during each stage was 1.8, 0.41, 1.21, 0.78, and 16.83 mg/(d m^2). The release of phosphorus was caused by the replacement of iron and aluminium phosphate ($FePO_4$, $AlPO_4$) with hydroxyl radical (OH^-) in water. When the DO concentration was less than 1 mg/L, the release of phosphorus was quick, which is the combined result of replacement by OH^- and reductive dissolution by iron [30].

When the pH was 9.1, the release rate of phosphorus during each stage was 3.38, 4.64, 4.84, 7.26, and 15.83 mg/(d m^2). When the DO concentration decreased from 5 to 2 mg/L, the release rates of phosphorus were stabilized at a low level. This was still the result of the replacement of iron and aluminium phosphate ($FePO_4$, $AlPO_4$) by hydroxyl radical (OH^-) in water. When the DO concentration decreased to 1–2 mg/L, the release of phosphorus was accelerated, indicating that the reductive dissolution by iron began to work. When the DO was less than 1 mg/L, the release of phosphorus was further accelerated, due to the stronger reductive dissolution by iron.

In conclusion, the critical dissolved oxygen concentrations for the anaerobic release of phosphorus are less than 1 mg/L when the pH <8 and less than 2 mg/L when the pH was 9.1. Therefore, under neutral or acidic conditions, the premise of restraining the release of phosphorus from sediments using water-lifting aeration is a dissolved oxygen concentration of less than 1 mg/L, and under alkaline conditions, the premise is a dissolved oxygen concentration less than 2 mg/L.

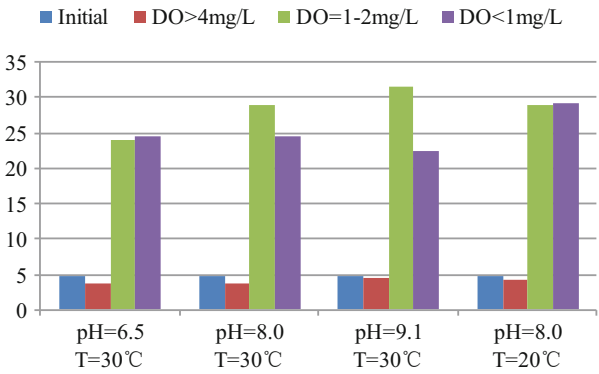

Fig. 16 Effects of dissolved oxygen concentration and pH on the release of organic matter *TOC*

4.3 Application Condition of Inhibiting the Release of Organic Matter

The release of organic matter from sediment is actually the accumulation of incomplete intermediate byproducts from the decomposition of organic matter under anaerobic conditions. While under aerobic conditions, these intermediate byproducts are decomposed into CO_2 and H_2O. Similar releasing experiments were performed. The dissolved oxygen concentrations were 4 mg/L for 6 days, from 4 to 1–2 mg/L for 6 days, and <1 mg/L for 6 days. The TOC concentrations in water were measured under different conditions of dissolved oxygen concentration. Figure 16 shows the results.

From Fig. 16, in the aerobic phase of DO >4 mg/L, the TOC concentration in each reactor did not increase but decreased to a certain degree, indicating that organic matter was not released from sediment to overlying water. Under aerobic conditions, aerobic decomposition of organic matter occurred in overlying water, reducing the concentration of organic matter.

In the anoxic stage of DO = 1–2 mg/L, a large amount of organic matter was released from sediment. During this stage of 6 days, the TOC concentration in each reactor significantly increased from 4.3 mg/L to 31.6 mg/L. This shows that, under anoxic conditions of DO = 1–2 mg/L, anaerobic bacteria began to multiply. The insoluble organic matter in sediments was degraded to soluble organic acids, and then released to overlying water. After reaching the state of being completely anaerobic (DO<1 mg/L), the TOC concentration did not further increase in overlying water, but instead decreased. This is because the methane-producing bacteria began to multiply, and the organic acids were biodegraded to methane [30].

The application condition for inhibiting the release of organic matter from sediment using water-lifting aeration is dissolved oxygen concentration less than 2 mg/L.

4.4 Application Conditions of Inhibiting the Release of Iron and Manganese

The release of iron and manganese is by reducing Fe^{3+} and Mn^{4+} in the precipitated state to Fe^{2+} and Mn^{2+} in the dissolved state under anaerobic conditions. As described in Sect. 3.4.3, iron and manganese will be rapidly released from sediment when the dissolved oxygen concentration is less than 1 mg/L.

In conclusion, the release of the phosphorus, iron, and manganese from sediment can be inhibited when the DO concentration in the lower water is increased to more than 1 mg/L using water-lifting aeration. The release of ammonia nitrogen and organic matter from sediment can be inhibited simultaneously when the DO is increased to more than 2 mg/L.

5 Algae Inhibition by Water-Lifting Aeration

5.1 Application Conditions of Algae Inhibition

5.1.1 Water Depth

With the help of mixing by water-lifting aeration, the algae in the upper water can be transported to the lower water of a reservoir, and will die due to the unfavorable environment for photosynthetic. The light intensity decreases with increasing water depth, so the production capacity of chlorophyll-*a* in unit concentration (O_2mg/L/(Chl-*a* μg/L)) decreases with the increase of water depth. Figure 17 shows the variation of the net production capacity of chlorophyll-*a* against the water depth. The value of the net production capacity above the compensation point is positive. The area enclosed by the curve above the compensation point and the axes is the positive accumulative net production capacity. And the value of the net production capacity below the compensation point is negative. The area enclosed by the curve below the compensation point and the axes is the negative accumulative net production capacity (respiratory capacity). The summation of the two areas is the net production capacity of the water body when the distribution of the content of chlorophyll-*a* is uniform and the content is of unit value.

There are two ways to reduce the net production capacity of water. One is to change the situation where the content of chlorophyll-*a* in the upper layer is greater than that in the lower layer to one where the distribution of chlorophyll-*a* in each water layer is uniform. The other is to ensure that the required water is deep enough and to extend the depth of the lower "black zone", since this can strengthen the algal respiration. Extending the curve plotted in Fig. 17, it can be calculated that the depth needed to achieve zero net production capacity in the water is 12 m. This can be decreased slightly, because of the impact of other factors, such as overcast and

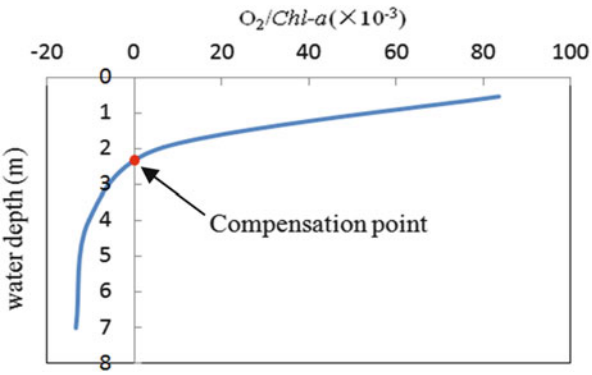

Fig. 17 Productivity of units of chlorophyll-*a* concentration in relation to depth changes

rainy weather. In conclusion, the applicable depth for using water-lifting aeration devices to restrain algal growth is at least 10 m.

5.1.2 Mixing Conditions

Microcystis aeruginosa is the dominant species of algae in most drinking water source reservoirs and it can float upwards with a typical velocity of 0.000275 m/s in water [14, 48, 49]. The mechanism of inhibiting algal growth by water-lifting aeration is achieved through a circulated flow from top to bottom caused by water-lifting aeration [20]; the algae are transported to the lower water layer and eventually die due to unfavorable growing conditions. To inhibit the algal growth, a minimum downward flow velocity of 0.000275 m/s is required.

5.2 Spatial Distance Between Two Water-Lifting Aerators

The mixing intensity is great enough to meet the requirements of the downward flow velocity within a certain zone outside a water-lifting aerator. Beyond the certain zone outside a water-lifting aerator, the mixing strength is decreased, and then the algal growth cannot be inhibited. Under certain boundary conditions, the flow field outside a water-lifting aerator can be numerically simulated with the computational fluid dynamics (CFD) method. The powerful CFD simulation software of Fluent can be used [50]. Based on the flow field outside a water-lifting aerator and the typical floating velocity of *Microcystis aeruginosa*, the effective algae inhibition zones can be numerically determined under different hydrological and operational conditions. Hence, the spatial distance between two water-lifting aerators can be determined.

Based on the typical operational conditions of the water-lifting aeration system used to improve the water quality of Jinpen Reservoir (Fig. 18), the flow field and algae concentration profiles outside the water-lifting aerator under different

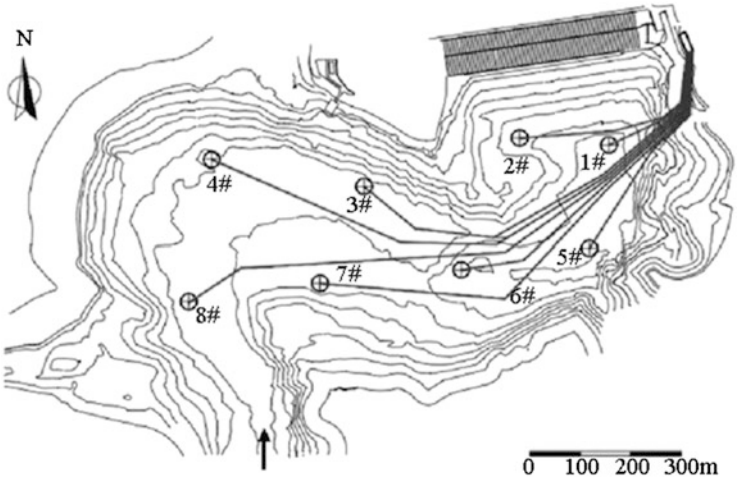

Fig. 18 Layout of water-lifting aerators in Jinpen Reservoir

conditions were numerically simulated, and the effects of the water temperature gradient and water depth on the algae inhibition zone were analyzed [29, 51].

5.2.1 Simulation Methods

The water body outside the water-lifting aerator was simplified as a two-dimensional axisymmetrical simulation model of the flow domain, and the right half of the simulation model was taken into consideration. The water-lifting aerator was simplified as a cylinder with a radius of 0.375 m, and its central line was set as the axis of the simulation domain. The water-lifting aerator was considered as a block body in which no flow entered or exited. The inlet of the water-lifting aerator was 6 m away from the reservoir bottom and the outlet was 0.5 m below the water surface. The inlet and outlet were considered to be the outlet and inlet of the simulated flow domain, respectively.

Boundary conditions: Velocity-inlet was used to describe the water-inlet of the simulated region. Under typical operational conditions, the velocity increased from 0 to 2.5 m/s linearly within 15 s, then decreased linearly to 0 m/s at 30 s, and then remained at 0 m/s until 270 s in a single cycle [20]. This periodic distribution of velocity was defined by a user-defined function (UDF) of Fluent [52]. The temperature of water-inlet of the simulated region defined by a UDF was the average value of the temperature of water-outlet of the simulation region at the previous simulation time. Pressure-outlet was used to describe the water-outlet of the simulation region and the pressure was decided from the water depth.

Initial conditions: The average water depths before the dam of Jinpen Reservoir are 50–110 m. The observed water temperature in Jinpen Reservoir decreased in linearly from the surface to a depth of 30 m. The seasonal temperature gradients

were 0, 0.17, 0.47, and 0.73 °C/m, respectively. The relationship between water temperature and thermal structure, density, and viscosity were defined by a UDF before simulation. The water depths were 50, 80, and 110 m.

Solving methods: The renormalization-group (RNG) κ–ε model was used to model turbulence. The algae concentration was calculated by a multicomponent model. Heat transfer of the surface and subsurface water was considered [53], and the heat transfer conditions were given by the UDF. The first-order upwind scheme was used to discretize the equations, and PISO (pressure implicit splitting of operator) and pressure-based implicit solver were applied to solve the unsteady equations.

Analysis methods of the algae inhibition zone: The zone where the downward vertical velocity is greater than 0.000275 m/s is defined as the core zone of algae inhibition. The area of the zone was calculated using Photoshop software. The percentage of the area of the zone was defined as the ratio of the core zone of algae inhibition to the whole simulation flow domain. The larger the radius of the algae inhibition zone, the better the algae inhibition. The bigger the percentage of the core algae inhibition zone, the better the algae inhibition.

Radius of simulation domain: The preliminary simulated results showed that the core zone of algae inhibition was roughly within 150 m using a water body with a radius of 1600 m. To ensure the reliability and efficiency of the numerical computation, the radius of the subsequent simulation domain was selected as 300 m.

The weakest algae inhibition moment: The preliminary simulated results also showed that the weakest area ratio of the core algal inhibition zone to the whole domain within one period was that at the starting point (endpoint). The following analysis was performed using the starting point data.

5.2.2 Verification of the Simulated Results of Algae Inhibition

The #4 aerator in Jinpen Reservoir was minimally affected by outflow and was taken as the object of verifying the simulated results. A test section was established between #4 and #6 aerators, where the terrain was relatively flat and roughly similar to that of the computational grid. Vertical variations of eight conventional water quality indexes, such as chlorophyll-*a* and water temperature etc., were measured daily using a Hydrolab DS5X multiprobe sonde (Hach, USA), and algae concentrations of water samples at 0.5 m from the surface, 30 m underwater, and 5 m from the bottom were analyzed in the laboratory twice a week during operation of the aerators. The monitoring profile was 50 m away from #4 aerator.

The flow field outside the water-lifting aerator was measured by three-dimensional acoustic Doppler profilers (ADP, LAUREL company WH600kHz, USA). An ADP measures the flow velocity with the principle of acoustic Doppler [54, 55]. According to the simulated results, the flow out of the aerator was unsteady, and the flow field 50 m away from the aerator was substantially independent of the periodic flow after running for a period of time. Figure 19a shows the simulated algae inhibition zone. Based on the data of vertical flow velocity derived

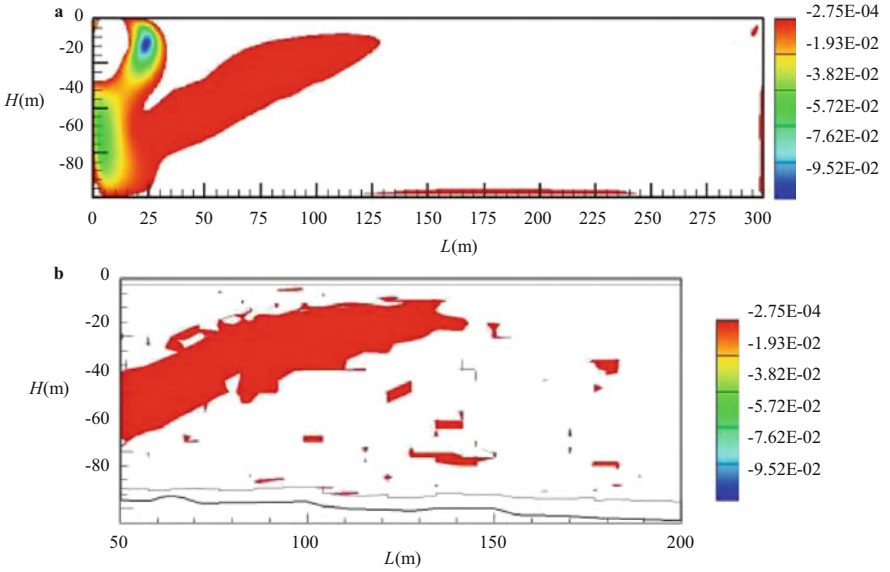

Fig. 19 Comparison of the predicted and measured core algae inhibition zones ($H = 80$ m): (**a**) predicted zone, (**b**) measured zone

from the ADP, the actual algae inhibition zone is drawn in Fig. 19a. By comparing Fig. 19a, b, the measured and simulated algae inhibition zones were substantially similar, indicating that the simulated vertical velocities and the measured velocities were in good agreement.

5.2.3 Effect of Temperature Gradient on the Algae Inhibition Zone

Figure 20 shows the simulated flow fields outside a water-lifting aerator under different temperature gradients.

The flow field was characterized as a clockwise flow under non-stratified conditions (Fig. 20a); however, the flow field was characterized as a clockwise flow near the domain inlet and a counter-clockwise flow in the other regions under stratified conditions (Fig. 20b, c). Different flow patterns under non-stratified and stratified conditions were mainly caused by the density differences between the inflow and background water. When the water was not stratified, water from the domain inlet initially moved horizontally with its own kinetic energy; a clockwise flow was finally formed outside the aerator under the influence of the right boundary and outlet flow. When the water was stratified, the low-temperature water from the domain inlet initially moved horizontally, and then moved downwards due to its greater density. However, the water flow changed its direction and moved upwards because of the buoyancy resistance from the stratification [56], and, as a result, a partial clockwise flow developed near the domain inlet. The low-temperature water

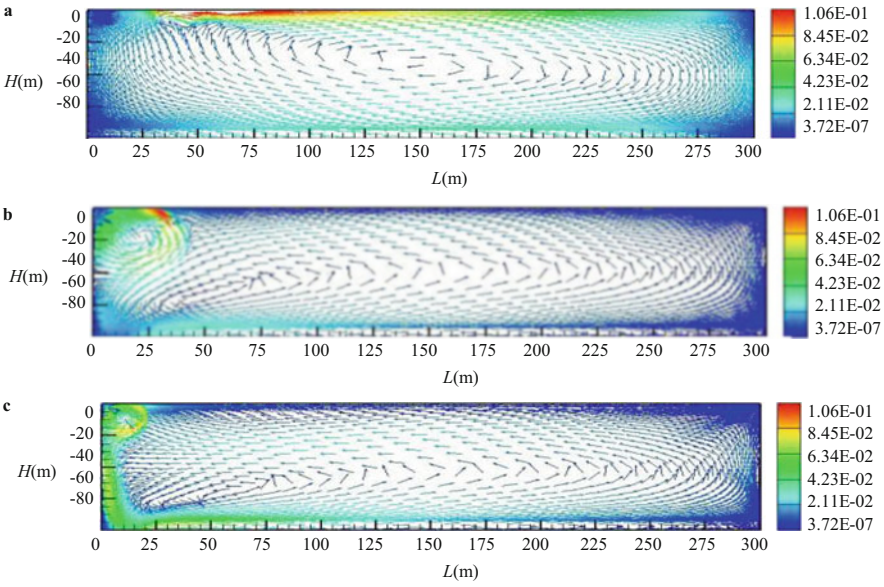

Fig. 20 Flow fields outside a water-lifting aerator under different water temperature gradients: (**a**) 0 °C/m, (**b**) 0.170 °C/m, (**c**) 0.730 °C/m

from the domain inlet formed a large counter-clockwise flow on the right side of the aerator.

The temperature gradient affected the flow outside the aerator. When the temperature gradient gradually increased from 0.17 to 0.73 °C/m, the radius of the clockwise flow near the domain inlet decreased from 40 to 25 m, and the maximum velocity of the clockwise flow decreased from 10.5 to 8.5 cm/s. As the kinetic energy of the inflow water and the volume of the water body were all constant, this phenomenon was caused by the difference in buoyancy resistance due to the stratification. As the temperature gradient increased, more energy was consumed when the clockwise flow near the domain inlet moved downwards.

Figure 21 shows the contour lines of the vertical velocity of flow outside the water-lifting aerator, and the colored region is defined as the core zone of algae inhibition.

The core zone of algae inhibition depended directly on the flow outside the water-lifting aerator; therefore, the shape of the zone under stratified conditions was different from that under non-stratified conditions (Fig. 21). The percentage of the core zone under non-stratified conditions was about 63.95 %, and it increased slightly from 25.2 to 28.6 % when the temperature gradient increased from 0.17 to 0.73 °C/m. The radius of the core inhibition zone increased with the temperature gradient. The radius of the core inhibition zone increased from 100 to 150 m when the temperature gradient increased from 0.17 to 0.73 °C/m. Firstly, a higher temperature gradient led to stronger buoyancy resistance, which restricted the development of clockwise flow near the domain inlet and promoted the

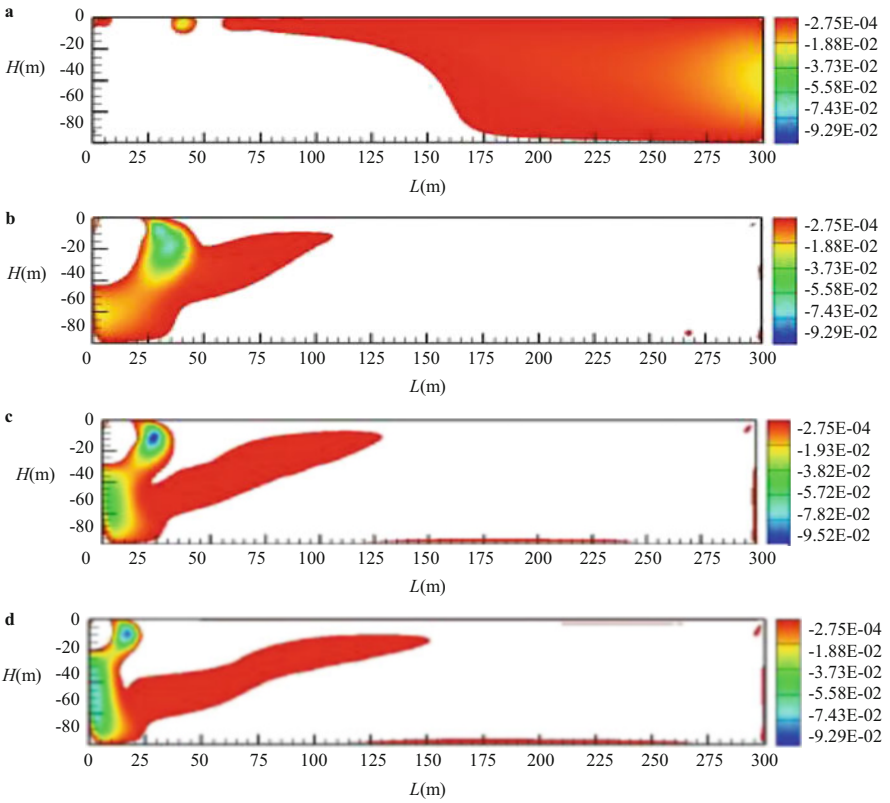

Fig. 21 Core algae inhibition zones under different temperature gradients: (**a**) 0 °C/m, (**b**) 0.170 °C/m, (**c**) 0.470 °C/m, (**d**) 0.73 °C/m

development of strong counter-clockwise flow in the other regions. Secondly, as the water temperature at the bottom was almost 6 °C, the water temperature increased with a higher temperature gradient when the upper and bottom waters became completely mixed, and this led to increased water fluidity due to the decreased water viscosity.

5.2.4 Effects of Water Depth on the Algae Inhibition Zone

Figure 22 shows the simulated flow fields outside the water-lifting aerator under water depths of 50, 80, and 110 m. Under a water temperature gradient of 0.73 °C/m, the flow was characterized as a clockwise flow at the inlet and a counter-clockwise flow in other regions, which was similar to that shown in Fig. 20.

Figure 22 illustrates that range and strength of the inlet clockwise flow did not changed obviously with water depth. This was because the inlet clockwise flow was mainly influenced by the water temperature gradient, and temperature gradients

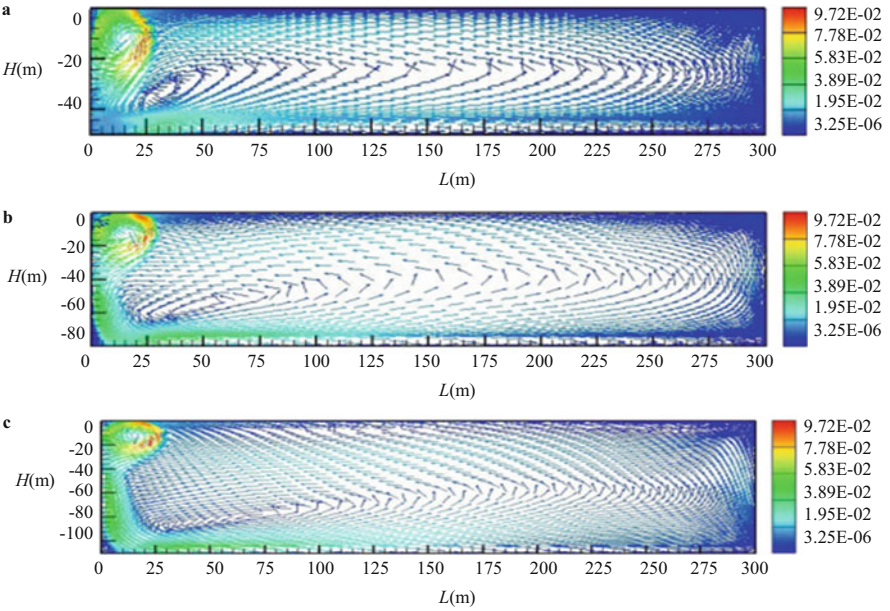

Fig. 22 Flow fields outside the water-lifting aerator under different water depths: (**a**) 50 m, (**b**) 80 m, (**c**) 110 m

within the range of 30 m under different depths were identical, and the buoyancy resistance of inlet water with lower temperature was the same too. The vertical velocity of the flow was increased gradually with the increasing water depth, and this was mainly because the ratio of the width to the depth of the water was decreased when the water depth was increased, and the wall effect on the flow structure across the section was gradually enhanced [57].

Figure 23 shows the contour lines of the vertical velocity of flow outside the water-lifting aerator. Although the water depths were different, the shapes of the core zone of algae inhibition were almost the same when the temperature gradient within 30 m was 0.7 °C/m. This was because the core zone depended directly on flow outside the aerator and the flow mainly depended on the temperature gradient. The water depth mainly affected the size of the core zone.

The percentage of the core zone increased from about 12.5 to 30.6 % when the water depth increased from 50 to 110 m. The radius of the core zone increased with water depth. The radius of the core zone increased from about 60 to 175 m when the water depth increased from 50 to 110 m. Because under the condition that the flow domain was not wide enough to limit the flow, the water depth is an important factor affecting the flow when the depth increased within a certain range. Under the condition of constant velocity of the inlet flow, the distance between the inlet and outlet of the flow domain would drive its movement direction to turn left from the right after the inlet flow entered the flow domain outside the aerator. With increasing water depth, the effect of the water outlet became weaker, and the maximum

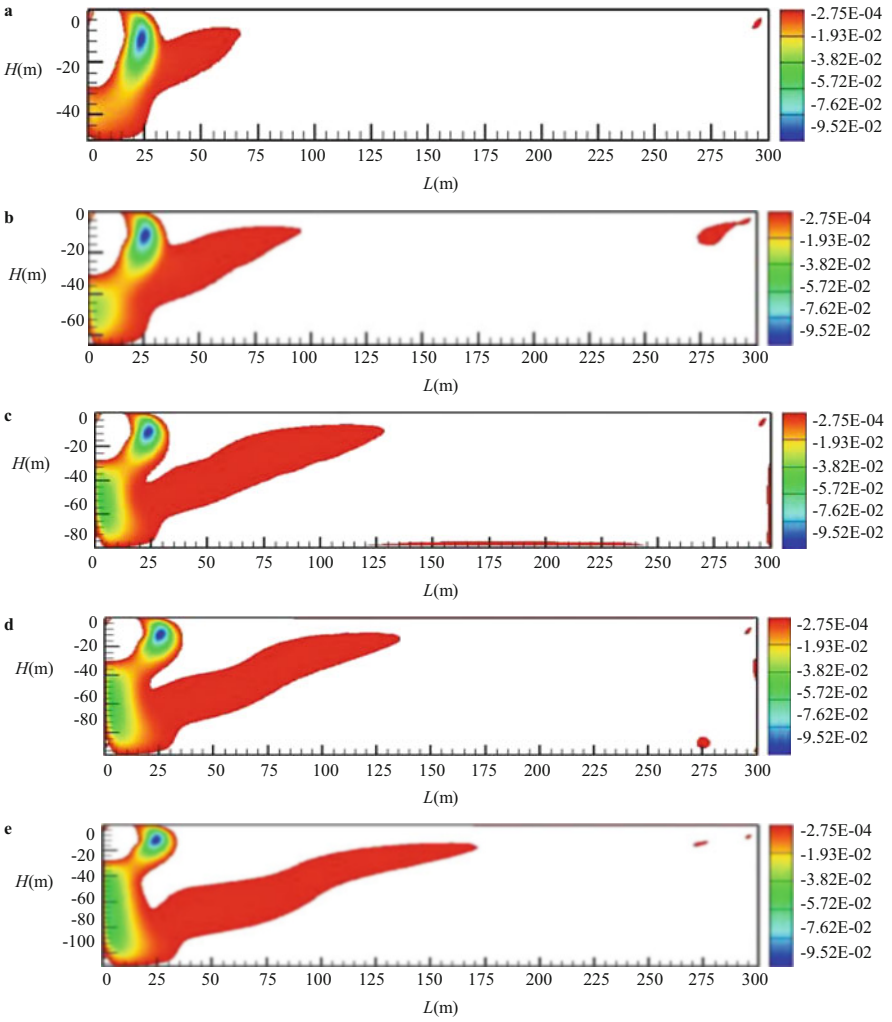

Fig. 23 Core algae inhibition zones under different water depths: (**a**) 50 m, (**b**) 65 m, (**c**) 80 m, (**d**) 95 m, (**e**) 110 m

movement distance of the inlet flow gradually increased, manifesting as an increasing core zone of algae inhibition.

Based on the above simulated results, the proper design interval of two water-lifting aerators can be proposed as 250–300 m.

5.3 Installation Height of a Water-Lifting Aerator

The installation height is defined as the vertical distance between the bottom of a water-lifting aerator and the reservoir bottom. To enhance and improve the oxygenation performance of a water-lifting aerator in the bottom water of a reservoir, the installation height should be low. On the other hand, the installation height also influences the suspension of sediment. A proper installation height for a water-lifting aerator needs to be determined.

5.3.1 Simulation Method

To determine the proper installation height of a water-lifting aerator, the flow fields outside a water-lifting aerator under different installation heights were simulated with the Euler–Euler model using Fluent software. The installation heights were 2, 1, and 0.5 m. The water-lifting aerator system installed in Jinpen Reservoir was taken as a study case, and the typical air flow rate of 25 m^3/h was used for each simulation case. According to the previous research results of incipient velocity for sediment transport, the water flow velocities above the sediment under different installation heights were compared with the proposed incipient velocity for sediment transport, and the proper installation height of a water-lifting aerator was determined.

5.3.2 Characteristics of Flow Inside and Outside a Water-Lifting Aerator

Under the conditions of an air flow rate of 25 m^3/h, a water depth of 80 m, and an installation height of 2 m, the simulated release period of an air piston is about 165 s. The outflow velocity changed periodically within a cycle of about 165 s; it increased linearly from 0 to 4.8 m/s as the time increased from 0 to 15 s, then decreased linearly from 4.8 to 0 m/s as the time increased from 15 to 45 s, and then remained at 0.5 m/s until 165 s.

Because the numerical simulation aimed to evaluate whether the circulated flow can cause the suspension of sediment or not, only the flow fields near the reservoir bottom were analyzed. The bottom water flow is jointly caused by the water flow in the ascending tube and the bubble flow in the aeration chamber of a water-lifting aerator, so the bottom water flow is characterized as the coexistence of multiple circulations, but the flow velocities are usually low due to the large cross-section at the reservoir bottom.

The centerline of the first grid above the reservoir bottom, 0.0795 m from the reservoir bottom, was chosen for analysis of the velocity. Figure 24 shows the temporal variations of the water flow velocity at the specified vertical position. In Fig. 24, the horizontal axis in the figure represents the distance from the water-

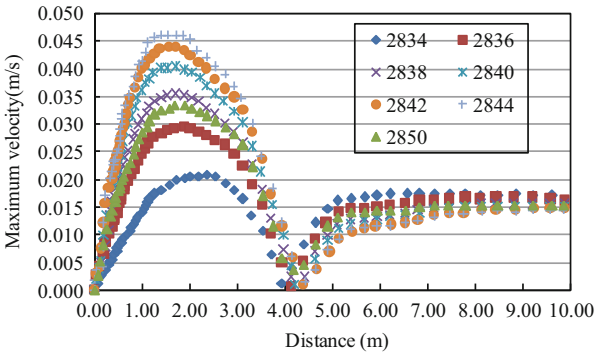

Fig. 24 Maximum velocities at different aeration times along the centerline of the first grid above the reservoir bottom

lifting aerator's central axis and the time period is one release period of an air piston. Figure 24 shows that the water flow velocity always maximized at a distance of 2 m and always minimized at a distance of 4.25 m.

To analyze the possibility of the generated water flow disturbing and suspending the bottom sediment, the maximum water flow velocities at the specified vertical position were plotted against the aeration time in Fig. 25. The maximum flow velocity at the specified vertical position varied synchronously with the average flow velocity in the ascending tube of a water-lifting aerator, but the maximum bottom flow velocity was only about 1 % of that in the ascending tube, and the maximum velocity was only 0.0417 m/s.

5.3.3 Flow Characteristics Under Different Installation Heights

Under installation heights of 2, 1, and 0.5 m, the temporal variations of the water flow velocity at the specified vertical position were similar in pattern, but the peak velocities were different. The maximum velocity increased from about 0.02 to 0.23 m/s in 15 s under an installation height of 1 m, but the maximum velocity increased from about 0.1 to 2.1 m/s in 15 s under an installation height of 0.5 m. From Figs. 25 and 26, the maximum water flow velocities at the centerline of the first grid above the reservoir bottom under installation heights of 2, 1, and 0.5 m were about 0.041, 0.23, and 2.1 m/s, respectively.

5.3.4 Proper Installation Height

At present, the incipient movement of sediment is usually evaluated by three methods, namely, the incipient friction velocity formula, the incipient shear stress formula, and the incipient velocity formula. As shown in Fig. 27, the incipient velocity is dependent on the diameter of the sediment and minimizes in the diameter range of 0.1–1 mm [58]. Under a typical air flow rate of 25 m^3/h, the maximum water flow velocities were 0.042, 0.22, and 2.1 m/s for installation

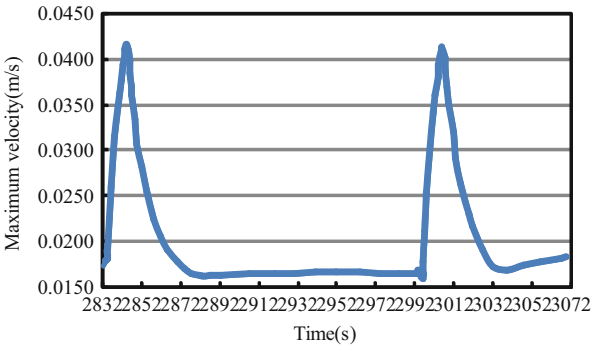

Fig. 25 Relationship between the maximum velocity along the centerline of the first grid above the reservoir bottom and aeration time (installation height of 2 m)

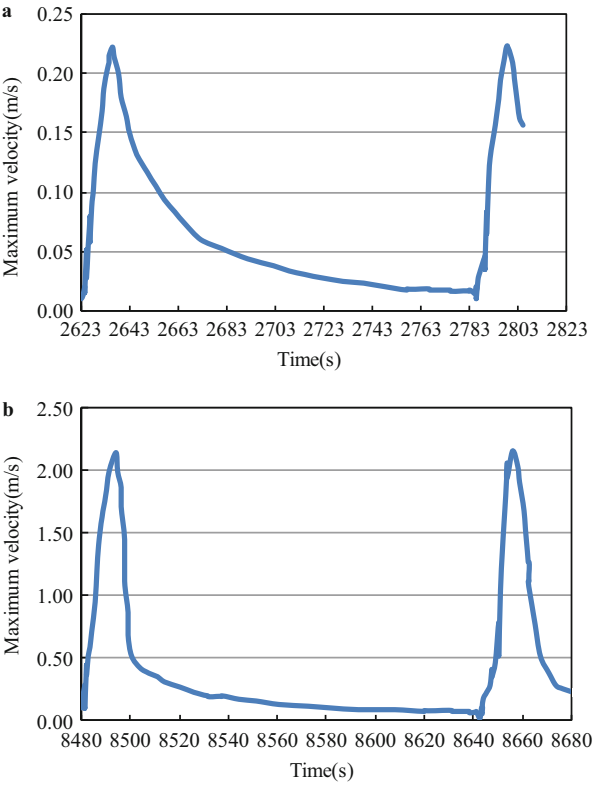

Fig. 26 Relationship between the maximum velocity along the centerline of the first grid above the reservoir bottom and aeration time: (**a**) installation height of 1 m, (**b**) installation height of 0.5 m

heights of 2, 1, and 0.5 m, respectively. Based on the incipient velocities as shown in Fig. 27, it can be deduced that running water-lifting aerators with installation heights greater than 1 m will not cause the suspension and movement of reservoir sediment, regardless of the sediment diameter, which will not increase the water turbidity and deteriorate the water quality of the reservoir. Considering the actual geometry of the reservoir bottom, the installation technology, and the total

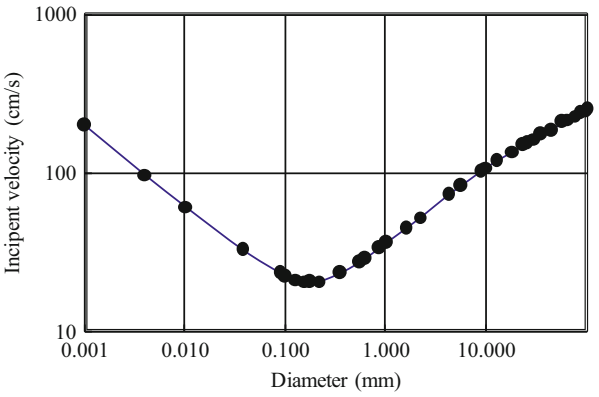

Fig. 27 Relationship between the incipient velocity and sediment diameter

comprehensive installation cost, the proper installation height of a water-lifting aerator can be suggested as 2 m.

5.4 Effects of Water-Lifting Aerator Type on Algae Inhibition

Two types of water-lifting aerators have been developed to improve the water quality in reservoirs: submerged [13, 20] and non-submerged [5, 6]. From the perspective of economic costs, the initial investment and operating costs of a submerged aerator are about one-third of that of a non-submerged aerator. Moreover, it is also easier to install and maintain. From the perspective of water quality improvement, the function of hypolimnetic aeration is the same for each type of aerator, but the mixing between the upper and lower water bodies will be different, so the effectiveness of mixing as a means of algae inhibition will also be different for the two types of aerator.

To choose the proper type of water-lifting aerator, the effectiveness of algae were numerically compared using non-submerged and submerged water-lifting aerators under the same operational conditions [15, 35]. A water-lifting aerator with an optimized outlet configuration was used. The water depths were 77.25, 87.25, and 97.25 m. The outlet of the submerged aerator was 70 m above the domain bottom and the outlet of the non-submerged aerator was 1.1 m below the water surface. The other simulation methods are the same as those in previous sections.

5.4.1 Algae Inhibition Under Non-stratified Conditions

Figure 28 shows the contour lines of the vertical velocity of flow outside the water-lifting aerators, with the colored region defined as the core algae inhibition zone.

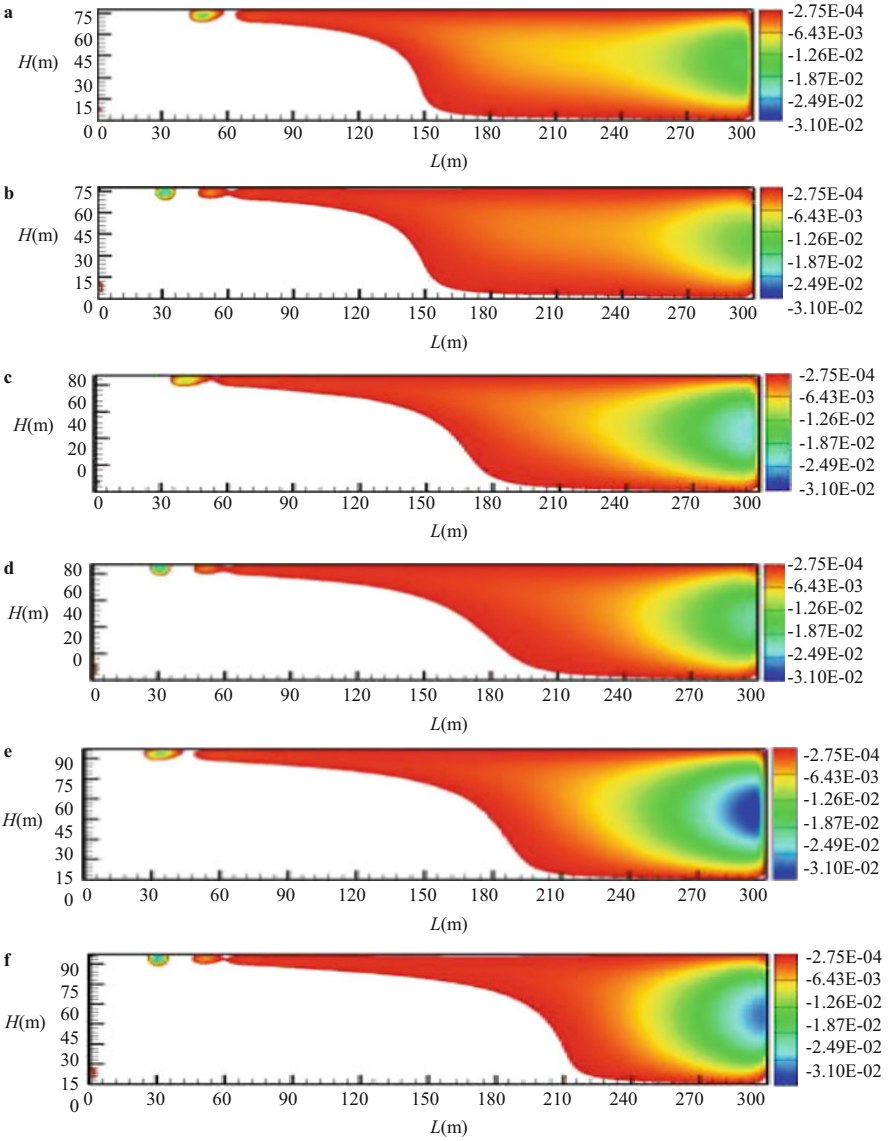

Fig. 28 Core algae inhibition zones outside submerged and non-submerged water-lifting aerators at different water depths: (**a**) submerged, $H = 77.25$ m, (**b**) non-submerged, $H = 77.25$ m, (**c**) submerged, $H = 87.25$ m, (**d**) non-submerged, $H = 87.25$ m, (**e**) submerged, $H = 97.25$ m, (**f**) non-submerged, $H = 97.25$ m

From Fig. 28, when the water depth was increased from 77.25 to 97.25 m, the percentage of the core algae inhibition zone to the whole domain was decreased from 56.01 to 47.34 % for the submerged case, while that for the non-submerged

case was decreased from 55.48 to 40.15 %. This indicates that the percentage of the core algae inhibition zone for the submerged case is larger than that for the non-submerged case under each water depth. That is because the water from the outlet of the submerged aerator interacts with the background water in the domain from the depth of 77.25 m, which is wider in space and earlier in time than for the non-submerged case; the clockwise flow initially generated from entrainment develops laterally in a wider area. On the contrary, the water from the outlet of the non-submerged aerator interacts with the background water in a narrower area. As the input energy is fixed, the core algae inhibition zone is pushed closer to the right wall of the domain.

It can also be seen from Fig. 28 that the area of the core algae inhibition zone was obviously decreased with increasing depth. The main reason for this is that the boundary effect becomes more evident as the ratio of the depth to the width increases. The stronger the boundary effect, the bigger the vertical velocity, hence the closer the core algae inhibition zone is to the right wall.

5.4.2 Algae Inhibition Under Stratified Conditions

In the study, Jinpen Reservoir is a typical stratified reservoir [5, 6]. The thermocline lies between depths of 0 and 30 m, the temperature reduced from 28 to 6 °C when the depth increased from the water surface to 30 m, the zone below 30 m was an isothermal layer, with the temperature there remaining at 6 °C, and the temperature gradient was 0.73 °C/m.

1. Effects of aerator type on the core algae inhibition zone

   Figure 29 shows the simulated core algae inhibition zone under different water depths, with the colored region defined as the core algae inhibition zone. From Fig. 29, when the water depths were 77.25, 87.25, and 97.25 m in the submerged water-lifting aerator case, the percentages of the core algae inhibition zones to the whole flow domain were 39.71, 41.14, and 42.73 %, respectively. For the non-submerged water-lifting aerator case, the percentages were 33.83, 37.46, and 41.58 %, respectively. This indicates that the percentage of the core algae inhibition zone for the submerged case was larger than that for the non-submerged case at each water depth. This is because the core algae inhibition zone is mainly determined by the velocity field. The effect of aerator type on the core algae inhibition zone was consistent with the effect on the flow outside the water-lifting aerators.

   Figure 29 also shows that the core algae inhibition zone area increased with increasing depth. The main reason for this is that, when the width cannot sufficiently limit the development of the circulation, the water depth acts as a major factor affecting the flow development. For a non-submerged aerator, when the inlet velocity was certain, the water flow from the inlet of the domain was equivalent to a horizontal jet, the distance between the inlet and the bottom would affect the direction of motion, and with increasing water depth, the

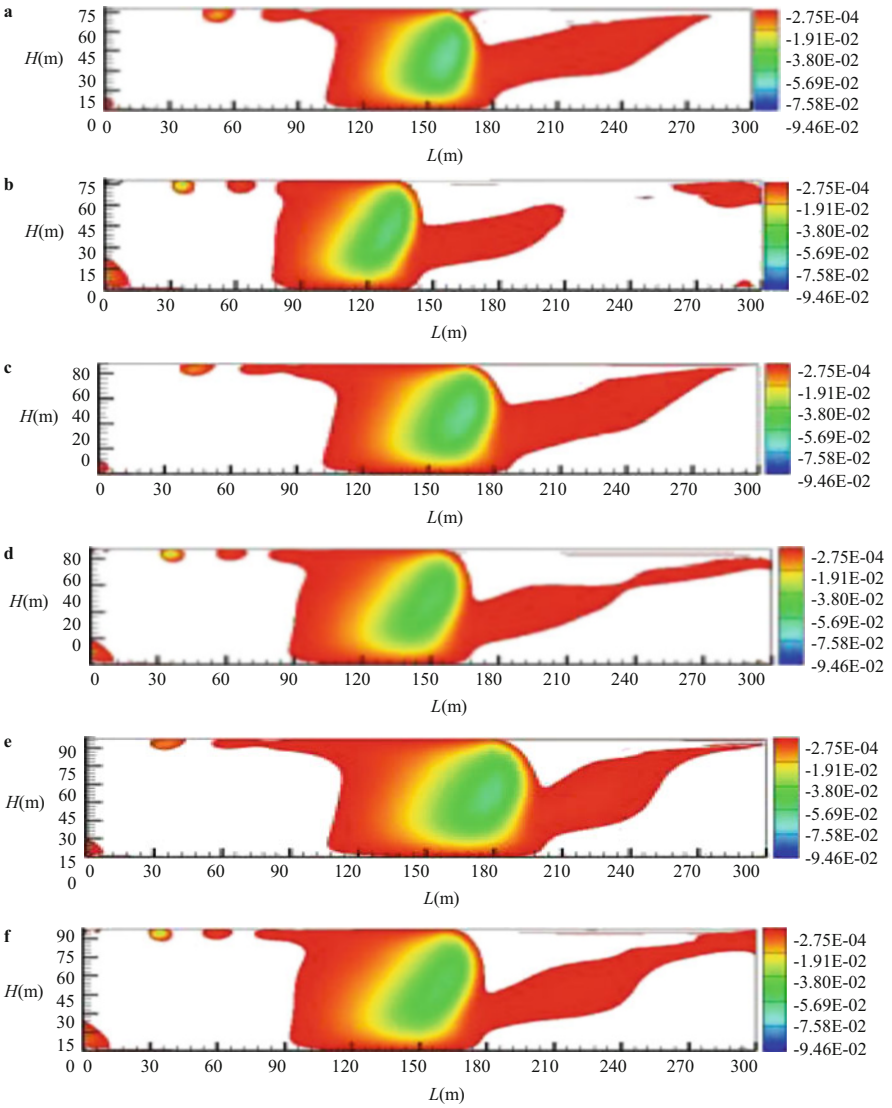

Fig. 29 Core algae inhibition zones outside submerged and non-submerged water-lifting aerators at different water depths: (**a**) submerged, $H = 77.25$ m, (**b**) non-submerged, $H = 77.25$ m, (**c**) submerged, $H = 87.25$ m, (**d**) non-submerged, $H = 87.25$ m, (**e**) submerged, $H = 97.25$ m, (**f**) non-submerged, $H = 97.25$ m

maximum distance of movement rightward of the inlet flow increased accordingly, which was manifested as the enlargement of the core algae inhibition zone area. For the submerged type, the upper surface was the main factor limiting the flow development, so the deeper the water, the weaker the effect of the upper surface and the further the flow circulation developed.

2. Mixing time of algae

The algae concentration decreasing to a constant value was taken as a sign of complete mixing of algae. The times required for complete algal mixing in three vertical directions and one lateral direction were analyzed. The distances were 20, 100, and 200 m from the aerator and 3 m below the water surface, respectively. As shown in Fig. 30, the *x*-axis represents the running time in hours. In Fig. 30a–c, the *y*-axis represents the simulated average algae concentration in the vertical direction, while in Fig. 30d, it represents the simulated average algae concentration in the horizontal direction. In the submerged aerator case, the times required for complete algal mixing in the three water depth conditions were roughly 10, 12, and 14 days, respectively. In the non-submerged case, the corresponding times were about 18, 19, and 20 days, respectively. In the non-submerged case, a longer time was needed for algae to completely mix compared to that in the submerged case. Complete mixing of algae in the submerged case could be achieved earlier, an effect that was very obvious in the vertical direction.

Therefore, as shown in Fig. 30a–c, the greater the water depth, the lower the algae concentration after complete mixing. In addition, at the beginning, the nearer to the aerator, the higher the algae concentration. That is because, in early operation, the circulation near the aerator side of the velocity field was small, influenced by the flow circulation. Algae far from the aerator were swept closer, so the algae concentration in the area close to the aerator was larger. For the adaptability of the flow, the water circulation to the right would react to the movement of the circulation near the aerator and spontaneously supplement the area near the aerator, where the algae concentration was lower, so the algae concentration in this flow area far from the aerator was further diluted. With the circulation developing more widely, the mixing of algae was more efficiently characterized by the algae concentration tending to be stable in every direction. As can be seen from Fig. 30d, the algae fraction near the surface was effectively reduced.

Considering the advantages of more effective algal inhibition, lower initial investment, and easier operational management, the submerged water-lifting aerator was suggested for engineering applications in stratified reservoirs.

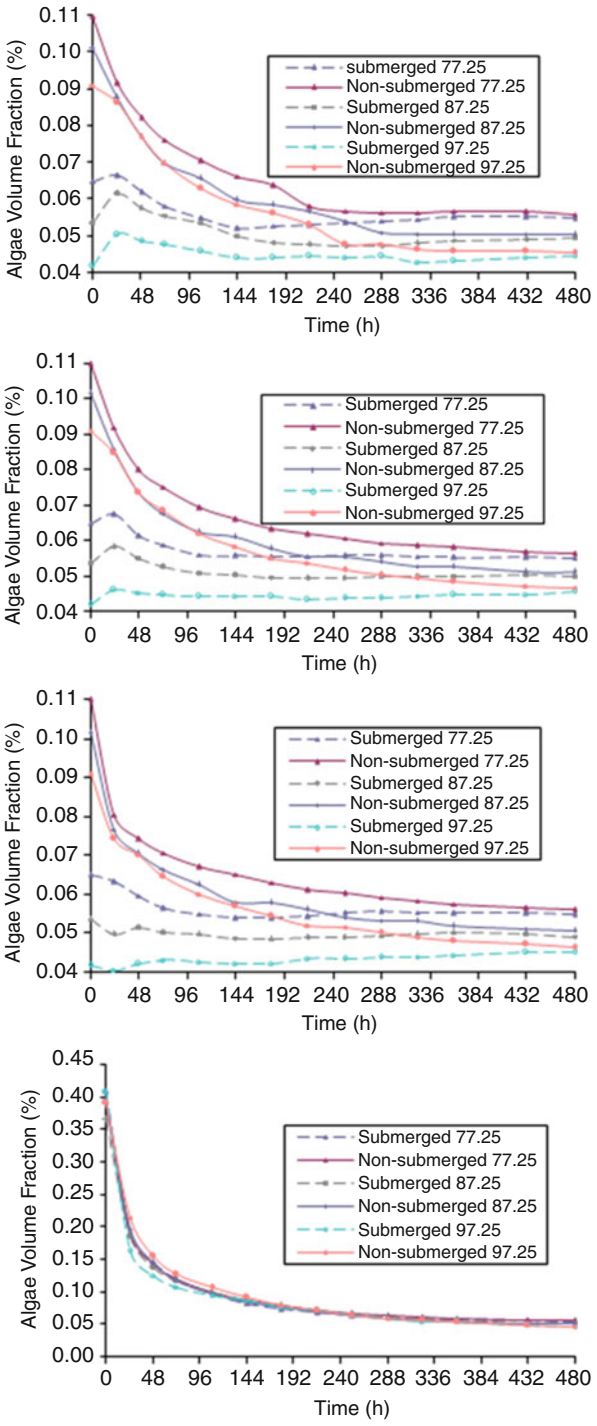

Fig. 30 Simulated times required for algae to completely mix for different aerator types: (**a**) 20 m horizontally from the aerator, (**b**) 100 m horizontally from the aerator, (**c**) 200 m horizontally from the aerator, (**d**) 3 m below the water surface

References

1. Kraus TEC, Bergamaschi BA, Hernes PJ et al (2011) How reservoirs alter drinking water quality: organic matter sources, sinks, and transformations. Lake Reservoir Manage 27 (3):205–219
2. Lui YS, Hong HC, Zheng GJS et al (2012) Fractionated algal organic materials as precursors of disinfection by-products and mutagens upon chlorination. J Hazard Mater 209:278–284
3. Zhang P, Zhai CM, Chen RQ et al (2012) The dynamics of the water bloom-forming *Microcystis aeruginosa* and its relationship with biotic and abiotic factors in Lake Taihu, China. Ecol Eng 47:274–277
4. Huang TL, Cong HB, Chai BB (2009) Source water quality pollution and control. China Architecture & Building Press, Beijing
5. Huang TL, Li X, Rijnaarts H et al (2014) Effects of storm runoff on the thermal regime and water quality of a deep, stratified reservoir in a temperate monsoon zone, in Northwest China. Sci Total Environ 485–486:820–827
6. Huang TL, Ma Y, Cong HB et al (2014) Application of the technology of water lifting and aeration on improving water quality in a Deep Canyon Reservoir – a case study from northern China. Desalin Water Treat 52(7–9):1636–1646
7. Sun X, Huang TL (2013) Water pollution control of lakes and reservoirs. Hubei Scientific and Technical Press, Wuhan
8. Lawson R, Anderson MA (2007) Stratification and mixing in lake Elsinore, California: an assessment of axial flow pumps for improving water quality in a shallow eutrophic lake. Water Res 41(19):4457–4467
9. Xu Y, Yang J, Ou M et al (2007) Study of Microcystis aeruginosa inhibition by electrochemical method. Biochem Eng J 36(3):215–220
10. Kotopoulis S, Schommartz A, Postema M (2009) Sonic cracking of blue-green algae. Appl Acoust 70(10):1306–1312
11. Cao CJ, Zheng BH, Chen ZL (2011) Eutrophication and algal blooms in channel type reservoirs: a novel enclosure experiment by changing light intensity. J Environ Sci 23 (10):1660–1670
12. Lundgren VM, Roelke DL, Grover JP et al (2013) Interplay between ambient surface water mixing and manipulated hydraulic flushing: implications for harmful algal bloom mitigation. Ecol Eng 60:289–298
13. Cong HB, Huang TL, Chai BB (2009) A new mixing–oxygenating technology for water quality improvement of urban water source and its implication in a reservoir. Renew Energy 34(9):2054–2060
14. Cong HB, Huang TL, Chai BB (2011) Research on applying a water-lifting aerator to inhibit the growth of algae in a source-water reservoir. Int J Environ Pollut 45(1–3):66–175
15. Sun X, Li XL, Zhang MD et al (2014) Comparison of water-lifting aerator type for algae inhibition in stratified source water reservoirs. Ecol Eng 73(12):624–634
16. Heo WM, Kim B (2004) The effect of artificial destratification on phytoplankton in a reservoir. Hydrobiologia 524(1):229–239
17. Liu L, Liu D, Johnson DM et al (2012) Effects of vertical mixing on phytoplankton blooms in Xiangxi Bay of Three Gorges Reservoir. Water Res 46(7):2121–2130
18. Simmons J (1998) Algal control and destratification at Hanningfield reservoir. Water Sci Technol 37(2):309–316
19. Jungo E, Visser PM, Stroom J (2001) Artificial mixing to reduce growth of the blue-green alga Microcystis in Lake Nieuwe Meer, Amsterdam: an evaluation of 7 years of experience. Water Sci Technol Water Supply 1(1):17–23
20. Cong HB, Huang TL, Chai BB (2011) Water-circulating aerator: optimizing structure and predicting water flow rate and oxygen transfer. J Hydraul Eng 137(6):659–667
21. Burris VL, Mcginnis DF, Little JC (2002) Predicting oxygen transfer and water velocity in airlift aerators. Water Res 36(18):4605–4615

22. Gantzer PA, Bryant LD, Little JC (2009) Effect of hypolimnetic oxygenation on oxygen depletion rates in two water-supply reservoirs. Water Res 43(6):1700–1710
23. Bryant LD, Hsu-Kim H, Gantzer PA et al (2011) Solving the problem at the source: controlling Mn release at the sediment–water interface via hypolimnetic oxygenation. Water Res 45 (19):6381–6392
24. Tofflon M, Ragazzi M, Righetti M et al (2013) Effects of artificial hypolimnetic oxygenation in a shallow lake. Part 1: phenomenological description and management. J Environ Manage 114:520–529
25. Zboray R, Cachard FD (2005) Simulating large-scale bubble plumes using various closure and two-phase turbulence models. Nucl Eng Des 235(8):867–884
26. Visser PM, Ketelaars HAM, Mur LR (1995) Reduced growth of the cyanobacterium microcystis in an artificially mixed lake and reservoir. Water Sci Technol 32(4):53–54
27. Goldyn R, Podsiadlowski S, Dondajewska R et al (2014) The sustainable restoration of lakes—towards the challenges of the Water Framework Directive. Ecohydrol Hydrobiol 14(1):68–74
28. Seo D, Jang DS, Kwon OH (1995) The evaluation of effects of artificial circulation on Daechung Lake, Korea. In: Proceedings of 6th international conference on the conservation and management of lakes, vol 11. pp 336–339
29. Sun X, Xu Y, Wang X et al (2014) Effects of water depth on algae control in stratified reservoirs by in-situ water-lifting aeration technology. Acta Sci Circumst 34(5):1166–1172
30. Cong HB (2007) Studies on source water quality improvement technology of water-lifting and aeration. Dissertation, Xi'an University of Architecture and Technology
31. Zhang YJ, Wang HY, Zhang ZP (1987) Two-phase fluid dynamics. Beihang University Press, Beijing
32. Little JC (1995) Hypolimnetic aerators: predicting oxygen transfer and hydrodynamics. Water Res 29(11):2475–2482
33. Zhang WS (2009) Modeling and Simulating of oxygen transfer and water flow rate in the aeration chamber of Water-lifting Aerator. Dissertation, Xi'an University of Architecture and Technology
34. Sun X, Duan FF, Huang TL et al (2013) Development and sensitivity analysis of model for aeration chamber in water-circulating aerator. Appl Mech Mater 261–262:663–668
35. Sun X, Zhang MD, Zhao WL et al (2013) Comparison of water-lifting aerator type for algae inhibition in deep reservoirs. Appl Mech Mater 295–298:1053–1056
36. Brodkey RS, Hershey HC (1988) Transport phenomena-a unified approach. McGraw-Hill, New York
37. Fried E, Idelchick IE (1989) Flow resistance: a design guide for engineers. Hemisphere Publishing, New York
38. Wüest A, Brooks NH, Imboden DM (1992) Bubble plume modeling for lake restoration. Water Resour Res 28:3235–3250
39. Trimmer M, Nicholls JC, Deflandre B (2003) Anaerobic ammonium oxidation measured in sediment along the Thames estuary, United Kingdom. Appl Environ Microbiol 69 (11):6447–6454
40. Zehr JP, Ward BB (2002) Nitrogen cycling in the ocean: new perspectives on processes and paradigms. Appl Environ Microbiol 68(3):1015–1024
41. Casey RE, Taylor MD, Klaine SJ (2004) Localization of denitrification activity in macropores of a riparian wetland. Soil Biol Biochem 36:563–569
42. Boatman CD, Murray JW (1982) Modeling exchangeable NH4+ adsorption in marine sediments: process and controls of adsorption. Limnol Oceanogr 27:99–100
43. Morin J, Morse JW (1999) Ammonium release from re-suspended sediment in the Laguna Madre estuary. Mar Chem 65:97–100
44. Beutel MW (2006) Inhibition of ammonia release from anoxic profundal sediments in lakes using hypolimnetic oxygenation. Ecol Eng 28(3):271–279
45. Bostom B, Andersen JM, Fleischer S, Jansson M (1988) Exchange of phosphorus across the sediment–water interface. Hydrobiologia 170:229–244

46. Kim LH, Choi E, Stenstrom MK (2003) Sediment characteristics, phosphorus types and phosphorus release rates between river and lake sediments. Chemosphere 50:53–61
47. Kim LH, Choi E, Gil KI et al (2004) Phosphorus release rates from sediments and pollutant characteristics in Han River, Seoul, Korea. Sci Total Environ 321:115–125
48. Cao HS, Tao Y, Kong FX et al (2008) Relationship between temperature and cyanobacterial recruitment from sediments in laboratory and field studies. J Freshw Ecol 23:405–412
49. Catherine Q, Susannac W, Isidoraa ES et al (2013) A review of current knowledge on toxic benthic freshwater cyanobacteria – ecology, toxin production and risk management. Water Res 47(15):5464–5479
50. Fluent Inc. (2006) FLUENT user's guide. Fluent Inc.
51. Sun X, Ye LL, Zhao WL et al (2014) Effect of temperature gradient on algal inhibition by in-situ water-lifting aeration in a stratified reservoir. China Environ Sci 34(2):352–358
52. Fluent Inc. (2006b) FLUENT user defined function manual. Fluent Inc.
53. Hodges BR (1999) Heat budget and thermodynamics at a free surface. Centre for Water Research, The University of Western Australia
54. Sun X, Shiono K, Chandler JH et al (2010) Discharge estimation in small irregular river using LSPIV. Proc Inst Civ Eng Water Manage 163(5):247–254
55. Gunawan B, Sun X, Sterling M (2012) The application of LS-PIV to a small irregular river for inbank and overbank flows. Flow Meas Instrum 24:1–12
56. Fischer HB, List JE, Koh CR et al (1979) Mixing in inland and coastal waters. Academic Press, London
57. Sun X, Shiono K (2009) Flow resistance of one-line emergent vegetation along the floodplain edge of a compound open channel. Adv Water Resour 32(3):430–438
58. Dou GR (1999) Incipient motion of coarse and fine sediment. Shuili Xuebao/J Hydraul Eng 6:1–9

Application of Water-Lifting Aerators in Reservoirs

Tinglin Huang, Xuan Li, Weixing Ma, Haibing Cong, and Jianchao Shi

Abstract Based on the water quality problems in three typical Chinese reservoirs, this chapter introduces the functions of water-lifting aerator (WLA) technology used in these reservoirs for water quality improvement and its engineering solutions. The main contents include: the composition of WLA systems, the layout and installation of WLAs and the compression pipeline, operation conditions, and parameters of WLA systems, and the improvement of WLA systems in order to solve the problems that occur during the operation period.

Keywords Water-lifting aerators • Water quality problems • Operation conditions • Technical parameters • System improvement

1 Application of Water-Lifting Aerators in Fenhe Reservoir

1.1 Background

Fenhe Reservoir is located 83 km to the northwest of the City of Taiyuan, Shan'xi Province, China, and it is the most important raw water source for the city. It serves as the regulating reservoir of the Wanjiazhai water diversion project from the Yellow River, which is the third hydraulic and second water diversion project in China. The water from the Yellow River is lifted 648 m by a five-step water pumping station, and delivered through 236 km of tunnels and conduit pipes to the Fenhe Reservoir. The water is then piped over 58 km to the Huyan drinking water treatment plant in Taiyuan City. From May 2004, the reservoir began to supply raw water to the drinking water treatment plant, and, currently, it supplies 200,000 m^3/day.

The ammonia concentration in the raw water increased abruptly to 1.6 mg/L on March 17, 2005, excessively exceeding the specified 0.5 mg/L raw water quality

T. Huang (✉) • X. Li • W. Ma • H. Cong • J. Shi
School of Environmental and Municipal Engineering, Xi'an University of Architecture and Technology, Yanta Road 13, 710055 Xi'an, Shaanxi Province, P. R. China
e-mail: huangtinglin@xauat.edu.cn

T. Huang (ed.), *Water Pollution and Water Quality Control of Selected Chinese Reservoir Basins*, The Handbook of Environmental Chemistry 38,
DOI 10.1007/978-3-319-20391-1_10

standard. With normal chlorine dosage, the concentration of the residual chlorine in the processed water from the Huyan Water Treatment Plant was zero. To meet the drinking water standard, a large amount of chlorine was added to the treated water. Unfortunately, the fishy and iron rust odors in the treated water raised a lot of complaints from consumers, and the plant was forced to stop the raw water supply from the Fenhe Reservoir until mid-May 2005 and turned to the groundwater as a temporary solution during that period.

The Fenhe Reservoir freezes in December every year and thaws in mid-March, with a freezing time of about 100 days and an ice layer thickness of about 45 cm. When the superficial water of the Fenhe Reservoir freezes in winter, the water is in a rest condition and water stratification occurs. The dissolved oxygen concentration in the lower-layer water decreases because of the oxygen consumption by the sediments and the lower-layer water gradually becomes anoxic. Under these conditions, the nitrogenous organic matter deposited in the reservoir's bed decomposes to form ammonia, which is then released into the lower-layer water [1]. Lacking any mixing, the released ammonia stays in the lower-layer water until the surface ice thaws in spring. The outlet to the water treatment plant is located within the surface layer; thus, the ammonia concentration in the outlet is not very high in winter. After the spring thaw, the ammonia concentration in the outlet suddenly rose because of wind–wave mixing. It was confirmed by the fact that the Fenhe Reservoir water thawed on March 16, 2005, and the ammonia concentration in the outlet water rose on March 17, 2005.

Clearly, in order to restrain the ammonia release from the sediments of the Fenhe Reservoir, the concentration of dissolved oxygen in the lower layer must be increased. So, a water-lifting aerator was used to solve this problem. The water-lifting aerator used in the Fenhe Reservoir has the following functions [2]:

1. To destroy water stratification by mixing the lower and upper layer waters; thus, the dissolved oxygen concentration in the lower-layer water can be increased.
2. To directly oxygenate the lower-layer water with the help of the aeration chamber.
3. To defreeze superficial water in the area around the water-lifting aerator; thus, oxygen can dissolve in the superficial water.
4. To allow the wind–wave mixing of the upper and lower-layer waters by stopping the water surface around the aerator from freezing.

1.2 The Water-Lifting Aerator System in the Fenhe Reservoir

1.2.1 System Layout

In the area within 2.5 km from the dam of the Fenhe Reservoir, the water is comparatively deeper, and it is about 13 m deep during the winter time. However, in the area beyond 2.5 km from the dam, the depth sharply decreases to between

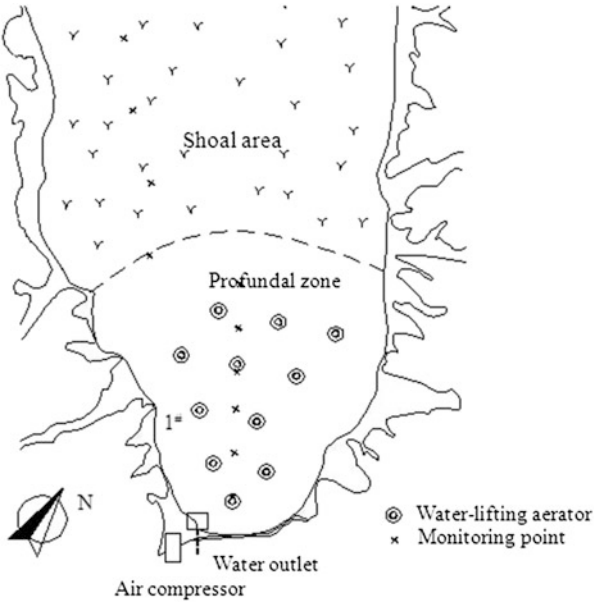

Fig. 1 Arrangement of the water-lifting aerators in the Fenhe Reservoir

2 and 5 m. A lot of aquatic plants are found in the shoal areas that grow well in winter. The dissolved oxygen concentration at the bottom of the shoal area is high because of the oxygenation caused by plant photosynthesis. So, the 11 water-lifting aerators are deployed only in the area near the dam and there is a 400-m spacing between the adjacent aerators. Figure 1 shows the deployment map.

As Fig. 2 shows, the water-lifting aerator has a diameter of 800 mm and a maximum length of 12 m, and can automatically adjust its length with the water level. Most of the aerator is made of steel panels, and only the sliding tube that moves with the water level is made of plastic. Each aerator is fixed to an anchor pier by non-rust steel wire ropes, with its inlet 1.5 m from the reservoir bed. The air-releasing tube is an annular pipe with a diameter of 80 mm and perforated with 564 holes with a diameter of 3 mm each. The air compressor, which forces the filtered air to the water-lifting aerator, sits on the bank. Each water-lifting aerator has a dedicated air supply duct made of DN75 polyethylene plastic pipe. The air supply ducts are settled on the reservoir bed, and they are bound with concrete blocks every 4 m.

1.2.2 Operation of the Water-Lifting Aerator

The Fenhe Reservoir froze on December 5, 2005. The water-lifting aerators began partial operation on January 17, 2006, and completely stopped on March 18, 2006, when the ice thawed. The air rate supplied to every water-lifting aerator was 2 m^3/min. The rate of circulating water flow produced by the water-lifting aerators was

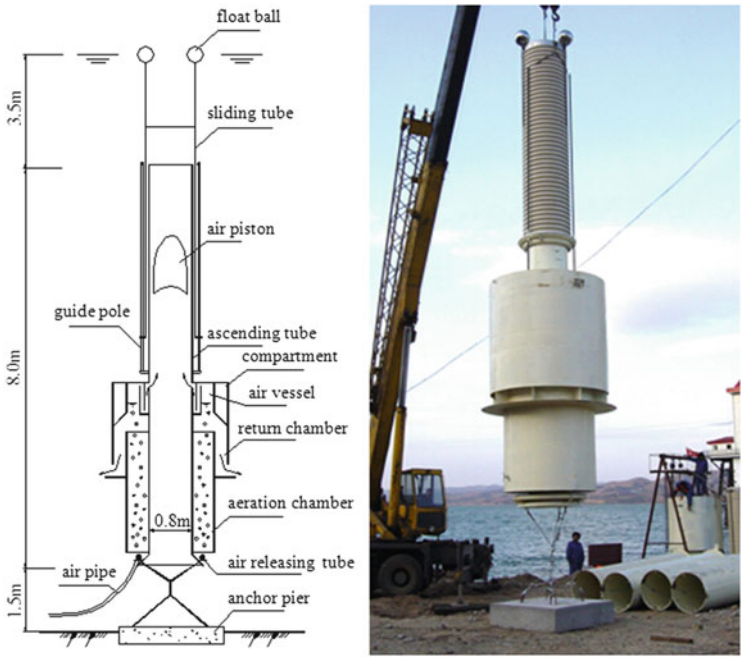

Fig. 2 Schematic diagram of the water-lifting aerator and its locale photo (used in the Fenhe Reservoir)

4.5×10^4 m^3/day according to the water-lifting model, and the oxygen quantity oxygenated by every aeration chamber was 70 kg/day, as calculated by the oxygenation model under the condition that the air supply rate was 2 m^3/min [3, 4].

After 8 h of operation, the ice layer had been broken by the flow coming from the water-lifting aerator's outlet which was 3 m below the water surface, and the water was jetted to a height of 2 m above the surface. The blast wave produced by the water-lifting aerator below the ice layer was detected 500 m away from the aerator, where the water surface fluctuated significantly when the ice was broken factitiously. Figure 3 shows a photograph of the scene when the water-lifting aerator is in operation.

The water waves produced by the water-lifting aerator continuously punched and broke the ice brim around water-lifting aerator, and the brim gradually expanded outward. After 10 days, there was no ice within a 40-m diameter centered on the water-lifting aerator. After 17 days, this increased to 80 m, and, 30 days later, it became 120 m. The wind energy also helped increase the ice-free area. The reservoir is located in a windy area with a prevailing northwest wind, which is in the same direction as the long axis of the reservoir. The windy season starts in December and ends in the following April. The waves caused by the wind causes the ice to shrink more quickly along the wind blowing direction. After 30 days, the length of ice-free area was 250 m, while the width was only 120 m. The waves also have an intense mixing effect on the water below the ice layer.

Fig. 3 The water-lifting aerator in operation

2 Application of the Water-Lifting Aerators in Jinpen Reservoir

2.1 Background

The Jinpen Reservoir is located in the City of Xi'an, Shaanxi Province, China, and it is the most important raw water source for the city, with a daily water supply of 8.0×10^5 m^3. The storage capacity of the Jinpen Reservoir is 2.0×10^8 m^3, with watershed area of 1481 km^2. In recent years, the environmental problem aroused by eutrophication has become severe, which certainly causes the increasing content of organic matter and algae, leading to an acute water quality problems considering that the urban drinking water is mainly supplied by this reservoir. According to the Chinese national drinking water standard, a large amount of chlorine had to be added into the treated water, which results in lots of complaints from consumers. After a series of investigations, the reservoir has the following water quality problems:

1. Increase of total nitrogen concentration. The total nitrogen in the Jinpen Reservoir was relatively low in 2005 (0.66–0.93 mg/L), with an annual average of 0.83 mg/L. The annual average total nitrogen increased to 0.91 mg/L in 2006, with a maximum of 0.98 mg/L, which could still meet the water quality standard of surface water environment (specified 1.0 mg/L). However, the concentration of TN increased rapidly in 2007, with an annual average of 1.18 mg/L, and the maximum concentration reached 2.55 mg/L in September. The increase of nutrients resulting in reservoir eutrophication represents a deterioration in water quality, and the restoration of eutrophic water bodies can be challenging [5, 6].
2. Harmful cyanobacterial blooms. Phytoplankton biomass was low, with an average chlorophyll-*a* concentration of less than 5 μg/L during the initial filling of Jinpen Reservoir. The increase of nutrients in the reservoir since 2006 led to intense blooms of cyanobacteria from July to October. A large number of green

flocs appeared on the surface of Jinpen Reservoir in July 2011, with an algal cell density of up to 30 million/L and the chlorophyll-*a* concentration exceeded 30 μg/L, including microcystis accounting for 78 %, seriously affecting the ecological balance of the reservoir. Thus, the Jinpen Reservoir can be categorized as a eutrophication reservoir [7, 8].

3. The release of endogenous pollutants from bottom sediments. Under anoxic conditions, pollutants in the sediments, such as organics, nitrogen (N), phosphorus (P), iron (Fe), and manganese (Mn), will be released into the water. A series of problems may be caused, such as color and odor [9, 10], the pH level may decrease, and the algae's multiplication may be accelerated. The Jinpen Reservoir has a long, stable period of stratification characterized by high stability of the water column, due to its location in a warm temperate climate and its canyon-shaped morphometry with a maximum depth of 80–95 m. This leads to a long period of anaerobic conditions at the bottom and, correspondingly, results in a significant deterioration of water quality as reduced chemical species continue to be released from the sediments and enter the hypolimnion [11, 12].

The water-lifting aerator used in the Jinpen Reservoir has the following functions:

- To reduce the quantity of algae in the upper layer of water whilst increasing it in the lower layer, thus making the algal distribution much more uniform. The decrease in algae in the upper layer reduced its production capacity, while the increase in algae in the lower layer accelerated algal death [13, 14].
- To resist the flotation of cyanobacteria, reduce the harmful competitive advantage of algae, and, thus, change the structure of the phytoplankton community [15].
- To destroy the water stratification by mixing the lower and upper-layer waters; thus, the entire vertical dissolved oxygen concentration can be increased.
- To directly oxygenate lower-layer water and promote the diffusion of dissolved oxygen, thus inhibiting the release of endogenous pollutants from the bottom sediments.

2.2 The Water-Lifting Aerator System in Jinpen Reservoir

The water-lifting aerator system in Jinpen Reservoir was improved from the submerged water-lifting aerator system used in the Fenhe Reservoir. It combined with the actual impoundment situation and the dynamic characteristics of the Jinpen Reservoir. The core component includes an aeration chamber, gas chamber, return chamber, watertight compartment, air release, and the working principle of water-lifting aerators in the Jinpen Reservoir (WLA-J) are essentially the same as the water-lifting aerators in the Fenhe Reservoir (WLA-F). The main differences between them included the following three points:

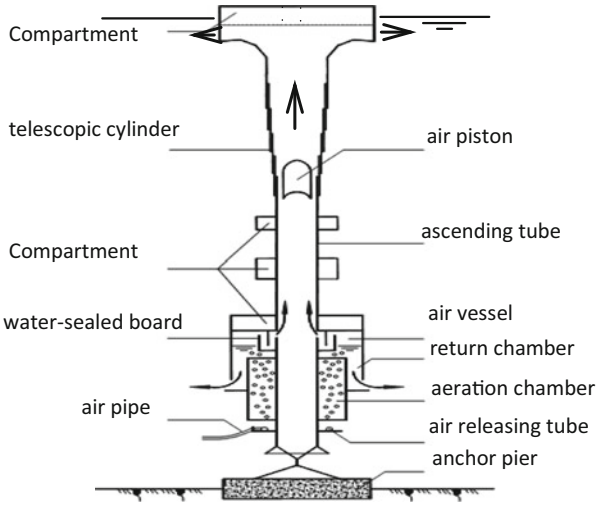

Fig. 4 Diagram of the water-lifting aerator configuration

1. Effluent type: The outlet of WLA-F is submersed in the water. The gas bomb produced by the aerator promotes water rising, which rushes vertically out of the equipment (Fig. 2). The outlet of WLA-J is located at the top and around the watertight compartment with a horizontal radial baffle. When it is in operation, the outlet is exposed above the water surface and we can see the effluent from the horizontal and vertical currents (Fig. 4). In deep water, the upflow has a large kinetic energy at the outlet. If there is no improvement, the water injection and spray vertically but are limited in horizontal agitation. This improvement aims to increase the water gravitational potential energy into horizontal energy and expands the working scope for the surface flow field (Fig. 5). This is important for algae control.
2. Buoyancy regulating: WLA-F is based on the watertight compartment in the cylinder to adjust the buoyancy. The upper sliding tube is made of plastic, though there is a float device, but its main function is to keep the equipment in the vertical position in water, not to provide buoyancy for it. And it also does not have the function of changing the direction of the outflow. WLA-J has a watertight compartment like a "mushroom head" with a diversion function. On the one hand, it can keep the equipment in overall vertical suspension; on the other hand, it can provide buoyancy for the massive telescopic cylinder using its large volume (2.6–2.8 m^3). Actually, in a deep reservoir, the main structure of the basic equipment uses carbon steel or stainless steel materials because of their strength and working stability. So, the equipment's weight is increased and the lower cylinder is of a fixed length, though its weight can balanced by the watertight compartment, but the upper stainless steel telescopic cylinder does not have buoyancy by itself, instead relying on other components to provide enough buoyancy to ensure balance.

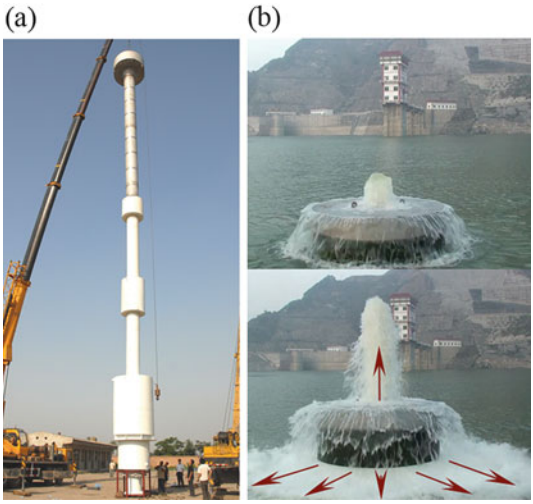

Fig. 5 The assembled water-lifting aerator (**a**) and the operation scene (**b**)

3. Adaptability of water level fluctuation: Both WLA-F and WLA-J use a telescopic device in response to water level changes. WLA-F is used at shallow water depth (10–30 m), its telescopic principle is based on a sliding tube along a vertical slider, and its adjustable range is relatively limited. WLA-J is used in deep reservoirs, such as Jinpen Reservoir. As the water level changes, the amplitude is bigger in a deep reservoir, so the adjustable range needs to increase correspondingly. The equipment uses a multilayer concentric cylindrical tube nested to make up the telescopic cylinder device, but it also invokes a greater requirement on the strength of the components. The minimum adjustable length is 6 m, and the maximum adjustable length is 34 m. It can automatically adjust with the water level fluctuation.

When the WLA-F is working, compressed air continues to be transferred into the annular air release tube, and releases air bubbles into the aeration chamber by the microporous pipe. The bubble rising process will dissolve oxygen diffusion into the water. At the same time, it will drive the flow upwards, and the oxygen-filled water is added to the bottom of the reservoir via the return chamber. The residual gas rises directly into the air chamber. When the air chamber is filled, it will instantaneously release into the cylinder and produce a gas bomb piston flow, which drives the water column in an accelerated motion until the gas bomb completely escapes out of the cylinder. Then, the water in the cylinder, under the inertial forces, continues to slowly rise, until the next gas bomb formation. The bottom water of Jinpen Reservoir is pumped by the water-lifting aerator onto surface, which mixes with the surface water and spreads horizontally, so the bottom water and surface water mixing cycle can continue.

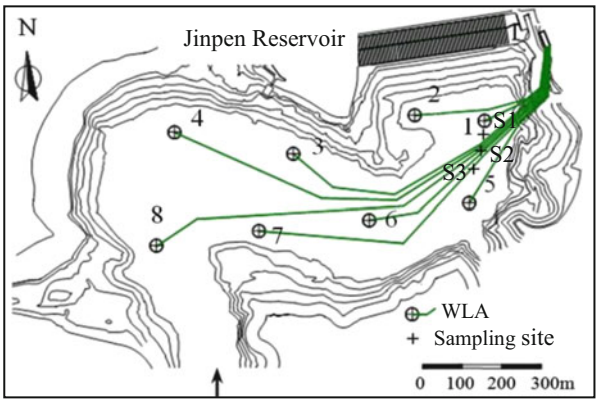

Fig. 6 Layout of water-lifting aerators in the Jinpen Reservoir

Table 1 The design parameters of the water-lifting aerator

Parameter		High water level (EL 594 m)	Low water level (EL 570 m)	Remark
Depth (m)		78.3–99.8	54.3–75.8	
Equipment height (m)		73.3–94.8	56.3–70.8	
Equipment diameter (mm)		750		Part 2100
Air flow (m^3/min)	Single	6.9		
	Total (8)	55.2		
Average flow rate (m/s)		2.8–2.9	2.7–2.8	
Water yield ($\times 10^4$ m^3/day)	Single	10.7–11.1	10.3–10.8	
	Total (8)	85.6–88.8	82.4–82.4	
Oxygenate (kg/day)	Single	100	100	The background DO content was 3 mg/L
	Total (8)	800	800	

2.3 *The Layout of the Water-Lifting Aerator System in Jinpen Reservoir*

The in situ restoration of water quality in Jinpen Reservoir is composed of water-lifting aerators, an air compressor system, and a pipeline system. Eight water-lifting aerators are deployed separately in the area within 1.1 km from the dam of the reservoir, and there is 250–300-m spacing between the adjacent aerators. The layout of the water-lifting and aeration system in Jinpen Reservoir is shown in Fig. 6, and the design parameters of the water-lifting aerator are detailed in Table 1.

Figure 7 shows a flow chart of the water-lifting aerator system in Jinpen Reservoir. The air compressor, which forces the filtered air into the water-lifting aerator, sits on the bank, connected to each water-lifting aerator with an air supply

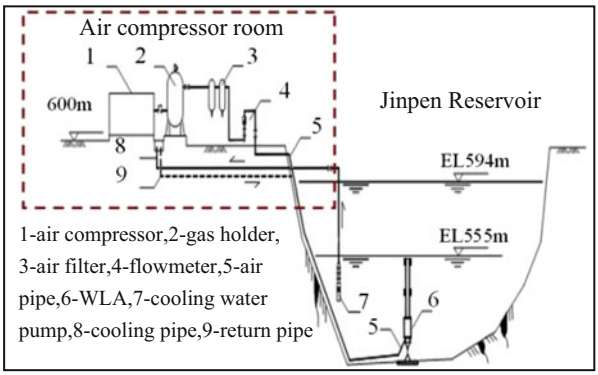

Fig. 7 Flow chart of the water-lifting aerator system

pipeline made of stainless steel for the onshore part and polyethylene for the underwater part. The water-lifting aerators begin partial operation from June to December every year. The air flow for each water-lifting aerator is 20–30 m^3/h with a supply pressure of 0.7–1 MPa. The rate of circulating water flow produced by the water-lifting aerators is 4.5×10^4 m^3/day.

2.4 Improvement of the Water-Lifting Aerators in Jinpen Reservoir

2.4.1 Reason for Water-Lifting Aerators Improvement in Jinpen Reservoir

1. The operation water level is lower than the design water level

   The rapid development of Xi'an City led to a sharp increase in urban water consumption. As the main water source, Jinpen Reservoir is run at full capacity. In recent years, extreme rainfall events occurred more often, which prolonged dry periods before rainfall events, as the total rainfall was not substantially changed in a short period of time. The long period of drought caused the water level decline rapidly before storm events. The lowest water level in 2010 was 564 m, in 2011 557.8 m, in 2012 556 m, and in 2013, it dropped to 551 m. But the design water level of the water-lifting aeration system is 570–594 m. Under the actual lowest water level condition, the equipment runs off the straight and cannot operate normally. If the equipment is forced to run under such conditions, it will increase the wear on the sliding components, and lead to failure of the sliding components and damage to the bottom air line. And because it is running off the straight, it will directly affect the uniformity of the equipment's inlet and outlet flows; it can even damage the water-lifting aeration system.

   In addition, though the guiding device at the top of the equipment uses streamlining to improve the surface water's mixing effect, the high-speed floating gas flares carry water; therefore, the gravitational potential energy

changes into horizontal flow energy and is consumed by the equipment on vertical impact (invalid work). This will cause the equipment to undergo periodic vertical stretching vibrations and the fluctuation amplitude can reach up to 1 m. It will affect the safe and stable operation of the entire equipment, so it needs to be improved.

2. Flood peak affects the normal operation of the system

   Existing equipment cannot achieve deep aeration oxygenation alone; this affects the normal operation in flood season. The design running condition of the water-lifting aeration system is all layers mixed; that is, from bottom to surface, the water is in full-thickness vertical mix. This operation mode is very difficult to improve water quality and control pollution with the conditions that change the water quality in different seasons.

   In recent years, significant turbid density flows followed large rainfall events, leading to the deterioration of reservoir water quality (3000 NTU, 2012), thus influencing the operation of water-lifting aerators during the flooding season. The water managers of the Heihe Reservoir suspend operation of the water-lifting aerators during storm runoff periods to avoid increasing the water turbidity of the upper layers, meanwhile selecting the appropriate intake height to avoid high outflow turbidity. However, anoxic conditions reappeared after the storm runoff ended, caused by the increase of the oxygen consumption rate, which could accelerate the release of pollutants from the bottom sediment [16, 17]. In addition, the reservoir surface algae means less breeding in the spring and early summer, but the bottom water is anaerobic. During this period, we should focus on the problem of the bottom water's aeration oxygen filling; the function of algae control is secondary. But existing equipment cannot achieve deep aeration oxygenation alone; this will lead to an increase in the energy consumption. In conclusion, to solve the problem of different water quality improvement, we must solve the bottom water aeration oxygen filling problem alone to ensure that the water quality is up to standard in the reservoir.

3. The installation height influences the aeration effect

   The device installation height was 5 m, which makes it difficult to achieve higher oxygenation rates. The running results show that the direct aeration functions of the water-lifting aerator was not effective below an installation height of 5 m. While the bottom water has direct contact with the sediment, the anoxic or anaerobic degree is the most serious. The key point of controlling internal pollution was to improve the water-dissolved oxygen at the bottom; thus, it can inhibit the release of Fe, Mn, nitrogen, and phosphorus from the sediment. In the normal operation of the water-lifting aerators, without causing sediment resuspension, inadequate equipment installation height should be reduced as much as possible, so as to improve the efficiency of oxygenation.

4. The high external pressure can destroy the air pipe when the water-lifting aerator system is stopped

   The maximum depth of Jinpen Reservoir is nearly 100 m. The internal pressure of the air pipe can reach 1.0–1.2 MPa and the hydrostatic pressure outside the pipe is about 0.9–1.1 MPa when the water-lifting and aeration system

operates at a high water level, while the inner and outer pressure is about 0.1 MPa, thus the air pipe can basically maintain the internal and external pressure balance. There was no adverse effect on the air pipe when the system is in operation. However, when the water-lifting aerator is stopped running, the water plug pipe formations cause a rapid reduction in the internal pressure of the air pipe, and the external hydrostatic pressure is constant, so the pressure difference increases sharply. The polyethylene air pipe is easily compressed and deforms at high pressure, which seriously influences the security and stability of the water-lifting and aerator system.

2.4.2 The Improved Method of the Water-Lifting Aerator System in Jinpen Reservoir

1. Adjust the design level by removing the slide adjuster and other components from the top.

   After the improvement, the lowest operation water level was reduced to 553 m. The elevation of the top of each water-lifting aerator was 549–551 m, with a submerged depth of 2–4 m at the lowest water level (553 m).
2. Replace the perforated aeration tube with a microporous aeration device

   Replace the perforated aeration tube with a microporous aeration device to strengthen the oxygenation to the isothermal layer.
3. Improve the gas chamber structure

   Improve the gas chamber structure for achieving single aeration with a small volume of gas (<20 m^3/h), and achieving the full layer's mixing and oxygenation functions with huge volumes of gas.
4. Reduce the installation height and improve the connection method of the anchor pier

   The water-lifting aerator equipment was 5.5 m from the sediment before being improved. In order to improve the oxygenation effect at the bottom, the installation height of each water-lifting aerator from the sediment needed to the reduced. Meanwhile, the installation height was high enough to avoid disturbance of the sediment at the bottom, which can increase water turbidity. Through hydraulic calculation, when the water-lifting aerator installation height was 2 m above the reservoir bottom, it will not disturb sediment at the bottom. Considering sediment deposition in Jinpen Reservoir, and having the security of surplus, the water-lifting aerator installation height was reduced from 5.5 to 3 m.
5. Improve and maintain the air pipe system

   Improve the compressed air line into the water connection and extend the stainless steel pipes for ensuring the long running life of the polyethylene tube at low water operating levels. Add a water injection system into the air pipe to maintain stability of the pipeline pressure. Improve the fixing method of the underwater air pipe in order to keep the underwater pipeline running stably (Fig. 8).

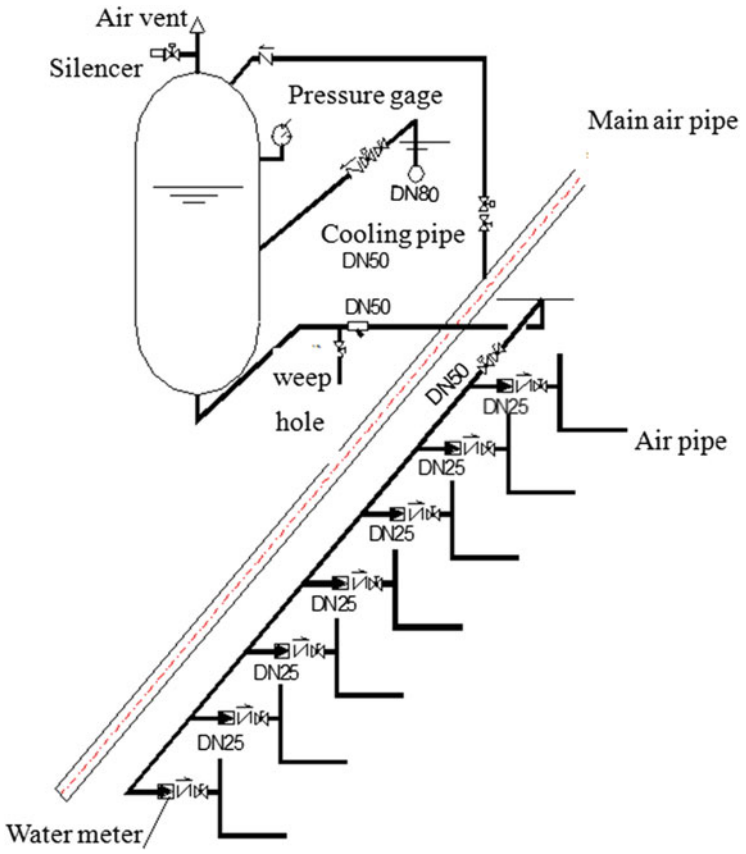

Fig. 8 Water injection system diagram

3 Application of the Water-Lifting Aerators in Shibianyu Reservoir

3.1 Background

The Shibianyu Reservoir is a stratified, eutrophication reservoir with annual average total nitrogen (TN) and total phosphorus (TP) concentrations of 2.8 and 0.041 mg/L, respectively [16, 17]. Summer stratification leads to the release of endogenous pollutants from the bottom sediment, accompanied by cyanobacteria blooms in the upper water that seriously affect the reservoir water quality [18, 19]. Two water-lifting aerators were installed in the reservoir for the experimental study to improve the water quality.

The water-lifting aerators used in Fenhe Reservoir were mainly made of steel panels, and only the sliding tube that moved with the water level was made of

plastic. This material was prone to severe electrochemical corrosion and pitting problems, which affect the long-term stable operation of the equipment. Stainless steel material was used for processing the water-lifting aerators that were applied in Jinpen Reservoir, in order to solve the corrosion problems. However, this increased the production cost and caused difficulties with installation and maintenance. To solve these problems, the water-lifting aerators employed in Shibianyu Reservoir use FRPP as the main material and 304 stainless steel as the auxiliary material. Equipment made of this material was easy to install and maintain, and it can also resist corrosion in water compared with the previously used steel panels.

3.2 The Water-Lifting Aerator System in the Shibianyu Reservoir

3.2.1 System Layout

WLA #1was located close to the dam. The water depth of this region is relatively shallow, but experiences serious cyanobacterial blooms. WLA #2 was located at the deepest point of the reservoir, which experiences stable summer stratification.

3.2.2 Operation of the Water-Lifting Aerators

The installation of water-lifting aerators was completed in late August 2012. The reservoir experienced heavy rainfall prior to the operation of the water-lifting aerators. This heavy rain lasted for 2 days and generated a total rainfall of 134.1 mm. The reservoir level rose by 12.8 m due to this storm runoff, which strongly influenced the stratification structure. As Fig. 9a shows, the water temperature difference between the surface and the lower layer decreased due to the rainstorm runoff. After the heavy rain, the temperature gradient at a water depth of 45 m or less was only 0.1 °C/m, while a large temperature gradient was observed from 45 m to the bottom (approximately 1.3 °C/m). This storm runoff did not affect the water temperature and anoxic condition in the bottom water (Fig. 9b).

Due to the high nutrient input into the reservoir by the heavy rain, cyanobacteria blooms appeared again approximately 1 week after the heavy rain [20, 21]. The two water-lifting aerators then began to operate to improve the water quality for this study. Figure 10b, c show a photograph of the scene when the water-lifting aerators were in operation. The water-lifting aerators operated from September 10 to October 22, and the initial 10 days were the debugging stage (the water-lifting aerators only operated in the daytime to investigate the stability of the new material). The submerged depth, compressed air flow, and time interval of the air piston during regular operation (24 uninterrupted hours) were approximately 15 m, 14 m^3/h, and 4.1 min for WLA #1 and 35 m, 28 m^3/h, and 2.3 min for WLA #2, respectively.

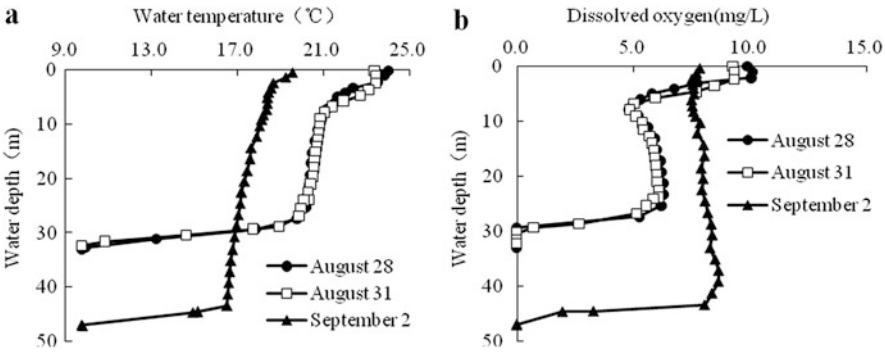

Fig. 9 Vertical distributions of water temperature (**a**) and dissolved oxygen (**b**) at the deepest monitoring site in the Shibianyu Reservoir before and after storm runoff

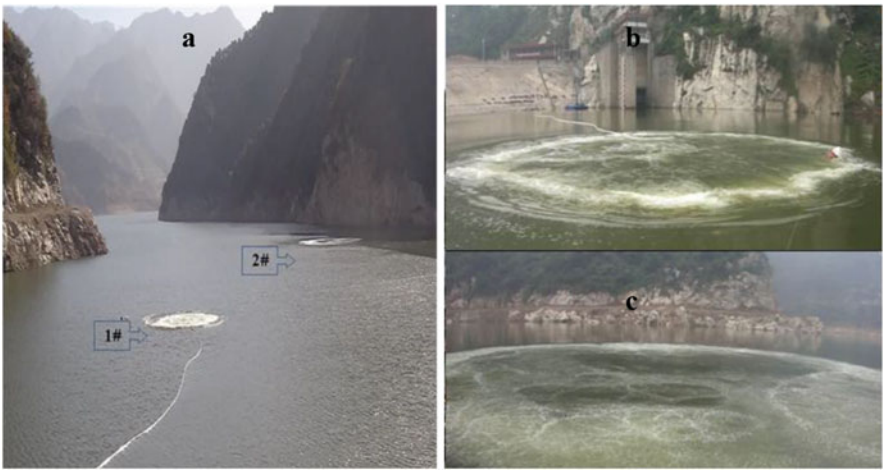

Fig. 10 Arrangement of the water-lifting aerators in the Shibianyu Reservoir (**a**) and the scene when 1# water-lifting aerator (**b**) and 2# water-lifting aerator (**c**) were in operation

References

1. Beutel MW (2006) Inhibition of ammonia release from anoxic profundal sediments in lakes using hypolimnetic oxygenation. Ecol Eng 28:271–279
2. Cong HB, Huang TL, Chai BB, Zhao JW (2009) A new mixing–oxygenating technology for water quality improvement of urban water source and its implication in a reservoir. Renew Energy 34:2054–2060
3. Burris VL, McGinnis DF, Little JC (2002) Predicting oxygen transfer and water flow rate in airlift aerators. Water Res 36:4605–4615
4. Cong HB, Huang TL, Chai BB (2010) Water-circulating aerator: optimizing structure and predicting water flow rate and oxygen transfer. J Hydraul Eng 137:659–667

5. Conley DJ, Paerl HW, Howarth RW, Boesch DF, Seitzinger SP, Havens KE, Lancelot C, Likens GE (2009) Controlling eutrophication: nitrogen and phosphorus. Science 323:1014–1015
6. Girmay G, Singh B, Nyssen J, Borrosen T (2009) Runoff and sediment-associated nutrient losses under different land uses in Tigray, Northern Ethiopia. J Hydrol 376:70–80
7. Paerl HW, Xu H, McCarthy MJ, Zhu G, Qin B, Li Y, Gardner WS (2011) Controlling harmful cyanobacterial blooms in a hyper-eutrophic lake (Lake Taihu, China): the need for a dual nutrient (N & P) management strategy. Water Res 45:1973–1983
8. O'Neil J, Davis T, Burford MA, Gobler C (2012) The rise of harmful cyanobacteria blooms: the potential roles of eutrophication and climate change. Harmful Algae 14:313–334
9. Pettersson K (2001) Phosphorus characteristics of settling and suspended particles in Lake Erken. Sci Total Environ 266:79–86
10. Zaw M, Chiswell B (1999) Iron and manganese dynamics in lake water. Water Res 33:157–164
11. Branco CWC, Kozlowsky-Suzuki B, Sousa-Filho IF, Guarino AWS, Rocha RJ (2009) Impact of climate on the vertical water column structure of Lajes Reservoir (Brazil): a tropical reservoir case. Lakes Reserv Res Manag 14:175–191
12. Beutel MW, Leonard TM, Dent SR, Moore BC (2008) Effects of aerobic and anaerobic conditions on P, N, Fe, Mn, and Hg accumulation in waters overlaying profundal sediments of an oligo-mesotrophic lake. Water Res 42:1953–1962
13. Upadhyay S, Bierlein KA, Little JC, Burch MD, Elam KP, Brookes JD (2013) Mixing potential of a surface-mounted solar-powered water mixer (SWM) for controlling cyanobacterial blooms. Ecol Eng 61:245–250
14. Kim HK, Kim JM, Lee YJ (2007) Vertical profile of algal distribution during aeration prior to intake tower for safe drinking water. Water Sci Technol 55:321–327
15. Liu L, Liu D, Johnson DM, Yi Z, Huang Y (2012) Effects of vertical mixing on phytoplankton blooms in Xiangxi Bay of Three Gorges Reservoir: implications for management. Water Res 46:2121–2130
16. Huang TL, Li X, Ma WX, Qin CH, Zhang YT (2014) Dynamic characteristics of nutrients and causal analysis in eutrofic reservoir: a case study of Shibianyu reservoir. Dsealination Water Treat 52:1636–1646
17. Huang TL, Li X, Rijnaarts H, Grotenhuis T, Ma WX, Sun X, Xu JL (2014) Effects of storm runoff on the thermal regime and water quality of a deep, stratified reservoir in a temperate monsoon zone, in Northwest China. Sci Total Environ 485–486:820–827
18. Wang S, Qian X, Han BP, Luo LC, Hamilton DP (2012) Effects of local climate and hydrological conditions on the thermal regime of a reservoir at Tropic of Cancer, in southern China. Water Res 46:2591–2604
19. Burford MA, Johnston SA, Cook AJ, Packer TV, Taylor BM, Townsley ER (2007) The relative importance of watershed and reservoir characteristics in promoting algal blooms in subtropical reservoirs. Water Res 41:4204–4214
20. Piehler MF, Dyble J, Moisander PH, Chapman AD, Hendrickson J, Paerl HW (2009) Interactions between nitrogen dynamics and the phytoplankton community in Lake George, Florida, USA. Lake Reserv Manag 25:1–14
21. Rueda FJ, Fleenor WE, de Vicente I (2007) Pathways of river nutrients towards the euphotic zone in a deep-reservoir of small size: uncertainty analysis. Ecol Model 202:345–361

Water Quality Improvement by Water-Lifting Aerators

Tinglin Huang, Xuan Li, Weixing Ma, and Haibing Cong

Abstract This chapter presents the results of water quality improvement performed in three different types of Chinese reservoirs after the installation of water-lifting aerators and the improved equipment during the period of 2006–2013. The results showed that the technology of water-lifting aerators can effectively control the release of endogenous pollutants, inhibit algal blooms, remove volatile contaminants (VOC), and reduce the pollution load in reservoirs. Compared to the same conditions, the algae can be reduced by 75–90 %, ammonia can be reduced by 69–95 %, TP can be reduced by 63–97 %, Fe/Mn can be reduced by 67–90 %, VOC can be reduced by 80–90 %, TN can be reduced by 19–32 %, and COD_{Mn} can be reduced by 16–26 %.

Keywords Mixing • Aeration • Stratification • Endogenous pollution • Cyanobacterial blooms

1 Water Quality Improvement in Fenhe Reservoir

Two sorts of data were collected to evaluate the water quality improved by water-lifting aerators in Fenhe Reservoir. One is the water quality distribution around the #1 water-lifting aerator, and the other is the water quality distribution over the whole deep-water area. Tests of the dissolved oxygen (DO), ammonia (NH_4-N), and temperature were carried out. The tests of the dissolved oxygen and temperature took place on-site, while the ammonia test was done in the laboratory with samplings. All on-site tests were performed from January 16 to March 1, 2006, during which the ice of the test site was thick enough to allow access for the test personnel.

T. Huang (✉) • X. Li • W. Ma • H. Cong
School of Environmental and Municipal Engineering, Xi'an University of Architecture and Technology, Yanta Road 13, 710055 Xi'an, Shaanxi Province, P. R. China
e-mail: huangtinglin@xauat.edu.cn

T. Huang (ed.), *Water Pollution and Water Quality Control of Selected Chinese Reservoir Basins*, The Handbook of Environmental Chemistry 38,
DOI 10.1007/978-3-319-20391-1_11

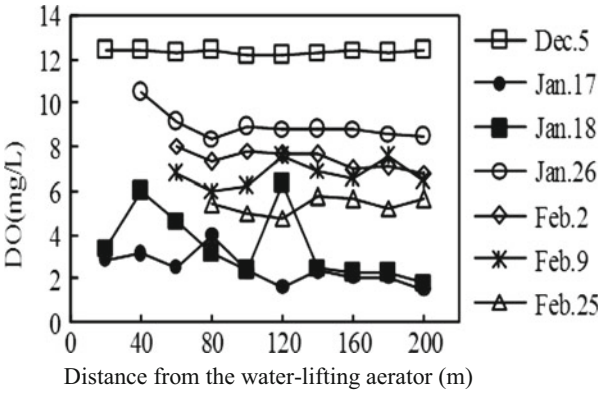

Fig. 1 DO distribution around the #1 water-lifting aerator at 0.5 m above the sediment surface

1.1 The Water Quality Distribution Around the Water-Lifting Aerator

1.1.1 The Distribution of Dissolved Oxygen Around the Water-Lifting Aerator

The monitoring sites were set up every 20 m along the east radial direction of the #1 water-lifting aerator. The dissolved oxygen concentration at different depths was tested through holes made through the ice surface. The concentration of dissolved oxygen above the sediment surface has an important effect on the release of ammonia. The concentrations of dissolved oxygen within 0.5 m above the sediment surface are plotted in Fig. 1.

As seen in Fig. 1, before freezing on December 5, 2005, the water was saturated with dissolved oxygen because the persistent and intensive wind-wave mixing made the entire water body homogeneous. After 42 days, namely on January 17, 2006, the dissolved oxygen concentration in the water 0.5 m above the sediment surface was only 1.5–3 mg/L. It was an appropriate time to start the operation of the water-lifting aerators. Consequently, the dissolved oxygen concentration in the lower layer started to rise and increased more quickly in the area close to the aerator. The dissolved oxygen concentration in the water 0.5 m above the sediment layer stayed above 3 mg/L until the ice melted. The concentration of dissolved oxygen in the lower layer increased to 8 mg/L in a short time due to the additional effects of the intensive wind-wave mixing.

The vertical distribution of the dissolved oxygen around the water-lifting aerator is shown in Fig. 2. As can be seen from this graph, before freezing, the dissolved oxygen concentration had a uniform vertical distribution with an average concentration of 12.4 mg/L. Forty-two days later, as the water-lifting aerator started to operate, an obvious change in the vertical distribution can be seen.

The dissolved oxygen concentration at the sediment surface had fallen to 1–2 mg/L, while that at the water surface was slightly changed. This indicates that the sediment oxygen consumption caused the rapid decrease in the lower layer water's

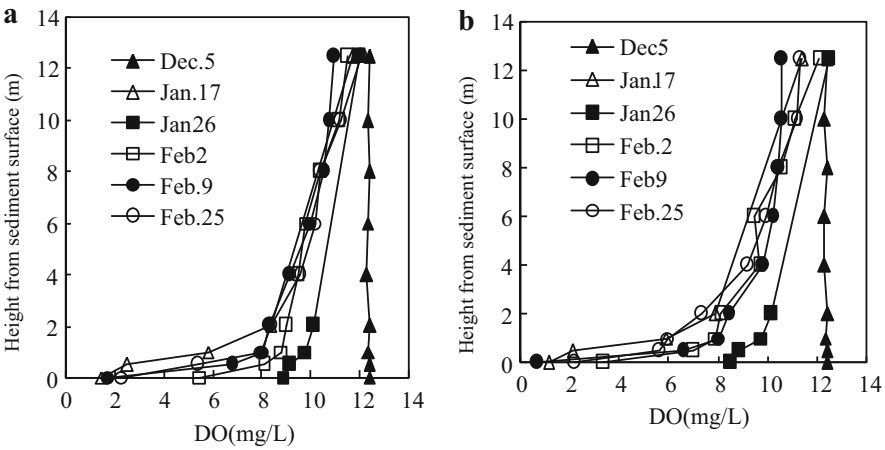

Fig. 2 Vertical distribution of dissolved oxygen at 60 m (**a**) and 160 m (**b**) from the #1 water-lifting aerator

dissolved oxygen concentration. The variation in the dissolved oxygen concentration from the water surface to 2 m above the sediment surface was not sharp, being 11.5–8 mg/L. Yet, in the lowest 2 m above the sediment, the variation is sharp, and the concentration decreased rapidly from 8 to 1–2 mg/L. This illustrates that, without the influence of external mixing, the diffusion of the dissolved oxygen was slow. However, through aerating and mixing by the water-lifting aerators and wind-wave mixing, the difference in the dissolved oxygen concentration between the upper and lower layers was reduced and the nearer to the water-lifting aerator, the better the effects. However, the difference between the upper and lower layers was still large.

1.1.2 Ammonia Distribution Around the Water-Lifting Aerator

The change of ammonia concentrations around the water-lifting aerator at the sediment surface is shown in Fig. 3, and the vertical distributions of the ammonia concentration at 60 m and 160 m from the water-lifting aerator are shown in Fig. 4. As seen from the two graphs, in general, the values of the ammonia concentration are low. At the beginning of water-lifting aerator operation, the ammonia concentration in the lower layer is apparently higher than that in the upper layer. As the water-lifting aerator operated, the ammonia concentration in the lower layer decreased gradually, and the rate of decrease in the ammonia concentration near the aerator was slightly greater than those farther away. The ammonia concentration in the upper layer increased slightly, and the concentration in the upper and lower layers became more uniform. This indicates that the release of ammonia from the sediment was restrained by the operation of the water-lifting aerator and that the mixing made the ammonia concentration in the upper and lower water layers homogeneous.

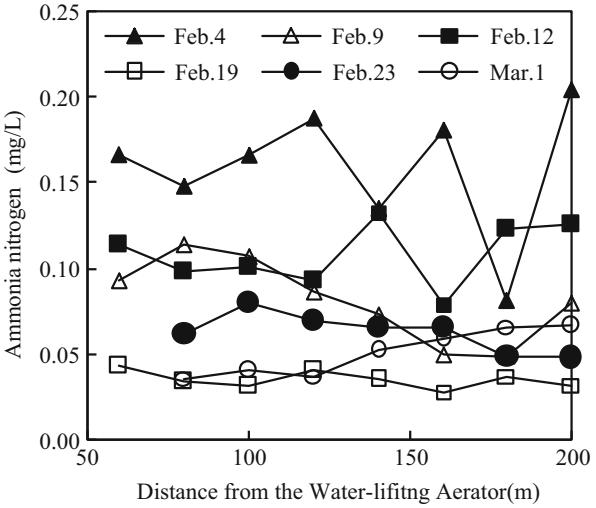

Fig. 3 NH_4-N distribution around the #1 water-lifting aerator at the sediment surface

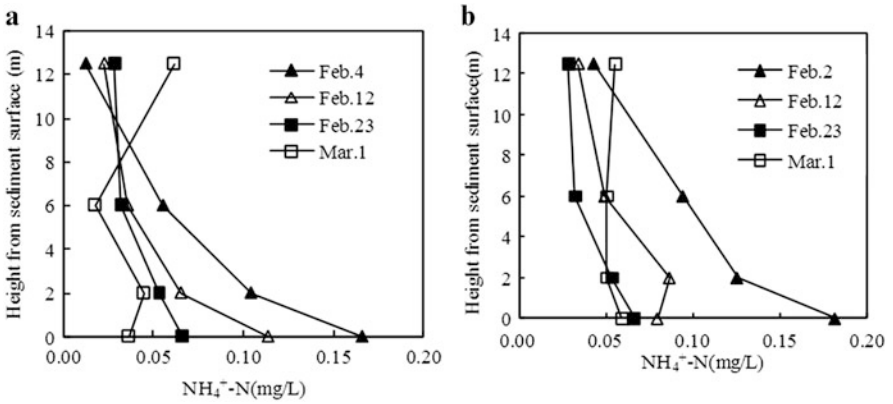

Fig. 4 Vertical distribution of NH_4-N at 60 m (**a**) and 160 m (**b**) from the #1 water-lifting aerator

1.1.3 Water Temperature Distribution Around the Water-Lifting Aerator

The vertical distributions of the water temperature on February 2, 13, and 25, 2006 are shown in Fig. 5. As seen from the graph, at the beginning of water-lifting aerator operation, the water temperature in the lower layer was apparently higher than that in the upper layer. Because of mixing by the water-lifting aerator, the difference in water temperature between the upper and lower layer waters near the water-lifting aerator was smaller than those farther away. As the water-lifting aerator operated, the water temperature in the upper layer increased gradually, while that in the lower layer was always about 4 °C because the water density is the greatest at this temperature.

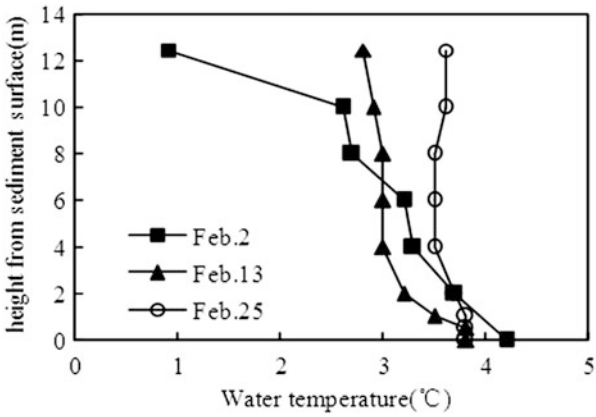

Fig. 5 NH_4-N distribution around the #1 Water-lifting aerator at the sediment surface

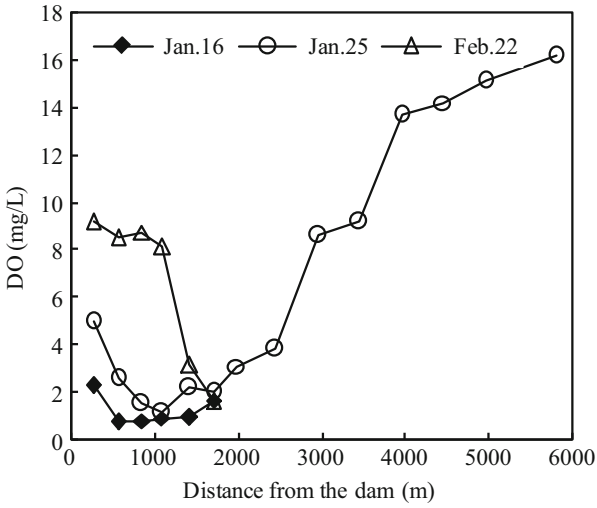

Fig. 6 Distributions of dissolved oxygen at the sediment surface along the reservoir's long axis

1.2 Water Quality Distribution in the Reservoir

The monitoring points were distributed along the axial direction of the reservoir every 300–500 m, as shown in Fig. 1 of the chapter entitled "Application of Water-Lifting Aerators in Reservoirs". The concentrations of dissolved oxygen at these monitoring points are shown in Fig. 6. As seen in the graph, when the water-lifting aerator started to operate, the dissolved oxygen concentration at the sediment surface began to increase, and the increase in the area near the dam is greater than that of other areas. This is because this area was in the wind direction, and it experienced intensive mixing by wind-waves in the ice-free area. In addition, the dissolved oxygen concentration in the shoal area was tested on January 25, 2006 and the value for the area beyond 2.5 km from the dam was relatively higher at 9–

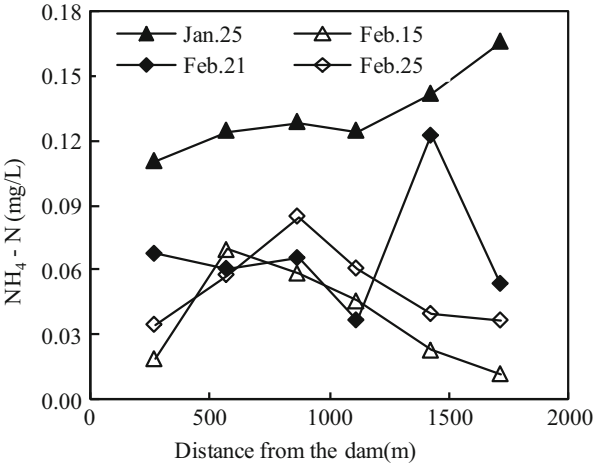

Fig. 7 Distributions of ammonia concentration at the sediment surface along the reservoir's long axis

16 mg/L. The more shallow the water, the higher the dissolved oxygen concentration. This is because there was a lot of aquatic plants, which photosynthesized and produced oxygen to saturate the water.

The test results of ammonia concentration at the sediment surface along the reservoir's longitudinal axis are plotted in Fig. 7. As seen in the graph, the ammonia concentration in the sediment decreases and maintains a very low level after the water-lifting aerator began operation.

1.3 Outlet Water Quality of the Reservoir

A gale lasted for several days following the thaw of Fenhe Reservoir on March 18, 2006. This wind-wave made the upper and lower layer waters mix adequately. The ammonia nitrogen concentration at the reservoir outlet was continually monitored from March 13 to March 27, 2006. The results show that the ammonia concentration in the outlet water was very low at 0.02–0.05 mg/L, which is a remarkable reduction of 95 % as compared to the same period in 2005. The sudden rise of the ammonia concentration in the reservoir did not reoccur in 2006 (Fig. 8).

1.4 Advantage Analysis

The water-lifting aerator system in Fenhe Reservoir operates for 2 months every year before the surface ice thaws. The operation cost, which is mainly the electricity cost of the air compressor, is about 0.016 Yuan RMB/m^3. Another scheme to solve the problem of ammonia concentration exceeding the quality standard was designed

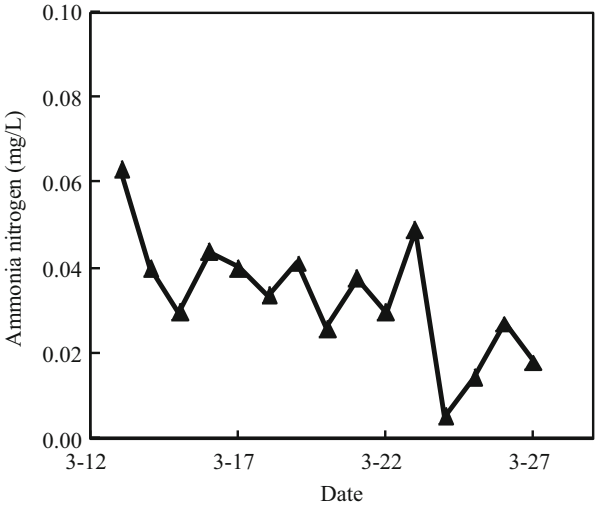

Fig. 8 Distribution of ammonia in outlet water after the reservoir thawed

while the water-lifting aerator system was being constructed. In the scheme, chlorine and powder active carbon would be put into raw water at the water supply duct before it enters the water treatment plant. This treatment technology would operate for 2 months after the ice thaws. The operation cost, which is mainly composed of chlorine and powder active carbon spending and electricity cost, is about 0.07 Yuan RMB/m^3. Compared with traditional treatment technology, the water-lifting aerator water quality improvement technology has some advantages as follows:

1. Energy-saving and saves costs of 77 %. With the help of wind energy, the water-lifting technology uses less energy to mix the upper and the lower layers.
2. Sanitary and has no side effects. The Water-lifting technology prevents the problem from arising, while traditional technology solves the problem after it has occurred. Adding chlorine into raw water will produce disinfection by-products and odors [1, 2].
3. No reaction on subsequent treatment processes. Adding powder active carbon into raw water will increase turbidity and append additional burden on the flocculation and sedimentation processes in the water treatment plant.

Consequently, the water-lifting water quality improvement technology is a sanitary, energy-saving, and continuable technology.

2 Water Quality Improvement in Jinpen Reservoir (2010)

The water-lifting aerators are in partial operation from June to December every year. The supplied rate of each water-lifting aerator is 20–30 m^3/h, with a supply pressure of 0.7–1 MPa. The rate of circulating water flow produced by the water-lifting aerators is 4.5×10^4 m^3/day.

Two sorts of data were collected to evaluate the water quality improved by the water-lifting aerator. One is the water quality distribution at monitoring point S1, 20 m from the #3 water-lifting aerator (which is a typical aerator selected for investigating the effect of water quality improvement around water-lifting aerators; the location of the #3 aerator is shown in Fig. 2); the other is the water quality distribution over the whole deep-water area: S2 (20 m from the #5 water-lifting aerator); S3 (200 m from the #8 water-lifting aerator); S4 (400 m from the #8 water-lifting aerator).

2.1 Water Quality Improvement at Monitoring Point S1: the Distribution of Dissolved Oxygen Around the Water-Lifting Aerator

The variation in the vertical distribution of dissolved oxygen was significantly influenced by the thermal stratification in Jinpen Reservoir (Fig. 9). During the mixed period (January to early March), the structure of stratification disappears, the entire reservoir stayed in the aerobic condition, and the water quality tended to be uniform. From mid-March, the stratification pattern of dissolved oxygen gradually emerged. In June, the vertical water exchange was severely limited by the stable stratification structure. The oxygen consumed could not be compensated and the dissolved oxygen began to decrease rapidly. As shown in the Fig. 9a, b, during the period from June to December in 2008 and 2009, the concentration of dissolved oxygen at the point S1 decreased rapidly with the increasing water depth and the average variation gradient at the fracture surface reached 0.06–0.12 mg/L m^{-1}. The concentration of dissolved oxygen at the sediment surface decreased from 5–6 mg/L in June to around 2 mg/L in mid-July, achieving the anoxic condition (Fig. 10). After September, the dissolved oxygen concentrations continued to decline and the entire bottom of the reservoir became anaerobic. Since the water-lifting aerators were put into operation, the vertical dissolved oxygen concentration improved significantly over the same period of 2008 and 2009 (Fig. 9c). With the depth range from 0 to 50 m, the dissolved oxygen concentration decreased slowly and remained relatively stable above 7 mg/L; with a water depth greater than 50 m, the dissolved oxygen concentrations stay around 2.5 mg/L, without attaining anoxic or anaerobic concentrations.

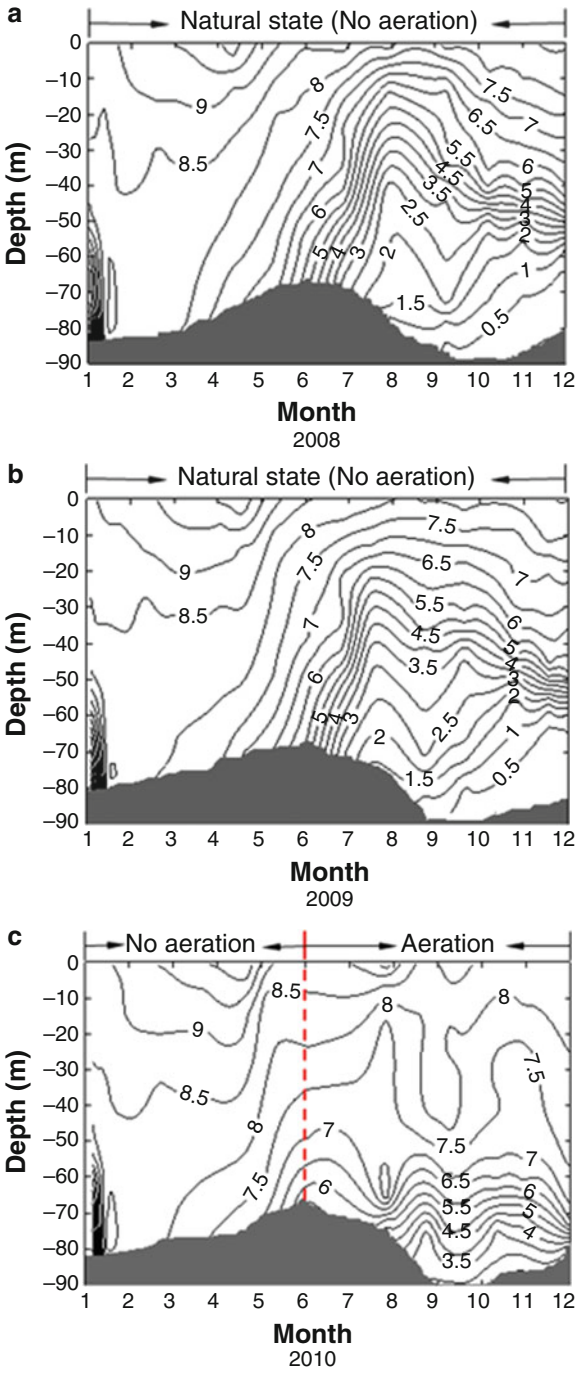

Fig. 9 Vertical dissolved oxygen distribution in Jinpen Reservoir from 2008 to 2010

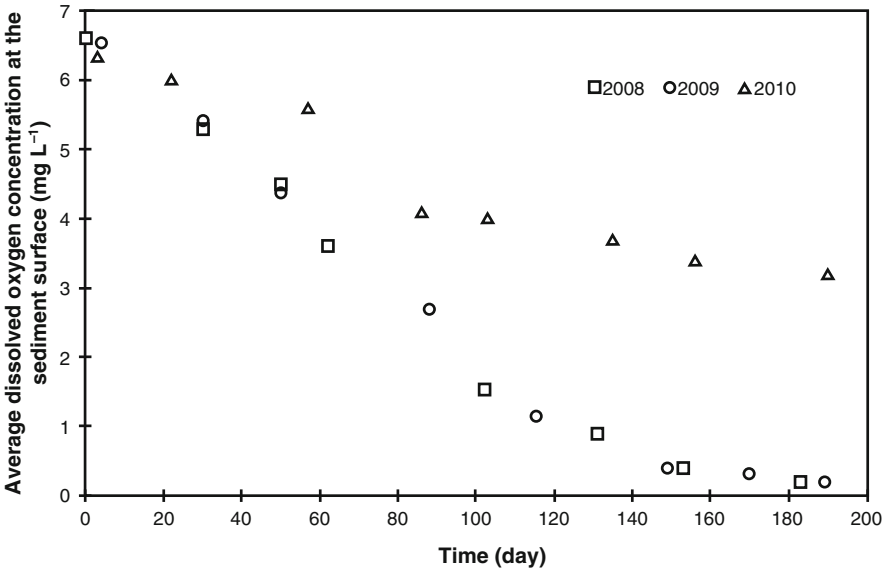

Fig. 10 Variance of dissolved oxygen concentrations at the sediment surface from 2008 to 2010

2.1.1 Effects on Inhibiting the Release of Endogenous Pollution

The ammonia and phosphorus concentrations around the water-lifting aerator at three different depths from 2008 to 2010 are shown in Fig. 11a, b. The results indicated that, during the mixed period of 2008 and 2009, the release of pollutants from the sediment remains shortly stagnant and the homogeneity of ammonia and phosphorus concentrations in different layers was observed. After the thermostratification, the concentrations of ammonia and phosphorus augment with increasingly severe anoxic and anaerobic conditions, extending towards the upper layers until attaining the maximum concentrations of 0.24–0.27 mg/L and 0.63–0.73 mg/L, respectively. As the water-lifting aerator operated in 2010, the total phosphorus and ammonia concentrations in the lower layer decreased remarkably and remained stable at around 0.01–0.06 mg/L and 0.05–0.12 mg/L, respectively, which indicated that the release of the phosphorus and ammonia from the sediment was restrained by the operation of the water-lifting aerator and that the water mixing made the phosphorus and ammonia concentrations in the upper and lower water layers homogeneous.

Anaerobic condition is the determining factor for the release of ammonia and phosphorus from the sediment. But, up to now, little has been known about the critical value of dissolved oxygen to trigger the massive release of these pollutants. The nitrification is inhibited and begins to accumulate when the concentration of dissolved oxygen is below 2 mg/L, and the phosphorus begins to release when the concentration of dissolved oxygen is below 1 mg/L in acidic and neutral conditions or 2 mg/L in alkaline conditions [3, 4]. Based on this theory, the dissolved oxygen

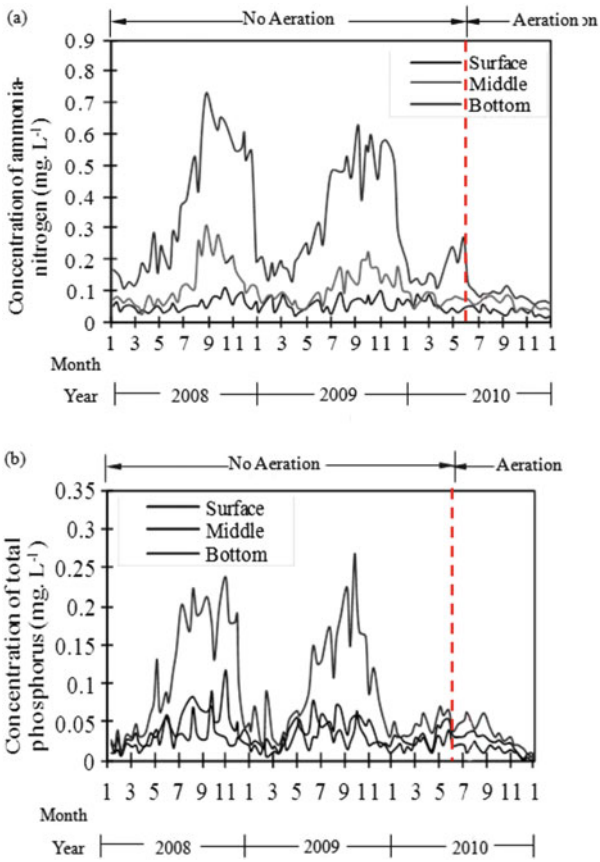

Fig. 11 Concentration variance of ammonia (**a**) and total phosphorus (**b**) at different depths from 2008 to 2010

concentration should be kept below 2 mg/L in order to control and restrict the release of phosphorus and ammonia from the sediment. As shown in Figs. 9, 10, and 11, the water-lifting aeration effectively enhanced the dissolved oxygen concentration level of the sediment–water interface in the reservoir (DO > 2.5 mg/L) in order to prevent the high-loaded pollution problems caused by the seasonal anoxic environment in the reservoir.

2.1.2 Effects on Inhibiting Algae Growth

Eutrophication causes the generation of toxic algae which, in addition to causing the deoxygenation of water, is harmful to other organisms and destroys the ecological balance. The variance of concentration and community composition indicates and affects directly the dynamics of the reservoir water quality.

As Fig. 12 shows, during the period of 2008 and 2009, the seasonal variance in quantity and composition of algae showed a typical “saddle-type” distribution. For

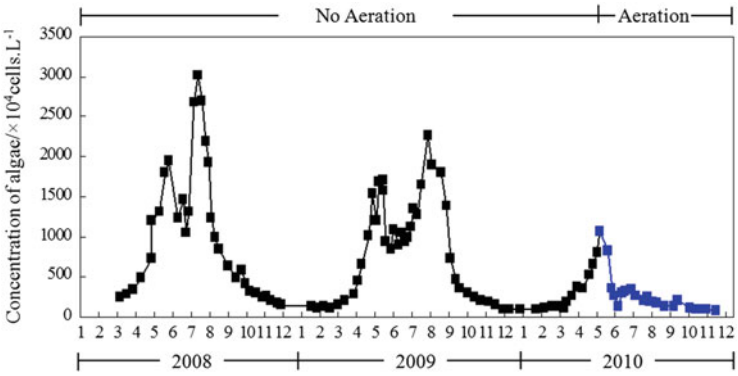

Fig. 12 Seasonal variations of algal abundance in the surface water layer of Jinpen Reservoir

the first peak in spring, the diatom species dominated, with a concentration greater than 10×10^6 cells/L. After the second peak in summer, the proportion of cyanobacteria increased rapidly and became the dominant population, with a concentration of $22–30 \times 10^6$ cells/L. However, after the aeration in 2010, the quantity of algae decreased substantially compared with previous years ($<4.5 \times 10^6$ cells/L) and continued to decline with the system running. This inhibitory effect was caused by multiple or combined mechanisms: (1) The mixing caused by the vertical circulation has an influence on the light climate of the algae by carrying large amounts of algae to the lower layer and decreasing the proportion of the population residing in the euphotic zone, reducing the effect of photosynthesis [5]. (2) The decrease of the surface water temperature, reducing the cyanobacteria competitive advantage [6, 7]. (3) At the same time, the aeration inhibits the sediments from releasing organic pollutants, especially the content of phosphorus, reducing the nutrient supply for the algae [8, 9].

2.1.3 Effects on Removing Volatile Halocarbons

Volatile halocarbons (VHC), most of which have strong physiological toxicity, are carcinogenic, teratogenic, and there exists a mutation of the endocrinal system risk serious harm to the environment and the health of residents [10]. They caught the attention of the US Environmental Protection Agency (EPA) and is the focus of one of the items called "preferred controlled pollutant in water" established by the Department of Environmental Protection of our country.

We found that the methylene chloride (CH_2Cl_2) concentrations exceeded the limit of the surface water environmental quality standard in China (the limit value was 20 μg/L) by up to 8–11 times in the spring of 2010 (Table 1).

As shown in Table 1, the CH_2Cl_2 concentration increased with water depth and it reached the highest value at the bottom, which indicated that the presence of CH_2Cl_2 may be related to the deposition of organic matter in the sediment. One

Table 1 Monitoring results of CH_2Cl_2 concentration in the water of Jinpen Reservoir (μg/L)

Date	April 2010	May 2010	July to December 2010		
Sites	S_1	S_1	S_1	S_2	S_3
0.5 m under surface	6.1	2.3	$<3 \times 10^{-4}$	$<3 \times 10^{-4}$	$<3 \times 10^{-4}$
30 m under surface	13.1	9.5	$<3 \times 10^{-4}$	$<3 \times 10^{-4}$	$<3 \times 10^{-4}$
70 m under surface	218.5	191.3	$<3 \times 10^{-4}$	$<3 \times 10^{-4}$	$<3 \times 10^{-4}$

Remarks: ① The date was from the national urban water supply water quality monitoring station network in Xi'an. ② The monitoring sites increased from one (S_1) to three (S_1, S_2, S_3) from July 2010

possible reason for this may be the natural organic components of sediment decomposition of halogenated or dear electrophilic addition reaction under anaerobic conditions. Another possible reason was that, with long-term exogenous low load input persistent pollutants which contain halogenated organic compounds (such as pesticides), there is continuous accumulation at the bottom of the reservoir and decomposition into low halogenated organic compounds in anaerobic conditions.

After the water-lifting aerator operated in 2010, the concentration of CH_2Cl_2 decreased in Jinpen reservoir and it was less than 3×10^{-4} μg/L.

The mechanism of removal of CH_2Cl_2 by the water-lifting aerator could be reflected in three aspects. The first is physical removal (the main way), i.e., the mixing and oxygenation enhanced the contact of water and air, which can improve the evaporation rate of CH_2Cl_2. The second is biochemical degradation, where the operation of the water-lifting and aeration system improves the metabolic activity of microorganisms in water, which can speed up the biodegradation rate of CH_2Cl_2 under oxygen environment. The third is controlling the source; the bottom anaerobic conditions are changed after the operation, which can inhibit the anaerobic decomposition and conversion of chlorinated organic compounds.

2.2 *Water Quality Improvement of Different Regions in Jinpen Reservoir*

The data of monitoring point S1 was taken as an example to demonstrate the results which show that, from August to December 2010, the water quality near the monitoring points was significantly improved compared to that in 2008 and 2009: the dissolved oxygen concentration in the bottom water was maintained above 2 mg/L and the concentrations of pollutants (ammonia, phosphorus, and algae) were also reduced by varying degrees (Fig. 13). The changes in water quality distribution were consistent for monitoring points S1 and S2 because they were the same distance from the aerator (20 m): the dissolved oxygen concentration in the bottom water was between 2.5 and 3.3 mg/L, while the concentrations of total phosphorus, ammonia, and chlorophyll-*a* in the whole reservoir were around 0.02–

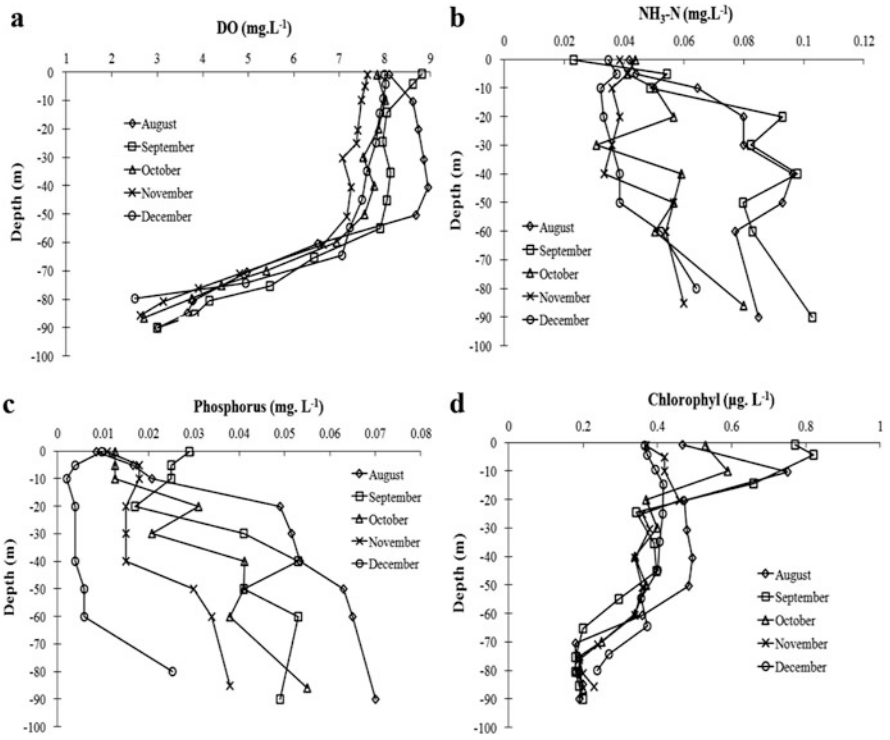

Fig. 13 Vertical water quality variance of monitoring point S1 from August 2010 to December 2010: (**a**) dissolved oxygen, (**b**) ammonia, (**c**) phosphorus, (**d**) chlorophyll-*a*

0.08 mg/L, 0.06–0.12 mg/L, and 0.8 μg/L, respectively. In contrast, the monitoring points S3 and S4 were less affected because of their greater distances from the aerators: the dissolved oxygen concentration at the sediment surface was maintained between 2.1 and 2.5 mg/L, while the concentration fluctuations of total phosphorus, ammonia, and chlorophyll-*a* were 0.05–0.12 mg/L, 0.08–0.25 mg/L, and 0.6–3 μg/L, respectively. The comparisons of the vertical water quality in November at monitoring points S1 and S4 are shown in Fig. 14. A much better effect observed in monitoring point S1 was clearly shown. Therefore, the closer the monitoring point is to the aerators, the better the effect of aeration, leading to a faster reduction of pollutants concentrations and a better improvement of water quality.

2.3 Water Quality Improvement at the Reservoir Outlet

In order to investigate the improvement of water quality during the operation of the water-lifting aerator, the water quality at the reservoir outlet was continually

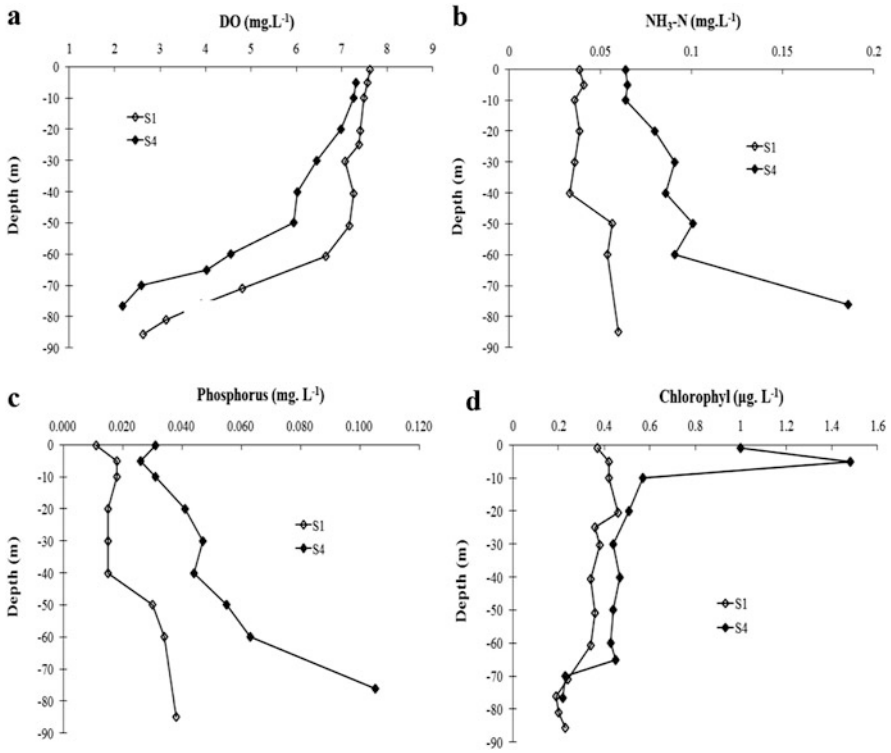

Fig. 14 Comparison of vertical water quality in November between monitoring points S1 and S4: (**a**) dissolved oxygen, (**b**) ammonia, (**c**) phosphorus, (**d**) chlorophyll-*a*

monitored for 6 months from July 1, 2010. The results are shown in Table 2, which indicated that the improvement was obvious, in which the total phosphorus, ammonia, and COD concentrations were maintained lower than 0.05, 0.1, and 4 mg/L, which were reduced remarkably by 47.3, 68.7, and 24.2 % as compared to the same period during 2008 and 2009, which accorded with the Chinese national surface water quality standard (GB 3838–2002) types III, I, and II, respectively, as well as showing a significant reduction of chlorophyll-*a* concentrations by 53.6 %.

3 Water Quality Improvement by the Improved Water-Lifting Aerator in Jinpen Reservoir

3.1 The Operation of the Improved Water-Lifting Aerator and the Layout of Monitoring Sites

Improvement of the water-lifting aerator system began in early May 2013 and was completed in early July of the same year. The commissioning of the improved

Table 2 Water quality variance at the outlet of Jinpen Reservoir

Water quality index	Month	Reduction level of the water pollutants						
					Reduction (%)		Average reduction (%)	
		2008	2009	2010	Compared to 2008	Compared to 2009	Compared to 2008	Compared to 2009
Total phosphorus (mg/L)	July	0.06–0.07	0.06–0.08	0.04–0.05	30.8	35.7	46.7	47.2
	August	0.07–0.08	0.06–0.07	0.03–0.04	53.3	46.2		
	September	0.06–0.07	0.05–0.06	0.03–0.04	46.2	36.4		
	October	0.04–0.05	0.05–0.06	0.02–0.04	33.3	45.5		
	November	0.04–0.05	0.03–0.05	0.01–0.02	66.7	62.5		
	December	0.02–0.04	0.03–0.04	0.01–0.02	50	57.1		
Ammonia (mg/L)	July	0.11–0.16	0.1–0.18	0.05–0.07	55.6	57.1	69.5	67.1
	August	0.20–0.25	0.11–0.17	0.06–0.08	68.9	50		
	September	0.24–0.26	0.18–0.25	0.07–0.09	68.0	62.8		
	October	0.18–0.25	0.2–0.23	0.03–0.06	79.5	79.1		
	November	0.14–0.16	0.17–0.19	0.04–0.05	70	75		
	December	0.10–0.14	0.12–0.16	0.02–0.04	75	78.6		
COD_{Mn} (mg/L)	July	4.12–4.36	4.78–5.01	3.22–3.54	20.3	30.9	22.4	25.8
	August	4.14–4.78	4.23–4.89	3.43–3.67	20.4	22.1		
	September	4.82–5.26	4.86–5.14	3.72–3.94	24.0	23.4		
	October	4.12–4.35	4.08–4.53	3.39–3.54	18.2	19.5		
	November	3.78–4.00	3.93–4.02	2.65–3.33	23.1	24.8		
	December	3.14–3.72	3.58–3.87	2.34–2.58	28.3	34		
Chlorophyll-*a* (μg/L)	July	0.88–1.02	0.91–1.05	0.32–0.38	63.2	64.3	53.6	56
	August	1.09–1.28	1.11–1.32	0.40–0.53	60.8	61.7		
	September	0.86–1.05	0.91–1.08	0.44–0.47	52.4	54.3		
	October	0.74–0.82	0.83–0.96	0.37–0.44	48.1	54.7		
	November	0.65–0.72	0.71–0.76	0.34–0.36	48.9	52.4		
	December	0.55–0.65	0.52–0.68	0.28–0.34	48.3	48.3		

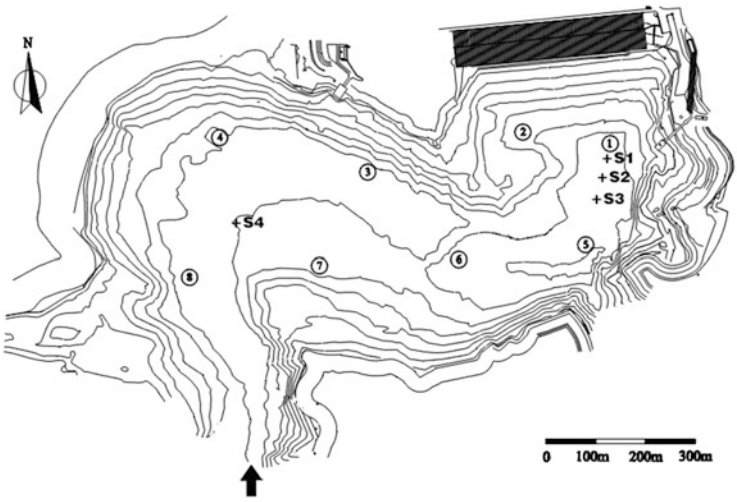

Fig. 15 The layout of monitoring sites in Jinpen Reservoir

water-lifting aerator started from July 2, 2013 to July 19, 2013. During the period of commissioning, the volume of compressed air was increased gradually from 10 to 40 m^3/h. The improved water-lifting aerator achieves single aeration with a small volume of gas (<20 m^3/h) and achieves full layer mixing and oxygenation functions at huge volumes of gas. All eight water-lifting aerators were running well and stably during the commissioning period, which was in accordance with our goal.

Influenced by the storm runoff that occurred on July 19 and July 23 in 2013, the dissolved oxygen in the bottom water increased from 0 to 6.3 mg/L. Thus, the favorable conditions induced by storm runoff were exploited by suspending the operation of the WLAs to reduce power consumption. On September 12, 2013, the dissolved oxygen in the bottom water decreased to 2 mg/L. Then, the improved water-lifting aerator began operation on September 13 to inhibit the release of pollutants from the bottom sediment. According to the vertical distribution of water turbidity, the WLAs were first run at a small air flow rate to avoid causing the increase of turbidity in the upper water. When the turbidity fell to below 50NTU, the equipment was then operated with an air flow of approximately 40 m^3/h.

Four monitoring sites were set at the main reservoir, as shown in Fig. 15. Sites S1, S2, and S3 were arranged between the #1 and #5 water-lifting aerators. S4 was located in the center among the #4, #8, and #7 water-lifting aerators. According to the results of the four monitoring points, the improvement of the water quality at the main reservoir was investigated.

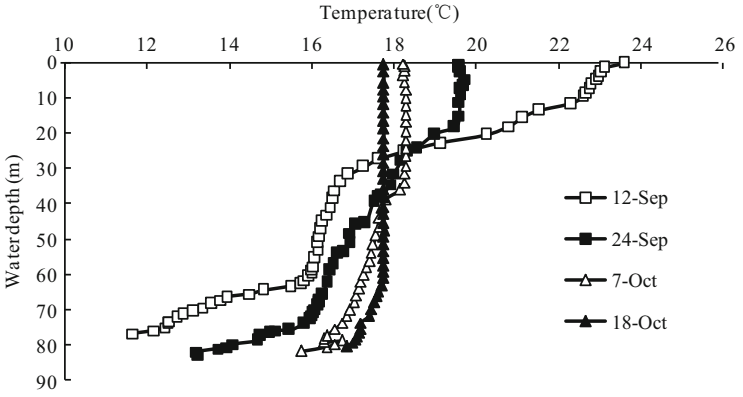

Fig. 16 Vertical temperature distribution at S1 during the operation period

3.2 Mixing Effects

The mixing ability of the improved water-lifting aerator was enhanced; thus, the mixing effect was significantly improved.

The vertical distribution of the temperature at monitoring site S1 during the operation period is shown in Fig. 16. Temperature changes at the surface and bottom waters and vertically during the operation period is shown in Table 3.

As shown in Fig. 16, the surface water temperature was 23.59 °C, while the water temperature at the bottom was 11.67 °C before the water-lifting aerators were running. Stable natural thermal stratification was maintained with a high temperature difference between the surface and bottom. The water-lifting aerators began to run on September 12. The surface water temperature decreased to 4 °C, while the bottom water temperature increased to 1.59 °C till September 24, and the vertical temperature difference decreased to 5.59 °C. The aeration system displayed a good mixing effect during the period of initial operation, effectively reducing the vertical temperature difference of Jinpen Reservoir.

With the operation of the water-lifting aerators, the strong mixing effects made the vertical temperature difference become smaller. The surface water temperature dropped to 18.22 °C, while the bottom temperature increased to 15.75 °C, and the vertical temperature difference narrowed to 2.47 °C on October 7.

After the water-lifting aerators were running for about 5 weeks, the surface water temperature dropped to 17.75 °C, while the bottom temperature increased to 16.87 °C. The water body was completely mixed, and the vertical temperature difference narrowed to 0.88 °C (October 18).

The mixing effects of the water-lifting aerator could effectively reduce the vertical temperature difference and enabled complete mixing of the reservoir, which have already occurred at the end of October in 2013. Mixed in advance can effectively inhibit further release of pollutants from the bottom sediment.

Table 3 Temperature changes at the surface and bottom during the operation period

Date	Items					
	Surface		Bottom		Vertical	
	Temperature (°C)	Temperature decrease (°C)	Temperature (°C)	Temperature increase (°C)	Temperature difference (°C)	Temperature decrease (°C)
September 12	23.59	–	11.67	–	11.92	–
September 24	19.59	↓4.00	13.26	↑1.59	6.33	↓5.59
October 07	18.22	↓1.37	15.75	↑2.49	2.47	↓3.86
October 18	17.75	↓0.47	16.87	↑1.12	0.88	↓1.59
October 22	17.52	↓0.23	17.06	↑0.19	0.46	↓0.42

"↑" Increase of water temperature
"↓" Decrease of water temperature

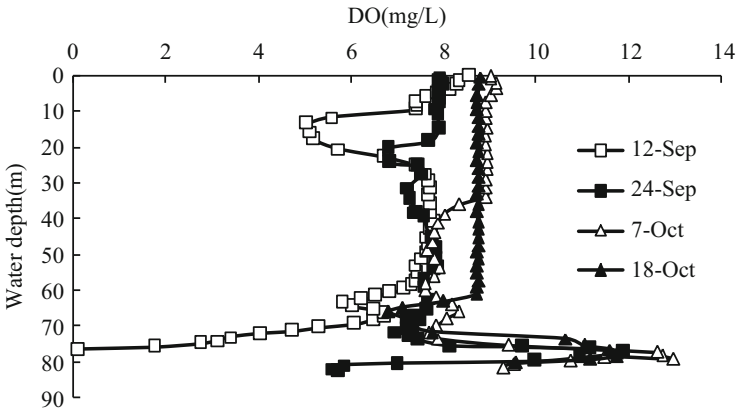

Fig. 17 Vertical dissolved oxygen distribution at S1 during the operation period

The WLAs stopped running on October 22. The reservoir was completely mixed by October 18, which was 3 months ahead of the natural mixing time and the vertical temperature was about 17 °C. With the coming of winter, the air temperature would reduce and the reservoir surface water temperature would continue to decline; thus, the density of the surface water would be increased. The low temperature, high density, and oxygen-rich surface water would continuously be transferred to the lower layer, which can form a continuous mixing process at the natural state. The natural mixing process could continue until the surface temperature no longer dropped (estimated at about 6 °C) and reached a steady state.

3.3 Changes of Dissolved Oxygen

Microporous aerators were installed at the bottom of the improved water-lifting aerator They can release compressed air into tiny bubbles with small size which enlarge the contact area of air and water during the process of small air bubbles rising in the aeration chamber; thus, the oxygen transfer efficiency significantly improved, and the exchange rate of oxygen-enriched water was improved at the same time. The water-lifting aerator can directly oxygenate lower-layer water and lessen the circulation in the lower, anoxic, water, thus promoting the diffusion of dissolved oxygen. Changes of dissolved oxygen at site S1 during the period of running is shown in Fig. 17.

As Fig. 17 shows, the available dissolved oxygen in the bottom water was almost completely consumed before the water-lifting aerators began running. With the operation of the aeration system, the dissolved oxygen concentration in the bottom water gradually improved. After the aeration system was run for 12 days (September 24), the dissolved oxygen in the bottom water increased to 5.75 mg/L and the dissolved oxygen concentration in the upper water column was further increased.

After the water-lifting aerators had been running for 25 days (October 7), along with the destruction of the reservoir temperature stratification, dissolved oxygen in the bottom water of Jinpen Reservoir was increased to 9.28 mg/L and the dissolved oxygen in the upper body water (water depth of 10–30 m) also improved to 2 mg/L or so.

During this period, the dissolved oxygen concentration of the bottom water remained at 9 mg/L or more and the dissolved oxygen content in the upper water body (extended down to the 60 m depth zone) was also improved.

3.4 Effects on Inhibiting Algae Growth

3.4.1 Effects on Inhibiting Algae Cell Density

The algae growth peak in Heihe Reservoir occurs from July to September every year in the natural state and the dominant species is cyanobacteria. Table 4 gives the maximum algae cell density at the surface of 2008–2012 during July to September, from which we can make comparison and analysis to the effects on inhibiting algae growth by water-lifting aerators.

Table 4 shows that the algae cell density at the surface reached 30,900,000/L in July 2008 and 22,700,000/L in August 2008,

The operation of the water-lifting and aeration system in 2010 effectively inhibited the reproduction of algae, the peak algae cell density dropped to 3,300,000/L, and the algae cell density was maintained at a relatively low level during the operation period of the water-lifting and aeration system.

The algae cell density at the surface reached 15,900,000/L in July 2011 because of the non-operation of the water-lifting and aeration system.

The algae cell density fell to relatively low levels (<200,000/L) during the commissioning period in early July 2013. The algae cell density increased to 3,500,000/L at the end of July after the water-lifting and aeration system stopped running in the middle of July. The amount of algae continued to rise from the end of

Table 4 Surface algae cell density from 2008 to 2013 (×10,000/L)

	Month				
Year	July	August	September	October	Notes
2008	3090	1001	630	420	Nature
2009	1352	2270	1382	352	Nature
2010	**330**	**235**	**124**	**201**	**Operation**
2011	1590	1200	560	320	Nature
2012	1150	980	580	240	Nature
2013	**350**	**680**	**617**	**88**	**Operation**

Bold values stands for Algae surface cell density during the operation period of the water-lifting aerators

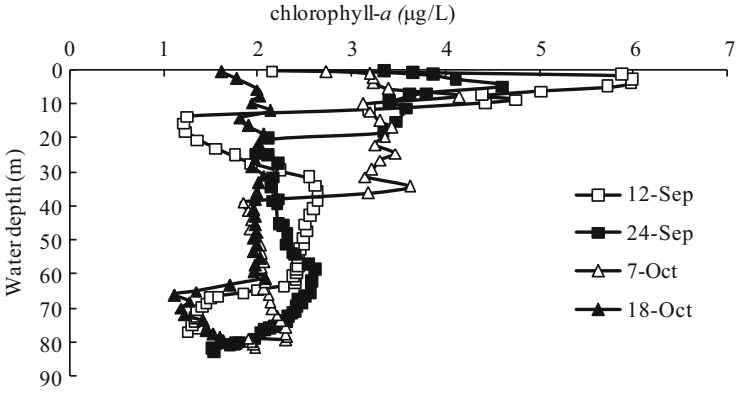

Fig. 18 Vertical chlorophyll-*a* distribution during the operation period

July and the algae cell density at the surface reached 6,170,000/L before the operation of the water-lifting aerator in September. The algae cell density decreased to 1,180,000/L when the water-lifting aerator operated for about 2 weeks at the end of September, and the algae cell density decreased with operation of the water-lifting aerator. The algae cell density decreased to 880,000/L at the end of the operation period on October 22 and the decay rate reached 85 % compared to before the operation period.

3.4.2 Changes of Chlorophyll-*a*

Chlorophyll-*a* is the main pigment of phytoplankton for photosynthesis; most of the green plants contain chlorophyll-*a*, which can reflect the primary productivity conditions in water. The concentration of chlorophyll-*a* along the depth can characterize well the vertical distribution of algae in water. The change in chlorophyll-*a* at the monitoring point is shown in Fig. 18.

The content of chlorophyll-*a* from the surface to a depth of 10 m ranged from 4.40 to 5.99 μg/L, and the average concentration was 5.28 μg/L before the operation of the water-lifting aerator. The concentration of chlorophyll-*a* was lower at the bottom of the reservoir, with a value of 1.25 μg/L.

The growth of algae was restrained after the operation of the water-lifting aerator. The content of chlorophyll-*a* from the surface to a depth of 10 m ranged from 3.36 to 4.62 μg/L, the average concentration was 3.78 μg/L, the maximum concentration was at a depth of 5 m with a value of 4.62 μg/L, and the content of chlorophyll-*a* at the bottom of the reservoir increased a little, with a value of 1.53 μg/L on September 24.

The content of chlorophyll-*a* from the surface to a depth of 10 m ranged from 2.73 to 4.15 μg/L, the average concentration was 3.28 μg/L, the maximum concentration was at a depth of 8 m with a value of 4.15 μg/L, and the content of

Table 5 The change in content of chlorophyll-*a* during the operation period

Date	Item			
	Range from surface to the depth of 10 m (μg/L)	Average (μg/L)	Maximum concentration depth (m)	Maximum concentration (μg/L)
September 12	4.40–5.99	5.28	3	5.99
September 24	3.36–4.62	3.78	5	4.62
October 7	2.73–4.15	3.28	8	4.15
October 18	1.62–2.13	1.91	10	2.13
October 22	1.46–1.55	1.5	Well-distributed	1.55

chlorophyll-*a* at the bottom of the reservoir reached 1.95 μg/L on October 7. The content of chlorophyll-*a* from the surface to a depth of 10 m ranged from 1.62 to 2.13 μg/L, the average concentration was 1.91 μg/L, the maximum concentration was at a depth of 10 m with a value of 2.13 μg/L, and the content of chlorophyll-*a* at the bottom of the reservoir reached 1.64 μg/L on October 18. The change in content of chlorophyll-*a* is shown in Table 5.

As is shown in Table 5, owing to the artificial mixing process, the content of chlorophyll-*a* from the surface to a depth of 10 m continued to be reduced and the algae were brought to the dark layer, where they died. When the water-lifting aerator operated till October 18, the thermal stratification structure was destroyed and the vertical distribution of chlorophyll-*a* was well distributed. The concentration of chlorophyll-*a* was reduced to 1.5 μg/L.

3.5 Effects on Reducing Total Nitrogen

The operation of the water-lifting aerator changed the original water environmental conditions. The metabolic activity of denitrification bacteria was enhanced due to the temperature and dissolved oxygen at the bottom of the reservoir was increased, thus enhancing the effect of nitrogen denitrification bacteria [11, 12]. The vertical total nitrogen (TN) distribution during the operation period is shown in Fig. 19.

The concentration of TN reached 1.51 mg/L at the lower layer before the operation of the water-lifting aerator.

The concentration of TN reduced to 1.33 mg/L at the bottom after the water-lifting aerator operated for 11 days (September 24). With the increase of temperature and dissolved oxygen at the lower layer, the metabolic activity of denitrification bacteria was enhanced and the concentration of TN reduced to 1.29 mg/L at the bottom after the water-lifting aerator operated for 24 days (October 7) [13, 14]. The vertical total nitrogen reduced to 0.96–1.22 mg/L after the water-lifting aerator operated for 35 days (October 18), and it was reduced by 20.5 % compared to the TN concentration before the operation.

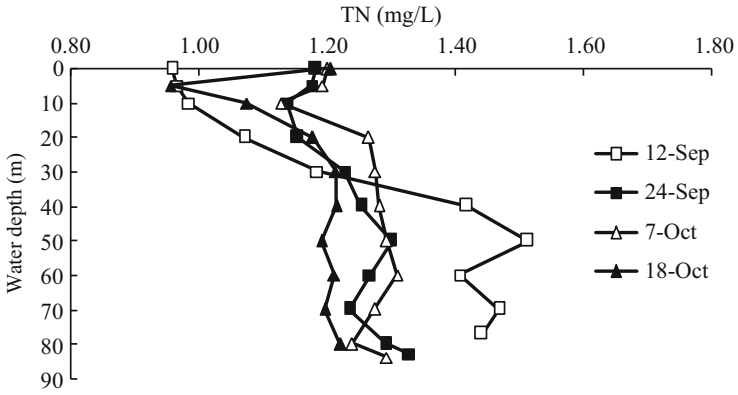

Fig. 19 Vertical total nitrogen distribution at S1 during the operation period

The vertical total nitrogen distribution during September to December from 2008 to 2013 is shown in Table 6.

As shown in Table 6, the vertical distribution of total nitrogen was high in the natural state. The highest value of total nitrogen reached 2.54 mg/L and the vertical averaged value was 1.58 mg/L in 2008. The highest value of total nitrogen reached 2.23 mg/L and the vertical averaged value was 1.72 mg/L in 2009. The operation of the water-lifting aerator in 2010 reduced the concentration of total nitrogen significantly. The concentration of total nitrogen remained at a higher level in 2011 and 2012.

The operation of the improved water-lifting and aeration system in 2013 enhanced the metabolic activity of denitrification bacteria and water self-purification ability; thus, the concentration of total nitrogen was reduced. The vertical TN value reduced by 19, 24, 17, and 15 % compared to the non-operation periods in 2008, 2009, 2011, and 2012, respectively.

3.6 Effects on Inhibiting the Release of Internal Pollutants

Due to the thermal stratification in summer and autumn, the dissolved oxygen at the bottom of Heihe Reservoir can decrease to less than 2 mg/L and even decrease to an anaerobic state, which can lead to the release of nitrogen, phosphorus, iron, manganese, and sulfide from the sediment, and, thus, can cause the deterioration of water quality. The lack of oxygen at the bottom is a key factor in causing endogenous pollution in the reservoir; therefore, improving the dissolved oxygen content at the bottom of the reservoir can effectively inhibit the release of pollutants from the sediment.

Table 6 Vertical total nitrogen distribution from 2008 to 2013

	Year											
	2008		2009		2010		2011		2012		2013	
Depth	21/9	25/12	28/10	25/12	24/9	11/12	22/9	18/12	2/9	25/12	12/9	18/10
0.5 m	1.32	1.54	1.60	1.32	1.31	1.03	1.47	1.43	1.08	1.48	0.96	1.21
10 m	1.31	1.52	1.71	1.89	1.24	0.97	1.35	1.44	1.19	1.42	0.97	0.96
20 m	1.27	1.09	1.66	1.60	1.20	1.08	1.67	1.33	1.30	1.39	0.98	1.07
30 m	1.22	1.13	1.88	1.19	1.24	0.97	1.34	1.47	1.40	1.44	1.07	1.18
40 m	1.47	1.39	1.38	1.56	1.18	0.95	1.40	1.34	1.41	1.35	1.19	1.21
50 m	1.19	1.05	1.58	1.41	1.14	0.97	1.30	1.37	1.26	1.35	1.42	1.21
60 m	1.60	1.55	1.63	1.50	1.16	0.97	1.63	1.39	1.46	1.36	1.51	1.19
70 m	2.28	1.78	1.67	1.53	1.15	1.01	1.73	1.49	1.51	–	1.47	1.21
80 m	–	–	1.77	1.50	1.23	–	1.53	1.32	1.43	–	–	1.20
90 m	–	–	1.76	–	1.03	–	1.51	–	–	–	–	–
Bottom	2.54	1.87	2.23	1.76	1.14	0.86	1.52	1.56	1.28	1.34	1.44	1.22
Depth	78 m	73 m	92 m	88 m	95 m	78 m	91 m	85 m	89 m	69 m	76 m	80.5 m
Average	1.58	1.44	1.72	1.53	1.18	0.98	1.50	1.41	1.33	1.38	1.24	1.17
Reduction (%)	26	19	32	24	–	–	22	17	12	15	6	–
State	Nature		Nature		Operation		Nature		Nature		Operation	

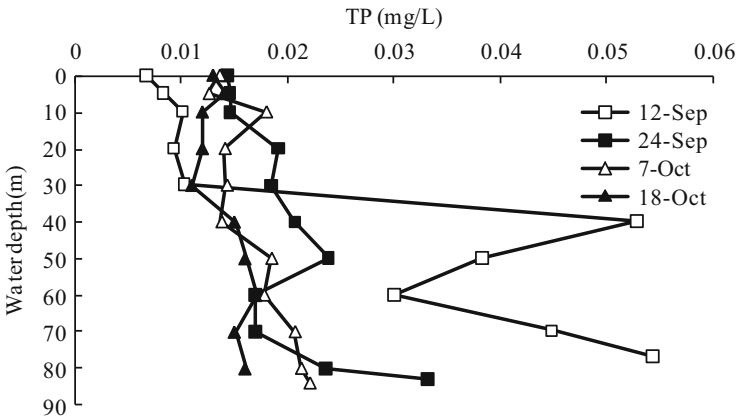

Fig. 20 Vertical total phosphorus distribution during the operation period

3.6.1 Effects on Inhibiting the Release of Total Phosphorus from Sediment

With the operation of the water-lifting aerator, the concentration of dissolved oxygen at the bottom increased, which inhibited the release of internal pollutants from the sediment effectively

The vertical total phosphorus distribution during the operation period is shown in Fig. 20.

The concentration of TP reached 0.049–0.054 mg/L at the bottom before the operation of the water-lifting aerator (September 12) and the concentration of TP at the lower layer was higher. The average vertical concentration of TP reached 0.026 mg/L.

With the operation of the water-lifting aerator, the oxygen content at the bottom increased and the release of P was inhibited. The concentration of TP reduced to 0.033 mg/L at the bottom and the average vertical concentration of TP decreased to 0.019 mg/L after the water-lifting aerator operated for 11 days (September 24). The concentration of TP reduced to 0.022 mg/L at the bottom and the average vertical concentration of TP decreased to 0.017 mg/L after the water-lifting aerator operated for 25 days (October 7). The vertical TP reduced to 0.014 mg/L after the water-lifting aerator operated for 35 days (October 18). The whole reservoir was mixed and TP was reduced by 74 % compared to the TP concentration at the bottom of the reservoir before the operation of the water-lifting aerator.

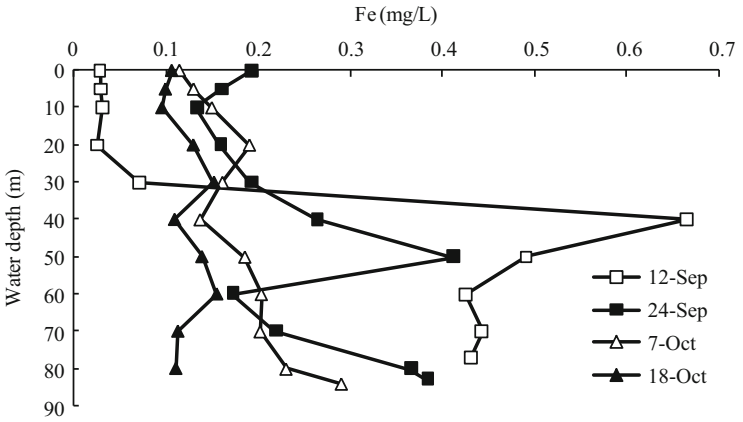

Fig. 21 Vertical iron distribution during the operation period

3.6.2 Effects on Inhibiting the Release of Iron and Manganese from Sediment

The concentration of Fe reached 0.67 mg/L at the bottom before the operation of the water-lifting aerator (September 12). The vertical total iron distribution during the operation period is shown in Fig. 21.

As shown in Fig. 21, the content of Fe at the lower layer was decreasing with the operation time of the water-lifting aerator. The maximum Fe content at the vertical column decreased to 0.417 mg/L after the water-lifting aerator operated for 11 days (September 24) and it decreased to 0.30 mg/L after the water-lifting aerator operated for 25 days (October 7). The vertical distribution of iron decreased to 0.10–0.16 mg/L after the water-lifting aerator operated for 36 days (October 18).

The operation of the water-lifting aerator inhibited the release of iron significantly, and it was reduced by over 80 % compared to the iron concentration before the operation. After the operation of the water-lifting aerator, the manganese concentration was lower than 0.05 mg/L.

3.6.3 Comparison to Other Years

The concentration of iron, manganese, and TP at the bottom of the reservoir from 2008 to 2013 is shown in Table 7. The thermal stratification from September to December hinders the vertical transfer in the natural state. The oxygen at the bottom was consumed by the water and the sediment, which cause pollutants to be released from the sediment.

As shown in Table 7, the concentration of iron, manganese and TP was higher and exceeded the surface water environmental quality standard in China (GB 3838–2002). The concentrations of Fe, Mn, and TP at the bottom of the reservoir at the

Table 7 The concentration of iron, manganese, and TP at the bottom of the reservoir from 2008 to 2013 (mg/L)

Content	Index					
	Fe		Mn		TP	
Date	Content	Over class III (%)	Content	Over class III (%)	Content	Over class III (%)
2008-09-21	0.478	59	0.213	113	0.063	26
2008-12-25	1.529	409	0.618	518	0.172	244
2009-10-28	0.782	160	0.512	412	0.092	84
2009-12-25	1.612	437	0.716	616	0.122	144
2010-09-24	0.112	–	0.015	–	0.029	–
2010-12-11	0.106	–	0.012	–	0.016	–
2011-09-22	0.115	–	0.103	3	0.019	–
2011-12-08	0.825	175	0.282	182	0.082	64
2012-09-02	0.382	27	0.208	108	0.064	28
2012-10-17	1.778	492	0.413	313	0.178	256
2012-11-08	1.113	271	0.125	25	0.104	108
2013-09-12	0.431	43	<0.05	–	0.054	8
2013-10-18	0.111	–	≤0.05	–	0.016	–

The limit Fe value is 0.3 mg/L and the limit Mn value is 0.1 mg/L in the surface water environmental quality standard in China (GB 3838–2002)
The limit TP value in the surface water environmental quality standard in China (GB 3838–2002) for lakes and reservoirs: class I: 0.01 mg/L, class II: 0.025 mg/L, class III: 0.05 mg/L
The underlined data were obtained during the water-lifting aerator operation period

end of December in 2009 exceeded the class III standards by 437, 616, and 144 %, respectively.

The operation of the water-lifting and aeration system in 2010 inhibited the release of pollutants from the sediment. The concentrations of iron, manganese, and TP decreased to 0.1, 0.01, and 0.016 mg/L, respectively, which reached the class II water standard.

Influenced by the rainstorm in 2012, the turbidity was high at the bottom of the reservoir and the water-lifting aerator was not operated so as to avoid increasing the turbidity in the whole column. After the rainstorm, the high concentration of

suspended solids caused the oxygen to be consumed quickly. The bottom water became severely anaerobic a few days later and pollutants began to be released from the sediment. The concentrations of iron, manganese, and TP reached 1.78, 0.41, and 0.18 mg/L, respectively, and exceeded the class III standards by 492, 313, and 256 %, respectively.

In early November 2012, the reservoir mixed in advance and the vertical water iron content reached 0.8–1.2 mg/L, which caused the launch of the emergency plan by Xi'an Environmental Protection Bureau.

The improved water-lifting and aeration system began to operate in September 2013. The water quality significantly improved after it was in operation for 40 days. The operation of the water-lifting and aeration system effectively inhibited the release of pollutants. The iron concentration decreased to 0.1 mg/L, the manganese concentration was lower than 0.05 mg/L, and the TP concentration reduced to less than 0.025 mg/L during the late operation period.

In conclusion, the improved water-lifting aerator could effectively inhibit the release of pollutants from the bottom sediment and control the endogenous pollution, thus improving the reservoir water quality.

4 Water Quality Improvement in Shibianyu Reservoir

To investigate the effects of the WLAs on the water quality of Shibianyu Reservoir, 12 monitoring sites were set up around the WLAs. S1 to S6 were arranged along the west radial direction at distances of 10, 20, 40, 60, 80, and 100 m from the #1 WLA. S7 to S12 were arranged along the south radial direction 10, 20, 40, 60, 80, and 100 m away from the #2 WLA (Fig. 22).

4.1 Mixing Effects

The large air piston formed in the ascending tube promptly ascended and then accelerated the water in the ascending tube, which continued to rise until the air piston exited the outlet of the ascending tube. Subsequently, the bottom water continued to rise under the effect of inertia and moved horizontally due to its inherent kinetic energy upon arrival at the water surface. In a stratified reservoir during summer, the water at the bottom was denser than the surface water. Low-temperature water reached the surface and initially moved horizontally in all directions due to its inherent kinetic energy; the water then moved downwards because it was denser than the background water. However, the water changed direction and moved upwards because of the buoyancy resistance from the stratification [13, 14]. The temperature gradient is an important factor that influences the mixing depth of the WLA [15]. As the water temperature gradient decreased, the buoyancy resistance decreased, which increased the mixing depth. The temperature gradient near the WLAs at a water depth of 45 m or less was only 0.1 °C/m, while a

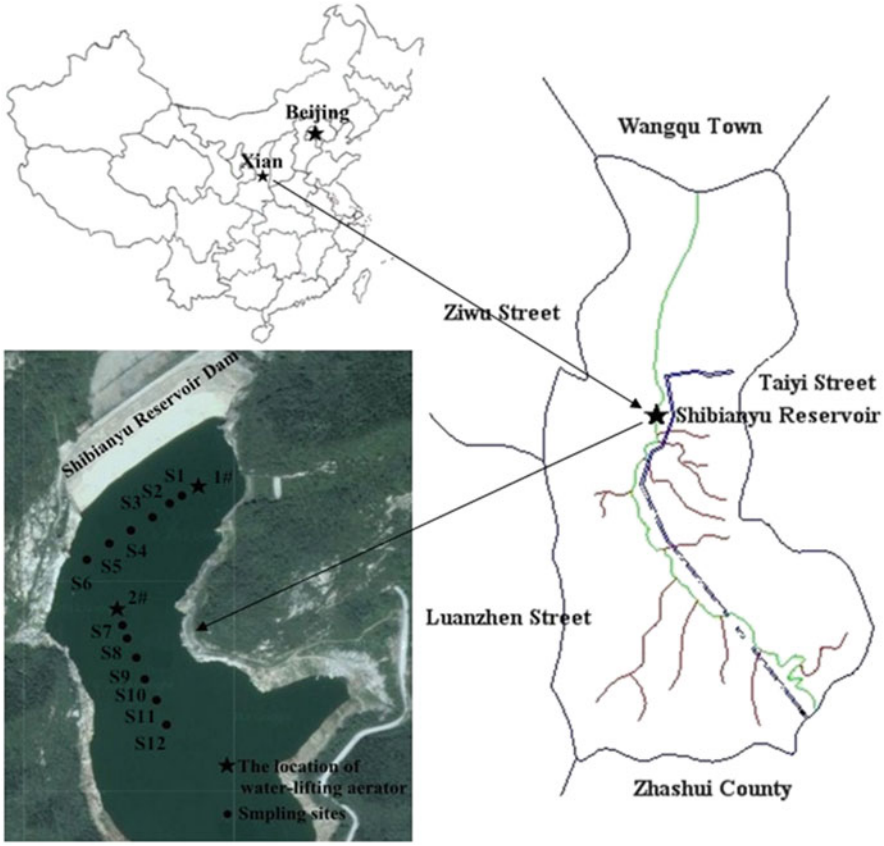

Fig. 22 The layout of monitoring sites in Shibianyu Reservoir

large temperature gradient was observed between 45 and 50 m (approximately 1.3 °C/m) after the storm runoff (Fig. 23a, c). The water temperature is an important index to measure the mixing effects of the WLAs. As shown in Fig. 23b, d, the water body was completely mixed (the water temperature difference between the surface and bottom waters was less than 0.5 °C) at depths of 40 m or less near the WLAs after the aerators operated for 3 weeks, while a relatively stable temperature stratification structure persisted within 5 m of the bottom sediment at S7 (the deepest monitoring site). The bottom water at S7 was completely mixed after 6 weeks, which is discussed in the following section. The effective radius of the WLAs was the main factor to determine the installation of WLAs. Many factors influence the effective radius of WLAs, such as the submerged depth, pressed airflow, WLA structure, etc. The #1 and #2 WLAs were submerged at depths of approximately 15 and 35 m, respectively. The pressed airflows of the #1 and #2 WLAs were 14 and 28 m^3/h, respectively. After operation for 3 weeks, the radius of the two WLAs reached 60 and 80 m, respectively (Fig. 23b, d).

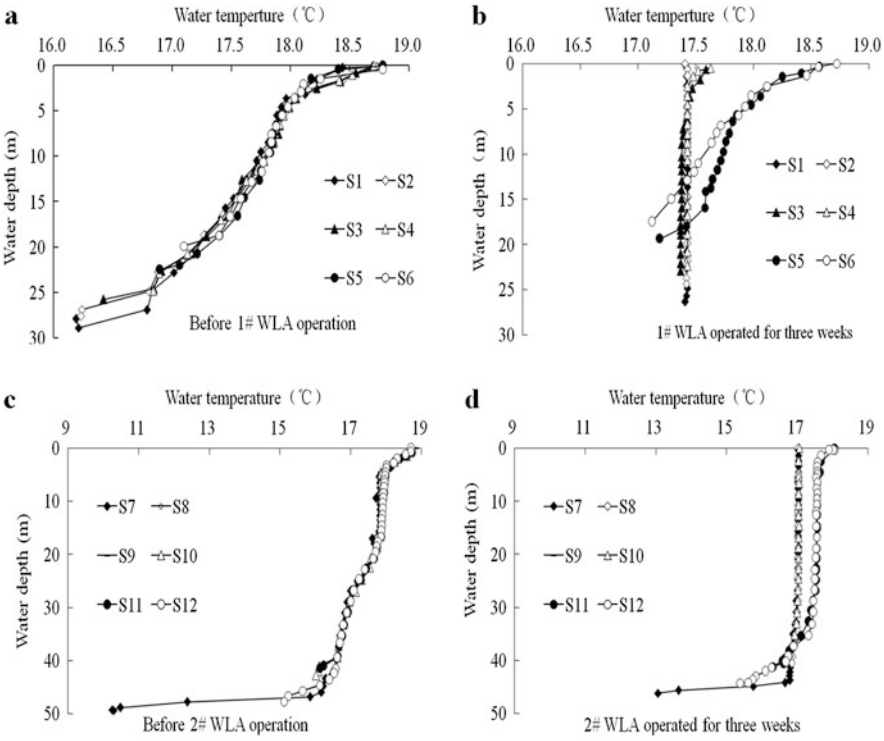

Fig. 23 The vertical distribution of water temperature before and after the operation of the two water-lifting aerators

4.2 Oxygenation of the Water in the Lower Layer

The WLA can increase the concentration of dissolved oxygen of water in the lower layer in two ways: (1) Destroy the water stratification by mixing the lower and upper water layers, which increases the dissolved oxygen concentration in the lower layer; (2) Directly oxygenate water in the lower layer and decrease the circulation in the lower, anoxic water, which promotes the diffusion of dissolved oxygen. As shown in Fig. 24a, the water temperature difference was approximately 4 °C within 3 m of the bottom 10 m from the #2 WLA before the operation of the aerator. The mixing function of the WLA continuously increased the water temperature of the lower layer. The water temperature difference in the lower layer water influences the diffusion rate of dissolved oxygen. As shown in Fig. 24b, the dissolved oxygen content increased more slowly near the reservoir bottom at the beginning of the operation of the #2 WLA. As the water temperature difference decreased, the diffusion rate of dissolved oxygen significantly increased. After 1 month of WLA operation, the dissolved oxygen 0.2 m above the reservoir bottom increased from 0 to 5 mg/L. Due to the rainstorm runoff, the water temperature increased to approximately 16 °C and the oxygen dissolved in the bottom water increased

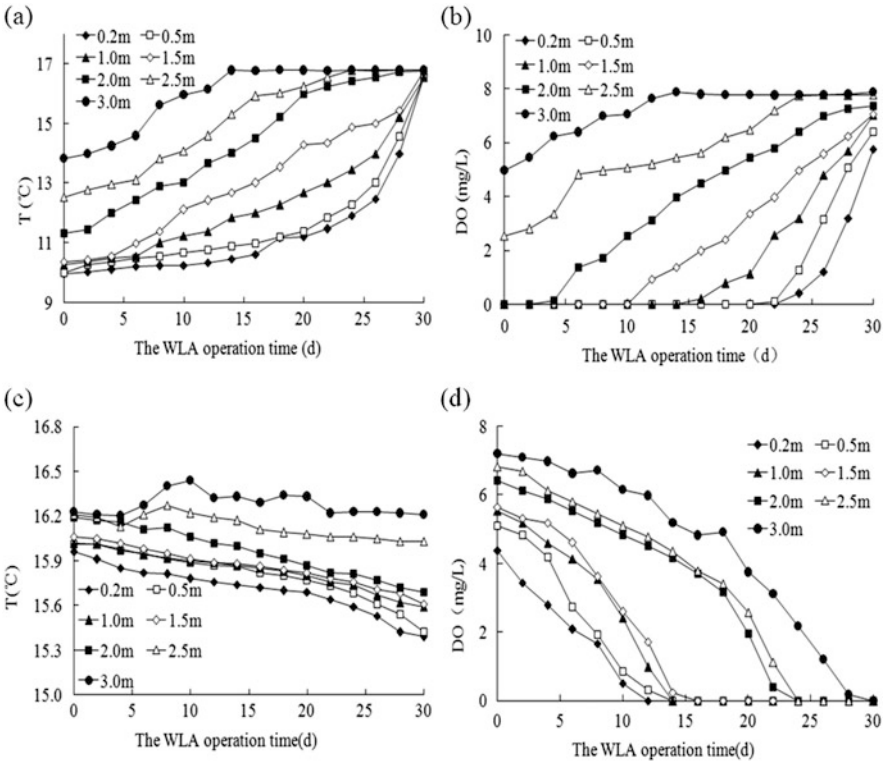

Fig. 24 Changes of water temperature and dissolved oxygen in the deep layer water at S7 (**a**, **b**) and S12 (**c**, **d**) after the WLA operation

from 0 to 4.2 m/L at the S12 monitoring point (100 m from the #2 WLA) after the heavy rain. During the operating period of the WLA, the water temperature slightly decreased, while the dissolved oxygen content rapidly decreased in the lower layer (Fig. 24c, d).

4.3 Effect on Inhibiting the Release of Internal Pollutants

Anaerobic conditions can lead to the release of pollutants from the sediment. The WLA can effectively restrain the release of pollutants from the sediment by increasing the dissolved oxygen content in the hypolimnion. As shown in Fig. 25, the concentrations of dissolved phosphorus, nitrogen from ammonia, iron, and manganese in the overlying water reached 0.116, 0.63, 0.51, and 0.61 mg/L, respectively, prior to the operation of the WLA. As the dissolved oxygen content at the bottom increased, the release of pollutants from the sediment was effectively suppressed after the operation of the WLA. The mixing due to the WLA rapidly

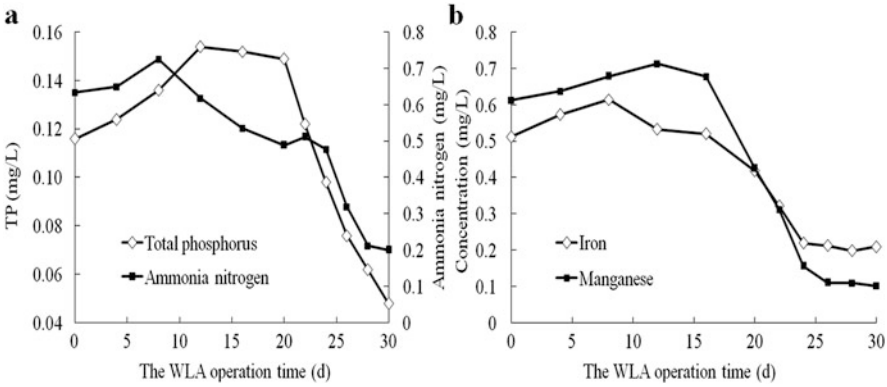

Fig. 25 Dynamic changes of total phosphorus and ammonia nitrogen (**a**), and total iron and manganese (**b**) at the bottom of S7 after the WLA operation

decreased the concentrations of pollutants in the water at the bottom of the reservoir. After the operation of the #2 WLA for 1 month, the concentrations of dissolved phosphorus, nitrogen from ammonia, iron, and manganese in the overlying water decreased to 0.048, 0.20, 0.21, and 0.10 mg/L, respectively.

4.4 Effects on Inhibiting Algae Growth

According to the distribution and growth characteristics of phytoplankton, the WLA aims to control algal growth by reducing the quantity of algae in the upper layer of the water, while increasing it in the lower layer, which homogenizes the algal distribution. The decrease in algae in the upper layer reduces their production capacity, while the increase in algae in the lower layer accelerates algal death due to the unfavorable growing conditions. As shown in Fig. 26a, the algae were mainly concentrated in the upper layer of the reservoir prior to the operation of the #1 WLA. After the operation of the #1 WLA, the quantity of algae in the upper water layer markedly decreased, while the number of algae at the bottom increased (Fig. 26b–d). The algae growth within 60 m of the #1 WLA was effectively suppressed after operation of the aerator for 4 weeks, while the algae number reached 100 million/L at a distance of 100 m from the #1 WLA.

The algae reduction efficiencies at different distances from the #1 water-lifting aerator are shown in Table 8. Compared with the unaffected area, the total number of algae at distances of 10, 20, 40, and 60 m from the WLA were reduced by 90.8, 90.2, 88.1, and 83.6 %, respectively. The nearer the WLA, the higher the algae growth reduction efficiency. In addition, the reduction of algae caused by the mixing function of the WLA was decreased with water depths due to the differences in the vertical distribution of algae.

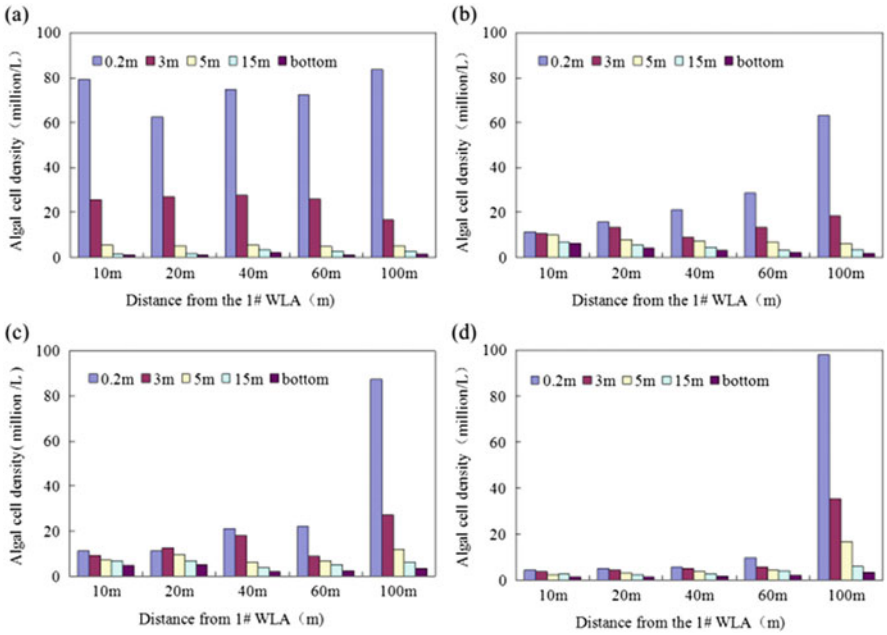

Fig. 26 Vertical distribution of algae at different distances from the aerator before (**a**) and after the #1 WLA was in operation for 1 week (**b**), 2 weeks (**c**), and 4 weeks (**d**)

Cyanobacteria can adjust their buoyancy to exploit nutrients, light, and inorganic carbon resources over a wider range [16, 17]. The vertical circulation caused by the operation of the aerator can effectively resist the flotation of cyanobacteria, reduce the harmful competitive advantage of algae, and, thus, change the structure of the phytoplankton community [18, 19]. As shown in Fig. 27, the algal cell density decreased to less than 10 million/L, of which only 16 % consisted of cyanobacteria at S1. The quantity of algae reached 100 million/L, of which 91 % consisted of *Microcystis* at S6 after the aerator had been in operation for 3 weeks. Thus, the operation of a WLA can both reduce the number of algae and change the phytoplankton community structure.

4.5 Effects on Accelerating Organic Matter Degradation

4.5.1 The Removal of Volatile Organic Compounds (VOCs)

In general, the concentration of VOCs in Shibianyu Reservoir was very low. Algae growth and metabolism could result in a higher concentration VOCs in the upper water, while the increase of VOCs in the bottom water was mainly caused by the release of organic pollutants from sediment under anaerobic conditions (Fig. 28a).

Table 8 Algae reduction efficiency after the #1 WLA was in operation for 4 weeks

	Algae inhibition efficiency at different water depths (%)					
Distance from the WLA (m)	0.3 m	3 m	5 m	15 m	Bottom	Total
10	95.4	89.2	86.7	55.9	56.5	90.8
20	95	88.1	81.2	62.7	65.2	90.2
40	94.2	86.1	77	52.5	53.6	88.1
60	90.1	83.5	73.3	33.9	39.1	83.6

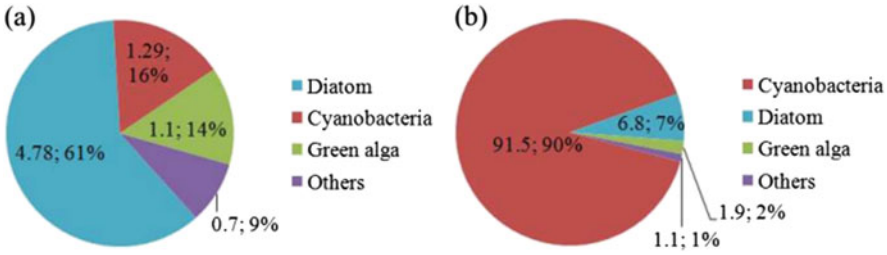

Fig. 27 Phytoplankton community structure and quantity at the surface of S1 (**a**) and S6 (**b**) after the aerator was in operation for 3 weeks

The mixing function of the WLA could effectively remove the VOCs from the reservoir water. As shown by Fig. 28 and Table 9, the VOC removal rate was above 90 % within a distance of 60 m from the #2 WLA after it was in operation for 4 weeks.

4.5.2 Accelerating Organic Matter Degradation

The concentration of organic matter increased because of the large amount of suspended matter that entered the reservoir via storm runoff. Prior to the operation of WLAs, the concentration of COD_{Mn} reached approximately 7 mg/L in the SBYR. Due to the aerobic biodegradation, the concentration of COD_{Mn} consistently decreased (Table 10). Compared to the sites located 100 m away from the WLA, the average organic degradation rate was higher at sites close to the WLA. The results demonstrated that the activity of microbial metabolism was improved, which can accelerate the rate of organic matter degradation to 0.11 mg/L·day after the operation of the WLA [20].

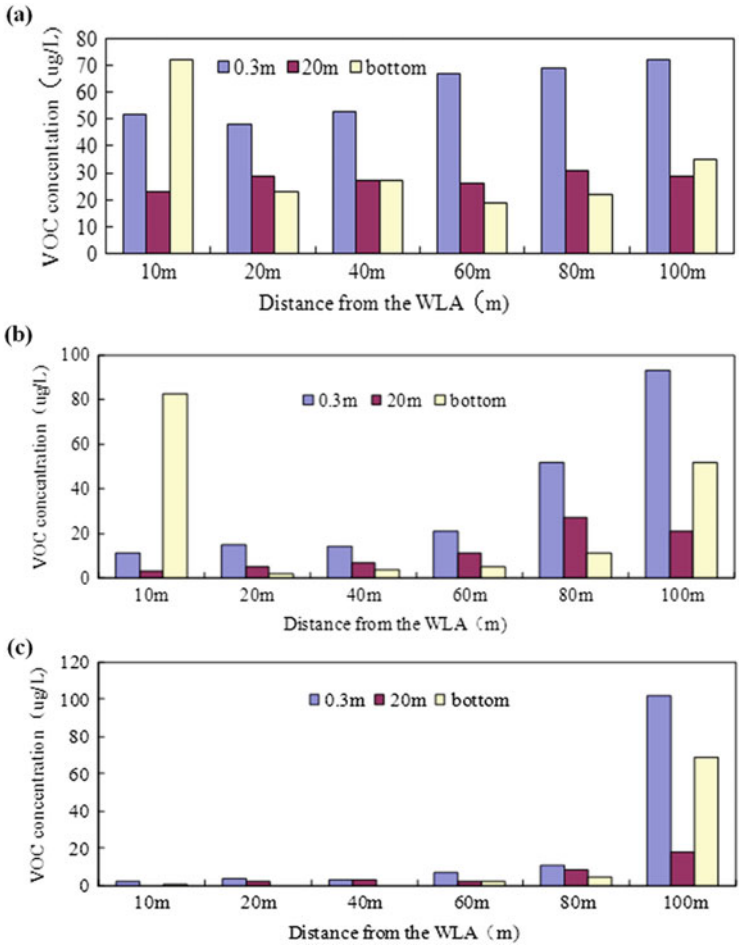

Fig. 28 Vertical distribution of VOC at different distances from the aerator before (**a**) and after the #2 WLA was in operation for 2 weeks (**b**) and 4 weeks (**c**)

Table 9 The removal rate of VOCs after the #2 WLA was in operation for 4 weeks

	The removal rate of VOCs at different distance from the WLA (%)				
Water depth	10 m	20 m	40 m	60 m	80 m
0.5 m	96.2	91.7	94.3	89.6	85.1
20 m	100	93.1	90.1	92.3	82.0
Bottom	98.6	100	100	89.5	82.3
Total	98.0	94	94.4	90.2	82.8

Table 10 The concentration and averaged degradation rate of COD_{Mn} during the WLA operation time

Distance from the WLA (m)	WLA operation duration (day)							Average degradation rate (mg/L·day)
	0	5	10	15	20	25	30	
10	6.98	6.12	5.38	4.98	4.25	4.15	3.62	0.1120
20	7.18	6.28	5.47	5.11	4.36	4.22	3.78	0.1133
40	6.98	6.23	5.52	5.09	4.42	4.32	3.82	0.1053
60	7.02	6.15	5.73	5.23	4.57	4.49	3.79	0.1077
100	6.89	6.32	6.02	5.67	5.25	5.11	4.92	0.0657

References

1. Richardson SD, Plewa MJ, Wagner ED, Schoeny R, DeMarini DM (2007) Occurrence, genotoxicity, and carcinogenicity of regulated and emerging disinfection by-products in drinking water: a review and roadmap for research. Mutat Res Rev Mutat Res 636:178–242
2. Gunten UV (2003) Ozonation of drinking water: Part II. Disinfection and by-product formation in presence of bromide, iodide or chlorine. Water Res 37:1469–1487
3. Chiaro PS, Burke DA (1980) Sediment oxygen demand and nutrient release. J Environ Eng Div 106:177–195
4. Kim LH, Choi E, Stenstrom MK (2003) Sediment characteristics, phosphorus types and phosphorus release rates between river and lake sediments. Chemosphere 50:53–61
5. Chen X, He S, Huang Y, Kong H, Lin Y, Li C, Zeng GQ (2009) Laboratory investigation of reducing two algae from eutrophic water treated with light-shading plus aeration. Chemosphere 76:1303–1307
6. Davis TW, Berry DL, Boyer GL, Gobler CJ (2009) The effects of temperature and nutrients on the growth and dynamics of toxic and non-toxic strains of *Microcystis* during cyanobacteria blooms. Harmful Algae 8:715–725
7. Jiang Y, Ji B, Wong RNS, Wong MH (2008) Statistical study on the effects of environmental factors on the growth and microcystins production of bloom forming cyanobacterium-Microcystis aeruginosa. Harmful Algae 7:127–136
8. Paerl HW, Xu H, McCarthy MJ, Zhu G, Qin B, Li Y, Gardner WS (2011) Controlling harmful cyanobacterial blooms in a hyper-eutrophic lake (Lake Taihu, China): the need for a dual nutrient (N & P) management strategy. Water Res 45:1973–1983
9. Havens KE, James RT, East TL, Smith VH (2003) N:P ratios, light limitation, and cyanobacterial dominance in a subtropical lake impacted by non-point source nutrient pollution. Environ Pollut 122:379–390
10. Comba ME, Kaiser KL (1985) Volatile halocarbons in the Detroit River and their relationship with contaminant sources. J Great Lakes Res 11:404–418
11. Yao S, Ni J, Chen Q, Borthwick AG (2013) Enrichment and characterization of a bacteria consortium capable of heterotrophic nitrification and aerobic denitrification at low temperature. Bioresour Technol 127:151–157
12. Takaya N, Catalan-Sakairi MAB, Sakaguchi Y, Kato I, Zhou ZM, Shoun H (2003) Aerobic denitrifying bacteria that produce low levels of nitrous oxide. Appl Environ Microbiol 69:3152–3157
13. Huang TL, Li N, Zhang HH, Wang K, Liu TT (2013) Denitrification characters and safety of communities of cold tolerant oligotrophic and aerobic denitrifying bacteria. Chin J Environ Eng 7:2419–2423 (in Chinese)
14. Huang TL, Sun X, Zhao WL (2013) Effects of water depth on algae control in stratified reservoirs using in situ water-lifting aeration technology. Adv Mater Res 663:977–981

15. Sun X, Zhao WL, Zhang MD, Huang TL (2013) Effects of temperature gradient on algae inhibition zone in source water reservoirs using in situ water-lifting aeration technology. Adv Mater Res 663:870–875
16. Paerl HW, Paul VJ (2012) Climate change: links to global expansion of harmful cyanobacteria. Water Res 46:1349–1363
17. O'Neil J, Davis T, Burford MA, Gobler C (2012) The rise of harmful cyanobacteria blooms: the potential roles of eutrophication and climate change. Harmful Algae 14:313–334
18. Becker V, Caputo L, Ordóñez J, Marcé R, Armengol J, Crossetti LO, Huszar VLM (2010) Driving factors of the phytoplankton functional groups in a deep Mediterranean reservoir. Water Res 44:3345–3354
19. Liu L, Liu D, Johnson DM, Yi Z, Huang Y (2012) Effects of vertical mixing on phytoplankton blooms in Xiangxi Bay of three Gorges Reservoir: implications for management. Water Res 46:2121–2130
20. Whitworth KL, Baldwin DS, Kerr JL (2012) Drought, floods and water quality: drivers of a severe hypoxic blackwater event in a major river system (the southern Murray–Darling Basin, Australia). J Hydrol 450:190–198

Part IV
Microbial Remediation Method for Polluted Source Water

Functional Microbial Composition

Haihan Zhang

Abstract Reservoir water qualities are regulated by sediment/water microbial functional communities harbored in the drinking water reservoir ecosystem. However, little is known about reservoir sediment-/water-associated bacterial, fungal, archaeal, sulfate reducing bacterial, and actinomycetes populations. In this chapter, we used nested polymerase chain reaction (PCR) denaturing gradient gel electrophoresis (DGGE), substrate utilization profiling (named BIOLOG), quantitative PCR, clone sequencing, and high-throughout pyrosequencing methods to describe the microbial functional composition in drinking water reservoir ecosystems. Based on these backgrounds, there are five parts in this chapter, as follows: (1) Microbial metabolic activity in the sediments of drinking water reservoirs; (2) Bacterial composition in drinking water reservoir sediments; (3) Fungal composition in drinking water reservoir sediments; (4) Archaeal composition in drinking water reservoir sediments; (5) Carbon utilization patterns of reservoir water bacterial communities. The results from this chapter will undoubtedly broaden our understanding of reservoir functional microbial species harbored in these freshwater environmental conditions. The specific microbial species might be used for reservoir water bioremediation engineering processes.

Keywords Drinking water reservoir • Microbial composition • DNA • Pyrosequencing • Metabolic activity

1 Microbial Metabolic Activity in Drinking Water Reservoirs

Sediment microbial communities act as an important role in the aquatic ecosystem by influencing nutrient cycling, organic matter metabolism, heavy metal transportation, and organic pollutant transformation [1]. Previous publications have

H. Zhang (✉)
School of Environmental and Municipal Engineering, Xi'an University of Architecture and Technology, Yanta Road 13, 710055 Xi'an, Shaanxi Province, P. R. China
e-mail: zhanghaihan@xauat.edu.cn

T. Huang (ed.), *Water Pollution and Water Quality Control of Selected Chinese Reservoir Basins*, The Handbook of Environmental Chemistry 38,
DOI 10.1007/978-3-319-20391-1_12

recorded sediment microbial communities from the sea [2], lakes [3–7], rivers [8–10], wetlands [11], freshwater ponds [12], and drinking water reservoirs [13–16].

Drinking water reservoirs, either manmade or natural, are the main source of drinking water supply for cities in the northwest China area with low groundwater stocks [17]. During the past several decades, to ensure the safety of urban water supply, several manmade drinking water reservoirs have been built by the Chinese government. The raw water quality of a drinking water reservoir is regulated by the complex interactions between surface sediment and overlying water. To monitor the raw water quality of a reservoir, much attention has been paid to phosphorus release [18, 19], heavy metals and organic contaminants [20], and cyanobacterial water blooms [21]. Wei et al. [22] reported that denitrifying and ammonia oxidizing bacteria played a major role in the process of nitrogen release from the sediments of drinking water reservoirs through a static simulation experiment. However, little is known about the microbial community functional diversity harbored in the sediments of drinking water reservoirs.

Sediment microbial community diversity is also closely related to enzyme activities [16]. The mineralization of organic material by microbial communities is initiated by the activities of enzymes. Enzymes are inherently more sensitive to environmental conditions and employed as a biological parameter for sediment fingerprinting [23]. However, only a few studies of enzymatic activity from the sediment of reservoirs have been carried out [24]. Therefore, in this part of the chapter, we report on the sediment microbial community functional diversity determined using the substrate utilization profiling (BIOLOG) method and the activities of enzymes involved in phosphorus (alkaline phosphatase) and nitrogen (urease, protease) cycling from the reservoirs in northwest China.

1.1 Sampling Program

In this work, two drinking water reservoirs were selected to evaluate the microbial community functional diversity and enzyme activities. Sediment cores were collected from Shibianyu (SBY) and Tangyu (TY) Reservoirs, located in Chang'an District and Lantian County of Xi'an City, Shaanxi Province, China. The reservoirs were described in detail by Huang et al. [18, 19]. SBY and TY Reservoirs play an important role in the Xi'an urban water supply. In November 2011, surface sediments (0–30 cm) were collected using a Peterson sampler and transported to the laboratory within 4 h. The sediments were taken in three replicates and then subdivided for BIOLOG and enzyme activity determination. In this work, BIOLOG and enzyme activities were examined within 24 h after sampling.

1.2 Enzyme Activity Determination

To explore the sediment enzyme activity profiles, four enzyme activities, including sucrase activity, urease activity, dehydrogenase activity, and alkaline phosphatase

activity, were determined. The sediment enzyme activities were measured by the method developed by Guan Songyin [25], and with a little modification. Sucrase activity was examined using sucrose as the substrate. Urease activity was examined using urea as the substrate and measured spectrophotometrically at 578 nm. The sediment dehydrogenase activity was measured by 2,3,5-triphenyl tetrazolium chloride reduction, and the results were expressed as TF μg/(g · 24 h). Alkaline phosphatase activity was examined as the amount of phenol, and the activity was expressed as phenol mg/(g · 24 h). Sediment enzyme activities were examined with three replicates. Blank assays without sediment suspension and without substrate were also examined at the same time and acted as controls. The results of sediment enzyme activities were determined on the dry weight (*d.w.*).

1.3 Microbial Community Functional Diversity Determination

To explore the microbial community functional diversity profiles, bacterial and fungal communities were measured using BIOLOG ECO and FF MicroPlates (Biolog Inc., Hayward, CA, USA). According to the methods described by Zhang et al. [26], sediment samples (10.0 g *d.w.*) were shaken in 90 mL of sterile 0.85 % sodium chloride for 30 min at 120 rpm. The sediment suspension was diluted to 10^{-3} and 150 μL of sediment suspension was added into every well in the ECO and FF plates using eight-way electronic pipettes (Bio-Rad, USA). The BIOLOG ECO plate contains 31 different carbon sources: ten carbohydrates, two phenolic compounds, four polymers, seven carboxylic acids, two amines, and six amino acids (Table 1). The FF plate contains 95 different carbon sources.

The absorbance at 590 nm (ECO) and 750 nm (FF) was recorded every 12-h interval. The microbial activity in ECO and FF plates was expressed as the average well color development (*AWCD*). The *AWCD* was assessed using the formula [16]:

$$AWCD = \sum (Y - Y_0)/31 \text{ or } 95$$

Community functional diversity was expressed as species richness (R) and Shannon's diversity (H). R was the number of oxidized carbon substrates in the ECO or FF plates. H was calculated using the following formula:

$$H' = -\sum_{i=1}^{S} Pi \ln Pi = -\sum_{i=1}^{S} (Ni/N)\ln(Ni/N)$$

where Pi is the proportional color development of the ith well over the total color development of all wells of a plate. According to the *AWCD* curve, 96-h data were

Table 1 The 31 different carbon sources located on the BIOLOG ECO plate

Carbohydrates	Carboxylic acids	Amino acids	Polymers	Phenolic compounds	Amines
D,L-a-Glycerol	Pyruvic acid methyl ester	Arginine	a-Cyclodextrin	4-Hydroxy benzoic acid	Phenyl ethylamine
a-D-L-lactose			Glycogen	2-Hydroxy benzoic acid	Putrescine
b-Methyl-D-glucoside	g-Hydroxy butyric acid	Threonine	Tween40		
Phosphate	D-Galacturonic acid	Serine	Tween80		
i-Erythritol	a-Ketobutyric acid	Phenylalanine			
D-Cellobiose	D-Glucosaminic acid	Asparagine			
D-Mannitol	D-Malic acid	Glycyl-L-glutamic acid			
D-Xylose	Itaconic acid				
Glucose-1-phosphate					
N-Acetyl-D-glucosamine					
D-Galactonic acid lactone					

used for principle component analyses (PCA) of the microbial community diversity.

1.4 Statistical Analyses

The results are expressed as means and standard errors (SE). Means were compared by one-way analysis of variance and the Tukey–Kramer honestly significant difference (HSD) test at the 5 % level of significance ($P < 0.05$). PCA was carried out with SPSS (version 17.0) software for Windows.

1.5 Enzyme Activities in the Sediments

As shown in Fig. 1a, the sucrase activity in TY Reservoir was 329.77 mg glucose/$g \cdot 24$ h, which is significantly higher than that of SBY Reservoir ($F = 31.85$, $P = 0.0049$). The dehydrogenase activities in SBY and TY Reservoirs were 63.21 and 104.78 μg TF/h, respectively (Fig. 1b). The higher urease activity, 1.024 mg NH_2-N/$g \cdot 24$ h, was recorded in SBY Reservoir, which was 5.72 % higher than that

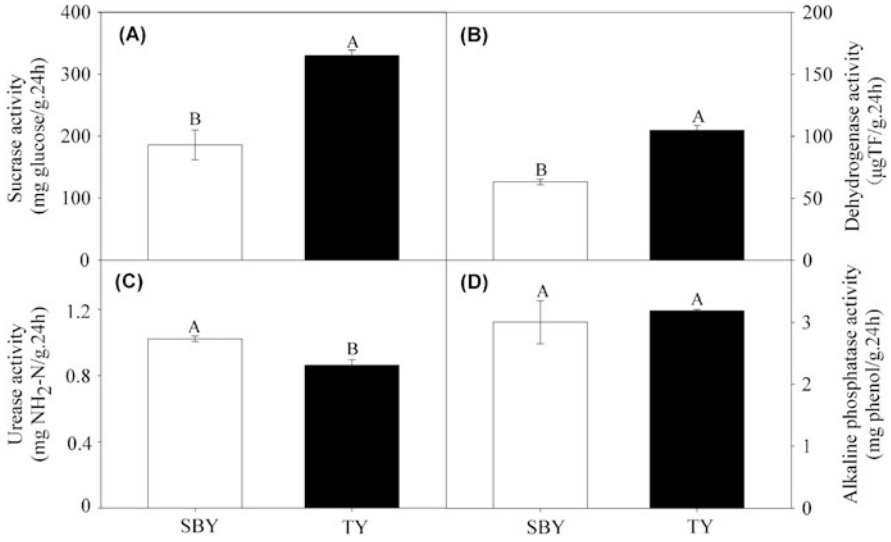

Fig. 1 (**a**) Sucrase activity, (**b**) dehydrogenase activity, (**c**) urease activity, (**d**) alkaline phosphatase activity in the sediments of SBY and TY Reservoirs. The data are shown as means and standard errors ($n = 3$). The same letter indicates no significant difference by the Tukey–Kramer HSD test ($P < 0.05$)

of TY Reservoir, being 0.968 mg NH_2-N/g · 24 h ($P < 0.05$). There were no significant differences in the alkaline phosphatase activity between SBY and TY Reservoirs ($P = 0.622$) (Fig. 1d).

1.6 Microbial Community Functional Diversity in the Sediments

As shown in Fig. 2, the *AWCD* was recorded. The *AWCD* of the bacterial community ($AWCD_{590nm}$) in the sediment of TY Reservoir was higher than that of SBY Reservoir (Fig. 2a). The $AWCD_{590nm}$ was lower before the early incubation process (0–12 h), it then increased rapidly during 24–72 h, and became steady after 96 h with values of 1.75 and 1.58 in TY and SBY Reservoirs, respectively. The total $AWCD_{590nm}$ in TY was 32.25, which is 8.55 % higher than that of SBY Reservoir. No significant different was found in species richness (*R*) ($P > 0.05$) (Table 2). Whilst the fungal community was express as $AWCD_{750nm}$, the results showed that the total $AWCD_{750nm}$ were 0.32 and 0.37 in SBY and TY Reservoirs, respectively ($P < 0.05$). The species richness and Shannon's diversity in TY were also higher than that of SBY ($P < 0.05$) (Table 2).

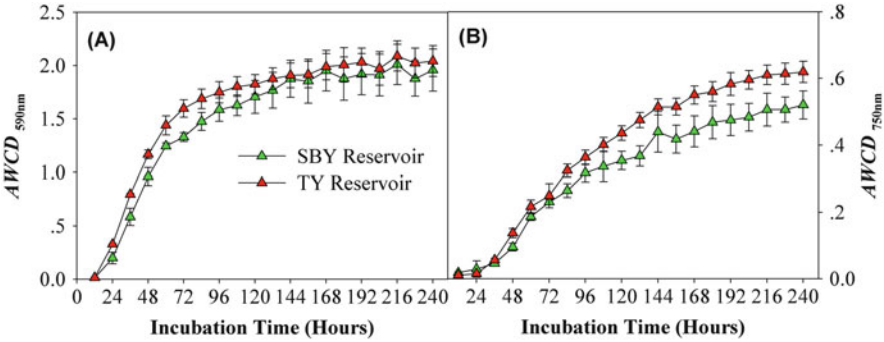

Fig. 2 Average well color development (*AWCD*) of: (**a**) bacterial community ($AWCD_{590nm}$) and (**b**) fungal community ($AWCD_{750nm}$) in the sediments of SBY and TY Reservoirs, respectively. The data are shown as means and standard errors ($n = 3$)

Table 2 The $AWCD_{(590nm,\ 750nm)}$, species richness (R), and Shannon's diversity (H) index of sediment microbial communities in the sediments of SBY and TY Reservoirs, respectively

Sediment microbe	Reservoirs	$AWCD_{(590nm,\ 750nm)}$	Species richness (R)	Shannon's diversity (H)
Bacterial community	SBY	1.58 ± 0.06 B	28 ± 1 A	3.21 ± 0.03 B
	TY	1.75 ± 0.05 A	29 ± 1 A	3.36 ± 0.01 A
Fungal community	SBY	0.32 ± 0.01 B	41 ± 2.31 B	4.11 ± 0.02 B
	TY	0.37 ± 0.01 A	51 ± 1.53 A	4.36 ± 0.03 A

The data are shown as means and standard errors ($n = 3$). The same letter indicates no significant difference by the Tukey–Kramer HSD test ($P < 0.05$)

PCA revealed that PC1 and PC2 explained 35.92 and 22.63 % of the total variation for the bacterial community, and 31.27 and 23.62 % for the fungal community, respectively (Table 3).

There is a significant difference in the carbon source utilization pattern in bacterial and fungal communities harbored in the sediments of SBY and TY Reservoirs (Fig. 3).

Meanwhile, the numbers of carbon substances with loadings ≥ 0.50 grouped by the sediment bacterial and fungal community for PC1 and PC2 are listed in Table 4.

In this work, the bacterial and fungal community diversity and enzyme activities revealing specific patterns of metabolic potentials in the sediments of SBY and TY Reservoirs were evaluated. The sucrase activity in TY Reservoir was 329.77 mg glucose/g · 24 h, which is significantly higher than that of SBY The reservoir. Dehydrogenase activities in SBY and TY Reservoirs were 63.21 and 104.78 μg TF/h, respectively. However, there were no significant differences in the alkaline phosphatase activity between SBY and TY Reservoirs. There was a significantly different carbon source utilization pattern in the bacterial and fungal communities harbored in the sediments of SBY and TY Reservoirs.

Table 3 PCA of latent root, percent of variance, and percent of total variance of sediment microbial communities in the sediments of SBY and TY Reservoirs, respectively

Sediment microbe	Item	Latent root	Percent of variance (%)	Percent of total variance (%)
Bacterial community	PC1	11.134	35.916	35.916
	PC2	7.016	22.631	58.547
	PC3	5.958	19.220	77.767
	PC4	4.378	14.123	91.890
	PC5	2.514	8.111	100
Fungal community	PC1	29.398	31.274	31.274
	PC2	22.198	23.615	54.889
	PC3	16.526	17.581	72.470
	PC4	13.610	14.479	86.949
	PC5	12.268	13.051	100

PCA principle component analyses

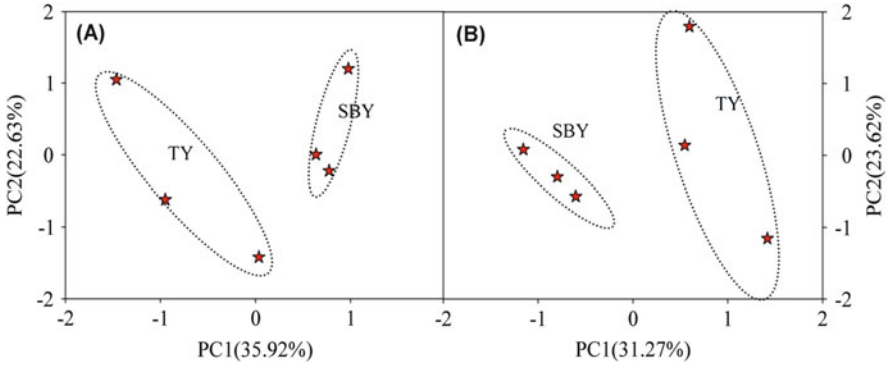

Fig. 3 PCA of (**a**) bacterial community functional diversity and (**b**) fungal community functional diversity in the sediments of SBY and TY Reservoirs. (**a**) Data were calculated based on substrate utilization patterns using BIOLOG ECO MicroPlates after an incubation period of 96 h. PC1 explained 35.92 % of the total variance, while PC2 explained 22.63 %. (**b**) Data were calculated based on substrate utilization patterns using BIOLOG FF MicroPlates after an incubation period of 96 h. PC1 explained 31.27 % of the total variance, while PC2 explained 23.62 %

1.7 Conclusion and Further Reading

Sediment microbial communities act as an important role in the aquatic ecosystem by influencing nutrient cycling, organic matter metabolism, heavy metal transportation, and organic pollutant transformation. In this work, the microbial community functional diversity and enzyme activity in the sediments of two drinking water reservoirs were examined. The functional diversities of sediment bacterial and fungal communities were determined using the substrate utilization profiling (BIOLOG) method. Sucrase, dehydrogenase, urease, and alkaline phosphatase activities were measured spectrophotometrically. The results showed that the

Table 4 Numbers of substances with loadings ≥0.50 grouped by the sediment bacterial and fungal community for PC1 and PC2

Sediment microbial communities	Carbon sources	PC1	PC2
Bacterial community	Carbohydrates	5	3
	Carboxylic acids	5	2
	Amino acids	4	2
	Polymers	3	1
	Phenolic compounds	1	0
	Amines	2	0
Fungal community	Carbohydrates	17	8
	Carboxylic acids	10	6
	Amino acids	11	4
	Polymers	1	0
	Phenolic compounds	0	0
	Amines	1	0

sucrase activity in TY Reservoir was 329.77 mg glucose/g · 24 h, which is significantly higher than that of SBY Reservoir. The dehydrogenase activities in SBY and TY Reservoirs were 63.21 and 104.78 μg TF/h, respectively. However, there were no significant differences in the alkaline phosphatase activity between SBY and TY Reservoirs. The *AWCD* of bacterial and fungal communities in the sediment of TY was higher than that of SBY. PCA revealed that PC1 and PC2 explained 35.92 and 22.63 % of the total variation, respectively. There is a significant difference in the carbon source utilization patterns of bacterial and fungal communities harbored in the sediments of SBY and TY Reservoirs.

In aquatic ecosystems, sediment enzymes play an important role in organic matter decomposition and the nutrition biogeochemical cycles, e.g., nitrogen and phosphorus cycling [27]. The esterases, phosphatases, glucosidases, and aminopeptidases activities in the sediments of the four reservoirs in Saxony (Germany) were reported by Wobus et al. [16], who suggested that different trophic states and catchment have different sediment enzyme activities. Meanwhile, Curticapean and Dragan-Bularda [24] also reported on the enzymatic activity from the sediment of Gilau Reservoir. Phosphatase, actual and potential dehydrogenase, catalase, urease, and protease were measured, revealing that the highest activities were observed at the tail of the reservoir. Enzyme activity can, therefore, be used as a biological characteristic of sediment in reservoir ecosystems.

The microbial community in the sediments of aquatic ecosystems also plays a vital role in monitoring the history of pollution of the sea, rivers, lakes, and reservoirs. However, compared with the massive literature available on lakes, the microbial community function diversity in the sediments of reservoirs is poorly understood. In this study, we used the BIOLOG method to examine the functional diversity of bacterial and fungal communities and found that there was a significant difference in the carbon source utilization patterns in bacterial and fungal communities harbored in the sediments of SBY and TY Reservoirs. Notwithstanding its

limitations, this study does, indeed, suggest microbial community functional diversity; the microbial community genetic diversity should be evaluated in the future. In previous studies, molecular methods were employed to explore the microbial compositions in sediment from aquatic ecosystems. Based on the PCR-DGGE method, Qu et al. [28] determined the bacterial diversity in the sediment of Guanting Reservoir, China; the results showed that the communities of bacterial types were very different in different layers of sediment. However, the structures of specific functional microbial communities should also be determined in the future. The results of this part of the chapter were first published in Desalination and Water Treatment [29]. Reprint with kind permission from Taylor & Francis Ltd.

2 Bacterial Composition in Drinking Water Reservoir Sediments

Microbial consortia play major roles in aquatic production and cycling of nutrients, and, particularly, the sediment-associated microbial community is vital for the maintenance of ecosystem function and health in aquatic environments [30]. Due to their important contributions in driving primary nutrient cycling and regulating water quality in the sediment–water interface, the sediment microbial community has attracted great attention from microbial ecologists [16, 28, 31–33]. Moreover, the sediment host distinct microbial communities and their populations may be greatly driven by changes in the nutritional status of water quality due to the variations of hydrological regimes [29, 34, 35]. However, given the importance of sediment microbes in regulating water quality through their roles in mediating biogeochemical cycles, we know very little of the bacterial community profiles [29]. Our recent studies provided preliminary knowledge of the sediment bacterial and fungal carbon utilization profiles of drinking water reservoirs, and revealed that there was a significant difference in the carbon source utilization patterns of bacterial communities harbored in reservoir sediments [29, 36–38], so these results received some qualifying statements.

Reservoir thermal stratification, a natural physical feature, creates physicochemical gradients from the surface water to the bottom sediment and forms an anoxic zone [39–41]. Sediment is, therefore, one of the most seasonally affected regions by lower oxygen and temperature due to vertical thermal stratification during the warmer months [42, 43]. Previous studies demonstrated that different temperatures and oxygen concentrations significantly altered the freshwater sediment microbial community composition [44, 45]. Compared with the massive amount of literature focused on exploring the patterns of microbial communities in sediment systems from oceans [46], lakes [44], and springs [46], investigations of drinking water reservoir sediments are limited [1, 36–38]. Meanwhile, a fundamental understanding of how the sediment bacterial groups are distributed during the thermal

stratification phase is still scare. Therefore, the present study was conducted with the aim of filling this gap.

Reservoir sediment-associated functional microbial groups such as ammonia-oxidizing bacteria (AOB) and ammonia-oxidizing archaea (AOA) have been broadly studied by molecular methods [47, 48]. In recent years, the high-throughput sequencing method has emerged as a powerful approach capable of exploring complex microbial communities in environmental samples such as sediments [33, 36–38]. The Roche 454 pyrosequencing approach has been widely used to reveal complex microbial community structures in the oxygen minimum zone of deep oceans [49] and subzero spring [50] sediments. Recently, we examined the sediment archaeal communities in thermal stratified SBY, ZC, and JP Reservoirs using Illumina MiSeq high-throughput sequencing and found that there was a distinct difference in the abundance and community composition of archaea among three water supply reservoirs [36–38]. However, the abundance and structure of sediment bacterial communities in this special and stressful environmental condition was not studied in detail by using advanced molecular methods such as quantitative PCR (qPCR) and high-throughput sequencing.

Therefore, the objective of this part of the chapter was to describe the community composition and abundance of sediment-associated bacteria present in three reservoirs by 454 pyrosequencing of 16S rRNA gene and qPCR methods. The reservoirs selected for this study have different geochemical parameters. The specific aims of the present work were: (1) to determine the abundance of sediment bacteria in ZC, SBY, and JP drinking water reservoirs, (2) to explore and compare the sediment bacterial community structure diversity in these three reservoirs, and also (3) to investigate the main sediment chemical characteristics which sustain the bacterial groups in these stressful water environmental conditions. Furthermore, the bacterial community sustained under this water ecosystem with complicated parameters is discussed.

2.1 Study Sites and Sampling

This study was conducted in three seasonally stratified reservoirs named ZCR, SBYR, and JPR. The ZCR Reservoir is located in Zaozhuang City, Shandong Province, eastern China, whereas the other two reservoirs are located in Xi'an City, Shaanxi Province, northwest China. JP and SBY Reservoirs serve as important drinking water sources for Xi'an City [40, 51] and ZC Reservoir is a large reservoir used for agricultural irrigation, drinking water, and recreational activities [29, 36–38]. Our research team has been studying the water quality of these oligotrophic reservoirs for a while, and the previous findings have been reported elsewhere [40, 51, 52]. Here, we report on the microbial diversity in sediments of the pronounced trophic gradient drinking water reservoirs. and the detailed conditions of these three reservoirs are listed in Tables 5 and 6.

Table 5 The main geochemical parameters of the three reservoirs observed during the sampling

Reservoirs	Reservoirs ID	Latitude (N)	Longitude (E)	Surface area (km^2)	Maximum depth (m)	Mean depth (m)	Temperature of surface sediment (°C)	Oxygen level of surface sediment (mg/L)
ZCR	ZCR	34°56′	117°40′	6.46	18	13	10	0.2
SBYR	SBYR	34°00′	108°95′	3.38	50	35	8	0.2
JPR	JPR	34°07′	108°20′	4.55	90	60	9	0.2

Table 6 The physicochemical properties of sediments in the ZCR, SBYR, and JPR Reservoirs

Reservoirs	pH	Organic matter (mg/g)	Total phosphorus (mg/g)	Total nitrogen (mg/g)	Total potassium (g/kg)	Available nitrogen (mg/kg)	Available phosphorus (mg/kg)	Available potassium (mg/kg)
ZCR	6.9 ± 0.8 B	42.72 ± 2.87 A	1.34 ± 0.01 A	2.97 ± 0.08 A	32.87 ± 0.47 C	102.10 ± 1.99 C	125.43 ± 2.75 A	612.48 ± 3.20 A
SBYR	8.1 ± 0.9 A	39.75 ± 0.92 A	1.02 ± 0.00 B	1.08 ± 0.01 B	44.93 ± 0.26 B	139.29 ± 0.87 A	63.01 ± 0.54 B	456.70 ± 13.69 B
JPR	7.8 ± 0.6 A	23.74 ± 1.55 B	1.01 ± 0.01 B	0.56 ± 0.03 C	50.74 ± 1.23 A	115.99 ± 0.38 B	38.01 ± 2.02 C	368.71 ± 11.82 C
ANOVA *F*-value	135**	81*	189**	1853***	412***	655***	1530***	406***

The data represent means and standard deviations. Values followed by different capital letters among reservoirs are significantly different.
*Statistically significant at $P < 0.05$, **statistically significant at $P < 0.01$, ***statistically significant at $P < 0.001$

ZCR, SBYR, and JPR were stratified at the time of sampling. The dissolved oxygen and temperature of the overlying water were determined using a Hydrolab DS5 multiprobe sonde (Hach, USA). Surface sediments were collected at a deep layer of 0–30 cm using a sterilized Petersen stainless steel grab sampler [29, 36–38], as mentioned in the method described by Zhang et al. [36–38]. For each reservoir, the sediment cores were taken in triplicate at 90–100-m intervals along the central length of each site [36–38]. The sediment samples were sieved by using a 2-mm mesh to remove stones and plant roots, and placed into sterile plastic bags and sealed. The samples were placed on ice and transported to the Key Laboratory of Northwest Water Resource, Environment and Ecology, Xi'an University of Architecture and Technology, China (KLNWR-ER-XAUAT). In the laboratory, each sample was divided into two halves and one half was used for physicochemical analysis, while the other half was put into sterilized screw-capped vials and stored at −20 °C until use for sediment microbial DNA extraction.

2.2 Determination of Sediment Chemical Characteristics

Sediments were air dried to a constant weight and then sieved a using 2- mm mesh [53]. Sediment chemical characteristics such as pH, organic matter, total nitrogen, total phosphorus, total potassium, available nitrogen, available phosphorus, and available potassium were analyzed in the Soil Environmental Testing Laboratory at Northwest A & F University (SETL-NWSUAF, China), as per the method described by Bao [53], with minor modifications.

2.3 Extraction of Sediment Microbial DNA

The total microbial genomic DNA from sediment samples was extracted using the Soil DNA Kit (Omega Bio-Tek, Norcross, GA, USA), according to the manufacturer's instructions. The DNA was extracted from 1.0 g (wet weight basis) of sediment in triplicate individually and then they were pooled together [36–38]. Extracted DNA was purified using the DNA Clean-Up Kit (Omega Bio-Tek, Norcross, GA, USA), according to the manufacturer's instructions, eluted in a final volume of 60 μL, and frozen at −80 °C until further analysis. The quantity (A_{260}/A_{280}) was determined using a NanoDrop ND2000 (Thermo Scientific, Waltham, MA, USA), and the concentration of the DNA was examined on 0.8 % agarose gel electrophoresis, stained with ethidium bromide (0.5 mg/L) and visualized by UV excitation (Bio-Rad Gel Doc™ XR^+, USA).

2.4 Determination of 16S rRNA Gene Copy Numbers by qPCR

To determine the abundance of bacteria in sediment samples, 16S rRNA gene copy numbers were examined using qPCR. The universal bacterial primer sets F357 (5′-CCTACGGGAGGCAGCAG-3′) and R518 (5′-ATTACCGCGGCTGCTGG-3′) were used for qPCR [54]. The qPCR reaction (25 μL) contained 12.5 μL of 2 × SYBR Green qPCR Master Mix (Tiangen Biotech Co., Ltd., Beijing, China), 0.5 μL of 10 μM of each F357 and R518 primer, 9.5 μL of ultrapure water, and 2 μL of DNA template (2 ng). Real-time qPCR was performed on an IQ5 thermo cycler (Bio-Rad Laboratories, Hercules, CA, USA), using a program of 2 min at 95 °C, followed by 40 cycles of 95 °C for 10 s, annealing for 40 s at 60 °C, and extension at 72 °C for 30 s. Melting curve analysis was performed from 60 to 95 °C.

To test the specificity of the qPCR, the melting curve profile and 1 % agarose gel electrophoresis of the PCR products suggested single specific amplicons of the predicted sizes (~170 bp). Amplification inhibition effects were determined according to Dumonceaux et al. [55]. The average amplification efficiency was 93.83 % and the amplification was linear ($R^2 = 0.999$). A qPCR standard was performed by amplifying the 16S rRNA gene of *Escherichia coli* genomic DNA [34, 35]. Amplification of a tenfold serial dilution of standard template from 10^7 to 10^1 copies was used to create standard curves. Based on the standards, bacterial 16S gene copy numbers were calculated by using a regression equation of the cycle threshold (*Ct*) value ($r^2 = 0.999$). The qPCR amplification of sediment sample, standard, and control containing no DNA template was performed in triplicate ($n = 3$).

2.5 Roche 454 Pyrosequencing

To better understand the specific profile of the bacterial community living in reservoir sediments, 454 pyrosequencing was performed on a 454 GS FLX Titanium sequencer platform (Roche Diagnostics Corporation, Branford, CT, USA), as previously described [49]. Briefly, the V1–V3 region of the 16S rRNA gene from different sediment samples with replicates was amplified using the primer sets designed by adding the adaptor barcode to the forward primer 8F (5′-454 adapterA-MID-AGAGTTTGATCCTGGCTCAG-3′) and reverse primer 533R (5′-454 adapterB-TTACCGCGGCTGCTGGCAC-3′) [49]. Adapters A and B represented (5′-GCCTCCCTCGCGCCATCAG-3′) and (5-′-GCCTTGCCAGCCCGCTCAG-3′), respectively. The total reaction (25 μL) contained 2.5 μL of 10 × buffer, 2.0 μL of dNTPs (2 mM), 2.0 μL of DNA (20 ng/μL), 1.0 μL of each forward (10 μM 8F) and reverse primers (10 μM 533R), and 0.125 μL of Taq DNA polymerase (5 U/μL) (TaKaRa, Japan). PCR was performed on a C1000 Thermal Cycler Gradient (Bio-Rad, USA) using a

program of 4 min at 94 °C, followed by 27 cycles of 30 s at 94 °C, 45 s at 55 °C, and 1 min at 72 °C, with a final extension for 7 min at 72 °C. For each sample, PCR was examined three times and pooled together to minimize PCR bias. Meanwhile, a negative control reaction was examined and revealed to be negative for the amplicon. All PCR products were verified by 1 % agarose gel electrophoresis with DL2000 DNA ladder (Kangwei Biotech Co., Ltd., Beijing, China) as a size standard.

The PCR products were purified with a DNA purification kit (DP209, Tiangen Biotech Co., Ltd., Beijing, China) according to the manufacturer's protocol, and then eluted in 60 μL of double-distilled water (ddH_2O). Small fragments were removed using beads (Beckman Coulter, Brea, CA, USA). The DNA concentration was quantified on an Agilent Bioanalyzer 2100 (Agilent Technologies, CA, USA), and an equimolar mix of three amplicon libraries was diluted to a concentration of 2.0×10^6 molecules/μL for emulsion PCR (emPCR). A full sequence run was performed on the Roche GS FLX 454 pyrosequencing platform (454 Life Sciences/Roche Applied Biosystems, Nutley, NJ, USA) by Shanghai Personal Biotechnology Co., Ltd. (Shanghai, China).

After the sequencing process, raw 454 pyrosequencing data were processed using Quantitative Insights Into Microbial Ecology (QIIME) software [56]. The standard primers and barcodes in the raw sequences were trimmed off. Sequences shorter than 200 bp, having a read quality score <25, and possessing homopolymers longer than 8 bp were also removed [57]. The sequencing reads were denoised and checked for chimeras [58]. After the filtration, the number of high-quality sequences of the three samples was 34,971. The average length of sequences without primer was 420 bp. In order to compare the three reservoirs, normalization of the sequence number was performed. The taxonomic classification of effective sequences was determined using the Ribosomal Database Project (RDP) database [59].

2.6 Nucleotide Sequence Accession Numbers

454 pyrosequencing data have been deposited at the NCBI Sequence Read Archive database (NCBI-SRA), under accession number SRP033486.

2.7 Data Analysis

Differences in sediment physical and chemical properties and bacterial 16S rRNA gene numbers of each reservoir were analyzed by one-way ANOVA with the Tukey–Kramer HSD test ($P < 0.01$), using SPSS for Windows version 16.0 (SPSS Inc., Chicago, IL, USA).

For 454 pyrosequencing bioinformatics analysis, high-quality sequences were classified into operational taxonomic units (OTUs) based on a 97 % sequence similarity using the mothur software package (version 1.7.0) (http://www.mothur.org/). The Shannon diversity index (H'), *Chao* 1 richness estimates, and abundance-based coverage estimator (ACE) were calculated using the ESTIMATES software package [60]. Coverage was calculated using the equation $C = 1 - N_1/N_2$, where N_1 is the number of singleton phylotypes and N_2 is the total number of sequencing reads.

The relative abundances of the top 85 abundant bacterial communities at the genus level were used to generate a heat map using vegan in the *R* package (version 2.1.1) [61]. A parsimony test was also used to analyze whether or not the sediment bacterial communities of two reservoirs have the same structure at the phylum level [62]. The bacterial cytoscape network clustering diagram was generated by Cytoscape software (version 2.8.0).

To reveal the main sediment chemical characteristics which sustain the bacterial groups, redundancy analysis (RDA) was performed to measure sediment chemical properties that had the most significant influence on the bacterial community. The significant correlations of the sediment chemical parameters were examined by a Monte Carlo permutation. The biplot was generated by CANOCO 4.5 software (Biometrics, Wageningen, The Netherlands). The figures were generated by SigmaPlot 10.0 for Windows (Systat Software Inc.) and the *R* package (version 2.1.1).

2.8 Chemical Characteristics of Sediments

The chemical composition of the reservoir sediments is summarized in Table 2. The selected chemical characteristics of sediments were significantly different among the three reservoirs ($P < 0.05$). The sediment pH values varied from 6.9 to 8.1, with the lowest value found in ZCR and the highest in SBYR. The ZCR sediment was nearly neutral. The available phosphorus was significantly higher in ZCR (125.43 ± 2.75 mg/kg) and significantly lower in JPR (38.01 ± 2.02 mg/kg) ($F = 1530$, $P < 0.0001$). The total nitrogen in ZCR was 5.3 times higher than that of JPR ($F = 1853$, $P < 0.0001$). Sediment organic matter, total phosphorus, and available potassium were in the ranges 23.74–42.72 mg/g, 1.01–1.34 mg/g, and 368.71–612.48 mg/kg, respectively (Table 6).

2.9 Abundance of Bacteria in Sediments

As shown in Fig. 1, the abundance of bacterial 16S rRNA gene in sediments was 9.13×10^6, 1.14×10^7, and 6.35×10^6 copies/ng DNA for SBYR, ZCR, and JPR,

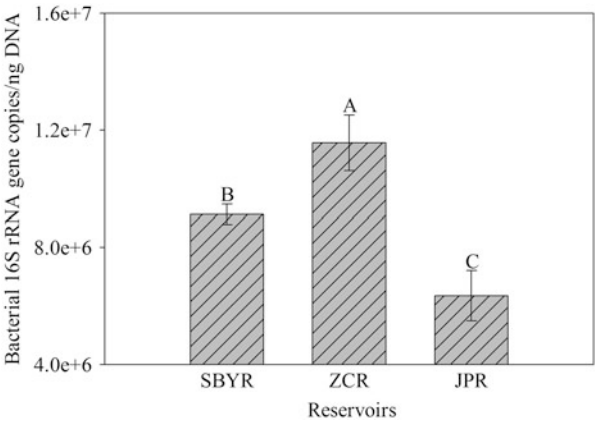

Fig. 4 The abundance of bacteria observed in sediments from SBYR, ZCR, and JPR. The *bars* with different upper letters are significantly different at the 0.01 levels. The *error bars* represent standard deviations. SBYR, ZCR, and JPR represent Shibianyu, Zhoucun, and Jinpen Reservoirs, respectively

respectively. The gene copy numbers were significantly higher in ZCR compared to SBYR and JPR ($P < 0.01$) (Fig. 4).

2.10 Bacterial Community Structure in Sediments

PCR-based 454 pyrosequencing produced 39,525 raw reads from the sediment samples of the three reservoirs, and 34,971 high-quality reads were used for further analysis. To assess the sediment bacterial community diversity, we chose to employ richness estimators. Table 7 shows the community diversity index values at a cut-off level of 3 %. The *Chao* 1 richness estimate in SBYR was 14.30 % higher than that of ZCR. The highest H' was observed in ZCR, and the lowest was in JPR, with a value of 6.57. The coverage of SBYR was slightly higher than that of ZCR (Table 7).

A total of 9673 OTUs were generated and the shared OTUs at different reservoirs were further determined via a Venn diagram. The values of OTUs were slightly higher in SBYR than the JPR and ZCR samples, and 212 OTUs were shared among the sediments of the three reservoirs. A total of 451 OTUs were shared between SBYR and JPR, accounting for 15.24 and 16.11 % of the total 2960 OTUs and 2800 OTUs, respectively (Fig. 5). At the phylum level, the sediment bacterial communities from the different reservoirs were similar to one another in terms of community composition; however, the percent of each phylum was distinct.

Figure 6 provides an overview of the bacterial community composition in the reservoir sediments. The dominant phyla in SBYR were *Proteobacteria* (40.38 %) and *Firmicutes* (30.96 %). In ZCR, *Proteobacteria* (39.56 %) were dominant, followed by *Firmicutes* (12.50 %), *Bacteroidetes* (17.62 %), and *Chloroflexi* (12.73 %). However, *Firmicutes* (56.83 %) and *Proteobacteria* (18.87 %) were the dominant phyla in JPR samples (Fig. 6 and Table 8).

Table 7 Sediment bacterial diversity and richness indices measured based on the 16S rRNA 454 pyrosequencing data retrieved from ZCR, SBYR, and JPR

Reservoirs	Number of effective sequences	Number of high-quality sequences	*Chao* 1 richness estimate	Abundance-based coverage estimators (ACE) index	Shannon's diversity index (H')	Coverage
ZCR	10,823	9106	7069	9486	7.52	0.77
SBYR	11,915	10,757	8080	11,379	7.22	0.78
JPR	16,787	15,108	7123	9466	6.57	0.86

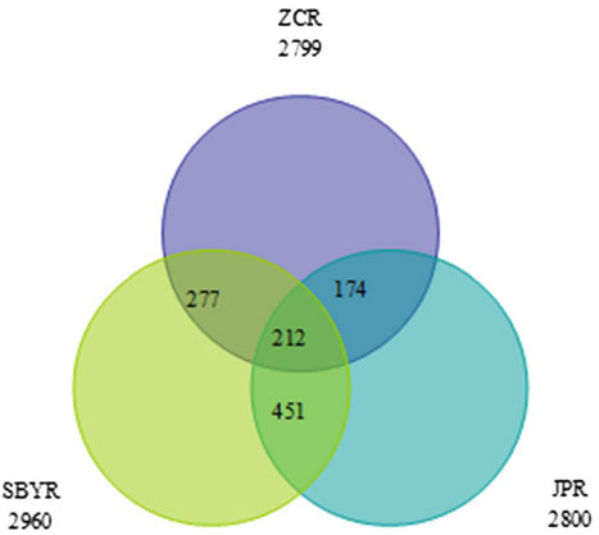

Fig. 5 Venn diagrams of shared and unique operational taxonomic units (OTUs) of bacteria in sediments at a 3 % distance level among the three reservoirs

The heat map diagram was drawn with the top 85 abundant bacterial communities at the genus level; throughout the whole profiles, the sediment bacterial communities in the three reservoirs were more diverse and different (Fig. 7). *Clostridium* (42.15 %) and *Bacillus* (20.44 %) were the dominant genera in JPR, whereas *Dechloromonas* (14.80 %) and *Smithella* (7.20 %) were dominant in ZCR. In ZCR, *Bacillus* (45.45 %) and *Acinetobacter* (5.15 %) were dominant (Fig. 7). The cytoscape network showed the most abundant OTUs across the sediments of the ZCR (cyan), JPR (red), and SBYR (green) reservoirs.

Multivariate analysis agrees with the heat map to indicate the distinct features among the three reservoirs. RDA was performed to assess the relationship between sediment chemical characteristics and the composition of the bacterial community based on 454 sequencing data. RDA performed on 454 sequencing data showed that RDA1 and RDA2 could explain 74.13 % of the total variation (Fig. 8) and the samples dispersed away from each other. RDA reveals that SBYR bacterial community in the top left of graph along RDA1, whereas the communities in the JPR and the ZCR in third quadrant and fourth quadrant in the plot, respectively (Fig. 8).

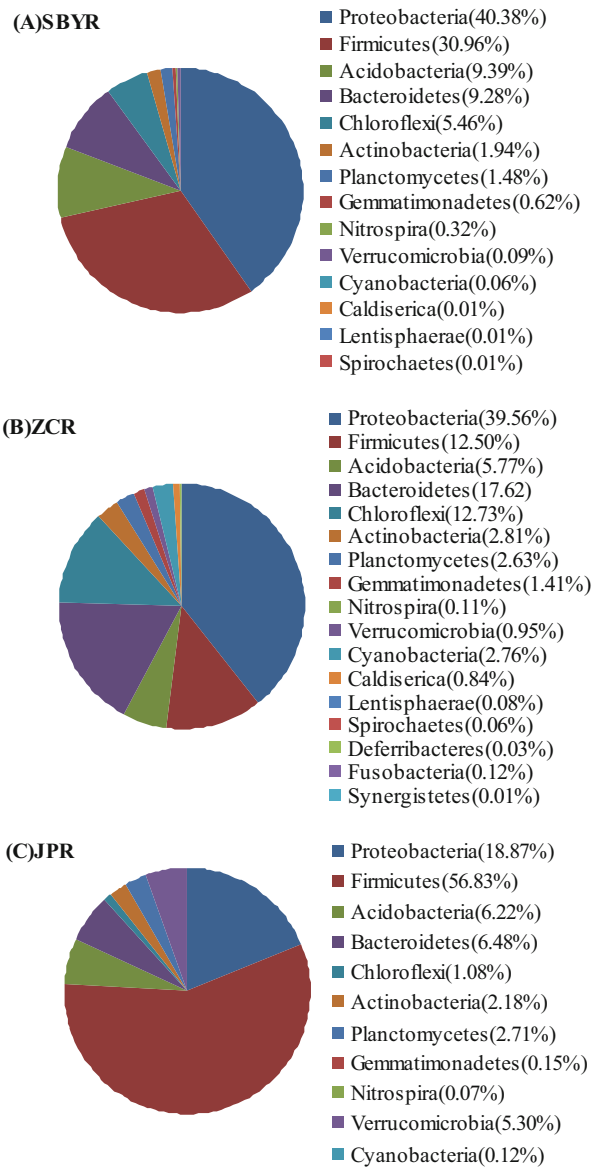

Fig. 6 Taxonomic classification of the bacterial community reads of 454 pyrosequencing from SBYR, ZCR, and JPR into phylum levels using the Ribosomal Database Project (RDP) classifier

RDA also showed that the composition of sediment bacterial communities in the JPR, SBYR, and ZCR Reservoirs were significantly correlated to the pH ($P < 0.01$, Monte Carlo permutation), organic matter ($P < 0.01$), total nitrogen ($P < 0.05$), and available phosphorous ($P < 0.05$). Organic matter, available potassium, available phosphorous, total nitrogen, total phosphorous, and total potassium accounted for a large amount of the variation in the distribution of samples along RDA1, and, thus, with the ZCR and JPR reservoirs. The pH and available nitrogen were significant in

Table 8 The results of parsimony test (*P*-test) for the sediment bacterial community structure in ZCR, SBYR, and JPR samples

Taxon at the phylum level	SBYR vs. ZCR (*P*-value)	ZCR vs. JPR (*P*-value)	JPR vs. SBYR (*P*-value)
Acidobacteria	NS	NS	NS
Actinobacteria	NS	NS	NS
Bacteroidetes	NS	<0.05	NS
Caldiserica	0.05	0.01	0.05
Chloroflexi	NS	0.05	0.05
Cyanobacteria	0.01	0.01	0.05
Deferribacteres	0.01	0.01	NS
Firmicutes	0.05	0.05	NS
Fusobacteria	0.01	0.01	NS
Gemmatimonadetes	NS	0.05	0.05
Lentisphaerae	0.05	0.01	0.01
Nitrospira	0.05	NS	0.05
Planctomycetes	NS	NS	NS
Proteobacteria	NS	NS	0.05
Spirochaetes	0.05	0.01	0.01
Synergistetes	0.01	0.01	NS
Verrucomicrobia	0.05	0.05	0.01

NS not significant, $P > 0.05$

explaining the variation in the microbial community composition along RDA2 ($P < 0.05$).

2.11 Conclusion and Further Reading

In summary, the bacterial abundance was 9.13×10^6, 1.14×10^7, and 6.35×10^6 copies/ng DNA in the sediments of SBYR, ZCR, and JPR, respectively. The pyrosequencing revealed a total of 9673 OTUs, which were affiliated with 17 phyla. The dominant phylum was *Firmicutes* (56.83 %) in JPR, whereas the dominance of *Proteobacteria* was observed in SBYR with 40.38 % and ZCR with 39.56 %. The Shannon–Wiener diversity (H') was high in ZCR, whereas the *Chao* 1 richness was high in SBYR. The dominant genera were *Clostridium* with 42.15 % and *Bacillus* with 20.44 % in JPR. Meanwhile, *Dechloromonas* with 14.80 % and *Smithella* with 7.20 % dominated in ZCR, and *Bacillus* with 45.45 % and *Acinetobacter* with 5.15 % in SBYR. The heat map profiles and RDA indicated substantial differences in the sediment bacterial community composition among the three reservoirs. Moreover, it appears from the results that physicochemical variables of sediments, including pH, organic matter, total nitrogen, and available phosphorous, played key roles in shaping the bacterial community diversity. The results obtained from this study will broaden our understanding on the bacterial

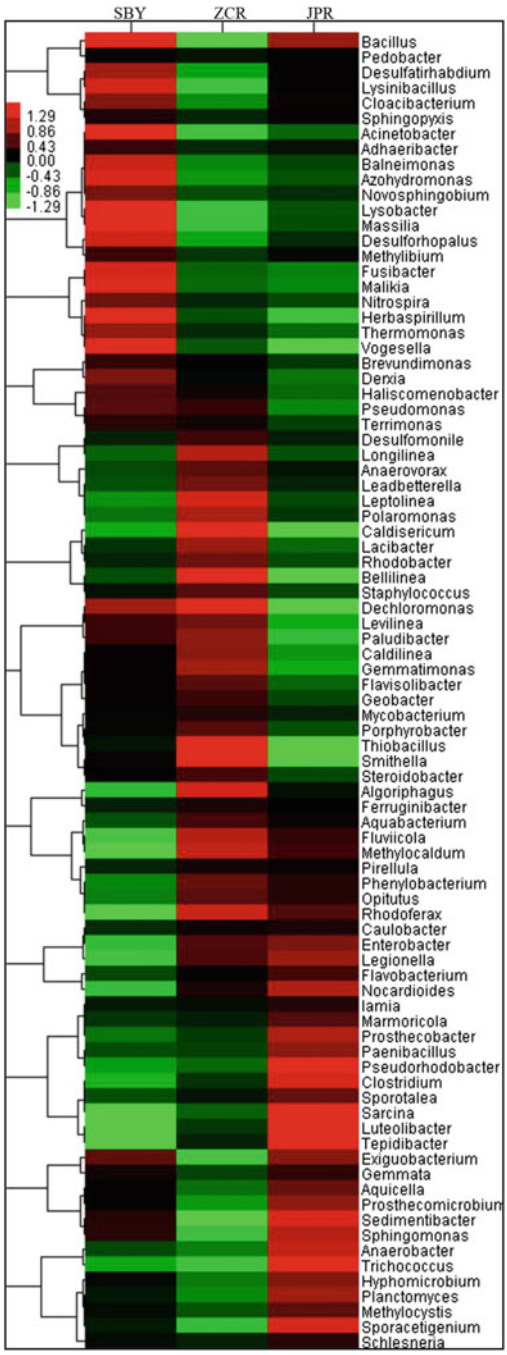

Fig. 7 A color scale heat map showing the 85 representative predominant 16S rRNA gene-based sequences classified at the genus level. *Red colors* indicate higher abundance; *green colors* indicate lower abundance

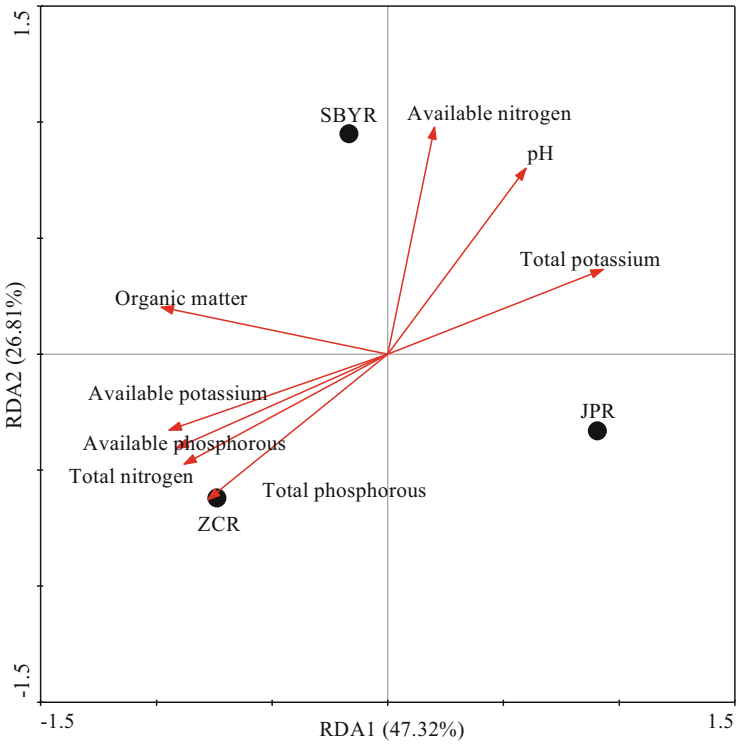

Fig. 8 RDA of sediment bacterial communities in SBYR, ZCR, and JPR Reservoirs. RDA1 explained 47.32 % and RDA2 explained 26.81 % of the total variance

community structure of sediments in oxygen minimum and stressful freshwater environments. The low oxygen concentrations, nutrient deficiency, and low food-to-mass conditions might be selective for individual special bacterial groups in stratified reservoirs.

Reservoirs play a pivotal role for urban areas by serving as drinking water sources and they are hydrologically distinct from other freshwater bodies, such as shallow lakes, subzero springs, and suboxic freshwater ponds [12, 31, 63]. Since the reservoir sediments are periodically threatened by low oxygen, due to seasonal thermal stratification [36–38, 42, 43], our present study investigated the abundance and diversity of bacteria present in oxygen minimum drinking water reservoir sediments.

The physicochemical characteristics of the sediments varied among the sampling locations. The pH was nearly neutral in ZCR, whereas the values were significantly high in sediments collected from the other two locations. The nutrients, both total and available nitrogen, phosphorous, and potassium varied significantly among the three sampling locations (Table 6). The organic matter, total phosphorus, total nitrogen, available phosphorus, and potassium levels were significantly high in ZCR as compared to the other two locations, due to the fact that

fish farming was intensely performed in ZCR in the last 20 years, so more nutrient substances were deposited into the bottom sediment. Compared with other similar studies, we found that the total phosphorous values observed were comparable to the values observed in the shallow Antoniek Reservoir in Cybina River, western Poland [64] and the tropical Kariba Reservoir, Zambia [65]. However, the total nitrogen values observed in this study were lower than the values observed in a reservoir located on the border between Zambia and Zimbabwe, in the middle Zambezi [65].

Sediment nitrogen and phosphorus cycling was influenced by thermal stratification. During the thermal stratification period, with lower oxygen concentration in the bottom of reservoir, more phosphorus can be released from the bottom sediment. Hupfer and Lewandowski reported that the oxygen level controls the phosphorus release in sediments [66]. Fan and Morohiro also determined the effect of aerobic and anaerobic conditions on the exchange of nitrogen and phosphorus across the sediment–water interface in Lake Kasumigaura and found that the nutrients release in sediment was more under anaerobic conditions as opposed to aerobic conditions [67]. It is might be that nitrogen and phosphorus released from the sediment can regulate the bacterial community structure.

The bacterial abundance (assessed by the calculation of 16S rRNA gene copy numbers) was significantly higher in ZCR as compared to SBYR and JPR (Table 2), and the results revealed that a high abundance of bacteria was observed in anoxic sediments of the reservoirs. The total numbers of bacterial cells observed in sediments may be influenced by the trophic state of the reservoir [68]. The bacterial abundance in terms of bacterial 16S rRNA gene copy numbers observed in this study was comparable to the data observed for other drinking water reservoirs [33] and a hypersaline lake [6]. High values observed in the previous studies were consistent with the hypothesis that sediment bacteria adapt to lower temperature and oxygen stress conditions for survival. Huang et al. reported that the bacterial abundance was highest in the surface sediment collected from Pearl River, whereas the abundance decreased significantly below 20 cm and the active bacteria were present in 7.5–46.7 % of the total bacterial number, which decreased with the sediment depth [18, 19].

The H' values ranged from 6.57 to 7.52 and the highest value was observed in ZCR. However, the ACE index did not show much difference. While studying the microbial diversity of sediments in a drinking water reservoir in Saidenbach, Germany, Röske et al. found that the Shannon diversity values were in the range 6.7–7.1 [33]. However, Wobus et al. observed low diversity values ranging from 3.6 to 4.5 while studying the microbial community of reservoir sediments from different trophic states [16]. The coverage values observed in the present study (0.77–0.86) indicate the presence of high microbial diversity in reservoir sediments.

In the present study, the sediment bacterial communities in ZCR, JPR, and SBYR belonged to 17 phyla and similar results were previously observed by Song et al. while studying the sediment microbial communities in a shallow lake in Dongping, China [63]. We observed that the globally distributed bacterial species within the phyla *Proteobacteria* and *Flavobacteria* were highly abundant

in the drinking water reservoir sediments. The dominant phylum in ZCR and SBYR samples were *Proteobacteria*. Similar results were found by Röske et al. [32] in the sediments of a mesotrophic drinking water reservoir in Saidenbach, Germany, where *Proteobacteria* were dominant in sediments, particularly the *Betaproteobacteria* and *Deltaproteobacteria*. Our findings are consistent with previous studies which reported the dominance of *Proteobacteria* in Neunzehnhain, Muldenberg, Saidenbach, and Quitzdorf Reservoir sediments [30] and hypersaline lakes [18, 19]. *Flavobacterium* was found to be dominant in JPR. The members of *Flavobacterium* have been frequently detected in various environments, such as soil and sediments [5]. Several clades which were not previously reported in reservoir sediments were found to be present exclusively within JPR, including the *Spirochaetes* and *Verrucomicrobiales*, which were commonly found in riverine sediments [69]. Anammox bacteria were detected in reservoirs, including *Planctomyces*, *Pirellula*, and *Gemmata*, which play important roles in nitrogen cycling. The present study revealed an unexpectedly high degree of bacterial diversity and several new clades in sediments which were not previously found in reservoir sediment samples.

As reported previously for several reservoirs, the community compositions among the different types of reservoir sediments exhibited pronounced differences [29, 33]. The reservoir sediment bacterial communities varied greatly due to the differences in physical and chemical properties, such as organic matter, pH, redox potential, and nitrogen availability [16, 30]. Differences in sediment physicochemical parameters may influence the bacterial community composition [30, 43, 44]. To reveal the effects of environmental conditions on bacterial community diversity, it is necessary to determine the main factors which shape the reservoir sediment's bacterial community. Sediments are extremely complex environmental systems where bacteria have to adapt to different physical and chemical conditions. Previous reports suggested that the sediment bacterial community was significantly impacted by environmental conditions [48, 62]. In the present study, the results of RDA revealed that pH, organic matter, total nitrogen, and available phosphorous were significantly correlated with the sediment bacterial community structure and a total of 74.13 % of the variations significantly correlated. In this work, the highest organic matter content was found in ZCR and the lowest was in JPR. The significant difference reveals that a higher sediment organic carbon concentration might lead to higher sediment bacterial diversity in the reservoir. This is consistent with several previous studies which suggested that increasing organic carbon in sediment could enhance sediment bacterial metabolism [64]. We also used a Monte Carlo permutation (MCP)-based statistical test for detecting the main factors influencing the bacteria community, as the MCP method can be used to detect community stratification of genetic samples. The present study indicated that the total nitrogen and pH were the most important drivers for sediment bacterial community composition. However, this result is different from that found in Taihu Lake, which showed that the sediment total phosphorus concentration was significantly correlated with the diversity of sediment bacterial communities [62].

Functional groups of bacteria in sediments play an important role in regulating carbon, nitrogen, sulfur, iron, and manganese biogeochemical cycles [30]. Moreover, the aquatic sediments act as a reservoir for many microbes, including pathogens. In this study, *Clostridium* and *Bacillus* were dominant in the sediments of JPR and SBYR. The genera *Clostridium* and *Bacillus* are Gram-positive bacteria belonging to the *Firmicutes* and the members of the former genus are obligate anaerobes, whereas the members of the latter can be obligate aerobes or facultative anaerobes. The above genera include free-living forms and also some pathogenic organisms. Although it is difficult to explain the reasons for their dominance in sediment samples, it has been previously reported that sediments and also the sewer samples act as reservoirs for members of the *Clostridium*, such as *C. perfringens* [70]. Members of the *Bacillus* were reported to produce a large amount of endospores in order to survive under stressful conditions [71].

The color-coded heat map shows that the bacterial genera *Haliscomenobacter*, *Pseudomonas*, *Terrimonas*, *Dechloromonas*, *Levilinea*, and *Paludibacter* were abundant in SBYR and ZCR (Fig. 7), whereas the genera *Fluviicola*, *Methylocaldum*, *Phenylobacterium*, *Optitus*, and *Rhodoferax* were abundant in ZCR and JPR, and, interestingly, *Enterobacter* and *Legionella* were also found to be abundant in these locations. The bacteria *Exiguobacterium*, *Sedimentobacter*, and *Sphingomonas* were abundant in SBYR and JPR (Fig. 7). *Haliscomenobacter hydrossis* has been reported to be the only species for this genus and is commonly found in activated sludge [72]. Factors such as low oxygen concentrations, nutrient deficiency, and low food-to-mass conditions were found to be selective for *H. hydrossis* [73]. Although it is difficult to explain the reason for the abundance of all the above organisms, the water quality, nutrient availability, and low oxygen conditions of the river sediments might favor the growth of certain microorganisms. It is also clear that most of those organisms are found to be ubiquitous in environmental samples, including soil, sediment, and water, whereas some organisms were found to be common in wastewater and sludge samples (e.g., *Terrimonas* and *H. hydrossis*). Some bacteria like *Pseudomonas* and *Clostridium* were found to be involved in nutrient cycling, such as denitrification [74]. The genus *Dechloromonas* has been found to be ubiquitous in the environmental samples and soil bacterial species. *D. aromatica* was reported to have complex life cycle and cryptic anaerobic pathways for aromatic biodegradation [75, 76]. In addition, members of *Dechloromonas* have been reported to be involved in nitrate-dependent Fe (II) oxidation and the Fe–N redox reactions in sediments may be associated with the development of specific microbial populations based on the energy available [77]. The less abundant bacteria such as *Polaromonas* and *Rhodobacter* could be correlated with carbon cycling, while *Desulfatirhabdium* and *Desulfomonile* could be linked to sulfate reduction and *Thiobacillus* with iron and sulfur oxidation. The nitrifying bacteria, closely related to the *Nitrospira*, observed in this study were found to be present in other drinking water reservoirs [44] and Lake Taihu [67]. It is also noteworthy to mention that the genera *Enterobacter* and *Legionella* were found to be abundant in two reservoirs (ZCR and JPR). These two reservoirs serve as a drinking water source for Xi'an City and Zaozhuang City; therefore, several

suitable water treatment processes should be done prior to distribution to urban community consumers.

It is generally believed that the activity and growth of the bacterial community in reservoir sediments is controlled by the oxygen concentration [44], temperature [45], and availability of organic carbon [78], nitrogen, and phosphorus [79]. During thermal stratification, sediment beneath biotic ecosystems is thought to be controlled by very low oxygen concentrations near to zero. It is noteworthy that dramatic diversity of the sediment bacterial community was found in the present study and the bacterial community was significantly correlated to the environmental parameters such as organic matter, pH, total nitrogen, and total phosphorous. Functional bacterial groups in sediments play an important role in regulating carbon, nitrogen, sulfur, iron, and manganese cycling. In future work, the high-throughput and sensitive sequencing technologies, including PCR-based Roche 454 pyrosequencing, Illumina GA, and Ion Torrent PGM sequence platforms, should be combined with the stable isotope probing (SIP) technique to establish a relationship between nutrients biogeochemistry cycling and the function of sediment microbial communities in fresh drinking water reservoirs. The results of this part of the chapter were first published in Microbial Ecology [80]. Reprinted from Microbial Ecology, 2015, Vol. 69, pp. 618-629, with kind permission from Springer Science+Business Media.

3 Fungal Composition in Drinking Water Reservoir Sediments

Aquatic sediment hosts diverse microbial communities that are the main drivers of nutrient cycles and energy fluxes [81–83]. Over the past few decades, bacterial and archaeal communities from the sediment of various aquatic environmental systems have been widely examined [32, 33, 48, 84, 85]. Sediment carbon monoxide-oxidizing bacteria [83], methanobacteria [81], denitrifying bacteria [82], and sulfate-reducing bacterial community compositions clearly regulate the exchange and transformation of carbon (C), nitrogen (N), and sulfur (S) at the water–sediment interface of eutrophic lakes [83], constructed wetlands [86], and acidic mine-draining rivers [87]. In contrast, sediment fungal community structure and diversity are not well examined, although fungal species perform important services involved in organic matter decomposition and the food web [88].

Reservoirs provide water sources for several beneficial purposes, including agricultural irrigation, industrial cooling processes, and urban municipal water utilization [40]. To ensure the security of urban water supply, the determining of the harmful cyanobacterial toxins [89], antibiotic resistance genes [78], and endogenous pollutants (e.g., nitrogen, phosphorus, iron, and manganese) released from sediments [1] of water supply reservoirs have been routinely performed. From an aquatic ecological point of view, more comprehensive exploration of the microbial

diversity in sediment will improve our understanding of the major global biochemical processes in reservoirs [81]. Unfortunately, limited publications have revealed sediment microbial compositions [32, 33], and even fewer have described fungal abundance and communities [88].

Sediment fungi represent a significant component of the benthic microbial biomass in reservoirs, and these organisms are a vital biological force in regulating water quality through the decomposition of organically bound C and N deposited at the bottom of the reservoir [1, 29, 36–38]. Our previous studies of water supply reservoir sediments demonstrated that sediment fungal communities successfully utilize carbohydrates, phenolic compounds, and carboxylic acids as carbon sources [29, 36–38]. Furthermore, nested PCR-DGGE profiles suggested that the sediment fungal community was fairly complex; however, more specific taxonomically defined fungal populations have not yet been thoroughly explored due to technological limitations such as only predominant species are displayed in the DGGE gel fingerprints and the comigration of PCR fragments with different sequences [36–38].

With notable advances in molecular and bioinformatics technologies, several useful methods such as catalyzed reporter deposition fluorescence in situ hybridization (CARD-FISH), clone sequencing, and functional gene arrays (FGAs, GeoChip) have been widely employed for tracking sediment microbial diversity, and the application of high-throughput sequencing techniques (HTST) has provided insight into reservoir sediment microbial communities [32, 33, 90]. Röske et al. [32, 33] used CARD-FISH and 454 GS FLX pyrosequencing to investigate sediment bacterial and archaeal communities from a mesotrophic drinking water reservoir located in Saxony, Germany. Recently, Huerta et al. [78] also determined the sediment bacterial communities in three water supply reservoirs located near Barcelona, Spain using Roche 454 GS FLX pyrosequencing.

This part of the chapter will help to close this enormous "fungi gap" in our understanding of sediment microbial communities by using Roche 454 GS FLX pyrosequencing to provide detailed genetic fingerprints of sediment fungal community diversity in water supply reservoirs with different eutrophication levels. The main objective of this section was to determine the abundance and diversity of fungal community in the surface sediments from three water supply reservoirs (named JP, SBY, and ZC Reservoirs) with different eutrophication levels. To this end, we (1) utilized qPCR to examine the 18S rRNA gene copy numbers and (2) used 454 GS FLX pyrosequencing to determine the taxonomic diversity and composition of the fungal community compositions in the sediments of the JP, SBY, and ZC Reservoirs. The results from this work can give us greater insight into the aquatic fungal community diversity in the sediment at the bottom of the reservoir exposed to various degrees of eutrophication.

3.1 Sampling Sites Description and DNA Extraction

This study was conducted on three different water supply reservoirs (named JP, SBY, and ZC Reservoirs) in China. Our research group members typically monitor

the water quality of these seasonally stratified reservoirs, which are oligotrophic, although ZC Reservoir often exhibits a moderate eutrophication development trend [40, 51]. As shown in our previous reports [40, 51], the water quality of the ZC Reservoir is worse than that of the JP and SBY Reservoirs, due to the presence of intense fish farming 10 years ago.

The JP Reservoir, a potable water source reservoir, is located in Zhouzhi County (34°07′N, 108°20′E), Shaanxi Province, northwestern China. The annual average rainfall is approximately 900 mm. This reservoir was built in 1996 and includes 1481 km^2 of watershed and 4.55 km^2 of water surface. The maximum depth is 90 m, and the daily water supply ability for Xi'an City is about 8.0×10^5 m^3 [40].

The SBY Reservoir, which was built in 1976, is situated in Chang'an District (34°00′N, 108°95′E) and is 35 km from Xi'an City, Shaanxi Province, northwestern China. The maximum and minimum water levels are 731 m and 675 m above sea level, respectively. The maximum depth is about 50 m. The daily water supply for Xi'an City is about 4.0×10^5 m^3. The total storage capacity is 2.81×10^8 m^3. The height of the dam is 82.5 m, and the length of this dam is 285 m [51].

The ZC Reservoir, which was built before 1985, is located in Zaozhuang City (34°56′N, 117°40′E), Shandong Province, eastern China. The maximum depth is about 15–18 m, with an average depth of about 13 m, and the area of the water surface is 6.46 km^2 [36–38]. This reservoir serves as an important backup water source for Zaozhuang City municipal water utilization during the dry season.

In summer and autumn, stable thermal stratification is seasonally formed in these three water supply reservoirs [40, 51]. During the sampling periods, the dissolved oxygen concentration of sediment-overlying water was about 0.2 mg/L, and the bottom sediment experienced complete anaerobic conditions, with a temperature of approximately 8–10 °C [40]. As previously described [36–38], the surface sediment cores (~30 cm long) were sampled using a sterilized Peterson sampler. Sediment samples were collected randomly from three spatially separated sites in each reservoir with a minimum of 90–100 m interval. The upper 5 cm (0–5 cm depth) of the surface sediments from the triplicate samples in each reservoir was sliced and mixed, placed into sterile polyethylene bags (Corning, Biotechnology Co., Ltd., Shanghai, China), and then maintained at 8 °C in a cooler (SK-01A, XBY technology Co., Ltd., Beijing, China) until transfer to the laboratory of the School of Environmental and Municipal Engineering, Xi'an University of Architecture and Technology (SEME-XAUAT), within 24 h after the fieldwork.

Samples were sieved through a sterile stainless steel 2-mm sieve and then frozen at −20 °C before use for DNA extraction. Total microbial DNA was extracted from 0.5 g of sediment (wet weight), as reported previously [36–38], using the Soil Fast DNA® Extraction Kit (Omega Bio-Tek, Norcross, GA, USA), according to the manufacturer's protocol. The extracted DNA was purified using a DNA purification kit (DP209, Tiangen Biotechnology Co., Ltd., Beijing, China), and the DNA concentration and quality (OD_{260}/OD_{280} ratio) were determined using a NanoDrop ND2000 (Thermo Scientific, Waltham, MA, USA), and checked on 0.8 % agarose gel (Amresco, Solon, OH, USA), visualized by ethidium bromide (0.5 mg/L, Sigma, USA) staining and UV illumination (Bio-Rad, Gel Doc™ XR^+, USA).

The purified DNA was stored at −20 °C until qPCR and 454 pyrosequencing analysis.

3.2 qPCR Analysis

To examine the relative abundance of sediment fungi in the three reservoirs, we used the real-time qPCR (qPCR) method as described by Rousk et al. [91] and Dollive et al. [92], with minor modifications. In this work, an assay was used to determine the 18S rRNA gene. The qPCR was performed in a volume of 25 μL with 2× SYBR Green qPCR Master Mix (12.5 μL, TaKaRa, Japan), 1 μL of each primer (10 μM), ddH_2O (9.5 μL), and 2 μL of DNA template (45 ng/μL). The following primers were used in these studies: Fung (5′-ATTCCCCGTTACCCGTTG-3′) and NS1 (5′-GTAGTCATATGCTTGTCTC-3′). The qPCR was performed in an IQ 5 thermal cycler (Bio-Rad, Hercules, CA, USA), using the following amplification protocol: 95 °C for 2 min, followed by 40 cycles of 95 °C for 10 s, 60 °C for 40 s, and 72 °C for 30 s. Samples were then maintained at 4 °C and checked on the 0.8 % agarose gels (Amresco, OH, USA) with DL-2000 DNA Marker (Kangwei Biotech Co., Ltd., Beijing, China), stained with ethidium bromide (5 mg/L, Sigma, USA). The resultant qPCR product of 337 bp was obtained.

The standard curve was constructed using genomic DNA containing a full-length copy of the *Saccharomyces cerevisiae* 18S rRNA gene. Tenfold serial dilutions from 10^{-1} to 10^{-7} were used to generate the standard curve [91]. The calculated DNA melting curve ranged from 80 to 88 °C, with 0.5-°C increments. The average amplification efficiency (AAE) was 91.03 %, and amplification resulted in a good linear relationship ($R^2 = 0.998$). Based on the number of gene copies from the standard curve, the tested fungal 18S rRNA gene copy numbers were calculated according to cycle threshold (C_t) data [91]. All qPCR were repeated in triplicate using the DNA extracted from each sediment sample.

3.3 454 Pyrosequencing Analysis

To analyze the composition and diversity of the fungal communities in the three reservoirs, we used Roche's 454 GS FLX pyrosequencing technique. The nuclear ribosomal internal transcribed spacer (ITS) region has recently been used as the standard marker for fungal DNA barcoding, and more ITS sequences have been deposited in several databases, giving a large reference for the identification of fungal taxa [93–95]. Therefore, the ITS region was determined in the present study. The following primers were used: ITS1F (5′-454adapterA-MID-CTTGGTCATTTAGAGGAAGTAA-3′) and ITS4R (5′-454adapterB-TCCTCCGCTTATTGATATGC-3′) (amplifying both ITS1 and ITS2 introns). adapterA and adapterB represent 5′-GCCTCCCTCGCGCCATCAG-3′ and

5′-GCCTTGCCAGCCCGCTCAG-3′, respectively. MID was designed for the barcoding key. ITS1F and ITS4R are fungal-specific primers that correspond to the ITS1 and ITS2 regions, respectively [96].

Each PCR assay contained 2.5 μL of 10× reaction buffer, 2 μL of dNTPs (2.5 mM), 1 μL of DNA (20 ng/μL), 1 μL of primer ITS1F (10 μM), 1 μL of primer ITS4R (10 μM), and 0.125 μL of *Taq* DNA polymerase (5U/μL) (TaKaRa, Japan). PCR was carried out in a C1000 Thermal Cycler Gradient (Bio-Rad, USA) with the following cycling protocol: 4 min at 94 °C; 34 cycles of 30 s at 94 °C, 45 s at 47 °C, and 60 s at 72 °C; and a final extension for 7 min at 72 °C. Samples were then maintained at 4 °C until analysis. The resultant PCR products, which were 600–800 bp fragments of the fungal ITS region, were obtained and purified using a DP209® DNA purification kit (Tiangen Biotechnology Co., Ltd., Beijing, China), following the manufacturer's recommendations. Small fragments were removed using beads (Beckman Coulter, Brea, CA, USA). The quality and quantity were checked using a Bioanalyzer 2100 (Agilent, Santa Clara, CA, USA) and the Qubit® Fluorometer (Invitrogen, Carlsbad, CA, USA). Emulsion PCR (emPCR) was carried out using a GS FLX emPCR amplicon kit in accordance with streamlined protocols (454 Life Sciences/Roche Applied Biosystems, Nutley, NJ, USA). The ITS regions were sequenced using the Roche GS FLX 454 pyrosequencing platform (Roche Applied Science, USA) by the Shanghai Personal Biotechnology Co., Ltd., China.

After sequencing, the raw sequences obtained were processed using the QIIME toolkit [56]. The standard primer sets and barcodes were excluded. Sequences with a quality score lower than 25 were trimmed. Sequences with lengths of less than 200 bp or containing any unresolved nucleotides were removed. Pyrosequencing data were denoised and chimeras were identified and removed from the datasets. To identify potential chimeric sequences, mothur was used. After removing lower quality sequences, all good-quality sequences obtained by pyrosequencing were clustered into OTUs with 0.97 cut-off settings. The taxonomic statuses of the tested sequences were classified using the RDP classifier and the NCBI Taxonomy browser [59, 90].

3.4 Nucleotide Sequence Accession Number

454 GS FLX pyrosequencing data have been deposited in the NCBI-SRA under the accession number SRP 033487.

3.5 Data Analysis

The sediment fungal abundance data were analyzed by one-way ANOVA with the Tukey–Kramer HSD test ($P < 0.01$). For bioinformatics analysis, the *Chao*

1 diversity, ACE, and Shannon's (H) and Simpson (D) diversity indices were calculated by mothur (http://www.mothur.org/) [90, 91]. The parsimony test was used to determine the relatedness of the dominant fungal phyla between two reservoirs. Based on the pyrosequencing data, PCA was employed to reveal the relationships between the sediment samples and fungal genus data derived from 454 pyrosequencing using SPSS software (version 16.0, Systat Software, Inc., Chicago, IL, USA). Heat maps and rank-abundance curves were constructed with the *R* statistics software package (version 3.0.2, USA). The fungal cytoscape network clustering diagram was generated by Cytoscape (version 2.8.0, USA). The size of each circle indicates the OTU abundance, and the line color indicates the presence of the OTU in this sample. The PCA diagram was built with SigmaPlot for Windows (version 12.0, Systat Software, Inc., Chicago, IL, USA).

3.6 Sediment Fungal Abundance and Diversity

The abundance of sediment fungal communities from the JP, SBY, and ZC Reservoirs were determined by qPCR. The abundances of fungal 18S rRNA gene sequences in the three reservoir sediment samples are presented in Table 9. The fungal 18S rRNA genes ranged from 2610 ± 89 copies (g dry sediment)$^{-1}$ to 1991 ± 58 copies (g dry sediment)$^{-1}$ in the sediment samples. The fungal abundance in the JP Reservoir was 1.31 times higher than that of the ZC Reservoir ($P < 0.01$).

The present work validates the powerful and effective 454 pyrosequencing method for the survey of sediment fungal composition diversity. It revealed a high diversity of fungal compositions with a total of 43,123 raw ITS sequences (18,425, 11,554, and 13,144 for ZC, SBY and JP, respectively), with an average length of about 650 bp obtained from the three reservoir sediment samples. After filtering, 30,880 high-quality sequences were selected for the data analysis. As shown in Fig. 9, the rank-abundance curves indicated that the JP Reservoir had the highest species richness and evenness, whereas the SBY Reservoir showed the lowest species richness (shortest curve) and also the lowest species evenness (lowest curve).

To determine fungal diversity, OTUs were identified based on the fungal ITS sequence with a dissimilarity level of 3 %. In total, 945 OTUs were detected. As shown in Table 9, the JP Reservoir sample had the highest richness (ACE = 967, *Chao* 1 = 962), while the sample from SBY had the lowest richness (ACE = 190, *Chao* 1 = 170). Furthermore, the JP Reservoir sample exhibited the highest diversity ($H = 4.52$) among the three samples, and this diversity was 3.6 times higher than that of the ZC Reservoir ($H = 1.25$). The SBY Reservoir exhibited the lowest diversity ($H = 0.96$). The lowest Simpson diversity (D) was observed in the JP Reservoir (Table 9). In addition, the JP, ZC, and SBY Reservoirs had 682, 122, and 59 OTUs in common, respectively. The OTUs shared among the three reservoirs

Table 9 qPCR and fungal population diversity index based on the 454 pyrosequencing data from sediment samples from the JP, SBY, and ZC Reservoirs

Reservoirs	Fungal 18S rRNA gene copies per gram of sediment[a]	Abundance-based coverage estimators (ACE)	Shannon's diversity (H)	Simpson diversity (D)	*Chao* 1 diversity	Coverage
ZC Reservoir	1991 ± 58 B	307	1.25	0.50	328	0.975
SBY Reservoir	2473 ± 102 AB	190	0.96	0.57	170	0.994
JP Reservoir	2610 ± 89 A	967	4.52	0.05	962	0.993

[a]Data are shown are means ($n = 3$). The same letter (A or B) indicates no significant difference by the Tukey–Kramer HSD test ($P < 0.01$)

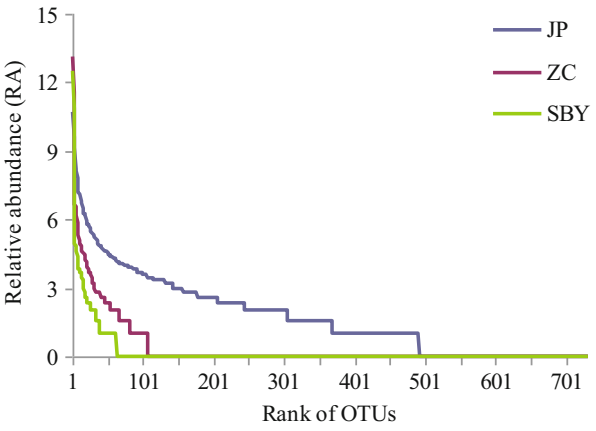

Fig. 9 Rank-abundance curve based on the fungal nuclear ribosomal internal transcribed spacer (ITS). OTUs at a dissimilarity level of 3 % in the sediments of the ZC, JP, and SBY Reservoirs

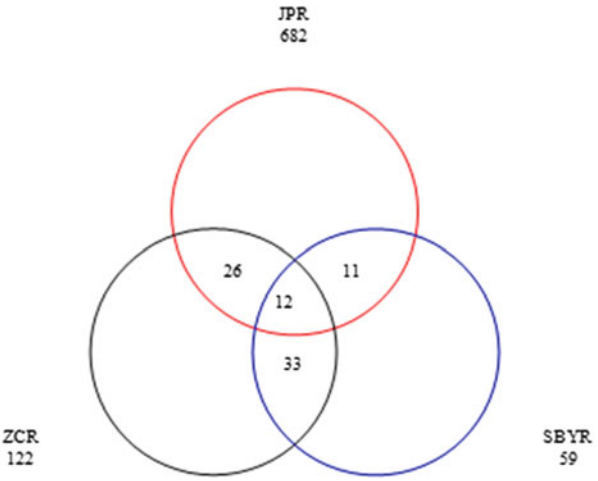

Fig. 10 Venn diagram depicting distinct and uniform fungal nuclear ribosomal internal transcribed spacer (ITS) OTUs at the 97 % similarity cut-off level for the sediment fungal populations from the ZC, SBY, and JP Reservoirs (ZCR, SBYR, and JPR, respectively)

were depicted using a mothur Venn diagram, and 12 OTUs were shared in the three reservoirs (Fig. 10).

3.7 Sediment Fungal Community Composition

As shown in Table 10, the taxa detected in our sampling cover a wide variety of organisms from the five main phyla and include Ascomycota, Basidiomycota, Chytridiomycota, Glomeromycota, Mucoromycotina, and unassigned. In the three reservoirs, the highest phylum is Chytridiomycota (12.71 % in JP, 9.43 % in SBY, 2 % in ZC), and the lowest phylum is Glomeromycota (1.50 % in JP, 0.83 % in ZC, 0.0 % in SBY). Unfortunately, at the phylum level, 66.38 % (JP), 85.41 % (ZC), and

Table 10 Parsimony test analysis for the taxonomic distribution of the sediment fungal community based on 454 pyrosequencing data for the ZC, SBY, and JP Reservoirs

Fungal phylum and class[a]	ZC vs. SBY (*P*-value)	JP vs. ZC (*P*-value)	JP vs. SBY (*P*-value)
Ascomycota	NS	<0.01	0.01
Dothideomycetes	NS	0.01	0.01
Eurotiomycetes	NS	0.01	0.01
Pezizomycetes	0.01	NS	0.01
Saccharomycetes	NS	0.01	0.01
Sordariomycetes	NS	<0.05	0.05
Basidiomycota	0.01	0.01	0.01
Agaricomycetes	0.01	NS	0.01
Agaricostilbomycetes	NS	0.01	0.01
Microbotryomycetes	NS	0.01	0.01
Tremellomycetes	NS	NS	NS
Chytridiomycota	NS	0.01	0.01
Blastocladiomycetes	NS	0.01	0.01
Chytridiomycetes	NS	0.01	0.01
Monoblepharidomycetes	NS	0.01	0.01
Glomeromycota	0.01	0.01	0.01
Glomeromycetes	0.01	0.01	0.01
Mucoromycotina	NS	0.01	0.01
Mortierellales[b]	NS	0.01	0.01
Mucorales	NS	0.01	0.01
Unassigned fungi	0.01	0.01	0.01

NS not significant, $P > 0.05$
[a]NCBI taxonomy
[b]Order

79.25 % (SBY) of the sequences could be identified as "unassigned fungi". Clearly, sediment harbors diverse ecosystems with a plethora of ignored fungal species. These lager proportions of "unassigned fungi" call for the curated International Nucleotide Sequence Database (INSD). Dominant classes among the Ascomycota were the Dothideomycetes, Eurotiomycetes, Pezizomycetes, Saccharomycetes, and Sordariomycetes. The fungal communities were dominated by OTUs belonging to the Chytridiomycota (33.90 % of OTUs). Dominant Chytridiomycota groups included the Blastocladiomycetes, Chytridiomycetes, and Monoblepharidomycetes. According to the parsimony test, no significant difference existed between the ZC and SBY Reservoirs for Ascomycota and Chytridiomycota ($P > 0.05$); however, the JP Reservoir was significantly different from the ZC and SBY Reservoirs at the phylum level ($P < 0.01$).

More specifically, *Rhizophydium* (relative frequency 30.98 %), *Placidium* (20.20 %), *Apophysomyces* (8.43 %), *Allomyces* (6.26 %), and *Rhodotorula* (6.01 %) were the dominant genera in the JP Reservoir, while *Elaphomyces*

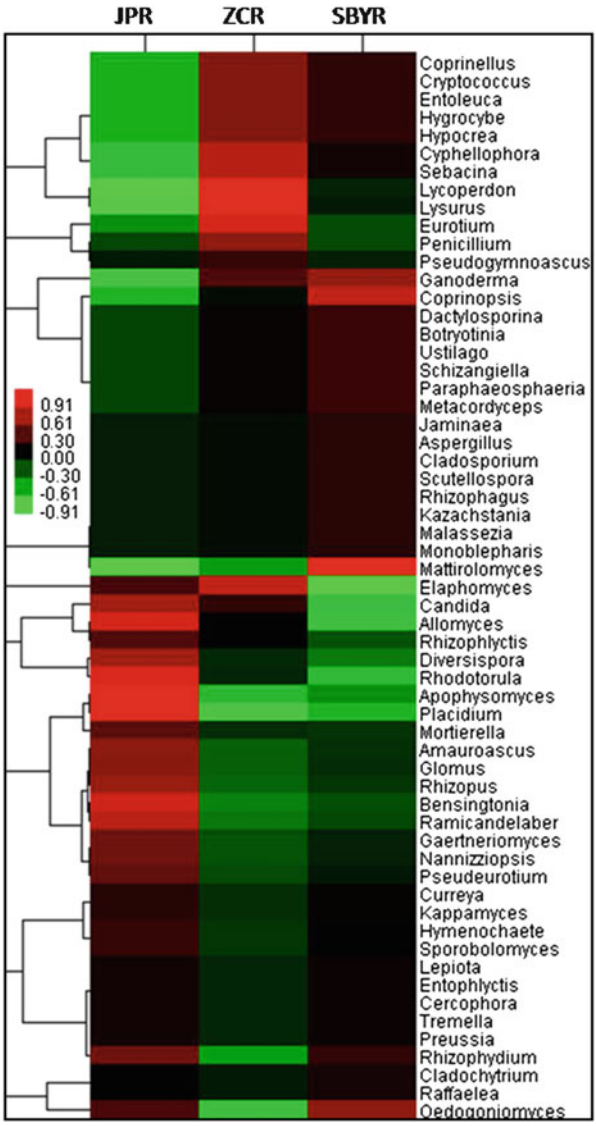

Fig. 11 Heat map diagram depicting sediment fungal populations. The *colors* (from −0.91 to 0.91) show the relative abundances of fungal nuclear ribosomal internal transcribed spacer (ITS) OTUs at the 97 % similarity cut-off level in the ZC, SBY, and JP Reservoirs (ZCR, SBYR, and JPR, respectively)

(20.00 %) and *Rhizophydium* (13.84 %) dominated in the ZC Reservoir, and *Rhizophydium* (77.78 %) and *Oedogoniomyces* (16.67 %) dominated in the SBY Reservoir. *Glomus* sp. was only found in the JP Reservoir. Based upon the relative percentages of the 59 main fungal types, we utilized heat map diagram colors to represent the relative percentages of the fungal classes within each reservoir (Fig. 11).

To better understand the distinct communities of the three reservoirs, we employed diagram clustering network analysis. These findings showed that

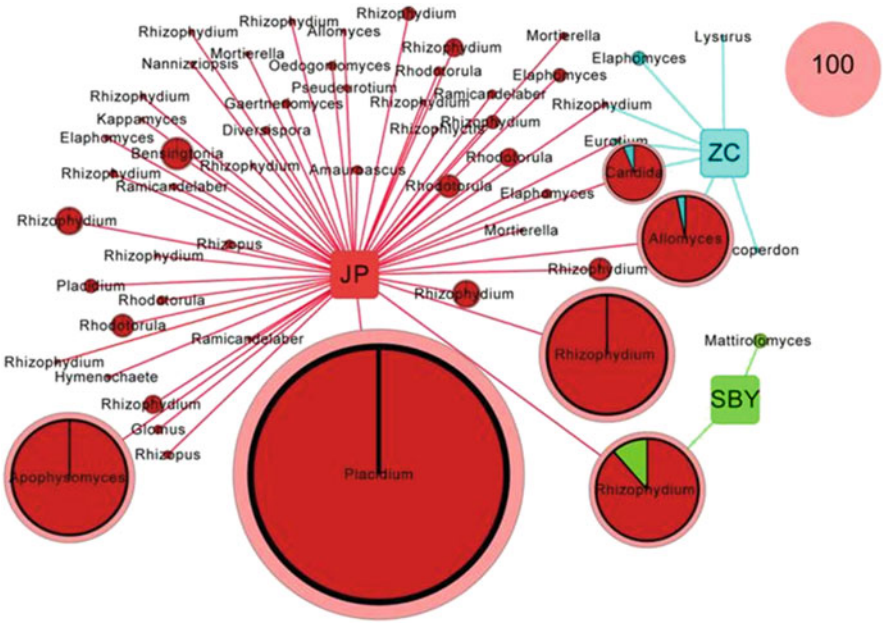

Fig. 12 Cytoscape network clustering diagram. The figure shows the dominant fungal nuclear ribosomal internal transcribed spacer (ITS) OTUs at the 97 % similarity cut-off level from the ZC (*azure*), SBY (*green*), and JP (*red*) Reservoirs. The node sizes represent relative abundance. The standard node indicates 100 reads

Placidium was the most ubiquitous fungal genus and was dominant in the JP Reservoir (Fig. 12).

Thus, these two types of dendrograms enabled us to visualize the entire dataset. Furthermore, as shown in the phylogenetic tree in Fig. 13, the abundant genera belonged to Ascomycota, Basidiomycota, Chytridiomycota, Glomeromycota, and Mucoromycotina.

PCA also revealed that the sediment fungal community structure varied significantly among the reservoirs. PC1 and PC2 explain 35.70 % and 25.32 % of the total variance, respectively. JPR was located in the third quadrant, and ZCR and SBYR were located in the fourth quadrant. *Lysurus* sp. and *Lycoperdon* sp. were present in ZCR, *Mattirolomyces* sp. was in SBYR, and *Placidium* sp., *Rhodotorula* sp., and *Glomus* sp. were abundant in JPR (Fig. 14).

3.8 Conclusion and Further Reading

Here, qPCR and the recently developed high-throughput 454 GS FLX pyrosequencing were combined to investigate the abundance and diversity of sediment fungal communities in three water supply reservoirs. These results

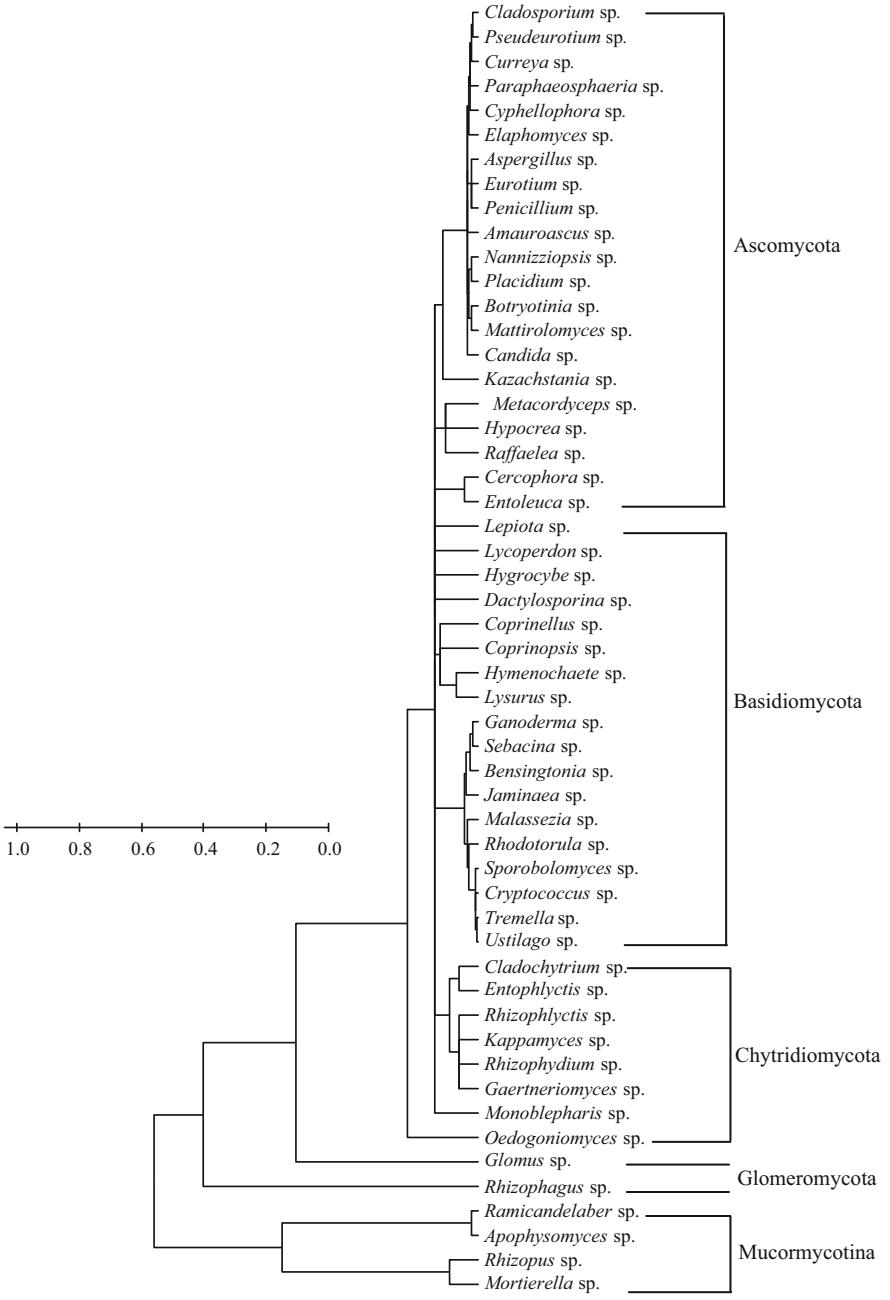

Fig. 13 Phylogenetic relationships among the 53 OTUs with internal transcribed spacer (ITS) sequences of known fungi based on the neighbor-joining analysis. Bootstrap values were based on 1000 replications

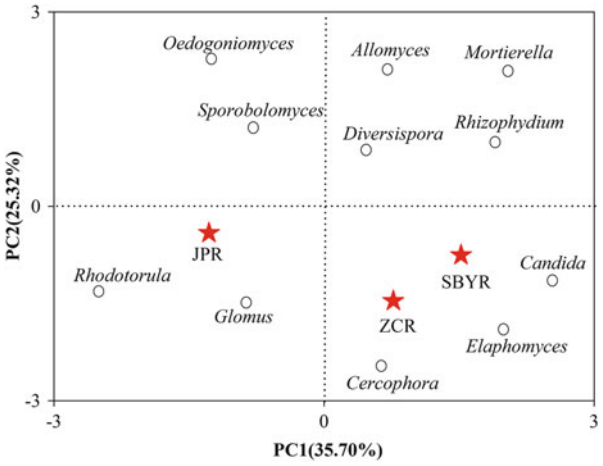

Fig. 14 PCA of sediment fungal populations. Sampling sites from ZC, SBY, and JP Reservoirs (ZCR, SBYR, and JPR, respectively). PC1 and PC2 explained 35.70 and 25.32 % of the total variance, respectively

revealed 1991, 2473, and 2610 copies of the 18S rRNA gene in the sediments from the ZC, SBY, and JP Reservoirs, respectively. The fungal abundance in JP Reservoir was 1.31 times higher than that of the ZC Reservoir. Fungal communities are extremely diverse. In general, 43,123 reads were recovered, corresponding to 945 distinct molecular OTUs (97 % similarity cut-off level). The majority of the fungal nuclear ribosomal internal transcribed spacer (ITS) region sequences were affiliated with Ascomycota, Chytridiomycota, Basidiomycota, Glomeromycota, and Mucoromycotina. Thus, the results of this research suggest that the combination of high-throughput Roche 454 GS FLX pyrosequencing and qPCR is successfully employed to decrypt reservoir sediment fungal communities. Diverse fungi occur widely in the sediments of water supply reservoirs. These findings will undoubtedly broaden our understanding of reservoir sediment fungal species harbored in this freshwater stressful environmental condition. Future research should be conducted to determine the potential for fungi to degrade pollutants and their secondary metabolites related to the water quality.

Compared with other freshwater bodies such as lakes, rivers, streams, and springs, reservoirs might be less explored. There is an abundance of literature showing that fungi contribute more to leaf breakdown than bacteria in other aquatic environments [97]. The environmental conditions of oligotrophic freshwater supply reservoir sediments are unique, with a temperature of about 8–10 °C, and during thermal stratification, the reservoir sediments are exposed to anaerobic conditions [51, 88]. Evidence has suggested that these allotrophic environments harbor great bacterial structures [33]; however, the enumeration of reservoir sediment fungal diversity is still lacking. Thus, additional works on the fungal community in the previously undocumented water supply reservoir sediments are required. Importantly, in reservoir ecosystems, microbial species, such as bacteria and archaea, are important for energy flow [29, 36–38]; however, microbial species are not limited to these species, and fungi are prevalent in freshwater reservoirs and play major roles in regulating the flow of organic carbon and nitrogen [1, 59]. Furthermore, the water quality and sediment physicochemical properties also shape the fungal

community in the sediment and in water overlying the sediment [32, 33]. Freshwater reservoir sediment fungi have only begun to be revealed in recent years [29, 36–38, 97]. To close this gap, this study presents the more comprehensive dataset on fungal community composition from the sediment of water supply reservoirs.

Over the past several decades, culture-dependent fungal analysis methods, such as the horse hair baiting method [88], bait method [98], Czapek Dox agar, Sabouraud dextrose media [99], and community-level physiological profiles (CLPPs) [29], have been used to examine the occurrence of fungi in sediments from rivers and reservoirs. The fungal species in reservoir sediments are mainly organisms with unknown physiological activity [88, 98]. Our previous study using BIOLOG FF MicroPlates to investigate sediment fungal community functional diversity from the SBY and TY Reservoirs suggested that tremendous fungal diversity with respect to carbon utilization profiles was present in sediments of the SBY and TY Reservoirs [29]. These studies reported a remarkable physiological metabolic potential of fungi that inhabit these sediments, although the phylogenetic diversity of these fungi are only beginning to be revealed.

Recently, much attention has been focused on HTST platforms including 454 GS Junior (Roche), Ion Torrent PGM (Life Technologies), and MiSeq (Illumina) [90]. The 454 GS FLX pyrosequencing techniques are quite powerful and are being increasingly explored to evaluate the aquatic microbial communities [33, 90, 100]. Our results suggest that sediment fungi are important benthic organisms that have previously been ignored because of the constraints of the available test methods. Culture-dependant techniques, such as plate-pouring and BIOLOG methods, have incompletely assessed the fungal landscape in sediments [29]. To this end, we utilized a next-generation, high-throughput 454 pyrosequencing approach to overcome these difficulties and reveal the sediment fungal community diversity from three different reservoirs in China. Furthermore, the abundance of fungal species was also examined based on the quantitation of fungal 18S rRNA genes using a qPCR assay.

The sediment fungal community in reservoirs was both taxonomically diverse and OTU-rich. Our results revealed the abundance of previously unknown fungi in the sediments. In addition, different fungal abundance was observed among the three reservoirs, which might be due to the fact that different reservoirs had distinct water quality and environmental conditions [97]. The 18S rRNA gene copy number obtained from this study was lower than that of the arable soils [91]. Rousk et al. [91] examined soils collected across a long-term liming experiment, and revealed 2000–8000 18S rRNA gene copy numbers. Next-generation sequencing allows a deeper insight into sediment fungal communities in the reservoirs. The result of PCA agrees with another study that revealed distinct fungal compositions in samples collected from five different trophic status reservoirs [101]. The fungal communities from the three reservoir sediments were characterized by specific and distinct structures. These oligotrophic water source reservoirs harbor a high diversity of largely unknown fungal species. The phylogenetic diversity of the fungal community is separated among the three reservoir sediments. Our results show that Chytridiomycota dominated over Basidiomycota and Ascomycota with respect to abundance in these sediments. In the present study, the results revealed that

Rhizophydium was the dominant genera in all of the reservoirs. *Rhizophydium* is one of two genera in the Chytridiales with more than 220 described species. This result may indicate that the presence of these fungal taxa play an important role in nutrient recycling in the sediment ecosystem meanwhile, the sediment fungal species were also mainly dependant on the degree of water contaminations [1, 29]. However, as shown in our previous studies, the water quality of JP Reservoir was better than SBY Reservoir and ZC Reservoir [51, 88]. It is suggested that the diversity of aquatic hyphomycetes is highest in relatively non-polluted reservoirs. Similarly, Sridhar et al. [51] also found lower fungal diversity in the more nutrient-enriched streams. The most probably explanation for this phenomenon was the high level of toxic organic and inorganic micropollutants typically associated with eutrophication, which might have decreased the fungal community diversity [97].

In this work, the JP Reservoir was dominated by *Rhizophydium*, while the ZC Reservoir was dominated by *Elaphomyces* and the SBY Reservoir was dominated by *Rhizophydium*, as well as *Oedogoniomyces*. The distinction in fungal abundance and community structure in this region may be related to sediment physicochemical characteristics [84, 102]. *Rhodotorula* sp. has been previously isolated from deep-sea sediments in the northwest Pacific Ocean [103]. The dominance of *Oedogoniomyces* was also found in high-elevation soils [104]. Our results are in agreement with the results of another study that examined reservoir samples [101]. For example, Ranković used culture-dependent methods to investigate the presence of fungi in Serbian reservoirs and found that *Penicillium*, *Rhizopus*, and *Rhizophydium* were popular [101]. Furthermore, we unexpectedly found that *Glomus* sp. was abundant in the JP Reservoir sediment samples, although *Glomus* sp. is a typical arbuscular mycorrhizal fungus (AMF), which typically penetrates the cortical cells of vascular plant roots [105]. As no plants were growing at the bottom of this deep reservoir, the most likely reason for this phenomenon is that various vascular plant species are growing on the mountains around this valley reservoir, especially in the water level fluctuation zone [36–38]. Previously, we found that *Setaria viridis* was the dominant plant grown in the middle of water level fluctuation zone in the JP Reservoir, and *Glomus* sp. consistently colonizes the root of *S. viridis* [36–38]. Storm runoff-induced water level changes may carry AMF spores, such as *Glomus* sp., from rhizosphere soils along with the roots into the reservoir, and then this matter settles down into the sediments. This result was consisted with Anderson et al. [106], who suggested that *Glomus* sp. had been identified from lake sediment cores from Gould Pond and Upper South Branch Pond, Maine, USA. As far as we know, this is the first report of *Glomus* sp. harbored in deep reservoir sediment environmental conditions.

Chytridiomycota dominated the fungal biodiversity in the SBY and JP sediments. A similar study performed by Kagami et al. [107], which employed DGGE and sequence analysis, demonstrated that a large proportion of the sequences belonged to chytrids in Inba Lake in Japan. Microscopic observations revealed that chytrids infect various algal species, such as *Aulacoseira granulata* and *A. ambigua* [107]. This observation is also in agreement with other work performed on high-elevation soils [104]. In the United States, for example, high

Chytridiomycota abundance was also detected in the high-elevation soils undergoing snowmelt. This environmental ecosystem has no plants and fewer carbon source inputs than the reservoir system. Freeman et al. [104] suggested that chytrids can utilize algae and cyanobacteria as carbon sources for survival. In agreement, various algae and cyanobacteria live in the reservoir water and sediments [51, 88]. The water content of sediment is high. Our previous study found that diatom species are very popular in reservoir sediments. Bertrand et al. [108] revealed that parasitic and saprotrophic chytrids are a significant component of freshwater fungi that inhabit the pelagic algal. *Rhizophydium* dominated in JP and SBY Reservoirs. Likewise, Fernández et al. [109] also found that the parasitism by *Rhizophydium couchii* played a vital role in the dynamics of the *Closterium aciculare* community in a eutrophic–hypertrophic reservoir from Argentina. It might be that freshwater reservoir sediment conditions were highly suitable for chytrids survival and growth due to direct parasitism in freshwater algal cells. The results of this part of the chapter were first published in BMC Microbiology. Reprinted from an open access article in BMC Microbiolgy, 2015, Vol. 15, pp. 44, with kind permission from Springer Science+Business Media.

4 Archaeal Compositions in Drinking Water Reservoir Sediments

Archaea is the most abundant and diverse group of sediment microbes [85, 110]. Compared with the abundance of literature on soil archaea, we understand little about archaea living in aquatic oxygen-deficient sedimentation conditions [111, 112]. The sediment microbial community represents the wondrous diversity of habitats in reservoirs and is central to water ecosystem ecological functioning and restoration [36–38]. Consequently, there is an increasing need to understand the composition of archaea in the sediment of oligotrophic water supply reservoirs.

In our previous studies, BIOLOG, PCR-DGGE, and clone sequence methods were combined to examine sediment bacterial and fungal community functional diversity from SBY, TY, and ZC water supply reservoirs [36–38]. However, these techniques have several limitations. For example, BIOLOG can be performed to determine aerobic cultivable bacterial and fungal species [36–38, 113]. There are fewer bands that can be shown in the DGGE gel. More information on the sediment microbial community was lost. With the development of molecular biological methods, real-time qPCR (RT-qPCR) and next generation sequencing technology (NGST) have been developed and they are powerful in determining the quantity and diversity of environmental microbial community composition. NGST allows us to deeply explore the structure and compositions of microbial communities based on the 16S or 18S ribosomal RNA sequences.

To date, there are three NGST platforms, including Roche 454 FLX pyrosequencing, Illumina MiSeq, and Ion Torrent (PGM) [90]. These techniques

have been commonly used to reveal various environmental microbial communities [114–116]. Meanwhile, numerous reports have demonstrated that archaea can live in several aquatic ecosystems, such as lakes, rivers, and seas [117–121]. Unfortunately, no report has been focused on the oxygen-deficient surface sediment of the water supply reservoir with poor nutrition characteristics.

It is, therefore, the primary goal of this part of the chapter to determine the quantity and composition of sediment archaeal community from three different water supply reservoirs. To this end, qPCR was used to investigate the sediment archaeal abundance, and Illumina MiSeq sequencing (IMS) was also employed to compare sediment archaeal communities from JP, ZC, and SBY Reservoirs.

4.1 Site Description and Sampling

The research was conducted in three different water supply reservoirs, named JPR, ZCR, and SBYR. JPR and SBYR are located in Xi'an City, Shaanxi Province, while ZCR is located in Zaozhuang City, Shandong Province, China. The greatest depths are 15–18 m, 45–50 m, and 95–100 m for ZCR, SBYR, and JPR, respectively [40, 51]. An oxygen-deficient area is formed. The dissolved oxygen concentration is near to zero. As described in our previous studies, the surface sediments (0–30 cm) were collected using a Petersen stainless steel grab sampler, placed in a small cooler which maintains the temperature at 8 °C, and then transported to the School of Environmental and Municipal Engineering, Xi'an University of Architecture and Technology (SEME-XAUAT) within 24 h. The sediment samples were stored at −20 °C until the microbial total DNA extraction process.

4.2 Sediment Microbial DNA Extraction

To extract sediment microbial total DNA, the Soil DNA Kit (Omega, USA) was selected [36–38]. As described in the manufacturer's recommendations, total sediment microbial DNA was extracted and examined by electrophoresis in 0.8 % agarose gels. The extracted DNA samples were stored at −20 °C.

4.3 qPCR Determination

To examine the relative abundance of archaea, we used RT-qPCR (SYBR Premix Ex Taq II, TaKaRa). In this work, the archaeal primer set was ARC-787 F (5-′-GATTAGATACCCSBGTAGTCC-3′) and ARC1059R (5-′-GCCATGCACCWCCTCT-3′). The total volume was 25 μL containing DNA template 0.5 μL, primers 0.5 μL, dNTP 0.5 μL, 10× Taq Buffer 2.5 μL, 25 mM

$MgCl_2$ 2 μL, Taq 0.2 μL, and H_2O18.3 μL. The PCR process was 95 °C for 3 min, 35 cycles of 94 °C for 30 s, 56 °C for 30 s, 72 °C for 30 s, and then 72 °C for 5 min, and the PCR products was 272 bp. Copy numbers of the archaeal 16S gene were examined using external standards. A standard curve and cycle threshold value was constructed using ten times serial dilutions. Melting curve (MC) analysis was determined from 55 to 95 °C. The average amplification efficiency was 84.76 % and the amplification was linear ($R^2 = 0.999$).

4.4 Illumina MiSeq Sequencing Determination

To determine the diversity of the archaeal community, we used the Illumina MiSeq sequencing technique [122]. The V5–V6 16S rRNA gene region was employed to identify the archaeal species. The primer sets are F: 5-′-AGGATTAGATACCCTGGTA-3′, R: CRRCACGAGCTGACGAC-3′. The fusion of primers is: F: 5′-Index + AGGATTAGATACCCTGGTA-3′, R: 5-′-CRRCACGAGCTGACGAC-3′. PCR reactions contained 10 × reactions buffer 2.50 μL, dNTP 2.00 μL, DNA 1.00 μL, primer F 1.00 μL, primer R 1.00 μL, and Taq DNA polymerase 0.125 μL. The PCR cycle parameters were 5 min at 94 °C; 25 cycles of 30 s at 94 °C, 30 s at 55 °C and 30 s at 72 °C; and a final extension for 7 min at 72 °C. The multiplexed DNA libraries (10 nM) were sequenced.

4.5 Statistical Analysis

In order to explore the diversity of the sediment archaeal community structure, the *Chao* index, ACE index, Shannon's diversity, and Simpson diversity were used. Based on the OTUs data (cut-off 0.03), diversity indexes were treated by mothur (http://www.mothur.org/) software. One-way ANOVA with the Tukey–Kramer HSD test was performed to evaluate the significant differences of archaeal abundance (RT-qPCR) using DPS software (version 6.4). A heat map was constructed by *R* software (version 3.0.2). PCA was used to compare the Illumina MiSeq sequencing data.

4.6 Abundance of Sediment Archaea

In this work, we found that there was an abundance of archaeal species in the sediments of water supply reservoirs. As shown in Fig. 15, the results revealed that the archaeal 16S RNA gene copy numbers per gram of sediment were 6.09×10^4, 6.19×10^5, and 1.94×10^5 for JPR, ZCR, and SBYR, respectively ($P < 0.01$) (Fig. 15).

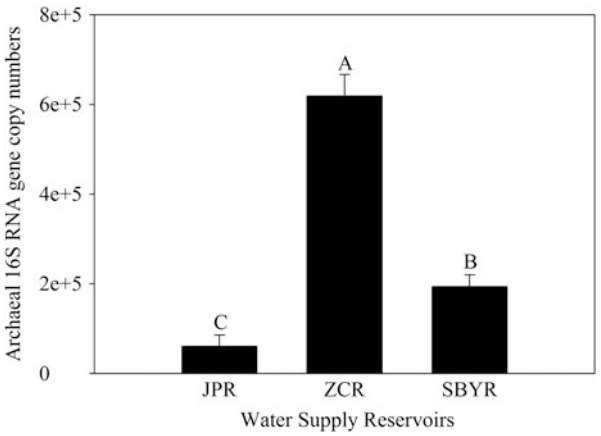

Fig. 15 Abundance of archaea species living in the sediment samples expressed as archaeal 16S RNA gene copy numbers per gram of sediment from ZC, SBY, and JP Reservoirs. Different capital letters above the bars indicate significant difference by the Tukey–Kramer HSD test ($P < 0.01$). The error bars represent the standard deviations of triplicates

4.7 Community Diversity of Sediment Archaea

According to the Illumina MiSeq sequencing data, the *Chao* indexes were 774, 245, and 276 for ZCR, SBYR, and JPR, respectively. The highest ACE index was observed in ZCR (1544) and the lowest was that observed in JPR. The Shannon's diversity of ZCR was 1.76 times higher than that of ZCR (1.634). However, the Simpson diversity indexes were 0.134, 0.139, and 0.487 for ZCR, SBYR, and ZCR, respectively (Table 11).

As shown in Fig. 16, *Methanosaeta*, *Methanospirillum*, *Methanosarcina*, *Methanobacterium*, *Methanosphaerula*, *Methanocella*, *Methanomethylovorans*, *Methanocorpusculum*, *Methanoculleus*, *Methanolinea*, *Methanosphaera*, and *Thermofilum* were the dominant archaeal species harbored in the sediments from the three reservoirs (Fig. 16, Table 11). *Methanobacterium* was not significantly different among the three samples (Table 12).

Methanosaeta was significantly different among the samples. As shown in Fig. 16, there were *Methanosaeta* (53.6 %), *Methanosarcina* (25.6 %), *Methanospirillum* (12.0 %), *Methanobacterium* (7.2 %), *Methanosphaerula* (0.8 %), and *Methanocella* (0.8 %) distributed in SBY Reservoir. Meanwhile, *Methanosarcina* (44.0 %), *Methanosaeta* (24.0 %), *Methanospirillum* (18.0 %), *Methanobacterium* (12.0 %), and *Thermofilum* (2.0 %) were observed in JP Reservoir. For ZC Reservoir, *Methanosaeta* (76.31 %), *Methanospirillum* (10.48 %), *Methanosarcina* (6.71 %), *Methanobacterium* (3.46 %), *Methanosphaerula* (1.68 %), *Methanocella* (0.32 %), *Methanomethylovorans* (0.32 %), *Methanocorpusculum* (0.21 %), *Methanoculleus* (0.21 %), *Methanolinea* (0.21 %), and *Methanosphaera* (0.11 %) were present. *Thermofilum* was not found. *Methanosaeta* was the dominant species in ZC and SBY Reservoirs. However, *Methanosarcina* was the dominant species in JP Reservoir. The sequencing data indicate that the ZC Reservoir can host species of archaea in numbers higher than the JP and SBY Reservoirs. ZC had significantly

Table 11 The richness index and phylogenetic diversity of the sediment archaeal community in ZC, SBY, and JP water supply reservoirs based on Illumina MiSeq sequencing

Reservoirs	*Chao* index	ACE index	Shannon's diversity	Simpson diversity	Coverage
ZCR	774	1544	2.869	0.134	0.957
SBYR	245	440	2.683	0.139	0.938
JPR	276	325	1.634	0.487	0.943

ACE index abundance-based coverage estimators. *ZCR*, *SBYR*, and *JPR* represent ZC, SBY, and JP water supply reservoirs, respectively

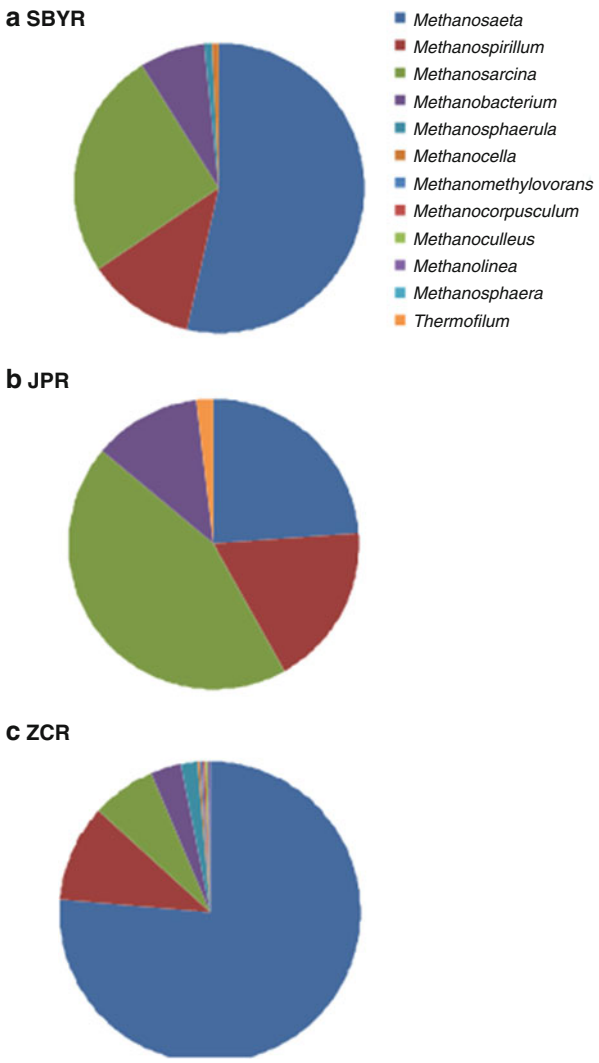

Fig. 16 Relative abundances of the dominant archaeal genus in the sediments of ZC, JP, and SBY reservoirs. The relative abundances are based on the proportional frequencies of archaeal 16S RNA sequences that can be classified at the genus level

Table 12 Summary of parsimony test (*P*-test) results for the comparison of archaeal communities among sediment samples from ZCR, SBYR, and JPR

Taxon	ZCR vs. JPR (*P*-value)	JPR vs. SBYR (*P*-value)	SBYR vs. ZCR (*P*-value)
Methanobacterium	NS	NS	NS
Methanocella	<0.01	0.01	NS
Methanocorpusculum	0.01	NS	0.01
Methanoculleus	0.01	NS	0.01
Methanolinea	0.01	NS	0.01
Methanomethylovorans	0.01	NS	0.01
Methanosaeta	0.05	0.05	0.05
Methanosarcina	NS	NS	0.05
Methanosphaera	0.01	NS	0.01
Methanosphaerula	0.01	0.01	0.05
Methanospirillum	0.05	NS	NS
Thermofilum	0.01	0.01	NS

NS not significant

greater OTU richness. The Venn diagram shows OTUs found exclusively in ZC (172), in JP (39), and in SBY (37) (Fig. 17).

Illumina MiSeq sequencing targeting the 16S rRNA gene of archaea showed shifts in the composition of the archaeal community. The heat map colors indicate the relative percentage of archaea ranging within each sample. High and low OTUs can be seen in Fig. 19a. The heat map and PCA score plot revealed that there was a significant difference in the sediment archaeal quantity and community compositions among the three drinking water reservoirs (Figs. 18 and 19).

4.8 Conclusion and Further Reading

Archaea is an important microorganism distributed in aquatic environmental conditions. To better understand the diversity of archaea in water supply reservoirs, the objective of this work was to evaluate and compare the sediment archaeal quantity and community diversity in three oligotrophic water supply reservoirs (JPR, ZCR, and SBYR) using RT-qPCR and high-throughput Illumina MiSeq Sequencing (IMS) techniques. The results showed that the archaeal 16S RNA gene copy numbers per gram of sediment were 6.09×10^4, 6.19×10^5, and 1.94×10^5 for JPR, ZCR, and SBYR, respectively ($P < 0.01$). Moreover, in total, 40,941, 36,552, and 31,234 effective sequence reads of the sediment archaeal 16S rRNA gene were obtained using the Illumina MiSeq sequencing method from sediments of the ZC, SBY, and JP Reservoirs, respectively. The highest *Chao* diversity index was observed in ZC Reservoir, which was 2.80 times higher than that of JP Reservoir, which had the lowest. *Methanosaeta*, *Methanospirillum*, *Methanosarcina*, *Methanobacterium*, *Methanosphaerula*, *Methanocella*, *Methanomethylovorans*,

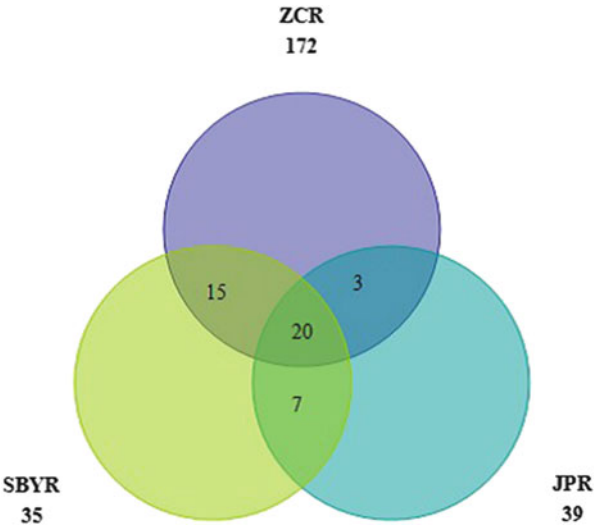

Fig. 17 Venn diagram showing the unique and shared OTUs of the archaeal community from ZC, SBY, and JP Reservoirs

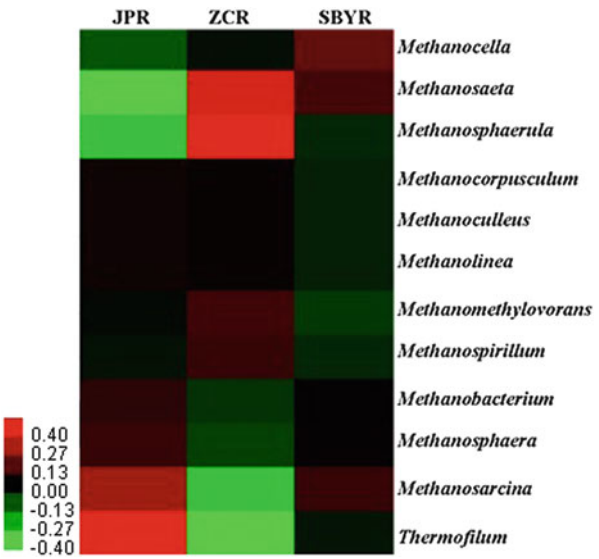

Fig. 18 Heat map diagram showing the sediment archaeal community diversity from ZC, SBY, and JP Reservoirs. *Red* and *green colors* (from −0.40 to 0.40) represent the relative abundance of high and low OTUs, respectively

Methanocorpusculum, *Methanoculleus*, *Methanolinea*, *Methanosphaera*, and *Thermofilum* were observed in the sediments from three reservoirs. *Methanosaeta* was the dominant species in ZC and SBY Reservoirs, and *Methanosarcina* was the dominant species in JP Reservoir. *Thermofilum* was only found in JP Reservoir. ZC Reservoir had significantly greater OTU richness. The heat map and PCA suggested that there were distinctly different sediment archaeal quantity and community compositions among the three water supply reservoirs, which may play an

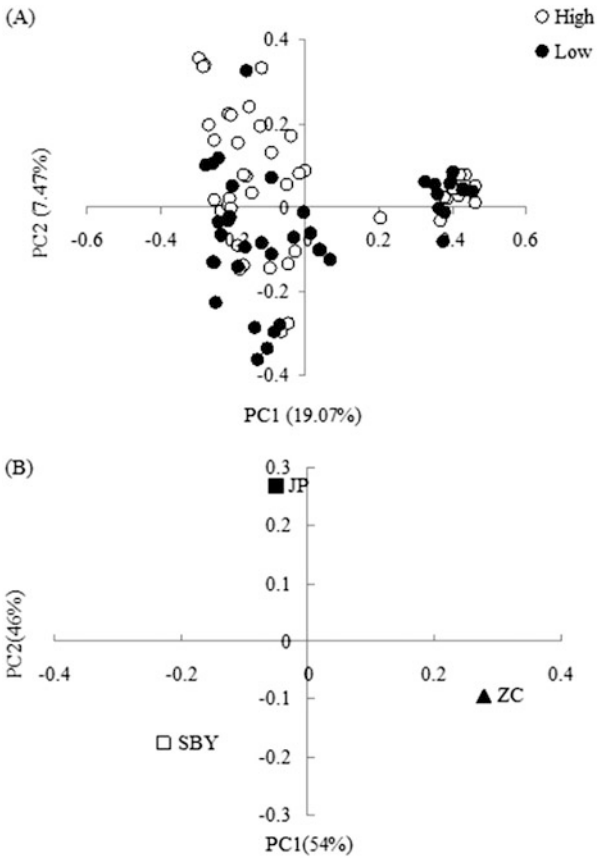

Fig. 19 PCA scatter plots of the sediment archaeal community diversity from ZC, SBY, and JP Reservoirs. (**a**) PC1 and PC2 explained the total variance for 19.07 and 7.47 %. (**b**) PC1 explained the total variance for 54 % and PC2 explained the total variance for 46 %

important role in driving nutrition transportation and shaping the water quality of reservoirs.

In the past few decades, several molecular approaches have been developed to measure the sediment microbial community diversity in various aquatic environmental conditions. An increasing number of researches have examined the archaeal species [117–121]. Consequently, there is an increasing need to understand archaea functioning. In aquatic ecosystems, sediment archaea is complex and varies in number and community composition. However, fewer works have been conducted to determine the quantity and diversity of the archaeal community from oligotrophic water supply reservoirs. In this study, we used molecular methods to explore the archaeal community; the composition of the archaeal community was monitored by Illumina MiSeq sequencing of 16S rRNA genes and several valuable data were obtained. Koizumi et al. [117] used PCR-DGGE to investigate the sediment archaeal community structure in a mesophilic freshwater lake and suggested that the diversity of the archaeal community did not drastically change through vertical changes, and the sediment archaeal community in low-temperature areas has been

underestimated. Similarly, Borrel et al. [123] studied the depth changes of anoxic freshwater sediments archaeal communities of the freshwater meromictic Lake Pavin in France. The results showed that dramatic changes were observed in the archaeal community diversity along the sediment core. Green et al. [81] examined sediment archaeal community diversity in a subtropical polymictic reservoir, Lake Wivenhoe, using cloning of the 16S rRNA gene method, and revealed that the sediment archaeal community structure was shaped by the delivery of dissolved oxygen. In this study, JP and SBY Reservoirs are near to each other, they are oligotrophic drinking water reservoirs, and the water quality has been recorded regularly. The sediment archaeal community might be influenced by water quality.

This work also provides further evidence that the Illumina MiSeq sequencing technology has shown great potential to reveal the freshwater sediment archaeal community. Sediment microbial species such as archaea, bacteria, and fungi also play an important role in regulation of the water quality and pollution released from the sediment to the surface water. It is necessary that sediment ammonia-oxidizing archaea, bacterial and fungal communities, and quantity should be determined simultaneously in the field experiments. In this section, reprint with kind permission from Editor (Dr. M. N. Khan) of Journal of Pure and Applied Microbiology.

5 Carbon Utilization Patterns of Reservoir Bacterial Composition

Microbial communities are ubiquitous inhabitants in various aquatic environments, contributing substantially to critical geological and ecological processes in water ecosystems, including breakdown of complex organic substances, circulation of nitrogen, and modification of water aesthetic properties [124]. In the past few decades, several functional microbes harbored in water environmental conditions have been investigated [99, 125]. Compared with the massive literature on seas [9, 10, 126, 127], lakes [128, 129], rivers [130, 131], wetlands [131, 132], and springs [133–135], research on drinking water reservoirs is limited, which represent only the sediment-associated microbial community [15, 136].

Drinking water reservoirs are the main source of drinking water supply for urban regions in arid and semiarid areas with lower groundwater stocks, such as northwest China [17]. Drinking water quality can be evaluated and quantified based on the evaluation of physical, biochemical, or microbial parameters. To monitor the raw water quality of reservoirs, much attention has been paid to taste, odor and color 18, phosphorus absorption and release [1], heavy metals [137], organic contaminants [133, 134], and cyanobacterial blooms and microcystins [129], but little is known about the microbial community living in this oligotrophic water body. In particular, detailed spatial sampling for bacterial community functional diversity has not been generally understood.

In drinking water sources, the microbial community can be used as an indicator of water quality [138]. Microbe growth can lead to the development of taste, odor,

and color in the drinking water. In drinking water reservoir ecosystems, a number of water microbial parameters such as microbial metabolic activity have the potential for use as diagnostic bioindicators of drinking water quality. Wilhelm et al. [129] reported the relationships between water nutrients and the structure of microbial communities in Lake Tai. Pereira et al. [99, 125] also examined the temporal variations in the filamentous fungal and yeast populations in three drinking water sources, including surface water, spring water, and groundwater. Recently, Lautenschlager et al. [139] determined the effect of overnight stagnation of drinking water in household taps on the structure of the bacterial community and growth. However, since the water bacterial functional communities change spatially in the drinking water reservoir, it has been poorly evaluated.

The objective of this part of the chapter was, therefore, to explore the spatial pattern of bacterial community functional diversity in a drinking water reservoir in northwest China using community-level physiological profiles (CLPPs), thus providing an experimental evaluation of the aquatic bacterial community diversity in a drinking water body that may constitute a potential health risk.

5.1 Study Site Description

The experiment was conducted in the Jinpen Reservoir, located in Zhouzhi County, Xi'an City, Shaanxi Province, northwest China (E108°11′, N34°02′). It is a large drinking water reservoir with a maximal depth of 90–105 m, average depth of 60–80 m [1], area of 4550 m^2, and has a water volume of 2×10^8 m^3, serving as municipal and domestic water supply sources for Xi'an City. The daily water supply capacity is 8×10^5 m^3.

5.2 Water Sampling Procedure

Polyethylene bottles (1 L) were carefully sterilized using ethanol disinfection for 5 min and rinsed with sterile distilled water three times before sampling. In order to evaluate the spatial pattern of microbial community functional diversity in the Jinpen drinking water reservoir, water samples were collected from three different sampling sites (site A, site B, and site C) (Table 13, GPS position) on July 6, 2012. In each site, three different depths (0.5, 30, and 65 m) were selected. All water samples were immediately put on ice and transported back to the lab within 5 h after collection. For BIOLOG analysis, each water sample (50 mL) was stored at 4 °C for less than 24 h until the BIOLOG profiles were analyzed, in order to minimize any changes in the bacterial communities.

Table 13 Location (longitude and latitude) and water depth of the three sampling sites (site A, site B, site C) in the Jinpen drinking water reservoir, Shaanxi Province, northwest China

Sampling sites	Longitude (E)	Latitude (N)	Water depth (m)
Site A	34°02′13.70″	108°11′33.92″	0.5
Site A	34°02′13.70″	108°11′33.92″	30
Site A	34°02′13.70″	108°11′33.92″	65
Site B	34°02′39.44″	108°11′52.86″	0.5
Site B	34°02′39.44″	108°11′52.86″	30
Site B	34°02′39.44″	108°11′52.86″	65
Site C	34°02′39.81″	108°12′20.55″	0.5
Site C	34°02′39.81″	108°12′20.55″	30
Site C	34°02′39.81″	108°12′20.55″	65

5.3 *Community-Level Physiological Profiles (CLPPs) Determination*

To examine the water bacterial community functional diversity, the BIOLOG ECO plate technique was used to explore the carbon source utilization pattern (functional diversity) of the bacterial community harbored in the water body [113]. The BIOLOG ECO plate contains 31 different carbon sources, including ten carbohydrates, two phenolic compounds, four polymers, seven carboxylic acids, two amines, and six amino acids. As described by Choi and Dobbs [113], and with a little modification, in the laboratory, using an eight-channel pipette (Bio-Rad, USA), water samples were added to each well of the ECO MicroPlate, with a quantity of 150 μL. All of the inoculated ECO plates were put into the polyethylene bag, and incubated at 25 ± 2 °C in the dark for 140 h. The absorbance at 590 nm was measured every 12-h interval, and optical density (OD_{590nm}) values that were negative were set to zero [9, 10].

The bacterial community activity in the BIOLOG ECO plate was expressed as the *AWCD*, and the diversity index as species richness (*R*) [9, 10, 113]. Ninety-six-hour values were used to calculate the *AWCD* and functional diversity index. The bacterial community activity in the ECO plate was expressed as the *AWCD*. The bacterial functional diversity was expressed as species richness (*R*) and Shannon's diversity (*H*).

5.4 *Statistical Analysis*

All data were analyzed with SPSS 16.0 (SPSS Inc., USA). The data were expressed as means and standard errors (SE) ($n = 3$). A parametric two-way ANOVA test, followed by the Tukey–Kramer HSD test, was employed to evaluate the significant differences in the microbial properties of sediment among different sampling sites and depth at the 5 % level ($P < 0.05$). PCA was used to analyze the water bacterial

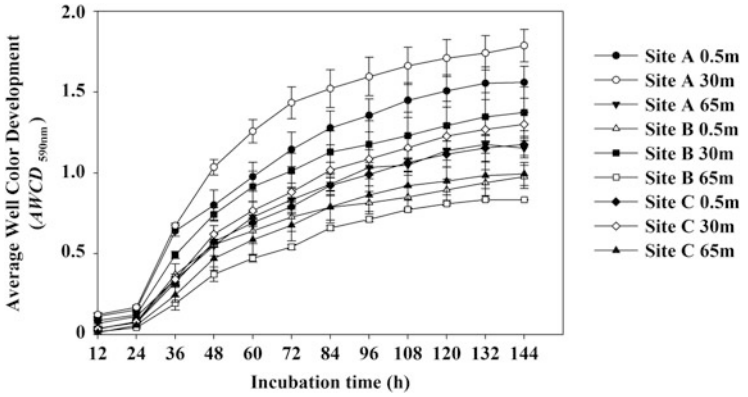

Fig. 20 $AWCD_{590nm}$ of the bacterial community in the water collected from different sampling sites (Sites A, B, and C) and depths (0.5, 30, and 65 m) of the Jinpen drinking water reservoir. The data are expressed by means and standard errors ($n = 3$)

community using the SPSS version 16.0 software package for Windows (SPSS Inc., USA). Graphical work was carried out using the SigmaPlot (version 10.0) software package.

5.5 AWCD *and Functional Diversity Index*

The water bacterial community activity was expressed the $AWCD_{590nm}$, and the curve is shown in Fig. 20. It can be seen that the $AWCD_{590nm}$ increased steadily during the cultural periods from 12 to 144 h.

Ninety-six-hour values were used to calculate the *AWCD* and functional diversity index. As shown in Fig. 21, the $AWCD_{590nm}$ varied significantly and reached the highest value (1.60 ± 0.12) at 30 m of Site A and the lowest value (0.71 ± 0.01) at 65 m of Site B. In each of the three different sampling sites, the $AWCD_{590nm}$ in the middle of the drinking water reservoir (30 m) were higher than those at the bottom (65 m) (Fig. 21a). The highest species richness (R) was 28 ± 1.76 at 30 m of Site A and the lowest R was 16 ± 1.15 at 65 m of Site B (Fig. 21b). Meanwhile, the Shannon diversity index (H) was determined for all samples. The value at 30 m of Site A was 3.26 ± 0.06, which was significantly higher than that at 65 m in Site A, with a value of 2.68 ± 0.06 ($P < 0.05$) (Fig. 21c).

These results revealed that the ability to utilize sole carbon substrates and functional diversity (metabolic diversity) for the drinking water bacterial community were stronger at 30 m than that at 65 m. The $AWCD_{590nm}$ varied for both sites and depths, as indicated by MANOVA (Table 14). The significant "sites" and "depth" indicate that the $AWCD_{590nm}$ and R and H indexes varied among the sites within the depth ($P < 0.01$). There were significant two-way interactions for

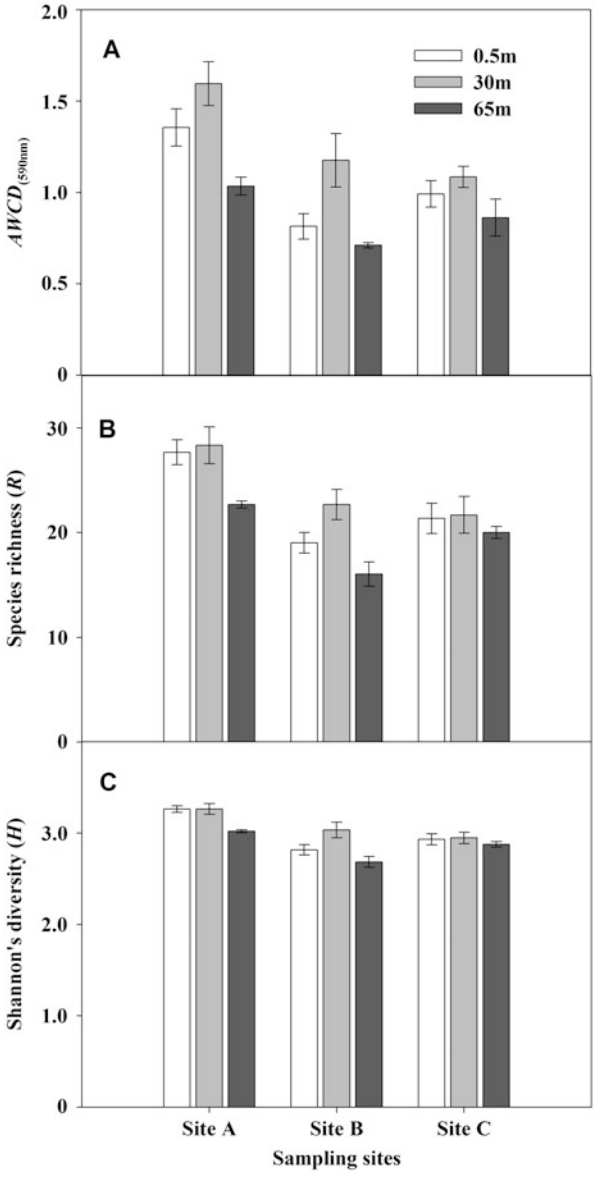

Fig. 21 $AWCD_{590nm}$, species richness (R), and Shannon's diversity (H) of the bacterial community functional diversity in the water collected from different sampling sites (Sites A, B, and C) and depths (0.5, 30, and 65 m) of the Jinpen drinking water reservoir. The data are expressed by means and standard errors ($n = 3$)

$AWCD_{590nm}$ ($P < 0.05$). However, there were no significant two-way interactions for the R and H indexes ($P > 0.05$).

Table 14 Two-way ANOVA significance levels for the main and interaction effects of sites (S) and depths (D) on the water bacterial community diversity of Jinpen drinking water reservoir, Shaanxi Province, northwest China

Parameters of the water bacterial community diversity	Site (S) (F-value)	Depth (D) (F-value)	Interaction (S*D) (F-value)
$AWCD_{(590nm)}$	17.73***	10.28**	3.48*
Species richness (R)	24.37***	9.64**	1.78 ns
Shannon's diversity (H)	30.95***	12.06***	2.55 ns
Carbohydrates	20.13***	13.27***	3.12*
Carboxylic acids	31.78***	10.11**	1.96 ns
Amino acids	21.62***	9.32**	3.05*
Polymers	29.93***	13.01***	2.43 ns
Phenolic compounds	25.11***	8.54**	1.82 ns
Amines	17.62***	10.17**	3.39*

ns non-significant $P > 0.05$, *$P < 0.05$, **$P < 0.01$,***$P < 0.001$

5.6 Carbon Sources Utilization

Carbon substrates were utilized by the drinking water bacterial community. The utilization of substrates of carbohydrates, polymers, and carboxylic acids was higher at 30 m than at 65 m, but that of phenolic compounds was similar between 30 and 65 m (data not shown). The F-values for two-way ANOVAs of the variables for different carbon sources are shown in Table 14. The significant "sites" and "depth" indicate that the carbon sources varied among the sites within the depth ($P < 0.001$). However, there were no significant two-way interactions in carboxylic acids, polymers, and phenolic compounds ($P > 0.05$). Thus, carbon sources utilized by the water bacterial community showed strong variations within depth in drinking water reservoirs. We found that, in the surface water, carbohydrates were easily utilized, while in the lower layers at 65 m, amino acids were utilized (data not shown).

5.7 PCA of Carbon Utilization Profiles

To analyze the BIOLOG profiles, PCA was used. PCA ordination revealed differences in the water bacterial community functional diversity among samples, with 32.96 % of the variability explained by PC1 and 23.22 % of the variability explained by PC2. Site B is located at the top of the graph. PCA showed that the water bacterial communities changed significantly throughout the site depending on depth (Fig. 22). Carbon substrates with significant correlation coefficients for PC1 were glucosaminic acid, L-lactose, hydroxy butyric acid, etc. D-mannitol, ketobutyric acid, and glucose-1-phosphate had higher significant correlation coefficients for PC2 (Table 15).

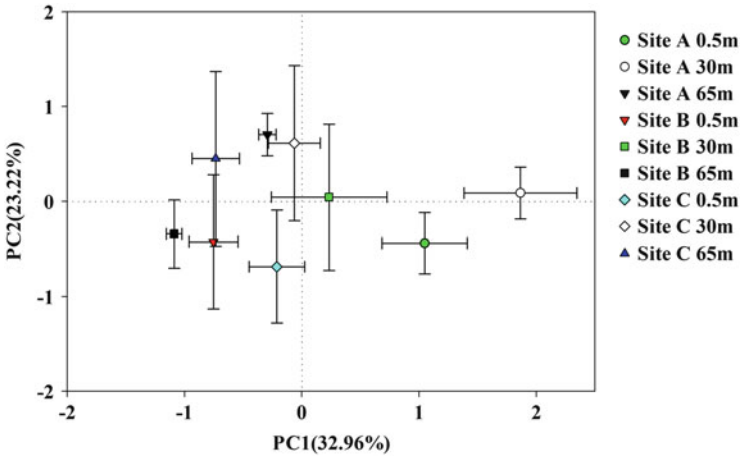

Fig. 22 PCA of carbon utilization profiles of the water bacterial community collected from different sampling sites (Sites A, B, and C) and depth (0.5, 30, and 65 m) of the Jinpen drinking water reservoir. PC1 explains 32.96 % of the variance of the data and PC2 explains 23.22 % of the variance of the data. The data are expressed by means and standard errors ($n = 3$)

Table 15 Carbon substrates with significant correlation coefficients (Pearson's correlation coefficient) for PC1 and PC2 in PCA of the water bacterial community functional diversity patterns for each sampling site. Carbon substrates with $r \geq 0.5$ are shown ($P < 0.05$)

PC1	*R*	PC2	*r*
a-Cyclodextrin	0.785	Glucose-1-phosphate	0.697
Glycogen	0.800	Phenyl ethylamine	0.633
a-D-L-lactose	0.874	Phenylalanine	0.755
i-Erythritol	0.748	D-Mannitol	0.873
D-Glucosaminic acid	0.854	Glucose-1-phosphate	0.838
D,L-a-Glycerol	0.767	Tween40	0.779
g-Hydroxy butyric acid	0.849	a-Ketobutyric acid	0.842
Itaconic acid	0.667		
Serine	0.777		
D-Cellobiose	0.805		

5.8 Conclusion and Further Reading

In this part of the chapter, the BIOLOG CLPP technique was employed to explore the bacterial community functional diversity at different depths (0.5, 30, and 65 m) and sites (Sites A, B, and C) of the Jinpen drinking water reservoir. The results showed that the highest bacterial community activities expressed as the $AWCD_{590nm}$ was observed at 30 m and the lowest was observed at 65 m. The significant "sites" and "depth" indicates that the $AWCD_{590nm}$ varied among the sites within the depth ($P < 0.01$). Whilst the species richness diversity (R) was

significantly higher at 30 m than that at 0.5 and 60 m, there were no significant two-way interactions for R and Shannon's diversity index ($P > 0.05$). Meanwhile, PCA of the BIOLOG profiles indicated that the bacterial community functional diversity changed at different depths and sites. Carbon substrates with the highest significant correlation coefficients for PC1 and PC2 were hydroxy butyric acid and mannitol. Overall, the findings increased our knowledge about the aquatic bacterial community diversity in drinking water constituting a potential health risk, because increased functional microbial communities may influence drinking water quality.

The water microbial community structure plays a vital role in defining drinking water quality and health, such as carbon, nitrogen, and phosphorus cycling, driving organic matter transformation [135, 136, 138]. However, significant gaps remain in our understanding of the spatial pattern of bacterial community functional diversity in a drinking water reservoir. This work provides substantial new insights into the bacterial community functional diversity in the drinking water reservoir. Water bacteria are important drivers for several biogeochemical cycles in aquatic ecosystems and play a critical role in most nutrient transformations in water and sediment [15]. Several techniques were used to determine the microbial community, such as BIOLOG, PLFA, PCR-DGGE, and pyrosequencing. In this survey, a cultural-dependent BIOLOG method was used. The BIOLOG method is based on explaining the profiles of sole carbon sources utilization represented by color development in a 96-well plate [113]. In previous reports, BIOLOG has been widely employed to determine the microbial community functional diversity from various environmental conditions, including soil [26], air [140], wetland [141], and so on.

Choi and Dobbs [113] compared the abilities of BIOLOG ECO and GN plates to distinguish the water bacterial communities from ballast water, Chesapeake Bay, tidal creek, oceanography pond, Tony's pond, groundwater, and suggested that BIOLOG is a fast and useful technique to explore the water bacterial community. The activity and structure of microbial communities affect water nutrient cycling. The main important reason for this is that the different water quality affects the water bacterial community diversity. The physical properties of water, such as temperature, dissolved oxygen, and pH may shape the water bacterial community metabolic characteristics.

In this study, we found that the water bacterial community activity and functional diversity were changed from the surface to the bottom of drinking water reservoir. A similar survey conducted by Comeau et al. [142] found that the marked differences in the water bacteria communities between the surface (2–12 m) and deeper (29–60 m) strata of a perennially stratified saline Arctic Lake using molecular method high-throughput 16S rRNA gene tag pyrosequencing was because of the strongly different limnological conditions. Meanwhile, the same phenomenon was also observed in other freshwater bodies. This result corresponded to a cultivation-independent study of Karlov et al. The distribution of water microbial community diversity in the upper (1.3 m) and bottommost horizons (367 m) of the Lake Radok water column was determined by Karlov et al. [143], and they suggested that exist distinct microbial stratification of the Lake Radok water

column with different microbial community composition. Previous studies indicated that water properties such as pH value or temperature are important drivers of the bacterial community structure. The water microbial community was dramatically driven by water physicochemical properties; therefore, it is possible that saline and limnological factors may also drive community composition. In this section, reprint with kind permission from Editor (Dr. M. N. Khan) of Journal of Pure and Applied Microbiology.

In this chapter, the results from the five parts give us more and more information on reservoir bacterial, fungal, actinomycic, and sulfate reducing bacterial compositions. Meanwhile, the reservoir microbial communities were related to water quality and water pollution transformation. Among these functional microbial species, aerobic denitrifying microbes, such as aerobic denitrifying bacteria, can be used as bioremediation for drinking water reservoir freshwater ecosystems. To this end, it follows that we will discuss the aerobic denitrifying bacteria in the next chapter, entitled "Screening and Cultivation of Oligotrophic Aerobic Denitrifying Bacteria".

References

1. Huang TL, Chai BB, Qiu ES, Zhou WH (2010) Microbial effects on phosphorus release from sediments on the multi-phase interface of water-sediment-biofacies. J Basic Sci Eng 18:61–70
2. Kohling T, Lara-Martín P, González-Mazo E, Amils R, Sanz JL (2011) Microbial community composition of anoxic marine sediments in the Bay of Cádiz (Spain). Int Microbiol 14:143–154
3. Jiang H, Dong H, Yu B, Liu X, Li Y, Ji S, Zhang CL (2007) Microbial response to salinity change in Lake Chaka, a hypersaline lake on Tibetan plateau. Environ Microbiol 10:2603–2621
4. Jiang H, Dong H, Zhang GX, Yu BS, Chapman LR, Fields MW (2006) Microbial diversity in water and sediment of Lake Chaka, an athalassohaline lake in northwestern China. Appl Environ Microbiol 72:3832–3845
5. Mesbah NM, Abou-El-Ela SH, Wiegel J (2007) Novel and unexpected prokaryotic diversity in water and sediments of the alkaline, hypersaline lakes of the Wadi An Natrun, Egypt. Microb Ecol 54:598–617
6. Swan BK, Ehrhardt CJ, Reifel KM, Moreno LI, Valentine DL (2010) Archaeal and bacterial communities respond differently to environmental gradients in anoxic sediments of a California hypersaline lake, the Salton Sea. Appl Environ Microbiol 76:757–768
7. Tamaki H, Sekiguchi YJ, Hanada S, Nakamura K, Nomura N, Matsumura M, Kamagata Y (2005) Comparative analysis of bacterial diversity in freshwater sediment of a shallow eutrophic lake by molecular and improved cultivation-based techniques. Appl Environ Microbiol 71:2162–2169
8. Droppo IG, Krishnappan BG, Liss SN, Marvin C, Biberhofer J (2011) Modelling sediment-microbial dynamics in the South Nation River, Ontario, Canada: towards the prediction of aquatic and human health risk. Water Res 45:3797–3809
9. Zhang Y, Wu E, Li CX, Yang SW, Jin XC, Liao JY, Wang SR (2011) Enzyme activity in sediments and its relation with eutrophication in the lakes along the Yangtze River. Chin J Appl Environ Biol 17:196–201 (in Chinese)

10. Zhang Y, Jiao NZ, Sun ZY, Hu AY, Zheng Q (2011) Phylogenetic diversity of bacterial communities in South China Sea mesoscale cyclonic eddy perturbations. Res Microbiol 162:320–329
11. Bossio DA, Fleck JA, Scow KM, Fujii R (2006) Alteration of soil microbial communities and water quality in restored wetlands. Soil Biol Biochem 38:1223–1233
12. Briée C, Moreira D, López-García P (2007) Archaeal and bacterial community composition of sediment and plankton from a suboxic freshwater pond. Res Microbiol 158:213–227
13. Chaerun S, Pangesti NPD, Jumiarni D (2010) Biogeochemical characterization of sediments from three largest dam reservoirs (Saguling, Cirata, Jatiluhur) in West Java Province, Indonesia. Proceedings of the 8th international symposium on southeast Asian water environment, pp 169–182
14. Mhamdi BA, Azzouzi A, Khattabi H, Mhamdi MA, Aleya L (2006) The bacteria in the sediment of the Sahela reservoir (Morocco): potential impacts on phosphorus budget. Environ Technol 27:1249–1256
15. Qu JH, Yuan HL, Wang ET, Li C, Huang HZ (2008) Bacterial diversity in sediments of the eutrophic Guanting reservoir, China, estimated by analyses of 16S rDNA sequence. Biodivers Conserv 17:1667–1683
16. Wobus A, Bleul C, Maassen S, Scheerer C, Schuppler M, Jacobs E (2003) Microbial diversity and functional characterization of sediments from reservoirs of different trophic state. FEMS Microbiol Ecol 46:331–347
17. Cong HB, Huang TL, Chai BB, Zhao JW (2009) A new mixing–oxygenating technology for water quality improvement of urban water source and its implication in a reservoir. Renew Energy 34:2054–2060
18. Huang S, Chen C, Wu YY, Wu QH, Zhang RD (2011) Characterization of depth-related bacterial communities and their relationships with the environmental factors in the river sediments. World J Microbiol Biotechnol 27:2655–2664
19. Huang TL, Yan S, Chai BB (2011) Phosphorus forms and its distribution in source water reservoir sediment. J Tianjin Univ 44:607–612 (in Chinese)
20. Schintu M, Kudo A, Sarritzu G, Contu A (1991) Heavy metal distribution and mobilization in sediments from a drinking water reservoir near a mining area. Water Air Soil Pollut 57–58:329–338
21. Palus J, Dziubałtowska E, Stańczyk M, Lewinska D, Mankiewicz-Boczek J, Izydorczyk K, Bonislawska A, Jurczak T, Zalewski M, Wasowica W (2007) Biomonitoring of cyanobacterial blooms in Polish water reservoir and the cytotoxicity and genotoxicity of selected cyanobacterial extracts. Int J Occup Environ Health 20:48–65
22. Wei W, Huang TL, Su JF (2010) Experimental study on effectiveness and influencing factors of biological denitrification via oligotrophic biofilm system. Chin J Environ Eng 10:2179–2184 (in Chinese)
23. Nosrati K, Govers G, Ahmadi H, Sharifi F, Amoozegar MA, Mrckx R, Vanmaercke M (2011) An exploratory study on the use of enzyme activities as sediment tracers: biochemical fingerprints? Int J Sediment Res 26:136–151
24. Curticapean MC, Dragan-Bularda M (2007) The enzymatic activity from the sediment of the Gilau dam reservoir—Cluj county. J Biochem Biophys Methods 69:261–272
25. Guan SY (1983) Soil enzyme and its analysis method. Agriculture Press, Beijing
26. Zhang HH, Tang M, Chen H, Zheng CL (2010) Inoculation with ectomycorrhizal fungi affects microbial biomass and bacterial functional diversity in the rhizosphere of *Pinus tabulaeformis* seedlings. Eur J Soil Biol 46:55–61
27. Boschker HTS, Cappenberg TE (1998) Patterns of extracellular enzyme activities in littoral sediments of Lake Gooimeer, The Netherlands. FEMS Microbiol Ecol 25:79–86
28. Qu JH, Yuan HL, Huang HZ, Wang ET (2005) Depth-related distribution of bacterial community in sediments of eutrophic Guanting reservoir. Sci China D 48:276–284

29. Zhang HH, Huang TL, Chen SN, Guo L, Liu TT, Yang X (2014) Microbial community functional diversity and enzymatic activity in the sediments of drinking water reservoirs, Northwest China. Desalination Water Treat 52(7–9):1608–1614
30. Paerl HW, Pinckney JL (1996) A mini-review of microbial consortia: their roles in aquatic production and biogeochemical cycling. Microb Ecol 31:225–247
31. Kranzioch I, Stoll C, Holbach A, Chen H, Wang L, Zheng B (2013) Dechlorination and organohalide-respiring bacteria dynamics in sediment samples of the Yangtze Three Gorges Reservoir. Environ Sci Pollut Res Int 20:7046–7056
32. Röske K, Roske I, Uhlmann D (2008) Characterization of the bacterial population and chemistry in the bottom sediment of a laterally subdivided drinking water reservoir system. Limnologica 38:367–377
33. Röske K, Sachse R, Scheerer C (2012) Microbial diversity and composition of the sediment in the drinking water reservoir Saidenbach (Saxonia, Germany). Syst Appl Microbiol 35:35–44
34. Liu CM, Aziz M, Kachur S, Hsueh PR, Huang YT, Keim P, Price LB (2012) BactQuant: an enhanced broad-coverage bacterial quantitative real-time PCR assay. BMC Microbiol 12:56
35. Liu J, Lin Z, Zhang H, Han BP (2012) Hydrodynamic change recorded by diatoms in sediments of Liuxihe reservoir, southern China. J Pale Limnol 47:17–27
36. Zhang HH, Huang TL, Liu TT (2013) Sediment enzyme activities and microbial community diversity in an oligotrophic drinking water reservoir, eastern China. PLoS One 8:e78571
37. Zhang HH, Huang TL, Yang X, Ma WX (2013) Soil dehydrogenase activity and bacterial community diversity in the water level fluctuation zone of a drinking water reservoir. J Pure Appl Microbiol 7:2451–2458
38. Zhang HH, Huang TL, Chen SN, Guo L, Yang X, Liu TT (2013) Spatial pattern of bacterial community functional diversity in a drinking water reservoir, Shaanxi province, northwest China. J Pure Appl Microbiol 7:1647–1654
39. Gantzer PA, Bryant LD, Little JC (2009) Controlling soluble iron and manganese in a water-supply reservoir using hypolimnetic oxygenation. Water Res 43:1285–1294
40. Ma Y, Guo QL, Huang TL, Tan P (2013) Response characteristics of water quality to the seasonal thermal stratification in Jin-pen reservoir along the Heihe river, Xi'an City in China. J Hydraul Eng 44:406–415
41. Wang S, Qian X, Han BP, Luo LC, Hamilton DP (2012) Effects of local climate and hydrological conditions on the thermal regime of a reservoir at Tropic of Cancer, in southern China. Water Res 46:2591–2604
42. Bryant LD, Gantzer PA, Little JC (2011) Increased sediment oxygen uptake caused by oxygenation-induced hypolimnetic mixing. Water Res 45:3692–3703
43. Huang TL, Li X, Rijnaarts H, Grotenhuis T, Ma WX, Sun X (2014) Effects of storm runoff on the thermal regime and water quality of a deep, stratified reservoir in a temperate monsoon zone, in Northwest China. Sci Total Environ 485–486:820–827
44. Bryant LD, Little JC, Bürgmann H (2012) Response of sediment microbial community structure in a freshwater reservoir to manipulations in oxygen availability. FEMS Microbiol Ecol 80:248–263
45. Wu YC, Ke X, Hernández M, Wang B, Dumont MG, Jia Z (2013) Autotrophic growth of bacterial and archaeal ammonia oxidizers in freshwater sediment microcosms incubated at different temperatures. Appl Environ Microbiol 79:3076–3084
46. Zhang HH, Huang TL (2013) Archaeal community structure and quantity in the oxygen deficient sediments from three water supply reservoirs. J Pure Appl Microbiol 7:2783–2789
47. Wang XY, Wang C, Bao LL, Xie SG (2014) Abundance and community structure of ammonia-oxidizing microorganisms in reservoir sediment and adjacent soils. Appl Microbiol Biotechnol 98:1883–1892
48. Zhao DY, Zeng J, Wan WH, Liang HD, Huang R (2013) Vertical distribution of ammonia-oxidizing archaea and bacteria in sediments of a Eutrophic Lake. Curr Microbiol 67:327–332

49. Zhu DC, Tanabe SH, Yang C, Zhang W, Sun J (2013) Bacterial community composition of south China sea sediments through pyrosequencing-based analysis of 16S rRNA genes. PLoS One 8:e7850
50. Lay CY, Mykytczuk NC, Yergeau É, Lamarche-Gagnon G, Greer CW, Whyte LG (2013) Defining the functional potential and active community members of a sediment microbial community in a high-arctic hypersaline subzero spring. Appl Environ Microbiol 79:3637–3648
51. Qin CH, Huang TL, Li X (2013) Studies on the seasonal variation and budget of nitrogen, phosphorus of the Shibianyu reservoir. J Xi'an Univ Arch Technol 45:111–116 (in Chinese)
52. Huang TL, Wei W, Su JF, Zhang HH, Li N (2012) Denitrification performance and microbial community structure of a combined WLA-OBCO system. PLoS One 7:e48339
53. Bao SD (1999) Soil and agricultural chemistry analysis. China Agriculture Press, Beijing, pp 125–150
54. Nielsen AT, Liu WT, Filipe C, Grady L, Molin S, Stahl DA (1999) Identification of a novel group of bacteria in sludge from a deteriorated biological phosphorus removal reactor. Appl Environ Microbiol 65:1251–1258
55. Dumonceaux TJ, Hill JE, Briggs SA, Amoako KK, Hemmingsen SM, Van Kessel AG (2006) Enumeration of specific bacterial populations in complex intestinal communities using quantitative PCR based on the chaperonin-60 target. J Microbiol Methods 64:46–62
56. Caporaso JG, Kuczynski J, Stombaugh J, Bittinger K, Bushman FD, Costello EK, Fierer N, Peña AG, Goodrich JK, Gordon JI, Huttley GA, Kelley ST, Knights D, Koenig JE, Ley RE, Lozupone CA, McDonald D, Muegge BD, Pirrung M, Reeder J, Sevinsky JR, Turnbaugh PJ, Walters WA, Widmann J, Yatsunenko T, Zaneveld J, Knight R (2010) QIIME allows analysis of high throughput community sequencing data. Nat Methods 7:335–336
57. Hamady M, Walker JJ, Harris JK, Gold NJ, Knight R (2008) Error-correcting barcoded primers for pyrosequencing hundreds of samples in multiplex. Nat Methods 5:235–237
58. Quince C, Lanzen A, Davenport R, Turnbaugh P (2011) Removing noise from pyrosequenced amplicons. BMC Bioinformatics 12:38
59. Cole JR, Chai B, Farris RJ, Wang Q, Kulam-Syed-Mohideen AS (2007) The ribosomal database project (RDP-II): introducing myRDP space and quality controlled public data. Nucleic Acids Res 35:169–172
60. Chao A, Bunge J (2002) Estimating the number of species in a stochastic abundance model. Biometrics 58:531–539
61. Oksanen J, Blanchet FG, Kindt R, Legendre P, Minchin PR (2012) Vegan: community ecology package, R package version, 20–23
62. Schloss PD, Handelsman J (2006) Introducing treeclimber, a test to compare microbial community structures. Appl Environ Microbiol 72:2379–2384
63. Song H, Li Z, Du B, Wang G, Ding Y (2012) Bacterial communities in sediments of the shallow Lake Dongping in China. J Appl Microbiol 112:79–89
64. Dondajewska R (2008) Seasonal and spatial changes in phosphorus and organic matter content in bottom sediments of a shallow reservoir. Limnol Rev 8:159–164
65. Kunz MJ, Anselmetti FS, Wüest A, Wehrli B, Vollenweider A, Thüring S (2011) Sediment accumulation and carbon, nitrogen, and phosphorus deposition in the large tropical reservoir Lake Kariba (Zambia/Zimbabwe). J Geophys Res Biogeosci 116:G03003
66. Hupfer M, Lewandowski J (2008) Oxygen controls the phosphorus release from lake sediments—a long-lasting paradigm in limnology. Int Rev Hydrobiol 4–5:415–432
67. Fan CX, Morihiro A (1997) Effects of aerobic and anaerobic conditions on exchange of nitrogen and phosphorus across sediment–water interface in Lake Kasumigaura. J Lake Sci 9:337–342
68. Maassen S, Röske I, Uhlmann D (2003) Chemical and microbial composition of sediments in reservoirs with different trophic state. Int Rev Hydrobiol 88:508–518

69. Ye W, Liu X, Lin S, Tan J, Pan J, Li D (2009) The vertical distribution of bacterial and archaeal communities in the water and sediment of Lake Taihu. FEMS Microbiol Ecol 70:263–276
70. Brinkmeyer R, Knittel K, Jurgens J, Weyland H, Amann R, Helmke E (2003) Diversity and structure of bacterial communities in Arctic versus Antarctic pack ice. Appl Environ Microbiol 69:6610–6619
71. Mueller-Spitz SR, Stewart LB, Klump JV, Mclellan SL (2010) Freshwater suspended sediments and sewage are reservoirs for enterotoxin-positive *Clostridium perfringens*. Appl Environ Microbiol 76:5556–5562
72. Mulder EG, Deinema MH (2006) The genus *Haliscomenobacter*. Proc Natl Acad Sci U S A 7:602–604
73. Gaval G, Pernelle JJ (2003) Impact of the repetition of oxygen deficiencies on the filamentous bacteria proliferation in activated sludge. Water Res 37:1991–2000
74. Smil V (2000) Cycles of life. Scientific American Library, New York
75. Coates JD, Chakraborty R, Lack JG, O'Connor SM, Cole KA, Bender KS, Achenbach LA (2001) Anaerobic benzene oxidation coupled to nitrate reduction in pure culture by two strains of *Dechloromonas*. Nature 411:1039–1043
76. Salinero KK, Keller K, Feil WS, Feil H, Trong S, Bartolo GD, Lapidus A (2009) Metabolic analysis of the soil microbe *Dechloromonas aromatica* str. RCB: indications of a surprisingly complex life-style and cryptic anaerobic pathways for aromatic degradation. BMC Genomics 10:351
77. Coby AJ, Picardal F, Shelobolina E, Xu HF, Roden EE (2011) Repeated anaerobic microbial redox cycling of iron. Appl Environ Microbiol 77:6036–6042
78. Huerta B, Marti E, Gros M, López P, Pompêo M (2013) Exploring the links between antibiotic occurrence, antibiotic resistance, and bacterial communities in water supply reservoirs. Sci Total Environ 456–457:161–170
79. Judd KE, Crump BC, Kling GW (2006) Variation in dissolved organic matter controls bacterial production and community composition. Ecol Lett 87:2068–2079
80. Zhang HH, Huang TL, Chen SN, Yang X, Lv K, Sekar R (2015) Abundance and diversity of bacteria in oxygen minimum drinking water reservoir sediments studied by quantitative PCR and pyrosequencing. Microb Ecol 69:618–629
81. Green TJ, Barnes AC, Bartkow M, Gale D, Grinham A (2011) Sediment bacteria and archaea community analysis and nutrient fluxes in a sub-tropical polymictic reservoir. Aquat Microb Ecol 65:287–302
82. Song K, Lee SH, Kong H (2011) Denitrification rates and community structure of denitrifying bacteria in newly constructed wetland. Eur J Soil Biol 47:24–29
83. Yang J, Jiang HC, Dong HL, Wu G, Hou WG (2013) Diversity of carbon monoxide-oxidizing bacteria in five lakes on the Qinghai-Tibet Plateau, China. Geomicrobiol J 30:758–767
84. Carolina C, Renato I, Franco V, Giulio P (2013) Bacterial communities in polluted seabed sediments: a molecular biology assay in leghorn harbor. Sci World J 2013:165706
85. Laurence H, Mauro T, Jakob Z, Peduzzi R, Wildi W (2011) Composition of bacterial and archaeal communities in freshwater sediments with different contamination levels (Lake Geneva, Switzerland). Water Res 45:1213–1228
86. Foulquier A, Volat B, Neyra M, Bornette G, Montuelle B (2013) Long-term impact of hydrological regime on structure and functions of microbial communities in riverine wetland sediments. FEMS Microbiol Ecol 85:211–226
87. Sanchez-Andrea I, Stams AJM, Amils R, Sanz JL (2013) Enrichment and isolation of acidophilic sulfate-reducing bacteria from Tinto River sediments. Environ Microbiol 5:672–678
88. Ulfig K (1995) A statistical evaluation of the occurrence of keratinolytic fungi in the sediments of two dam reservoirs. Rocz Panstw Zakl Hig 46:81–89

89. Douma M, Ouahid Y, del Campo FF, Loudiki M, Mouhri KH (2010) Identification and quantification of cyanobacterial toxins (microcystins) in two Moroccan drinking-water reservoirs (Mansour Eddahbi, Almassira). Environ Monit Assess 160:439–445
90. Loman NJ, Misra RV, Dallman TJ, Constantinidou C, Gharbia SE (2012) Performance comparison of benchtop high-throughput sequencing platforms. Nat Biotechnol J 30:434–439
91. Rousk J, Baath E, Brookes PC, Lauber CL, Lozupone C (2010) Soil bacterial and fungal communities across a pH gradient in an arable soil. ISME J 4:1340–1351
92. Dollive S, Chen Y-Y, Grunberg S, Bittinger K, Hoffmann C (2013) Fungi of the murine gut: episodic variation and proliferation during antibiotic treatment. PLoS One 8:e71806
93. Bellemain E, Carlsen T, Brochmann C, Coissac E, Taberlet P, Kauserud H (2010) ITS as an environmental DNA barcode for fungi: an in silico approach reveals potential PCR biases. BMC Microbiol 10:189
94. La Duc MT, Vaishampayan P, Nilsson HR, Torok T, Venkateswaran K (2012) Pyrosequencing-derived bacterial, archaeal, and fungal diversity of spacecraft hardware destined for Mars. Appl Environ Microbiol 16:5912–5922
95. Nilsson R, Ryberg M, Abarenkov K, Sjvist E, Kristiansson E (2009) The ITS region as a target for characterization of fungal communities using emerging sequencing technologies. FEMS Microbiol Lett 296:97–101
96. Porter TM, Schadt CW, Rizvi L, Martin AP, Schmidt SK (2008) Widespread occurrence and phylogenetic placement of a soil clone group adds a prominent new branch to the fungal tree of life. Mol Phylogenet Evol 46:635–644
97. Krauss GJ, Solé M, Krauss G, Schlosser D, Wesenberg D, Bärlocher F (2011) Fungi in freshwaters: ecology, physiology and biochemical potential. FEMS Microbiol Lett 35:620–651
98. Kiziewicz B (2004) Water fungi occurence in the water reservoir in Zarzeczany of Podlasie province. Wiad Parazytol 50:587–593
99. Pereira VJ, Basílio MC, Fernandes D, Domingues M, Paiva JM (2009) Occurrence of filamentous fungi and yeasts in three different drinking water sources. Water Res 43:3813–3819
100. Egge E, Bittner L, Andersen T, Audic S, de Vargas C (2013) 454 pyrosequencing to describe microbial eukaryotic community composition, diversity and relative abundance: a test for marine haptophytes. PLoS One 8:e74371
101. Ranković B (2005) Five Serbian reservoirs contain different fungal propagules. Mycologia 97:50–56
102. Hou DK, He J, Lü CW, Sun Y, Zhang FJ, Otgonbayar K (2013) Effects of environmental factors on nutrients release at sediment–water interface and assessment of trophic status for a typical shallow lake, Northwest China. Sci World J. Article ID 716342
103. Nagahama T, Hamamoto M, Horikoshi K (2006) *Rhodotorula pacifica* sp nov. a novel yeast species from sediment collected on the deep-sea floor of the north-west Pacific Ocean. Int J Syst Evol Microbiol 56:295–299
104. Freeman KR, Martin AP, Karki D, Lyncha RC, Mitter MS (2009) Evidence that chytrids dominate fungal communities in high-elevation soils. Proc Natl Acad Sci U S A 106:18315–18329
105. Hodge A (2000) Microbial ecology of the arbuscular mycorrhiza. FEMS Microbiol Ecol 32:91–96
106. Anderson RS, Homola RL, Davis RB, Jacobson GL Jr (1984) Fossil remains of the mycorrhizal fungal Glomus fasciculatum complex in postglacial lake sediments from Maine. Can J Bot 62:2325–2328
107. Kagami M, Amano Y, Ishii N (2012) Community structure of planktonic fungi and the impact of parasitic chytrids on phytoplankton in Lake Inba, Japan. Microb Ecol 63:358–368
108. Bertrand C, Couté A, Cazaubon A (2004) Fungal parasitism of the diatom *Asterionella formosa* Hassall (Bacillariophyceae) by Chytridiomycota. Ann Limnol Int J Limnol 40:63–69

109. Fernández C, Parodi ER, Cáceres EJ (2011) Impact of the fungal parasite *Rhizophydium couchii* (Chytridiomycota) on the population dynamics of the freshwater alga *Closterium aciculare* (Chlorophyta). Nova Hedwigia 93:1–2
110. Bates ST, Berg-Lyons D, Caporaso JG, Walters WA, Knight R (2011) Examining the global distribution of dominant archaeal populations in soil. ISME J 5:908–917
111. Cao HL, Hong YG, Li M, Gu JD (2011) Phylogenetic diversity and ecological pattern of ammonia-oxidizing archaea in the surface sediments of the Western Pacific. Microb Ecol 62:813–823
112. Leininger S, Urich DA, Schloter M, Schwark L, Qi J, Nicol GW (2006) Archaea predominate among ammonia oxidizing prokaryotes in soils. Nature 442:806–809
113. Choi KH, Dobbs FC (1999) Comparison of two kinds of Biolog microplates (GN and ECO) in their ability to distinguish among aquatic microbial communities. J Microbiol Methods 36:203–213
114. Christopher Q, Anders L, Thomas PC, Russell JD, Neil H, Ian MH, Fiona R, William TS (2009) Accurate determination of microbial diversity from 454 pyrosequencing data. Nat Methods 6:639–641
115. Luo C, Tsementzi D, Kyrpides N, Read T, Konstantinidis KT (2012) Direct comparisons of Illumina vs Roche 454 sequencing technologies on the same microbial community DNA sample. PLoS One 7:e30087
116. Wirth R, Kovács E, Maróti G, Bagi Z, Rákhely G, Kovács KL (2012) Characterization of a biogas-producing microbial community by short-read next generation DNA sequencing. Biotechnol Biofuels 5:41
117. Koizumi Y, Takii S, Fukui M (2004) Depth-related change in archaeal community structure in a freshwater lake sediment as determined with denaturing gradient gel electrophoresis of amplified 16S rRNA genes and reversely transcribed rRNA fragments. FEMS Microbiol Ecol 48:285–292
118. Li ZX, Jin WB, Liang ZY, Yue YY, Lv JH (2013) Abundance and diversity of ammonia-oxidizing archaea in response to various habitats in Pearl River Delta of China, a subtropical maritime zone. J Environ Sci Technol 25:1195–1205
119. Lloyd KG, Schreiber L, Petersen DG, Kjeldsen KU, Lever MA, Steen AD, Stepanauskas R, Richter M, Kleindienst S, Lenk S, Schramm A, Jørgensen BB (2013) Predominant archaea in marine sediments degrade detrital proteins. Nature 496:215–218
120. Tang C, Madigan MT, Lanoil B (2013) Bacterial and archaeal diversity in sediments of West Lake Bonney, McMurdo Dry Valleys, Antarctica. Appl Environ Microbiol 79:1034–1038
121. Wang P, Li T, Hu AY, Wei YL, Guo WT, Jiao NZ, Zhang CL (2010) Community structure of archaea from deep-sea sediments of the South China Sea. Microb Ecol 60:796–806
122. Andrea KB, Michael DJL, Jennifer CS, Gabriel MH, Josh DN (2011) Generation of multimillion-sequence 16S rRNA gene libraries from complex microbial communities by assembling paired-end Illumina reads. Appl Environ Microbiol 77:3846–3852
123. Borrel G, Lehours AC, Crouzet O, Jézéquel D, Rockne K, Kulczak A, Duffaud E, Joblin K, Fonty G (2012) Stratification of archaea in the deep sediments of a freshwater meromictic lake: vertical shift from methanogenic to uncultured archaeal lineages. PLoS One 8:e43346
124. Sanz-Montero ME, Rodríguez-Aranda JP (2012) Magnesite formation by microbial activity: evidence from a Miocene hypersaline lake. Sediment Geol 263–264:6–15
125. Pereira VJ, Fernandes D, Carvalho G, Benoliel MJ, San Romão MV, Barreto Crespo MT (2010) Assessment of the presence and dynamics of fungi in drinking water sources using cultural and molecular methods. Water Res 44:4850–4859
126. Gallina AA, Celussi M, Del Negro P (2011) Large-scale distribution and production of bacterioplankton in the Adriatic Sea. J Sea Res 66:1–8
127. Stabili L, Cavallo RA (2011) Microbial pollution indicators and culturable heterotrophic bacteria in a Mediterranean area (Southern Adriatic Sea Italian coasts). J Sea Res 65:461–469

128. Gentès S, Monperrus M, Legeay A, Maury-Brachet R, Davail S, André JM, Guyoneaud R (2013) Incidence of invasive macrophytes on methylmercury budget in temperate lakes: central role of bacterial periphytic communities. Environ Pollut 172:116–123
129. Wilhelm SW, Farnsley SE, LeCleir GR, Layton AC, Satchwell MF, DeBruyn JM, Boyer GL, Zhu GW, Paerl HW (2011) The relationships between nutrients, cyanobacterial toxins and the microbial community in Taihu (Lake Tai), China. Harmful Algae 10:207–215
130. Bouvy M, Arfi R, Bernard C, Carré C, Got P, Pagano M, Troussellier M (2010) Estuarine microbial community characteristics as indicators of human-induced changes (Senegal River, West Africa). Estuar Coast Shelf Sci 87:573–582
131. Yu Y, Wang H, Liu J, Wang Q, Shen TL, Guo WH, Wang RQ (2012) Shifts in microbial community function and structure along the successional gradient of coastal wetlands in Yellow River Estuary. Eur J Soil Biol 49:12–21
132. Sura S, Waiser M, Tumber V, Farenhorst A (2012) Effects of herbicide mixture on microbial communities in prairie wetland ecosystems: a whole wetland approach. Sci Total Environ 435–436:34–43
133. Li GY, Jiang HC, Hou WG, Wang S, Huang LQ, Ren HL, Deng SC, Dong HL (2012) Microbial diversity in two cold springs on the Qinghai-Tibetan Plateau. Geosci Front 3:317–325
134. Li WH, Tian YZ, Shi GL, Guo CS, Li X, Feng YC (2012) Concentrations and sources of PAHs in surface sediments of the Fenhe reservoir and watershed, China. Ecotoxicol Environ Saf 75:198–206 (in Chinese)
135. Niederberger TD, Ronimus RS, Morgan HW (2008) The microbial ecology of a high-temperature near-neutral spring situated in Rotorua. Microbiol Res 163:594–603
136. Kerstin R, Rene S, Carola S, Röske I (2012) Microbial diversity and composition of the sediment in the drinking water reservoir Saidenbach (Saxonia, Germany). Syst Appl Microbiol 35:35–44
137. Siba H, Schmieder K, Reinhard B (2010) Spatial patterns of submerged macrophytes and heavy metals in the hypertrophic, contaminated, shallow reservoir Lake Qattieneh/Syria. Limnologica 40:54–60
138. Chen C, Zhang ZC, Ding AZ, Wu JY, Xiao JF, Sun YJ (2011) Bar-coded pyrosequencing reveals the bacterial community during microcystis water bloom in Guanting Reservoir, Beijing. Procedia Eng 18:341–346
139. Lautenschlager K, Boon N, Wang YY, Egli T, Hammes F (2010) Overnight stagnation of drinking water in household taps induces microbial growth and changes in community composition. Water Res 40:4868–4877
140. Duan WW, Lou K, Zeng J, Hu R, Shi YW, He Q, Liu XC, Sun J, Chao QF (2012) Metabolic characteristics of air microbial communities from sandstorm source areas of the Taklamakan desert. Huan Jing Ke Xue 33:26–31 (in Chinese)
141. Salomo S, Münch C, Röske I (2009) Evaluation of the metabolic diversity of microbial communities in four different filter layers of a constructed wetland with vertical flow by Biolog analysis. Water Res 43:4569–4578
142. Comeau AM, Harding T, Galand PE, Vincent WF, Lovejoy C (2012) Vertical distribution of microbial communities in a perennially stratified Arctic lake with saline, anoxic bottom waters. Sci Rep 2:604
143. Karlov DS, Marie D, Chuvochina MS, Alekhina IA, Bulat SA (2011) Microbial communities of water column of Lake Radok, East Antarctica, dominated by abundant actinobacterium "Candidatus Planktophila limnetica". Microbiol Immunol 80:576–579

Screening and Cultivation of Oligotrophic Aerobic Denitrifying Bacteria

Haihan Zhang and Shilei Zhou

Abstract During the past few decades, more and more people have poured nitrogen into the fresh water ecosystem, leading to serious environmental problems, such as eutrophication, algal bloom, and unsafe water, especially in drinking water reservoirs. Nitrogen removal in freshwater ecosystems is important for water utilization processes. Physical (air stripping) and chemical techniques (chemical precipitation) are widely used to remove nitrogen from wastewater, as the traditional biological method (nitrification by autotrophs under aerobic conditions and denitrification by heterotrophs under anaerobic conditions) is impractical. Conventional biological denitrification only occurs under anaerobic or anoxic conditions with the reduction from nitrate to nitrogen gas. Oxygen inhibits the reaction steps, which makes them impractical in natural waters, especially in reservoirs. However, few studies have focused on aerobic denitrifiers' characteristics for removing nitrogen from oligotrophic drinking water reservoirs. To end this, we isolated several strains using enrichment and screening processes. We found that some strains have perfect performance on nitrogen removal in aerobic conditions with low pollutant concentration. Therefore, the objectives of the present work were to determine the taxonomic status using the 16S rRNA method, and to determine nitrogen removal performance in nutrient medium. The results can be useful for applications of aerobic denitrifiers for micropollution reservoir bioremediation. There are two parts in this chapter: (1) Screening and isolation of oligotrophic aerobic denitrifying bacteria; (2) Denitrification performance in pure culture conditions. The results of this part demonstrated that oligotrophic aerobic denitrifying bacterial species had aerobic denitrification ability, and resist a low carbon to nitrogen ratio, therefore, provided the scientific evidence for micropolluted source water bioremediation processes in situ.

Keywords Aerobic denitrifiers • Aerobic denitrification • Nitrogen removal • Source water • Reservoir

H. Zhang (✉) • S. Zhou
School of Environmental and Municipal Engineering, Xi'an University of Architecture and Technology, Yanta Road 13, 710055 Xi'an, Shaanxi Province, P. R. China
e-mail: zhanghaihan@xauat.edu.cn

T. Huang (ed.), *Water Pollution and Water Quality Control of Selected Chinese Reservoir Basins*, The Handbook of Environmental Chemistry 38,
DOI 10.1007/978-3-319-20391-1_13

1 Screening and Isolation of Oligotrophic Aerobic Denitrifying Bacteria

1.1 Reservoir Sediment Sampling

Reservoir sediment samples were collected from Zhoucun drinking water reservoir (#1, 34°56′38.85″N,117°40′27.42″E; #2, 34°57′9.84″N,117°39′34.17″E; #3, 34°57′21.50″N,117°39′48.67″E; #4, 34°57′3.03″N,117°40′4.78″E; #5, 34°57′19.59″N,117°40′51.69″E; #6, 34°56′35.16″N,117°41′04.09″E; #7, 34°56′31.41″N, 117°41′95.57″E). In June 2011, surface sediment samples were collected at a deep layer of 0–10 cm using a sterilized Petersen stainless steel grab sampler [1, 2]. The reservoir source water was also collected. The samples were stored in black plastic bags at 4 °C, and transferred to the Key Laboratory of Northwest Water Resource, Environment and Ecology, Xi'an University of Architecture and Technology (Fig. 1).

1.2 Enrichment Culturing and Isolation of the Aerobic Denitrifiers

The 100-mL sludge sample was added into 700 mL of heterotrophic enrichment denitrification broth medium (HEDM) (in (g/L)) [1, 2]: CH_3COONa 0.5; $NaNO_3$ 0.1; $K_2HPO_4 \cdot 3H_2O$ 0.1; $CaCl_2$ 0.05; $MgCl_2 \cdot 6H_2O$ 0.05; pH 7.0–7.5. Every three days, we threw out the liquid medium, reduced the concentration of the medium by

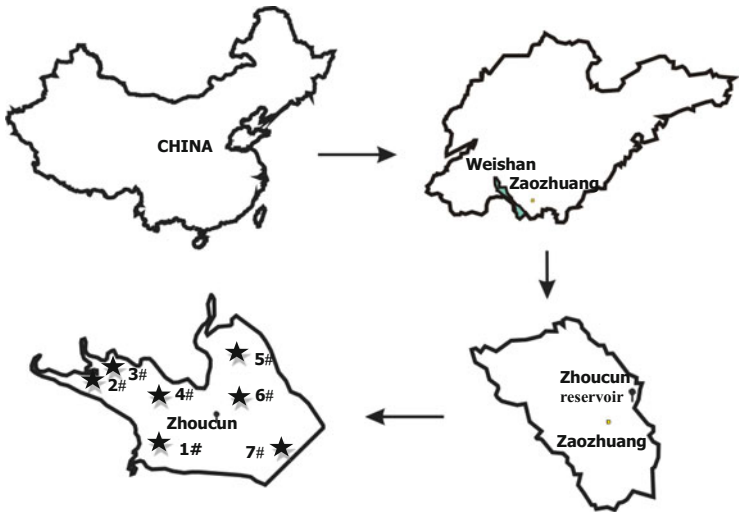

Fig. 1 The location of the sediment sample collection

Fig. 2 The enrichment and domestication of the aerobic denitrifiers

one-tenth, and put the new medium into the sludge sample, until the concentration of the HEDM became one-tenth of the first concentration (Fig. 2). The enrichment of aerobic denitrifiers lasted almost one month [3]. The temperature and the DO of the enrichment cultures were controlled to room temperature and nearly 5 mg/L, respectively. The enrichment sludge suspension was sampled via a series of gradient dilutions: 10^{-1}, 10^{-2}, 10^{-3}, 10^{-4}, 10^{-5}, 10^{-6}, and 10^{-7} dilutions. And the diluents were streaked on a screening medium (SM) [4–6] plate (g/L): CH_3COONa 0.1; $NaNO_3$ 0.02; $K_2HPO_4 \cdot 3H_2O$ 0.02; $CaCl_2$ 0.01; $MgCl_2 \cdot 6H_2O$ 0.01; agar 20; pH 7.0–7.5, which was incubated at 30 °C. Prominent growing single colonies were harvested and cultivated in SM medium with $NaNO_3$ as the sole nitrogen source in order to detect the aerobic denitrifying bacteria performance. To this end, in our primary works, 196 strains were isolated using enrichment and screening processes, and 14 strains have perfect performances on the nitrogen removal process under low pollutant concentration and aerobic conditions. The isolated strains with high nitrogen removal efficiency were stored on SM slant medium at 4 °C and on SM Glycerin medium at −20 °C, respectively.

1.3 Morphological Characteristics of Aerobic Denitrifiers

The 14 strains isolated from the oligotrophic reservoir have perfect performances on the nitrogen removal process under low pollutant concentration and aerobic conditions, and are named after ZHF2, ZHF3, ZHF5, ZHF6, ZHF8, ZMF2, ZMF5, ZMF6, N299, G107, 81Y, SF9, SF18, and SXF14. The morphological characteristics of aerobic denitrifiers were analyzed under a scanning electron microscope, and the results are shown in Fig. 3.

1.4 Analysis of 16S rRNA Gene Sequences

The 16S rRNA sequences of the 14 strains were obtained via polymerase chain reaction (PCR) and sequencing. The PCR primers [7] were F27,

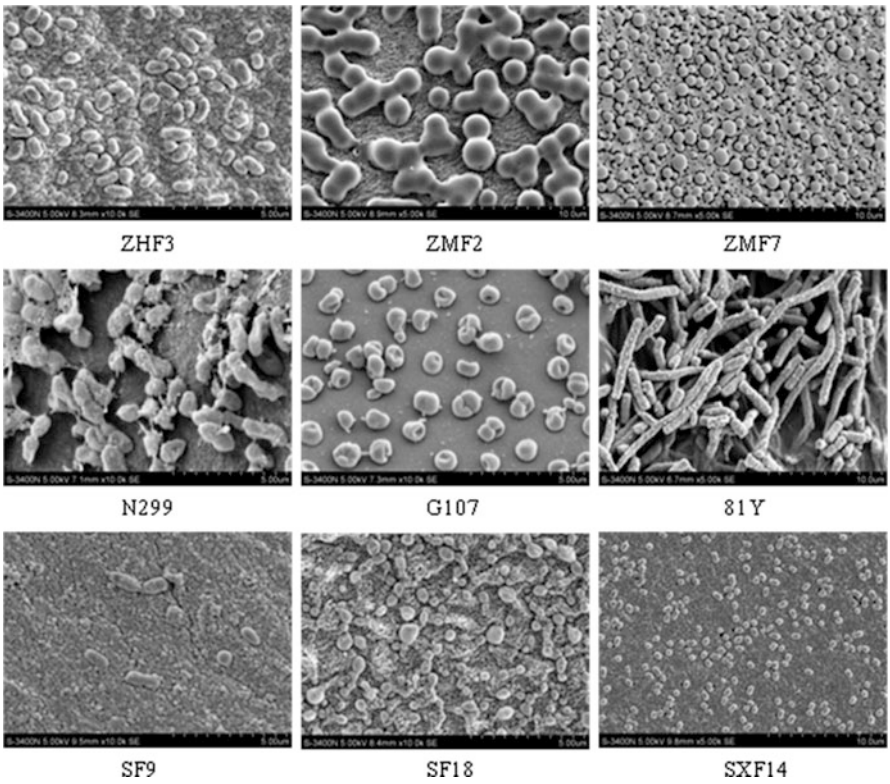

Fig. 3 Scanning electron microscope (SEM) images of aerobic denitrifiers

5′-AGAGTTTGATCATGGCTCAG-3′, and R1492, 5-′-TACGGTTACCTTGTTACGACTT-3′. The PCR reaction mix consisted of the following reagents: 10× Taq buffer (2.0 μL); 2.5 mM dNTP mix (1.6 μL); 5p primer 1 (0.8 μL); 5p primer 2 (0.8 μL); template (0.5 μL); 5u Ex Taq (0.2 μL); with the sterile nuclease-free water to 20 μL. PCR was carried out as follows: 95 °C for 5 min for 1 cycle, then denaturation at 95 °C for 30 s, annealing at 55 °C for 30 s, extension at 72 °C for 90 s, for 24 cycles. After a final extension at 72 °C for 10 min, reactions were held at 10 °C. Homologies searching of the sequences in GenBank by BLAST (http://blast.ncbi.nlm.nih.gov/Blast.cgi) were revealed. A neighbour-joining tree was constructed in the MEGA 5.0 program using the neighbor-joining (NJ) method with 1000 bootstrap replicates and the maximum composite likelihood model [2]. High similarity type culture strains to the genera are listed in Table 1.

An NJ tree based on the comparison of partial 16S rRNA gene sequences of 14 strains and other type culture strains sequences is shown in Fig. 4. The phylogenetic tree based on the 16S rRNA gene sequence of 14 strains with high nitrogen removal efficiency and other previously studied aerobic denitrifiers is shown in Fig. 5.

Table 1 The sequence results of the aerobic denitrifiers

Strains	GenBank no.	Sequence length	High similarity type culture strains	Similarity (%)
ZHF2	KP717095	1394	*Novosphingobium aromaticivorans* DSM 12444(T)	98.06
ZHF3	KP717089	1379	*Acinetobacter junii* CIP 64.5(T)	99.64
ZHF5	KP717094	1447	*Acinetobacter junii* CIP 64.5(T)	97.64
ZHF6	KP717088	1393	*Acinetobacter brisouii* CIP 110357(T)	96.34
ZHF8	KP717087	1399	*Novosphingobium aromaticivorans* DSM 12444(T)	97.28
ZMF2	KP717086	1380	*Acinetobacter junii* CIP 64.5(T)	99.64
ZMF5	KP717085	1434	*Aquabacterium citratiphilum* B4(T)	98.01
ZMF6	KP717084	1400	*Sphingomonas koreensis* JSS26(T)	96.99
N299	KP717093	1361	*Zoogloea caeni* EMB43(T)	97.85
G107	KP717096	1392	*Acinetobacter pittii* CIP 70.29(T)	99.57
81Y	KP717097	1315	*Acinetobacter pittii* CIP 70.29(T)	99.92
SF9	KP717092	1396	*Delftia lacustris* DSM 21246(T)	100
SF18	KP717091	1227	*Acinetobacter oryzae* B23(T)	98.45
SXF14	KP717090	1362	*Acinetobacter johnsonii* CIP 64.5(T)	99.71

Based on 16S rRNA gene sequences, strains ZHF3, ZHF5, ZHF6, ZMF2, G107, 81Y, SF18, and SXF14 clustered with species from *Acinetobacter* sp., strains ZHF2 and ZHF8 clustered with species from *Novosphingobium* sp., strain ZMF5 clustered with species from *Aquabacterium* sp., strain ZMF6 clustered with species from *Sphingomonas* sp., strain N299 clustered with species from *Zoogloea* sp., and strain SF9 clustered with species from *Delftia* sp. Therefore, the aerobic denitrifiers were identified as *Acinetobacter* sp. ZHF3, *Acinetobacter* sp. ZHF5, *Acinetobacter* sp. ZHF6, *Acinetobacter* sp. ZMF2, *Acinetobacter* sp. G107, *Acinetobacter* sp. 81Y, *Acinetobacter* sp. SF18, *Acinetobacter* sp. SXF14, *Novosphingobium* sp. ZHF2, *Novosphingobium* sp. ZHF8, *Aquabacterium* sp. ZMF5, *Sphingomonas* sp. ZMF6, *Zoogloea* sp. N299, and *Delftia* sp. SF9.

An NJ phylogenetic tree based on the 16S rRNA gene sequences of 14 strains with high nitrogen removal efficiency and other previously studied aerobic denitrifiers was constructed in Fig. 5 of Chap. 1. The results showed that strains ZHF5, ZMF2, and SF18 were in the same group; strains ZHF2, ZHF6, ZHF8, and ZMF6 were in the same group; strain ZHF3 and *Acinetobacter* sp. N22 were in the same group; strains SXF14 and *Acinetobacter* sp. CGMCC 6052 were in the same group; strains G107, 81Y, and *Acinetobacter* sp. M9 were in the same group; strains SF9 *Delftia* sp. WXZ-15, *Delftia tsuruhatensis* strain WXZ-1, *Delftia tsuruhatensis* strain P18, and *Delftia tsuruhatensis* strain WYLW2–3 were in the same group; and strains N299, ZMF5, and *Comamonas testosteroni* strain GAD4 were in the same group.

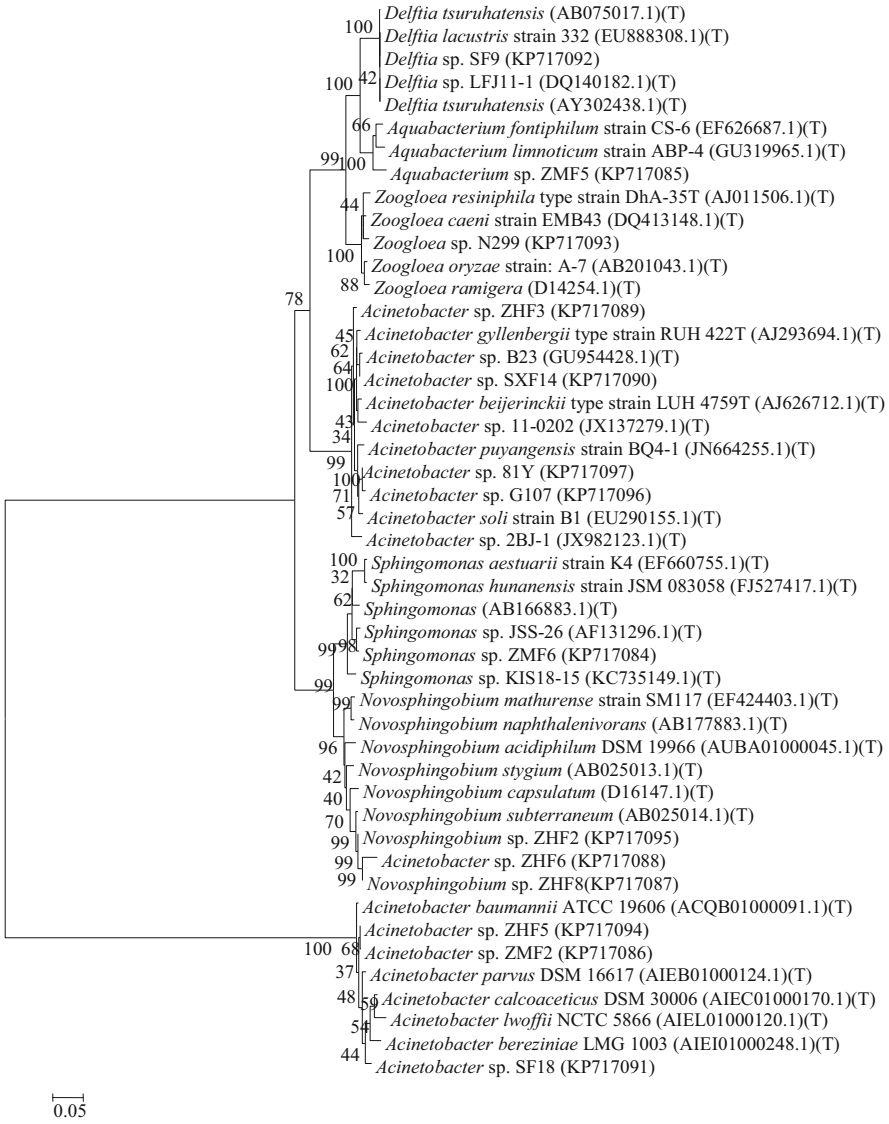

Fig. 4 Phylogenetic tree based on the comparison of partial 16S rRNA gene sequences of 14 strains and other type culture strains sequences

1.5 Summary

We isolated the aerobic denitrifiers from an oligotrophic reservoir water system and studied the taxonomic status. The oligotrophic aerobic denitrifiers were obtained, based on enrichment, domestication, and screening processes, and taxonomic

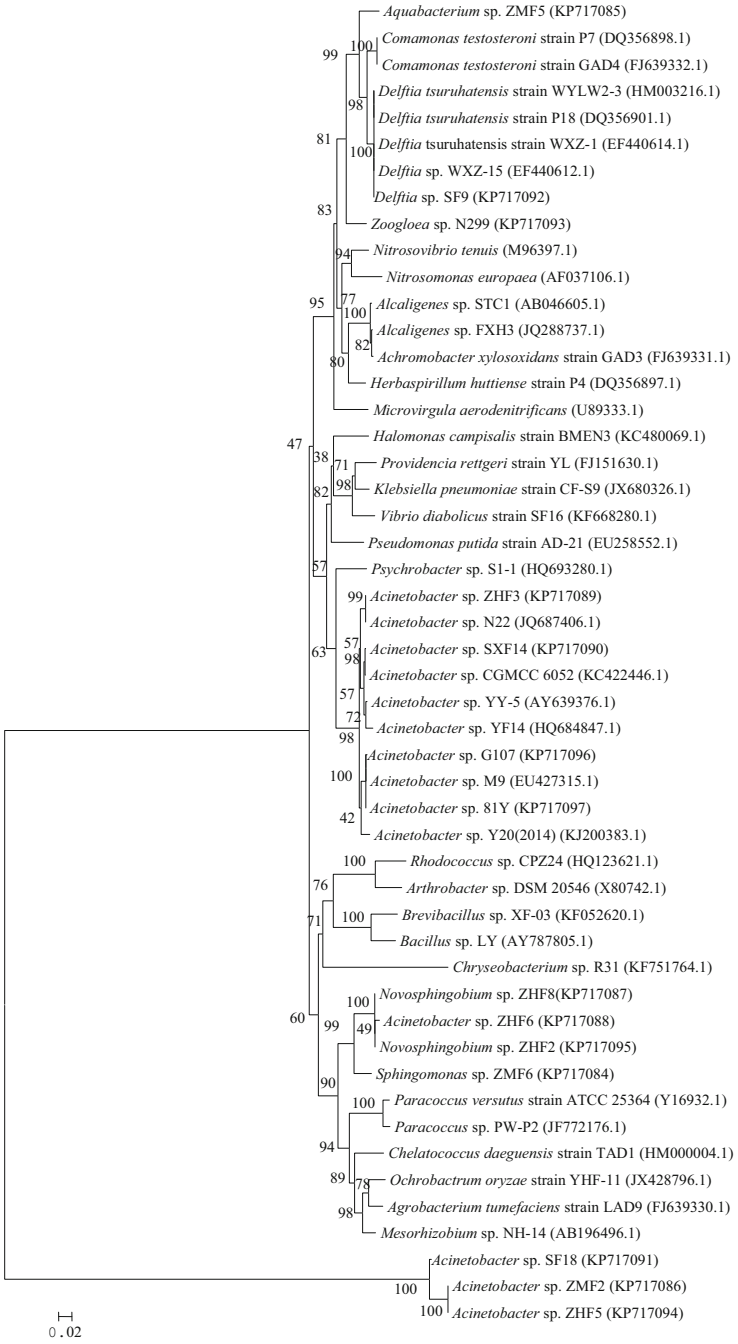

Fig. 5 Phylogenetic tree based on the 16S rRNA gene sequences of 14 strains with high nitrogen removal efficiency and other previously studied aerobic denitrifiers

statuses were determined by 16S rRNA. In the preliminary experiment with enrichment culture isolation, 196 strains were isolated, and 14 strains (ZHF2, ZHF3, ZHF5, ZHF6, ZHF8, ZMF2, ZMF5, ZMF6, N299, G107, 81Y, SF9, SF18, and SXF14) demonstrated perfect nitrogen removal ability. Based on morphological and phylogenetic analyses, ZHF3, ZHF5, ZHF6, ZMF2, G107, 81Y, SF18, and SXF14 were identified as *Acinetobacter* sp.; ZHF2 and ZHF8 were identified as *Novosphingobium* sp.; ZMF5 was identified as *Aquabacterium* sp.; ZMF6 was identified as *Sphingomonas* sp.; N299 was identified as *Zoogloea* sp.; and SF9 was identified as *Delftia* sp. The isolation of oligotrophic aerobic denitrifiers enriched the species of aerobic denitrification bacteria, and the perfect nitrogen removal performances of oligotrophic aerobic denitrifiers provided a significant parameter to remediate the micropolluted reservoir water system.

2 Denitrification Performance in Pure Culture

During the past few decades, more and more nitrogen has been discarded into the fresh water environmental ecosystem, leading to many serious environmental problems [8–11], such as eutrophication, algal bloom, and lack of drinking water safety [12, 13], especially in the drinking water reservoirs [14, 15]. Nitrogen removal processes in freshwater ecosystems is a hot topic. Physical [16] and chemical techniques [4–6] have been widely used to removal nitrogen in wastewater, and the traditional biological method also has practical application [17]. Conventional biological denitrification only occurs under anaerobic or anoxic conditions with the reduction from nitrate to nitrogen gas [18]. Oxygen inhibits the reaction steps, which makes them impractical in natural waters, especially reservoirs [19].

The discovery of the first aerobic denitrification bacteria *Thiosphaera pantotropha* strain was done by Robertson and Kuenen [20] from a denitrifying, sulfide-oxidizing wastewater treatment plant. There is a new novel method of nitrogen removal, and it is not limited to oxygen [21, 22]. Aerobic denitrification has attractive advantages when compared to conventional denitrification under anaerobic conditions: (1) the nitrification and denitrification can occur in the same treatment system [23] and (2) the denitrification can produce alkalinity to balance the acid of nitrification [24]. There are recent reports of aerobic denitrification bacteria isolated from canals [25], ponds [26, 27], and soils [28], and the dominant species included *Thiosphaera pantotropha* [29], *Alcaligenes faecalis* [30], *Citrobacter diversus* [31], *Pseudomonas stutzeri* [32], and *Rhodococcus* sp. [33].

Compared with strains isolated in massive amounts from other environmental systems [25–28], aerobic denitrifiers are rarely isolated from reservoirs, and there is limited research to date on the use of aerobic denitrifiers to denitrify and bioremediate reservoir ecosystems [26, 27, 34]. Several studies have illustrated the difficulties in removing nitrogen from source water, owing to its low

concentration as a pollutant [35, 36]. Our research team has been researching the water quality of aerobic denitrifiers for a while, and the findings have been reported elsewhere [1, 2, 4–6, 37, 38]. However, fewer studies have focused on exploring the nitrogen removal characteristics of aerobic denitrifiers from oligotrophic drinking water reservoirs.

To end this, in our primary works, 196 strains were isolated using enrichment and screening processes, and 14 strains have perfect performance on the nitrogen removal process under low pollutant concentrations and aerobic conditions. The nitrogen removal performance of *Zoogloea* sp. N299, *Acinetobacter* sp. G107, and 81Y were explored. Therefore, the objectives of the present work were to: (1) determine the growth characteristics of oligotrophic aerobic denitrifiers, (2) investigate the denitrification performances in a pure culture medium system, and (3) examine the nitrification performances in a reservoir source water medium system.

2.1 *Growth Characteristics of* Zoogloea *sp. N299,* Acinetobacter *sp. G107, and* Acinetobacter *sp. 81Y*

To evaluate the growth characteristics of the isolated strain N299, G107, and 81Y, their growth conditions were investigated with a shake flask experiment. 400-mL of the liquid SM medium was placed in 1000-mL shake flasks, inoculated with 4 mL preculture of the strain, and then cultivated at 30 °C. During incubation, 3 mL of culture was removed periodically for the determination of the cell optical density. The aerobic denitrifying bacteria N299, G107, and 81Y were precultured for 24 h in 50 mL of liquid medium (without agar) in a 100-mL Erlenmeyer flask at 30 °C and120 rpm, in order to be activated [4–6]. Then, the N299, G107, and 81Y were inoculated at 1 % (v/v) into 400 mL of liquid SM medium ((in g/L): CH_3COONa 0.1; $NaNO_3$ 0.02; $K_2HPO_4 \cdot 3H_2O$ 0.02; $CaCl_2$ 0.01; $MgCl_2 \cdot 6H_2O$ 0.01; pH 7.0–7.5.) in a 1000-mL Erlenmeyer flask in order to study the cell growth characteristics through measuring the OD_{510}.

Figure 6 shows the growth curve of the N299 strain as a sigmoid curve. The first 18 h comprised the lag phase, followed by a 16-h logarithmic growth phase, and the last 34 h was the stationary phase. During the growth period, the OD_{510} of the strain N299 increased from 0.004 to 0.062. Figure 7 shows the growth curve of isolate G107 as a sigmoid curve. The first 6 h comprised the lag phase, followed by a 24-h logarithmic growth phase, and the last 38 h was the stationary phase. During the growth period, the OD_{510} of the strain G107 increased from 0.009 to 0.052. Figure 8 shows the growth curve of isolate 81Y as a sigmoid curve. The first 15 h comprised the lag phase, followed by a 155-h logarithmic growth phase, and the last 50 h was the stationary phase. During the growth period, the OD_{510} of the strain 81Y increased from 0.003 to 0.081.

The logistic growth equation [39], $y(t) = a/[1 + (a/c - 1)\exp(-bt)]$, describes the cell growth curve, where t is time (h), y is the bacterial cell growth rate (h^{-1}), and

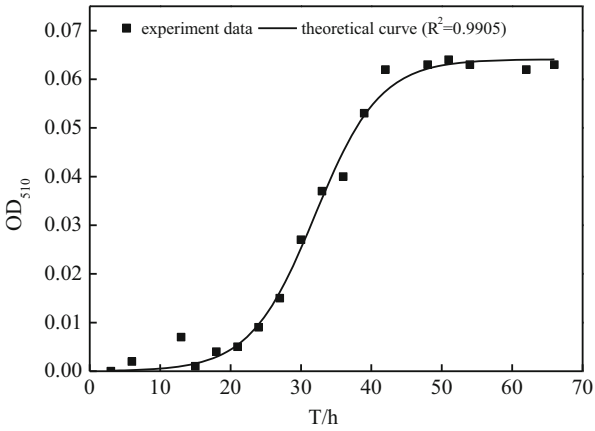

Fig. 6 Growth curve of strain N299 in the liquid SM medium

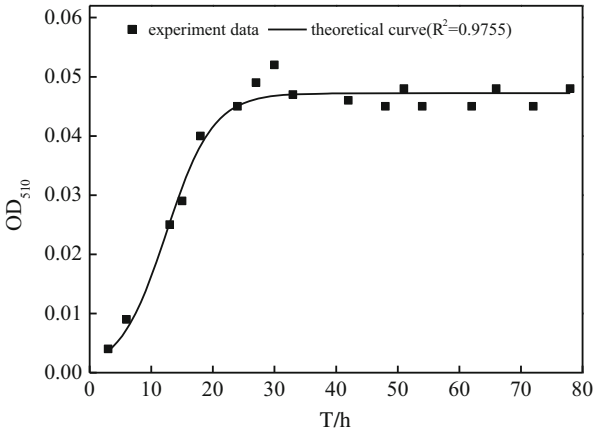

Fig. 7 Growth curve of strain G107 in the liquid SM medium

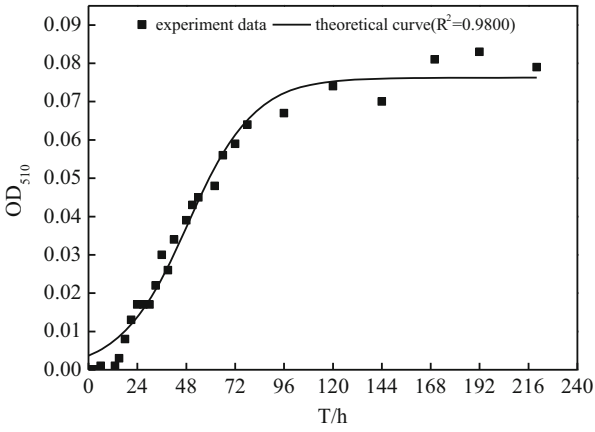

Fig. 8 Growth curve of strain 81Y in the liquid SM medium

a is the maximum bacterial cell density (OD). Correlation analysis of the strain N299 using OriginPro (Version 8.0) yielded $a = 0.064$, $c = 0.004$, and $b = 0.22\ h^{-1}$, with a correlation coefficient of 0.9905. The generation time for N299 was 3.15 h, and the generation time for G107 was 2.67 h ($b = 0.26\ h^{-1}$). T he generation time for the strain 81Y was 11.55 h ($b = 0.06\ h^{-1}$). The heterotrophic aerobic denitrification bacteria possessed higher growth rates and shorter growth cycles. The specific growths of N299, G107, and 81Y are 0.22, 0.26, and 0.06 h^{-1}, respectively. Comparing *N. europaea* (0.03–0.05 h^{-1}) [40], *Pseudomonas denitrificans* (0.19–0.23 h^{-1}), and *T. pantotropha* (0.28–0.45 h^{-1}) under different growth conditions [21, 22], and the specific growth rate of *A. faecalis* no. 4 was 0.2 h^{-1} [18], because the aerobic denitrifiers N299, G107, and 81Y were cultured in the oligotrophic SM medium, then the results demonstrated the strong growth and substrate utilization abilities of the isolated aerobic denitrifiers in the present work.

2.2 *The Relationship Between OD and Colony Numbers of* Zoogloea *sp. N299,* Acinetobacter *sp. G107, and* Acinetobacter *sp. 81Y*

In order for the OD to represent the numbers of colonies in the medium, it is necessary to study the relationship between the OD and colony numbers. The aerobic denitrifying bacteria N299, G107, and 81Y were precultured. The N299, G107, and 81Y were inoculated at 2 %(v/v) into a 150-mL or 250-mL Erlenmeyer flask for 24 h. The cell pellet was prepared by centrifuging a 10-mL sample of broth culture at 5000 rpm for 10 min and then decanting the supernatant after washing twice with distilled water. Then, by adding the distilled water, we obtained a series of ODs. The numbers of colonies of every OD suspension was counted via gradient dilution.

From the data series, Fig. 9 shows the relationship between OD and the colony numbers of the N299, G107, and 81Y strains. We obtained the relationships between OD and colony as follows: strain *Zoogloea* sp. N299, $y(\lg(\text{colony})) = 5.23 + 38.51x(OD_{600})$, correlation coefficient $R^2 = 0.9497$; strain *Acinetobacter* sp. G107, $y(\lg(\text{colony})) = 6.63 + 44.17x(OD_{600})$, correlation coefficient $R^2 = 0.8247$; strain *Acinetobacter* sp. 81Y, $y(\lg(\text{colony})) = 6.46 + 43.53x\ (OD_{600})$, correlation coefficient $R^2 = 0.9266$. Therefore, we can obtain the number of colonies of the medium by measuring the OD_{600}.

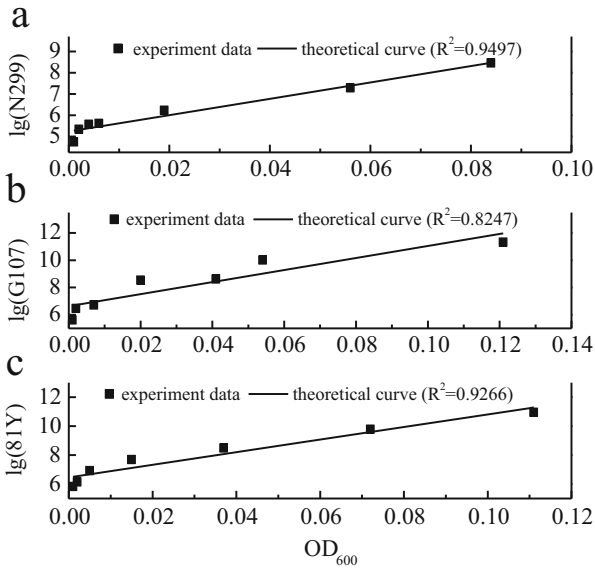

Fig. 9 The relationship between OD_{600} and colony numbers of *Zoogloea* sp. N299, *Acinetobacter* sp. G107, and 81Y

2.3 *The Denitrification Performances of* Zoogloea *sp. N299,* Acinetobacter *sp. G107, and* Acinetobacter *sp. 81Y in Nitrate Medium*

The precultured N299, G107, and 81Y were inoculated in 10 % (v/v) into 150 mL of liquid SM medium, in an Erlenmeyer flask at 30 °C and 120 rpm. The nitrate, nitrite, TN, TDN, and TOC concentrations, and cell optical density (OD) were measured to reflect the denitrification performances of strains N299, G107, and 81Y. All parameters were measured in triplicate ($n = 3$). SM medium (in g/L): CH_3COONa 0.1; $NaNO_3$ 0.02; $K_2HPO_4 \cdot 3H_2O$ 0.02; $CaCl_2$ 0.01; $MgCl_2 \cdot 6H_2O$ 0.01; pH 7.0–7.5.

Under aerobic conditions (dissolved oxygen, DO = 7.0–8.0 mg/L), *Zoogloea* sp. N299, *Acinetobacter* sp. G107, and *Acinetobacter* sp. 81Y demonstrated clear denitrification performance. As shown in Figs. 10, 12, and 14, at 72 h, the nitrate concentrations of N299, G107, and 81Y decreased from 3.54 ± 0.03 mg/L to 0.87 ± 0.06 mg/L, 0.41 ± 0.02 mg/L, and 0.52 ± 0.07 mg/L, and the nitrite increased from 0 mg/L to 0.02 ± 0.00 mg/L, 0.08 ± 0.01 mg/L, and 0.08 ± 0.01 mg/L, with no nitrite accumulation. As shown in Figs. 11, 13, and 15, the TN (total nitrogen) and TDN (total dissolved nitrogen) concentrations decreased from 3.63 ± 0.03 mg/L to 1.93 ± 0.01 mg/L, 2.18 ± 0.05 mg/L, and 2.41 ± 0.06 mg/L; from 3.63 ± 0.03 mg/L to 1.00 ± 0.02 mg/L, 1.63 ± 0.09 mg/L, and 1.72 ± 0.07 mg/L at 120 h, respectively. The removal rate of TN and TDN reached 46.79 ± 0.30 %, 39.90 ± 1.45 %, and 33.72 ± 1.78 %; and 72.30 ± 0.52 %, 55.15 ± 2.43 %, and 52.71 ± 1.97 % at 120 h, respectively. The TOC of N299 and

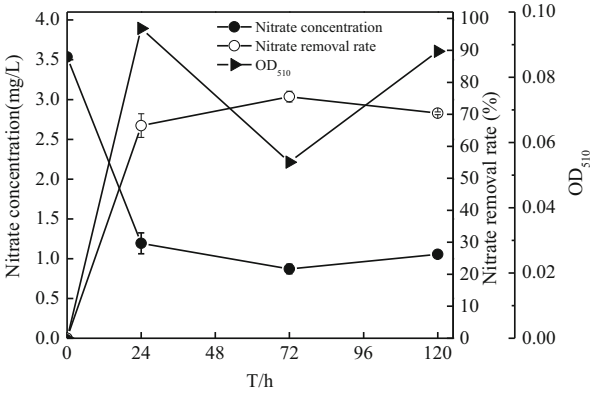

Fig. 10 Changes in nitrate, nitrate removal rates, and OD_{510} of strain N299 growth in nitrate nitrogen medium

G107 decreased to 1.62 mg/L and 2.48 mg/L in 24 h. The TOC of 81Y decreased from 28.38 ± 0.69 mg/L to 24.61 ± 0.27 mg/L at 0–24 h, and 2.00 ± 0.03 mg/L at 72 h. After that, the denitrification of 81Y became obvious, which was consistent with the characteristics of the isolate. It was suggested that the utilization of organic matter and the degradation of nitrate nitrogen took place simultaneously, indicating it was a true heterotrophic process. The denitrification of N299, G107, and 81Y became weak at low C/N. Because carbon is essential for cell growth and nitrate reduction processes, the optimal quantity of carbon is a key parameter in the denitrification process. However, Zhu et al. [26, 27] showed that the removal rate of nitrate and TN reached 31.7 and 45.0 % at low substrate levels (TOC 48 mg/L and nitrate 4 mg/L), respectively. At the same nitrate level, N299, G107, and 81Y demonstrated strong denitrification performance.

2.4 The Denitrification Performances of Zoogloea *sp. N299,* Acinetobacter *sp. G107, and* Acinetobacter *sp. 81Y in Nitrite Medium*

The precultured N299, G107, and 81Y were inoculated at 10 % (v/v) into 150 mL of short SM medium in a 250-mL Erlenmeyer flask at 30 °C and 120 rpm. The nitrate, nitrite, TN, TP, and TOC concentrations, and cell optical density (OD) were measured to reflect the denitrification performance of the N299, G107, and 81Y strains. All parameters were measured in triplicate ($n = 3$). Short SM medium (in (g/L)): CH_3COONa 0.1; $NaNO_2$ 0.018; $K_2HPO_4 \cdot 3H_2O$ 0.02; $CaCl_2$ 0.01; $MgCl_2 \cdot 6H_2O$ 0.01; pH 7.0–7.5 [3].

Few aerobic denitrifiers using nitrite as the sole nitrogen source were identified. Using nitrite as the sole nitrogen source, this experiment assessed the denitrification activity of N299, G107, and 81Y. Figures 16, 17, 18, 19, 20, and 21 show the time courses of the concentration, TN, nitrite, nitrate, TP, OD_{510}, and TOC levels at the

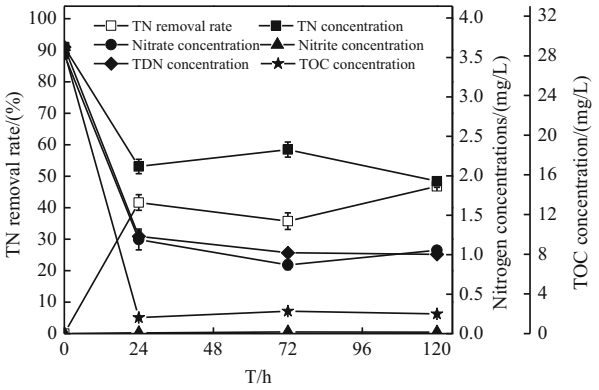

Fig. 11 Changes in TN, TDN, nitrate, nitrite, and TOC concentrations of strain N299 in nitrate nitrogen medium

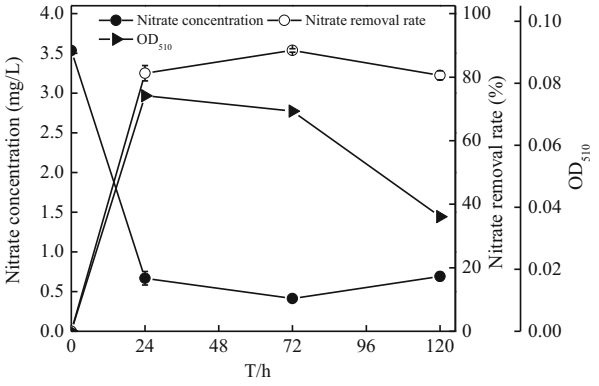

Fig. 12 Changes in nitrate, nitrate removal rates, and OD_{510} of strain G107 growth in nitrate nitrogen medium

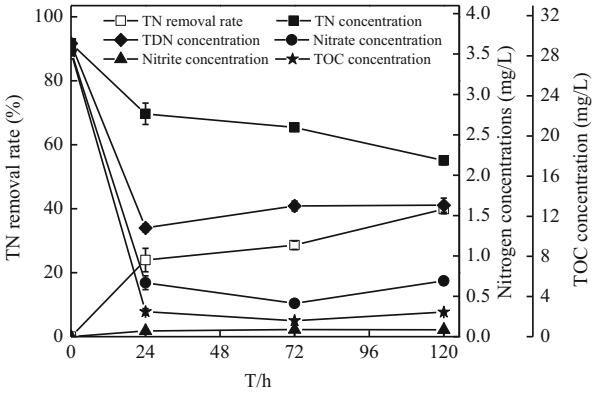

Fig. 13 Changes in TN, TDN, nitrate, nitrite, and TOC concentrations of strain G107 in nitrate nitrogen medium

initial 3.76 mg/L of nitrite. The removal of nitrite and TOC correlated strongly with the growth rates of isolate N299, G107, and 81Y in Figs. 12, 14, and 16 of Chap. 2, with the fastest removal rates occurring during the log phase. The nitrite and TOC

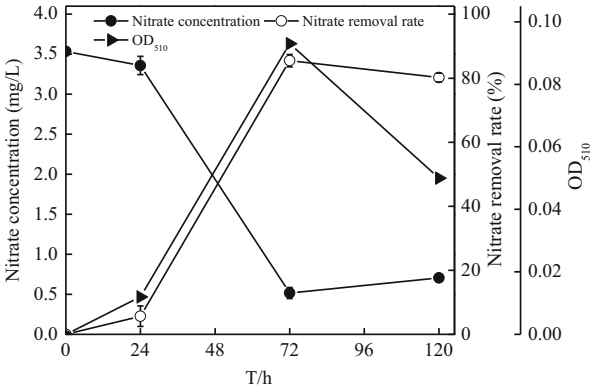

Fig. 14 Changes in nitrate, nitrate removal rates, and OD_{510} of strain 81Y growth in nitrate nitrogen medium

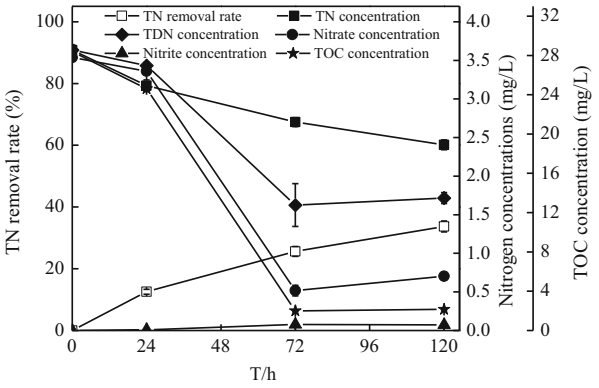

Fig. 15 Changes in TN, TDN, nitrate, nitrite, and TOC concentrations of strain 81Y in nitrate nitrogen medium

were decreased from 3.76 ± 0.08 mg/L and 27.70 ± 0.75 mg/L to 1.56 ± 0.01 mg/L, 1.25 ± 0.05 mg/L, and 1.60 ± 0.12 mg/L; and 0 mg/L, 4.95 ± 0.17 mg/L, and 0.16 ± 0.14 mg/L at 120, 24, and 72 h, respectively. Meanwhile, with the strain's growth, the TN and TP were consumed, and the TN and TP removal rates reached 21.38 ± 9.22 %, 48.98 ± 12.91 %, and 45.37 ± 4.66 %; and 15.97 ± 1.25 %, 12.91 ± 0.98 %, and 17.42 ± 3.76 %, respectively. At the end of the experiment, the nitrate only was increased to 0.19 ± 0.11 mg/L, 0.08 ± 0.04 mg/L, and 0.35 ± 0.04 mg/L. From all of the results, N299, G107, and 81Y clearly demonstrated the denitrification of utilizing the nitrite as the sole nitrogen source.

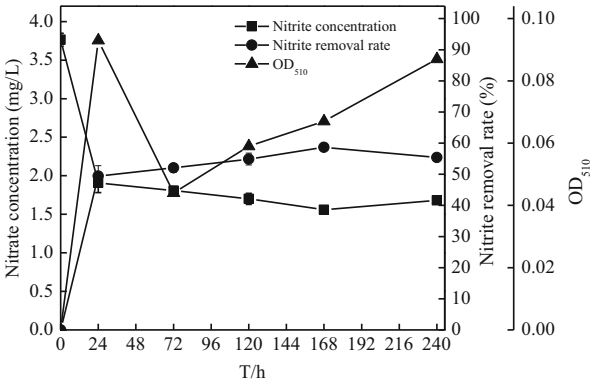

Fig. 16 Changes in nitrite, nitrite removal rates, and OD_{510} of strain N299 growth in nitrite nitrogen medium

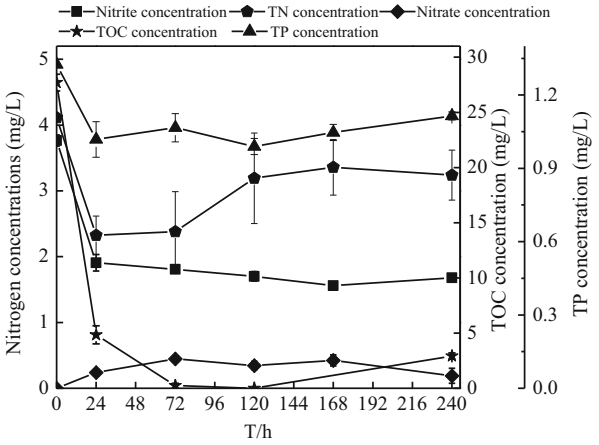

Fig. 17 Changes in TN, nitrate, nitrite, TP, and TOC concentrations of strain N299 in nitrite nitrogen medium

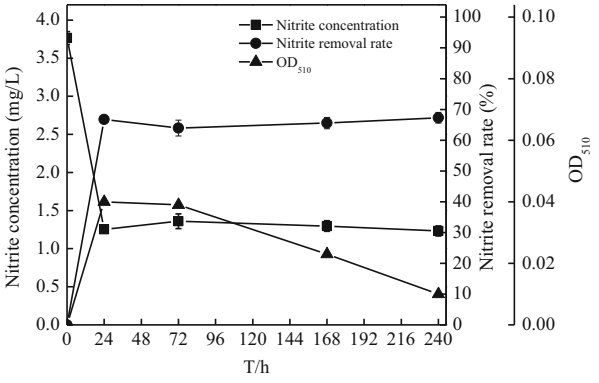

Fig. 18 Changes in nitrite, nitrite removal rates, and OD_{510} of strain G107 growth in nitrite nitrogen medium

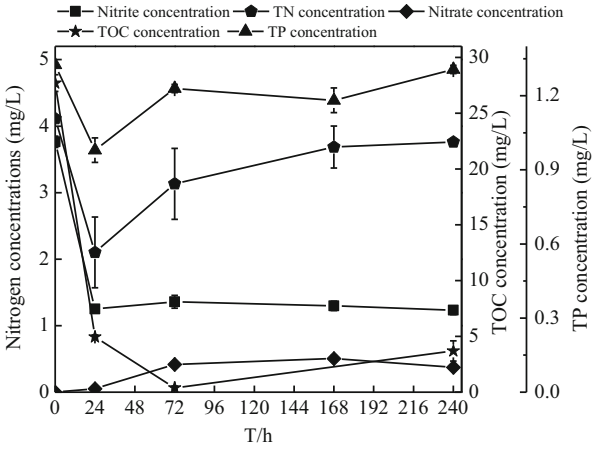

Fig. 19 Changes in TN, nitrate, nitrite, TP, and TOC concentrations of strain G107 in nitrite nitrogen medium

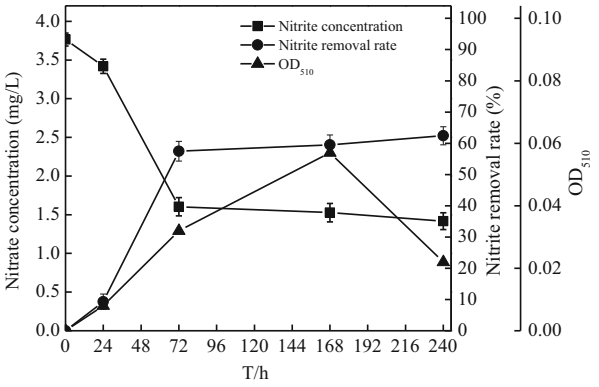

Fig. 20 Changes in nitrite, nitrite removal rates, and OD_{510} of strain 81Y growth in nitrite nitrogen medium

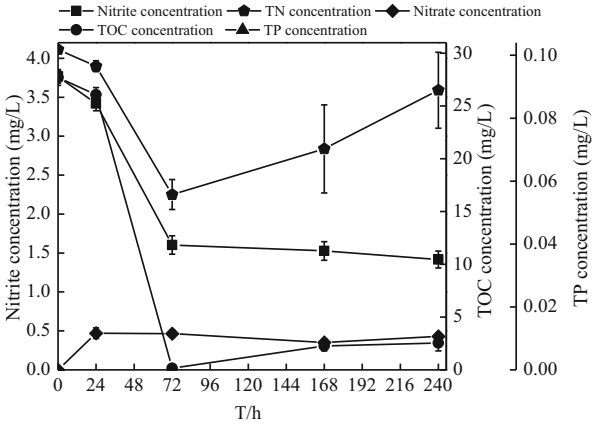

Fig. 21 Changes in TN, nitrate, nitrite, TP, and TOC concentrations of strain 81Y in nitrite nitrogen medium

2.5 *The Nitrification Characteristics of* Zoogloea *sp. N299,* Acinetobacter *sp. G107, and* Acinetobacter *sp. 81Y in Ammonia Medium*

The precultured N299, G107, and 81Y were inoculated at10 % (v/v) into 150 mL liquid HNM in a 250-mL Erlenmeyer flask at 30 °C and 120 rpm. The nitrate, nitrite, TN, ammonia, TP, and TOC concentrations, and cell optical density (OD) were measured to reflect the denitrification performance of the N299, G107, and 81Y strains. All parameters were measured in triplicate ($n = 3$). Heterotrophic nitrification medium (HNM) (in (g/L)): CH_3COONa 0.5; NH_4Cl_4 0.1; $K_2HPO_4 \cdot 3H_2O$ 0.1; $CaCl_2$ 0.05; $MgCl_2 \cdot 6H_2O$ 0.05; pH 7.0–7.5.

The changes of various components in the flask culture are shown in Figs. 22, 23, 24, 25, 26, and 27. The concentration of ammonia decreased significantly, as did TN. The same trend could be seen in the removal of TOC. This indicates that active nitrification occurred largely with a decrease of TOC. At the same time, nitrate and nitrite began to accumulate by nitrification, and remained as denitrification occurred simultaneously, without any nitrate and nitrite accumulation. At the end of the experiment, the ammonia and TN of N299, G107, and 81Y decreased from 28.27 ± 0.14 mg/L and 30.68 ± 0.06 mg/L to 15.79 ± 0.45 mg/L, 18.57 ± 0.99 mg/L, 18.41 ± 2.08 mg/L; and 18.40 ± 0.63 mg/L, 19.41 ± 1.45 mg/L, 19.41 ± 1.45 mg/L, respectively. The removal rate of ammonia and TN reached 44.12 ± 1.61 %, 34.31 ± 3.51 %, 34.31 ± 3.51 %; and 40.05 ± 2.04 %, 36.75 ± 4.73 %, 26.85 ± 7.18 %, respectively. The TOC of N299, G107, and 81Y decreased from 146 ± 0.04 mg/L to 77.90 ± 0.31 mg/L, 24.21 ± 0.68 mg/L, and 24.12 ± 0.93 mg/L. The nitrate and nitrite reached 0.13 ± 0.02 mg/L, 0.15 ± 0.02 mg/L, 0.27 ± 0.06 mg/L; and 0.01 ± 0.00 mg/L, 0.01 ± 0.00 mg/L, respectively. With the growth of N299, G107, and 81Y, the removal rate of TP also reached 22.77 ± 3.90 %, 5.99 ± 0.20 %, and 6.38 ± 1.03 %. From all of the results, it can be seen that N299, G107, and 81Y showed significant nitrification performance. The ability of heterotrophic organisms to oxidize ammonium to nitrate has generally been linked to aerobic denitrification. Therefore, the utilization of ammonium by isolates was investigated. Previous reports found that the aerobic denitrification bacteria usually possessed nitrification ability [26, 27, 32]. Most of the aerobic denitrification bacteria possessed nitrification; however, *Pseudomonas stutzeri* C3 [41] could not exhibit ammonia. In this study, N299, G107, and 81Y could utilize the ammonia as the sole nitrogen source to grow, and, therefore, have heterotrophic nitrification ability. Like other previous aerobic denitrifiers [2], N299, G107, and 81Y demonstrated a good nitrification and no nitrate or nitrite accumulation.

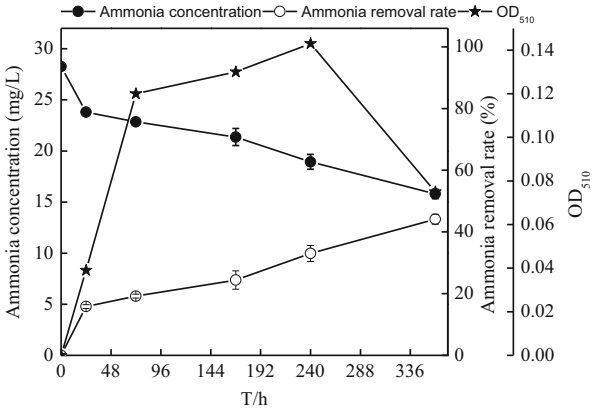

Fig. 22 Changes in ammonia, ammonia removal rates, and OD_{510} of strain N299 growth in ammonia nitrogen medium

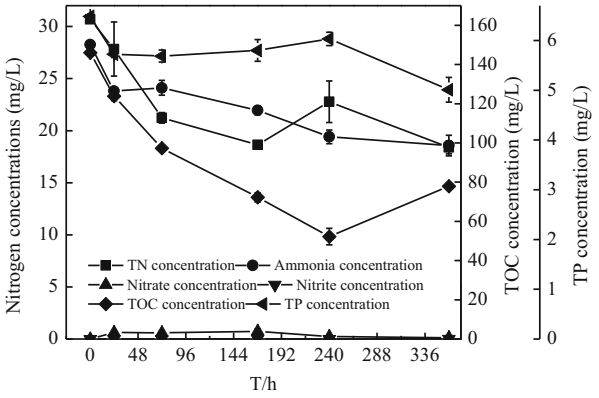

Fig. 23 Changes in TN, ammonia, nitrate, nitrite, TP, and TOC concentrations of strain N299 in ammonia nitrogen medium

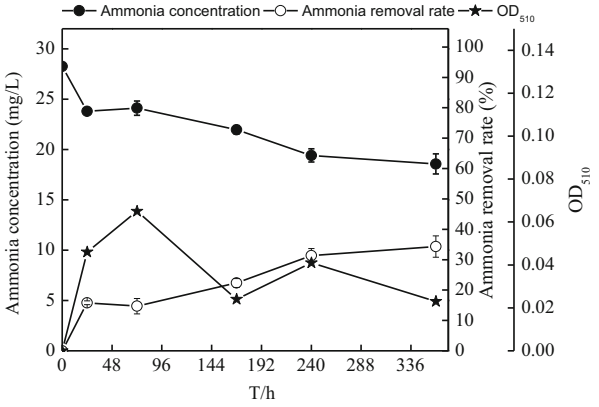

Fig. 24 Changes in ammonia, ammonia removal rates, and OD_{510} of strain N299 growth in ammonia nitrogen medium

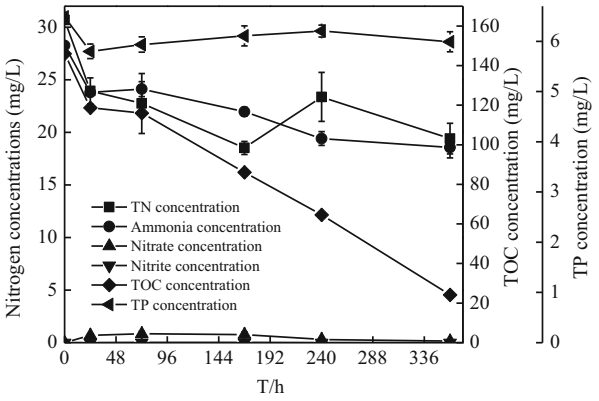

Fig. 25 Changes in TN, ammonia, nitrate, nitrite, TP, and TOC concentrations of strain G107 in ammonia nitrogen medium

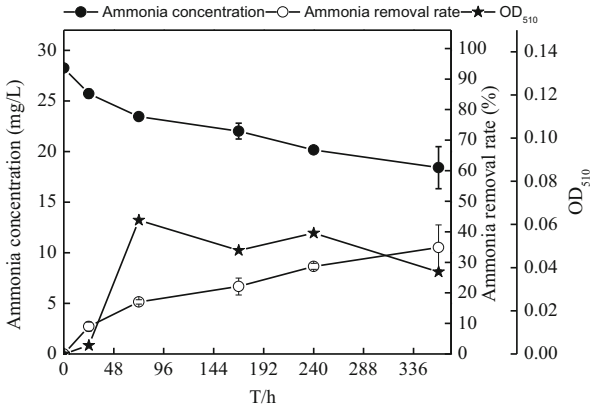

Fig. 26 Changes in ammonia, ammonia removal rates, and OD_{510} of strain 81Y growth in ammonia nitrogen medium

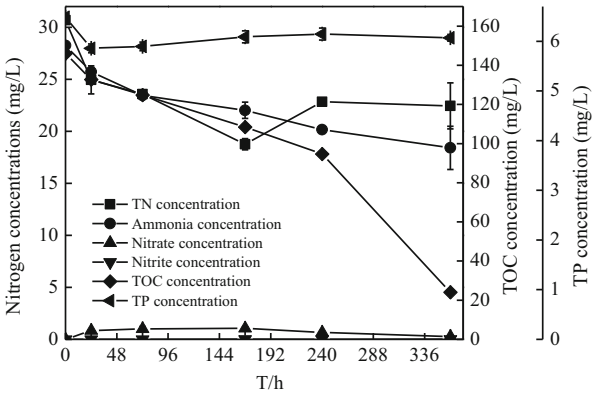

Fig. 27 Changes in TN, ammonia, nitrate, nitrite, TP, and TOC concentrations of strain 81Y in ammonia nitrogen medium

2.6 Summary

The newly isolated indigenous aerobic denitrifiers, N299, G107, and 81Y, were named as *Zoogloea* sp. N299, *Acinetobacter* sp. G107, and *Acinetobacter* sp. 81Y. The specific growths of N299, G107, and 81Y are 0.22, 0.26, and 0.06 h^{-1}, respectively. We discovered the relationship between OD and colony: strain N299, $y(\lg(\text{colony})) = 5.23 + 38.51x(OD_{600})$, correlation coefficient $R^2 = 0.9497$; strain G107, $y(\lg(\text{colony})) = 6.63 + 44.17x(OD_{600})$, correlation coefficient $R^2 = 0.8247$; strain 81Y, $y(\lg(\text{colony})) = 6.46 + 43.53x(OD_{600})$, correlation coefficient $R^2 = 0.9266$. Therefore, we can obtain the number of colonies of the medium by measuring the OD_{600}. The strains showed the ability to utilize the nitrate and enabled nitrite nitrogen. The removal rates of nitrate of strains N299, G107, and 81Y reached 75.53, 88.4, and 85.31 %, respectively, with no nitrite accumulation. Comparing with the study conducted by Zhu et al. [26, 27], they showed that the removal rates of nitrate and TN reached 31.7 and 45.0 % at a low substrate level (with a TOC of 48 mg/L) under the same nitrate level (4 mg/L). The N299, G107, and 81Y showed further powerful advantages. The nitrite of strains N299, G107, and 81Y were decreased from 3.76 ± 0.08 mg/L to 1.56 ± 0.01 mg/L, 1.25 ± 0.05 mg/L, and 1.60 ± 0.12 mg/L, respectively. In this study, the strains N299, G107, and 81Y could utilize the ammonia as the sole nitrogen source, and they possessed heterotrophic nitrification ability.

References

1. Huang TL, Li N, Zhang HH, Wang K, Liu TT (2013) Denitrification characters and safety of communities of cold tolerant oligotrophic and aerobic denitrifying bacteria. Chin J Environ Eng 7:2419–2423 (in Chinese)
2. Wei W, Huang TL, Su JF, Wang CY, Huang Z, Li N (2010) Isolation and identification of an oligotrophic and aerobic denitrification and its denitrification characteristics. Ecol Environ Sci 19:2166–2171 (in Chinese)
3. Wei W (2011) Properties and experiments of enhanced in-situ biological nitrogen removal by lifting water and aeration for micro-polluted raw water, pp 26–27 (D) (in Chinese)
4. Huang HM, Song QW, Wang WJ, Wu SW, Dai JK (2012) Treatment of anaerobic digester effluents of nylon wastewater through chemical precipitation and a sequencing batch reactor process. J Environ Manage 101:68–74
5. Huang TL, Wei W, Su JF, Zhang HH, Li N (2012) Denitrification performance and microbial community structure of a combined WLA–OBCO system. PLoS One 7:e48339
6. Huang TL, Wei W, Wang CY, Huang Z, Su JF, Zhi L (2012) Pilot research on micropollutants removal in the raw water by combined process of water-lifting aeration and oligotrophic biofilm. J Chongqing Univ 35:125–146 (in Chinese)
7. Heuer H, Krsek M, Baker P, Smalla K, Wellington E (1997) Analysis of actinomycete communities by specific amplification of genes encoding 16S rRNA and gel-electrophoretic separation in denaturing gradients. Appl Environ Microbiol 63:3233–3241
8. Camargo JA, Alonso A (2006) Ecological and toxicological effects of inorganic nitrogen pollution in aquatic ecosystems: a global assessment. Environ Int 32:831–849

9. Duce RA, Laroche J, Altieri K, Arrigo KR, Baker AR, Capone DG, Cornell S, Dentener F, Galloway J, Ganeshram RS (2008) Impacts of atmospheric anthropogenic nitrogen on the open ocean. Science 320:893–897
10. Galloway JN, Townsend AR, Erisman JW, Bekunda M, Cai Z, Freney JR, Martinelli LA, Seitzinger SP, Sutton MA (2008) Transformation of the nitrogen cycle: recent trends, questions, and potential solutions. Science 320:889–892
11. Tilman D, Cassman KG, Matson PA, Naylor R, Polasky S (2002) Agricultural sustainability and intensive production practices. Nature 418:671–677
12. Qin BQ, Zhu GW, Gao G, Zhang YL, Li W, Paerl HW, Carmichael WW (2010) A drinking water crisis in Lake Taihu, China: linkage to climatic variability and lake management. Environ Manage 45:105–112
13. Zhou Q, Takenaka S, Murakami S, Seesuriyachan P, Kuntiya A, Aoki K (2007) Screening and characterization of bacteria that can utilize ammonium and nitrate ions simultaneously under controlled cultural conditions. J Biosci Bioeng 103:185–191
14. Cai Q, Hu Z (2006) Studies on eutrophication problem and control strategy in the Three Gorges Reservoir. Acta Hydrobiol Sinica 30:11
15. Jiang CL, Zhu LQ, Hu XQ, Cheng JY, Xie MH (2011) Reasons and control of eutrophication in new reservoirs. In: Ansari AA, Singh Gill S, Lanza GR, Rast W (eds) Eutrophication: causes, consequences and control. Springer, Berlin, pp 325–340
16. Li L, Wang HW, Lu JH (2006) Nitrogen removal using air stripping tower in urban wastewater treatment plant. China Water Wastewater 22:92 (in Chinese)
17. Zhu GB, Peng YZ, Li BK, Guo JH, Yang Q, Wang SY (2008) Biological removal of nitrogen from wastewater. In: Whitacre D (ed) Reviews of environmental contamination and toxicology. Springer, New York, pp 159–195
18. Joo HS, Hirai M, Shoda M (2005) Characteristics of ammonium removal by heterotrophic nitrification-aerobic denitrification by *Alcaligenes faecalis* No. 4. J Biosci Bioeng 100:184–191
19. Van Rijn J, Tal Y, Schreier HJ (2006) Denitrification in recirculating systems: theory and applications. Aquac Eng 34:364–376
20. Robertson LA, Kuenen JG (1983) *Thiosphaera pantotropha* gen. nov. sp. nov., a facultatively anaerobic, facultatively autotrophic sulphur bacterium. J Gen Microbiol 129:2847–2855
21. Arts PM, Robertson LA, Gijs Kuenen J (1995) Nitrification and denitrification by *Thiosphaera pantotropha* in aerobic chemostat cultures. FEMS Microbiol Ecol 18:305–315
22. Robertson LA, Kuenen JG (1984) Aerobic denitrification: a controversy revived. Arch Microbiol 139:351–354
23. Joo HS, Hirai M, Shoda M (2006) Piggery wastewater treatment using *Alcaligenes faecalis* strain No. 4 with heterotrophic nitrification and aerobic denitrification. Water Res 40:3029–3036
24. Carter JP, Hsaio Y, Spiro S, Richardson DJ (1995) Soil and sediment bacteria capable of aerobic nitrate respiration. Appl Environ Microbiol 61:2852–2858
25. Zhang DY, Li WG, Huang XF, Qin W, Liu M (2013) Removal of ammonium in surface water at low temperature by a newly isolated *Microbacterium* sp. Strain SFA13. Bioresour Technol 137:147–152
26. Zhu L, Ding W, Feng LJ, Dai X, Xu XY (2012) Characteristics of an aerobic denitrifier that utilizes ammonium and nitrate simultaneously under the oligotrophic niche. Environ Sci Pollut Res 19:3185–3191
27. Zhu L, Ding W, Feng LJ, Kong Y, Xu J, Xu XY (2012) Isolation of aerobic denitrifiers and characterization for their potential application in the bioremediation of oligotrophic ecosystem. Bioresour Technol 108:1–7
28. Kim M, Jeong SY, Yoon SJ, Cho SJ, Kim YH, Kim MJ, Ryu EY, Lee SJ (2008) Aerobic denitrification of *Pseudomonas putida* AD-21 at different C/N ratios. J Biosci Bioeng 106:498–502

29. Su JJ, Liu BY, Liu CY (2001) Comparison of aerobic denitrification under high oxygen atmosphere by *Thiosphaera pantotropha* ATCC 35512 and *Pseudomonas stutzeri* SU2 newly isolated from the activated sludge of a piggery wastewater treatment system. J Appl Microbiol 90:457–462
30. Ozeki S, Baba I, Takaya N, Shoun H (2001) A novel C1-using denitrifier *Alcaligenes* sp. STC1 and its genes for copper-containing nitrite reductase and azurin. Biosci Biotechnol Biochem 65:1206–1210
31. Huang HK, Tseng SK (2001) Nitrate reduction by *Citrobacter diversus* under aerobic environment. Appl Microbiol Biotechnol 55:90–94
32. Zhang JB, Wu PX, Hao B, Yu ZN (2011) Heterotrophic nitrification and aerobic denitrification by the bacterium *Pseudomonas stutzeri* YZN-001. Bioresour Technol 102:9866–9869
33. Chen PZ, Li J, Li QX, Wang YC, Li SP, Ren TZ, Wang LG (2012) Simultaneous heterotrophic nitrification and aerobic denitrification by bacterium *Rhodococcus* sp. CPZ24. Bioresour Technol 116:266–270
34. Guo LY, Chen QK, Fang F, Hu ZX, Wu J, Miao AJ, Xiao L, Chen XF, Yang LY (2013) Application potential of a newly isolated indigenous aerobic denitrifier for nitrate and ammonium removal of eutrophic lake water. Bioresour Technol 142:45–51
35. Heaton T, Talma A, Vogel J (1983) Origin and history of nitrate in confined groundwater in the western Kalahari. J Hydrol 62:243–262
36. Wilson G, Andrews J, Bath A (1990) Dissolved gas evidence for denitrification in the Lincolnshire Limestone groundwaters, eastern England. J Hydrol 113:51–60
37. Huang TL, Wei W, Su JF, Zhi L, Liu Y (2010) Biological denitrification for micro-polluted source water via in situ oligotrophic bio-contact oxidation system. Technol Water Treat 36:95–99 (in Chinese)
38. Wei W, Huang TL, Li N (2012) Denitrification characteristics of in-situ biological inoculation under conditions of low temperature and poor nutrient. Water Technol 6:8–12 (in Chinese)
39. Wan CL, Yang X, Lee DJ, Du MA, Wan F, Chen C (2011) Aerobic denitrification by novel isolated strain using as nitrogen source. Bioresour Technol 102:7244–7248
40. Gupta AB, Gupta SK (2001) Simultaneous carbon and nitrogen removal from high strength domestic wastewater in an aerobic RBC biofilm. Water Res 35:1714–1722
41. Ji B, Yang K, Wang HY, Zhou J, Zhang HN (2014) Aerobic denitrification by *Pseudomonas stutzeri* C3 incapable of heterotrophic nitrification. Bioprocess Biosyst Eng 38:407–409

Effect and Ecological Assessment of Microbial Remediation

Haihan Zhang and Xiao Yang

Abstract In situ biological purification technology has been widely used in the engineering of environmental pollution treatment, since it is a more convenient and effective approach, with low cost. Therefore, the potential risk to the safety of biological agents should be seriously taken into consideration. The efficient aerobic denitrifying bacteria strain HF3, which is isolated and cultured in a low-nitrogen medium in order to remove nitrogen under oligotrophic conditions, has been used for bioremediation treatment, with effective and reliable ability in removing the nutrients of aquatic environments. Different to other biological agents, the efficient strain used for biological purification was cultured from raw water, and was isolated among indigenous bacteria. It is, therefore, the inferior species, and pathogenic bacteria had been excluded during the isolation. In addition, non-native application of the efficient strains which had a high environmental risk could be avoided during the application. In this chapter, we discuss the safety of the efficient strain HF3 by three aspects: biological safety on drinking water quality, ecological safety on indigenous microorganisms, and toxicological safety on aquatic animals. The results showed that the efficient aerobic denitrifying bacteria strain HF3 had no significant effect on the microbial community, and had no toxicity on mice, luminescent bacteria, or zebrafish. The efficient strain HF3 could be inactivated without any influence on the inactivation efficiency. The results suggest that the biological agent used for bioremediation treatment is safe and poses no risks to the urban drinking water supply, which could provide theoretical guarantees for the security of a wider range of application. It is important to reveal the effect and ecological assessment of microbial remediation. Therefore, in this chapter, we describe the effect and ecological assessment of the microbial remediation process.

Keywords WLA-OBCO system • DGGE analysis • Ecological security toxicity test • Aquatic animal • Zebrafish

H. Zhang (✉) • X. Yang
School of Environmental and Municipal Engineering, Xi'an University of Architecture and Technology, Yanta Road 13, 710055 Xi'an, Shaanxi Province, P. R. China
e-mail: zhanghaihan@xauat.edu.cn

T. Huang (ed.), *Water Pollution and Water Quality Control of Selected Chinese Reservoir Basins*, The Handbook of Environmental Chemistry 38,
DOI 10.1007/978-3-319-20391-1_14

1 Effects of Oligotrophic Aerobic Denitrifying Bacterial Agents on Nitrogen Removal from Reservoir Water

Surface water resources are often contaminated by nitrogen and organic matter due to the excessive use of fertilizers and uncontrolled on-land discharge of raw and treated water, resulting in severe reductions in water quality, as well as eutrophication. This limits the direct use of surface water for drinking water purposes [1]. Eutrophication in lakes and reservoirs has become an increasingly serious problem worldwide, affecting not only function and quality, but also destroying the ecological balance of water bodies. Thus, it is necessary to remove excess nitrogen from contaminated water in order to meet criteria for usage as potable water.

Denitrification is a microbially facilitated process of nitrate reduction that may ultimately produce molecular nitrogen (N_2) through a series of intermediate products such as NO and N_2O. In general, denitrification occurs where oxygen is depleted. This process is called anaerobic denitrification. However, when oxygen exists, some genera of microorganisms simultaneously use O_2 as oxidizing agents. This process is called aerobic denitrification. Much research on the denitrification of source water has been conducted, but most processes only convert nitrogen from one form to another, and fail to completely remove nitrogen from water sources [2, 3]. Moreover, there are many problems associated with the biological pretreatment of surface water sources through the use of anaerobic denitrifying bacteria:

Firstly, denitrification of surface water is mostly based on ectopic bioremediation techniques, and biological contact time is a major limiting factor for biological denitrification [4–10].

Secondly, most bioremediation techniques require the addition of an electron donor, such as an organic substrate, which tends to increase water treatment costs. Moreover, some studies have shown certain residual concentrations of carbonaceous compounds in the effluent, a finding that could be problematic for certain aquaculture species [11–13]. Finally, water in deep layers is often found in anaerobic conditions, which tends to accelerate the release of nutrients accumulated in sediment into the water, resulting in high nutrient loading and nutrient-rich water [14, 15]. It is difficult to fundamentally solve eutrophication with biological purification methods alone. It must be combined with other technologies in order to form an efficient, economic, and stable combined technology for the purification of lakes and reservoirs.

Water-lifting and aeration (WLA) technology has been widely applied for improving the quality of reservoir water in China [16, 17]. This technique mixes and oxygenates water, which may facilitate the growth of aerobic denitrifiers and enhance the denitrification of water by aerobic microorganisms.

In this research, a multifunctional device, which combines water-lifting and aeration with oligotrophic biological contact oxidation (OBCO), was used for the denitrification of raw water. The main objective was to investigate the feasibility and efficiency of micropollutant removal using the combined system with a pilot

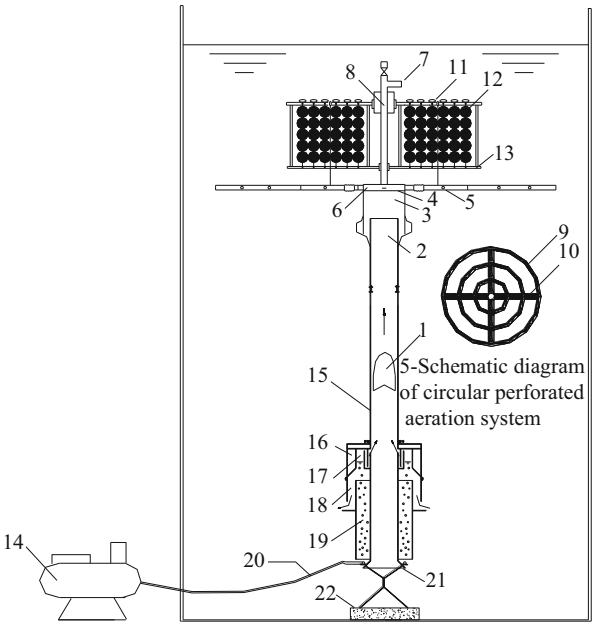

Fig. 1 Schematic representation of the pilot experiment: (*1*) aeroelasticity; (*2*) outlet; (*3*) aeroelasticity collective chamber; (*4*) perforated regulator plate; (*5*) cyclic aeration system; (*6*) pressure stabilization chamber; (*7*) valve; (*8*) voltage regulator pipe; (*9*) aeration branch (DN15); (*10*) aeration trunk (DN15); (*11*) float; (*12*) suspended carrier; (*13*) filler bracket; (*14*) air compressor; (*15*) up-flow cylinder; (*16*) water-tight compartments; (*17*) air chamber; (*18*) back flow chamber; (*19*) aeration chamber; (*20*) inlet pipe; (*21*) air releaser; (*22*) anchor block

scale in situ, which could provide a theoretical basis and technical support for field tests.

1.1 WLA-OBCO System

A combined WLA-OBCO system is shown in Fig. 1. The WLA-OBCO system was placed in a cylindrical Plexiglas container with an inner diameter of 1.8 m and a height of 4.4 m. The container was filled with 10 m^3 of raw water to simulate natural reservoir conditions. The volume of the aeration chamber of the WLA device was 2487 cm^3 and the up-flow cylinder had a diameter of 50 mm and a height of 3.5 m.

The air releaser, aeration chamber, backflow chamber, air chamber, up-flow cylinder, water-tight compartments, gas pipeline, and anchoring device were part of the WLA device, as shown in Fig. 1. The WLA device was vertically installed in the water and was fixed to the bottom of the container with an anchor block and suspended by a float.

Compressed air was continuously insufflated into the air releaser as a driving force and released into the aeration chamber in the form of small bubbles. Air-mixed water was pushed into the lower water levels through the backflow chamber and local circulation was observed at the bottom layers. Gas collected in the air chamber was released into the up-flow cylinder after filling the air chamber, resulting in the appearance of a large gas bubble. The bubble pushed water up into the up-flow cylinder until it exited the device. Water in the up-flow cylinder

continued to rise until the next gas bubble was formed. Water from the bottom of the container was continuously transported to the surface by the up-flow cylinder and mixed with surface water, resulting in a desirable water cycle.

The WLA device increased the dissolved oxygen concentration at lower water levels through direct mixing and oxygenation. This improved the water quality by creating a more suitable aerobic environment for aquatic organisms that inhibited the release of pollutants from the sediment. The biological contact oxidation system included a cyclic aeration system and suspended packing. The cyclic aeration system consisted of four aeration trunks connected with a pressure stabilization chamber and three aeration branches. Each branch contained 0.25-cm aeration holes every 4 cm. The aeration pipes were aluminum/plastic pipes with a diameter of 15 mm. The biological carrier was placed in an angle bracket with a diameter of 0.4 m and a height of 0.5 m. The bracket was then placed above the perforated aeration system 0.2 m below the surface of the water. Compressed air collected in the air chamber was released, resulting in a gas bubble entering the cyclic perforated aeration pipe.

1.2 Blank System

One system without biological carrier or WLA device was used as the blank control group in order to compare it with the purification effect of the WLA-OBCO system. The blank system was a cylindrical Plexiglas container with an inner diameter of 0.45 m and a height of 4.4 m.

1.3 Source Water

Water samples for this study were taken from a reservoir in Xi'an City, China (water source characteristics: COD 3.140 mg L^{-1}, TOC 3.012 mg L^{-1}, N-NH_4^+ 0.230 mg L^{-1}, N-NO_3^- 1.125 mg L^{-1}, N-NO_2^- 0.010 mg L^{-1}, TN 2.010 mg L^{-1}).

1.4 Bacterial Source and Culture Medium

The bacterial agents used in this study consisted of efficient aerobic denitrifiers isolated and cultured in a low-nitrogen medium in order to remove nitrogen under oligotrophic conditions. Many studies have illustrated the difficulties of removing nitrogen from source water, owing to its low concentration as a pollutant [18]. For this purpose, a special method was used for the culturing of aerobic denitrifying bacteria in our laboratory. During two months of domestication, the target bacteria became dominant under oligotrophic and aerobic conditions. As a result, oligotrophic

denitrifying bacteria were isolated and subjected to ecological combination experiments in order to obtain optimal oligotrophic aerobic denitrifying functional bacteria groups (W3, W5, and W8). Through the analysis of their physiological and biochemical properties, and through sequence analysis of 16S rDNA, strains W3, W5, and W8 were identified as *Rhizobium* sp., *Pseudomonas* sp., and *Pseudomonas* sp., respectively. The pure strains of W3, W5, and W8 were inoculated individually into a denitrification medium solution and cultivated under conditions of rotary shaking at 120 rpm, temperature 30 °C, and incubation period of 48 h. The above bacterial suspensions with 2 % of the total inoculation volume were placed into sterilized raw water for the adaptive culture. The preculture that was obtained was then used for biofilm cultivation.

Denitrification culture medium (g L^{-1}): CH_3COONa 0.1, $NaNO_3$ 0.02, K_2HPO_4 0.02, $MgCl_2$ 0.01, and $CaCl_2$ 0.01, pH 7.0–7.5.

1.5 Biological Packing Material

The biological packing material was mainly made of polypropylene and polyethylene. This material had the advantages of having both a high specific surface area and hydrophilic properties, which favored the development and establishment of microorganisms. The suspended carrier had a specific gravity of about 1 after inoculation and rotated freely under the aeration and could make good use of the oxygen by colliding and cutting the air bubbles. Indicators of physical and chemical properties were as follows: diameter 10 mm; height 10 mm; bulk density 150 kg m^3; specific surface area more than 500 m^2 m^{-3}; porosity about 75 %; application temperature −35 to 65 °C; and accumulation number 760,000 m^{-3}.

1.6 Analytical Equipment and Methods

NH_4-N, NO_2-N, NO_3-N, and TN concentrations were determined according to the standard method using an ultraviolet spectrophotometer (Hach, Model DR5000, USA). Temperature and pH values were measured with a glass electrode pH meter (Eutech, Model pH510, USA). The DO concentration was estimated by a DO meter (Hach, Model HQ30d, USA). The TOC concentration was determined by an IL500 type TOC analyzer (Hach Company, USA).

Biofilm samples were observed under a BX51 fluorescence microscope (Olympus Company, Japan) and a TS5136XM scanning electron microscope (VEGA Company, Germany). The dilution plate method was employed for counting oligotrophic denitrifying bacteria cultured in denitrification solid medium for 168 h at 28 °C.

1.7 Determination of the Microbial Community Structure

Bacterial DNA was extracted following the method of Tsai and Olson [19], with slight modification. 30 mL of biofilm suspension was filtered with a polycarbonate filter (Millipore, pore size 0.2 μm) to collect bacteria cells. The filter was added to 5 mL of TE buffer (0.1 M Tris · Cl, 0.1 M EDTA-Na_2, 0.2 M NaCl, 2 % CTAB, pH 8.0) and incubated at 37 °C for 45 min with agitation (100 rpm). 0.75 mL of 20 % SDS (w/v) was added, followed by a water bath at 65 °C for 1 h. These samples were centrifuged for 10 min at 12,000 × *g*. The supernatant was transferred to a new tube and further extracted twice with an equal volume of phenol-CIAA (phenol:chloroform:isoamyl alcohol, 25:24:1). Finally, nucleic acids in the extracted supernatant were precipitated with sodium acetate (final concentration 0.3 M, pH 5.2) and 2.0 volumes of 100 % ethanol for 1 h at room temperature. The pellet of crude nucleic acids was obtained by 20 min of centrifugation at 12,000 × *g*. The pellet was washed with 70 % ethanol, dried for 10 min under a vacuum, and dissolved in 50 μL TE buffer.

The V3 variable region of bacterial 16S rDNA was amplified using two primers described by Muyzer et al. [20]: F338-GC (5′-CGCCCGCCGCGCGCG GCGGGCGGGGCGGGGGCACGGGGGGCCTACGGGAGGCAGCAG-3′) and R518 (5′-ATTACCGCGGCTGCTGG-3′). A GC clamp of 40 nucleotides was added to the forward primer 5′ of F338 in order to ensure that DNA fragments would remain partially double stranded [21]. The polymerase chain reaction (PCR) system (50 μL) included 0.5 μL 100 ng of template DNA, 0.25 μL of Taq polymerase (5 U), 1 μL of primer F338-GC, 1 μL of R518 (10 μM), 5 μL of tenfold PCR buffer (containing 2.0 mM $MgCl_2$), 1 μL of dNTP (10 mM), and 41.25 μL of UV-sterile water. The following PCR program was used: an initial denaturation at 94 °C for 4 min, followed by 30 cycles of 94 °C for 30 s, 56 °C for 1 min, 72 °C for 30 s, and a final extension at 72 °C for 7 min. The final extension for 7 min was performed to eliminate the occurrence of artificial double bands in the subsequent denaturing gradient gel electrophoresis (DGGE) analysis [22].

The expected size of the amplified fragment was 250 bp. DGGE analysis was performed in a DGGE apparatus (Bio-Rad, Richmond, CA, USA). Approximately 3 μL of PCR products were loaded onto an 8.0 % (w/v) polyacrylamide gel cast in 1× TAE buffer. The polyacrylamide gels (acrylamide:bisacrylamide, 37.5:1) were made with denaturing gradients ranging from 30 to 60 %. 100 % denaturant contained 7 M urea and 40 % formamide. Electrophoresis was carried out at 60 °C with a voltage of 150 V in 1× TAE buffer for 4 h. Bands were visualized using a UV transilluminator after staining the gel with ethidium bromide (EB) and photographed.

1.8 Cloning and Sequencing

The dominant bands in the DGGE gel were excised. Each excised piece was washed twice with 1 mL of sterilized distilled water. A small chip (less than 1 mm^3) of each piece was used as a direct template for PCR to recover the DNA fragment.

The selective bands on the EB-stained DGGE gel were assigned to different species after their isolation, reamplification by PCR, and sequencing. The selective bands were incised and then placed in a 1.5-mL tube to reclaim the DNA. DNA was reclaimed using the DNA reclaim kit (Shanghai Sangon: SK1135), according to the manufacturer's instructions. The reclaimed DNA was used as a template to reamplify the bands with the same pair of primers (not containing the GC clamp) and the same PCR conditions as described earlier. Amplicons were then purified by the SK1191 UNIQ-10 DNA Gel Extraction Kit (Shanghai Sangon), according to the manufacturer's protocol, and sequenced with one of the amplification primers. These sequences were finally compared with similar sequences in the GenBank DNA database using BLAST analysis (Basic Local Alignment Search Tool, BLAST at NCBI) [23].

1.9 Operating Conditions

Samples were taken 1.7 m from the bottom of the Plexiglas container due to the mixing effect of the WLA system. Source water was purified by the WLA-OBCO system under conditions of dissolved oxygen 5.0–7.0 mg L^{-1} and temperature 10–23 °C. All pollutant removal efficiencies were calculated at the cumulative removal rate because there were no influent and effluent pollutants in the container during the operation from July 30 to December 16, 2009.

Biofilm cultivation could be accelerated artificially by adding bacteria liquid according to the method in Sect. 2.3. The preculture obtained above was added to a sterile liquid medium and incubated at 30 °C for 3–4 days. Fillers were then placed into the cultures. Microorganisms were cultured under conditions of aeration, and attached to the biological packing material for growth and reproduction. The biofilm was gradually forming on the biological packing material after a few days. The fillers with biofilm were then set into the bracket fixed in the pilot experimental system.

1.10 Denitrification Effects of the WLA-OBCO Combined System

The WLA-OBCO combined system showed a desirable denitrification effect for source water under conditions of COD_{Mn}/TN 1.56, temperature 10–23 °C, and

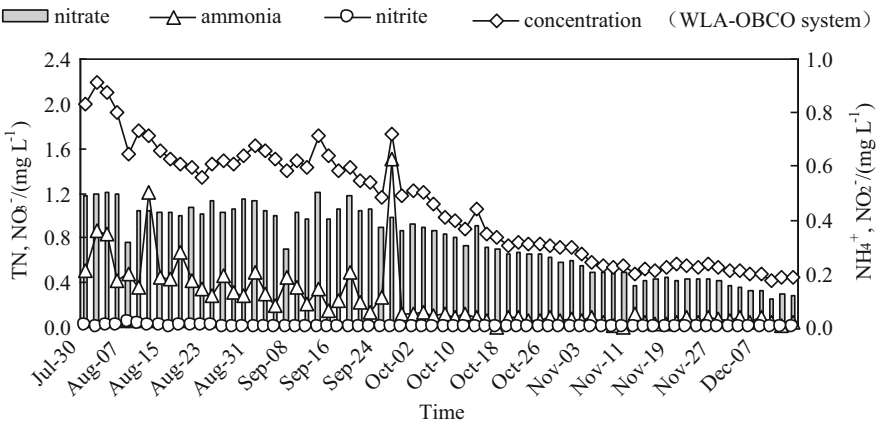

Fig. 2 Variation of nitrogen pollutants concentrations for the WLA-OBCO combined system during operation

dissolved oxygen 5.0–7.0 mg L^{-1}. Since aerobic denitrifiers were used in the system, the denitrification process could not be inhibited by oxygen. NO^{3-} and O_2 could be used as the final electron receptors and reduced at the same time. Therefore, NO^{3-} could still be reduced to nitrogen gas or other gaseous oxides of nitrogen by the microorganisms in the combined system.

The experimental results for ammonium, nitrate, nitrite, and total nitrogen concentration variations are illustrated in Fig. 2. Nitrogen pollutants were adsorbed quickly by the biofilm at the beginning of the experiment, resulting in a slight decrease of the ammonium, nitrate, and total nitrogen concentrations on the eighth day. However, for approximately two months after the beginning of operation of the WLA-OBCO system, the nitrate and total nitrogen removal rates increased slowly (in the range of 5–20 % and 10–35 %, respectively), which suggested that the bacterial population adapted to the low nutrition environment over a long period of time. The microorganisms acclimatized themselves to the diminished nutriment level by reducing their metabolic levels, extending their specific areas, and utilizing a larger number of substrates. During this period, the morphology and physiology of oligotrophic bacteria experienced a significant change, resulting in a steady starvation–survival state, with the cell size remaining almost constant. Additionally, the metabolic efficiency of the microorganisms improved due to energy deficiency [24].

Rapid removal of nitrogen pollutants followed these adaptations. The removal rates of ammonium, nitrate, and total nitrogen in a steady running period were in the ranges 82–100 %, 62–79 %, and 71–80 %, respectively. Since the total nitrogen concentration was only 0.418 mg L^{-1} during the late experiment period, it was less than the limits of 1.0 mg/L for class III surface water quality according to GB 3838–2002. These results indicate the necessity of establishing a longer biological contact time for enhancing denitrification efficiency, one of the most attractive advantages

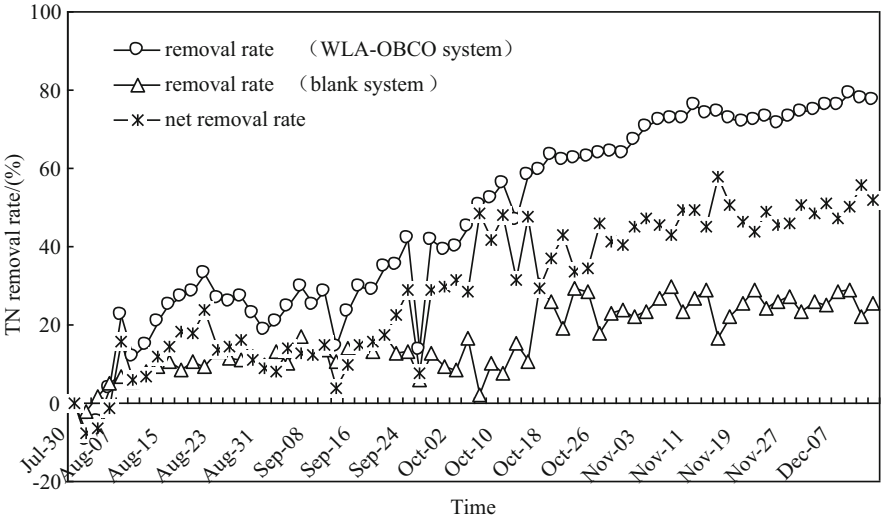

Fig. 3 Denitrification effects of the WLA-OBCO combined system during operation

of the WLA-OBCO combined system. The nitrite concentration changed little during the entire operation period, and was not detected after November 3, 2009. Thus, the unique design of the WLA-OBCO system ensured dependable water quality with regard to ammonium, nitrite, nitrate, and total nitrogen.

The removal rate and net removal rate of total nitrogen for the WLA-OBCO combined system is shown in Fig. 3. The total nitrogen removal rate of the WLA-OBCO system was almost always higher than that of the blank system during the entire operation. The total nitrogen removal rate of the blank system was only 29 % when the total nitrogen removal rate of the WLA-OBCO system reached the maximum of 79 %. The net total nitrogen removal rate of 50 % was obtained for the WLA-OBCO system. These results show that the desirable denitrification performance can be obtained absolutely under the combined effects of the biodegradation of the OBCO system and the aeration of WLA.

1.11 The Effect of Water Treatment on TOC

Total organic carbon (TOC) was often used to evaluate the degree of organic pollution in water. As shown in Fig. 4, a desirable removal efficiency of TOC was achieved during the entire operation. The consumption of TOC mainly resulted from the metabolic activities of microorganisms, such as oxidation, reduction, and synthesis, and the biological flocculation and adsorption process. Biodegradable organic matter served as electron donors and carbon sources for heterotrophic bacteria, and was beneficial for the propagation of oligotrophic microorganisms.

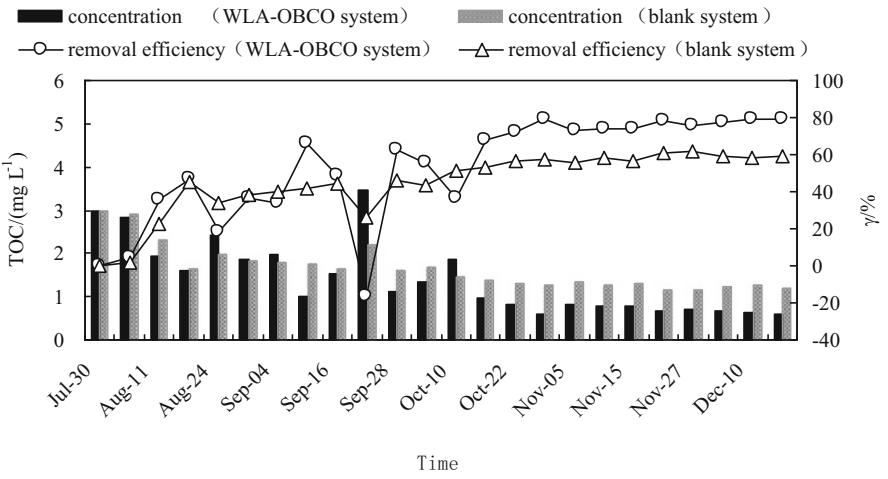

Fig. 4 Variation of TOC concentration and removal efficiency during the operation

The biofilm applied in micropolluted raw water was mainly composed of oligotrophic bacteria, which helped consume and remove organic matter from the surrounding environment. Figures 2 and 4 show that the trend for organic matter and total nitrogen concentrations were similar, since oligotrophic denitrifiers could use organic matter as electron donors and use carbon sources in denitrification and cell synthesis. Therefore, the denitrification effect had a direct relationship with organic matter. The degradation of organic matter was not obvious and TOC removal efficiency was in the range of 18–37 % between July 30 and August 29, 2009. The metabolic efficiency of oligotrophic microorganisms improved following adaptation of the biofilm system to the source water. Consequently, the efficiency of organic matter utilization also increased. The organic matter removal rate was higher than 70 % during the stable operation phase, reaching a maximum removal rate of 80 % for TOC, and more than the TOC maximum removal rate of 57 % for the blank system. The TOC concentration fell from an initial value of 2.979 mg L^{-1} down to 0.609 mg L^{-1}. These results also show a sharp increase in TOC concentration to 3.46 mg L^{-1} on September 22, 2009. This increase seemed to have been caused by a lack of organic matter, which led microbial cells on the fillers to develop into an endogenous metabolic phase, which consequently resulted in death or hydrolysis, and an increase of organic matter. However, this part of the organic matter was mostly biodegradable and was beneficial for biological denitrification.

1.12 Changes of Oligotrophic Denitrifying Bacteria

Figure 5 summarizes the changes in the number of oligotrophic denitrifying bacteria on the biofilm during the entire experimental period. When organic

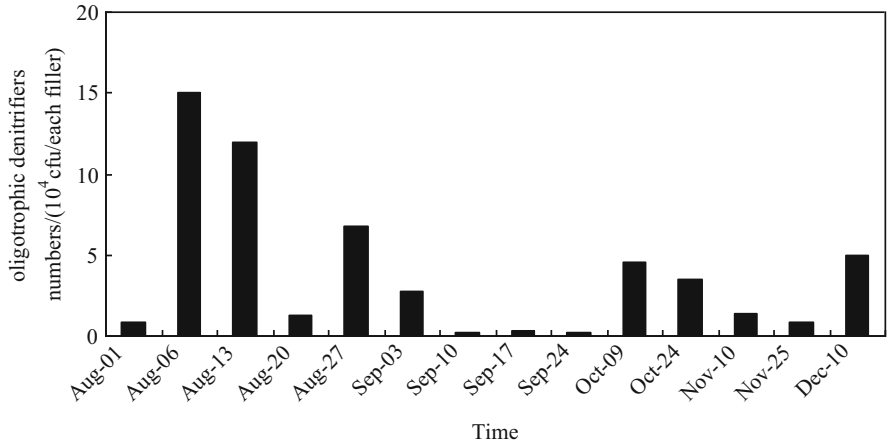

Fig. 5 Changes of in the number of oligotrophic denitrifiers on the fillers during operation

nutrients in the raw water were relatively abundant, oligotrophic denitrifying bacteria used organic carbon as energy and as electron donors for the purpose of achieving microbial growth, removal of organic and nitrogen pollutants in the process of metabolism, and synthesis of cell and denitrification. As indicated in Fig. 5, the number of oligotrophic denitrifying bacteria could increase on the order of 10^3 to 10^5 cells per filler, owing to the relatively abundant sources of carbon during the early part of the operation. As the experiment ran on and as nutrients in raw water were consumed, the microorganisms would utilize their own stored nutrients through endogenous respiration. However, as stored nutrients were exhausted, the cells began to die or break down, causing the number of denitrifying bacteria to decline to $(2.0–3.6) \times 10^3$ cells per filler during the second month. Figure 4 shows that the TOC value suddenly increased in late September due to the death of some bacteria. The remaining bacteria would continue to use part of this organic matter as a substrate for growth and reproduction, allowing the number of denitrifying bacteria to increase to 4.5×10^4 cells per filler in early October. In the middle and late period, the microorganisms gradually adapted to the oligotrophic environment, with the structure of the biological community on the biofilm trending stable. The number of denitrifying bacteria changed little, with bacteria growth and death at a state of dynamic equilibrium.

1.13 Diversity of Microbial Community Structure Analysis

Samples taken from the biofilm in different periods were prepared for DGGE analysis. DGGE separation of PCR products were isolated for different electrophoretic bands on different locations, and were used to identify the diversity of the microbial community structure and biological diversity for different samples. The

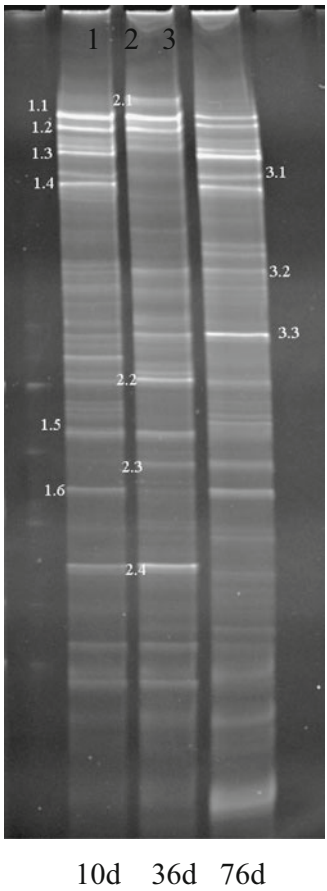

Fig. 6 DGGE profiles of the 240-bp PCR fragment of 16S rDNA genes (V3 region) amplified from different biofilm samples

diversity of the bacterial community in each sample was studied by PCR-DGGE analysis of the amplified V3 region of 16S rDNA genes. The DGGE banding patterns showed that the number and intensity of migrating bands of the DNA profiles of all samples were changeable during the operation (Fig. 6). Each sample showed a specific profile. Some bands disappeared, and new bands appeared during the operation, indicating not only the demise of the original species, but also the growth of new species. Twelve bright and representative main bands were selected for tapping, DNA elution, recycling, re-amplification, and electrophoresis after isolation. Each re-amplified band was purified, underwent ligation, transformation, cloning, and sequencing. Homology analysis of sequences was made by searching in GenBank with NCBI BLAST in order to find the bacteria having the closest relationship with each sequence, as shown in Table 1.

The 12 dominant bands analyzed could be divided into α-*proteobacterium*, β-*proteobacterium*, γ-*proteobacterium*, and *Actinobacteria*s. However, α-*proteobacterium* and β-*proteobacterium* were the two main bacterial groups,

Table 1 Closest relative species or isolated oligotrophic denitrifying bacteria of the selected clones (determined by an NCBI BLAST search)

Band	Sequence length (bp)	The bacterial species searched in GenBank or isolated oligotrophic denitrifying bacteria having the closest relationship with the dominant bands (base sequence similarity)
1.1	193	*Eubacterium* WD229; AJ292593 (92 %)
1.2	195	W8 (100 %)
1.3	194	*Beta proteobacterium* HTCC304; AY429720 (96 %)
1.4	194	*Beta proteobacterium*; Z32M51B; FJ484386 (100 %)
1.5	169	*Magnetospirillum* sp.; MSM-4; Y17390 (94 %)
1.6	169	Uncultured bacterium; JG35-K2-AG47; AM116752 (92 %)
2.2	169	*Mesorhizobium* sp. Acj 104; AB480752 (97 %)
2.3	174	Uncultured bacterium; FC04A09; FM873233 (99 %)
2.4	174	Uncultured bacterium; nbu202c02c1; GQ020041 (100 %)
3.1	193	W3 (100 %)
3.2	194	*Pseudomonas geniculata* (T); ATCC 19374 T; AB021404 (100 %)
3.3	194	*Comamonas testosteroni*; Q10; AF519533

constituting 33 and 25 % of all bands, respectively. Bacteria belonging to the Proteobacteria accounted for 75 % of all bands. Some studies have shown that the α-*proteobacterium* outline contains many bacteria genera that have a high adaptability to nutrient-poor environments; thus, it was expected that α-*proteobacterium* would appear in the biological pretreatment system for drinking water. Chen et al. studied the microbial community structure for drinking water treatment using a reverse osmosis membrane reactor using 16S rDNA clone library and FISH methods, and the results of these two methods were consistent with the findings that the bacteria belonging to α-*proteobacterium* could account for 50 % of all bacteria [25]. Another bacterial group appearing in the tapping bands was β-*proteobacterium*, one of the major groups of the bacteria domain. Studies have shown β-*proteobacterium* to be the most dominant group in wastewater treatment systems. However, β-*proteobacterium* was not the largest group in our experimental results, probably due to variations in the bacterial community structure owing to differences in the types and concentrations of pollutants in water supply versus wastewater treatment. Sequencing analysis indicated that the two main types of nitrifying bacteria, *Nitrosomonas* and *Nitrospira*, did not appear in the tapping band due to the low concentration of ammonium in the raw water.

In addition, the sequence of band 1.2 was 100 % identical with that of strain W8, and the sequence of band 3.1 showed 100 % similarity to the gene of strain W3 by sequencing and NCBI analysis. These results imply that there were other dominant bacteria—other types of aerobic denitrifiers or other bacteria that were better adapted to the environment—in the biofilm system besides the oligotrophic denitrifying bacteria. These may form a stable system by synergic competition effects to remove the nitrogen and organic pollutants. Reprinted from an open access article in PLoS ONE, with kind permission from Springer Science+Business Media.

1.14 Summary

Pilot research on the WLA-OBCO combined process showed potential for the system as an alternative to drinking water purification, as it reduced the risk of nitrogen contamination and did not require high operational costs. The removal rates of ammonium, nitrate, total nitrogen, and TOC in the steady running period were in the ranges 82–100 %, 62–79 %, 71–80 %, and 70–80 %, respectively, under the conditions of dissolved oxygen 5.0–7.0 mg L^{-1}, temperature 10–23 °C, and C/N ratio 1.56 for source water. Nitrite could not be detected. The nitrogen removal effects could meet the requirements of class III surface water quality according to GB 3838–2002. The number of oligotrophic denitrifying bacteria on the biofilm changed regularly during the running period. The number of oligotrophic denitrifying bacteria could increase to the order of 10^4 to 10^5 cells per filler when the carbon source was relatively abundant in raw water. The denitrifying bacteria number changed little and bacteria growth and death were basically in a state of dynamic equilibrium in steady operation. The PCR-DGGE profiles showed that the number and intensity of migrating bands of the DNA profiles of all samples were changeable. The sequencing results revealed that α-*proteobacterium* was the largest bacterial group, and strains W8 and W3 became the dominant bacteria and played their role in achieving the purpose of water purification with other bacteria.

2 Evaluation of the Ecological Security of Effective Oligotrophic Aerobic Denitrifying Bacterial Strains

In this part, we discussed the biological safety of in situ bioremediation technology by inactivated biological experiments and the acute toxicity test. The results indicated that the biological agents used in this study can be inactivated totally under a low concentration of available chlorine, and there is no influence on the inactivation efficiency on microorganisms in the conventional water treatment by addition biological agents in raw water. In addition, the biological has no toxicity on mice and luminescent bacteria. This result suggests that the efficient aerobic denitrifying bacteria HF3 had high biological safety, and the in situ bioremediation technology had no risk to the safety of the urban drinking water supply.

2.1 Disinfectant Process

Potassium permanganate ($KMnO_4$) is an efficient oxidizer which has a special function in causing microbe tissue damage due to oxidation and killing the bacteria. It has been used as a substitute for chlorinated disinfectant in drinking water

treatment. Moreover, potassium permanganate can decrease the concentration of trichloromethane in the water as a preoxidation treatment [26].

Sodium hypochlorite (NaClO) has been widely used as a bactericidal and virucidal agent with high efficiency and safety. The hydrolyzed oxygen atom can denature the protein of bacteria and virus and kill the pathogenic microorganisms by forming hypochlorous acid from the hydrolyzing of sodium hypochlorite. Sodium hypochlorite can also be mixed with water in any proportion with high safety due to its good solubility. Moreover, sodium hypochlorite would able to combine with ammonia nitrogen in water to form chloramine, which has the ability of maintaining disinfection for longer. In addition, sodium hypochlorite would avoid producing disinfection by-products and, therefore, it has been widely used in urban drinking water supply [26].

At present, water treatment management has focused on a new kind of substitute of disinfectant, chlorine dioxide (ClO_2), which is more effective in decreasing the trihalomethane in the treated water and removing the odor produced by algae and phenolic compounds when compared with chlorine. Being both a powerful disinfectant and oxidizer, chlorine dioxide has great ability to adsorb on and penetrate the cell walls, and kills cells by rapidly inhibiting protein biosynthesis. In addition, chlorine dioxide has longer sustaining capabilities and a stronger ability to resist disturbing factors of pH value, due to its hydrolysis resistance. However, the by-products of chlorine dioxide disinfectant can oxidize hemachrome and cause hemolytic anemia, which is very harmful to the blood of animals, as well as their reproductive function. Therefore, chlorine dioxide is unusually combined with sodium hypochlorite at a ratio of 0.14:0.36 to improve the disinfectant effect in engineering applications [27].

2.2 *Luminescent Bacteria*

The luminescent bacteria toxicity test is a sensitive, stable, and rapid method to detect the concentration variation of toxic pollution in aquatic ecosystems based on the negative correlation between the light intensity of luminescent bacteria and the toxicity of the component [28]. The test can not only be used as environmental monitoring, but it can also provide useful information of the different components in the water. Thus, this method has been widely used in heavily polluted wastewater monitoring, surface water resource monitoring, and evaluation for the safety of drinking water quality. There are currently two types of luminescent bacteria toxicity test: the marine luminescent bacterium method and the fresh luminescent bacterium method.

Marine luminescent bacterium includes *Vibrio fischeri* sp. and *Photobacterium phosphoreum*. However, a concentration of 2–3 % NaCl has to be added to its culture medium, which may change the inherent properties of freshwater samples. In contrast, the fresh luminescent bacterium can work well without any salinity; therefore, the fresh luminescent bacterium is more advantageous in testing drinking

water [29]. *Vibrio qinghaiensis* sp. Q67 (Q67), a freshwater luminescent bacterium, had been extracted in fresh fish body from Qinghai Lake, China, and it had been proved that the bioassay with Q67 to determine the toxicity of various chemicals and water samples is as effective and reliable as the standard ecotoxicological bioassay with *V. fischeri* [30]. The cell of the Q67 strain is in the shape of a rod or a slightly curved rod, with a size of 1.5–2.0 μm. The bioluminescence can work under pH values in the range 6.5–11, with the highest light intensity at pH 9.

2.3 Inactivated Biological Experiments

The instruments used in this experiment included analytical balance, water bath, acidity meter, autoclave, constant temperature bath oscillator, electrothermostat, and bacteria-free workbench.

An R2A medium (w/v) was prepared for viable bacteria counting with a pH value of 7.2 ± 0.2 as follows: yeast extract powder (0.5 %), casein hydrolysates (0.5 %), soluble starch (0.5 %), $MgSO_4$ (0.024 %), tryptone (0.25 %), peptone (0.25 %), glucose (0.5 %), sodium pyruvate (0.3 %), KH_2PO_4 (0.3 %), and agar (18 %) [31].

To 100 mL of inoculated raw water was added the efficient aerobic denitrifying bacteria strain HF3 into a 250-mL sterile Erlenmeyer flask. The disinfectant was added into the flask, as described in Table 2, and then the flask was incubated at 25 °C. After incubating, 1 mL of water sample was pipetted into a tube with 9 mL of neutralizer (10 g/L of sodium thiosulfate) to react for 10 min. The sample was placed onto agar plates by gradient dilution for viable bacteria counting, and the plates were placed in an electrothermostat at 28–30 °C for 7 days. The colony-forming units were counted to calculate the total bacteria inactivation rate.

2.4 Luminescent Bacteria Toxicity Test

The tested samples used the efficient aerobic denitrifying bacteria strain HF3, which is isolated and cultured in a low-nitrogen medium in order to remove nitrogen under oligotrophic conditions. The efficient strain HF3 was cultured at 37 °C for 24 h using the FJ liquid medium. One group was tested using the inoculated liquid medium. In order to remove the interferences of the culture

Table 2 Dosage and reacting time of the disinfectant used in this study

Disinfectant	Dosage (available chlorine) (mg/L)	Reacting time (min)
$KMnO_4$	0.5, 1.0, 2.5, 5.0, 10.0, 20.0	10, 30, 60, 120
NaClO	0.5, 1.0, 2.5, 5.0, 10.0, 20.0	10, 20, 30
$NaClO + ClO_2$	0.5, 1.0, 2.5, 5.0, 10.0, 20.0	10, 20, 30

medium, another three groups were prepared by collecting the strain cells. The inoculated liquid medium was centrifuged (2300 *g*, 4 °C, 10 min), the supernatant discarded, and then the cells were resuspended by PBS into 1×10^7, 1×10^8, and 1×10^9 cfu/mL for the acute toxicity tests, respectively.

For the acute toxicity test, luminescent bacterium Q67 was purchased from Beijing Hamamatsu Photon Techniques Inc. The Q67 was grown in the culture medium that could produce a larger quantity of bacteria with fluorescence enzyme. The culture medium consisted of tryptone (0.5 %), yeast extract (0.5 %), glycerin (0.3 %), $MgCl_2$ (0.32 %), KBr (0.02 %), $CaSO_4$ (0.01 %), NaCl (0.4 %), and KCl (0.4 %), pH 8.5 ± 0.5, and was cultured at 22 ± 1 °C. The bacteria strains from a stock culture medium which was maintained at 4 °C were inoculated to a liquid medium. The bacteria were grown in the liquid medium up to the logarithmic growth stage after 10–12 h at 22 ± 1 °C while shaking at 120 rpm.

The acute toxicity test was then conducted using a Modulus™ Single Tube Multimode Reader. For each test, four testing tubes were prepared, three for parallel samples and one for the blank control. 100 μL of luminescent bacterial suspension was added into each tube, and the same volume of sample or blank control liquid (0.5 % DMSO) was added at a 15-s interval. After 15 min of exposure of the luminescent bacteria to the sample at 22 ± 1 °C, the relative light unit (RLU) of Q67 was measured on the Modulus™, and the acute toxicity of the sample on Q67 was expressed as the percentage inhibition value [29].

The toxicity of efficient strain HF3 on Q67 is expressed as the inhibition value (I), which is calculated as follows:

$$I = (R_0 - R)/R_0 \times 100\%$$

where R_0 is an average of the RLU of Q67 exposed to the blank controls and R is an average of the RLU exposed to the test substance.

In order to quantitatively compare the ecotoxicity of different water samples, the concentration (times) corresponding to the inhibition value of 50 %, namely, effective concentration (EC_{50}), was used. By definition, the higher the EC_{50} value, the lower the toxic effect.

2.5 Mice Acute Oral Toxicity Test

For the acute toxicity test, 20 Kunming mice weighing 18–24 g, with half males and half females, were purchased from the Laboratory Animal Unit of The Fourth Military Medical University, China (manufacturing license number: SCXK 2007–007). The mice were raised at an animal laboratory (license number: SYXK 2007–994) with a temperature of 20–22 °C and a relative humidity of 50–55 %.

The acute toxicity test was performed as per the standard method ordained by the Chinese Ministry of Health. Before the test, the mice were kept from eating for 16 h. The testing samples used the efficient aerobic denitrifying bacteria strain HF3. The

efficient strain HF3 was cultured at 37 °C for 24 h using the FJ liquid medium. The inoculated liquid medium (2300 *g*, 4 °C, 10 min) was centrifuged, the supernatant discarded, and then the cells were resuspended by PBS. A dosage of 5500 mg/kg bw was used for the gavage experiment in mice. After intragastric infusion, the toxic effects of the mice were successively observed and recorded for 14 days.

2.6 Inactivated Biological Experiments

The results indicated that, while the disinfectant dosages and the duration of disinfectant increases, the percentage of inactivated microorganisms also increases. Unfortunately, the inactivation efficiency only reached 84.07 % under the condition of 1.0 mg/L available chlorine (the concentration of potassium permanganate should not be over 2.0 mg/L to prevent excessive amounts of manganese) and 30 min of reacting time, with a higher viable bacteria count of 3250 cfu/mL. This is mainly because potassium permanganate is usually used in the preoxidation treatment as a strong oxidizer with a lower disinfectant ability (Fig. 7).

The inactivation rate of sodium hypochlorite treatment is shown in Fig. 8. Similar to the potassium permanganate experiment, the inactivation efficiency had an increasing trend with increasing dosages and duration. However, sodium hypochlorite had a higher percentage of inactivated microorganisms. Specifically, under the condition of room temperature and a total cell count of 2.0×10^4 cfu/mL, the value of the inactivation rate at 30 min was 99.44 % with an available chlorine concentration of 0.5 mg/L while the viable count was 85 cfu/mL, and the value at 30 min reached 99.58 % with an available chlorine concentration of 1.0 mg/L while the viable count was 65 cfu/mL. According to the drinking water standards ordained by the United States Environmental Protection Agency (USEPA) [26], the viable bacteria count measured by R2A medium must not be over 500 cfu/mL;

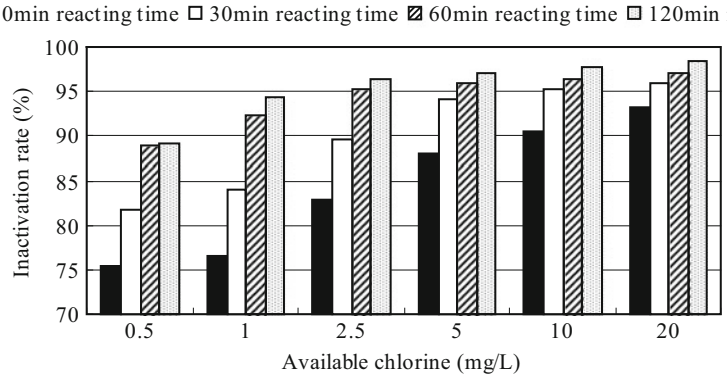

Fig. 7 Total bacteria inactivation rate of potassium permanganate of raw water inoculated with the efficient strain HF3

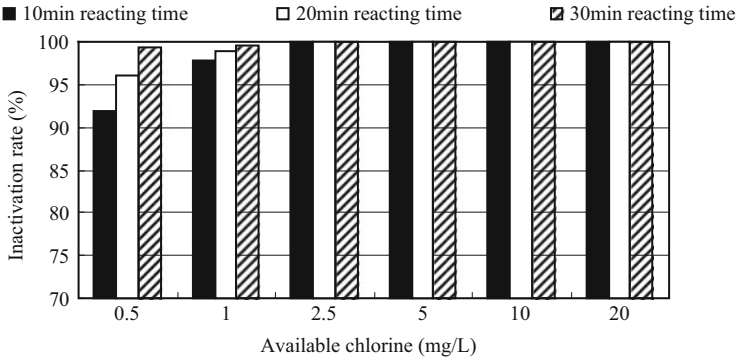

Fig. 8 Total bacteria inactivation rate of sodium hypochlorite of raw water inoculated with the efficient strain HF3

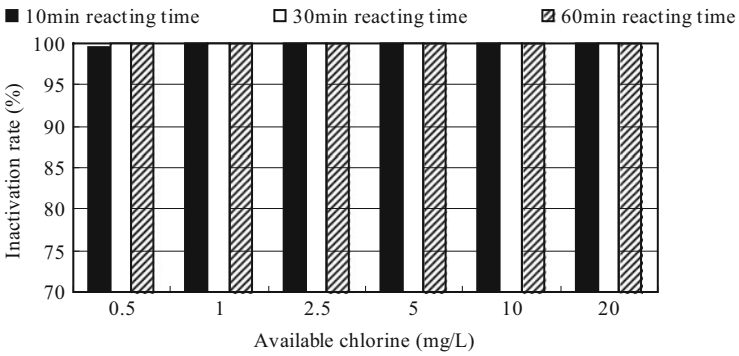

Fig. 9 Total bacteria inactivation rate of chlorine dioxide and sodium hypochlorite of raw water inoculated with the efficient strain HF3

therefore, the inactivated result can meet the drinking water requirements. Moreover, the inactivation efficiency reached 100 % with just 20 min of reacting time under 5 mg/L available chlorine.

The total bacteria inactivation rate of chlorine dioxide combined with sodium hypochlorite treatment is shown in Fig. 9. The treatment had the highest value of inactivation rate due to the powerful oxidized ability of chlorine dioxide. Clearly, the percentage of inactivated microorganisms reached 99.5 % after only 10 min following the addition of 0.5 mg/L of available chlorine, with only 80 cfu/mL viable bacteria count. The value also increased when the disinfectant dosages and reacting times increased. The total bacteria had been inactivated completely just 20 min after the addition of 2.5 mg/L of available chlorine, which was only half the concentration of the available chlorine of the sodium hypochlorite treatment.

The result of inactivated biological experiments showed that, except for potassium permanganate treatment, both sodium hypochlorite and chlorine dioxide

treatment under conventional disinfectant conditions can inactivate both the biological agents used in this study and the other microorganisms found in the water. The biological agents can be inactivated with relatively low available chlorine. It is suggested that the efficient strain HF3 has no safety risk on urban drinking water, and the in situ bioremediation technology applied in this study has relatively high safety.

2.7 Luminescent Bacteria Toxicity Test

The inhibition value of the luminescent bacteria toxicity test is shown in Table 3. The results showed that the inhibition value of each test on efficient strain HF3 was negative. It is suggested that efficient aerobic denitrifying bacteria HF3 had no negative influence or toxicity against the luminescent bacteria Q67. In contrast, the efficient stain had a relatively positive influence on Q67. Specifically, the inhibition value after 15 min of exposure of the luminescent bacteria to the efficient strain HF3 liquid medium was negative more than three times. After removing the distractions of culture medium and salinity from the luminescent bacteria, all the efficient strain HF3 bacterial suspensions had more than 16 times the negative inhibition value. In addition, there is no obvious relation between the inhibition value and the density of efficient strain HF3 cells. Therefore, there was no EC_{50} value in this test. This result indicated that, efficient aerobic denitrifying bacteria HF3 as a biological agent has high biological safety for drinking water quality.

2.8 Mice Acute Oral Toxicity Test

After 14 days of successive observation, there were no obvious toxic symptoms or death among mice (Table 4) under the nearly maximum tolerant dosage of mice. According to the grading standard of the acute toxicity test, the efficient strain HF3 was actually non-toxic by the acute oral toxicity test.

Table 3 Inhibition value of luminescent bacteria by the addition of the efficient strain HF3

Gender	Dosage (mg/kg bw)	Amount of testing	Mortality	Mortality rate (%)
Male	5500	10	0	0
Female	5500	10	0	0

Table 4 Effects of the efficient strain HF3 on mice by the acute oral toxicity test

Testing group	Inoculated liquid medium	1×10^7 cfu/mL	1×10^8 cfu/mL	1×10^9 cfu/mL
Inhibition value (%)	−345.896	−1697.3	−1612.3	−1604.0

3 The Ecological Safety on Indigenous Microbial Communities

In this part, we determine the influence of indigenous microorganisms' population diversity by the addition of efficient strain HF3. The results showed that there is no significant impact by inoculating the efficient aerobic denitrifying bacteria HF3 on bacterial, fungal, actinomycic, and sulfate-reducing bacterial group diversity. This implies that the efficient aerobic denitrifying bacteria HF3 had no significant effect on the ecological flora structure and had high ecological safety.

3.1 Experimental Design

In this study, the raw water was collected from Jinpen Reservoir in Xi'an City, China. The raw water was divided into two groups for treatment. The blank group used raw water without any addition, and the efficient strain was added to raw water for the experimental group. The efficient strain used in this study was efficient aerobic denitrifying bacteria HF3, which is isolated and cultured in a low-nitrogen medium in order to remove nitrogen under oligotrophic conditions. Each group was placed into an amber bottle (5 L) and sealed with parafilm. Samples were collected at 14 and 42 days after the inoculation treatment, respectively. The DGGE approach was then performed to explore the influence of the addition of the efficient strain HF3 to the indigenous microorganism community, including bacteria, fungus, actinomyces, and sulfate-reducing bacteria.

3.2 DNA Extraction

Microbial DNA was extracted from the water samples using the Water DNA Extraction Kit (Omega, USA), following the manufacturer's instructions [32–35].

- Filter each water sample with a volume of 1 L using a microporous filter paper (0.45 μm). Take the filter membrane from the filter adapter and cut the membrane into pieces. Insert the filter membrane to a 50-mL centrifuge tube and add 3 mL SLX buffer and 500-mg glass beads to the tube. Vortex the tube at maximum speed for 3 min.
- Incubate at 70 °C for 10 min and mix the samples 2–3 times during incubation by vortexing the tube. Incubate on ice for 5 min.
- Centrifuge at 4000 *g* for 10 min at 4 °C.
- Transfer the cleared supernatant (about 3 mL) to a new 10-mL tube and add 0.7 volume (about 2 mL) of isopropanol (incubate at −20 °C for at least 30 min). Mix thoroughly by inverting the tube 20 times.

- Centrifuge at 4000 *g* for 10 min at 4 °C.
- Carefully remove and discard the supernatant, making sure not to disturb the DNA pellet.
- Add 400 μL of elution buffer (incubate at 65 °C for 10 min) to the tube and mix thoroughly by inverting the tube 20 times.
- Incubate the tube at 65 °C for 20 min to dissolve the DNA.
- Transfer the sample to a new 2-mL micro tube and add 100 μL of HTR Reagent. Mix thoroughly by inverting the tube 20 times.
- Incubate the tube for 2 min at room temperature. Centrifuge at 10,000*g* for 3 min at 4 °C.
- Transfer the cleared supernatant to a new 2-mL microtube carefully. Add an equal volume (about 400 μL) of Buffer XP1. Mix thoroughly by inverting the tube 20 times.
- Place a DNA column into a 2-mL collection tube. Apply the entire sample to the DNA column inserted into the collection tube. Centrifuge at 10,000*g* for 1 min at room temperature. Discard the flow-through liquid and reuse the collection tube in the next step.
- Place the column back into the collection tube. Add 300 μL of Buffer XP1 to the column. Centrifuge at 10,000*g* for 1 min at room temperature. Discard the flow-through liquid and the collection tube.
- Place the column into a new 2-mL collection tube. Add 500 μL of DNA Wash Buffer (diluted with ethanol) and centrifuge at 10,000*g* for 30 s at room temperature. Discard the flow-through liquid and reuse the collection tube in the next step.
- Place the column back into the collection tube. Centrifuge at 12,000*g* for 2 min at 4 °C to dry the column. Discard the collection tube and place the column on an aseptic bench with air drying for 30–60 min to remove any trace of ethanol.
- Place the DNA column into a new 2-mL microtube. Apply 30 μL of Elution Buffer (incubate at 65 °C for 10 min) to the center of the membrane in the column. Incubate at 65 °C for 10–15 min. Centrifuge at 10,000*g* for 1 min at room temperature to elute DNA.
- Apply another 30 μL of Elution Buffer (incubate at 65 °C for 10 min) to the center of the membrane in the column. Incubate at 65 °C for 10–15 min. Centrifuge at 10,000*g* for 1 min at room temperature.
- Apply the total of 60 μL of flow-through liquid back to the center of the membrane in the column. Incubate at 65 °C for 10–15 min. Centrifuge at 10,000*g* for 1 min at room temperature. Discard the DNA column and store the elute DNA sample at −20 °C.

DGGE: The quality of the extracted DNA was assessed by performing electrophoresis in 1 % weight per volume (w/v) agarose gels stained with GelRed (Biotium, USA). The primer and the PCR conditions in this study are listed in Table 4 for PCR amplification [36–39]. Nested PCR was performed for both bacterial and fungal DNA amplification.

The PCR products were analyzed by DGGE fingerprinting using a DCode system (Bio-Rad, USA). Acrylamide gels (8 % [w/v]; acrylamide-*N*, *N*-′-methylenebisacrylamide ratio, 37.5:1) with a denaturing gradient in the range 30–70 % (w/v) (where 100 % [w/v] denaturant corresponded to 7 M urea and 40 % [v/v] formamide) were used for the analysis, following the manufacturer's instructions [33–35, 40].

- Firstly, place the gasket tilt rod on the gel caster and secure the glasses with clamps for assembling the gel sandwich for a perpendicular gradient gel. Make sure that the shorter glass faces outwards and seal the gap with gel around the sandwich. Label one of the syringes LO (for the low-density solution) and the other HI (for the high-density solution).
- For this step, it is critical to be quick in order to avoid any gel polymerization. Ensure that the tubing is free of any gel material by pushing water through the tubing with the syringe. The tubing should be free of material before casting. Remove any remaining water from the tubing. Transfer the 30 and 70 % gels to a centrifuge tube. Add 80 μL of a final concentration of 10 % (v/v) ammonium persulfate and 18 μL of TEMED to each tube. Cap and mix by inverting several times. With the syringe connected to the tubing, withdraw all of the high-density solution into the HI syringe. Do the same for the low-density solution into the LO syringe. Carefully remove air bubbles from the syringes by gently tapping. Place the syringes into the gradient delivery system syringe holder (LO and HI density side, respectively). Rotate the cam wheel slowly and steadily to deliver the gel solution from the bottom to the top of the sandwich. It is important to deliver the gel solution at a steady pace in order to avoid disturbances between gel solutions within the sandwich. Carefully level the gel sandwich by adjusting the gasket tilt rod when the cam wheel has reached the stop position. Place the comb gasket on top of the sandwich. Let the gel polymerize for about 6 h. After polymerization, remove the comb by pulling it straight up slowly and gently.
- Preheat the tris-acetate-EDTA buffer (TAE buffer; 40 mM Tris, 20 mM acetic acid, and 1 mM EDTA; pH 8.0) to 58 °C before electrophoresis. Place the gel sandwich into the electrophoresis tank.
- Add 5 μL of loading buffer into each PCR product and mix the PCR products by absorption back and forth. Approximately 40 μL of the mixed liquid were loaded onto a gel for each sample. And then electrophoresis was carried out for 13 h at a constant voltage of 70 V at 58 °C in TAE buffer.
- After electrophoresis, the gels were stained using GelRed (Biotium, USA) for 20 min and photographed under UV light on a Gel Doc XR+ Image Lab System (Bio-Rad, USA). Excise the lightest or unique DNA bands from the DGGE gels into microtubes, and add 30 μL of deionized water. Store the DNA band sample at 4 °C for further clone analysis.

3.3 DGGE Profiles and Principle Component Analyses

The DGGE profiles of the influence of indigenous microorganisms' population diversity by the addition of efficient strain HF3 are shown in Fig. 10. The results of the DGGE profiles suggested that there are a greater number of DNA bands detected in the bacterial and fungal gels with a higher brightness. Moreover, the fungus has the highest number and the most diverse bands. Specifically, after electrophoresis, the microbial communities have been separated at different positions, and each microbial species has different profiles. As shown in Fig. 10, there is a huge abundance and diversity of bacteria and fungus communities in the raw water, while actinomycetes and sulfate-reducing bacteria have significantly fewer numbers and lower brightness of DNA bands, which suggested that both actinomycetes and sulfate-reducing bacteria are rare in the raw water.

The banding patterns of the DGGE fingerprints were analyzed using the Quantity One software (Version 4.5, Bio-Rad, USA) to calculate the microbial community species richness (Table 5). Since species richness is an index used to evaluate the abundance and diversity of microbial communities, it plays a significant role in biological assays and has been widely used. The results indicated that there is no significant impact in species richness by inoculating the efficient aerobic denitrifying bacteria HF3 into raw water. Specifically, the bacterial species richness of inoculation and non-inoculation in 14 days after treatment are 30 and 28, respectively, while the indexes in 42 days after treatment are 42 and 42, respectively. Interestingly, there is larger species richness in 42 days after treatment than 14 days of bacterial species in the raw water with non-inoculation. This is likely because some bacterial species are rare in the early treatment, so they cannot be detected by the DGGE method, whereas during the treatment, the microbial communities

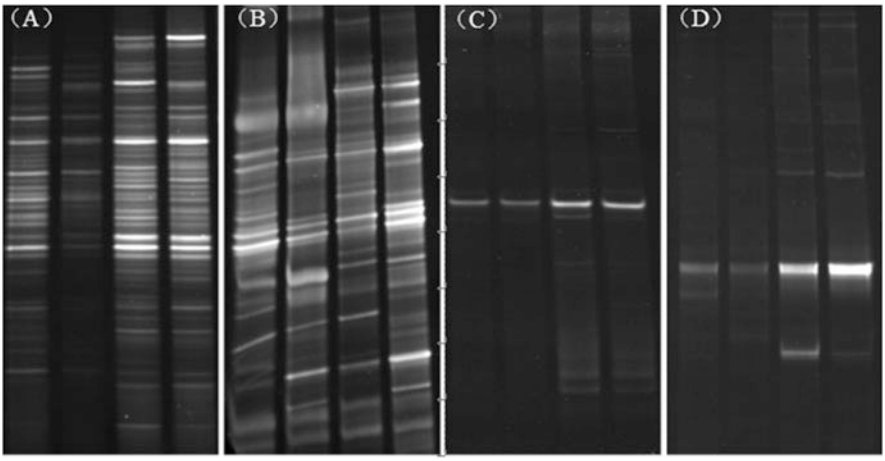

Fig. 10 Profiles of DGGE of: (**a**) bacterial, (**b**) fungal, (**c**) actinomycetic, and (**d**) sulfate-reducing bacterial communities in raw water inoculated with effectively oligotrophic aerobic denitrifying bacterial isolate HF3

Table 5 Effects of effectively oligotrophic aerobic denitrifying bacteria isolate HF3 inoculation on the species richness of raw water microbial communities

Time (days)	Treatment	Bacteria	Fungus	Actinomycetes	Sulfate-reducing bacteria
14	(I) Inoculation	30	23	4	2
	(NI) Non-inoculation	28	24	4	2
42	(I) Inoculation	42	30	12	8
	(NI) Non-inoculation	42	31	12	7

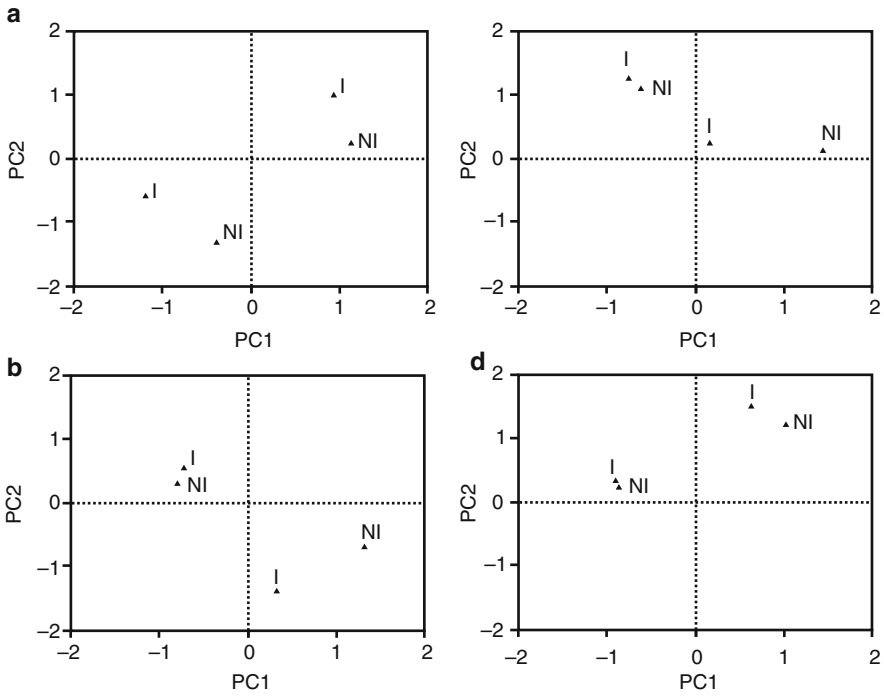

Fig. 11 Principle component analysis (PCA) of: (**a**) bacterial, (**b**) fungal, (**c**) actinomycetic, and (**d**) sulfate-reducing bacterial communities in the raw water inoculated with effectively oligotrophic aerobic denitrifying bacterial isolate HF3

maintained a stable increasing trend, and there became more species which could be detected. There is no difference in the species richness of actinomycetes between inoculation and non-inoculation samples at both 14 and 42 days after treatment, and the early treatment raw water has a smaller number of actinomycetes species. Moreover, sulfate-reducing bacterial communities have the smallest species richness, with very little impact of inoculation.

The peak density (relative intensity) of each gel band was recorded for principle component analysis (PCA), as shown in Fig. 11. The results indicate that, although

the diversity of microbial communities in the raw water has an obvious shift over time, the treatment by the addition of inoculation efficient strain HF3 has no significant influence on the indigenous microorganisms' population diversity. It suggests that the efficient aerobic denitrifying bacteria HF3 would not change the microbial community structure of raw water, and has high ecological safety.

4 Toxicological Safety on Aquatic Animals

Fish play a significant role in the aquatic food chain as the most important economic animal in aquatic environments. Among the different aquatic organisms' toxicity evaluation experiments, fish acute toxicity tests play an important role in water environmental risk assessment and hazard classification. Zebrafish is a popular aquarium fish, with a small size (4–6 cm length), a short generation time (3 months), a high reproductive rate, and a cheap and convenient feeding condition. It can live in the environments of wide pH and temperature ranges, and is sensitive to toxicity in water. Thus, it has been widely used in aquatic toxicology tests, developmental biology, and molecular genetics [41, 42]. Microcystin-LR (MC-LR) is a naturally occurring toxin produced by cyanobacteria, and is considered the most toxic compound of the microcystins. MC-LR is extremely stable in water and can withstand chemical breakdown, such as hydrolysis or oxidation. The toxicity of MC-LR is very diverse and includes neurotoxicity, hepatotoxicity, cytotoxicity, and dermatotoxicity. The toxic effect of MC-LR is due to its inhibition of protein phosphatases [43].

4.1 Experiment Setup

For the toxicity test, MC-LR was purchased from Beijing Puhuashi Technology Ltd., and the zebrafish were purchased from a pet market in Xi'an, China. The tested samples using the efficient aerobic denitrifying bacteria strain HF3, which was isolated and cultured in a low-nitrogen medium in order to remove nitrogen under oligotrophic conditions. Before the experiment, the zebrafish were acclimated for at least 14 days in conditions of 25 ± 1 °C and a light/dark photoperiod of 16/8 h. Well-aerated water to remove the chlorine was used for acclimation. The fish were fed regularly every day and the water renewal procedure was chosen to minimize handling stress and disturbances for the fish. The zebrafish can be used for testing only if the death rate of the fish was below 10 % during the 12 days after 48 h of acclimation. The fish must be prevented from feeding for 24 h just before the test begins, for complete defecation [44].

4.2 Acute Toxicity Test

The acute toxicity test was performed as per the Chinese standard. Well-aerated water to remove the chlorine was used for the tests. Zebrafish with health and activity were randomly selected for the experiment. The experimental setup consisted of seven water controls, including five testing controls, a blank control, and a toxic control.

The efficient strain HF3 was cultured at 37 °C for 24 h using the FJ liquid medium. Add the inoculated liquid medium into the testing water controls with a concentration of 30, 100, 300, 900, and 2700 mg/L, respectively. The blank control used FJ liquid medium without inoculation, and the toxic control had MC-LR added, with a concentration of 200 μg/L. Each test group had three parallel samples and a volume of 3 L of testing water in a 5-L beaker (Fig. 12), with ten zebrafish exposed inside. The experiment lasted 96 h at 25 ± 1 °C and a light/dark photoperiod of 16/8 h without any feeding, aeration, or water renewal. The toxic effects of the efficient strain HF3 after exposure of 3, 6, 12, 24, 48, 72, and 96 h were observed and recorded.

4.3 Short-Term Histological Toxicity Test

The efficient strain HF3 was cultured at 37 °C for 24 h using the FJ liquid medium. Then, the strain cells were collected by centrifuging at 2300*g* and 4 °C for 10 min. The collected cells were resuspended by PBS at a concentration of 1×10^6 cfu/mL. The short-term toxicity test consisted of three tanks of each water control, testing control (1×10^6 cfu/mL of efficient strain HF3), blank control (equivalent of PBS), and toxic control (200 μg/L of MC-LR). Thirty fish per control were randomly

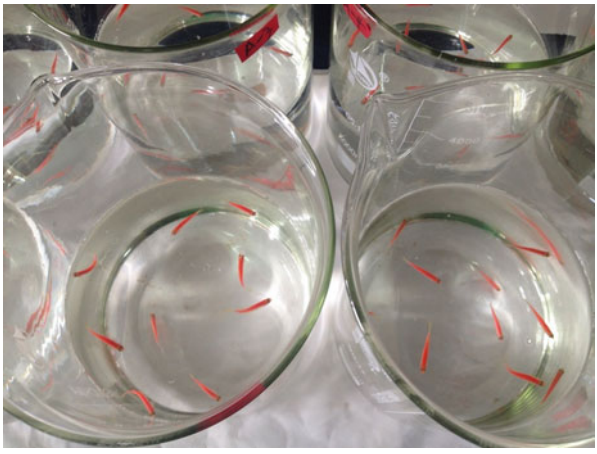

Fig. 12 Water controls of the acute toxicity test by the addition of effectively oligotrophic aerobic denitrifying bacterial isolate HF3

selected and assigned to well-aerated tanks at 25 ± 1 °C and a light/dark photoperiod of 16/8 h without any feeding, aeration, or water renewal for 96 h.

Three fish per control were randomly selected for histological observation at 3, 6, 12, 24, 48, and 96 h after exposure. Gonads, livers, brains, intestines, and kidneys were immediately excised. The excised tissues were frozen in liquid nitrogen for 10–20 s and then stored at −80 °C. For the histological examination, tissues were embedded in Tissue-Tek OCT Compound (Sakur Ltd., USA). Sections were taken along the long axis of the tissues at 10-μm intervals by CM1850 Freezing Microtome (Leica Biosystems, Germany) and stained with hematoxylin and eosin as follows [44–46].

- Fix sections in 4 % paraformaldehyde (w/v) for 30–60 s.
- Rinse sections under running water for 10 s.
- Stain sections with hematoxylin for 3–5 min.
- Rinse sections under running water for 10 s.
- Place sections in 1 % hydrochloric acid alcohol for 3–5 s for differentiation.
- Rinse under running water for 10 s.
- Place sections in 0.5 % dilute ammonia for 20 s.
- Rinse sections under running water for 10 s.
- Stain sections with eosin for 10–20 s.
- Rinse sections under running water for 10 s.
- Dehydrate sections in graded ethanol and xylene.
- Seal sections with neutral balsam.

The obtained sections were microscopically examined to reveal histological changes by a Nikon 90i Microscope (Nikon, Japan).

4.4 Long-Term Toxicity Test

For the long-term toxicity test, raw water from Shibianyu Reservoir of Xi'an City, China, was used to simulate the in situ condition. The efficient strain HF3 was cultured at 37 °C for 24 h using the FJ liquid medium. Then, the inoculated liquid medium were mixed with an equivalent amount of the raw water and cultured at 37 °C for 5 days for acclimation. The acclimated liquid was inoculated into new 100 % raw water and cultured at 37 °C for another 5 days for secondary acclimation. The two rounds of acclimation would ensure the efficient strain HF3 to be effective and reliable in simulating the in situ condition. The long-term toxicity test consisted of two water controls: testing control (0.1 mg/L of secondary acclimated liquid) and blank control. Thirty zebrafish per control were randomly selected and assigned for three months to simulate the hydraulic retention time. The fish were fed regularly every day and each water control was aerated with a dissolved oxygen concentration of 9.6 mg/L at 15 °C. During the test, mortality and abnormal behavior were recorded daily. Three zebrafish per water control were randomly

selected for histological examination at the end of the experiment. Sections were obtained and stained as per the short-term histological toxicity test.

4.5 Results of the Acute Toxicity Tests

During the 96-h acute experiment, the zebrafish in both testing controls and the blank control had active behavior and were in good condition without any mortality. There was no abnormal behavior, such as loss of balance, dyspnea, muscle dysfunction, and pigmentation at different concentrations of the efficient strain HF3. In contrast, the fish exposed to toxic control with an MC-LR concentration of 200 μg/L were obviously poisoned. After 48 h of exposure, the fish in the toxic control group were observed to have loss of physical function, lethargy, and listlessness. Mortality had been detected after 96 h of exposure. The result indicated that, besides the concentration of 2700 mg/L of biological agent, there are no negative influences on the zebrafish by the addition of efficient strain HF3 at different concentrations. This suggests that the efficient aerobic denitrifying bacteria HF3 had high safety on the acute aquatic animal toxicity tests.

4.6 Short-Term Histological Toxicity Test

There were no obvious changes of the intestine tissue in either the blank controls or the testing controls during the 96-h exposure. As shown in Fig. 13a, leafy or columnar villi consisted of intestinal mucosa and mucosa lamina propria, and goblet cells can be occasionally found on intestinal mucosa. However, in toxic controls, necrosis and shedding occurred in the intestinal villus epithelial cells, and the normal morphological structure of the mesenchyme disappeared (Fig. 12b).

None of the obvious changes of hepatic tissue had been observed in either the blank or testing controls. The hepatic cells were of a polygon shape with uniform cytoplasm, the edges between hepatocytes were clouding, and the nuclei were big and round (Fig. 14a). In contrast, there was vacuolar degeneration, with different sizes between hepatocytes (Fig. 14b).

As MC-LR is not a nerve poison, there was no obvious damage of brain tissue in all three water controls during the 96-h exposure (Fig. 15).

There were no obvious histological changes in renal tissue in either the blank or testing controls (Fig. 16a), while the mortality of renal cells and disappearance of the normal structure of the kidney were observed in toxic controls (Fig. 16b).

The zebrafish exposed in the testing control inoculated by the efficient strain HF3 had no histological difference in gonads tissue compared with the fish exposed in the blank control. As shown in Fig. 17a, mature follicles had been observed under the microscope with uniform and big nuclei, and clouding edges in the gonads tissue of the testing control after 96 h of exposure. However, in the gonads sections

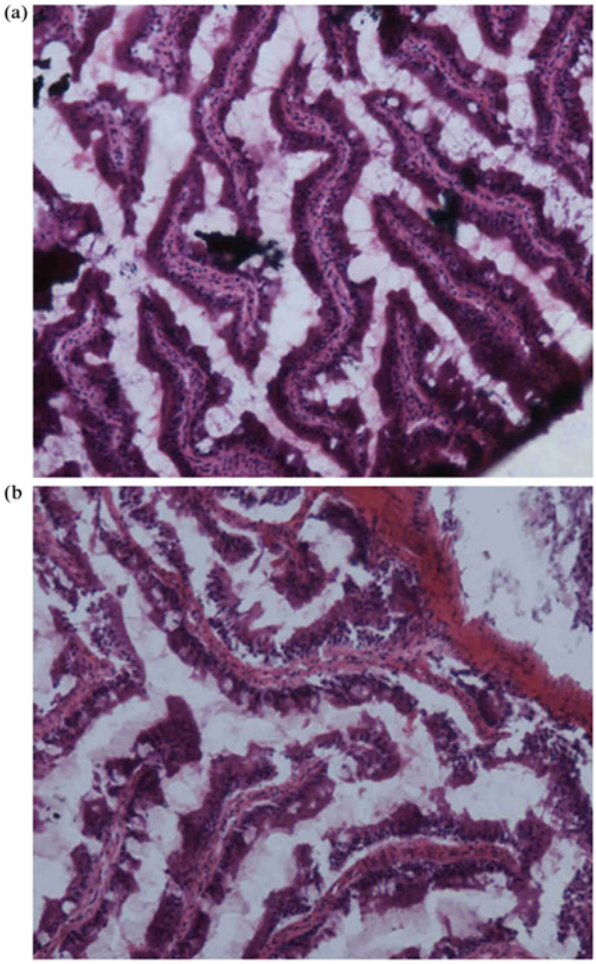

Fig. 13 Micrograph of zebrafish intestine tissue sections in: (**a**) testing control, (**b**) toxic control after 96 h of exposure

of the toxic control, there were obvious disappearances of nuclei and cytoplasms (Fig. 17b).

MC-LR can inhibit the growth of fish embryos and cause pathological changes, especially in the liver and kidney. The results of the short-term histological toxicity tests showed that there will not be any similar or other damage to the zebrafish during the 96-h exposure of the biological agent used in this study, even with a relatively high concentration of 1×10^6 cfu/mL. It is suggested that the efficient strain HF3 has high toxicological safety on aquatic animals. In addition, as HF3 is an efficient aerobic denitrifying bacteria, it can inhibit the growth of cyanobacteria by removing the nitrogen nutrients in water. Therefore, the efficient strain HF3 may alleviate the histological damages caused by MC-LR to the fish under certain conditions.

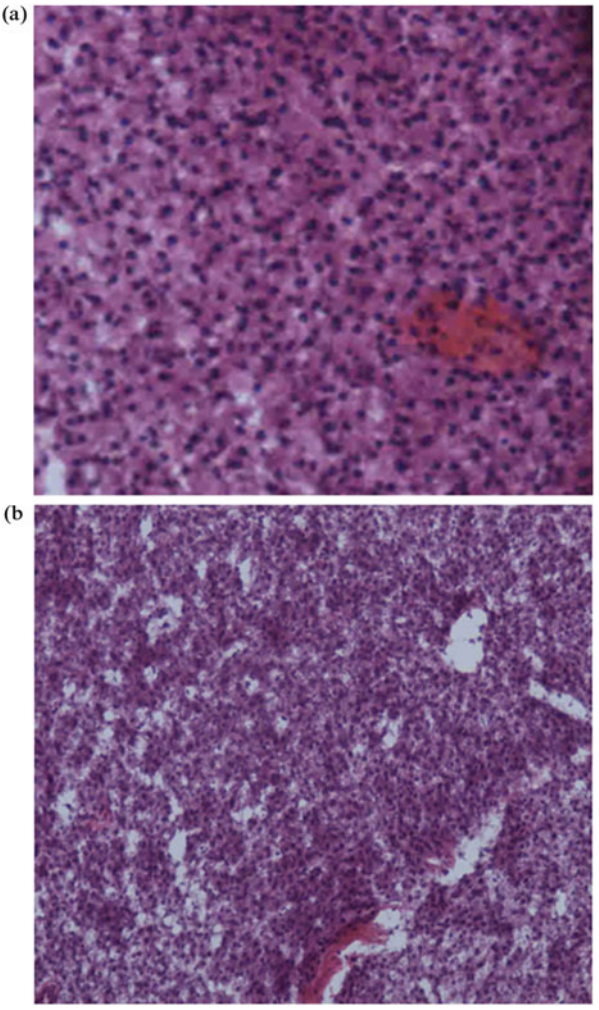

Fig. 14 Micrograph of zebrafish hepatic tissue sections in: (**a**) testing control, (**b**) toxic control after 96 h of exposure

4.7 Long-Term Toxicity Test

During the three-months experiment, there were no obvious differences between the zebrafish in the testing control and the blank control. The fish were in good condition during the exposure, with active and group behavior, and normal sexual maturity and spawning. No mortality or abnormal behaviors were detected in either of the water controls. In addition, there were no pathological changes in the histological examination at the end of exposure. The results of the long-term test indicated that a symbiosis between the efficient strain HF3 and the zebrafish is definitely possible under the simulated in situ conditions, as the biological agent will not cause any damage or inhibiting effects on the aquatic animals.

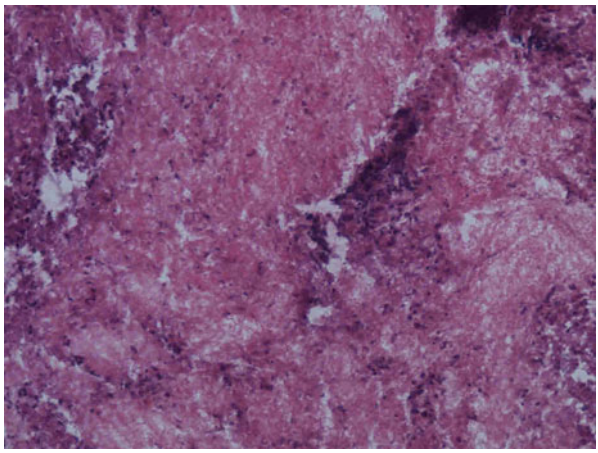

Fig. 15 Micrograph of zebrafish brain tissue sections in testing control after 96 h of exposure

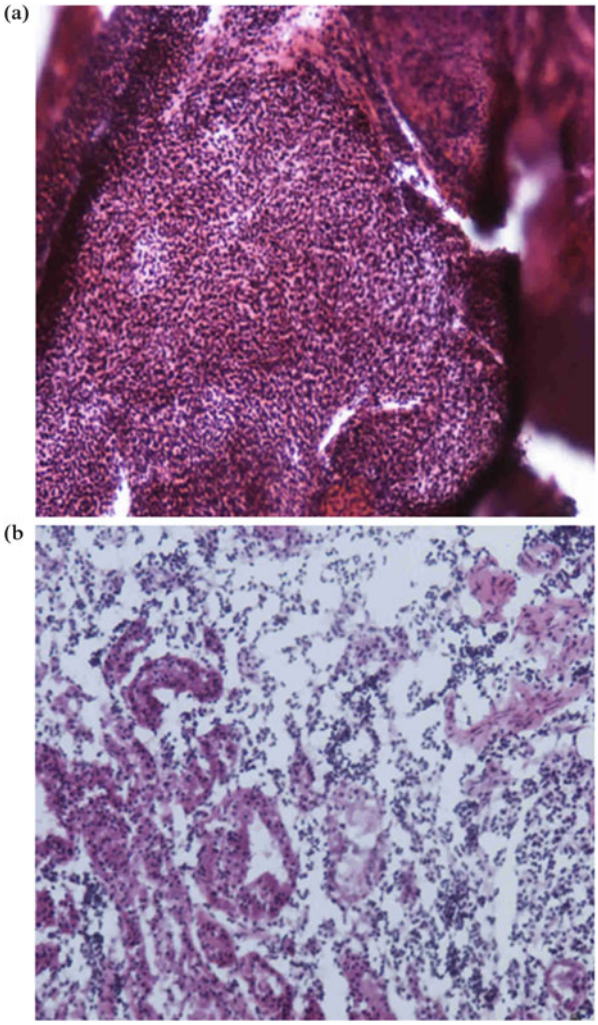

Fig. 16 Micrograph of zebrafish renal tissue sections in: (**a**) testing control, (**b**) toxic control after 96 h of exposure

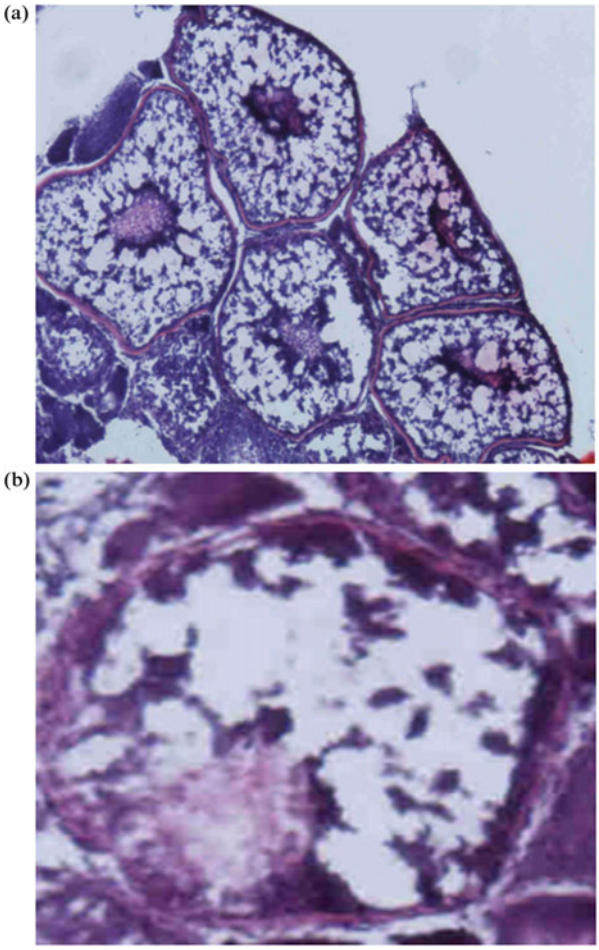

Fig. 17 Micrograph of zebrafish ovarian tissue sections in: (**a**) testing control, (**b**) toxic control after 96 h of exposure

4.8 Summary

This study discussed the toxicological safety of in situ biological purification technology on aquatic animals by acute, short-term, and long-term toxicity tests. The results showed that the efficient aerobic denitrifying bacteria strain HF3 used in this study had no toxic symptoms or caused death among zebrafish. In addition, the biological agents may decrease the damage caused by microcystins by restraining the algal growth. The results suggested that the efficient strain HF3 has a high safety for the animals in reservoir ecosystems.

References

1. Shrimali M, Singh KP (2001) New methods of nitrate removal from water. Environ Pollut 112:351–359
2. Tian WJ, Hao FH, Zhai JB (2008) Elasticity plastic filler for purification of polluted streams in situ entering lake. Environ Sci 29:1308–1312
3. Ji M, Zhou J, Ren ZY (2002) Comparison on bio-contact oxidation tank and ceramic bio-filter process for micro-polluted raw water pre-treatment. Water Wastewater 28:26–29
4. Lee KC, Rittmann BE (2002) Applying a novel autohydrogenotrophic hollow-fiber membrane biofilm reactor for denitrification of drinking water. Water Res 36:2040–2052
5. Janez V, Milenko R (2006) Denitrification of groundwater in the biofilm reactor with a specific biomass support material. Acta Chim Slov 53:396–400
6. Fabbricino M, Pettab L (2007) Drinking water denitrification in membrane bioreactor/membrane contactor systems. Desalination 210:163–174
7. Singer A, Parnes S, Gross A, Sagi A, Brenner A (2008) A novel approach to denitrification processes in a zero-discharge recirculating system for small-scale urban aquaculture. Aquacult Eng 39:72–77
8. Ovez B, Ozgen S, Yuksel M (2006) Biological denitrification in drinking water using *Glycyrrhiza glabra* and *Arunda donax* as the carbon source. Process Biochem 41:1539–1544
9. Buttiglieri G, Malpei F, Daverio E, Melchiori M, Nieman H, Ligthart J (2005) Denitrification of drinking water sources by advanced biological treatment using a membrane bioreactor. Desalination 178:211–218
10. Fan B, Qu JH, Liu SX (2001) Nitrate removal from drinking water by three-dimension electrode electrochemical-biofilm reactors. Acta Sci Circum 21:39–43
11. Luo QF, Tan YM, Wang L (2003) Research on drinking water denitrification. J Safety Environ 3:58–61
12. Shnel N, Barak Y, Ezer T (2002) Design and performance of a zero-discharge tilapia recirculating system. Aquacult Eng 26:191–203
13. Gómez MA, González-López J, Hontoria-García E (2000) Influence of carbon source on nitrate removal of contaminated groundwater in a denitrifying submerged filter. J Hazard Mater 80:69–80
14. Rivas Z, Medina HL, Gutierrez J, Gutierrer E (2000) Nitrogen and phosphorus levels in sediments from tropical catatumbo river (Venezuela). Water Air Soil Pollut 117:27–37
15. Beutel MW (2006) Inhibition of ammonia release from anoxic profundal sediments in lakes using hypolimnetic oxygenation. Ecol Eng 28:271–279
16. Huang TL, Cong HB, Zhou ZM, He WJ, Yin PJ (2006) The onsite experiment study of enhanced bio-contact oxidation process for pretreatment of Luanhe River water. Acta Sci Circum 26:786–790
17. Huang TL, Jia SJ, Cong HB (2008) Experimental study on the water-lifting aerator enhanced chemical oxidation process for polluted raw water. Water Wastewater Eng 34:52–55
18. Heaton THE, Talma AS, Vogel JC (1983) Origin and history of nitrate in confined groundwater in the western Kalahari. J Hydrol 62:243–262
19. Tsai YL, Olson BH (1991) Rapid method for direct extraction of DNA from soil and sediments. Appl Environ Microbiol 57:1070–1074
20. Muyzer G, De Waal EC, Uitterlinden AG (1993) Profiling of complex microbial populations by denaturing gradient gel electrophoresis analysis of polymerase chain reaction-amplified genes coding for 16S rRNA. Appl Environ Microbiol 59:695–700
21. Sheffield VC, Cox DR, Lerman LS (1989) Attachment of 40-base-pair G + C-rich sequence (GC-clamp) to genomic DNA fragments by the polymerase chain reaction results in improved detection of single-base changes. Proc Natl Acad Sci U S A 86:232–236
22. Janse I, Bok J, Zwart G (2004) A simple remedy against artifactual double bands in denaturing gradient gel electrophoresis. J Microbiol Methods 57:279–281

23. Li MY, Zhou GH, Xu XL, Li CB, Zhu WY (2006) Changes of bacterial diversity and main flora in chilled pork during storage using PCR-DGGE. Food Microbiol 23:607–611
24. Xu M (2005) Study on biological contact oxidation process under oligotrophic conditions. Environmental Engineering Department, Guangdong University of Technology, China
25. Chen CL, Liu WT, Chong ML, Wong MT, Ong SL, Seah H, Ng WJ (2004) Community structure of microbial biofilms associated with membrane-based water purification processes as revealed using a polyphasic approach. Appl Microbiol Biotechnol 63:466–473
26. Hoff JC (1986) Inactivation of microbial agents by chemical disinfectants. USEPA, Washington, DC
27. Hao ZM, Shi H, Zhou WJ (2009) Application of javel water in aquatic product processing. Mod Food Sci Technol 25:286–290 (in Chinese)
28. Zhu XW, Liu SS, Ge HL, Liu Y (2009) Comparison between the short-term and the long-term toxicity of six triazine herbicides on *photobacteria* Q67. Water Res 43:1731–1739
29. Ma XY, Wang XC, Liu YJ (2011) Study of the variation of ecotoxicity at different stages of domestic wastewater treatment using *Vibrio-qinghaiensis* sp.-Q67. J Hazard Mater 190:100–105
30. Ma M, Tong Z, Wang Z, Zhu W (1999) Acute toxicity bioassay using the freshwater luminescent bacterium *Vibrio-qinghaiensis* sp. Nov.—Q67. Bull Environ Contam Toxicol 62:247–253
31. Uhl W, Schaule G (2004) Establishment of HPC(R2A) for regrowth control in non-chlorinated distribution systems. Int J Food Microbiol 92:317–325
32. Zhou JZ, Bruns M, Tiedje JM (1996) DNA recovery from soils of diverse composition. Appl Environ Microbiol 62:3216–3221
33. Ma WK, Siciliano SD, Germida JJ (2005) A PCR-DGGE method for detecting arbuscular mycorrhizal fungi in cultivated soils. Soil Biol Biochem 37:1589–1597
34. Liang ZB, Drijber RA, Lee DJ, Dwiekat IM, Harris SD, Wedin DA (2008) A DGGE-cloning method to characterize arbuscular mycorrhizal community structure in soil. Soil Biol Biochem 40:956–966
35. Zhang HH, Huang TL, Liu TT (2013) Sediment enzyme activities and microbial community diversity in an oligotrophic drinking water reservoir, eastern China. PLoS One 8:e78571
36. Helgason T, Daniell TJ, Husband R, Fitter AH, Young JPW (1998) Ploughing up the wood-wide web? Nature 394:431
37. Schwarzott D, Schussler A (2001) A simple and reliable method for SSU rRNA gene DNA extraction, amplification, and cloning from single AM fungal spores. Mycorrhiza 10:203–207
38. Kowalchuk GA, De Souza FA, Van Veen JA (2002) Community analysis of arbuscular mycorrhizal fungi associated with *Ammophila arenaria* in Dutch coastal sand dunes. Mol Ecol 11:571–581
39. Cornejo P, Azcon-Aguilar C, Barea JM, Ferrol N (2004) Temporal temperature gradient gel electrophoresis (TTGE) as a tool for the characterization of arbuscular mycorrhizal fungi. FEMS Microbiol Lett 241:265–270
40. Zheng GQ, Zheng ZY, Xu X, Hu ZH (2010) Variation in fruit sugar composition of Lycium barbarum L. and Lycium chinense Mill. of different regions and varieties. Biochem Syst Ecol 38:275–284
41. Hill AJ, Teraoka H, Heideman W, Peterson R (2005) Zebrafish as a model vertebrate for investigating chemical toxicity. Toxicol Sci 86:6–19
42. Xiang J, Yang H, Che C, Zou H, Yang H, Wei Y, Quan J, Zhang H (2009) Identifying tumor cell growth inhibitors by combinatorial chemistry and zebrafish assays. PLoS One 4:e4361
43. Pereira S, Vasconcelos V, Antunes A (2013) Computational study of the covalent bonding of microcystins to cysteine residues – a reaction involved in the inhibition of the PPP family of protein phosphatases. FEBS J 280:674–680
44. Westerfield M (2007) The zebrafish book: a guide for the laboratory use of zebrafish (Danio Rerio). University of Oregon Press, Eugene

45. Christen V, Zucchi S, Fent K (2011) Effects of the UV-filter 2-ethyl-hexyl-4-trimethoxy-cinnamate (EHMC) on expression of genes involved in hormonal pathways in fathead minnows (*Pimephales promelas*) and link to vitellogenin induction and histology. Aquat Toxicol 102:167–176
46. Zhu B, Liu T, Hu X, Wang G (2013) Developmental toxicity of 3,4-dichloroaniline on rare minnow (*Gobiocypris rarus*) embryos and larvae. Chemosphere 90:1132–1139

Index

T. Huang (ed.), *Water Pollution and Water Quality Control of Selected Chinese Reservoir Basins*, The Handbook of Environmental Chemistry 38,
DOI 10.1007/978-3-319-20391-1